PREPARATION, CHARACTERIZATION AND INTRAMOLECULAR ELECTRON-TRANSFER STUDIES OF RUTHENIUM-MODIFIED CYTOCHROMES *c*

Thesis by

Deborah Sharon Wuttke

In Partial Fulfillment of the Requirements

for the Degree of

Doctor of Philosophy

California Institute of Technology

Pasadena, California

1994

(Submitted October 7, 1993)

Acknowledgments

I am indebted to many extraordinary individuals for both their academic and personal support and encouragement during my graduate years. I only regret that I can single out just a few of them here.

First and foremost, I thank Harry Gray for sharing his unbounded enthusiasm for science and providing me the freedom to explore and develop independence. Although I will always remain grateful for all Harry has taught me, most of all I will always value his kindness and friendship.

At Caltech I have enjoyed and benefited from many stimulating scientific interactions with experts in their fields. I thank Jay Winkler for generously sharing his expertise with the laser measurements and their interpretation, David Beratan for kind assistance with the pathway analysis on the elephants, Dimitrios Morikis and Peter Wright for their collaboration on the NMR work, and Stewart Fisher and Barbara Imperiali for their collaboration on the bipyridyl-alanine project. I am especially grateful to Jackie Barton for her encouragement and insightful advice.

I am extremely fortunate to have been a member of the talented and everchanging Gray group. I am grateful to have had the opportunity to learn from and work alongside Brad, Bruce, Mike T., Danny, Luet, Jeff, Gary, I-Jy, Morten, Angelo, Jorgé, Kara, Jack, Bill, Jens, Tim, and Yi. I especially thank Adrienne for introducing me to semisynthesis and preparing me for the trials and tribulations of life in the Gray group. Much more important, however, is the friendship and support offered by these and other colleagues. In particular, I will happily remember the times spent with Adrienne, Angelo, Bill, Brad, Don, Eric, Eva, Gary, Jack, Jay, Jens, Jim, Jorgé, Julia, Kara, H. Mark, Mike H., Anne, Mike T., Morten, Ramy, and Toshi.

Several people have played a special part in my Caltech experience. I thank my parents whose caring and unwavering support have made this all possible. Chris, Sandi and Martha are wonderful friends, celebrating the good times and consoling me

otherwise. I especially thank Julia for hours of free counseling and her creative excuses for having "just one." I will desperately miss our Friday lunch dates! Finally, I reserve a special thanks for Bill for giving me his continual support, advice and friendship.

Abstract

Redox-active ruthenium complexes have been covalently attached to the surface of a series of natural, semisynthetic and recombinant cytochromes *c*. The protein derivatives were characterized by a variety of spectroscopic techniques. Distant Fe^{2+} - Ru^{3+} electronic couplings were extracted from intramolecular electron-transfer rates in $Ru(bpy)_2(im)HisX$ (where X = 33, 39, 62, and 72) derivatives of cyt *c*. The couplings increase according to 62 (0.0060) < 72 (0.057) < 33 (0.097) < 39 (0.11 cm^{-1}); however, this order is incongruent with histidine to heme edge-edge distances [62 (14.8) > 39 (12.3) > 33 (11.1) > 72 (8.4 Å)]. These results suggest the chemical nature of the intervening medium needs to be considered for a more precise evaluation of couplings. The rates (and couplings) correlate with the lengths of σ-tunneling pathways comprised of covalent bonds, hydrogen bonds and through-space jumps from the histidines to the heme group. Space jumps greatly decrease couplings: one from Pro71 to Met80 extends the σ-tunneling length of the His72 pathway by roughly 10 covalent bond units. Experimental couplings also correlate well with those calculated using extended Hückel theory to evaluate the contribution of the intervening protein medium.

Two horse heart cyt *c* variants incorporating the unnatural amino acids (*S*)-2-amino-3-(2,2'-bipyrid-6-yl)-propanoic acid (6Bpa) and (*S*)-2-amino-3-(2,2'-bipyrid-4-yl)-propanoic acid (4Bpa) at position 72 have been prepared using semisynthetic protocols. Negligible perturbation of the protein structure results from this introduction of unnatural amino acids. Redox-active $Ru(2,2'\text{-bipyridine})_2^{2+}$ binds to 4Bpa72 cyt *c* but not to the 6Bpa protein. Enhanced ET rates were observed in the $Ru(bpy)_2^{2+}$-modified 4Bpa72 cyt *c* relative to the analogous His72 derivative. The rapid (< 60 nanosecond) photogeneration of ferrous Ru-modified 4Bpa72 cyt *c* in the conformationally altered alkaline state demonstrates that laser-induced ET can be employed to study submicrosecond protein-folding events.

Table of Contents

List of Figures

List of Tables

List of Abbreviations

1-D	one-dimensional
2-D	two-dimensional
4Bpa	(*S*)-2-amino-3-(2,2'-bypyrid-4-yl)propanoic acid
6Bpa	(*S*)-2-amino-3-(2,2'-bypyrid-6-yl)propanoic acid
a	ammine
bpy	2,2'-bipyridine
CD	circular dichroism
C. k.	*Candida krusei*
cyt *c*	cytochrome *c*
CZE	capillary zone electrophoresis
DEPC	diethylpyrocarbonate
EDTA	ethylenediaminetetraacetic acid
EPR	electron paramagnetic resonance
ET	electron transfer
FPLC	fast protein liquid chromatography
H-bond	hydrogen bond
HEPES	*N*-2-hydroxyethylpiperazine-*N'*-2-ethanesulfonic acid
Hse	homoserine
im	imidazole
k_d	observed rate constant for excited-state decay
k_{ET}*	rate constant for electron transfer from a Ru excited state to the heme
k_{ET}^{mm}	rate constant for electron transfer from ferric heme to a Ru^{3+} species
mg	milligram
ml	milliliter
MW	molecular weight
NaPi	sodium phosphate buffer

NHE	normal hydrogen electrode
NMR	nuclear magnetic resonance
PC	personal computer
PMT	photomultiplier tube
py	pyridine
Rua_5	pentaaminеruthenium
s	second
S. c.	*Saccharomyces cerevisiae*
SCE	saturated calomel electrode

Standard three-letter abbreviations are used for the amino acids (*Pure Appl. Chem.* **1984**, *56*, 595).

Chapter 1

Introduction

I. Introduction and Overview

Electron transfer (ET) is the fundamental process underlying energy storage and utilization in biological systems.[1] It is the basis for the conversion of light into chemical energy in photosynthetic reaction centers and the reduction of dioxygen to water with the concomitant production of ATP in the mitochondrial respiratory chain. Observed biological ET rates span at least thirteen orders of magnitude, with the fastest observed ET occurring in 3 ps in the photosynthetic reaction center. Developing an understanding of the factors which govern biological ET rates will lead to synthetic and engineered systems that can mimic the energy utilization and enzymatic properties inherent in reduction / oxidation active (redox) proteins. Now that it has been firmly established that ET occurs between well-separated and specifically oriented redox centers within proteins and protein complexes,[2,3] attention has turned to the role of the polypeptide in controlling both the ET process and the properties of the participating redox centers. Semisynthesis in conjunction with site-directed mutagenesis and site-specific modification has been used to prepare novel ET proteins; theoretical and experimental work on these proteins has contributed to the elucidation of the factors that modulate ET through polypeptide structures.

A. Electron-Transfer Theory

The intrinsic simplicity of an ET reaction between two redox centers results in a theoretically tractable problem. Marcus has derived a semiclassical expression based on transition state theory relating observed rates of ET to thermodynamic driving force, reorganization energy, and electronic coupling between redox sites for nonadiabatic ETs at fixed distance and medium between donor and acceptor:[4]

$$k_{ET} = \sqrt{\frac{4\pi^3}{h^2 \lambda k_b T}}\,[H_{AB}]^2\,\exp\left(\frac{-(\Delta G^\circ + \lambda)^2}{4\lambda k_b T}\right)$$

where k_b is Boltzmann's constant, T is temperature, *h* is Planck's constant, H_{AB} is the electronic coupling term, ΔG^o is the change in free energy for the reaction, and λ is the sum of the inner and outer sphere contributions to the reorganization energy. The one-dimensional potential energy surfaces illustrating this model for ET are presented in Figure 1.1.

The exponential term, referred to as the nuclear or Franck-Condon term, imparts the dependence of the observed ET rate on driving force and reorganization energy. The reorganization energy is free energy associated with bond-length changes (inner sphere) and solvent dipole adjustments (outer sphere) between the equilibrium conformations of the reactant and product molecules. The free energy of reaction can be obtained from the electrochemical potentials of the redox species involved in the reaction. If the reactant and product nuclear configurations are approximated as harmonic oscillators (as shown in Figure 1.1), the activation energy for the ET reaction is:

$$\Delta G^* = \frac{-(\Delta G^o + \lambda)^2}{4\lambda}$$

ET can only occur when vibrational fluctuations bring the system into the transition state conformation (the crossing point, C, of the product and reactant curves). The quadratic dependence of ΔG^* on ΔG^o results in the so-called "inverted" region of ET. As the driving force ($-\Delta G^o$) for an ET reaction (at constant λ) increases from zero to λ, the predicted rate increases reaching a maximum value at $-\Delta G^o = \lambda$. At this point the exponential term is unity and the ET reaction is activationless. As $-\Delta G^o$ increases in the region $-\Delta G^o > \lambda$, the observed rate of ET *decreases* with increasing driving force. This counterintuitive prediction was first experimentally verified by Closs, Miller, and

Figure 1.1 One-dimensional potential energy surfaces as a function of an arbitrary nuclear coordinate for ET in the "normal" region, where $-\Delta G^{o} < \lambda$. $-\Delta G^{o}$, ΔG^{*}, and λ are indicated. Dotted lines indicate the avoided crossing (C) present in the absence of any electronic interaction. Solid lines indicate the electronically coupled states.
Figure not drawn to scale.

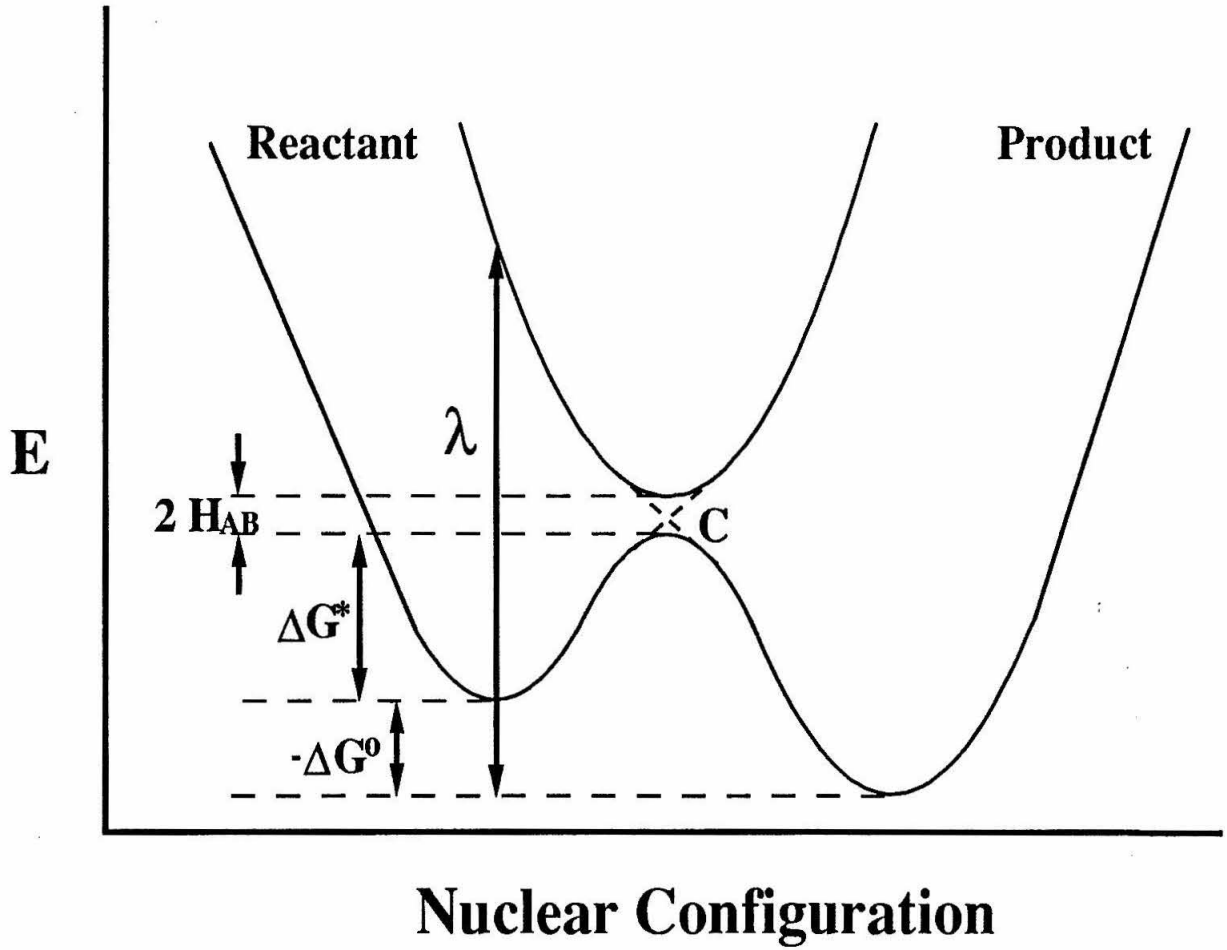
Reactant
Product
E
λ
2 H_{AB}
C
ΔG^*
$-\Delta G^o$
Nuclear Configuration

coworkers in steroid-bridged donor / acceptor systems by studying ET rates at a fixed distance as a function of $-\Delta G^{o}$.[5]

In the transition state conformation, the electron must have some probability of residing on both the donor and acceptor for ET to occur, necessitating some electronic interaction between the donor and acceptor. This electronic coupling (H_{AB}) of the donor and acceptor species causes a splitting of the product and reactant states at the crossing point by $2\ H_{AB}$. Even though this coupling is formally a function of all the electrons in the system, it can be approximated as a one-electron resonance integral.[6] In the case of significant electronic coupling between donor and acceptor ($\geq 80\ cm^{-1}$), this splitting is large enough to ensure that once the system reaches the transition state, electron transfer will occur (adiabatic case). However, frequently in biological systems the electronic coupling is small, on the order of $0.1\ cm^{-1}$ or less. This is the nonadiabatic regime where, at the transition state configuration, the small electronic coupling translates into a small probability that the system can cross onto the product curve to yield productive ET. Therefore, in the nonadiabatic case, ET rates are mainly limited by poor electronic coupling.

B. Donor / Acceptor Systems

There are inherent complexities in studying bimolecular ET between two species in solution due to the transient formation of an encounter complex. Thus, it is desirable to study ET rates in covalently linked donor / acceptor complexes (donor-bridge-acceptor) to elucidate the parameters that govern ET reactions. Factors such as driving force, distance and the chemical nature of the intervening medium must be carefully controlled to obtain relevant data to evaluate theoretical models. Studies of ET in such systems have validated Marcus-theory predictions.[1d,5]

These covalently linked systems are well suited for the systematic study of the interactions that mediate electronic coupling between donor and acceptor. At close

contact of the donor and acceptor species, H_{AB} will be directly proportional to the overlap of the electronic wavefunctions of the donor and acceptor. However, because these wavefunctions decay sharply and exponentially with distance, at separation distances larger than the van der Waals contact distance, the electronic coupling due to this direct interaction decays rapidly with donor-acceptor distance. However, if the donor and acceptor species are separated by some intervening medium instead of a vacuum, the medium can couple the donor and acceptor. The question then becomes precisely how the intervening medium between donor and acceptor facilitates the electronic coupling necessary for ET. A first-order model[7] treats the intervening matrix as a square potential barrier through which the electron tunnels, predicting that H_{AB} will decay exponentially with increasing intervening distance. In this model, H_{AB} is formulated as:

$$H_{AB} = H_{AB}^{o} \exp [-1/2 \beta (R - R_o)]$$

where H_{AB}^{o} is the electronic coupling at van der Waals contact, R is the donor-acceptor distance, R_o is the contact distance, and β is an attenuation factor describing the magnitude of the rate decay with distance.

In model systems constructed with rigid homogeneous chemical bridges between the donor and acceptor species, *e.g.*, steroid bridges or norbornyl bridges,[1d] H_{AB} varies exponentially with donor-acceptor distance. In simple donor / acceptor systems, the square potential barrier model describes observed rates well if the chemical nature of the bridge is conserved. However, the *magnitude* of β depends on the chemical composition of the bridge.[1d] For example, in systems where the bridge is saturated, β is on the order of 0.5 to 1.0 $Å^{-1}$. If the bridging group contains filled π levels, the medium can be thought of as "conducting" electrons more readily (lowering the tunneling barrier) and β is on the order of 0.1 to 0.5 $Å^{-1}$. Bridge-mediated superexchange arises from the localized wavefunction of the donor and acceptor both coupling to the medium.

Extended Hückel (superexchange type) calculations on rigid donor / acceptor model systems confirm that electronic couplings are a function of the chemical nature of the bridging species and predict βs that are in reasonable agreement with experimentally derived values.[8]

C. Electronic Coupling in Protein-Mediated Electron Transfer

Nonadiabatic electron transfer is known to occur between redox centers separated by 5 - 20 Å in proteins;[1,2] these distances are far too large for direct coupling. Therefore, the redox centers are electronically coupled *via* the protein medium. It seems reasonable to postulate that the intrinsic heterogeneity of the protein structure can enhance or inhibit coupling.[10,11] However, the contribution of the precise molecular and electronic structure of the intervening medium to the overall coupling may be minor, such that the protein medium can be considered essentially homogeneous. If H_{AB} is insensitive to the nature of the intervening protein medium, an exponential dependence on distance analogous to that observed in covalently-linked model systems is anticipated.[12] Such an experimental result would allow one to derive a universal value of β for the protein medium and thus predict electronic couplings based on merely the distance between redox centers.

Recent technical advances in molecular biology, chemical synthesis, and laser technology have made it possible to systematically engineer, structurally characterize and measure ET rates in biological systems. Initially, ET rates measured in protein:protein complexes indicated that the protein medium is not homogeneous with regard to its potential to couple redox sites. Heme-heme ET studies of the cyt *c*:cyt *c* peroxidase complex[13] using genetically engineered mutants of cyt *c* implied that intervening electron-rich aromatic side chains of tyrosine, phenylalanine, and tryptophan were required for strong couplings. This conclusion was intuitively attractive because the presence of energetically accessible HOMO and LUMO levels of the intervening aromatic groups could facilitate electron tunneling *via* a superexchange mechanism.

Additionally, it was consistent with the lower β values measured in model compounds with unsaturated bridges. However, it was subsequently found that the mutations made to non-aromatic residues needed for the systematic study perturbed the nature of the complex, so the ET measurements were made in a series of complexes with different conformations, donor-acceptor distances, and intervening medium.[14] Similar perturbation of the protein:protein complex geometry has been observed in the putidaredoxin:cyt P-450$_{cam}$ complex upon mutagenesis of the C-terminal Trp residue of putidaredoxin.[15] Therefore, to obtain high quality data regarding the molecular interactions that mediate electronic coupling, it is necessary to use a well-defined protein structure for which the distance and intervening medium between redox centers is unambiguously known.

Gray and co-workers have pioneered the study of ET in structurally characterized metalloproteins containing a single redox center by appending a second redox agent to the protein surface.[9] This creates a well-defined donor / acceptor system which is used to investigate ET at known driving force, distance and intervening medium. Although the proteins and protein complexes responsible for ET in biological systems are far more complicated than the covalently linked model systems, by varying the position and electrochemical and photochemical properties of the redox probe, it is possible to evaluate biological ET rates within the context of semiclassical Marcus theory.

Modification of surface histidine residues of proteins with ruthenium complexes has led to significant insights into the mechanism of biological ET.[9] Early studies used a Ru(bpy)$_3^{2+}$ (bpy = 2,2'-bipyridine) flash system to bimolecularly initiate ET in Rua$_5$-modified (a = NH_3) iron-heme proteins.[16] However, in the low driving force regime (for this ET: λ = 1.2 eV, $-\Delta G^o$ = 0.2 eV[9a,b]), the observed rates are extremely sensitive to small changes in driving force, leading to large errors in the derived values of H_{AB}, β and λ. Additionally, in this experiment a microsecond flash is needed to generate detectable ET, precluding resolution of fast ET events. Substitution of the iron in the heme with

zinc allows one to initiate ET directly between the long-live photogenerated excited state of the Zn-porphyrin and a $Rua_4(X)$-complex (X = ammine, pyridine, isonicotinimide) bound to a surface His residue at driving forces near the reorganization energy ($-\Delta G^o$ = 0.6 - 1.0 eV).[17] These studies provided the first indication that, in heme proteins with biological ET activity, electronic couplings are not consistent with a strictly distance-dependent model but rather correlate well with a σ-bond tunneling formulation.[10]

Comparison of rates obtained from ruthenium-modified His33 (horse heart),[16,17] His39 (*Candida krusei (C. k.)*),[18] and His62[19] (genetically engineered *Saccharomyces cerevisiae(S. c.)*) cyts *c* provide evidence for a medium-dependent formulation of electronic coupling. It was observed that ET rates were enhanced 3-fold in a series of $Rua_4(X)$-His39 Zn-cyts *c* relative to rates obtained in $Rua_4(X)$-His33-Zn cyts *c*,[18a] even though His39 is located ~ 1.2 Å *further* from the heme (edge-edge distances: His39-heme = 12.3 Å, His33-heme = 11.1 Å). The rate enhancement is more dramatic at lower driving force. The Fe^{2+} to Ru^{3+} ET rate in Rua_5His39 cyt *c* is approximately ten-fold greater than that in the His33 derivative.[18b] Attributing the stronger donor-acceptor coupling in His39 at longer distance than His33 to a protein medium effect is problematic, as the interpretation is sensitive to the convention employed for measuring donor-acceptor distances. Specifically, it depends on the whether the Zn-porphyrin triplet excited state is considered to be fully delocalized on the porphyrin ring. The difference between the porphyrin-localized states of Zn cyt *c* and the metal-localized state of native cyt *c* may explain the additional rate enhancement in the Fe proteins. Also, the structure of the Zn porphyrin cyt *c* may be perturbed relative to the native protein[20] and aforementioned distances were obtained from the crystal structure of the unmodified native heme protein.

Analogous ET rates measured in native and Zn porphyrin Ru-modified *S. c.* His62 cyt *c* (edge-edge distance = 14.8 Å) indicate that intervening aromatic (Trp) and polarizable (Met) residues do not enhance electronic coupling. The observed 100-fold

decrease in H_{AB} can be attributed to the increase in edge-edge distance relative to His39 and His33 and is also consistent with a medium-dependent σ-bond tunneling model.[19] However, studies on a series of Fe-porphyrin-substituted derivatives of cyt b_5, in which a critical bond between the donor and acceptor is removed by systematically altering the chemical structure of the porphyrin ring, strongly support a medium-dependent formulation of H_{AB} and are entirely inconsistent with predicted electronic couplings based on simple donor-acceptor distance measurements.[21] However, small structural perturbations triggered by the heme substitution could also explain the kinetic data. Finally, ET rates obtained in Zn-porphyrin substituted recombinant human myoglobin are consistent with models for both distance-dependent and medium-dependent electronic coupling.[22]

Recently,[23] a methodology was introduced to study ET using protein derivatives singly modified with a photoactive redox species on the protein surface. ET can be initiated by a short-lived laser pulse, affording observation of photoinduced and thermal ET in iron heme proteins at thermodynamic driving forces on the order of the estimated value for the reorganization energy (0.8 eV).[23a] $Ru(bpy)_2(CO_3)$ undergoes substitution to $Ru(bpy)_2(H_2O)_2^{2+}$ in aqueous solution; the labile aquo ligand is displaced by the imidazole of a surface His residue. Subsequent treatment with excess imidazole affords a $Ru(bpy)_2(im)HisX^{2+}$ modified protein (X = residue number). The $Ru(bpy)_2(im)_2^{2+}$ model complex exhibits a ~70 ns lifetime upon excitation into the 490 nm MLCT transition. These derivatives, combined with the ability to manipulate the primary sequence of cyt *c* thus positioning the redox surface probe at any location with respect to the heme, set the stage for the systematic mapping of the surface of cyt *c* to determine if ET rates depend simply on distance or if the chemical and electronic nature of the medium can actively modulate electronic couplings between redox centers.

D. Thesis Research

Cyt *c* has been selected for ET mapping studies aimed at elucidating the role of the protein medium in mediating electronic coupling. Cyt *c* is an unusually stable, small (12.4 kD), water-soluble, heme-containing protein intimately involved in the mitochondrial electron-transport chain associated with oxidative phosphorylation.[1i, 24] As described previously, intramolecular ET has been probed extensively in cyt *c* using surface modification techniques developed by Gray[9,16-19,25] and others.[26] The protein structure is known at high resolution in both the oxidized and reduced forms.[27] Native proteins are commercially available and the methodology for readily altering the primary sequence has been perfected in the Gray group. The gene for yeast iso-1-cyt *c* has been expressed in yeast cells and is amenable to site-directed mutagenesis.[19] Additionally, it is possible to rebuild the horse heart protein using a semisynthetic methodology.[28] The ability to use semisynthesis in horse heart cyt *c* to engineer changes in the primary sequence unlimited by the twenty naturally occurring amino acids provides additional flexibility in the creation of macromolecular structures suited for the study of long-range biological ET.

Experimental data accompanied by preliminary theoretical interpretations are presented in this thesis supporting a model for ET in cyt *c* that considers the exact nature of the intervening medium between redox sites. Intervening aromatic residues do not contribute to the electronic coupling, however a σ-bond-tunneling model[10] that discounts hydrogen-bonding (H-bonding) interactions and through-space jumps is found to qualitatively agree with the data.[25] More sophisticated calculations that include the precise electronic composition of the intervening medium also correlate well with the data. Chapter 2 presents the semisynthesis, characterization and pentaammineruthenium modification of horse heart His72 cyt *c*, a crucial test for the electronic coupling analysis because the distance-dependent model predicts an ET rate that differs from the experimentally determined value by four orders of magnitude. Chapter 3 describes the

modification of semisynthetic horse heart His72 cyt *c*, as well as His62 and His39 of yeast cyt *c* with $Ru(bpy)_2(CO_3)$ to complete the mapping studies. Included in this Chapter is the methodology and kinetics data for the measurement of ET rates in all proteins studied. Chapter 4 details the analysis of the measured ET rates within the context of current theoretical treatments of electronic couplings. Chapter 5 presents the engineering of proteins containing unnatural metal-binding amino acids and their novel ET properties with potential application to the protein-folding problem. Finally, two appendices are included that detail smaller related projects; including 2-D NMR data supporting the conclusion that the mutations and modifications made to the proteins studied do not significantly perturb their three-dimensional structure (Appendix A). Appendix B contains spectroscopic characterization and ET activity of a Cys80 axial-ligand mutant of cyt *c*.

II. References

1. Recent general reviews of ET in biological and related systems: (a) Sigel, H.; Sigel, A. Eds. *Metal Ions in Biological Systems* (Dekker: New York) 1990, Vol. 27. (b) *Structure and Bonding* (Verlag: New York) 1991, Vol. 75. (c) Canters, G. W.; van de Kamp, M. *Curr. Opin. Struct. Biol.* **1992**, *2*, 859. (d) Bowler, B. E.; Raphael, A. L.; Gray, H. B. *Prog. Inorg. Chem.* **1990**, *38*, 259. (e) Gray, H. B.; Malmström, B. G.; Biochemistry **1989**, *28*, 7499. (f) McLendon, G. *Acc. Chem. Res.* **1988**, *21*, 160. (g) Gray, H. B. *Proceedings of The Robert A. Welch Foundation Conference on Chemical Research XXXI. Design of Enzymes and Enzyme Models* (The Robert A. Welch Foundation: Houston) 1988, pp 9 - 33. (h) Devault, D. *Quantum mechanical tunneling in biological systems* (Cambridge University Press: Cambridge) 1985. (i) Hatefi, Y. *Ann. Rev. Biochem.* **1985**, *54*, 1015. (j) Wuttke, D. S.; Gray, H. B. *Curr. Opin. Struct Biol.* **1993**, *3*, 555.

2. Diesenhofer, J.; Epp, O.; Miki, K.; Huber, R.; Michel, H. *J. Mol. Biol.* **1984**, *180*, 385. Diesenhofer, J.; Michel H. *Science* **1992**, *245*, 1463. DiMagno, T. J.; Wang, Z.; Norris, J. R. *Curr. Opin. Struct. Biol.* **1992**, *2*, 836.

3. Pelletier, H; Kraut, J. *Science* **1992**, *258*, 1748. Chen, L.; Durley, R.; Poliks, B. J.; Hamada, K.; Chen, Z.; Mathews, F. S.; Davidson, V. L.; Satow, Y.; Huizinga, E.;

Vellieux, F. M. D.; Hol, W. G. J. *Biochemistry* **1992**, *31*, 4959. McLendon, G.; Hake, R. *Chem. Rev.* **1992**, *92*, 481.

4. Marcus, R. A.; Sutin, N. *Biochim. Biophys. Acta* **1985**, *811*, 265. Marcus, R. A. *Nobel Lecture* **1992**. Marcus, R. A. *J. Chem. Phys.* **1956**, *24*, 966. Marcus, R. A. *J. Chem. Phys.* **1965**, *43*, 679.

5. Miller, J. R.; Calcaterra, L. T.; Closs, G. L. *J. Am. Chem. Soc.* **1984**, *106*, 3047. Closs, G. L.; Miller, J. R. *Science* **1988**, *240*, 440.

6. Newton, M. D. *J. Phys. Chem.* **1988**, *92*, 3049.

7. Hopfield, J. J. *Proc. Natl. Acad. Sci. USA* **1974**, *71*, 3640. Jortner, J. *J. Chem. Phys.* **1976**, *64*, 4860. McConnell, H. M. *J. Chem. Phys.* **1961**, *35*, 508. Halpern, J.; Orgel, L. E. *Discussion Faraday Soc.* **1960**, *29*, 32.

8. Siddarth, P; Marcus, R. A. *J. Phys. Chem.* **1990**, *94*, 2985. Siddarth, P.; Marcus, R. A. *J. Phys. Chem.* **1992**, *96*, 3213.

9. Reviewed in (a) Winkler, J. R.; Gray, H. B. *Chem. Rev.* **1992**, *92*, 369. (b) Gray, H. B.; Winkler, J. R. *Pure & Appl. Chem.* **1992**, *64*, 1257. (c) Mayo, S. L.; Ellis, W. R.; Crutchley, R. J.; Gray, H. B. *Science,* **1986**, *233*, 948.

10. Onuchic, J. N.; Beratan, D. N.; Winkler, J. R.; Gray, H. B. *Annu. Rev. Biophys. Biomol. Struct.* **1992**, *21*, 349. Beratan, D. N.; Onuchic, J. N.; Betts, J. N.; Bowler, B. E.; Gray, H. B. *J. Am. Chem. Soc.* **1990**, *112*, 7915. Beratan, D. N.; Onuchic, J. N.; Hopfield, J. J. *J. Phys. Chem.* **1987**, *86*, 4488. Beratan, D. N.; Betts, J. N.; Onuchic, J. N. *Science* **1991**, *252*, 1285. Onuchic, J. N.; Andrade, P. C. P.; Beratan, D. N. *J. Chem. Phys.* **1991**, *95*, 1131. Onuchic, J. N.; Beratan, D. N. *J. Chem. Phys.* **1990**, *92*, 722. Beratan, D. N.; Onuchic, J. N. *Photosynth. Res.* **1989**, *22*, 173. Betts, J. N.; Beratan, D. N.; Onuchic, J. N. *J. Am. Chem. Soc.* **1991**, *113*, 4043.

11. Siddarth, P.; Marcus, R. A. *J. Phys. Chem.* **1993**, *97*, 2400. Siddarth P.; Marcus, R. A. *J. Phys. Chem.* **1993**, *97*, 6111. Siddarth, P.; Marcus, R. A. *J. Phys. Chem.* **1990**, *94*, 8430. Christensen, H. E. M.; Conrad, L. S.; Mikkelsen, K. V.; Nielsen, M. K.; Ulstrup, J. *Inorg. Chem.* **1990**, *29*, 2808. Christensen, H. E. M.; Conrad, L. S.; Hammerstad-Pedersen, J. M; Ulstrup, J. *FEBS Lett.* **1992**, *296*, 141. Christensen, H. E. M.; Conrad, L. S.; Mikkelsen, K. V.; Ulstrup, J. *J. Phys. Chem.* **1992**, *96*, 4451. Ratner, M. A. *J. Phys. Chem.* **1990**, *94*, 4877. Todd, M. D.; Nitzan, A.; Ratner, M. A. *J. Phys. Chem.* **1993**, *97*, 29. Mikkelsen, K. V.; Ratner, M. A. *Chem. Rev.* **1988**, *87*, 113. Goldman, C. *Phys. Rev. A* **1991**, *43*, 4500. Larsson, S. *J. Am. Chem. Soc.* **1981**, *103*, 4034. Broo, A.; Larsson, S. *J. Phys. Chem.* **1991**, *95*, 4925. Broo, A. *Chem. Phys.* **1993**, *169*, 135. Broo, A. *Chem. Phys.* **1993**, *169*, 152. Grushus, J. M.; Kuki, A. *Chem. Phys.*

Lett. **1992**, *192*, 205. Grushus, J. M.; Kuki, A. *J. Phys. Chem.* **1993**, *97*, 5581. Newton, M. D. *Chem. Rev.* **1991**, *91*, 767.

12. Moser, C. C.; Keske, J. M.; Warncke, K.; Farid, R. S.; Dutton, P. L. *Nature* **1992**, *355*, 796. Farid, R. S.; Moser, C. C.; Dutton, P. L. *Curr. Opin. Struct. Biol.* **1993**, *3*, 225. Kuki, A.; Wolynes, P. G. *Science* **1987**, *236*, 1647.

13. Liang, N.; Pielak, G.; Mauk, A. G.; Smith, M.; Hoffman, B. M. *Proc. Natl. Acad. Sci. USA* **1987**, *84*, 1249. Liang, N.; Mauk, A. G.; Pielak, G; Johnson, J. A; Smith, M.; Hoffman, B. M. *Science* **1988**, *240*, 311.

14. Wallin, S. A.; Stemp, E. D. A.; Everest, A. M.; Nocek, J. M.; Netzel, T. L.; Hoffman, B. M. *J. Am. Chem. Soc.* **1991**, *113*, 1842. Everest, A. M.; Wallin, S. A.; Stemp, E. D. A.; Nocek, J. M.; Mauk, A. G.; Hoffman, B. A. *J. Am. Chem. Soc.* **1991**, *113*, 4337.

15. Davies, M. D.; Qin, L.; Beck, J. L.; Suslick, K. S.; Koga, H.; Horiuchi, T; Sligar, S. G. *J. Am. Chem. Soc.* **1990**, *112*, 7396. Stayton, P. S.; Sligar, S. G. *Biochemistry* **1991**, *30*, 1845.

16. (a) Yocum, K. M.; Shelton, J. B.; Shelton, J. R.; Schroeder, W. A.; Worosila, G.; Isied, S. S.; Bordignon, E.; Gray, H. B. *Proc. Natl. Acad. Sci. USA* **1982**, *79*, 7052. (b) Winkler, J. R.; Nocera, D. G.; Yocum, K. B.; Bordignon, E.; Gray, H. B. *J. Am. Chem. Soc.* **1982**, *104*, 5798. (c) Nocera, D. G.; Winkler, J. R.; Yocum, K. M.; Bordgnon, E.; Gray, H. B. *J. Am. Chem. Soc.* **1984**, *106*, 5145.

17. Meade, T. J.; Gray, H. B.; Winkler, J. R. *J. Am. Chem. Soc.* **1989**, *111*, 4353.

18. (a) Therien, M. J.; Selman, M.; Gray, H. B.; Chang, I-J.; Winkler, J. R. *J. Am. Chem. Soc.* **1990**, *112*, 2420. (b) Selman, M. A. Ph. D. Thesis, California Institute of Technology, **1989**. A lower limit of 170 s^{-1} was placed on the $Ru^{2+}a_5$His39 to Fe^{3+} ET rate compared to 30 s^{-1} measured in the analagous horse heart His33 cyt *c* derivative.[16b,c]

19. Bowler, B. E.; Meade, T. J.; Mayo, S. L.; Richards, J. H.; Gray, H. B. *J. Am. Chem. Soc.* **1989**, *111*, 8757. Therien, M. J.; Bowler, B. E.; Selman, M. A.; Gray, H. B.; Chang, I-J.; Winkler, J. R., in *ACS Advances in Chemistry Series* Bolton, J. R., Mataga, N., McLendon, G., Eds. (American Chemical Society: Washington DC) 1991; No. 228, pp. 191 - 200.

20. It is probable that the methionine axial ligand is no longer coordinated. Moore, G. R.; Williams, R. J. P.; Chien, J. C. W.; Dickson, L. C. *J. Inorg. Biochem.* **1980**, *12*, 1.

21. Jacobs, B. A.; Mauk, M. R.; Funk, W. D.; MacGillivray, R. T. A.; Mauk, A. G.; Gray, H. B. *J. Am. Chem. Soc.* **1991**, *113*, 4390.

22. Casimiro, D. R.; Wong L.-L.; Colón, J. L.; Zewert, T. E.; Richards, J. H.; Chang, I-J.; Winkler, J. R.; Gray, H. B. *J. Am. Chem. Soc.* **1993**, *115*, 1485. Siddarth, P.; Marcus, R. A. *J. Phys. Chem.* **1993**, *97*, 6111.

23. (a) Chang, I-J.; Gray, H. B.; Winkler, J. R. *J. Am. Chem. Soc.* **1991**, *113*, 7056. (b) Durham, B. D.; Pan, L. P.; Hahm, S.; Long, J.; Millett, F., in *ACS Advances in Chemistry Series* Johnson, M. K.; King, R. B.; Kurtz, D. M.; Kutal, C.; Norton, M. L., Scott, R. A. Eds. (American Chemical Society: Washington DC) 1990, Vol. 226, pp. 181 - 193.

24. Reviewed in Dickerson, R. E.; Timkovitch, R. in *The Enzymes*, Boyder, P. D. Ed. (Academic Press: New York) 1975, Vol. 6, 3rd ed., pp. 397 - 547. Moore, G. R.; Pettigrew, G. W. *Cytochomes c: Evolutionary, Structural and Physiochemical Aspects* (Verlag : Berlin) 1990. Moore, G. R.; Pettigrew, G. W. *Cytochomes c: Biological Aspects* (Verlag : Berlin) 1987.

25. Wuttke, D. S.; Bjerrum, M. J.; Winkler, J. R.; Gray, H. B. *Science* **1992**, *256*, 1007. Wuttke, D. S.; Bjerrum M. J.; Chang, I-J.; Winkler, J. R.; Gray, H. B. *Biochim. Biophys. Acta* **1992**, *1101*, 168.

26. Durham, B.; Pan, L. P.; Long, J. E.; Millett, F. *Biochemistry* **1989**, *28*, 8659. Pan, L. P.; Durham, B.; Wolinska, J.; Millet, F. *Biochemistry* **1988**, *27*, 7180. Millett, F.; Durham, B., in *Metals in Biological Systems* Sigel, H.; Sigel, A. Eds. (Dekker : New York) 1991, Vol. 27, pp. 223 - 264. Conrad, D. W.; Scott, R. A. *J. Am. Chem. Soc.* **1989**, *111*, 3461. Conrad, D. W.; Zhang, H.; Stewart, D. E.; Scott, R. A. *J. Am. Chem. Soc.* **1992**, *114*, 9909. Elias, H.; Chou, M. H.; Winkler, J. R. *J. Am. Chem. Soc.* **1988**, *110*, 429. Isied, S. S.; Kuehn, C.; Worosila, G. *J. Am. Chem. Soc.* **1984**, *106*, 1722. Bechtold, R.; Kuehn, C.; Lepre, C.; Isied, S. S. *Nature* **1986**, *322*, 286. Isied, S. S., in *ACS Advances in Chemistry Series* Johnson, M. K.; King, R. B; Kurtz, D. M.; Kutal, C.; Norton, M. L.; Scott, R. A. Eds. (American Chemical Society: Washington DC) 1990, Vol. 226, pp. 191 - 100. Isied, S. S., in *Metals in Biological Systems* Sigel, H.; Sigel, A. Eds. (Dekker : New York) 1991, Vol. 27, pp. 1-56. Isied, S. S., in *ACS Advances in Chemistry Series* Bolton, J. R.; Mataga, N.; McLendon, G. Eds. (American Chemical Society: Washington DC) 1991, No. 228, pp. 229 - 245. Zang, L.-H.; Maki, A. H. *J. Am. Chem. Soc.* **1990**, *112*, 4346.

27. Bushnell, G. W.; Louie, G. V.; Brayer, G. D. *J. Mol. Biol.* **1990**, *214*, 585. Louie, G. V.; Brayer, G. D. *J. Mol. Biol.* **1990**, *214*, 527. Berghuis, A. M.; Brayer, G. D. *J. Mol. Biol.* **1992**, *223*, 959.

28. Corradin, G.; Harbury, H. A. *Proc. Natl. Acad. Sci. USA* **1971**, 68, 3036. Chaiken, I. M. *CRC Critical Reviews in Biochemistry* **1981**, 255. Raphael, A. L.; Gray,

H. B. *J. Am. Chem. Soc.* **1991**, *113*, 1038. Raphael, A. L.; Gray, H. B. *Proteins* **1989**, *6*, 338. Wallace, C. J. A. *FASEB J.* **1993**, *7*, 505. Humphries, J.; Offord, R. E.; Smith, R. A. G. *Curr. Opin. Biotech.* **1991**, *2*, 539.

Chapter 2

Semisynthesis, Characterization and Pentaammineruthenium Modification of His72 Cytochrome *c*

I. Introduction

A. Cytochrome c

The mitochondrial respiratory chain links a series of electron transfer reactions that results in the net four electron reduction of dioxygen to water with the concomitant pumping of protons across the membrane. The resulting pH gradient drives the production of ATP. Cytochrome *c* is a critical link in this chain, shuttling electrons from cytochrome reductase to cytochrome oxidase. Cytochromes *c* are monomeric, water-soluble proteins of between 100 - 110 residues that contain an iron protoporphyrin IX (heme) prosthetic group that imparts the ET activity.[1] The heme is covalently linked through the 1-vinyl positions to Cys14 and Cys17[2] *via* a thioether bond and is additionally bound through two invariant axial ligands, His18 (εN) and Met80 (δS) in both the ferric and ferrous forms (between pH 2.5 - 9.3 and 4 -12 respectively). The primary sequence for horse heart cyt *c* (molecular weight (MW) = 12,364 Daltons) is given in Figure 2.1. The three-dimensional structure of cyt *c* has been determined to high resolution for numerous species in the ferric and ferrous forms[1,3] and is remarkably conserved. As shown in Figure 2.2 A, the characteristic cytochrome fold is a compact, globular structure with the polypeptide wrapped around the heme, leaving ~4% of the heme-edge solvent exposed. The protein is ~50% α-helical, with the helicity concentrated in a 12-residue N-terminal helix, a 17-residue C-terminal helix, and two helical regions encompassing residues 60 - 75. The remainder of the protein is comprised of random coil and β-turn structure. The nature of the axial ligands and the hydrophobic nature of the protein environment impart a relatively high redox potential for the Fe^{3+}/Fe^{2+} couple of +265 mV *vs.* NHE.

Minor structural changes have been noted (and their significance debated) between the ferric and ferrous forms by both crystallographic and nuclear magnetic resonance studies.[4] The current consensus is that, while no major positional changes in protein atoms occur, there is a 1.7 Å displacement of an internally bound water and the

Figure 2.1 The amino acid sequence of horse heart cyt *c*. The underlined region corresponds to the 66-104 CNBr cleavage fragment. Italics indicate the Cys residues involved in thioether linkages, and the axial ligands are in plain type.

1	**Ac - Gly - Asp - Val - Glu - Lys - Gly - Lys - Lys - Ile - Phe**
11	**Val - Gln - Lys - *Cys* - Ala - Gln - *Cys* - His - Thr - Val**
21	**Glu - Lys - Gly - Gly - Lys - His - Lys - Thr - Gly - Pro**
31	**Asn - Leu - His - Gly - Leu - Phe - Gly - Arg - Lys - Thr**
41	**Gly - Gln - Ala - Pro - Gly - Phe - Thr - Tyr - Thr - Asp**
51	**Ala - Asn - Lys - Asn - Lys - Gly - Ile - Thr - Trp - Lys**
61	**Glu - Glu - Thr - Leu - Met - Glu - Tyr - Leu - Glu - Asn**
71	**Pro - Lys - Lys - Tyr - Ile - Pro - Gly - Thr - Lys - Met**
81	**Ile - Phe - Ala - Gly - Ile - Lys - Lys - Lys - Thr - Glu**
91	**Arg - Glu - Asp - Leu - Ile - Ala - Tyr - Leu - Lys - Lys**
101	**Ala - Thr - Asn - Glu -OH**

Figure 2.2 (A) The crystal structure of ferric horse heart cyt *c*.[3a] The 1-65 region backbone is shown in blue, the 66-104 region backbone is in yellow, the heme is in red and the Met 80 and His18 axial ligands are pictured in teal. (B) The crystal structure of ferric horse heart cyt *c* with His72, introduced by semisynthesis, indicated in purple.

A

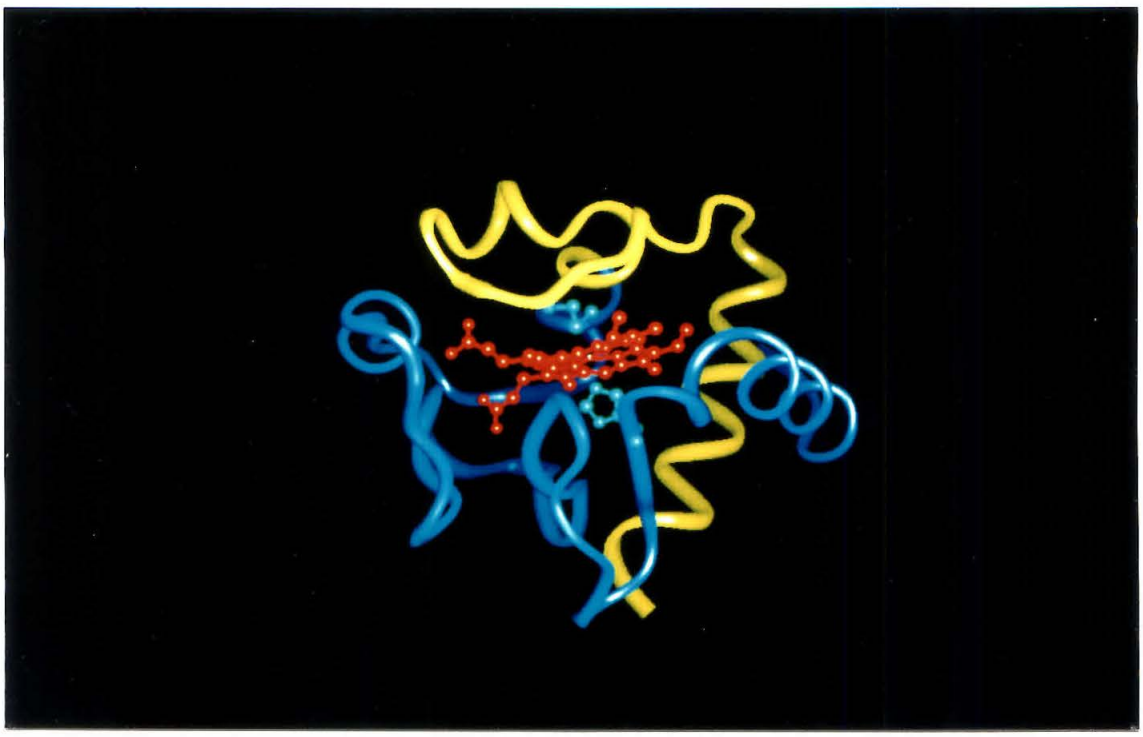

B

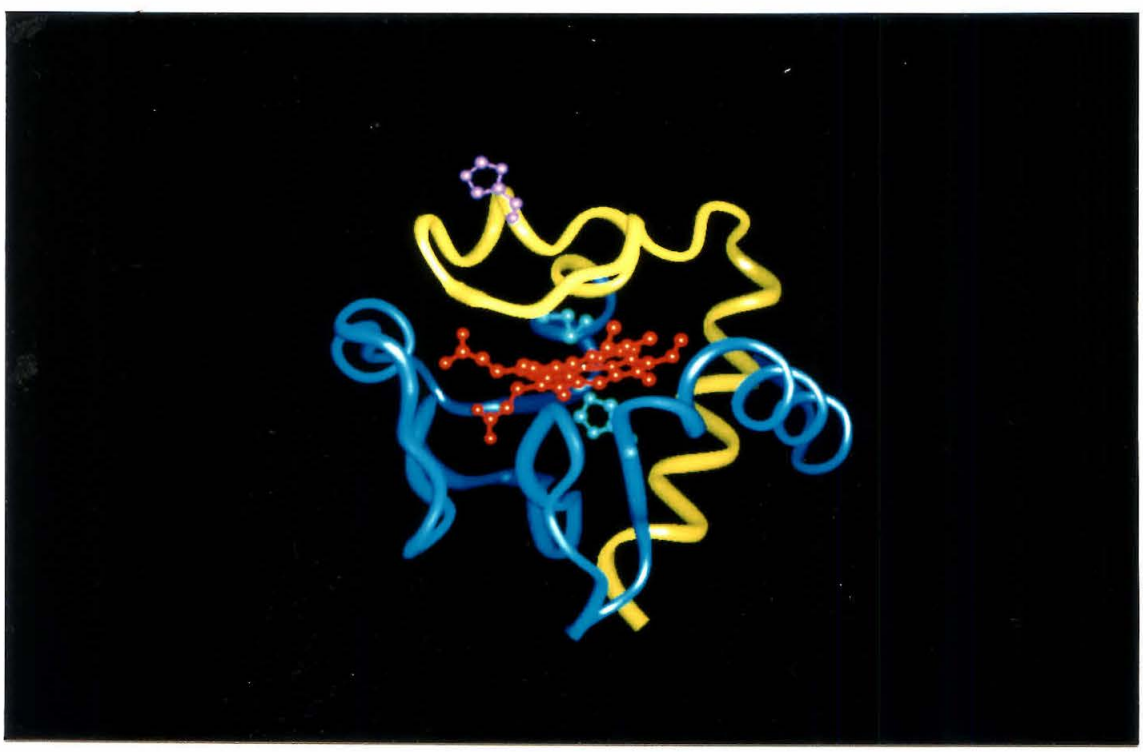

extensive H-bonding network on the Met80 face of the heme adjusts upon heme oxidation to stabilize the net positive charge by making the Met80 group less electron withdrawing (Figure 2.3). The ferrous state is thermodynamically more stable than the ferric state, as determined by denaturation in the presence of chaotropics or at extreme temperatures (T_m = 87° C ferric, 103° C ferrous), susceptibility to proteolysis, and side chain reactivities.[1a,b] This enhanced stability has been attributed to both the increased Met80-Fe bond strength[1f] and to the change in hydrophobicity of the heme. The heme propionates contribute a -2 charge, thus while the ferrous heme is neutral, the ferric heme has a net charge of +1 that must be buried within the hydrophobic interior of the protein.

The visible absorption spectrum is dominated by the presence of the porphyrin chromophore. Reduced and oxidized cyt *c* spectra are given in Figure 2.4.[5] Upon oxidation, the loss of Q-band structure and a 6 nm blue shift in the Soret from 416 to 410 nm is observed. Additionally, a weak band at 695 nm in the oxidized protein is assigned as a ligand to metal charge transfer (LMCT) transition from the sulfur of the ligation Met to Fe^{3+} and thus serves as a structural indicator for the presence of Met80 ligation and heme environment integrity.

B. Semisynthesis

In developing strategies for the construction of novel electron-transfer proteins in relatively large (milligram (mg)) quantities, semisynthesis of cyt *c* has been selected for the incorporation of natural and non-encoded (unnatural) metal-binding amino acids directly into the polypeptide backbone. Nearly thirty years ago Corradin and Harbury[6] discovered that the cyanogen bromide (CNBr) cleavage fragments of the protein (in the ferrous state) can associate to form a non-covalently bound complex that is structurally similar to the native intact protein. The C-terminus of one fragment is in close proximity to the N-terminus of the neighboring fragment, facilitating the aminolysis reaction at the cleavage point, thus reconstituting the intact protein. While this technique has been used

Figure 2.3 An illustration of the reorganization of the heme environment upon change in oxidation state in (A) reduced and (B) oxidized yeast iso-1-cyt *c*. Hydrogen bonds are shown by thin dashed lines. In the ferric protein the H-bond to Asn52 is broken and Wat166 shifts to within 5 Å of the heme iron atom. Borrowed from Reference 3c.

A

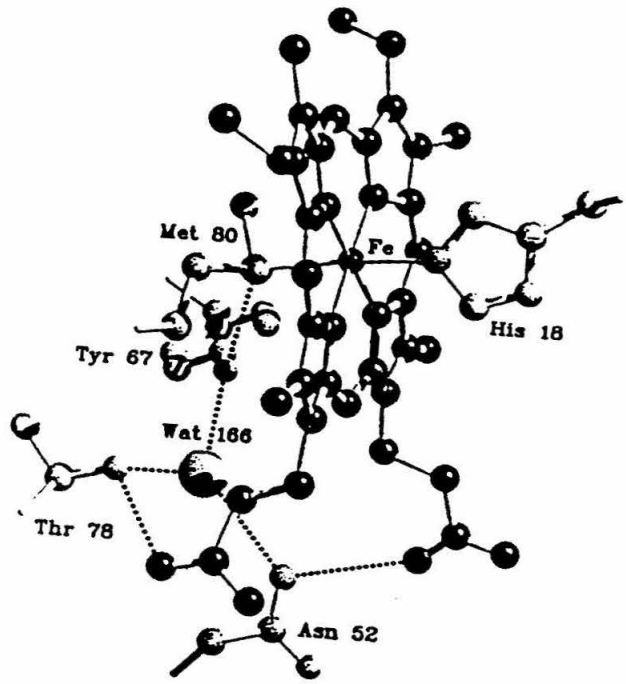
Met 80
Fe
His 18
Tyr 67
Wat 166
Thr 78
Asn 52

B

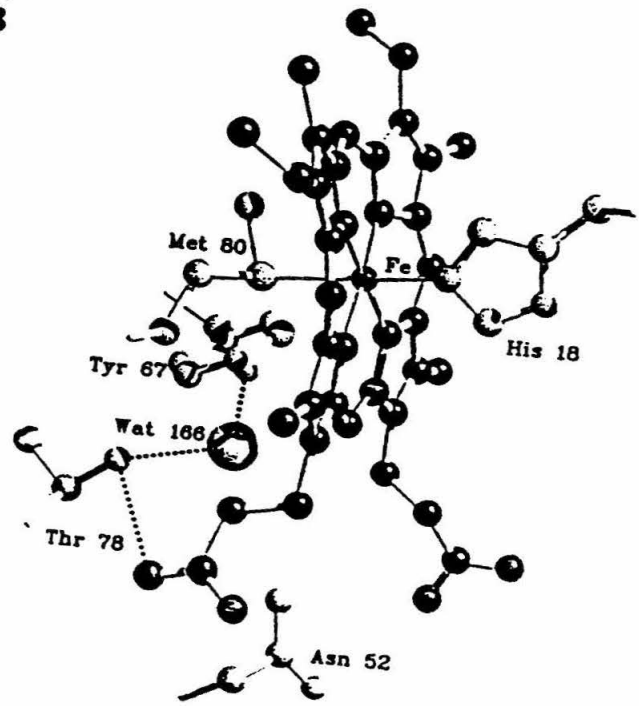
Met 80
Fe
His 18
Tyr 67
Wat 166
Thr 78
Asn 52

Figure 2.4 Measured electronic absorption spectra for native cyt *c* in the ferric (- - - -) and ferrous (——) states in 25 mM NaPi, pH 7.0. Protein was oxidized with Na[Co(EDTA)] prior to purification and reduced with sodium dithionite, which was removed by gel filtration, immediately prior to data acquisition.

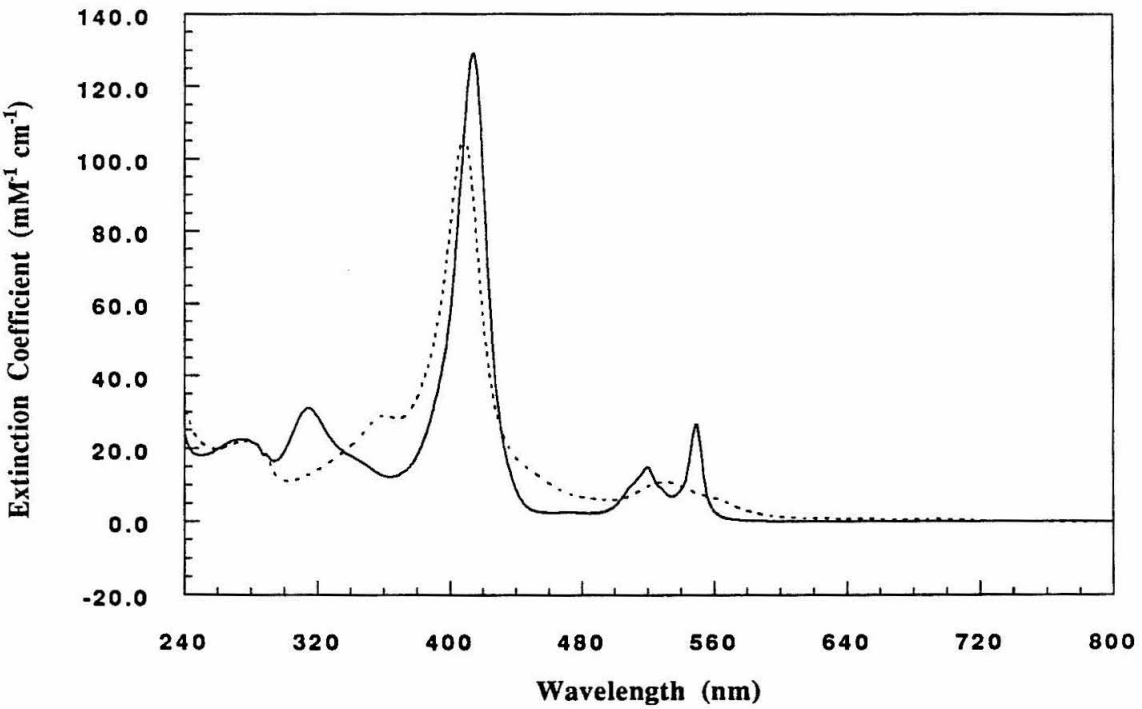
140.0
120.0
100.0
80.0
60.0
40.0
20.0
0.0
-20.0
Extinction Coefficient (mM-1 cm-1)
240
320
400
480
560
640
720
800
Wavelength (nm)

to probe structure / function relationships in cyt *c*,[7-9] it is only with the recent technical advances in solid phase peptide synthesis[10] that it has become feasible to obtain large quantities of semisynthetically generated mutants.[9]

The semisynthetic methodology is illustrated schematically in Figure 2.5. The mechanism for CNBr-mediated cyt *c* cleavage is given in Figure 2.6. In the cleavage reaction, the cyanogen group of CNBr electrophilically attacks the sulfur of Met, followed by nucleophilic attack on the sulfur by the carbonyl oxygen to form an iminolactone. The iminolactone hydrolyzes to yield the homoserine lactone and amino peptides.[11] The lactone can further hydrolyze to a homoserine carboxylate. Horse heart cyt *c* contains Met residues at positions 65 and 80, thus CNBr cleavage at denaturing conditions (70% formic acid or 0.1 M HCl) affords the 1-65, 1-80, 66-104, 66-80, and 81-104 fragments which are readily separated and purified using standard chromatographic techniques. The 1-65 and 1-80 fragments retain the covalently linked heme moiety and one His ligand. The intrinsic viscosity, and absorption and CD spectra of the 1-65 fragment indicate that it is neither fully unfolded nor globular, exhibits negligible residual helicity, and is low spin at neutral pH.[6a,12] His18 occupies one axial ligation site, and the absence of the signature 695 nm LMCT band indicates that Met ligation is absent. The unexpected low-spin character of the heme can be attributed to coordination of a nitrogenous species at the sixth coordination site, perhaps His26 or His33, either intramolecularly or *via* dimerization. The redox potential of the 1-65 fragment is low (*vide infra*), indicative of alternate coordination and/or greater solvent exposure of the heme.

Combination of the ferric 1-65 homoserine fragment with a 39-mer peptide corresponding to the native 66-104 sequence results in the formation of an ordered fragment:peptide complex that possesses properties that differ from those of the native protein (*i.e.*, absence of the 695 band).[6a] However, reduction of this nonproductive complex under anaerobic conditions results in the formation of a protein with

Figure 2.5 Schematic representation of the semisynthetic methodology. The native 66-104 fragment is discarded and a solid phase peptide synthesized 39-mer with modification(s) from the native sequence (indicated by the fragment with the asterisk) used for protein reconstitution. By this procedure, modifications can be directly incorporated into the polypeptide backbone.

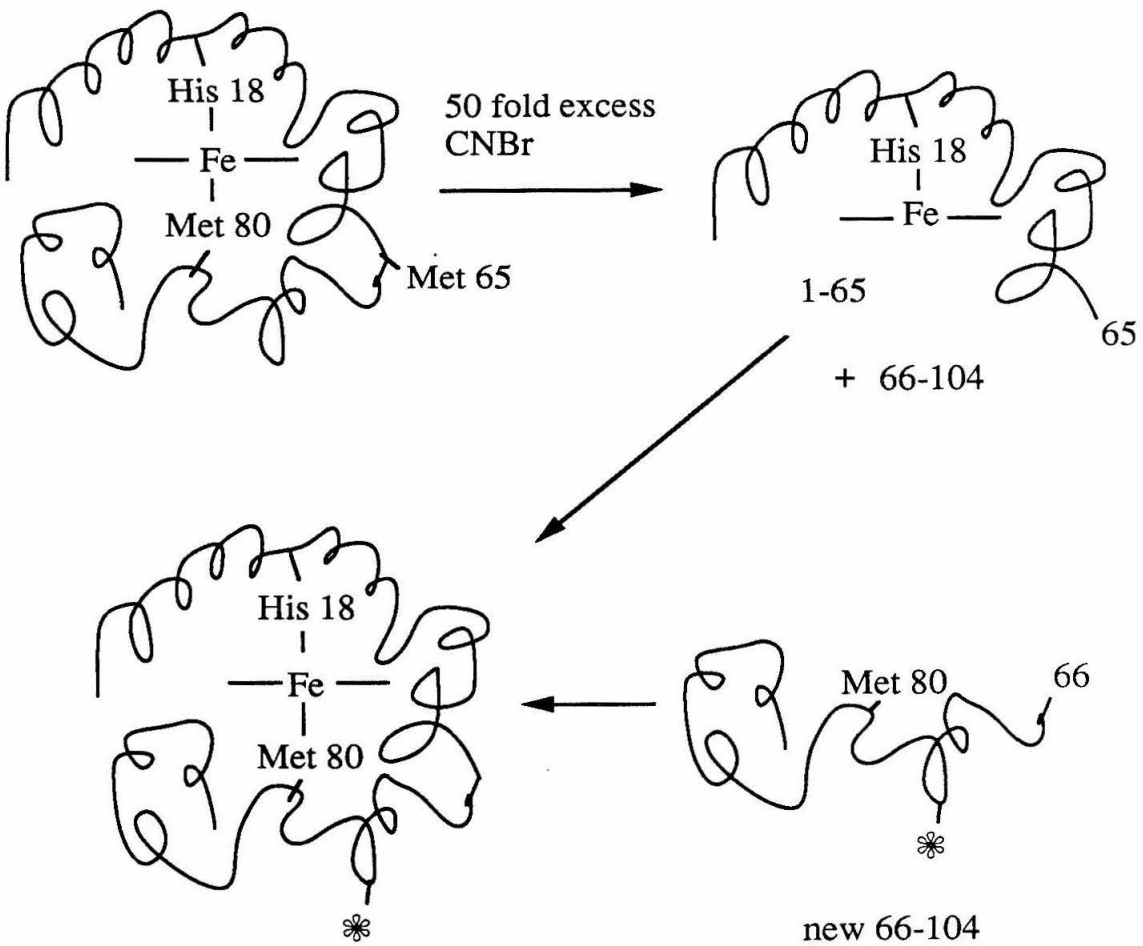
His 18
Fe
Met 80
Met 65
50 fold excess
CNBr
His 18
Fe
1-65
65
+ 66-104
His 18
Fe
Met 80
Met 80
66
new 66-104

Figure 2.6 Mechanism of CNBr-mediated cleavage at Met residues. The activated homoserine lactone and the homoserine carboxylate hydrolysis product are indicated.

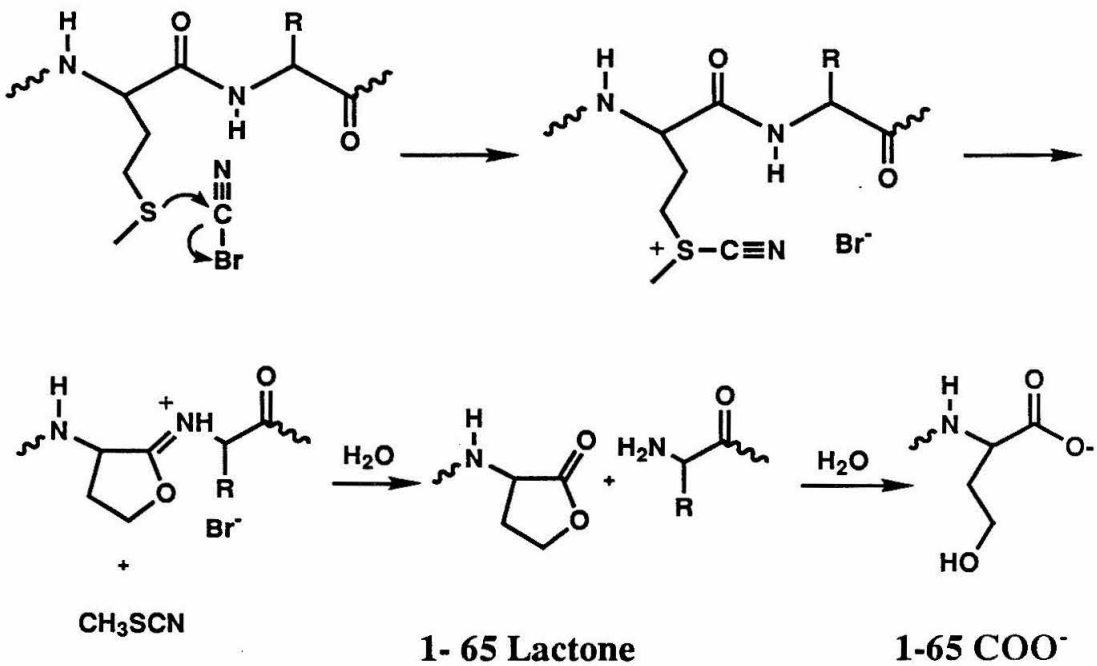

1- 65 Lactone **1-65 COO^-**

spectroscopic properties (absorption and circular dichroism (CD)) virtually identical with native protein. Moreover, isolation and oxidation of the reconstituted protein yields the ferric species that possesses an absorption spectrum (including the 695 nm band), CD spectrum and redox potential identical with native cyt *c*.[6,8h] The reduction of the 1-65:66-104 complex is believed to trigger a conformational change that brings the homoserine lactone at position 65 in close proximity with N-terminus of the 66-104 peptide (Figure 2.7), thus facilitating the aminolysis reaction that restitches the peptide bond. The reconstituted protein differs only in the identity of the residue present at position 65; in the native protein Met and in the semisynthetic protein homoserine (Hse). However, the identity of this surface residue has not been evolutionarily conserved and extensive characterization of Hse65 cyt *c* has failed to find any structural or functional differences relative to native horse heart cyt *c*. In addition to indistinguishable spectroscopic and electrochemical properties, the native and semisynthetic proteins share equal reactivity to anti-cyt *c* antibodies,[9a] similar biological activity in cyt *c*-depleted mitochondria,[8h] and virtually superposable NMR spectra in both the oxidized and reduced states.[13] The NMR result is especially significant; due to the presence of a paramagnetic center in the ferric form the NMR spectrum is excruciatingly sensitive to small perturbations of the heme environment. Therefore, if a native 66-104 peptide is used, the semisynthetic protocol introduces negligible structural changes in the protein. Site-specific changes can therefore be readily made in the primary sequence between residues 66 and 104 of cyt *c* using semisynthesis by altering the sequence of the 39-mer peptide. A limiting factor, however, is that modifications that radically alter the protein conformation will not lead to the productive complex formation required for protein reconstitution.

Semisynthesis is a complementary technique to genetic engineering for the introduction of site-specific changes in the protein structure. The gene for yeast iso-1-cyt *c* has been expressed in *Saccharomyces cerevisiae* (*S. c.*) and represents a viable approach to obtain 100 mg quantities of site-directed mutants.[14] Semisynthesis, which

Figure 2.7 (A) The geometry in the 65-66 region upon productive complex formation. Note the close proximity of the homoserine lactone at position 65 and the N-terminus of the 66-104 fragment. (B) The subsequent aminolysis reaction reforming the peptide bond between 65 and 66

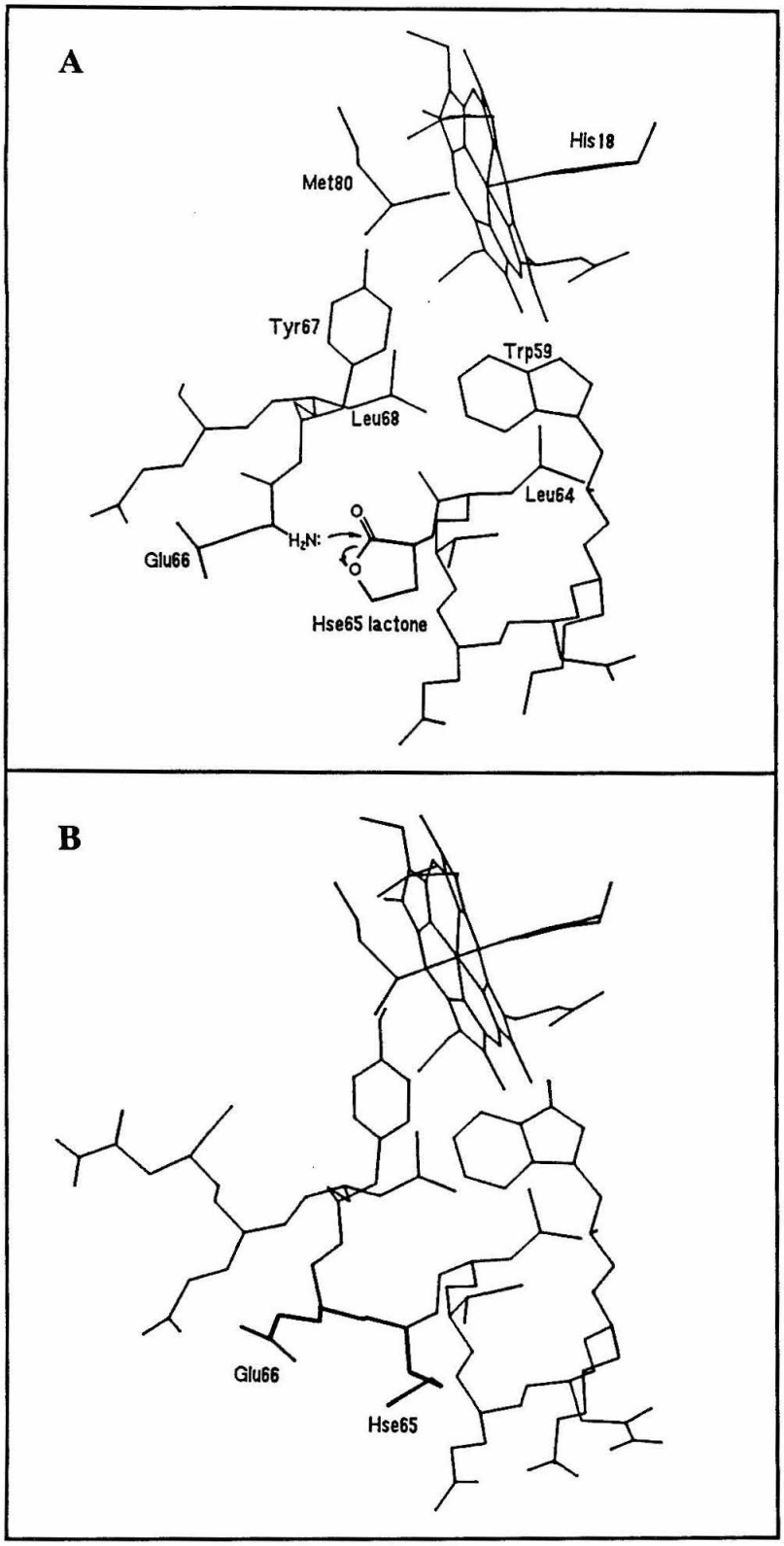
A
His18
Met80
Tyr67
Trp59
Leu68
Leu64
Glu66
H_2N:
Hse65 lactone
B
Glu66
Hse65

requires the synthesis of 100 mg quantities of the 39-mer peptide (the 1-65 fragment can be obtained in virtually infinite quantity due to the availability of native horse heart cyt *c* from Sigma at < $200 / gram), has the advantage of allowing the incorporation of non-naturally coded amino acids into the 66-104 region as long as the introduced amino acids do not preclude productive complex formation. Prior to and during the course of this work, *p*-fluorophenylalanine has been introduced at position 67,[8f,9e] modifications to unnatural amino acids made at positions 66[8i] and 78,[9f] and changes at position 80 to ethionine and methyl cysteine[8e] and a variety of other unnatural amino acids.[9d] Semisynthesis presents a methodology for systematically changing the axial ligand at position 80 for the study of the influence wielded by the axial ligand on the spectral and electrochemical properties of the heme.[8e,9b-d,g] An understanding of the effects of axial ligand substitution opens the way for the design and engineering of a heme enzyme possessing dramatically different properties than those of cyt *c*. Prior to a recent breakthrough,[15] it had been impossible to genetically produce and isolate axial-ligand mutants of cyt *c* with altered redox properties because the recombinant expression system requires a functional cyt *c* for survival.[16,17] Semisynthesis has been recently extended to the yeast proteins *via* the genetically engineered introduction of a Met residue at the position corresponding to 65 in the horse heart sequence.[18] Because semisynthesis does not work in native *S. c.* cyt *c* (which has a Met at position 64 rather than 65),[8h] it is clear that the formation of a productive complex is very sensitive to the precise nature of the fragments.

C. Position 72

Position 72 in horse heart cyt *c* was initially selected for the incorporation of metal-binding amino acids for the study of ET. Lysine is present at this position in 91 of the 92 sequences of cyts *c* determined to date (Ser is present in this position in *Tetrahymena pyriformis* cyt *c*[19]).[1,16] Lys72 is located on the surface of the protein ~8.4

Å above the coordinating sulfur of Met80 along a line coincident with the S-Fe bond (Figure 2.2 B, the position of the introduced His72 residue is indicated). This position in horse heart cyt *c* appears to be extremely solvent accessible in the crystal structure, and is among the most reactive of the 19 Lys residues in cyt *c* to modification with exogenous reagents.[20] Lys72 is specifically trimethylated in plant and fungal species; although it has been proposed that trimethylation imparts protection from proteolytic attack and is required for transport of the heme-deficient peptide into the mitochondrion,[21] the functional importance of trimethylation has not been established. Furthermore, the trimethylated Lys72 of *S. c.* iso-1-cyt *c* has been replaced with Arg with essentially no change in either activity *in vivo* or structure *in vitro*.[22]

Cyt *c* transfers electrons to and from its redox partners *in vivo* through the exposed heme edge within electrostatically bound protein:protein complexes.[1] The surface of cyt *c* is highly charged, with a total of 21 positive charges (excluding His residues) and 13 negative charges (including the C-terminus), resulting in an isoelectric point of 10.05.[1d] Extensive studies have implicated the positive charge at position 72 as mediating the interaction of cyt *c* with a number of its redox partners.[1,23] Specifically, this residue is important for the formation of an electrostatically bound complex with physiological redox partners cyt *c* peroxidase, cyt *c* reductase, and cyt *c* oxidase as well as a non-physiologically relevant complex with cyt b_5.[23,24] The recent crystal structure of the horse heart (and *S. c.*) cyt *c*:cyt *c* peroxidase complexes confirms that Lys 72 of horse heart cyt *c* forms a charge-charge H-bond with Glu290 of cyt *c* peroxidase.[25] In the *S. c.* cyt *c*:cyt *c* peroxidase complex structure, where Lys72 is trimethylated and thus incapable of forming a hydrogen-bond (H-bond), this residue is adjacent to the protein:protein interface.

To ensure that the essentially conserved Lys72 of horse heart cyt *c* was not crucial for maintaining the structural integrity of the protein, this position was replaced with a His residue *via* semisynthesis and the resulting His72 cyt *c* protein extensively

characterized prior to the incorporation of more precious unnatural amino acids (Chapter 5). During the course of this work, a new theoretical formulation for electronic coupling in proteins was developed (Chapter 4), and fortuitously initial calculations indicated that position 72 would serve as a dramatic test case delineating between a distance-dependent and medium-dependent model for electronic coupling. As ample quantities of His72 cyt *c* could be readily produced by semisynthesis, the ET properties of rutheniumpentaammine-modified His72 cyt *c* were studied.[26]

II. Experimental

A. Materials

Distilled water, passed through a Barnstead Nanopure purification system (No. 2794, specific resistance > 18 MΩ-cm) equipped with two ion-exchange filters, one organic-removal filter and one 0.22 μm filter, was used to prepare all aqueous solutions. Sodium phosphate (NaPi), sodium acetate, *N*-2-hydroxyethylpiperazine-*N'*-2-ethanesulfonic acid (HEPES), and ammonium bicarbonate buffers were prepared with analytical grade reagents, except in the NMR studies where ultrapure sodium phosphate buffer (J. T. Baker) was used. Horse heart cyt *c* (Type VI) was purchased from Sigma. CNBr (> 97%) was obtained from Aldrich. Chloropentaammineruthenium(III)chloride was supplied by Strem. Na[Co(EDTA)] was synthesized by the method of Kirschner,[27] substituting sodium carbonate for barium carbonate. 4,4'-bipyridine (Aldrich) was recrystallized from water before use in the electrochemical studies. Other reagents were of analytical or higher grade.

B. Instrumentation

Routine absorption measurements were made on a Hewlett-Packard diode array spectrophotometer (Model 8452) run by a personal computer (PC) or a Shimadzu model UV-260 spectrophotometer. High quality spectra were obtained on a Cary-14

spectrophotometer rebuilt and automated by On-Line Instruments Service (OLIS). All measurements were made at ambient temperature in 1 cm cells against a cell buffer baseline unless otherwise specified.

Circular dichroism measurements were made on a PC-driven JASCO-600 CD spectropolarimeter in jacketed 0.1 cm pathlength cells. Measurements were generally made with a 1 nm bandwidth, 0.5 time constant, and scanned at 50 nm/min with 0.2 nm step resolution. Data were the average of at least 8 acquisitions, subtracted from a cell baseline, and smoothed using a Fourier transform algorithm that removed high-frequency components. Melting curves were obtained by monitoring the loss of 222 nm CD signal as a function of temperature. Variable temperatures were obtained by incrementation of the temperature of the Brinkman Lauda K-2/R circulator and water bath, allowing the sample to equilibrate at each new temperature for five minutes before data collection .

Protein ^1H NMR spectra were obtained on a Bruker AM500 or AMX500 (Caltech, one-dimensional (1-D) experiments) or a Bruker AMX500 (Scripps, two-dimensional (2-D) experiments) spectrometer and were Gaussian enhanced. All experiments conducted at Caltech were performed on samples that were fully exchanged into D_2O buffers. pH measurements are those reported by a pH meter and are not corrected for the isotope effect. pH titrations were carried out in 50 mM NaPi and titrated with 1 N NaOD or DCl in buffer. Optimum resolution was obtained at 315 K in the 1-D experiments. Experiments at Scripps were designed for the observation of amide protons and were conducted in 90%/10% H_2O/D_2O, 100 mM NaPi, 150 mM NaCl, pH 5.7 at 293 K (refer to Appendix A for details).

Protein separations and purifications were performed using a Pharmacia FPLC apparatus equipped with two P-500 pumps, a MV7 valve with 0.2 to 10 ml injection loops, a UV-M monitor (Hg lamp) with 280 and 405 nm filters, an LCC-500 controller, a Pharmacia REC-482 strip chart recorder, and FRAC-100 fraction collector. Cation-exchange separations were performed with Pharmacia Mono S 5/5, 10/10, and 16/10

columns. Gel filtration chromatography was performed using the 10/30 Superose 12 column on the FPLC, various gravity columns using Sephadex G-25 (Pharmacia) resin, or prepared Sephadex G-25M 9-ml PD-10 columns (Pharmacia). Reversed phase liquid chromatography was performed with on the FPLC system with a PepRPC HR 5/5 column and flow restrictor. Buffers and protein samples were filtered through a 0.22 μm filter immediately prior to use. All chromatography columns were cleaned and equilibrated according to the manufacturers suggestions.

pH measurements were made with a Beckman model Φ32 pH meter, using either a Beckman combination electrode or an Ingold microelectrode. VWR buffer standards were used for calibration. pH measurements are reported for room temperature.

Isoelectric focusing gels were run on prefabricated Ampholine PAGplate pH 3.5 - 9.5 gels (Pharmacia) using an LKB 2117 Multiphor and 2197 DC power supply limited by a 15 mA current. The support plate was water cooled by a Masterline 2095 circulator and temperature bath maintained below 10° C.

Electron paramagnetic resonance (EPR) spectra were obtained in a 50 mM HEPES, 50% glycerol, pH 7.0 glass at 6.8 K. Spectra were measured on an ESP-300 Bruker spectrometer equipped with a liquid helium cryostat in the laboratories of Prof. David Goodin, the Scripps Research Institute, La Jolla, California.

Thermospray protein mass spectra were recorded on a Vestec Thermospray LC-Mass Spectrometer and analyzed using deconvolution algorithms developed at the laboratories of Prof. Curtis Monig, University of California, Riverside, California. Samples were prepared in 20 mM ammonium bicarbonate buffer (pH = 7.6) and diluted with 1N acetic acid.

Amino acid analysis and capillary zone electrophoretic (CZE) profiles were obtained at the Caltech Biopolymer Synthesis and Analysis Resource Center under the direction of Suzanna Horvath. Samples were provided in ammonium bicarbonate or another volatile buffer for analysis.

C. Methods

1. General

Protein samples were deoxygenated by at least 30 vacuum / purge cycles over the course of 0.5 to 1 hour on a dual-manifold vacuum / argon (manganese oxide scrubbed) line. Air-sensitive manipulations were performed under scrubbed argon or dinitrogen in a Vacuum Atmospheres Co. HE-493 Dri-Train glove box.

Proteins were stored at 4° C for routine use and were flash frozen in liquid nitrogen and stored at -50 to -80° C for long term storage. All proteins were repurified by cation-exchange chromatography within two weeks of use.

Protein solutions were concentrated in ultrafiltration cells (Amicon) with YM-3 (3000 MW cutoff), YM-5 (5000 MW cutoff), and YM-10 (10000 MW cutoff) filters or in Centricon-3 (3000 MW cutoff) and Centricon-10 (10000 MW cutoff) microconcentrators (Amicon).

Differential pulse polarography measurements were performed using a Princeton Applied Research Model 174A polargraphic analyzer with a 5.0 to 0.5 s^{-1} scan rate, 0.5 s drop time and 25 mV modulation amplitude. Applied potentials were monitored with a Keithley 177 microvoltmeter. A gold button (2 mm diameter) electrode (Bioanalytical Systems) was polished with 0.3 to 0.05 μm alumina (Buehler) or diamond paste (Bioanalytical Systems) and modified *in situ* with 4,4'-bipyridine.[28] A Pt wire was used as a counter electrode with a saturated KCl calomel reference (SCE = 242 mV *vs.* NHE). Measurements were made with 0.5 to 2 mM protein samples in 50 mM NaPi, 10 mM 4,4'-bipyridine, pH 7.0 unless otherwise specified. Solutions were degassed simultaneously with electrode modification *in situ* by occasional stirring under a blanket of Ar for a minimum of 30 minutes. Potential scans were initiated 300 mV cathodic of the anticipated wave and terminated ~300 mV anodic of the signal. Reported $E^{o'}$ values are the average of the forward and reverse peak potentials; peak separation was found to

be a function of scan rate with negligible peak separation at the slowest scan rates. The average of the forward and reverse waves, however, is independent of scan rate. Due to uncontrollable variations in the condition of the electrode from day to day, potentials obtained by this technique are adjusted using a small correction factor (not more than 20 mV) obtained by referencing the measured native horse heart cyt *c* potential to 265 mV *vs*. NHE. Measurements were made at ambient temperature.

Spectroelectrochemistry experiments were performed in home-built optically transparent thin layer (~0.03 cm pathlength) cells on a Cary-219 spectrophotometer. The cell specifications and construction are described in detail elsewhere.[28] The gold minigrid that served as the working electrode is 100 lines per inch, or 60% transmittance (Interconics). Potentials were applied with a Princeton Applied Research Model 174A polargraphic analyzer and monitored with a Keithley 177 microvoltmeter. The counterelectrode was Pt wire fitted in a glass tube to seal the cell and a miniature saturated calomel electrode (Sargent-Welch) was used as the reference electrode. Sample temperature was monitored within the cell directly *via* a microthermocouple (Omega Engineering) and a Fluke 2175A digital thermometer. 3 to 5-fold molar excess of $[Rua_5py]Cl_3$ ($E^{o'}$ = 298 mV *vs*. NHE[30]) (a gift of C. St. Clair) was present as a mediator for cyt *c* measurements. A cell baseline with buffer was obtained prior to each experiment. Typically, protein solutions were 0.5 mM in 50 mM NaPi; approximately one milliliter (ml) of degassed solution was needed to fill the cell without bubbles.

ET rates were measured in the pentaammineruthenium-modified proteins with a Caltech-built microsecond flash-photolysis system described in Milder[31] equipped with a Hamamatsu R928 photomultiplier tube (PMT), with some minor alterations.[32] Data were obtained using the $Ru(bpy)_3^{2+}$ flash system.[33] Data collection was conducted with a PC running UnkelScope (Unkel Software) and data were fit with SI-FIT (On-Line Instrument Systems). The samples were prepared in the glove box with thoroughly deoxygenated buffer (50 mM NaPi, 60 μM $[Ru(bpy)_3]Cl_2$, 7.25 mM Na_2EDTA, pH 7.0, subjected to at

least 5 freeze / pump / thaw cycles on a high vacuum line) in a 15 cm pathlength cell (11 ml total volume). Protein concentrations were 1 - 3 μM.

Modeling was performed using oxidized horse heart and oxidized and reduced *S. c.* cyt *c* structures[3] kindly provided by G. D. Brayer prior to Protein Data Bank release. Biograf (V 2.1) running on either a DEC microVax 3500 equipped with a PS340 Evans and Sutherland graphics system or a Silicon Graphics Personal Iris workstation was used to visualize the structures. The Dreiding force field was utilized for energy minimizations.

2. Cytochrome c Purification

The highest grade of horse heart cyt *c* available from Sigma is supplied partially reduced and contaminated with 1 - 10% deamidated forms. Therefore, cyt *c* was always purified as described below prior to use. 100 - 400 mgs of lyophilized protein was dissolved at a concentration of ~35 mg/ml in 25 mM NaPi, pH 7.0 with a 5 - 10-fold excess of Na[Co(EDTA)] added to fully oxidize the sample. Oxidation was effected overnight at 4° C with gentle stirring. 20 - 40 mgs could be purified per loading on the Mono S 16/10 FPLC column. The impurities could be readily separated using a slow 0 to 210 mM NaCl gradient in 25 mM NaPi, pH 7.0 (Figure 2.8), $Co(EDTA)^-$ elutes in the void volume. Protein concentrations were determined using molar extinction coefficients reported by Margoliash,[5] ε (410 nm) = 106100 M^{-1} cm^{-1} (ferric); ε (528) =11200 M^{-1} cm^{-1} (ferric) and ε (416) = 129100 M^{-1} cm^{-1} (ferrous); ε (520.5 nm) = 15900 M^{-1} cm^{-1} (ferrous); ε (550.25 nm) = 27700 M^{-1} cm^{-1}. Ferric / ferrous isosbestic points are at 339, 410, 434, 504, 526.5, 541.75, and 556.6 nm.

3. Preparation of the 1-65 Fragment

Horse heart cyt *c* was cleaved at Met65 and 80 by a procedure described previously with slight modifications.[9c] Purified horse heart cyt *c* was transferred into

Figure 2.8 Typical cation-exchange (FPLC Mono S 16/10, flow rate of 6 ml/min) chromatogram for the purification of native horse heart cyt *c* in 25 mM NaPi. Gradient represents the concentration of NaCl in mM. The main fraction is oxidized cyt *c* and impurities correspond to deamidated forms. Detection is on the 2.0 absorbance scale at 405 nm.

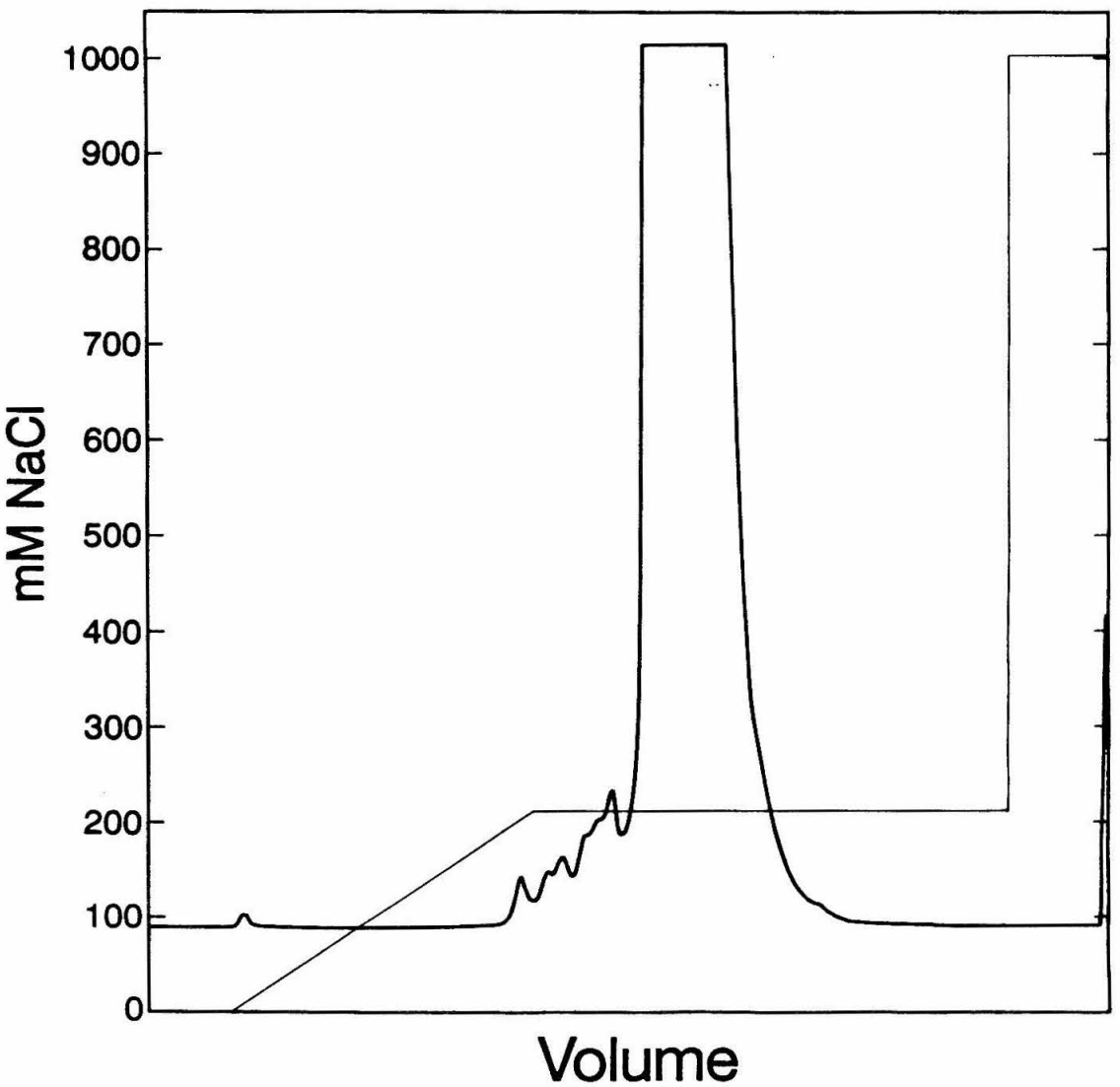
1000
900
800
700
600
500
400
300
200
100
0
mM NaCl
Volume

water *via* several ultrafiltration dilution / concentration cycles and diluted with 88% formic acid for a final solution of ~15 mg protein/ml of 70% formic acid. The protein is entirely denatured at these conditions; the color change from deep red to dark brown (Soret shifts from 410 to 394 nm) is due to the low- to high-spin state transition associated with the loss of heme axial ligation upon denaturation. Fifty-fold excess of CNBr is added as a solid to stirred, sealed roundbottom flask containing the protein. CAUTION: CNBr is extremely toxic (~150 mg is a lethal dose) and only some people can detect its almond scent.[34] This material was handled with extreme caution in the fume hood at all times except weighing, which was performed using Eppendorf tubes sealed in the hood. The cleavage reaction was allowed to proceed in the dark for 24 to 40 hours.

Cleavage was terminated by ultrafiltration. The reaction solution was first diluted with 25 mM NaPi, pH 7.0, to a final concentration of 21% formic acid to prevent Amicon filter decomposition evident at higher formic acid concentration. Ultrafiltration was carried out in the fume hood with the supernatant collected in a $AgNO_3$ solution to precipitate unreacted cyanide. The reaction solution was continuously diluted with neutral pH buffer until the solution was at neutral pH (~5 cycles). At ~pH 5.5 the fragment(s) undergo a high- to low-spin transition evidenced by the dramatic color change from brown to red. The small, non-heme protein fragments were not recovered.

Purification of the 1-65 lactone fragment was initially performed following literature methods:[9c,35] two gel-filtration steps (a 1.5 meter Sephadex G-50 gravity column followed by a Superose 12 FPLC purification in 7% formic acid) to remove uncleaved protein and small non-heme peptides followed by cation-exchange chromatography (FPLC Mono S 16/10 or 10/10) to separate the homoserine-lactone 1-65 fragment (1-65 lactone) from the hydrolyzed carboxylate-homoserine 1-65 fragment (1-65 COO^-). However, it soon became apparent that the resolution obtained by gel filtration chromatography was significantly inferior to that of cation-exchange

chromatography. Furthermore, under the conditions of cleavage employed, no evidence of a 1-80 heme-containing product was found. Therefore, midway through this work a streamlined purification strategy was introduced. Following ultrafiltration of the formic acid, CNBr, and non-heme fragments, two cation exchange purification steps were used (Figure 2.9) on the Mono S 16/10 or 10/10 column in 25 mM NaPi, pH 7.0 with a 0 to 400 mM NaCl gradient. Native cyt *c* is readily separable from the 1-65 fragment. The shoulder on the main 1-65 lactone band has been identified[36] as the 1-65 COO^- and can be 90% eliminated by judiciously selecting retained fractions. The 1-65 lactone hydrolyzes to this inactive form over time, however the only deleterious effect of its presence in reconstitution reactions is reduced product yield. The anamalously high retention time on cation exchange columns of the 1-65 fragment attests to its structural heterogeneity. The purified 1-65 fragment is unstable and precipitates from solution easily, thus samples were only used within a week of preparation without repurification. The 1-65 lactone fragment was routinely obtained in 50% yield in high purity.

4. Peptide Construction

Peptides containing natural amino acids were synthesized at the Caltech Biopolymer Synthesis and Analysis Resource Center under the direction of Suzanna Horvath. Peptides 66-104 with Lys and His at position 72 were synthesized using the stepwise solid phase method performed on an ABI 43A synthesizer with Caltech-developed *t*-BOC protocols.[10] The amide peptides were desalted on Dowex AG.1-X2 resin, purified by reversed-phase HPLC, and stored lyophilized. A representative HPLC trace indicating the quality of the 39-mers obtained from this facility is presented in Figure 2.10. The integrity of the peptides was confirmed by amino acid analysis and peptide microsequencing.

Figure 2.9 Typical cation-exchange (FPLC Mono S 16/10, flow rate of 6 ml/min) chromatograms for the first (A) and second (B) purifications of 1-65 fragment in 25 mM NaPi. Gradient represents the concentration of NaCl in mM. The main band at low ionic strength is uncleaved cyt *c* and the main band at high ionic strength is the 1-65 lactone product. The low ionic strength shoulder on the 1-65 lactone band corresponds to the 1-65 COO^- (see text for discussion). Detection is on the 2.0 absorbance scale at 280 nm.

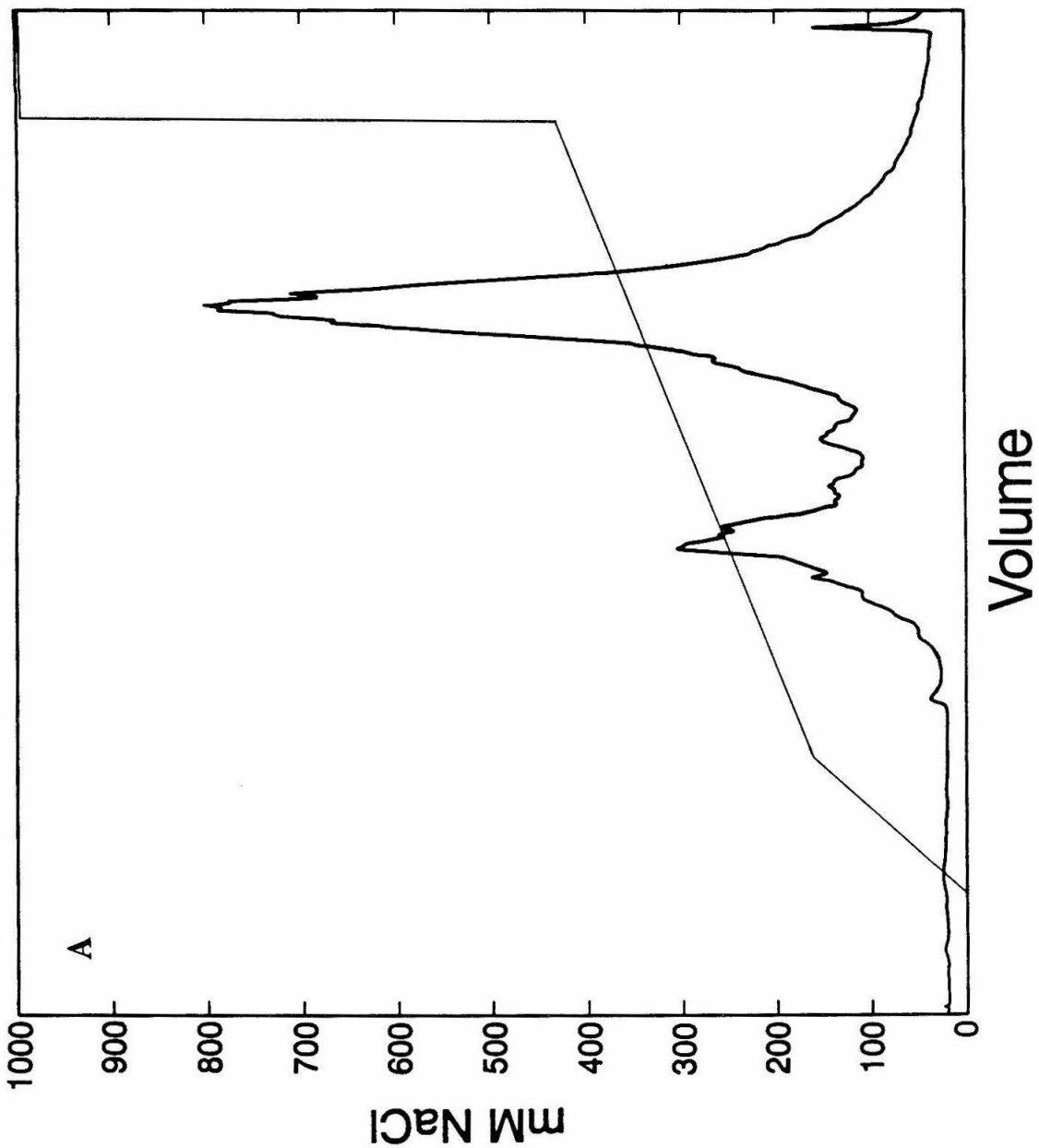
A
1000
900
800
700
600
500
400
300
200
100
0
mM NaCl
Volume

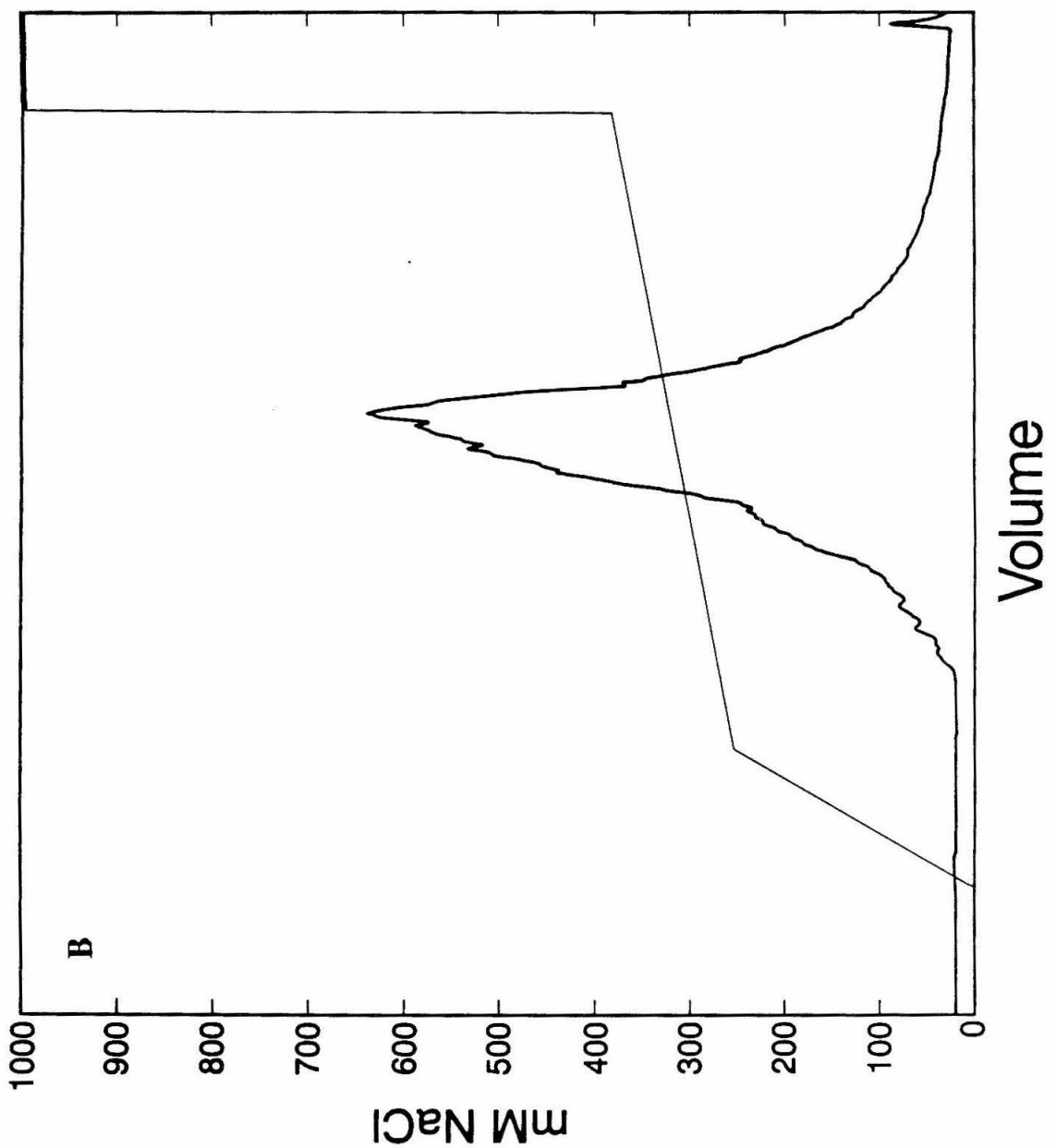
B
1000
900
800
700
600
500
400
300
200
100
0
mM NaCl
Volume

Figure 2.10 Reversed-phase HPLC trace of the final purification of 39-mer peptide for His72 cyt *c*. Detection at 214 nm. The peak with the retention time of 36.91 min. is the product. The shoulder is probably due to 38-mer impurities. The peaks eluting early from the column correspond to dithiothreitol and other small molecules.

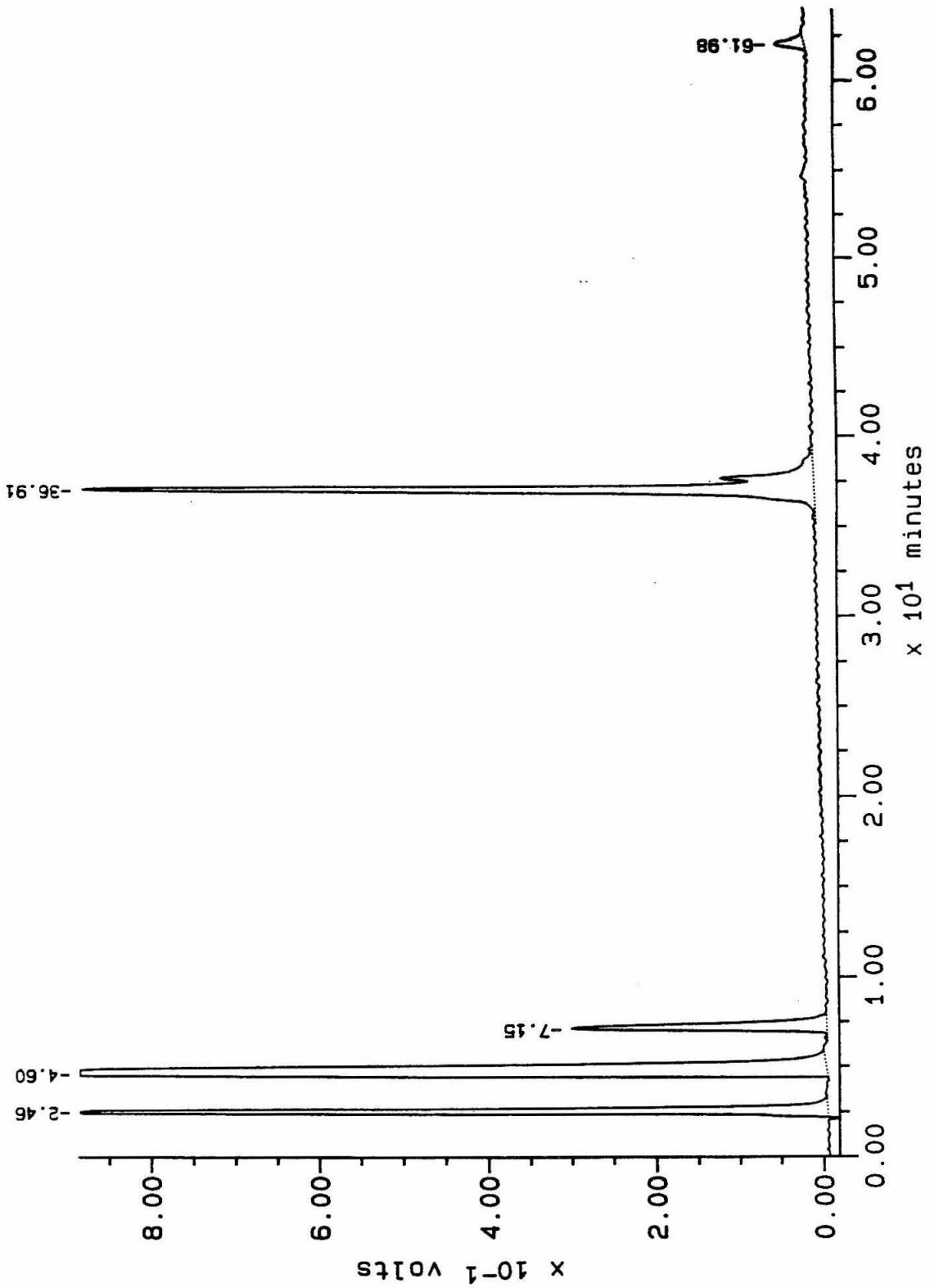
x 10⁻¹ volts
8.00
6.00
4.00
2.00
0.00
-2.46
-4.60
-7.15
-36.91
-61.98
0.00
1.00
2.00
3.00
4.00
5.00
6.00
x 10¹ minutes

5. Protein Reconstitution

Generally, a solution of 0.1 to 0.4 mM 1-65 lactone with 0.8 equivalent of 66-104 peptide in 25 mM NaPi, pH 7.0 was thoroughly deoxygenated using Schlenk techniques. A solution of the peptide was prepared prior to addition to the 1-65 lactone and occasionally required sonication or a slightly lower ionic strength to fully dissolve. Reduction was effected by anaerobic addition of a minimal amount of freshly prepared, deoxygenated sodium dithionite solution. Full reduction was gauged by a distinctive color change in solution. Best results were obtained if only 1 - 2 equivalents sodium dithionite were used for reduction. The reaction was allowed to proceed under rigorously anaerobic conditions for 24 to 40 hours. The presence of even a trace amount of dioxygen can lead to either premature oxidation of the 1-65 complex before bond reformation has occurred or reaction with the dithionite present to form radical species capable of heme degradation. Two techniques were employed to exclude oxygen during the course of the reaction. If the reaction flask was left on the Schlenk line under constant positive argon pressure, net oxidation was observed within 6 - 18 hours, necessitating additional sodium dithionite treatment. Significant protein degradation was observed. Cleaner reactions and higher product yields were obtained if, after deoxygenation and prior to reduction, the reduction and reconstitution reactions were carried out in the glove box under an inert atmosphere.

Reconstituted protein was isolated by cation-exchange chromatography (Figure 2.11) (Mono S 10/10 column) in 25 mM NaPi, pH 7.0 with a 100 to 300 mM NaCl gradient. The semisynthetic proteins eluted at similar volumes as native cyt *c*. The products are well separated from both the 1-65 lactone starting material and the inactive 1-65 COO^- impurity. Proteins were purified by cation-exchange chromatography at least two more times before use. Typical yields (based on peptide quantities used) were 50 -

Figure 2.11 Typical cation-exchange (FPLC Mono S 10/10, flow rate of 3.5 ml/min) chromatograms for a reconstitution reaction. Oxidized and reduced His72 cyt *c* products and 1-65 lactone and COO^- reactants are indicated. Gradient represents the concentration of NaCl in mM. Detection is on the 0.5 absorbance scale at 280 nm.

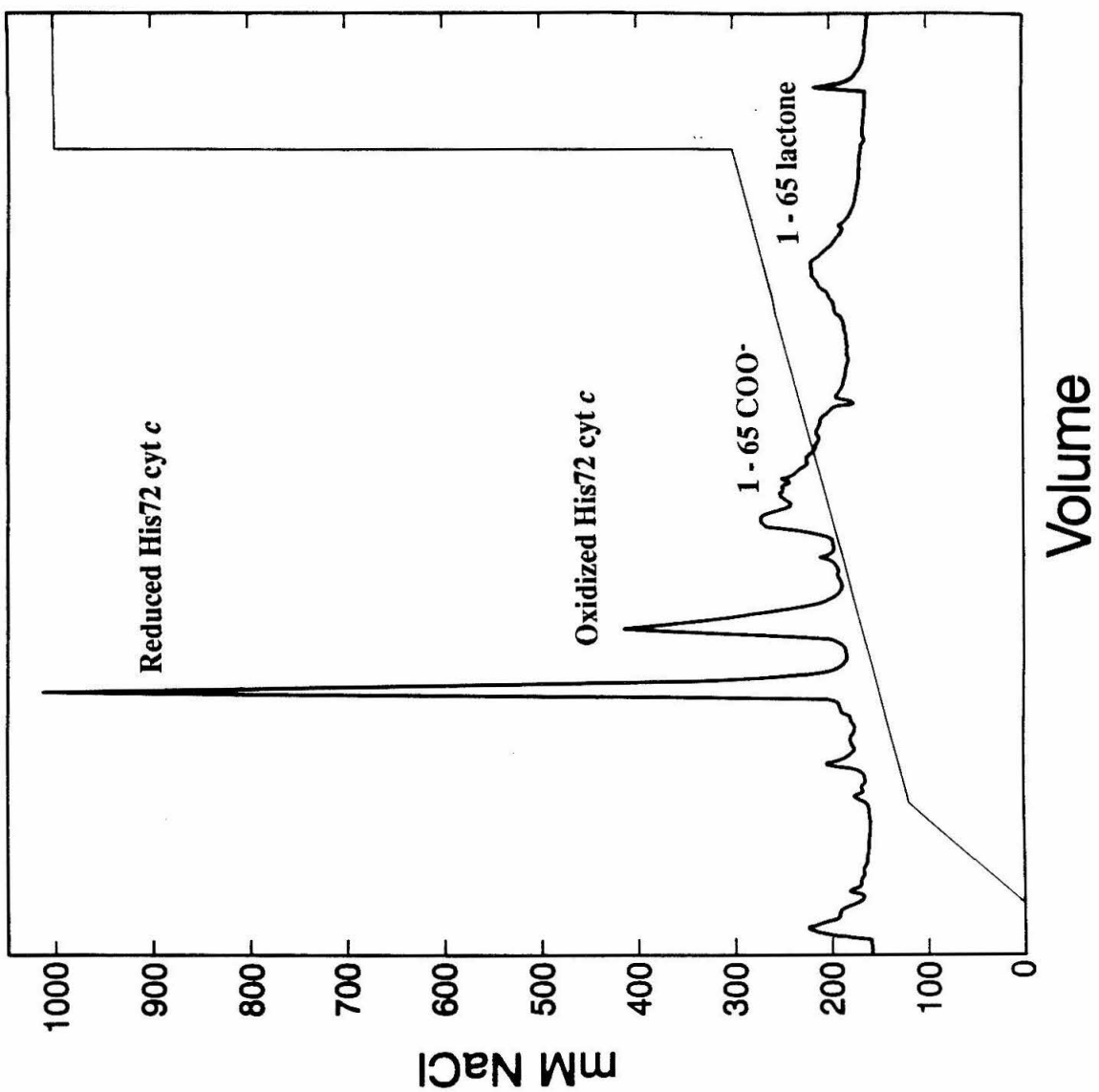
Reduced His72 cyt c
Oxidized His72 cyt c
1 - 65 COO-
1 - 65 lactone
mM NaCl
1000
900
800
700
600
500
400
300
200
100
0
Volume

75% and were similar for both the reconstitution of native and His72 cyt *c*. Peptide impurities (*i.e.*, small quantities of 38-mers) are not active in the reconstitution reaction.

6. Pentaammineruthenium Modification

Pentaammineruthenium derivatives of His33 of native and His72 of semisynthetic cyt *c* were obtained with slight modifications of previously reported protocols.[37] $[Rua_5(H_2O)]^{2+}$ was generated *in situ* or as the PF_6 salt by reduction of $[Ru(NH_3)_5Cl]Cl_2$ over a Zn / Hg amalgam using Schlenk and cannulae-transfer techniques. This compound was used only immediately following preparation due to its facile oxidation. Reactions were performed anaerobically with 49-fold excess of $[Rua_5(H_2O)]^{2+}$ (fifty equivalents added, one equivalent consumed in protein reduction) in a solution of 0.2 to 0.4 mM protein in 100 mM HEPES buffer pH 7.0. Aliquots were removed at fixed time intervals over the course of 30 hours to monitor the growth of products and optimize the reaction time. The modification reaction was quenched by gel filtration and oxidized overnight with excess $Co(EDTA)^-$ at room temperature to obtain the substitution inert Ru^{3+} complex. The products of the modification reaction were evaluated using analytical (5/5) and preparative (16/10) Mono S cation-exchange chromatography with 25 mM NaPi, pH 7.0 and a NaCl gradient. The yield of Rua_5His72 cyt *c* was 30%.

III. Results and Discussion

A. 1-65 Fragment Characterization

The biophysical characteristics of the 1-65 lactone fragment have been reported[6a,35] and are not the focus of this work. However, certain properties were investigated to verify the integrity of the reconstitution reaction. As alluded to earlier, this fragment probably exists as an ensemble of conformations, perhaps including dimerization along the exposed hydrophobic face, with some strong field ligand occupying the sixth coordination site of iron.

Absorption spectra of the 1-65 lactone fragment obtained at neutral and low pH agree well with reported values[6a] (observed at pH 7.0: ε_{max} = 407, 525 nm (ferric); 416, 520, and 550 nm (ferrous)). A value of ε (407 nm) = 101000 M^{-1} cm^{-1} was used. The absorption spectra for oxidized and reduced 1-65 lactone are similar to native cyt *c* in the Soret, α and β band region (a slight loss of intensity in the α and β band region is noted as well as a 3 nm blue-shift in the ferric Soret), however bands due to peptide backbone and aromatic absorption are proportionally less (220 and 280 nm). The 695 nm band is absent, as anticipated, and no additional charge transfer bands are observed.

Amino acid analysis was consistent with anticipated results and both isoelectric focusing (IEF) gel electrophoresis and capillary zone electrophoresis indicate the purified species is homogeneous with respect to molecular weight and total charge. IEF gel electrophoresis proved to be a particularly useful analytical technique as the 1-65 COO^-, 1-65 lactone and native protein focus as easily separable and identifiable bands.

Differential pulse polarography measurements taken on a freshly prepared sample indicate a reduction potential of 50 ± 20 mV *vs.* NHE (Figure 2.12). The measured potential varies over time, however, from -108[8e] to +300 mV,[38] indicating that changes are occurring in the heme environment. The ^1H NMR spectrum of ferric 1-65 lactone in pure D_2O exhibits broad and ill-defined resonances in the paramagnetically-shifted regime in comparison with the well-resolved peaks characteristic of native cyt *c* in this region.

Control reconstitution reactions were conducted with 1-65 lactone where the experimental manipulations necessary for protein reconstitution were mimicked (*i.e.*, degassing, reduction with sodium dithionite) in the absence of the 66 104 peptide. Significant degradation (5 to 20% depending on conditions) was noted by cation-exchange chromatography, with one degradation peak eluting near the anticipated retention time for native cyt *c*. Therefore, care was taken to purify reconstituted proteins at reducing and oxidizing conditions to ensure complete homogeneity of product proteins.

Figure 2.12 Differential pulse polarogram of freshly-made 1-65 lactone. $E^{o'}$ = 50(5) mV *vs.* NHE in 50 mM NaPi, 10 mM 4,4'-bipyridine, pH 7.0. Scan rate = 5 mV/sec.

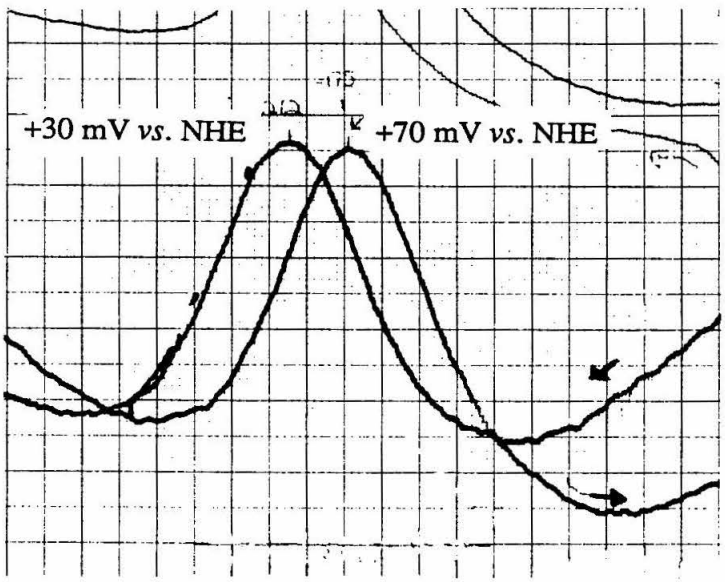
+30 mV *vs*. NHE
+70 mV *vs*. NHE

Since degradation is thought to be linked to sodium dithionite side reactions, alternative methods for reduction were explored. Ascorbate is not potent enough to affect reduction and dithiothreitol triggered a collapse of heme absorption. Mediated bulk electrolysis at a Pt basket electrode effectively reduced cyt *c* with one electron per heme, however the 1-65 lactone absorbed > 10 electrons per heme with no visible evidence of reduction. Significant degradation was also observed.

B. His72 Cytochrome c Characterization

Due to high yield from the reconstitution reaction, the His72 cyt *c* mutant has been extensively characterized. All measured biophysical characteristics indicate that the replacement of the invariant Lys at position 72 has no effect on the spectroscopic and structural features of the protein.

1. Chromatography and Electrophoresis

Both the ferric and ferrous form of His72 cyt *c* elute as sharp, distinct bands on cation-exchange columns well separated from the 1-65 lactone starting material (Figure 2.10). Ferric and ferrous His72 cyt *c* elute from a cation-exchange column at ionic strengths slightly lower than the corresponding redox state of native cyt *c*. The difference in elution ionic strength between native and His72 cyt *c* exactly corresponds to the separation between the ferric and ferrous forms, implying that His72 cyt *c* has effectively one less positive charge than native, as expected from the change in sequence if the pKa of His72 is less than 7.0 (pKa = 5.5, measured by NMR, *vide infra*). For example, on a Mono S 10/10 column, at identical conditions with identical elution programs, elution concentrations of NaCl in 25 mM NaPi, pH 7.0 are: Fe^{3+} native cyt *c*, 195 mM; Fe^{2+} native cyt *c*, 180 mM; Fe^{3+} His72 cyt *c*, 175 mM; Fe^{2+} His72 cyt *c*, 165 mM.

The homogeneity of the purified protein was confirmed by isoelectric focusing. The pI of His72 cyt *c* is slightly lower than native cyt *c* and much higher than 1-65

lactone and 1-65 COO^-. CZE also indicated a homogeneous product that eluted similarly with native cyt *c*.

2. Analytical Analysis

Amino acid analysis was consistent with anticipated results. Thermospray mass spectrometry was used to determine molecular weights. Data are presented below:

Table 2.1. Summary of protein mass spectrometry.

Sample	Calculated Mass (amu)	Measured Mass (amu)
Native horse heart cyt *c*	12,364	12,380(12)
His72 cyt *c*	12,343	12,360(12)

Parentheses indicate uncertainties in the preceding digit.

The data indicate that a fully reconstituted protein was formed with a mass consistent with a Lys to His and Met to Hse alteration.

3. Absorption Spectroscopy

The absorption spectrum of His72 cyt *c* in 25 mM NaPi, pH 7.0 is superposable with native cyt *c* in both the oxidized and reduced states (Figure 2.13). Extinction coefficients for native cyt *c* were therefore used to calculate concentrations. The 695 nm band was also present, indicating proper Met80 ligation (Figure 2.14).

4. Circular Dichroism Spectroscopy

Ambient temperature CD studies in the far UV region indicate that His72 cyt *c* possesses identical secondary structural features with native horse heart cyt *c* in 25 mM

Figure 2.13 (A) Measured electronic absorption spectra of His72 cyt *c* (——) and native cyt *c* (- - - -) in the ferric state in 25 mM NaPi, pH 7.0. Proteins were oxidized with Na[Co(EDTA)] prior to purification. (B) Measured electronic absorption spectra for His72 cyt *c* (——) and native cyt *c* (- - - -) in the ferrous state in 25 mM NaPi, pH 7.0. Proteins were reduced with sodium dithionite, which was removed by gel filtration, immediately prior to data acquisition. The His72 and native cyt *c* spectra are nearly identical in both the oxidized and reduced states.

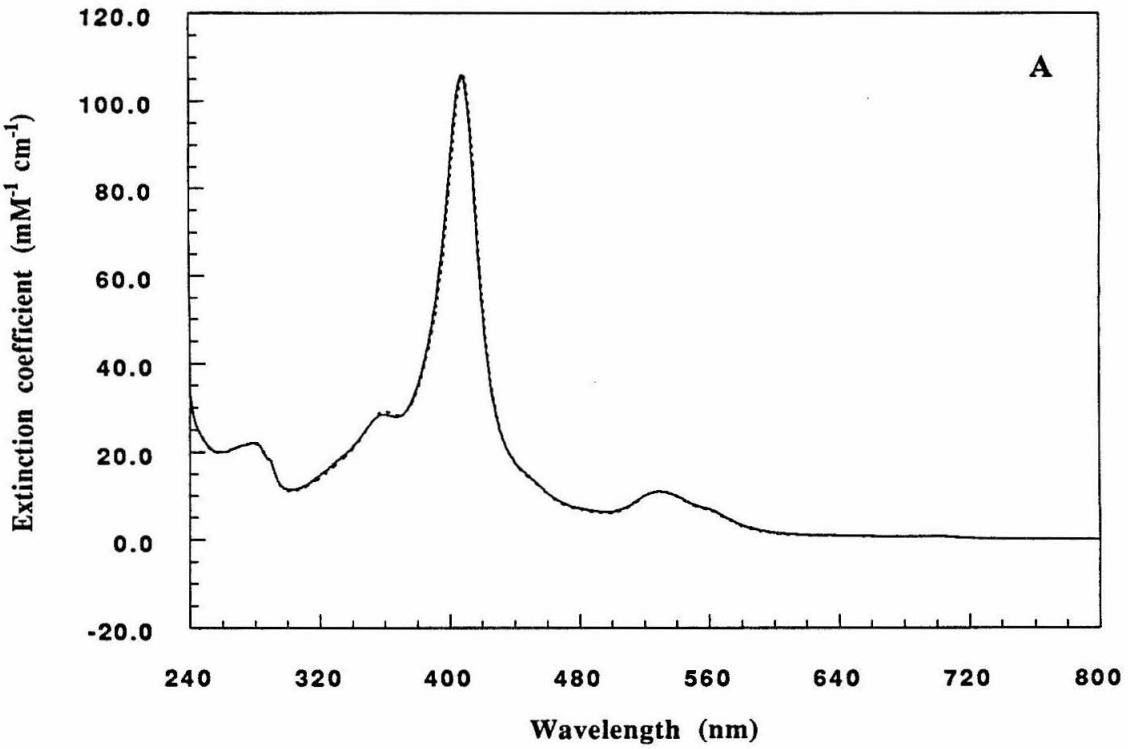
A
Extinction coefficient (mM-1 cm-1)
120.0
100.0
80.0
60.0
40.0
20.0
0.0
-20.0
240
320
400
480
560
640
720
800
Wavelength (nm)

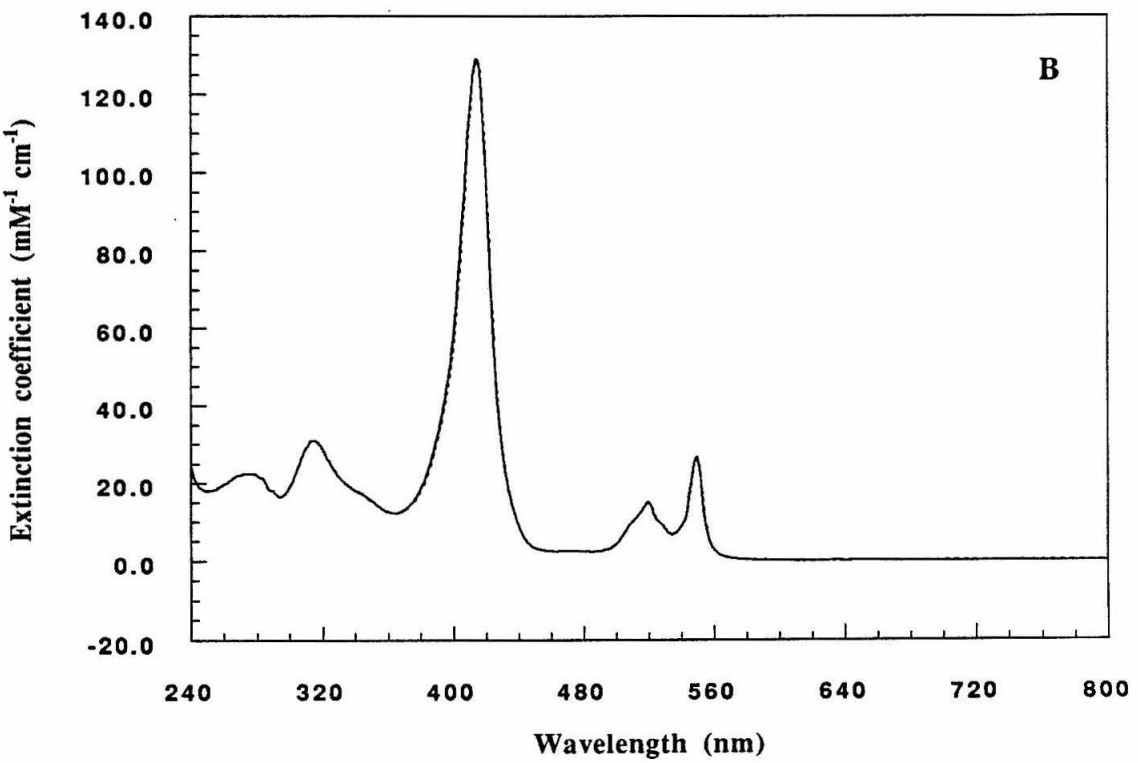
B
Extinction coefficient (mM-1 cm-1)
140.0
120.0
100.0
80.0
60.0
40.0
20.0
0.0
-20.0
240
320
400
480
560
640
720
800
Wavelength (nm)

Figure 2.14 Expansion of the measured electronic absorption spectra of His72 cyt *c* (——) and native cyt *c* (- - - -) in the ferric state in 25 mM NaPi, pH 7.0 in the region of the Met to Fe^{3+} charge transfer transition. Proteins were oxidized with Na[Co(EDTA)] prior to purification.

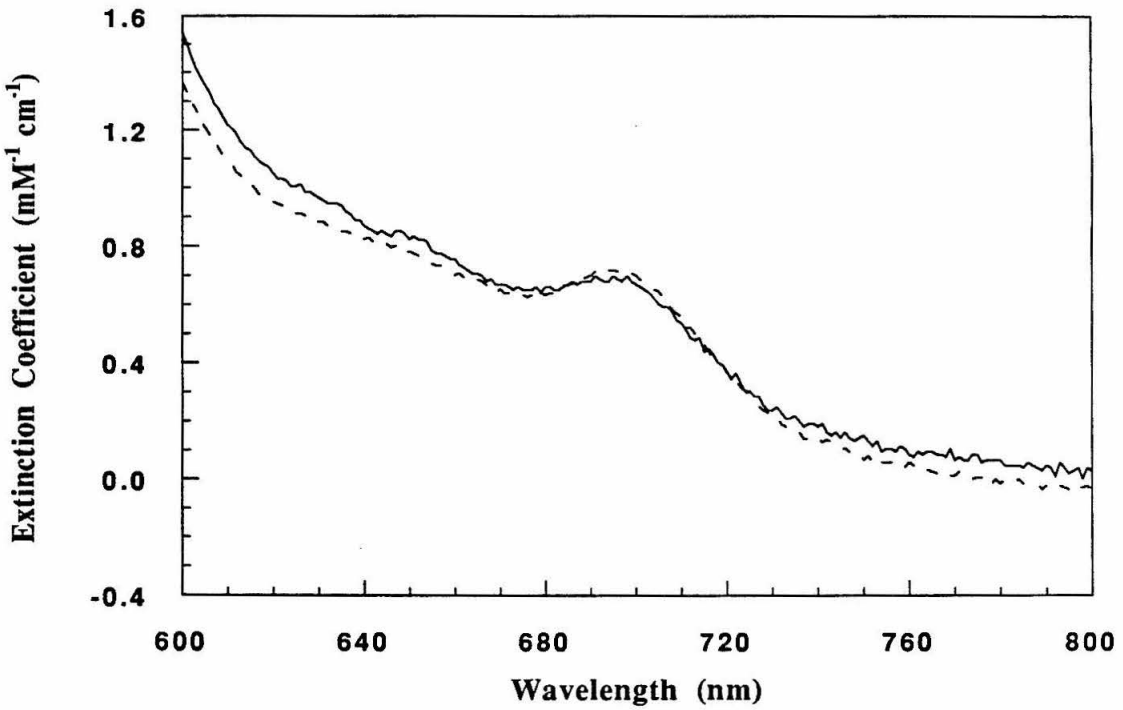
1.6
1.2
0.8
0.4
0.0
-0.4
Extinction Coefficient (mM-1 cm-1)
600
640
680
720
760
800
Wavelength (nm)

NaPi, pH 7.0 (Figure 2.15). The CD spectrum is typical of that for an α-helical protein with minima at 222 and 205 nm. Melting curves monitoring the loss of α-helix at 222 nm indicate that the midpoint for the melting transition is at 87° C for both native cyt *c* and His72 cyt *c* (Figure 2.16), indicating indistinguishable thermal stabilities for both proteins.

5. EPR Spectroscopy

The EPR spectrum of ferric His72 cyt *c* is nearly identical with that of native cyt *c* at 6.8 K (Figure 2.17). Measured *g* values for native cyt *c* are 3.03, 2.21, and 1.21 which are similar to published values at slightly different conditions, 3.06, 2.24, and 1.24.[39] *g* values obtained for His72 cyt *c* are 3.05, 2.23 and 1.21. These *g* values represent the tetragonal and orthorhombic distortions due to the ligand environment and are extremely sensitive to the electronic character of the ligands. Therefore, it can be concluded that the introduction of His at position 72 does not have any significant effect on heme ligation.

6. Electrochemistry

The redox potentials of native cyt *c*, reconstituted cyt *c* (Hse65 cyt *c*), and His72 cyt *c* were determined (exhaustively) by both spectroelectrochemistry with a $Rua_5py^{3+/2+}$ mediator and by differential pulse polarography at a 4,4'-bipyridine-modified gold electrode. The potentials obtained are summarized below. All potentials were measured in 50 mM NaPi, pH 7.0 at ambient temperature. Redox potentials were calculated from the differential pulse polarography data as described in Section II.C.1. Data for Hse65 cyt *c* and His72 cyt *c* are shown in Figure 2.18 A and B.

Figure 2.15 Far-UV circular dichroism spectra of His72 cyt *c* (——) and native cyt *c* (- - - -) in 25 mM NaPi, pH 7.0. Sample concentrations were ~14 μM and spectra were obtained in a 0.1 cm pathlength cell on the 20 mdeg sensitivity scale at ambient temperature.

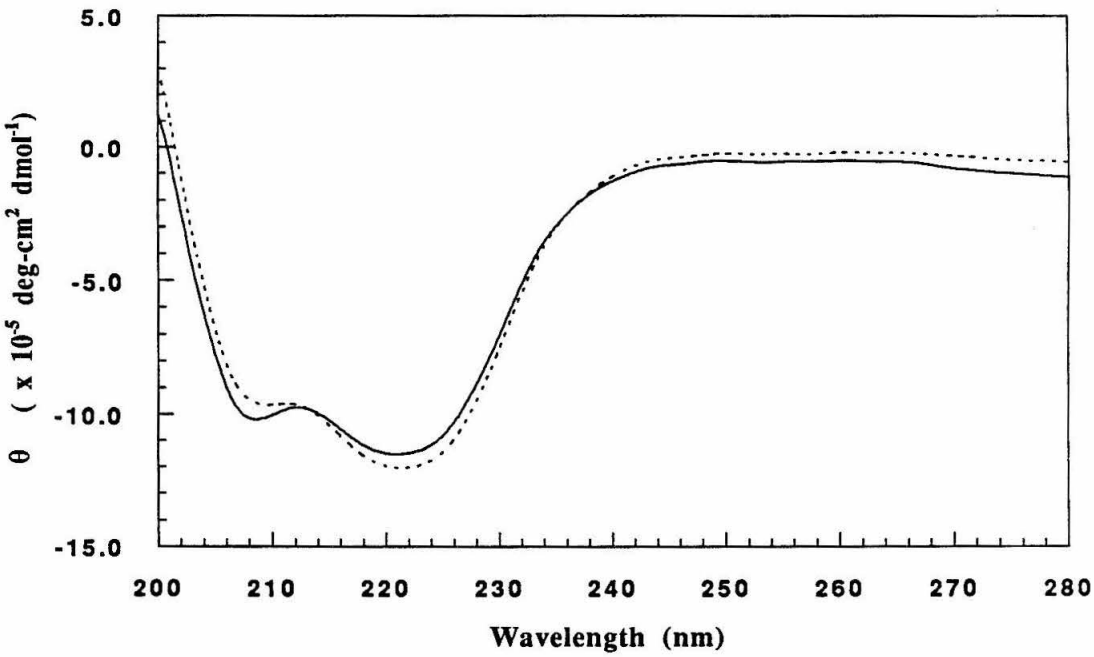
5.0
0.0
-5.0
-10.0
-15.0
θ (x 10-5 deg-cm2 dmol-1)
200
210
220
230
240
250
260
270
280
Wavelength (nm)

Figure 2.16 Melting curves for (A) native cyt *c* and (B) His72 cyt *c* in 25 mM NaPi, pH 7.0. Data plotted are the 222 nm signal of the CD spectrum. The signal at 222 nm was constant between 25° C and 60° C.

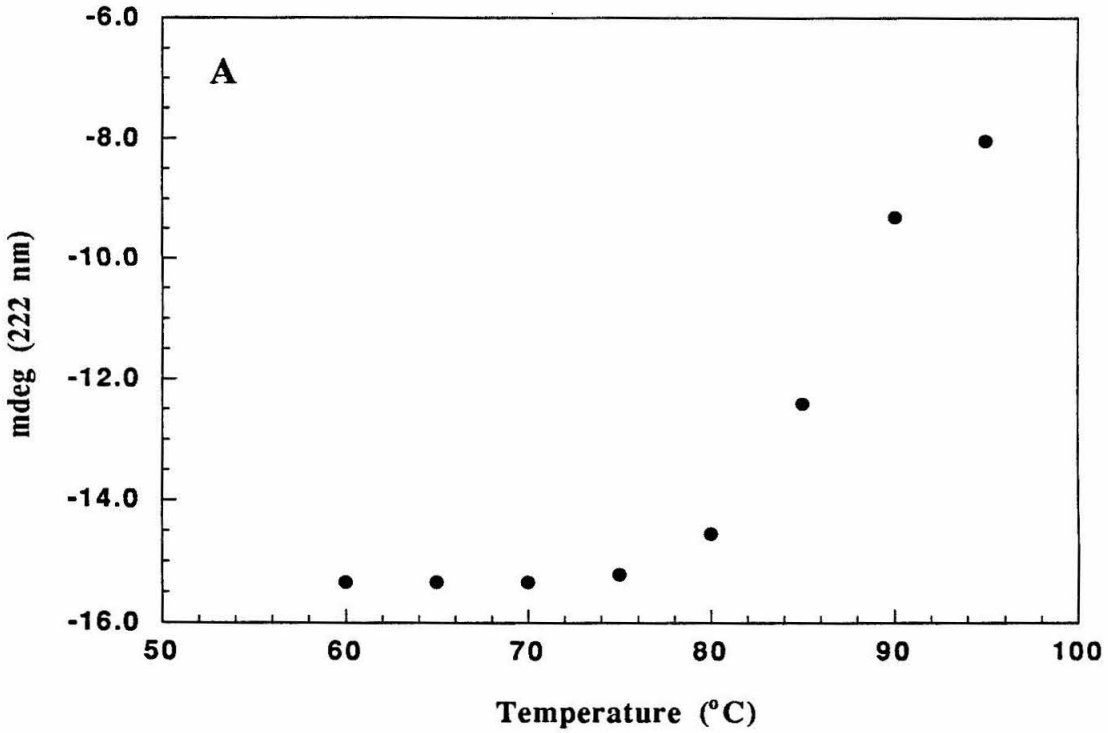
A
-6.0
-8.0
-10.0
-12.0
-14.0
-16.0
mdeg (222 nm)
50
60
70
80
90
100
Temperature (°C)

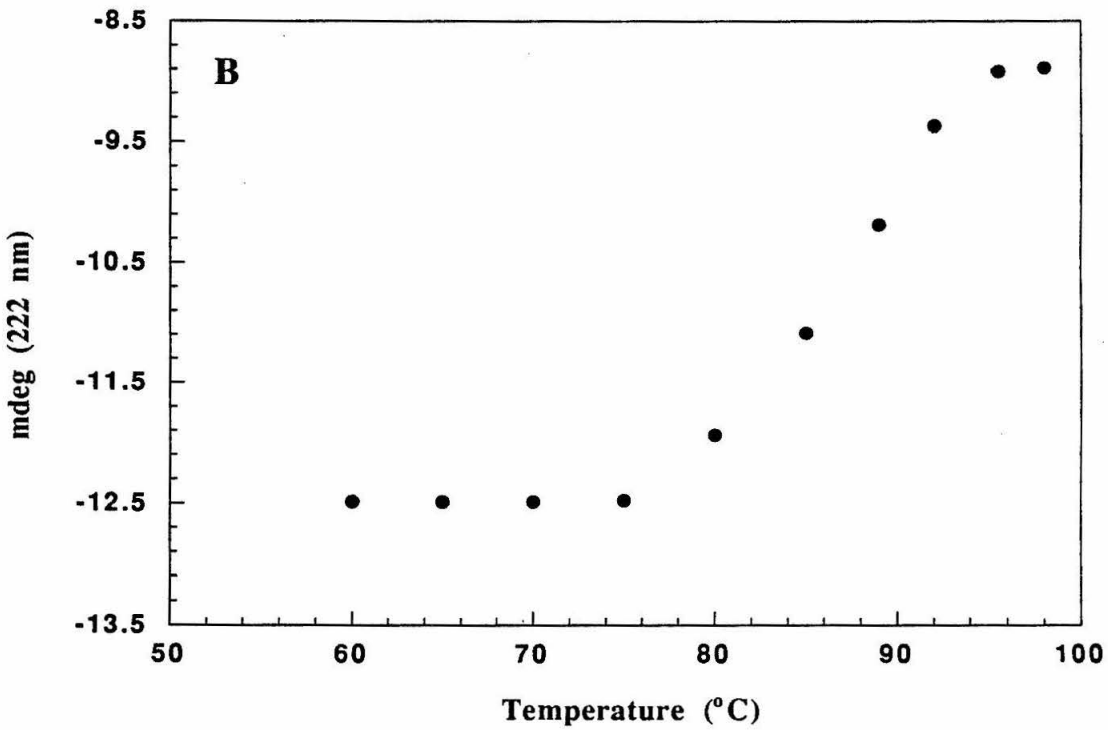
B
-8.5
-9.5
-10.5
-11.5
-12.5
-13.5
mdeg (222 nm)
50
60
70
80
90
100
Temperature (°C)

Figure 2.17 EPR spectra of ferric (A) native and (B) His72 cyt *c* in 50 mM HEPES, 50% glycerol, pH 7.0 glass at 6.8 K.

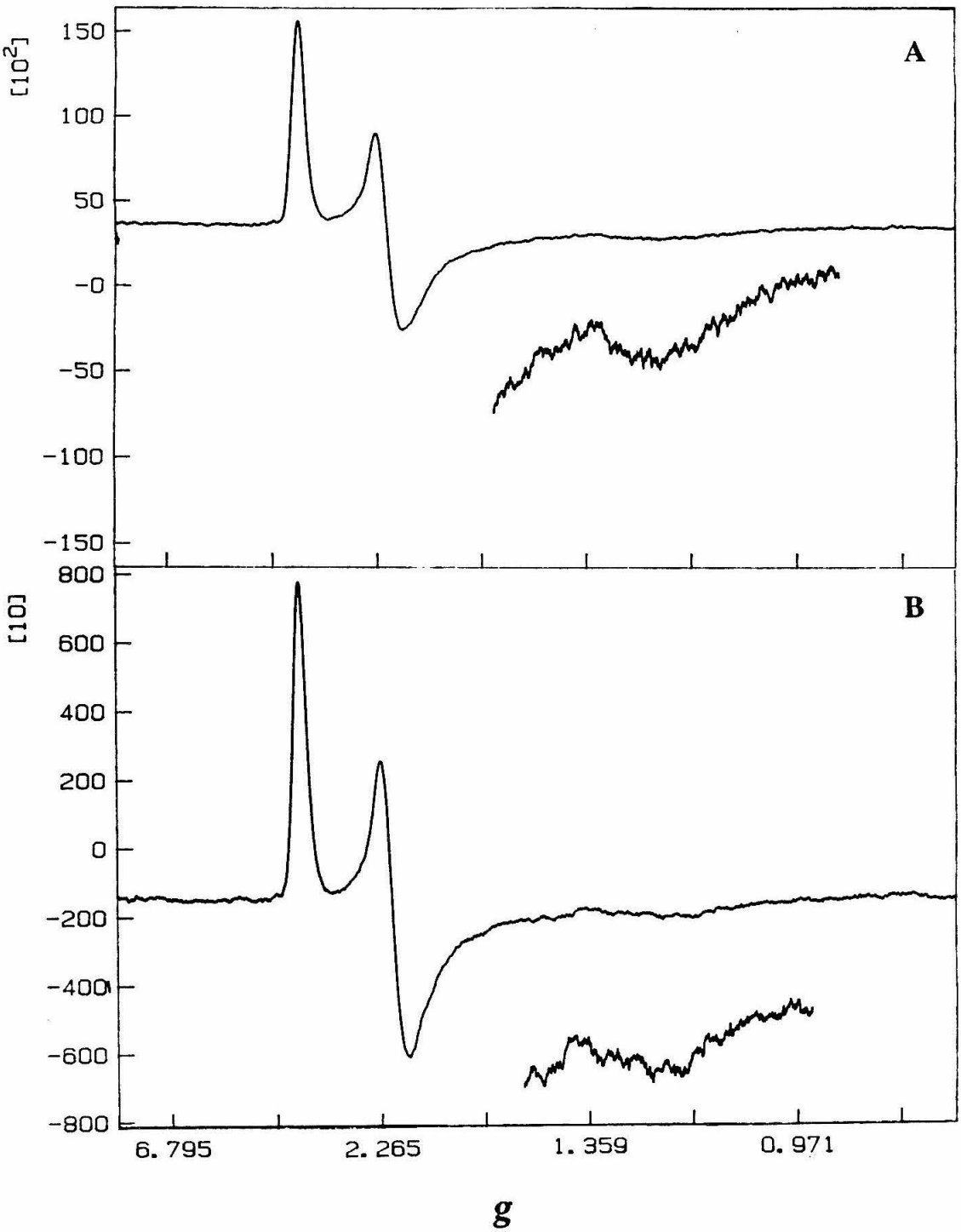
[10²]
150
100
50
-0
-50
-100
-150
A
[10]
800
600
400
200
0
-200
-400
-600
-800
B
6.795
2.265
1.359
0.971
g

Table 2.2. Summary of redox potentials obtained on unmodified proteins.

Sample	$E^{o'}$ ($Fe^{3+/2+}$)	
	Differential Pulse Polarography (mV *vs.* NHE)	Spectroelectrochemistry (mV *vs.* NHE)
Native cyt *c*	265(5)	265(2)
Hse65 cyt *c*	268(5)	263(2)
His72 cyt *c*	256(5)	255(2)

Spectroelectrochemistry data were obtained by monitoring the absorbance changes in the Q-band region of the spectrum as a function of applied potential. Representative raw data are presented in Figure 2.19. The mediator used possesses no spectral features in this region. At typical concentrations of protein (0.5 mM) and mediator (1.5 to 2.5 mM), the system requires 15 minutes to arrive at equilibrium and is independent of whether it is reached anodically or cathodically. The concentration of oxidized and reduced protein at each potential is calculated from the absorption using the difference in extinction coefficient of 18500 M^{-1} cm^{-1} at 550 nm between redox states. These values can be related to $E^{o'}$ using the Nernst equation:

$$E_{app} = E^{o'} - \frac{RT}{nF} \ln \frac{[red]}{[ox]}$$

E_{app}, R, T, n, and F are the applied potential, universal gas constant, temperature, numbers of electrons in the redox couple (1), and the Faraday constant, respectively. Thus a plot of log [red] / [ox] *vs.* applied potential will be linear with a slope of - 59 mV and a y-intercept of $E^{o'}$. Nernst plots of data obtained for Hse65 cyt *c* and His72 cyt *c* are presented in Figure 2.20.

Figure 2.18 Differential pulse polarograms of (A) reconstituted Hse65 cyt *c* ($E^{o'}$ = 268(5) mV *vs.* NHE) and (B) His72 cyt *c* ($E^{o'}$ =256(5) mV *vs.* NHE) in 50 mM NaPi, 10 mM 4,4'-bipyridine, pH 7.0. Scan rate = 1 mV/s.

A

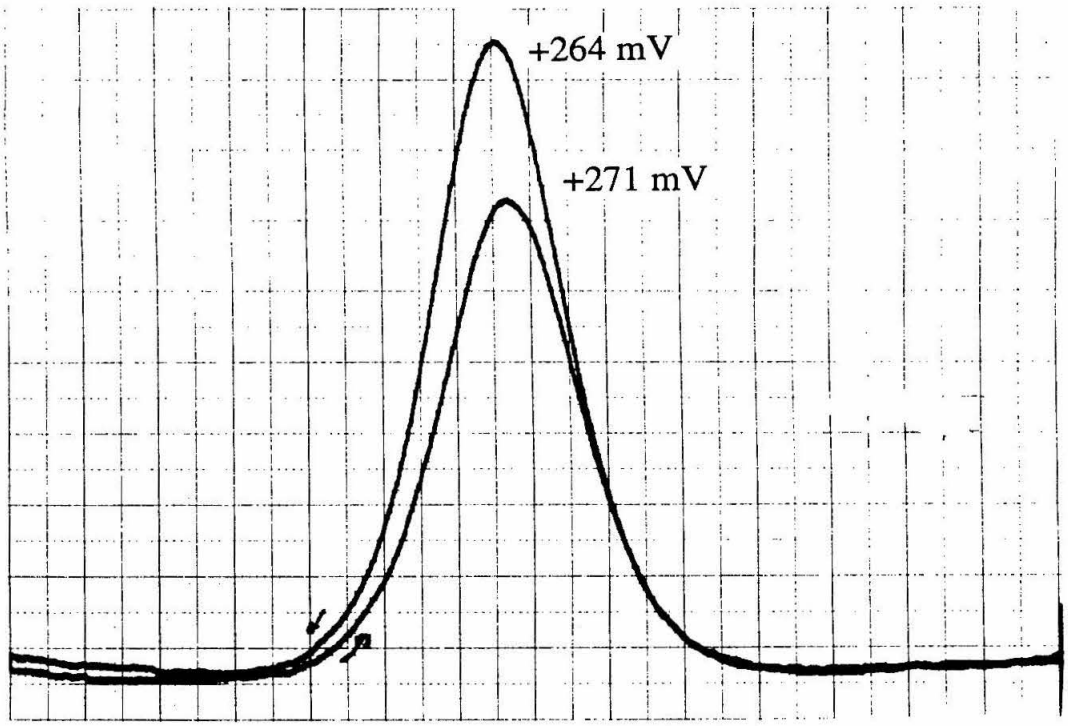

B

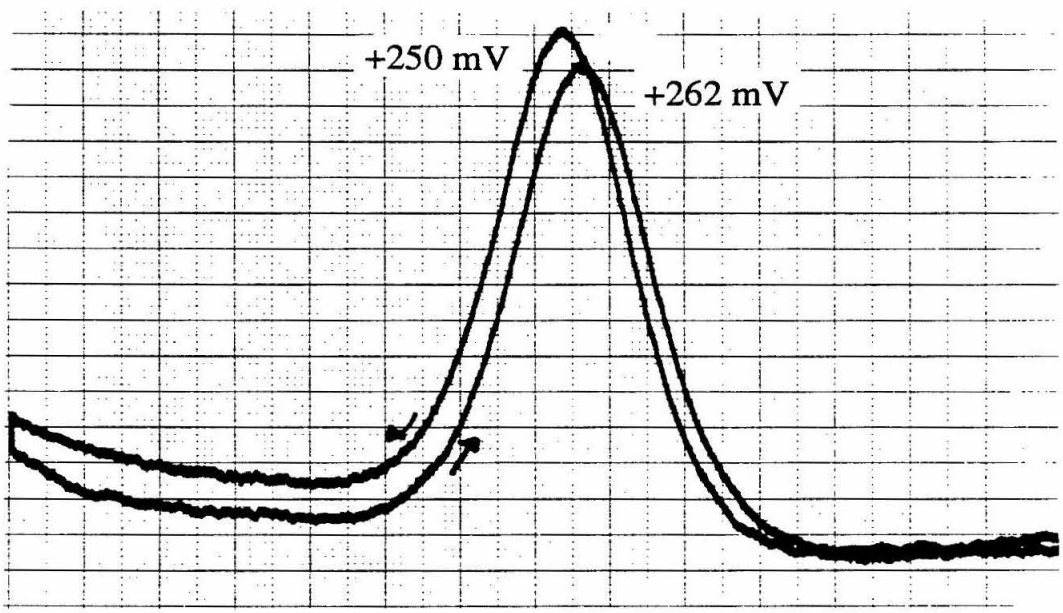

Figure 2.19 Typical raw data obtained in a spectroelectrochemical experiment. Traces correspond to absorption spectra in the Q-band region of a His72 cyt *c* sample at (with increasing absorption at 550 nm); 306, 75, 55, 35, 21, 6, -10, -20, and -350 mV *vs.* SCE. Isosbestic points are experimentally observed at 502, 526, 541, and 556 nm.

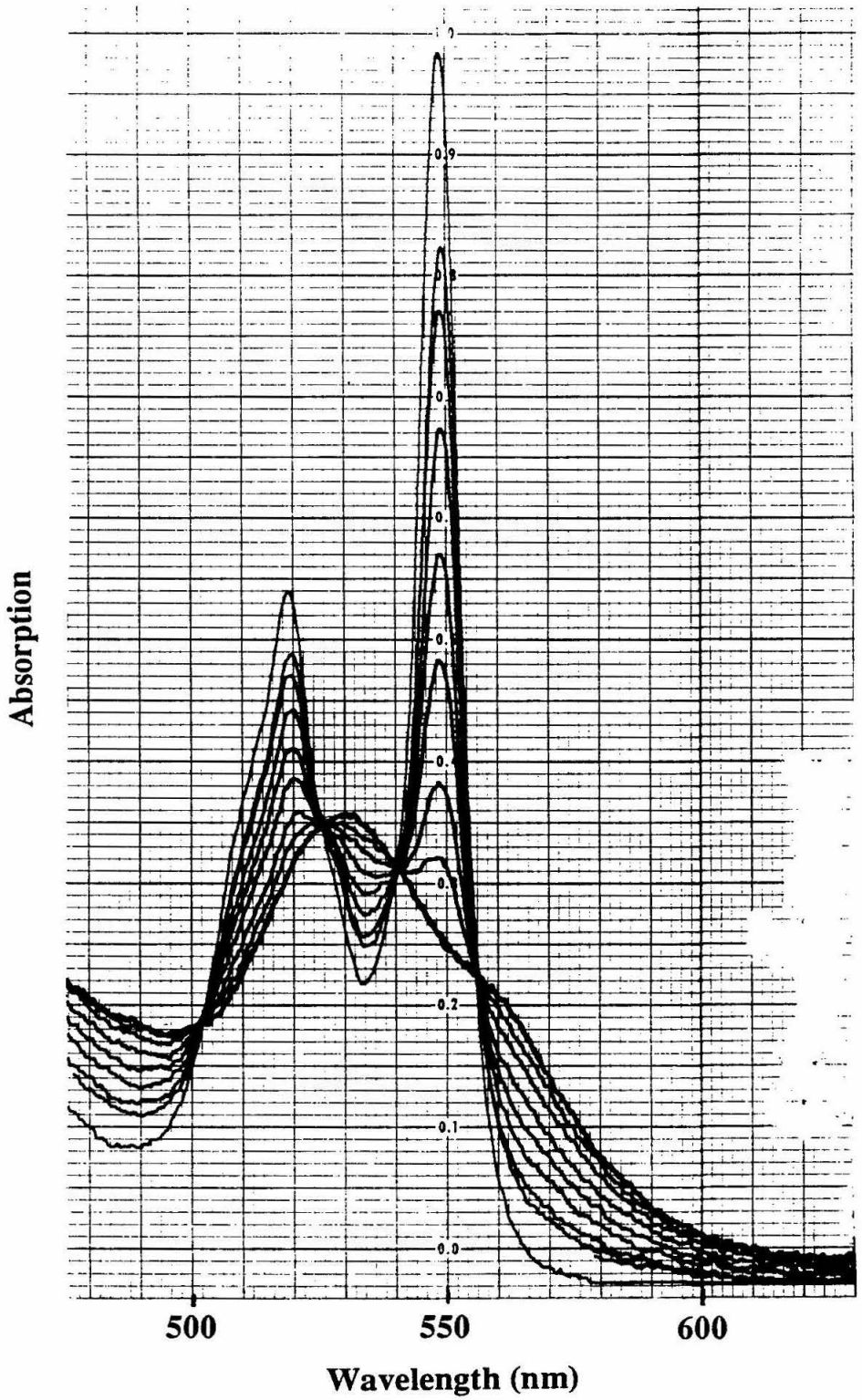
Absorption
1.0
0.9
0.2
0.1
0.0
500
550
600
Wavelength (nm)

Figure 2.20 Nernst plots for data obtained from (A) reconstituted Hse65 cyt *c* ($E^{o'}$ = 263(2) mV *vs.* NHE) and (B) His72 cyt *c* ($E^{o'}$ = 255(2) mV *vs.* NHE) in 50 mM NaPi , ~1 mM $[Rua_5py]^{3+}$, pH 7.0. Linear fits to the data are shown; potentials shown are *versus* the SCE reference. See text for details.

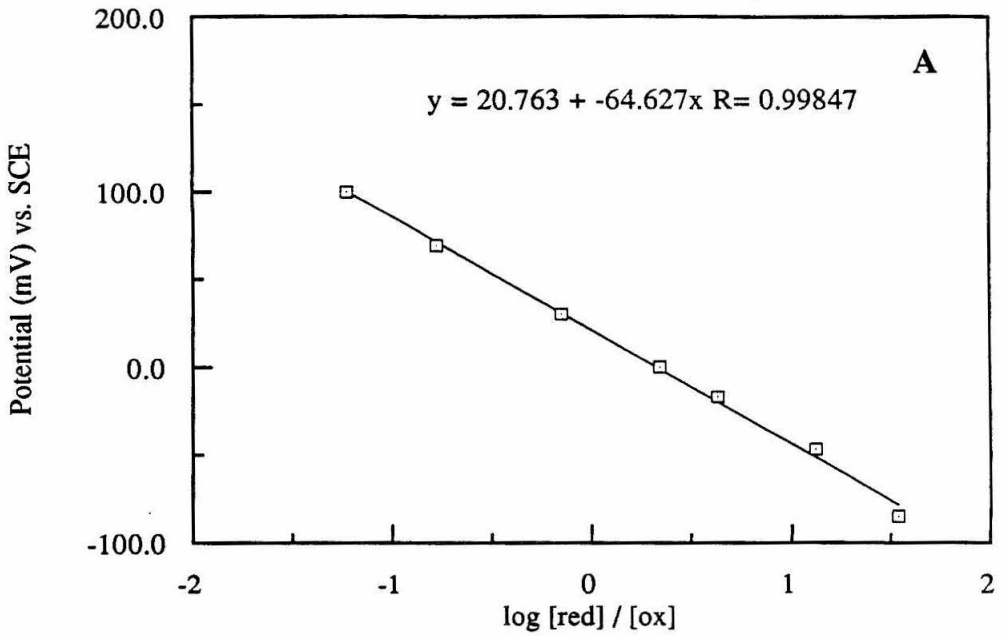
A
y = 20.763 + -64.627x R= 0.99847
Potential (mV) vs. SCE
200.0
100.0
0.0
-100.0
-2
-1
0
1
2
log [red] / [ox]

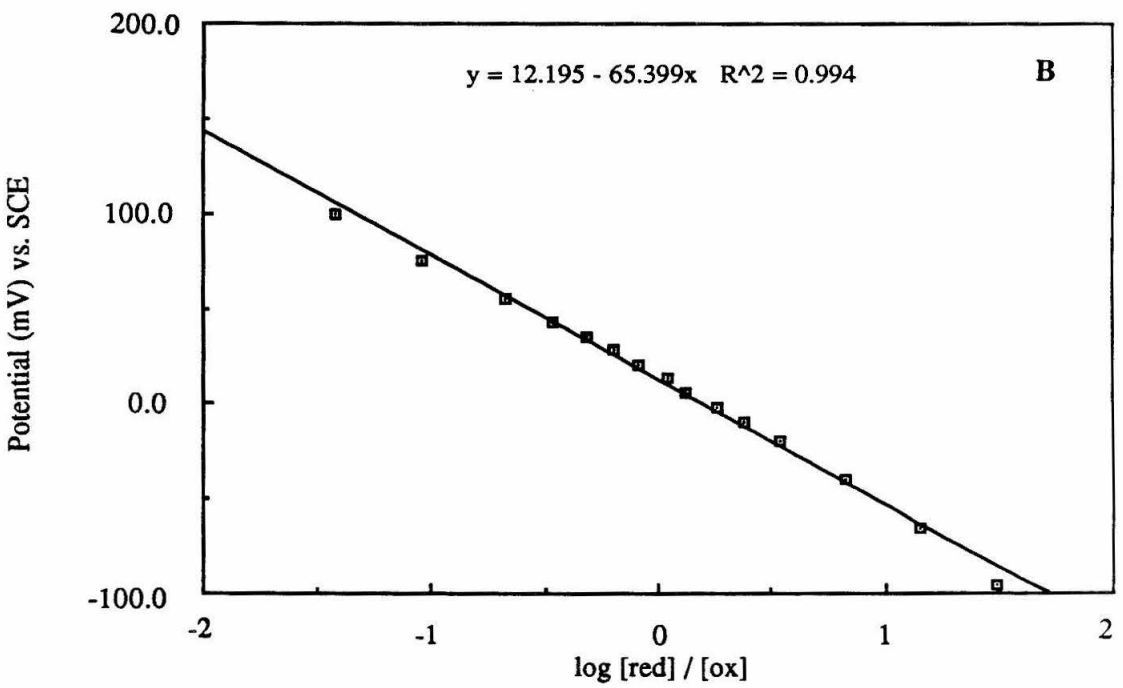
B
y = 12.195 - 65.399x R^2 = 0.994
Potential (mV) vs. SCE
200.0
100.0
0.0
-100.0
-2
-1
0
1
2
log [red] / [ox]

Spectroelectrochemical data obtained at pH 5.0 in 50 mM acetate buffer (below the pKa for His72) indicate that the redox potential of His72 cyt *c* also is ~10 mV lower (native cyt *c* = 272 mV, His72 cyt *c* = 263 mV *vs.* NHE) than that of native cyt *c* if His72 is protonated. The conclusion is that the slight decrease of the His72 cyt *c* redox potential relative to that of native is not due the electrostatic effect of replacing a charged with an uncharged residue at pH 7.0. This is consistent with lack of change in midpoint potential reported for a Lys79 to Ala mutation in *S. c.* iso-1-cyt *c*[40a] and inconsistent with small changes (~10 mV) observed in a series of cyt b_5 mutants due to alterations in surface charges.[40b]

7. *^{1}H NMR Spectroscopy*

To fully investigate minor structural changes that may be present in the His72 semisynthetic protein, 1-D ^{1}H NMR studies were conducted on the ferric state of protein. The paramagnetic center dramatically shifts resonances in close proximity by dipole / dipole and scalar coupling mechanisms, resulting in a characteristic pattern of chemical shifts outside the normal region that are extremely sensitive to the precise geometry of the heme environment. The ^{1}H NMR spectra of these well-resolved hyperfine shifted resonances for native cyt *c* and His72 cyt *c* are presented with assignments indicated in Figure 2.21. The spectra are virtually identical with published data,[41] and indicate the heme environment is not perturbed by the incorporation of His72.

A close comparison of the ^{1}H spectra in the 0 to 10 ppm regime showed many shared resonances, thus assignments for the native protein[42] were transferred to His72 cyt *c*. Spectra and relevant assignments are presented in Figure 2.22. In the His72 protein, two new singlets were noted in the aromatic regime at 8.32 and 9.01 ppm (pH 5.5) that were assigned to the C-2 and C-4 protons of the His72 imidazole ring. pH titrations, monitoring the chemical shift of these protons as a function of pH, confirmed this

Figure 2.21 ^1H NMR spectra of the hyperfine-shifted region of (A) native cyt *c* in D_2O, pH 6.8, 303 K (Reference 41) and (B) His72 cyt *c* in 50 mM NaPi (D_2O), pH 7.39, 287 K. Pertinent proton assignments are: A. heme methyl 8; B. heme methyl 3; C. heme methyl 5; D. thioether 2 methyl; E. Leu68 δCH_3; F. Met80 ε-CH_3; a. His18 C4; b. propionate7 αC; c. His18 βC; d. Met80 βC; e. propionate7 αC; f. Pro30 δC; g. Gly29 αC; h. Pro30 δC; i. His18 C2; k. Met80 γC.

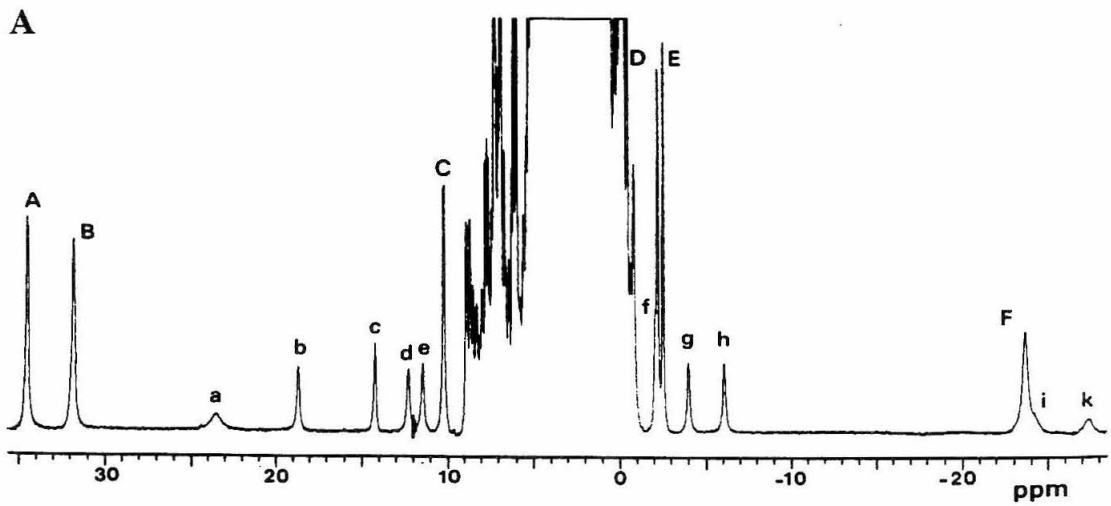
A
A
B
a
b
c
d
e
C
D
E
f
g
h
F
i
k
30
20
10
0
-10
-20
ppm

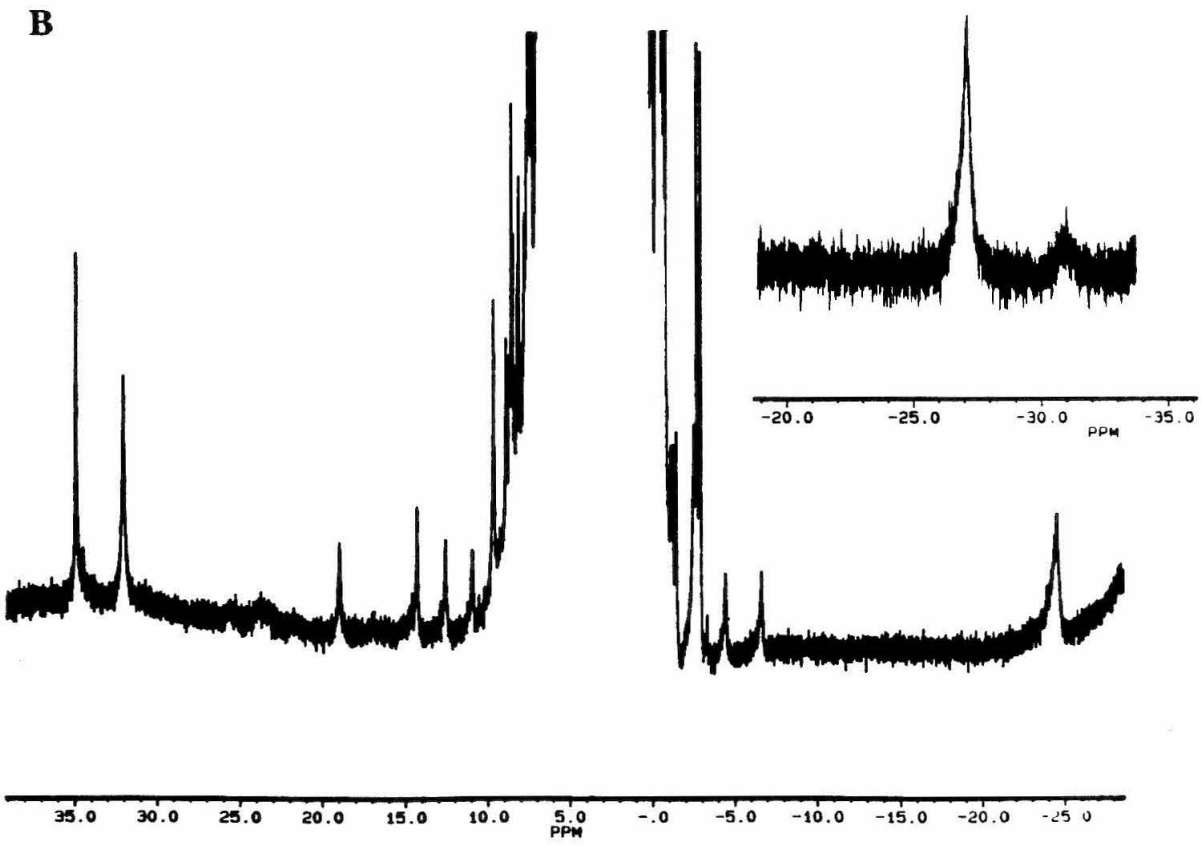
B
-20.0
-25.0
-30.0
-35.0
PPM
35.0
30.0
25.0
20.0
15.0
10.0
5.0
PPM
-.0
-5.0
-10.0
-15.0
-20.0
-25.0

Figure 2.22 ^{1}H NMR spectrum of the normal region of His72 cyt *c* in 50 mM NaPi (D_2O), pH 5.65, 315 K. Pertinent native protein assignments were obtained from Reference 42 and spectra obtained on the native protein at the experimental conditions. His72 assignments from this work are indicated.

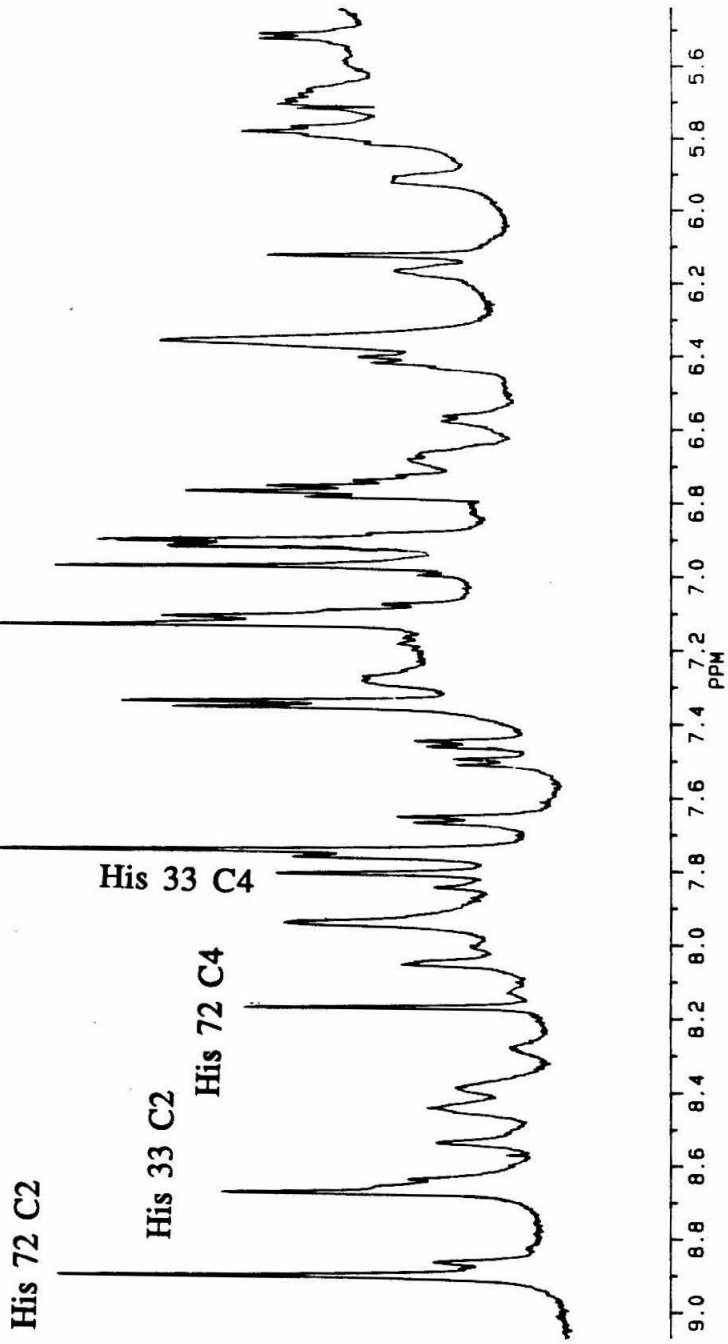
His 72 C2
His 33 C2
His 72 C4
His 33 C4
His 26 C2
His 26 C4
9.0
8.8
8.6
8.4
8.2
8.0
7.8
7.6
7.4
7.2
7.0
6.8
6.6
6.4
6.2
6.0
5.8
5.6
PPM

assignment, since only a titratable residue would be expected to shift. To determine the pKa of the imidazole ring, the following expression was used:[43]

$$pH = pKa + \log\left[\frac{(\delta^{+} - \delta)}{(\delta - \delta^{o})}\right]$$

with δ^{o} and δ^{+} as the chemical shift of the deprotonated and protonated species and δ is the chemical shift of the resonance when the concentration of the protonated and deprotonated species is equal (assumed to be $(\delta^{o} + \delta^{+}) / 2$). A graphical representation of the results of the pH titration of the C-2 and C-4 resonances is given in Figure 2.23. From these data a pKa of 5.5 for His72 was assigned. This value is reasonable for a surface imidazole on a positively charged protein. The pKa of His33 of cyt *c* is 6.4 and the pKa of His26 of cyt *c* is < 3.5 (due to a H-bonding interaction).[44]

Structural characterization of His72 cyt *c* was completed with 2-D double-quantum COSY NMR experiments aimed at comparing the "fingerprint" region ($C_{\alpha}H$ to NH proton-proton *J*-coupled crosspeaks) of His72 cyt *c* with native cyt *c*, as the spectrum of native horse heart cyt *c* is fully assigned.[42b] An in-depth discussion of this work is given in Appendix A. The conclusion of these studies is that most $C_{\alpha}H$ and NH resonances are not significantly shifted and 93% of the assignments can be transferred directly to the semisynthetic protein, indicating a high degree of structural homology. However, some resonances were either shifted by > 0.1 ppm or were not observed and were not reassigned. Although the disappearance of a resonance may be due to a lack of sensitivity, a pattern of unassigned and shifted resonances appeared when both the $C_{\alpha}H$ and NH chemical shift differences between native and His72 cyt *c* were calculated for each residue (Appendix A). Only minor alterations were observed from residues 1 through 60. The regions that appeared most affected were within the 65 - 90 section of the protein, indicating that substitution with His72 has either induced ring current

Figure 2.23 Chemical shift of the (A) C-2 and (B) C-4 protons of the His72 imidazole ring as a function of pH. Spectra taken in 50 mM NaPi (D_2O), data at 286 and 315 K are included.

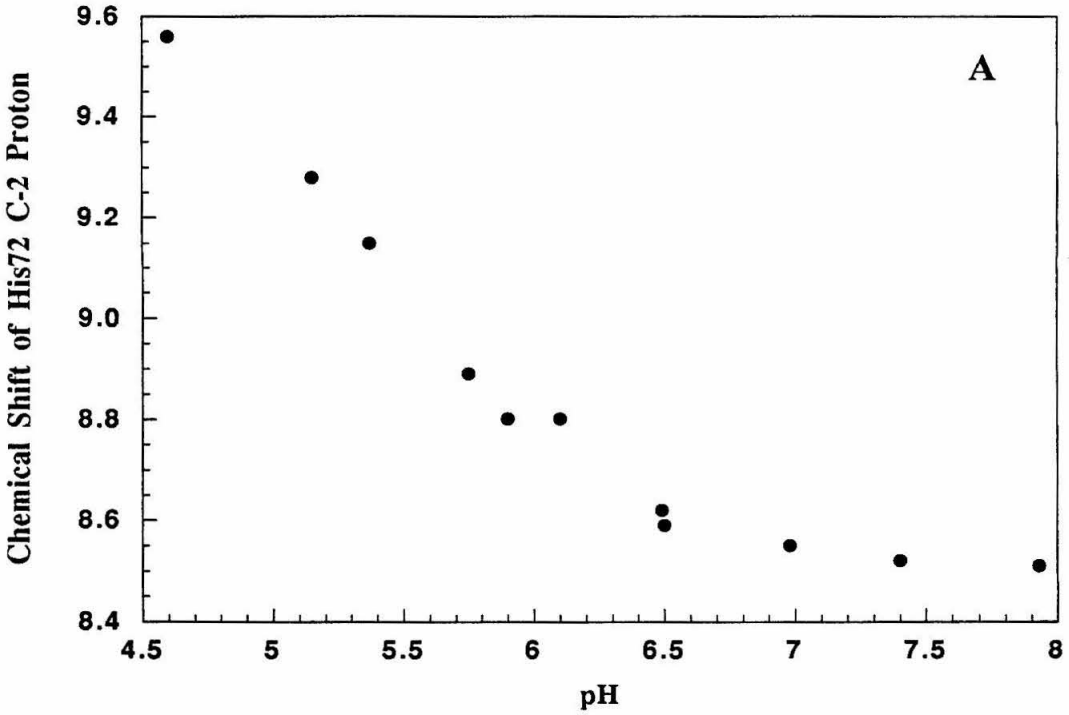
A
Chemical Shift of His72 C-2 Proton
9.6
9.4
9.2
9.0
8.8
8.6
8.4
4.5
5
5.5
6
6.5
7
7.5
8
pH

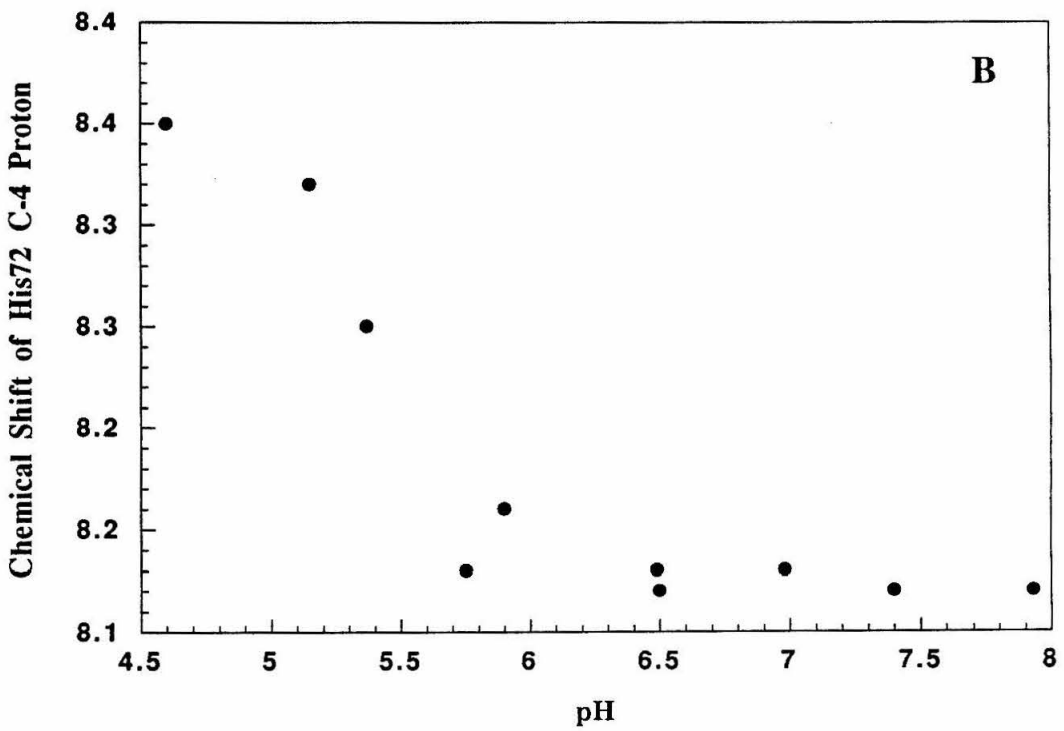
B
Chemical Shift of His72 C-4 Proton
8.4
8.4
8.3
8.3
8.2
8.2
8.1
4.5
5
5.5
6
6.5
7
7.5
8
pH

dependent shifts in neighboring residues or made some minor changes in the structure of the protein. Interestingly, in both the $C_\alpha H$ and NH chemical shift comparisons, the change in shifts is positive in the 60 - 70 and 80 - 90 regions, with a few of the resonances from 70 - 80 not observed (although position 72 could be assigned and was only slightly shifted). A more detailed analysis of the data is required to determine the origin of the observed chemical shifts.

C. $Ru(NH_3)_5$His72 Cytochrome c Characterization

1. Modification and Purification

The methodology previously developed for pentaammineruthenium modification of cyt *c* was used with few alterations.[37] HEPES buffer was used rather than NaPi to prevent precipitation of the ruthenium complex. It had been previously determined that the optimum reaction time for modification of His33 of native cyt *c* was 24 hours at room temperature with ~0.2 mM protein and 10 mM $[Rua_5(H_2O)]^{2+}$. However, since the rate of modification is related to the accessibility of the His residue and a new chromatographic protocol (FPLC Mono S cation-exchange chromatography) was to be used, a detailed study of the time evolution of the pentaammineruthenium modification reactions of native and His72 cyt *c* was undertaken. From these studies not only could the optimum reaction time for His72 be determined, but also a comparison of the chromatographic traces from the native and His72 cyt *c* reactions would afford unambiguous identification of the His72-modified derivative.

Cation-exchange chromatographic separations of the native cyt *c* reaction were similar to those reported, thus allowing identification of the His33 modified product. Modification of His72 cyt *c* afforded the same products observed in the native reaction, as anticipated since His33 and His26 are still present in the protein. However, a new peak was observed to grow in significantly faster than the His33 and His26 products that eluted at higher ionic strength than any product observed in the native cyt *c* modification

reaction. Figure 2.24 depicts product evolution as a function of reaction time as detected by analytical cation exchange chromatography. Products also present in the reaction with native protein are indicated. Since this new product is the first to appear, it can not correspond to a doubly labeled derivative and was tentatively assigned as Rua_5His72 cyt *c*. An optimum reaction time of 8 hours was determined at standard conditions. Preparative-scale reactions of Rua_5His72 cyt *c* were purified with similar separations.

2. *Absorption Spectroscopy*

The purified product possessed an absorption spectrum nearly identical with native, including the presence of the 695 nm band. Difference spectroscopy, however, indicated the presence of a weak absorption at 303 nm that corresponds to the absorption anticipated for Rua_5His^{3+} (Figure 2.25). Furthermore, using the extinction coefficient, ε (303 nm) = 2100 M^{-1} cm^{-1} for Rua_5His^{3+},[37] a 1:1 ratio of Fe:Ru (± 10%) is calculated, indicating isolation of a singly modified derivative.

3. *^{1}H NMR Spectroscopy*

The His site of Ru modification can be determined using ^{1}H NMR spectroscopy if the C-2 and C-4 resonances of all His residues have been assigned and are detectable. Rua_5His^{3+} is paramagnetic (^{99}Ru: 12.7% abundant, I = 3/2; ^{101}Ru: 17.1% abundant, I = 5/2) and will shift and broaden the C-2 and C-4 resonances of only the His residue to which it is bound. The ^{1}H NMR spectrum for Rua_5His72 cyt *c* is shown in Figure 2.26 A. While the His33 and His26 singlets are still present, the resonances due to His72 have disappeared (indicated by asterisks). The hyperfine shifted resonances due to the ferric heme are not perturbed in the Ru-modified protein (Figure 2.26 B). It has been reported that the contact-shifted His resonances reappear at -33 ppm in pentaammineruthenium(III)-modified myoglobin:[45] this may be the assignment of the new weak resonance seen at ~-27 ppm.

Figure 2.24 Cation-exchange (FPLC Mono S 5/5) time evolution of pentaammineruthenium modification of His72 cyt *c*. The first peak to elute is unmodified, and last peak is doubly modified. Short arrows indicate products also observed in the native cyt *c* modification reaction. The asterisk indicates the new product not observed in the native cyt *c* modification reaction.

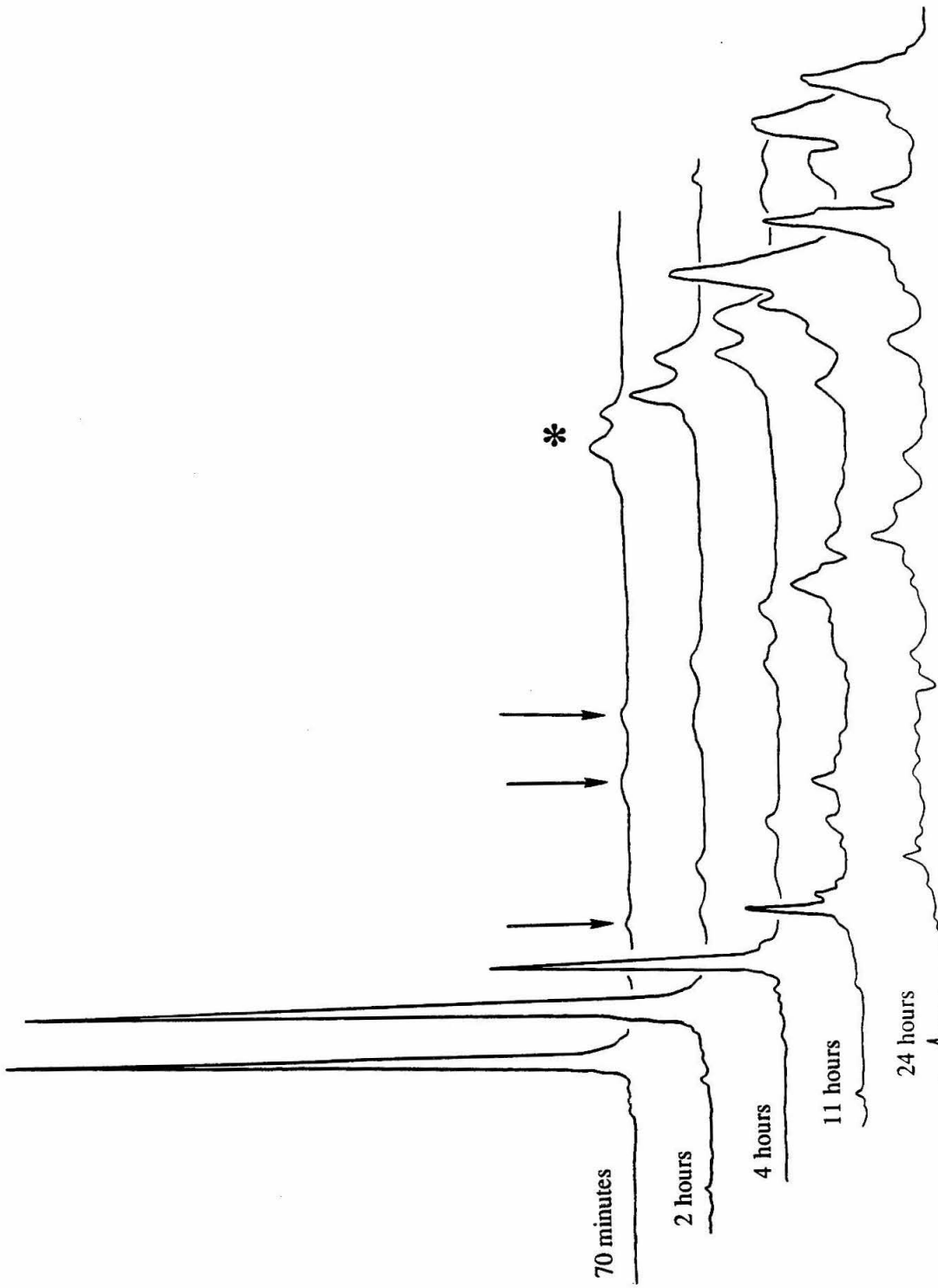
70 minutes
2 hours
4 hours
11 hours
24 hours
*

Figure 2.25 Absorption difference spectrum between ferric His72 cyt *c* and ferric Rua_5His72^{3+} cyt *c* in 25 mM NaPi, pH 7.0. Heme concentration = 13.4 μM, calculated Ru concentration = 14.8 μM. Additional peaks correlated with the ferrous heme spectrum and are attributed to incomplete heme oxidation.

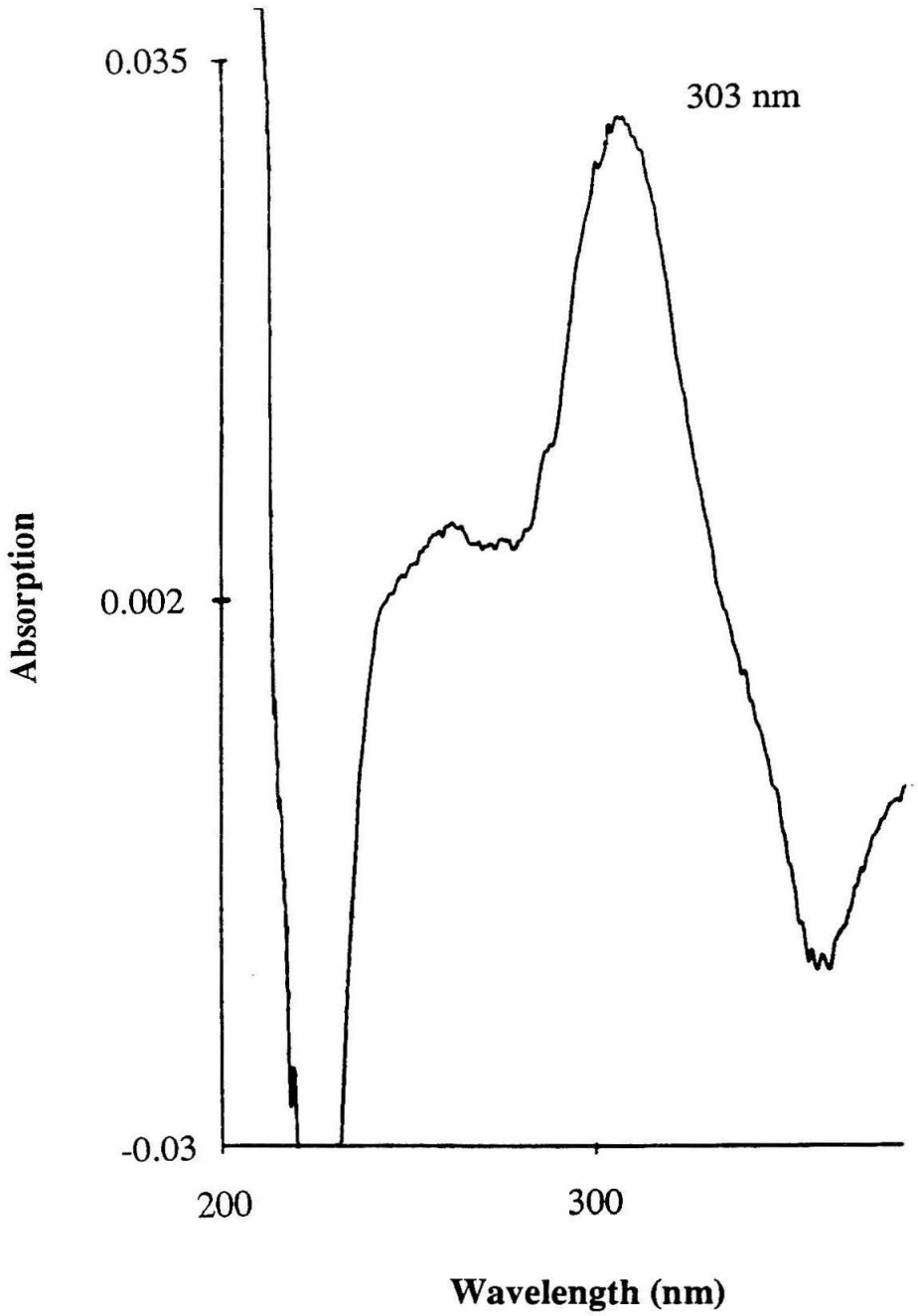
0.035
303 nm
0.002
Absorption
-0.03
200
300
Wavelength (nm)

Figure 2.26 ^{1}H NMR spectra of ferric Rua_5His72^{3+} cyt *c* in the (A) normal (50 mM NaPi, pH 5.7, 325 K) and (B) hyperfine-shifted (50 mM NaPi, pH 5.7, 298 K) regions of the spectrum. Note that there is little perturbation of the resonances in either region relative to the unmodified protein, with the exception of the disappearance of the His72 C-2 and C-4 protons, denoted by asterisks.

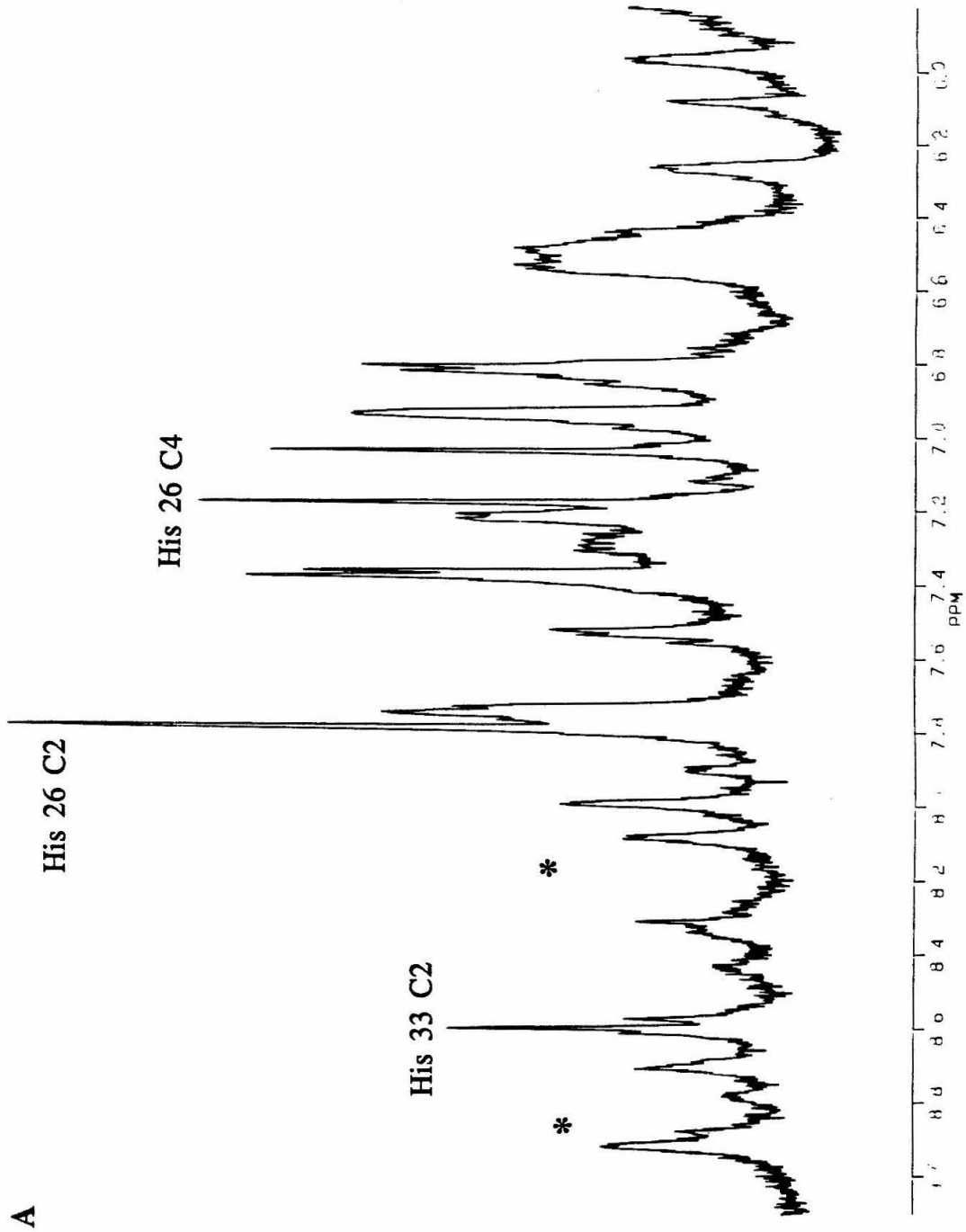
A
His 26 C2
His 26 C4
His 33 C2
*
*
ppm

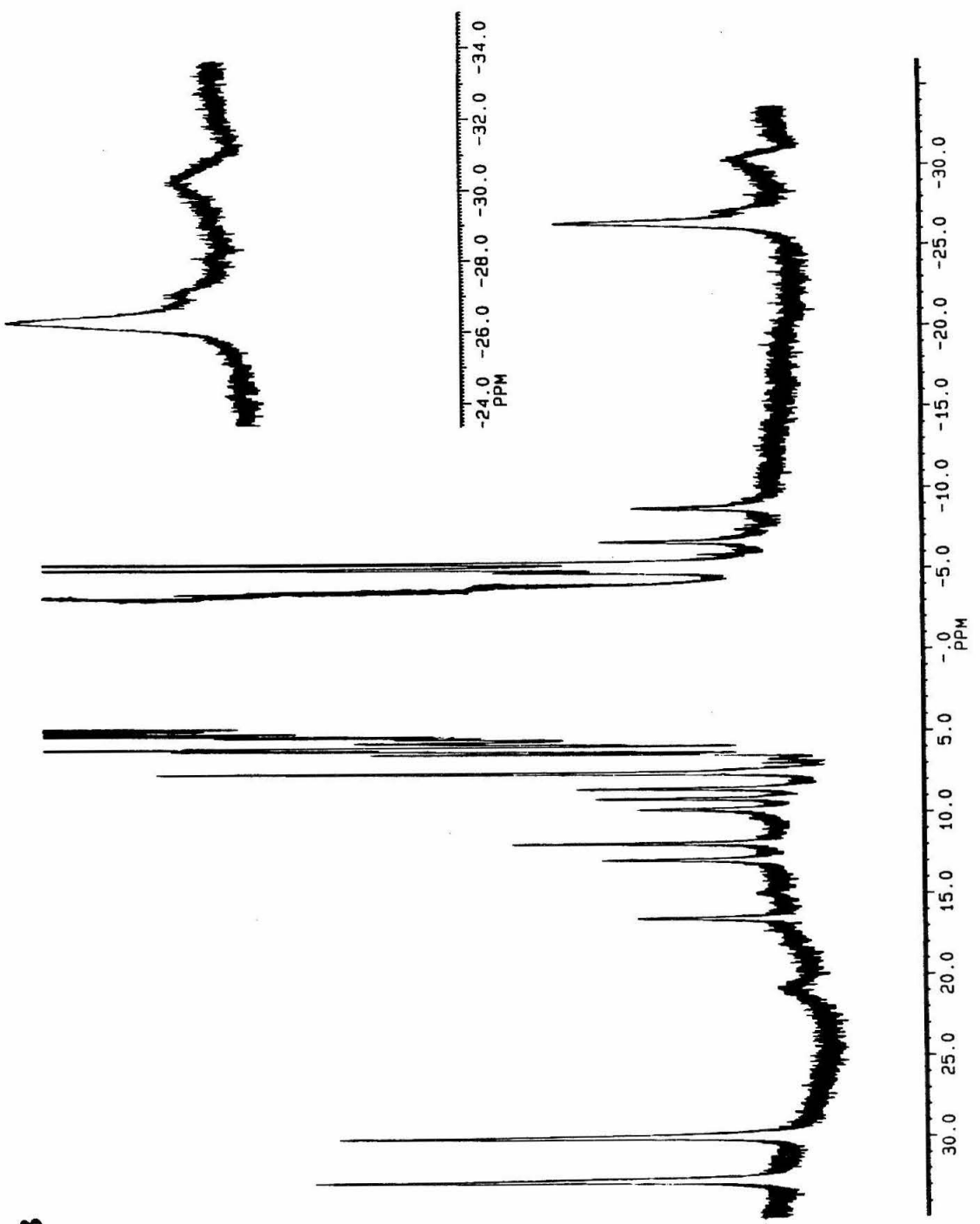
B
-24.0 -26.0 -28.0 -30.0 -32.0 -34.0
PPM
30.0 25.0 20.0 15.0 10.0 5.0 -.0 -5.0 -10.0 -15.0 -20.0 -25.0 -30.0
PPM

4. Electrochemistry

Differential pulse polarograms in 50 mM NaPi, 10 mM M 4,4'-bipyridine obtained for Rua_5His72 cyt *c* are presented in Figure 2.27. Two waves are seen that correspond to the heme and ruthenium site. Values obtained for E°' are consistent with anticipated results:

Table 2.3. Summary of redox potentials obtained on modified proteins.

Sample	E°' ($Ru^{3+/2+}$) (mV *vs.* NHE)	E°' ($Fe^{3+/2+}$) (mV *vs.* NHE)
Native cyt *c*	-	265
Rua_5His33 cyt *c*	80(5)	260(5)
His72 cyt *c*	-	255
Rua_5His72 cyt *c*	106(5)	284(5)

E°' for $Rua_5His^{3+/2+}$ is 110 mV *vs.* NHE. The $[Rua_5His]^{3+}$ complex in solution with native cyt *c* has an E°' of 108 mV vs. NHE.[37]

Based on the electrochemistry data, the measured driving force for ET from Rua_5His72^{2+} to the ferric heme is -178(5) mV.

D. Electron-Transfer Studies

Intramolecular ET rates in Rua_5His72 cyt *c* were measured using the flash photolysis protocol developed by Gray, Winkler and Nocera.[33] The reaction scheme is given in Figure 2.28. A microsecond white light flash generates a population of $*Ru(bpy)_3^{2+}$ excited state which can, *via* a bimolecular reaction, reduce (E°' for $Ru(bpy)_3^{3+/*2+}$ = -860 mV) both the heme and Rua_5His^{3+} centers on the protein. $EDTA^{2-}$

Figure 2.27 Differential pulse polarogram of Rua_5His72^{3+} cyt *c* in 50 mM NaPi, 10 mM 4,4'-bipyridine, pH 7.0. The $Fe^{3+/2+}$ wave is at 284(5) mV and the $Ru^{3+/2+}$ wave is at 106(5) mV *vs.* NHE. See text for details.

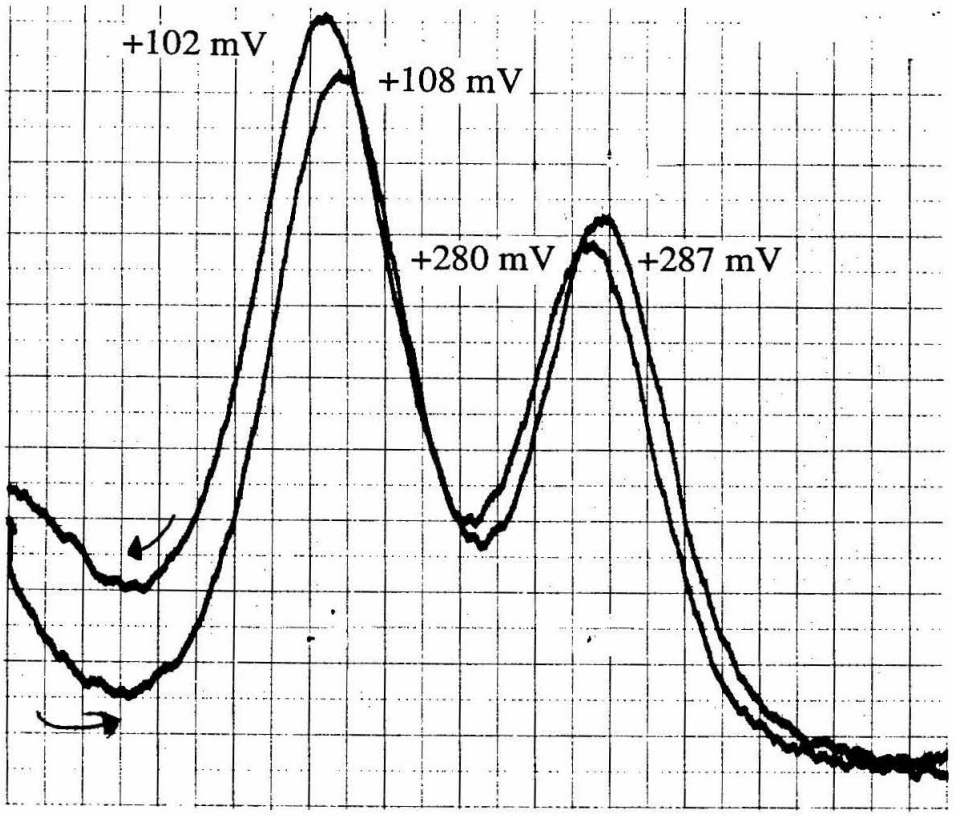
+102 mV
+108 mV
+280 mV
+287 mV

Figure 2.28 Reaction scheme for $Ru(bpy)_3^{2+}$-mediated reductive flash ET experiment.

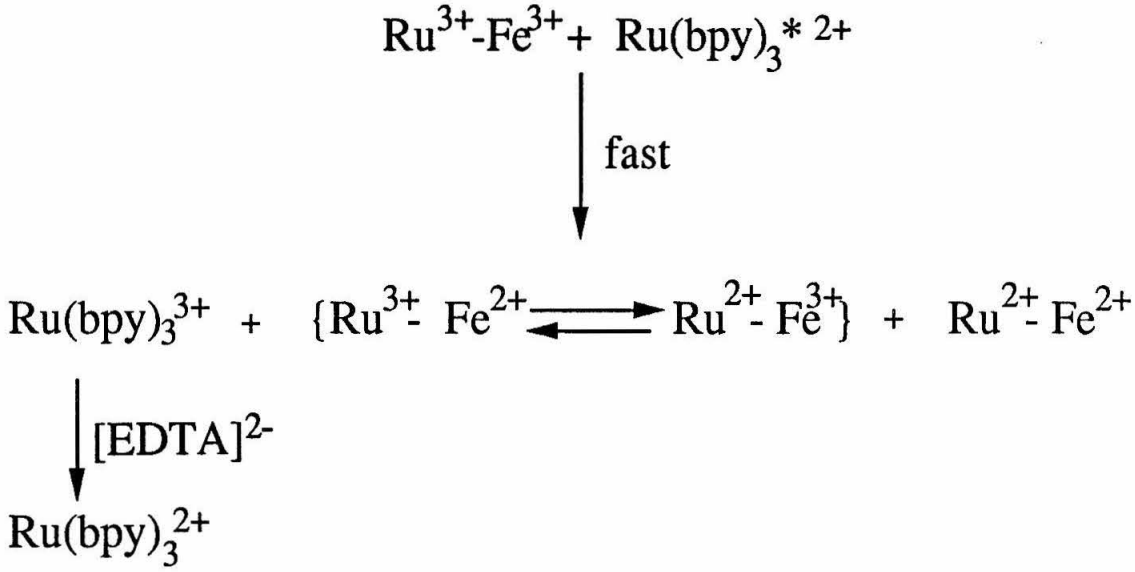
Ru^{3+}-Fe^{3+} + $Ru(bpy)_3^{*\,2+}$
fast
$Ru(bpy)_3^{3+}$ + {Ru^{3+}- Fe^{2+} Ru^{2+}- Fe^{3+}} + Ru^{2+}- Fe^{2+}
$[EDTA]^{2-}$
$Ru(bpy)_3^{2+}$

is present in solution to scavenge the $Ru(bpy)_3^{3+}$ product and prevent back ET from the protein. Since the $Ru(bpy)_3^{2+}$ excited state can reduce both metal centers in the protein, a non-equilibrium distribution of singly reduced Ru-modified proteins is generated. The transiently formed Rua_5His72^{2+} - Fe^{3+} cyt *c* species relaxes to the thermodynamically more stable Rua_5His72^{3+} - Fe^{2+} cyt *c* species *via* an electron transfer. This ET reaction is monitored by the increase in absorption at 550 nm due to the formation of reduced heme ($\Delta\varepsilon^{Fe^{2+}/Fe^{3+}} = 18500\ M^{-1}\ cm^{-1}$). Only rates < 200 s^{-1} can be measured due the recovery time needed for the photomultiplier tube (PMT) following the flash. A problem with this methodology is that it is not reversible, therefore only data from the first flash are usable. Caution was exercised to prevent sample exposure to room light prior to the flash.

Flash data are shown in Figure 2.29 A that represent a control reaction performed with unmodified ferric His72 cyt *c*. Irreversible reduction of the heme is complete within the flash duration. Kinetic data obtained on a 1.8 μM sample of ferric Rua_5His72^{3+} cyt *c* are presented in Figure 2.29 B. Following direct reduction of the heme by during the flash, a slow phase of reduction is observed and attributed to intramolecular Ru^{2+} to Fe^{3+} ET. The measured rate was fit to single exponential kinetics and determined to be 0.4(2) s^{-1}. This rate is independent of protein concentration over a range of 1 - 3 μM. A rate of 30(3) s^{-1} [33] has been measured for the analogous Rua_5His33 cyt *c* derivative at similar driving force (-180 mV) and presumably comparable reorganization energy since the redox centers are identical. Modeling indicates that the His72 residue is ~2.7 Å *closer* to the heme (edge-edge distances: His72-heme, 8.4 Å; His33-heme, 11.1 Å). Since no significant structural perturbation appears to have occurred in the His72 proteins, the slower ET rate observed between His72 and the heme relative to His33 is attributed to a decrease in electronic coupling that exhibits the exact opposite trend predicted by a distance-dependent model. These results imply that the intrinsic homogeneity of the protein medium can control protein couplings and triggered subsequent ET studies at higher driving force.

Figure 2.29 Flash-photolysis voltage / time traces at 550 nm for (A) ferric unmodified His72 cyt *c* (4.2 μM) and (B) ferric Rua_5His72^{3+} cyt *c* (1.8 μM) in 50 mM NaPi, 60 μM $[Ru(bpy)_3]Cl_2$, 7.25 mM Na_2EDTA, pH 7.0.

A

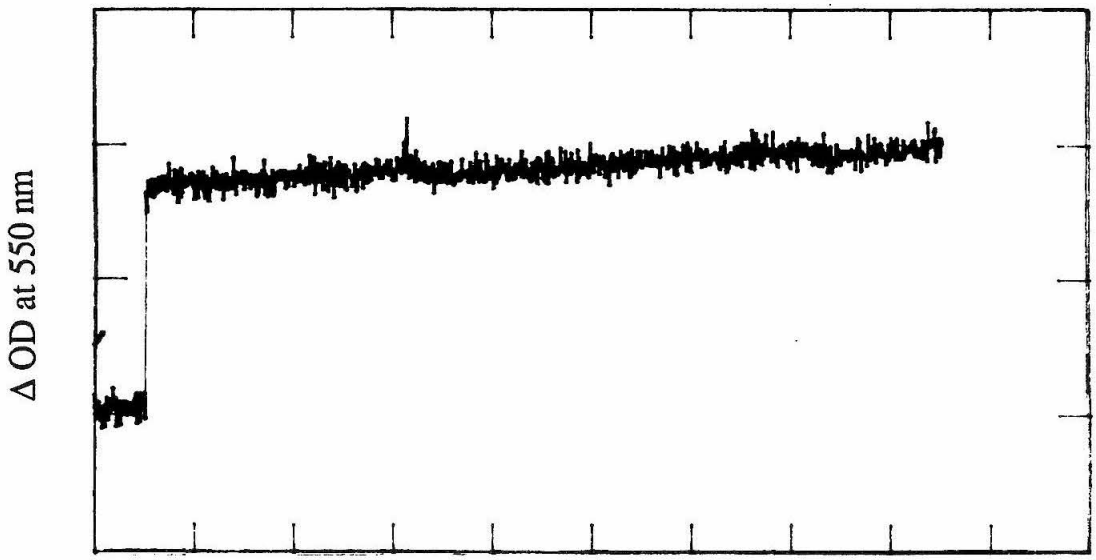

B

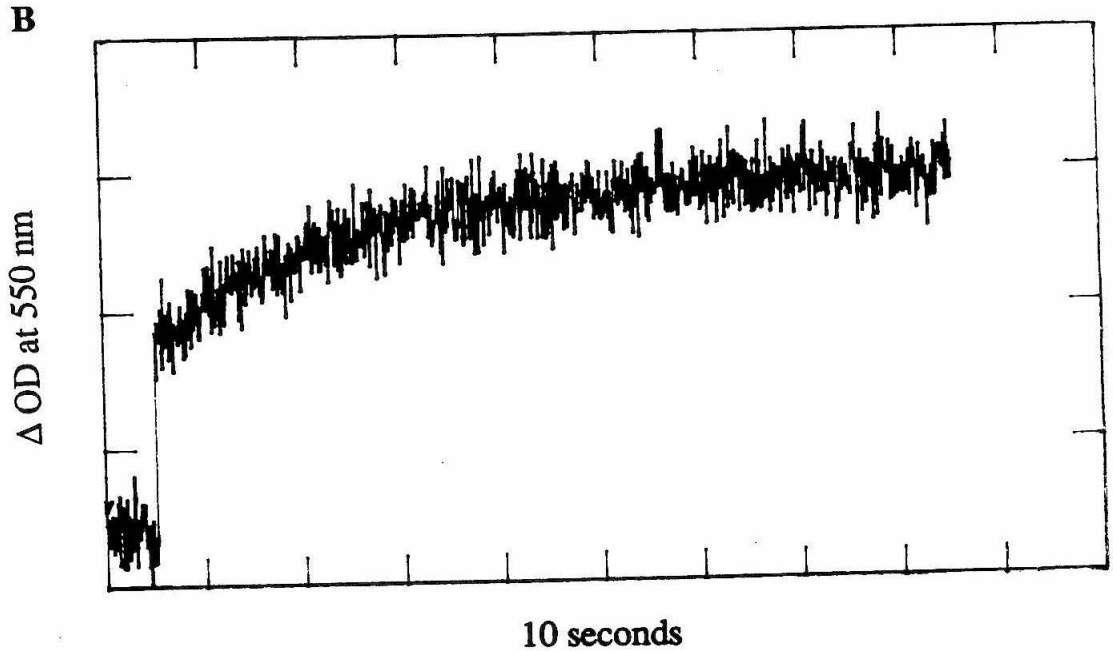

IV. Conclusion

Semisynthesis has been utilized to replace a lysine with a histidine residue at position 72 in horse heart cyt *c*. Measurements made from the oxidized horse heart crystal structure show that the edge-edge distance from His72 to the heme is 8.4 Å, 2.7 Å *closer* than the corresponding distance for His33. The mutant protein has virtually the same CD and absorption spectra as native as well as the same thermal stability (T_m = 87° C). The redox potential of His72 cyt *c* is 255(2) mV *vs.* NHE; native horse heart and semisynthetic Hse65 cyt *c* are 265 mV. The ^{1}H NMR of His72 cyt *c* is virtually identical with native in the aromatic and paramagnetic region, with the exception of two new singlets at 8.32 and 9.01 ppm that titrate with a pKa of 5.5 and are assigned to the C-2 and C-4 protons of the His72 imidazole ring. These data indicate that there is little structural perturbation of the overall protein structure.

His72 cyt *c* has been modified with a pentaammineruthenium(III) moiety and has been characterized by NMR, absorption spectroscopy and electrochemistry. The rate of intramolecular ET from Rua_5His72^{2+} to the Fe^{3+} heme was determined by flash photolysis to be 0.4(2) s^{-1} (ΔG^o = -178(5) mV); almost 100-fold slower than the rate of the corresponding His33-labelled protein (30 s^{-1}). The result implies that the inherently inhomogenous nature of the protein medium can mediate electronic coupling in a non-distance-dependent manner.

V. References

1. The structural and biological aspects of cytchromes *c* are reviewed in: (a) Dickerson, R. E.; Timkovitch, R., in *The Enzymes*, P. D. Boyder Ed. (Academic Press: New York) 1975, Vol. 6, 3rd ed., pp. 397 - 547. (b) Moore, G. R.; Pettigrew, G. W. *Cytochomes c: Evolutionary, Structural and Physiochemical Aspects* (Verlag : Berlin) 1990. (c) Moore, G. R.; Pettigrew, G. W. *Cytochomes c: Biological Aspects* (Verlag : Berlin) 1987. (d) Ferguson-Miller, S.; Brautigan, D. L.; Margoliash, E., in *The Porphyrins* Dolphin, D. Ed. (Academic Press: San Francisco) 1979, Vol. 7, Biochemistry

Part B. pp. 149 - 240. (e) Timkovich, R. In *The Porphyrins* Dolphin, D. Ed. (Academic Press: San Francisco) 1979, Vol. 7, Biochemistry Part B. pp. 241 - 294. (f) Williams, G.; Moore, G. R.; Williams, R. J. P. *Comment Inorg. Chem.* **1985**, *4*, 55.

2. Numbering is based vertebrate sequences. Yeast cyts *c* have 5 addiditonal amino acids at the N-terminus.

3. (a) Bushnell, G. W.; Louie, G. V.; Brayer, G. D. *J. Mol. Biol.* **1990**, *214*, 585. (b) Louie, G. V.; Brayer, G. D. *J. Mol. Biol.* **1990**, *214*, 527. (c) Berghuis, A. M.; Brayer, G. D. *J. Mol. Biol.* **1992**, *223*, 959.

4. Feng, Y.; Roder, H.; Englander, S. W. *Biochemistry* **1990**, *29*, 3494. Williams, G.; Clayden, N. J.; Moore, G. R.; Williams, R. J. P. *J. Mol. Biol.* **1985**, *183*, 447. Gao, Y.; Boyd, J.; Pielak, G. J.; Williams, R. J. P. *Biochemistry* **1991**, *30*, 1928.

5. Margoliash, E.; Frohwirt, N. *Biochem. J.* **1959**, *71*, 570.

6. (a) Corradin, G.; Harbury, H. A. *Proc. Natl. Acad. Sci. USA* **1971**, *68*, 3036. (b) Corradin, G.; Harbury, H. A. *Biochem. Biophys. Res. Comm.* **1974**, *61*, 1400.

7. Reviewed in: Wallace, C. J. A. *FASEB J.* **1993**, *7*, 505. Offord, R. E. *Protein Eng.* **1987**, *1*, 151. Chaiken, I. M.*CRC Critical Reviews in Biochemistry* **1981**, 225. Offord, R. E. *Semisynthetic Proteins* (John Wiley and Sons: New York) 1980. General semisynthetic and total synthesis: Humpries, J.; Offord, R. E.; Smith, R. A. G. *Curr. Opin. Biotech.* **1991**, *2*, 539. Tesser, G. I. *Kontakte (Darmstadt)* **1990**, *1*, 25. Kent, S. B. H. *Curr. Opin. Biotech.* **1993**, *4*,420.

8. (a) ten Kortenaar, P. B. W.; Adams, P. H. J. M.; Tesser, G. I. *Proc. Natl. Acad. Sci. USA* **1985**, *82*, 8279. (b) Wallace, C. J. A.; Offord, R. E. *Biochem. J.* **1979**, *179*, 169. (c) Boon, P. J.; van Raay, A. J. M.; Tesser, G. I.; Nivard, R. J. F. *FEBS Lett.* **1979**, *108*, 131. (d) Boon, P. J.; Tesser, G. I.; Nivard, R. J. F. *Proc. Natl. Acad. Sci. USA* **1979**, *76*, 61. (e) Wasserman, G. F.; Nix, P. T.; Koul, A. K.; Warme, P. K. *Biochim. Biophys. Acta* **1980**, *623*, 457. (f) Koul, A. K.; Wasserman, G. F.; Warme, P. K. *Biochem. Biophys. Res. Commun.* **1979**, *89*, 1253. (g) Nix, P. T.; Warme, P. K. *Biochim. Biophys. Acta* **1979**, *578*, 413. (h) Wallace, C. J. A.; Corradin, G.; Marchiori, F.; Borin, G. *Biopolymers* **1986**, *25*, 2121. (i)Wallace, C. J. A.; Corthésy, B. E. *Protein Eng.* **1986**, *1*, 23.

9. (a) Barstow, L. E.; Young, R. S.; Yakali, E.; Sharp, J. J.; O'Brien, J. C.; Berman, P. W.; Harbury, H. A. *Proc. Natl. Acad. Sci. USA* **1977**, *74*, 4248. (b) Raphael, A. L.; Gray, H. B. *J. Am. Chem. Soc.* **1991**, *113*, 1038. (c) Raphael, A. L.; Gray, H. B. *Proteins* **1989**, *6*, 338. (d) Wallace, C. J. A.; Clark-Lewis, I. *J. Biol. Chem.* **1992**, *267*, 3852. (e) Frauenhoff, M. M.; Scott, R. A. *Proteins* **1992**, *14*, 202. (f) Wallace, C. J. A.; Mascagni, P.; Chait, B. T.; Collawn, J. F.; Paterson, Y.; Proudfoot, A. E. I.; Kent, S. B. H. *J. Biol. Chem.* **1989**, *264*, 15199. (g) Bren, K. L.; Gray, H. B. *J. Am. Chem. Soc.* **1993**, in press.

10. Kent, S. B. H. *Annu. Rev. Biochem.* **1988**, *57*, 957. Merrifield, R. B. *J. Am. Chem. Soc.* **1963**, *85*, 2149.

11. Fortuna, A.; Gross, E. In *Practical Protein Chemistry: A Handbook.* A. Daibre, Ed. (Wiley: New York) 1986, pp. 83 - 88.

12. Babul, J.; McGowan, E. B.; Stellwagen, E. *Arch. Biochem. Biophys.* **1972**, *148*, 141.

13. Boswell, A. P.; Moore, G. R.; Williams, R. J. P.; Wallace, C. J. A.; Boon, P. J.; Nivard, R. J. F.; Tesser, G. I. *Biochem. J.* **1981**, *193*, 493.

14. Pielak, G. J.; Mauk, A. G.; Smith, M. *Nature* **1985**, *313*, 152. Cutler, R. L.; Pielak, G. J.; Mauk, A. G.; Smith, M. *Protein Eng.* **1987**, *1*, 95.

15. Yi, L.; Casimiro, D. R.; Bren, K. L.; Richards, J. R.; Gray, H. B., submitted.

16. Hampsey, D. M.; Das, G.; Sherman, F. *J. Biol. Chem.* **1986**, *261*, 3259.

17. An axial ligand mutant, His18 to Arg, in *S. c.* iso-2-cyt *c* has been made using site-directed mutagenesis. However, the redox potential is identical with native. Sorrell, T. N.; Martin, P. K.; Bowden, E. F. *J. Am. Chem. Soc.* **1989**, *111*, 766.

18. Wallace, C. J. A.; Guillemette, J. G.; Hibiya, Y.; Smith, M. *J. Biol. Chem.* **1991**, *266*, 21355.

19. Tarr, G. E.; Fitch, G. M. *Biochem. J.* **1976**, *159*, 193.

20. Bosshard, R.; Margoliash, E. *Trends Biochem. Sci.* **1983**, *8*, 316. Gorren, A. C. F.; Chan, M. L.; Crouse, B. R.; Scott, R. A. *Bioconjugate Chem.* **1992**, *3*, 291. Pan, L. P.; Durham, B.; Wolinska, J.; Millett, F. *Biochemistry* **1988**, *27*, 7180. Brautigan, D. L.; Ferguson-Miller, S.; Margoliash, E. *J. Biol. Chem.* **1978**, *253*, 130. Brautigan, D. L.; Ferguson-Miller, S.; Margoliash, E. *J. Biol. Chem.* **1978**, *253*, 140. Osheroff, N.; Brautigan, D. L.; Margoliash, E. *J. Biol. Chem.* **1980**, *255*, 8245. Smith, H. T.; Staudenmayer, N.; Millett, F. *Biochemistry* **1977**, *16*, 4971. Staudenmayer, N.; Ng, S.; Smith, M. B. *Biochemistry* **1977**, *16*, 600. Kim, C.-S.; Kueppers, F.; DiMaria, P.; Farooqui, J.; Kim, S.; Paik, W. K. *Biochim. Biophys. Acta* **1980**, *622*, 144.

21. Farooqui, J.; DiMaria, P.; Kim, S.; Paik, W. K. *J. Biol. Chem.* **1981**, *256*, 5041. DiMaria, P.; Polastro, E.; Delange, R. J.; Kim, S.; Paik, W. K. *J. Biol. Chem.* **1979**, *254*, 4645. Polatro, E.; Deconinck, M. M.; Devogel, M. R.; Mailer, E. L.; Looze, Y. B.; Schnek, A. G.; Leonis, J. *Biochem. Biophys. Res. Comm.* **1979**, *81*, 920. Paik, W. K.; Kim, S. *Protein Methylation* (John Wiley and Sons: New York) 1980.

22. Holzschu, D.; Principio, L.; Conklin, K. T.; Hickey, D. R.; Short, J.; Rao, R.; McLendon, G.; Sherman, F. *J. Biol. Chem.* **1987**, *262*, 7125. Cessay, K. J.; Bergman, L. W.; Tuck, M. T. *Int. J. Biochem.* **1991**, *23*, 761.

23. Reviewed in: McLendon, G.; Hake, R. *Chem. Rev.* **1992**, *92*, 481. Moore, G. R.; Eley, C. G. S.; Williams, G. *Adv. Inorg. Bioinorg. Mech.* **1984**, *1*, 1. Sudha, B. P.; Dixit, N.; Vanderkooi, J. M. *Current Topics in Bioenergetics* **1984**, *13*, 159.

24. Kornblatt, J. A.; Theodorakis, J.; Hoa, G. H. B.; Margoliash, E. *Biochem. Cell Biol.* **1992**, *70*, 539. Rieder, R.; Bosshard, H. R. *J. Biol. Chem.* **1980**, *255*, 4732. Pettigrew, G. *FEBS Lett.* **1978**, *86*, 14. Ahmed, A. J.; Smith, H. T.; Smith, M. B.; Millett, F. S. *Biochemistry* **1978**, *17*, 2479. Kang, C. H.; Brautigan, D. L.; Osherhoff, N.; Margoliash, E. *J. Biol. Chem.* **1978**, *254*, 6502. Ferguson-Miller, S.; Brautigan, D. L.; Margoliash, E. *J. Biol. Chem.* **1978**, *253*, 149.

25. Pelletier, H.; Kraut, J. *Science* **1992**, *258*, 1748.

26. The ET properties of Rua_5His72 cyt *c* are presented in this Chapter. Chapter 3 is devoted $Ru(bpy)_2(im)^{2+}$ derivatives of cyts *c*, including His72 cyt *c*, with ET measurements in those systems and their interpretation presented in Chapters 4 and 5.

27. Kirschner, S. *Inorg. Syn.* **1957**, *5*, 186.

28. Eddowes, M.; Hill, H. *J. Am. Chem. Soc.* **1979**, *101*, 4461.

29. Ellis, W. R. Ph. D. Thesis, California Institute of Technology, **1986**.

30. Matsubara, T.; Ford, P. *Inorg. Chem.* **1976**, *15*, 1107.

31. Milder, S. J.; Goldbeck, R. A.; Kliger, D. S.; Gray, H. B. *J. Am. Chem. Soc.* **1980**, *102*, 6761.

32. Jacobs, B. A. Ph. D. Thesis, California Institute of Technology, **1990**.

33. Nocera, D. G.; Winkler, J. R.; Yocum, K. M.; Bordignon, E.; Gray, H. B. *J. Am. Chem. Soc.* **1984**, *106*, 5145. Winkler, J. R.; Nocera, D. G.; Yocum, K. M.; Bordignon, E.; Gray, H. B. *J. Am. Chem. Soc.* **1982**, *104*, 5798.

34. First aid for CNBr exposure is amylnitrate inhalation; ampules are kept available in the laboratory at all times.

35. Corradin, G.; Harbury, H. A. *Biochim. Biophys. Acta* **1970**, *221*, 489.

36. The 1-65 lactone and 1-65 COO^- bands can be interchanged on an isoelectric focusing gel by treatment with acid or base. Raphael, A. L. unpublished results.

37. Yocum, K. M.; Shelton, J. B.; Shelton, J. R.; Schroeder, W. A.; Worosila, G.; Isied, S. S.; Bordignon, E.; Gray, H. B. *Proc. Natl. Acad. Sci. USA* **1982**, *79*, 7052. Yocum, K. M. Ph. D. Thesis, California Institute of Technology, **1982**.

38. Measurement taken by differential pulse polarography on an aged sample of 1-65 lactone.

39. Salmeen, I.; Palmer, G. *J. Chem. Phys.* **1968**, *48*, 2049.

40. (a) Ferrer, J. C.; Guillemette, J. G.; Bogumil, R.; Inglis, S. C.; Smith, M.; Mauk, A. G. *J. Am. Chem. Soc.* **1993**, *115*, 7507. (b) Rodgers, K. K.; Sligar, S. G. *J. Am. Chem. Soc.* **1991**, *113*, 9419.

41. Santos, H. Turner, D. L. *FEBS Lett.* **1987**, *226*, 179.

42. (a) Moore, G. R.; Williams, R. J. P. *Eur. J. Biochem.* **1980**, *103*, 493. (b) Feng, Y.; Roder, H.; Englander, S. W. *Biochemistry* **1989**, *28*, 195.

43. Selman, M. A. Ph. D. Thesis, California Institute of Technology, **1989**.

44. Cohen, J. S.; Hayes, M. B. *J. Biol. Chem.* **1974**, *249*, 5472.

45. Toi, H.; LaMar, G.; Margalit, R.; Che, C.-M.; Gray, H. B. *J. Am. Chem. Soc.* **1984**, *106*, 6213.

Chapter 3

Synthesis, Characterization and Electron-Transfer Studies of $Ru(bpy)_2(im)HisX$ Cytochromes *c* (X = 33, 39, 62, 72)

I. Introduction

A. Studies of Zn-substituted Cytochromes c

Early ET studies on ruthenium-ammine-modified heme cyts *c* led to significant insights into the factors controlling biological electron transfers.[1] However, as detailed in Chapter 1, this system is troubled by its low driving force that imposes difficulties in extracting accurate values for H_{AB} and λ from observed rates. In addition, the non-reversible bimolecular flash photolysis technique[2] necessary for rate measurements in this system to measure suffers from chemical irreversibility and poor resolution of fast rate components (> 200 s^{-1}). The replacement of heme with a non-native Zn-porphyrin in the $Rua_4(X)$ (X = ammine (a), pyridine (py), or isonicotinamide (isn))-modified proteins represented a breakthrough in ET studies.[3] In these systems, ET rates could be obtained at driving forces comparable to the estimated reorganization energy (1.2 eV).[1] This feature is crucial since, when $-\Delta G^o$ is near the value of λ, the dependence of the electron-transfer rate on driving force is minimal, thus accommodating a better estimation of H_{AB} and λ.

In the Zn cyt *c* studies, ET occurs from the highly reducing, long-lived Zn-porphyrin triplet excited state (Zn^{3*}, τ = 15 ms, $Zn^{3*/+\bullet}$ = -0.62 eV[4]) upon laser excitation at 532 nm. Both the Zn^{3*} to Ru^{3+} photoinduced ET rate and the subsequent Ru^{2+} to $Zn^{+\bullet}$ recombination ET rate could be readily determined using transient absorption spectroscopy due to monitor the different absorption properties of the species involved. Driving forces for the photoinduced and recombination ET reactions in $Rua_4(X)$His Zn cyts *c* are on the order of 0.7 to 1.1 eV, and observed rates were on the order of 10^4 to 10^7 s^{-1}. Fits of these rates obtained with a series of $Rua_4(X)$His33 Zn cyts *c* (X = a, py, isn), spanning a 0.39 eV range in driving force, yielded values of λ = 1.10 eV and H_{AB} = 0.12 cm^{-1} for the photoinduced reaction and λ = 1.19 eV and H_{AB} = 0.09 cm^{-1} for the recombination reaction.[1,3]

ET has been extensively studied between the heme and a Ru probe placed at two other surface His sites in heme and Zn porphyrin cyts *c*. Comparison of the rates obtained from these $Rua_4(X)$-modified surface sites with rates obtained from His33-modified derivatives allows for the evaluation of factors that contribute to electronic coupling. The first surface site, His39, is present in yeast species of cyt *c* and has been $Rua_4(X)$ labeled in the native and Zn-porphyrin *Candida krusei* (*C.k.*) protein.[5] The second site, His62, has been genetically engineered and expressed in *Saccharomyces cerevisae* (*S.c.*) iso-1-cyt *c*.[6] Maximum ET rates (*i.e.*, the ET rate at $-\Delta G^o = \lambda$) derived from the driving force studies in the heme and Zn porphyrin derivatives, calculated values for H_{AB} and edge-edge distances determined from horse heart or yeast iso-1-cyt *c* crystal structures[7] are set out in Table 3.1.

Table 3.1. Electron-transfer parameters for $Rua_4(X)$His Zn cyts *c*.[1]

Site	k_{max} (s^{-1})	edge-edge distance (Å)	H_{AB} (cm^{-1})
His39[5]	1.4×10^7	12.3	0.24
His33[2,3]	2.9×10^6	11.1	0.11
His62[6]	2.0×10^4	14.8	0.01

H_{AB} is somewhat larger between His39 and the heme than between His33 and the heme, even though His39 is situated slightly further away (1.2 Å) using the edge-edge distance correlation. The His62 derivative was designed to incorporate both an intervening aromatic (Trp) and polarizable sulfur (Met) to determine if either of these residues is capable of enhancing electronic couplings. The weak coupling observed correlates well with the long edge-edge distance and implies no special role for either the intervening Trp or Met residues in mediating electronic couplings. There are some

problems, however, associated with using these data to address protein-mediated electronic coupling. The first involves the determination of donor-acceptor distance. The transferred electron originates from the π-system of the porphyrin ring, since the Zn^{2+} ion is not able to participate in any redox reaction directly. Therefore, the relevant edge-edge distances are measured from the Ru complex to the closest point on the conjugated porphyrin ring. However, if the His33 to *porphyrin* (and not the His18 axial ligand used in the edge-edge convention) distance (14.8 Å) is used for the analysis, the H_{AB}s for this series correlate well with distance. It is not clear whether the His18 imidazole ring should be considered coupled to the Zn-porphyrin electron donor and acceptor. Secondly, it is not known if the substitution of zinc for iron alters the protein structure since the Zn porphyrin normally adopts a 5-coordinate geometry.

B. Protein-Surface Modification with a Photochemically Active Chromophore

In an effort to study intramolecular ET at higher driving force in proteins with a minimum probability of structural perturbation, several methodologies for the modification of surface amino acids with $Ru(bpy)_3^{2+}$ [8] derivatives have been developed by Durham, Millett and co-workers.[9-12] The basis for these studies was to use the long-lived (600 ns) MLCT excited state of $Ru(bpy)_3^{2+}$ to photoinduce ET from a specific residue on the surface of the protein to the ferric native heme. The first approach involved covalently attaching a dicarboxybipyridine (dcbpy) moiety to the ε-NH_2 group of Lys. Reaction with $Ru(bpy)_2(CO_3)$ creates a $Ru(bpy)_2(dcbpy)^{2+}$-Lys label.[9] Singly labeled Lys derivatives of horse heart cyt *c* at positions 7, 13, 25, 27 and 72 were isolated by ion-exchange chromatography and identified by tryptic digestion. Quenching of the $*Ru(bpy)_2(dcbpy)^{2+}$-Lys excited state in the ferric protein was observed and attributed to photoinduced ET from the $*Ru^{2+}$ to the Fe^{3+} heme. The rates for photoinduced ET and the subsequent back ET rates from the transiently generated ferrous heme to Ru^{3+} (see analogous reaction scheme, Figure 3.2) were determined by transient absorption

spectroscopy to be on the order of 1 to 20 x 10^6 s^{-1}. However, the attachment of the ET label to the end of the long methylene chain of a Lys residue precludes the determination of an accurate edge-edge distance measurement. Therefore, a range of edge-edge distances spanning 6 - 12 Å is reported for each modified derivative. Thus, while this system has demonstrated the applicability of direct covalent attachment of a photochemical probe to the surface of a protein for the study of biological ET, different chemistry needed to be developed to apply this methodology to the evaluation of protein-mediated electronic couplings.

It was demonstrated by the same group that, in aqueous solution, $Ru(bpy)_2(CO_3)$ would react with the surface His26 and His33 residues of horse heart cyt *c* to afford a $Ru(bpy)_2(H_2O)HisX^{2+}$ cyt *c* adduct (X = 26, 33) that exhibited no appreciable excited state lifetime in solution. Reaction of this modified protein with excess imidazole (im) resulted in $Ru(bpy)_2(im)HisX^{2+}$ derivatized cyts *c* that exhibited a 70 - 100 ns excited state lifetime with an emission maximum centered at 670 nm, comparable to that of the $Ru(bpy)_2(im)_2^{2+}$ model complex (~70 ns).[10a,b] The absorption spectrum of the derivatized protein precisely matches that of the sum of one equivalent of unmodified protein (ferric, (λ_{max} = 410 nm (ε = 106100 M^{-1} cm^{-1}) and 528 nm (ε = 11200 M^{-1} cm^{-1})) (Figure 2.4)) and one equivalent of the $[Ru(bpy)_2(im)_2]Cl_2$ model complex (λ_{max} = 292 nm (ε =56700 M^{-1} cm^{-1}) (π - π^*) and 490 nm (ε =87300 M^{-1} cm^{-1}) (MLCT)) (refer to Figure 3.7)). However, in these reports no quenching of the excited state due to photoinduced ET to the heme was observed, and it was concluded that the excited state lifetime was insufficient to accommodate a competing slow ET reaction. Additionally, a new photochemically active surface modifying reagent has been recently developed. $Ru(bpy)_2$(4-bromomethyl-4'-methylbipyridine) has been specifically bound to the surface Cys residues of *S. c.* iso-1-cyt c[11] and genetically engineered cytochrome b_5,[12] and used for the study of photoinitiated thermal ET within protein:protein complexes.

C. *Intramolecular Electron Transfer in Ru(bpy)$_2$(im)His Derivatives of Cytochrome c*

Chang, Gray and Winkler recognized that, if the lifetime of the ET active Ru(bpy)$_2$(im)HisX^{2+} label could be effectively lengthened, this system would be ideal for the study of intramolecular ET between a *well-defined position* on the surface of the protein and the *native* heme group at *high driving force* and *known intervening medium and distance.*[13] A flash / quench scheme (Figure 3.1) was devised to extend the window available for the observation of ET rates. In this scheme, ferrous Ru(bpy)$_2$(im)His33 cyt *c* is excited with a 480 nm laser pulse to generate the *Ru^{2+} - Fe^{2+} protein. The Ru excited state is bimolecularly quenched oxidatively (k_q = 4.9 x 10^8 M^{-1} s^{-1}) by a redox quencher, Q, (in this case Q = Ru(NH$_3$)$_6^{3+}$) to transiently generate the Ru^{3+} - Fe^{2+} species. This species then relaxes *via* a Fe^{2+} to Ru^{3+} ET (k_{ET}^{mm}) to the thermodynamically more favored (-ΔG^o = 0. 740 eV) (Table 3.2) Ru^{2+} - Fe^{3+} protein. On a much longer time scale (~0.1 s for 20 μM protein, 5 mM Rua$_6^{3+}$ (a = NH$_3$), the reduced quencher reduces the protein, regenerating the initial Ru^{2+} - Fe^{2+} state. Experiments can be performed with low concentration of protein and quencher due to the cyclic nature of this scheme that allows the signal averaging of many laser pulses.

Table 3.2. Summary of relevant reduction potentials. Ru(bpy)$_2$(im)$_2^{2+}$ data are from Reference 10c.

Redox Couple	E $^{o'}$ (aqueous solution, pH 7.0) (V)
cyt *c* (Fe$^{3+/2+}$)	+0. 265
Ru(bpy)$_2$(im)$_2^{3+/2+}$	+1.0
Ru(bpy)$_2$(im)$_2^{3+/*2+}$	-0.95

Figure 3.1 Reaction scheme for the flash / quench ET methodology. A $Ru(bpy)_2(im)^{2+}$-modified heme protein is depicted by the two overlapping spheres. The oxidative bimolecular quencher, Q, is Rua_6^{3+} in the described experiments. k_{ET}^{mm} is the rate of Fe^{2+} to Ru^{3+} ET.

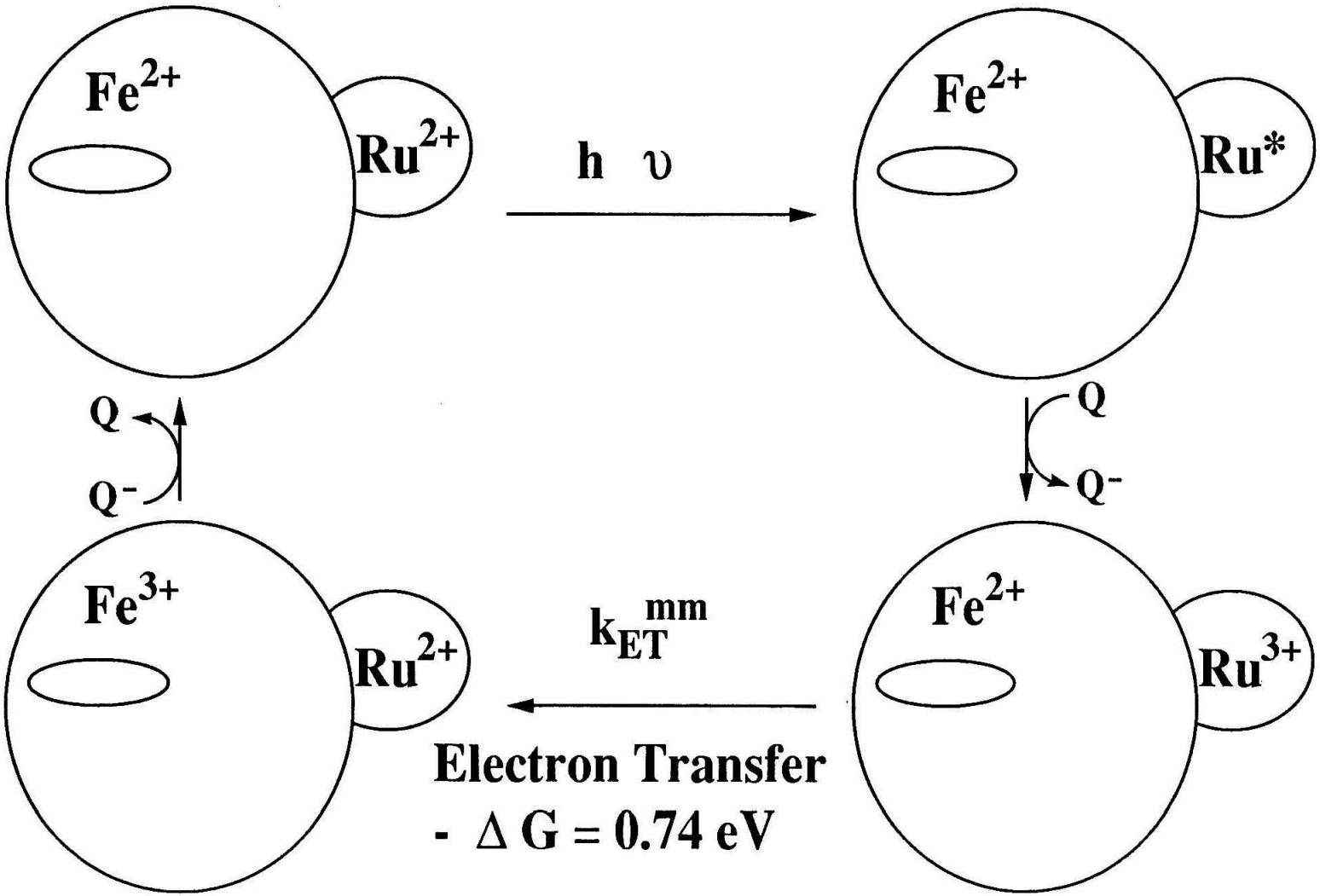
Fe2+
Ru2+
h υ
Fe2+
Ru*
Q
Q-
Q
Q-
Fe3+
Ru2+
k mm ET
Fe2+
Ru3+
Electron Transfer
- Δ G = 0.74 eV

The Fe^{2+} to Ru^{3+} ET rate (k_{ET}^{mm}) measured by the flash / quench technique described above is 2.6 x 10^6 s^{-1} for the His33-modified horse heart cyt *c* at 298 K in 50 mM NaPi, pH 7.0.[13] The $Ru(bpy)_2(im)His33^{2+}$ excited state lifetime is 80 ns in both the oxidized and reduced protein, in good agreement with the model complex at similar conditions. Approximately 5% of the excited state species in solution is oxidatively quenched to the ET-active Ru^{3+} - Fe^{2+} state at 20 μM protein with 5 mM Rua_6^{3+}. Identical kinetics are observed by transient absorption at wavelengths characteristic of both the heme and Ru oxidation states (306, 400, 500, and 550 nm).

The reorganization energy for the $Ru(bpy)_2(im)HisX$ - heme ET reaction should be lower compared to that observed in the Ru-ammine-modified proteins due to the difference in the self-exchange reorganization energies (λ_{11}) of Ru model complexes: λ_{11} = 1.20 eV for $Rua_5py^{3+/2+}$; λ_{11} = 0.57 eV for $Ru(bpy)_3^{3+/2+}$.[14] The reorganization energy (λ_{12}) for this ET can be estimated using the simplified Marcus cross relation:[15]

$$\lambda_{12} = 1/2\,\lambda_{11} + 1/2\,\lambda_{22}$$

λ_{12} for the ferrous heme to $Ru(bpy)_2(im)HisX^{3+}$ ET reaction can be estimated if λ_{11} and λ_{22} can be obtained for the two redox species. A self-exchange reorganization energy (λ_{22}) of 1.2 eV for cyt *c* is derived from the Zn cyt *c* driving force studies using the cross relation and λ_{11} for $Rua_5py^{2+/3+}$ = 1.2 eV. NMR studies give a λ_{22} value of 0.7 eV,[16] and calculations based on a microscopic model yield a value of 1.04 eV.[15] Because these measures of λ_{22} have large inherent errors, they are not necessarily mutually exclusive. Therefore, a compromise value of 1.0 eV for λ_{22} is used in these studies. Using the cross relation, this leads to an estimate of 0.80 eV for the reorganization energy of the ferrous heme to $Ru(bpy)_2(im)His^{3+}$ ET reaction using λ_{11} = 0.57 eV. This reorganization energy is near the measured driving force for the reaction, $-\Delta G^o$ = 0.74 eV, therefore ET is occurring near the anticipated activationless point ($-\Delta G^o = \lambda$). Preliminary results

indicate that the Fe^{2+} to Ru^{3+} ET is indeed temperature independent,[17] indicating that the estimate of λ_{12} is not far from the actual value. A driving force study using substituted bipyridl ligands is in progress to experimentally determine the reaction reorganization energy. A similar study has been recently reported[18] on recombinant cytochrome b_5 labeled with ruthenium(II) polypyridine complexes for which a λ value of 0.94 eV was estimated (λ_{11} cyt b_5 = 1.2 eV).[16]

Identical kinetics were observed for the Fe^{2+} to Ru^{3+} ET reaction when $Ru(bpy)_2(im)His33^{3+}$ - Fe^{2+} cyt *c* is produced in low yield from $*Ru(bpy)_2(im)His33^{2+}$ - Fe^{3+} cyt *c* by direct ET, providing an independent measure of the Fe^{2+} to Ru^{3+} rate.[13] Thus direct photoinduced ET from the $*Ru(bpy)_2(im)His33^{2+}$ excited state to the ferric heme does occur, albeit in sufficiently low yield that the observed excited state lifetime is not significantly affected. The reaction scheme for photoinduced ET followed by Fe^{2+} to Ru^{3+} ET is presented in Figure 3.2. Direct photoinduced ET ($-\Delta G^o$ = 1.2 eV (Table 3.2)) must compete with the intrinsic excited-state decay to transiently generate a $Ru(bpy)_2(im)His33^{3+}$ - Fe^{2+} protein. This species subsequently decays by Fe^{2+} to Ru^{3+} ET ($-\Delta G^o$ = 0.74 eV) back to the initial state, completing a cycle. The Fe^{2+} to Ru^{3+} ET rate measured directly from the rate of baseline recovery in the photoinduced scheme should be exactly the same as measured in the flash / quench experiment. Determination of the photoinduced $*Ru^{2+}$ to Fe^{3+} rate (k_{ET}*) is more complicated, since it is not observed directly. Rather, the rate of formation of the detectable Fe^{2+}-Ru^{3+} species corresponds to the excited state decay rate. The photoinduced ET rate is usually small ($\sim 10^5$ s^{-1}) relative to the observed decay rate ($k_d \sim 10^7$ s^{-1}), thus it cannot be reliably calculated by the small difference in the excited state lifetimes of the ferric and ferrous modified proteins. However, it can be estimated from the quantum of yield of ET product formed relative to the amount of excited state generated:

Figure 3.2 Reaction scheme for the photoinduced ET methodology. k_{ET}* is the rate of *Ru^{2+} to Fe^{3+} (photoinduced) ET and k_{ET}^{mm} is the rate of Fe^{2+} to Ru^{3+} (metal to metal) ET.

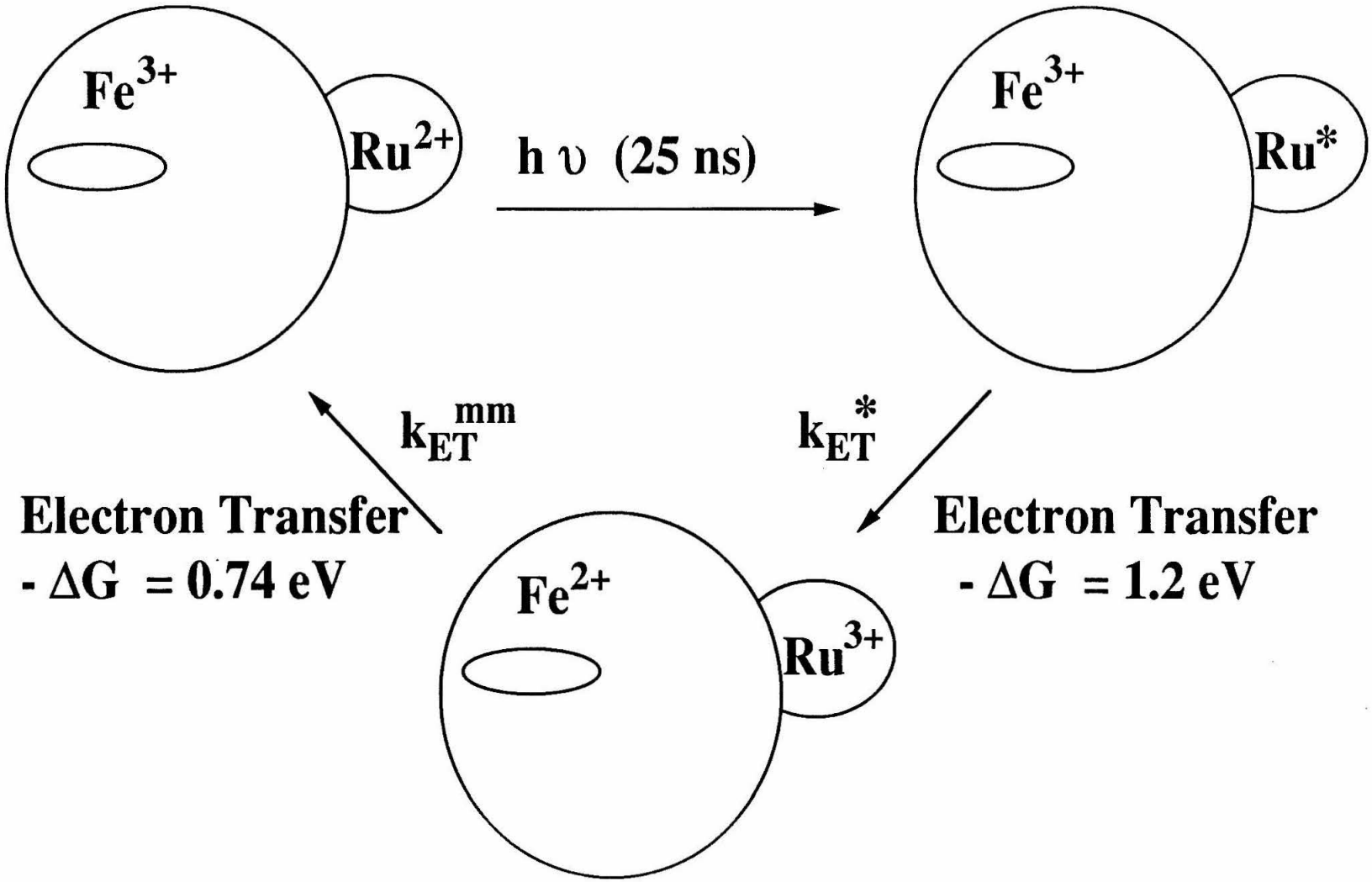
Fe^{3+}
Ru^{2+}
h υ (25 ns)
Fe^{3+}
Ru^*
k_{ET}^{mm}
k_{ET}^*
Electron Transfer
- ΔG = 0.74 eV
Electron Transfer
- ΔG = 1.2 eV
Fe^{2+}
Ru^{3+}

$$k_{ET}^{*} = \left\{ \frac{\text{[ET products]}}{\text{[excited state generated]}} \right\} k_d$$

k_{ET}^{*} is the rate constant of photoinduced ET from $*Ru^{2+}$ to Fe^{3+} and k_d is the observed excited-state decay rate constant. From this type of analysis, a photoinduced ET rate from $*Ru(bpy)_2(im)His33^{2+}$ to Fe^{3+} of 2.0×10^5 s^{-1} was determined in horse heart cyt *c*, corresponding to only a 2% yield of ET product. It should be noted that the character of the photoinduced ET reaction is significantly different from that of the Fe^{2+} to Ru^{3+} ET. In the latter reaction, the electron is transferred from a metal localized electronic orbital to another metal localized electronic orbital. However, the ET from the Ru excited state originates from a MLCT state, and the transferred electron therefore originates from a delocalized π^* orbital on the bipyridyl ligand. Thus these two fundamentally distinct ET reactions must be treated differently in the electronic coupling analysis.

With these ET tools in hand, the stage is set to investigate ET to and from various positions on the protein surface. In this chapter, mapping studies are described that extend the $Ru(bpy)_2(im)^{2+}$ labeling technique to other surface His residues on cyt *c*. $Ru(bpy)_2(im)^{2+}$ modification and both flash / quench and direct photoinduced ET data were obtained for *C. k.* His39, *S. c.* His62 and semisynthetic His72 cyts *c*. Discussion of these rates in the context of electronic couplings is relegated to Chapter 4.

II. Experimental

Most relevant instrumentation, methods, and materials were described in the experimental section of Chapter 2. Materials, methods and instrumentation introduced in this Chapter are presented below.

A. Materials

Native *C. k.* cyt *c* was obtained from Sigma (Type VII). The genetically engineered triple mutant Asn62 to His, His39 to Gln, and Cys102 to Ser mutant of *S. c.* cyt *c* was kindly provided by Dr. Bruce E. Bowler.[6] [*cis*-$Ru(bpy)_2]Cl_2$ was obtained from Strem. $Ru(bpy)_2(CO_3)$ was synthesized from [*cis*-$Ru(bpy)_2]Cl_2$ by the procedure of Johnson *et al.*[19] $[Ru(bpy)_2(im)_2]Cl_2$ was prepared by the method of Long *et al.*[20] Hexaammineruthenium(III)chloride was obtained from Strem and recrystallized from 1 M HCl. Diethylpyrocarbonate (DEPC) was obtained from Sigma and stored under argon. Trypsin (Type XIII), containing tosylamide-2-phenylethyl chloromethyl ketone, and ultrapure (99+) imidazole were obtained from Sigma.

B. Instrumentation

Luminescence spectra were recorded on an instrument constructed at Caltech that has been described previously, with some modifications.[21] The instrument is currently equipped with a Spex 1624 monochrometer for excitation spectra.

Time-resolved transient absorption and emission lifetime data were obtained on a Caltech-constructed nanosecond laser spectroscopy assembly in the Beckman Institute Laser Resource Center. A schematic of the system is presented in Figure 3.3. 25 ns full-width-half-maximum laser pulses were generated using a Lambda Physik LPX210i XeCl excimer-pumped Lambda Physik FL3002 dye laser. The excimer pump beam (308 nm, ~300 mJ) was attenuated with a partially reflecting beamsplitter (75% transmittance) before the dye laser. 480 nm pulses were obtained using Exciton Coumarin 480 dye dissolved in ultrapure Burdick & Jackson MeOH.

The output of the dye laser passed through a 4:1 beam expander then through two Glan-laser polarizers. Laser pulse energy was measured with a Scientech 372 Power and Energy Meter and the polarizer axes were adjusted relative to one another to discard a

Figure 3.3 Schematic diagram of the nanosecond resolution transient absorption apparatus at the Beckman Institute Laser Resource Center. The gas purifier for the XeCl excimer laser is not shown. The laser beam (- - -) and probe light (–·–·–·) are actually collinear at the sample, illustrated skewed for clarity. Figure courtesy of Andy Stevens.

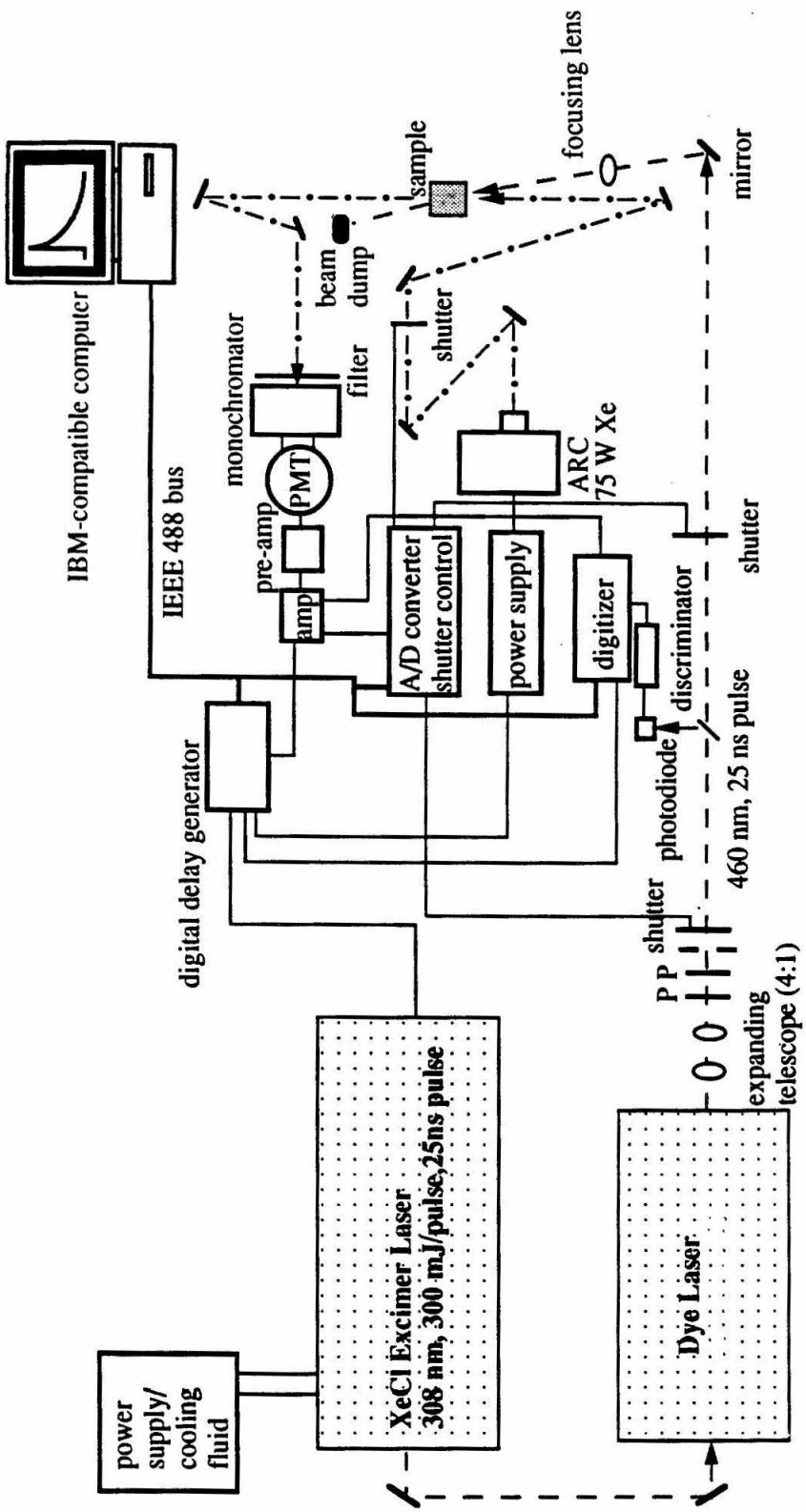
IBM-compatible computer
IEEE 488 bus
monochromator
filter
beam dump
sample
focusing lens
mirror
shutter
ARC 75 W Xe
pre-amp
PMT
amp
A/D converter shutter control
power supply
digitizer
discriminator
shutter
digital delay generator
photodiode
460 nm, 25 ns pulse
P P shutter
expanding telescope (4:1)
Dye Laser
XeCl Excimer Laser 308 nm, 300 mJ/pulse,25ns pulse
power supply/ cooling fluid

fraction of the pulse to obtain a 2 - 4 mJ final pulse energy. A small fraction of the pulse was selected with a glass plate and directed onto an Electro-Optics Technology ET2000 pin photodiode. The photodiode output was fed into a Phillips Scientific Model 6930 windowing discriminator. Only pulses that fell in a narrow energy range (E $\pm$ 12%) would pass though the discriminator and thereby trigger the digitizer for data collection. The beam was focused onto the sample cuvette with a 1-m focal length fused-silica lens.

The probe light source was a PTI 75-W Xenon arc lamp in a PTI A1010 (f/15 ellipsoidal reflector) end-on housing and powered by a PTI LPS-220 arc lamp supply. For most measurements, increased lamp intensity was desired for optimal signal-to-noise ratio. The lamp was simmered at 65 - 70 W then pulsed for 1 ms to 100 A using an Analog Modules 778P current pulser connected in parallel with the lamp power supply. Pulsed lamp intensity was flat for ~0.5 ms. The probe light was focused onto a 1-mm aperture. Light passing through the aperture was collected with a 50-cm radius-of-curvature (ROC) spherical-concave mirror (5 cm diameter, protected aluminum) then focused onto the sample. Light transmitted through the sample was collected by a second 50-cm ROC spherical mirror and then focused onto the entrance slit of a JY DH-10 double monochrometer. The excitation beam was directed through 1-cm holes in the center of the 50-cm ROC mirrors (Figure 3.3). Thus, with proper alignment, the pulse and probe light were collinear. Care was take to ensure that the probed region of the sample was fully within the laser beam profile. Single-wavelength transient absorption signals were detected using a R928 Hamamatsu photomultiplier tube housed in a Products for Research TEI77RF thermoelectrically cooled chamber. Voltage across the PMT was applied with a PC-driven LeCroy 2415 high voltage supply. Applied voltage was adjusted for maximum signal intensity within the 650 to 1200 V range.

Electronics were synchronized using an EG&G Princeton Applied Research Model 9650 Digital Delay Generator. The transient signal was amplified using either a Brookhaven National Labs-constructed quasi-differential amplifier (200 MHz, 7 μA/mV)

for kinetics on the 1.25 to 750 μs timescales, or a LeCroy DSP 1402E programmable amplifier for kinetics on the 1 to 500 ms timescales. The signal was digitized using a Sony Tektronix RTD710A digitizer and data were transferred to a PC *via* a GPIB interface.

C. Methods

1. Protein Purification

Cytochrome *c* proteins were oxidized and purified as described in Chapter 2 by cation-exchange chromatography (FPLC Mono S 10/10 and 16/10) in 25 mM NaPi, pH 7.0 with an NaCl gradient. *C. k.* cyt *c* elutes at 210 mM NaCl and *S. c.* cyt *c* elutes at 330 mM NaCl with the typical slow gradients used.

2. Modification of Surface Histidine Residues with $Ru(bpy)_2(CO_3)$

The method of Durham was used with some modifications.[10a] Typically, a degassed solution of 0.1 to 0.3 mM freshly purified ferric cyt *c* in 25 mM NaPi, pH 7.0 was prepared in a pear-shaped flask. Either solid or a concentrated solution in buffer of $Ru(bpy)_2(CO_3)$was added anaerobically to the reaction flask to make a final concentration of ~2 mM $Ru(bpy)_2(CO_3)$. Reactions were performed in the absence of oxygen to prevent the formation of intensely blue-colored oxidized ruthenium side products. $Ru(bpy)_2(CO_3)$ aquates to form the reactive $Ru(bpy)_2(H_2O)_2^{2+}$ species. The reaction was conducted at room temperature under positive argon pressure with gentle stirring. All manipulations from this point on were performed with minimal exposure to room light to avoid light-mediated degradation. Periodically aliquots of the reaction mixture were removed and quenched by gel filtration (PD-10) to separate excess Ru reagent from the protein. The remaining reaction mixture was quenched when the absorption spectrum of the aliquot indicated at 1:1 ratio of $Ru(bpy)_2$ to heme ($A_{292\,nm}$: $A_{410\,nm}$ = 1:1.7). This method of monitoring the progress of each reaction independently

yielded consistent modification results as the optimal reaction time appeared to be sensitive to the concentrations of reactants, temperature, and even stirring rate. After quenching by gel filtration in 25 mM NaPi, pH 7.0, the $Ru(bpy)_2(H_2O)$HisX cyt *c* species were converted to $Ru(bpy)_2$(im)HisX cyt *c* by incubation in 2M imidazole (not pH adjusted, final solution pH ~9.3) for 24 to 48 hours (the oxidation state of the Ru complex is 2+ unless otherwise indicated). The imidazole was removed by either gel filtration or extensive ultrafiltration washes. The reaction products were separated by cation-exchange chromatography (Mono S 5/5, 10/10, 16/10) in 25 mM NaPi, pH 7.0 with a NaCl gradient. Typical yields of the desired product were 10 - 30%. All singly modified proteins were repurified by cation-exchange chromatography before use in laser experiments. Overmodification was strictly avoided because multiply-modified proteins can not be recovered and also contaminate the chromatography columns. Recovered unmodified protein was routinely reused immediately in a second modification reaction to obtain higher net product yields.

3. *Diethylpyrocarbonate Reactions*

Under mild conditions (pH 6.5 to 7.0), diethylpyrocarbonate (DEPC) reacts exclusively with uncoordinated surface His residues to afford an adduct that absorbs at 240 nm ($\varepsilon = 2750\ M^{-1}\ cm^{-1}$).[22] Thus this reaction provides an independent test for the number of available surface His sites, and reports the status of Ru modification of surface His residues. A stock solution 0.2 M DEPC in ethanol was prepared fresh each day. A 100-fold excess of DEPC (10 µl of the stock solution) was introduced into a 1 cm pathlength cuvette with 1 ml of ~10 µM protein in 25 mM NaPi, pH 7.0. The absorbance at 220, 238, 240, 242, and 410 (control) nm was monitored as a function of time using the kinetics mode of the Hewlett-Packard Model 8542 photodiode array spectrophotometer. Scans were accumulated every 5 seconds for 30 minutes. Data obtained on the $Ru(bpy)_2(im)^{2+}$-modified proteins were complicated by the presence of an additional

band at 220 nm, perhaps corresponding to modification of the bipyridyl ring, and the ability of the DEPC to react with the pendant imidazole of the $Ru(bpy)_2(im)His^{2+}$ complex.

4. Luminescence-Decay and Transient-Absorption Measurements

Samples were prepared in 1 cm square precision quartz cuvettes (NSG Glassware) equipped with a glass blown bulb and Kontes 24/40 joints for degassing on a vacuum / argon Schlenk line. All samples were deoxygenated as described in Chapter 2. Samples were stirred continuously with a teflon microstirbar during data collection except on long time bases where the sample was stirred between laser shots. A laser repetition rate between 1 and 2 Hertz was used.

Luminescence decay and transient absorption data were obtained on the Beckman Institute Laser Resource Center nanosecond laser system operated by a 386 PC with software written by Dr. Jay R. Winkler. For luminescence decay measurements, an appropriate optical low pass filter was placed in front of the beam just before the monochrometer to reduce scattered laser light. Neutral density filters were also used, if necessary, to keep the signal below 0.1 intensity units. For transient absorption measurements, appropriate low pass or interference optical filters were placed before and after the sample. The PMT voltage, monochrometer slits, lamp power, and neutral density filters were adjusted to maximize the signal-to-noise ratio and wavelength resolution and to most effectively utilize the PMT dynamic range. Luminescence decay data for $Ru(bpy)_2(im)His^{2+}$ derivatives were obtained at 650 nm (λ_{max} = 670 nm, *vide infra*). Transients monitoring the oxidation state of the heme were routinely collected at 550, 425 and in the 395 to 400 nm region. As can be seen from the difference spectrum for reduced minus oxidized cyt *c* presented in Figure 3.4, these wavelengths represent large $\Delta\varepsilon$ for Fe^{2+}/Fe^{3+} ($\Delta\varepsilon_{550}$ = 18500 $M^{-1}cm^{-1}$; $\Delta\varepsilon_{425}$ = -31100 $M^{-1}cm^{-1}$; $\Delta\varepsilon_{395}$ = -21300 $M^{-1}cm^{-1}$). The difference absorption spectrum for the $*Ru(bpy)_2(im)_2^{2+}$ excited

Figure 3.4 Difference electronic absorption spectrum of reduced minus oxidized horse heart cyt *c* in 25 mM NaPi, pH 7.0. Extinction coefficients are from Margoliash, E.; Frohwirt, N. *Biochem. J.* **1959**, *71*, 570.

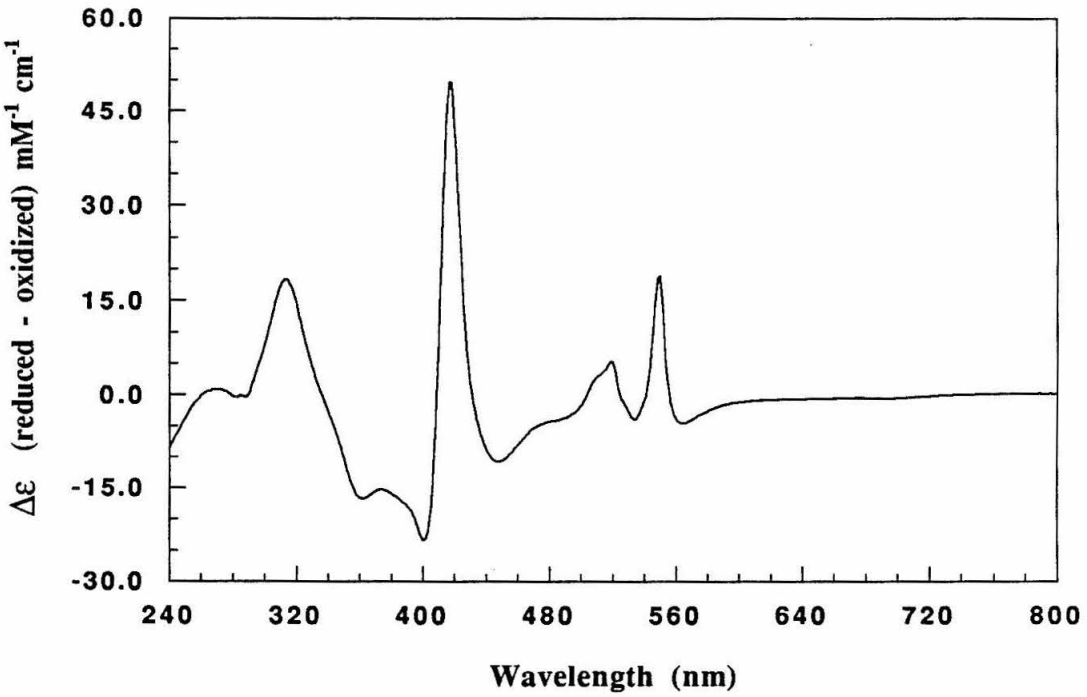
60.0
45.0
30.0
15.0
0.0
-15.0
-30.0
Δε (reduced - oxidized) mM-1 cm-1
240
320
400
480
560
640
720
800
Wavelength (nm)

state minus the $Ru(bpy)_2(im)_2^{2+}$ ground state is shown in Figure 3.5.[23] Data to be used for calculating the concentration of excited state generated by the laser pulse were collected at 370 nm ($\Delta\varepsilon_{370}$ = 11000 M^{-1} cm^{-1}, *vide infra*). To ensure that ET is occurring, it is advantageous to detect redox state changes directly at the Ru-label center. The $Ru(bpy)_2(im)_2^{3+}$ minus $Ru(bpy)_2(im)_2^{2+}$ difference spectrum is given in Figure 3.6.[23] Because the difference in ε values for the Ru^{3+}/Ru^{2+} species are fairly small relative to the changes observed in the heme chromophore in most regions of the spectrum, the Ru^{3+}/Ru^{2+} redox changes are most readily probed at Fe^{2+}/Fe^{3+} isosbestic points (*e.g.*, 434, 504, and 541 nm) and at 306 nm. For all Fe^{2+} to Ru^{3+} ET rates discussed, the rate constants measured at the Fe^{2+}/Fe^{3+} wavelengths exactly correspond to those observed at the Ru^{2+}/Ru^{3+} wavelengths, thus ensuring that ET between the Ru and Fe redox centers is being observed.

Photoinduced ET was observed in deoxygenated Ru-modified ferric protein samples ranging from 5 to 20 μM. Flash / quench ET was observed in deoxygenated Ru-modified ferrous protein samples 5 to 20 μm, which were also 4 to 7 mM in $[Rua_6]Cl_3$. The ferrous modified protein was generated immediately prior to the experiment by reduction with sodium dithionite followed by gel filtration (PD-10). All experiments were performed in 50 mM NaPi, pH 7.0 at ambient temperature. The integrity of all samples was routinely checked by absorption spectroscopy during the course of the laser experiments and by cation-exchange chromatography following the experiment. Typically, very little modified protein degradation was observed; the major laser-mediated degradation product being unmodified protein (~10%). Even so, samples were used for only one day of data collection. Suspect data were discarded.

The instrument response was obtained by collecting "luminescence decay" data on a sample of buffer at 480 nm. Collection of the scattered laser light represents the laser beam profile. NOTE: Neutral density filters up to 8.0 must be used to protect the PMT from the intense scattered laser light at this wavelength.

Figure 3.5 Difference electronic absorption spectrum of $*Ru(bpy)_2(im)_2^{2+}$ minus $Ru(bpy)_2(im)_2^{2+}$ from transient absorption studies in 50 mM NaPi, pH 7.0. Data scaled based on $\Delta\varepsilon = 11000\ M^{-1}\ cm^{-1}$ at 370 nm. Data courtesy of Dr. Morten J. Bjerrum.

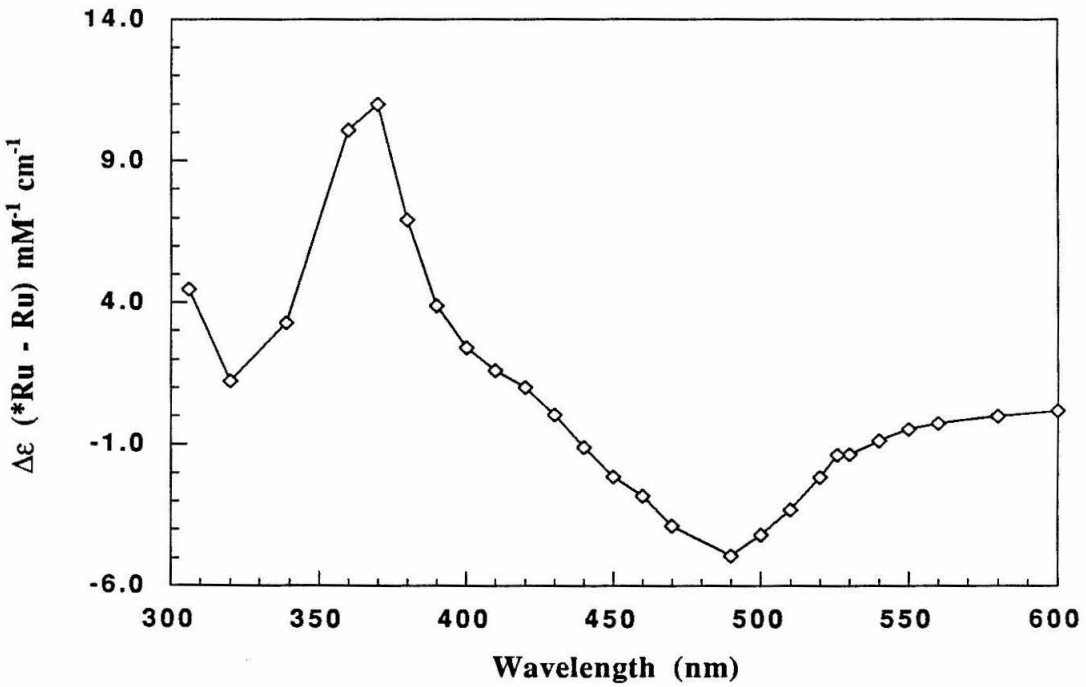
14.0
9.0
4.0
-1.0
-6.0
Δε (*Ru - Ru) mM-1 cm-1
300
350
400
450
500
550
600
Wavelength (nm)

Figure 3.6 Difference electronic absorption spectrum of $Ru(bpy)_2(im)_2^{3+}$ minus $Ru(bpy)_2(im)_2^{2+}$ from transient absorption studies in the presence of oxidative quencher in 50 mM NaPi, pH 7.0. Data courtesy of Dr. Morten J. Bjerrum.

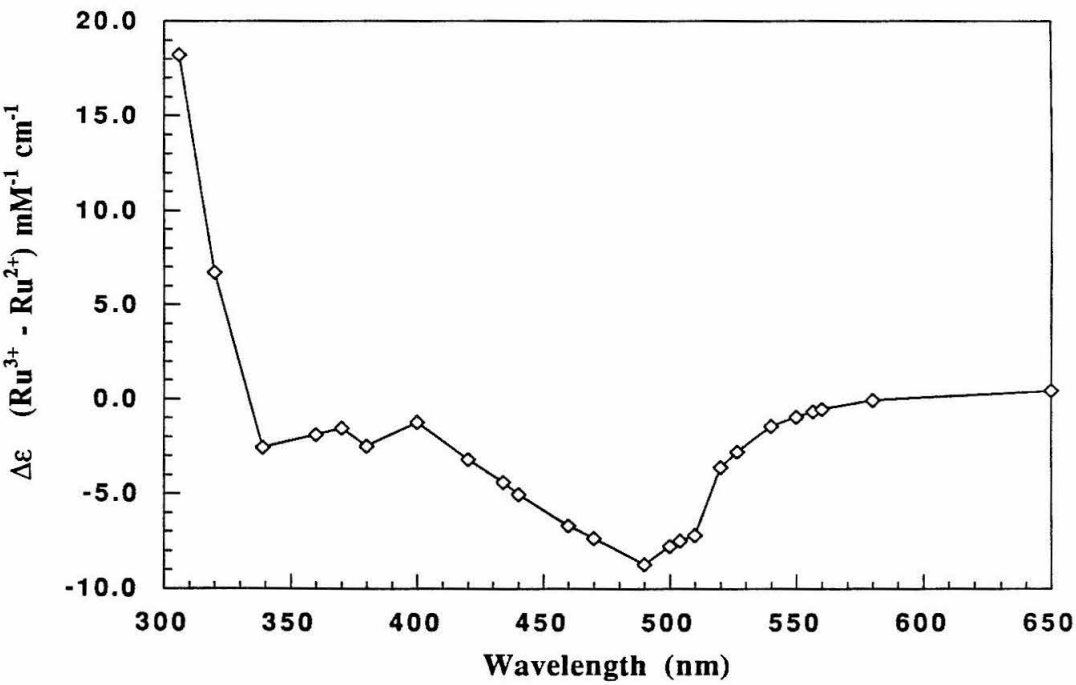
20.0
15.0
10.0
5.0
0.0
-5.0
-10.0
300
350
400
450
500
550
600
650
Δε (Ru3+ - Ru2+) mM-1 cm-1
Wavelength (nm)

5. Data Analysis

Data were fit with two different least squares fitting programs written by Dr. Jay R. Winkler. KINFIT allows one to select the region of the data set to be fit as well as define time zero (to obtain accurate values for the coefficients on the rate constants extrapolated to time zero (c_n)). The data can be fit using up to three exponential components according to (for a three-exponential fit):

$$y(t) = c_o + c_1 \exp(-k_1 t) + c_2 \exp(-k_2 t) + c_3 \exp(-k_3 t)$$

where t is time, c_n is the coefficient of the n^{th} component at t = 0, and k_n is the first-order rate constant for the n^{th} component. In this program, each parameter can be either set at a desired value, constrained to a given sign, or allowed to be optimized. Residuals were calculated and displayed to judge the goodness of fit. This fitting procedure was adequate on all timescales longer than 2.5 μs. On fast timescales, the laser pulse can no longer be treated as infinitely narrow and the data must be deconvoluted from the instrument response to obtain valid rate values. DECON deconvoluted the measured instrument response from a given data file while fitting up to three exponentials using a similar least squares procedure. On all but the 1.25 μs timescale, rates obtained using either KINFIT or DECON were identical within experimental error.

Photoinduced ET rate constants for $*Ru^{2+}$ to Fe^{3+} ET ($k_{ET}*$) were obtained using three independent data sets collected on the same sample at identical experimental conditions. First, the luminescence decay rate is obtained from the emission lifetime of the ferric $Ru(bpy)_2(im)^{2+}$-modified protein. This value was fixed in subsequent fits unless there is an additional signal due to scattered light in the transient absorbance data set. In this situation, the rate of reduced heme formation appears larger than it actually is and this variable was optimized in the fits. The c_n value for this component is meaningless in this case. The concentration of $*Ru^{2+}$ excited state generated by the laser

pulse is calculated by fitting the transient absorption signal at 370 with the luminescence decay rate (convolved with the instrument response) and extracting the c_n value for that component. Using a value of $\Delta\varepsilon$ ($^*Ru^{2+}$ - Ru(ground state)) =11000 M^{-1} cm^{-1}, c_n can be converted to concentration. Although there is some contribution to the signal at this wavelength due to Fe^{3+}/Fe^{2+} transient absorption ($\Delta\varepsilon$ = -13500 M^{-1} cm^{-1}) the quantum yield of ET products is usually much less than the quantum yield for excited state generation, and this second, slower, rate component is not significant. Typically, 70 to 90% of the available $Ru(bpy)_2(im)HisX^{2+}$ species are converted to the excited state, while < 10% of these excited-state species generate ET products. Fits of data sets probing the Fe^{2+}/Fe^{3+} kinetics (using k_{ET}^{mm} values obtained independently from flash / quench experiments and the photoinduced experiments for the Fe^{2+} to Ru^{3+} rate) extract a c_n value for electron transfer products that is converted to concentration using the appropriate $\Delta\varepsilon$ (Fe^{2+}/Fe^{3+}). The photoinduced ET rate is then the quantum yield of ET products formed ($[Fe^{2+}]$ / $[^*Ru^{2+}]$) multiplied by the luminescence decay rate. Quantum yields were not determined for the Ru^{2+}/Ru^{3+} couple.

As mentioned previously, all Fe^{2+}/Fe^{3+} rates were measured at a minimum of 2 independent wavelengths and Ru^{2+}/Ru^{3+} rates obtained by collecting data at at least one heme isosbestic wavelength to ensure that ET from/to the heme corresponded to ET from/to the heme. Full data sets (*i.e.*, transients obtained at multiple wavelengths) were obtained with at least two separate preparations of the modified proteins and usually on a total of more than eight samples at different concentrations for both the flash / quench and photoinduced experiments.

Values from data set fittings were analyzed using basic error analysis to obtain rate constants and their associated uncertainties.[24] Reported Fe^{2+} to Ru^{3+} rates were obtained by error-weighted averaging of all data obtained in both photoinduced and flash / quench experiments (for *i* individual measurements) according to:

$$\chi_{best} = \frac{\sum_{i=1}^{N} \omega_i \chi_i}{\sum_{i=1}^{N} \omega_i}$$

$$\omega_i = \frac{1}{\sigma_i^2}$$

with x_{best} as the reported rate constant, x as individual rate measurements, and σ as the estimated error associated with each measurement for i data sets. Thus, measurements with larger intrinsic errors contribute less to the final reported result. Uncertainties in the rate value from each individual measurement were estimated by inspection of the quality of fits (using the residuals) to a range of rate values. If not deconvoluted, only data collected after the complete decay of the pulse and excited state were used in the fits to avoid bias. The uncertainty of the reported rate constant was obtained using:

$$\sigma_{\chi_{best}} = \frac{1}{\sqrt{\sum_{i=1}^{N} \omega_i}}$$

For the analysis of the photoinduced rates, uncertainties in each individual rate determination (σ_{kET}*) are due to uncertainties in k_d, k_{ET}^{mm}, c_n, and $\Delta\varepsilon$ values. These uncertainties were propagated according to:

$$\frac{\left(\sigma_{k_{ET}^*}\right)^2}{\left(k_{ET}^*\right)^2} = \sum_{j=1}^{N} \frac{\left(\sigma_{\chi_j}\right)^2}{\left(\chi_j\right)^2}$$

k_{ET}* is function of N parameters, each with a value χ and an uncertainty σ_χ. Uncertainties in rates (k_{ET}^{mm} and k_d) were estimated from several fits as described, uncertainties in c_n were estimated from the magnitude of the noise (gauged in the residuals), and uncertainty in $\Delta\varepsilon$ for $*Ru^{2+}$ - Ru at 370 nm was estimated as 20%. Note that the values of c_n extracted from single and double exponential fits are extremely sensitive to the value of k_{ET}^{mm}. Therefore, the difference in the values of c_n calculated by fits using reasonable k_{ET}^{mm} rates was used as the uncertainty in c_n if this value was larger than the value estimated from the magnitude of noise. The uncertainty in the values of c_n dominated the error analysis, especially for faster k_{ET}^{mm} rates.

III. Results and Discussion

A. Model System: $Ru(bpy)_2(im)_2^{2+}$

The absorption spectrum of $Ru(bpy)_2(im)_2^{2+}$ in 25 mM NaPi, pH 7.0, is given in Figure 3.7 (λ_{max} = 292 nm (ε =56700 M^{-1} cm^{-1}) (π - π*) and 490 nm (ε =87300 M^{-1} cm^{-1}) (MLCT)). The strong absorption properties of this complex allow for unmodified, singly, and doubly $Ru(bpy)_2(im)^{2+}$-modified heme proteins to be readily distinguished from one another. The luminescence decay (λ_{ex} = 480 nm, λ_{obs} = 650 nm) is shown in Figure 3.8. The rate constant measured for excited-state deactivation (k_d) is 1.51(5) x 10^7 s^{-1} (τ = 66 ns) in 50 mM NaPi, pH 7.0.

A laser power saturation study of the transient absorption signal at 370 nm of the excited state lead to an estimate of $\Delta\varepsilon$ ($*Ru^{2+}$ - Ru(ground state)) of 11000 M^{-1} cm^{-1}. The signal of the 9.9 μM sample was fully saturated at 2 mJ energy. The intensity of the transient absorption signal was observed to decay (~20% with 1000 laser shots) with laser exposure, therefore a fresh sample was used at each power measured. This photodegradation may be due to loss of an imidazole ligand. However, the $Ru(bpy)_2(im)^{2+}$-modified proteins did not exhibit this photodegradation to a similar extent, although a small quantity of the label was lost over time.

Figure 3.7 Electronic absorption spectrum of $Ru(bpy)_2(im)_2^{2+}$ in 50 mM NaPi, pH 7.0.

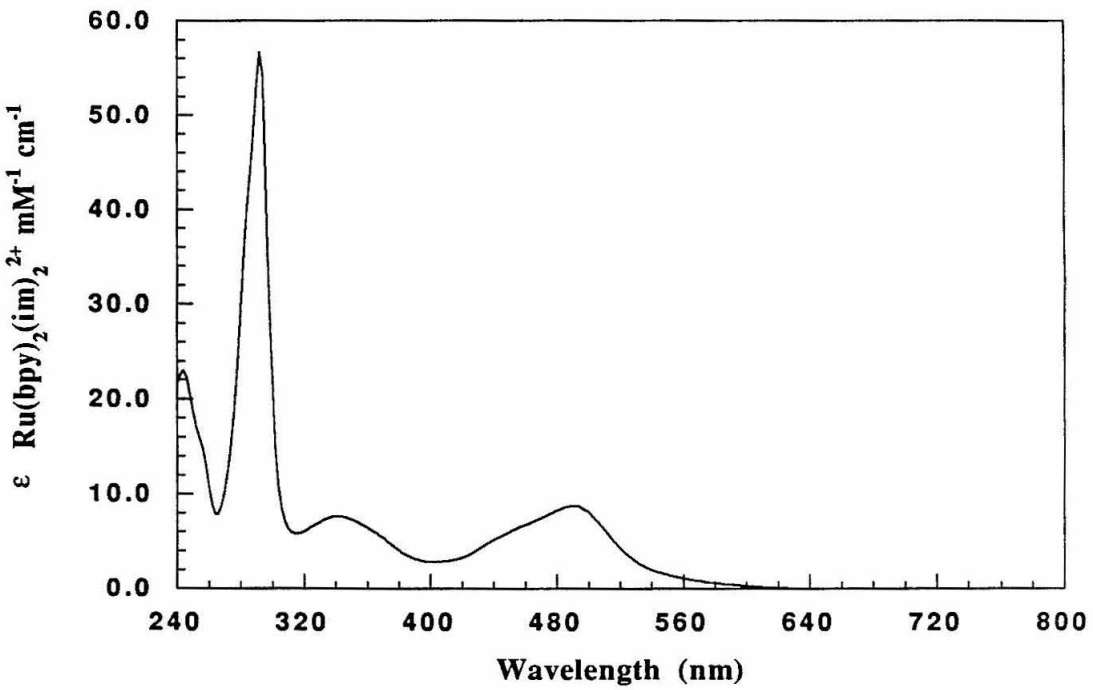
60.0
50.0
40.0
30.0
20.0
10.0
0.0
ε Ru(bpy)2(im)2 2+ mM-1 cm-1
240
320
400
480
560
640
720
800
Wavelength (nm)

Figure 3.8 Luminescence decay of a 9.9 μM sample of $Ru(bpy)_2(im)_2^{2+}$ in 50 mM NaPi, pH 7.0 observed at 650 nm following excitation at 480 nm (4 mJ pulse). The smooth line is the fit to a single exponential decay function convolved with the instrument response (shown); $k_d = 1.51(5) \times 10^7\ s^{-1}$.

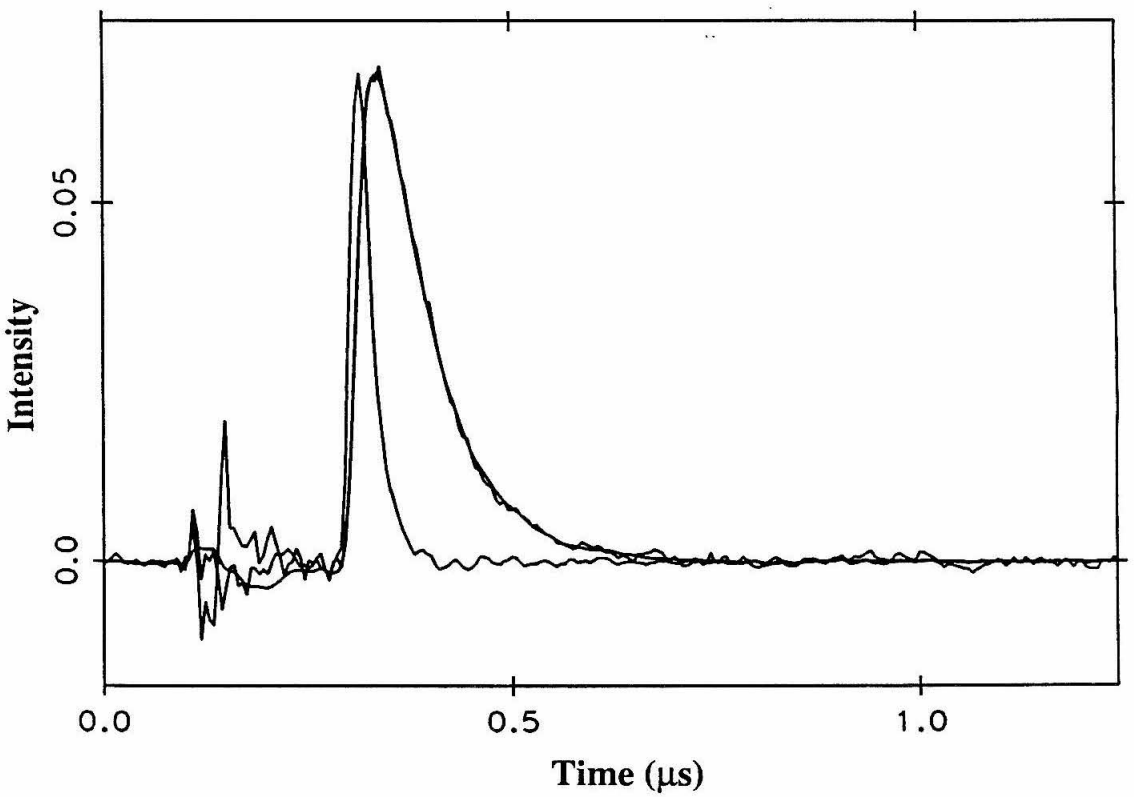
Intensity
0.05
0.0
0.0
0.5
1.0
Time (μs)

The excited state lifetime of the $Ru(bpy)_2(im)(H_2O)^{2+}$ complex was investigated by Dr. Angel Di Bilio. It was determined that this species has a luminescence lifetime that is too short to be resolved by the 25 ns laser pulse. Therefore, an impurity of the aquo complex on the $Ru(bpy)_2$-modified proteins due to incomplete reaction with imidazole (which cannot be separated by cation-exchange chromatography, *vide infra*) will not contribute to observed ET kinetics because this complex is photophysically inactive for ET *via* the methods used here.

B. Ru(bpy)$_2$(im)His33 cyt c (horse heart)

The modification and ET properties of horse heart $Ru(bpy)_2(im)$His33 cyt *c* have been studied in the Gray group by Dr. I-Jy Chang.[13] $Ru(bpy)_2(im)^{2+}$ modification of native protein was performed as part of this doctoral work to study the modification reaction and determine the biophysical properties of $Ru(bpy)_2(im)^{2+}$-modified heme proteins because ample quantities of protein could be readily generated.

1. Ru(bpy)$_2$(im)$^{2+}$-Modification Reaction

The modification reaction was conducted as described in General Methods. A trial reaction was initially performed to monitor the time course of the reaction. Aliquots removed during the course of the reaction and subsequently treated with imidazole were analyzed by analytical cation-exchange chromatography (FPLC Mono S 5/5). Four prominent singly-modified bands that elute at ionic strengths slightly higher than the native protein grow in with time, followed by numerous multiply-modified bands. A representative cation-exchange chromatogram of a modification reaction is shown in Figure 3.9 (Mono S 16/10). Band I is the native protein while bands II and III have been assigned to His33-modified species and bands IV and V to His26-modified species (*vide infra*). Band III was used for ET studies[13] and is used for the characterization described unless otherwise specified. Tryptic mapping confirms that band III contains

Figure 3.9 Typical cation-exchange (FPLC Mono S 16/10, flow rate of 6.0 ml/min) chromatogram for the native horse heart cyt *c* reaction products from the modification reaction with $Ru(bpy)_2(CO_3)$ in 25 mM NaPi, pH 7.0. Gradient represents the concentration of NaCl in mM. Band I corresponds to unmodified protein, bands labeled II - V represent the four prominent singly $Ru(bpy)_2(im)^{2+}$-modified cyt *c* products. The band that elutes with the void volume is $Co(EDTA)^-$, added to fully oxidize the sample prior to purification. Detection is on the 0.2 absorbance scale at 280 nm.

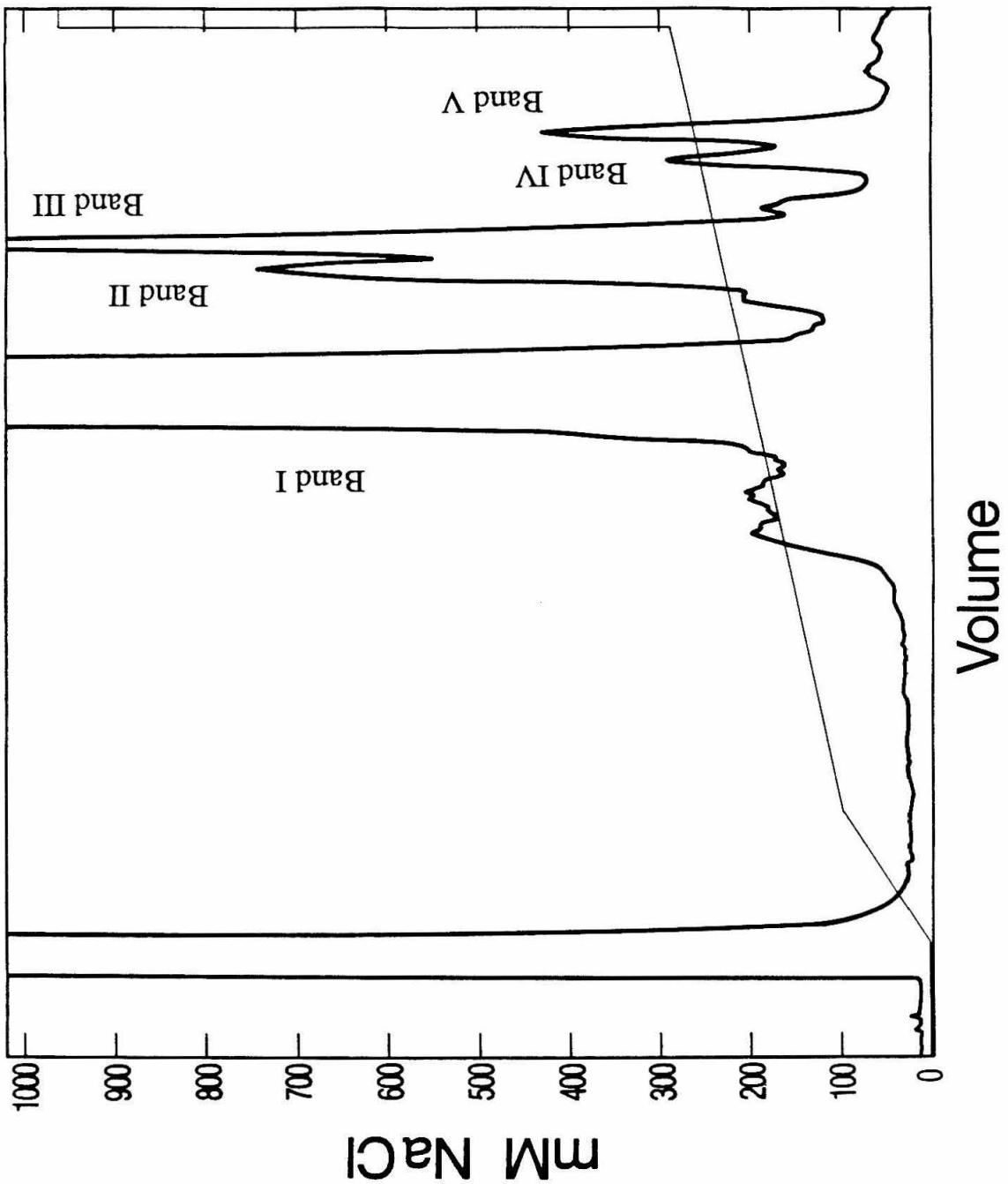
mM NaCl
1000
900
800
700
600
500
400
300
200
100
0
Volume
Band I
Band II
Band III
Band IV
Band V

$Ru(bpy)_2(im)$His33-modified cyt *c*.[17] Identical chromatograms were obtained for purification of the $Ru(bpy)_2(H_2O)$HisX cyt *c* adducts (*i.e.*, purification prior to incubation with imidazole), implying that the aquo and imidazole species cannot be resolved by cation-exchange chromatography. The product ratio of the 4 singly modified proteins isolated is extremely sensitive to experimental conditions; different ratios were obtained at different concentrations of product and reactant, ionic strength, and in reactions run on the ferrous protein. Typical reaction conditions were 0.4 mM purified horse heart cyt *c*, 3.0 mM $Ru(bpy)_2(CO_3)$ in 25 mM NaPi, pH 7.0 and reactions were quenched after 42 hours. Incubation in 2M imidazole was conducted at room temperature for 48 hours. The modified proteins were purified to homogeneity prior to use.

2. *Absorption Spectroscopy*

The absorption spectrum of $Ru(bpy)_2(im)$His33 Fe^{3+}cyt *c* (band III) in 25 mM NaPi, pH 7.0, is presented in Figure 3.10. It corresponds exactly to the sum of one equivalent ferric cyt *c* (Figure 2.4) and $Ru(bpy)_2(im)_2^{2+}$ (Figure 3.7), including the presence of the 695 nm band indicative of intact Met ligation (not shown). All singly modified $Ru(bpy)_2(im)^{2+}$ cyt *c* derivatives discussed in this chapter possess identical spectral features unless otherwise indicated.

3. *Electrochemistry*

Differential pulse polarography was performed on $Ru(bpy)_2(im)$His33 cyt *c* in 50 mM NaPi, 10 mM 4,4'-bipyridine, pH 7.0 at a gold button electrode as described in Chapter 2. The heme potential increases moderately (~15 mV) ($E^{o'}$ = 280(5) mV *vs.* NHE) upon $Ru(bpy)_2(im)^{2+}$ modification at position 33. However, scans in the region of the $Ru(bpy)_2(im)$His33$^{3+/2+}$ potential indicated no reversible wave present. Furthermore, after scanning at high potential, the heme wave at lower potential disappeared.

Figure 3.10 Electronic absorption spectrum of ferric $Ru(bpy)_2(im)His33^{2+}$ cyt *c* in 25 mM NaPi, pH 7.0. Absorption bands are assignments are given.

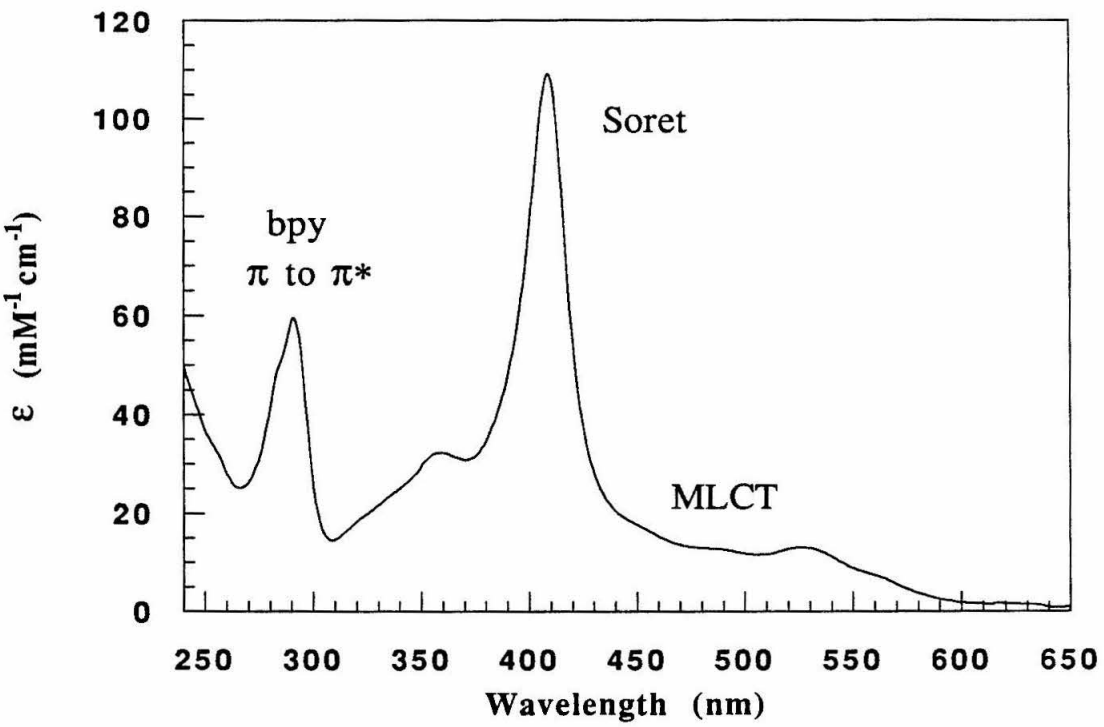
120
100
80
60
40
20
0
ε (mM-1 cm-1)
bpy
π to π*
Soret
MLCT
250
300
350
400
450
500
550
600
650
Wavelength (nm)

Differential pulse polarography at the 4,4'-bipyridine-modified gold electrode is therefore not a viable technique for the determination of the $Ru(bpy)_2(im)His33^{3+/2+}$ potential.

4. Diethylpyrocarbonate Modification

It has been reported that native horse heart cyt *c* possesses one DEPC-modifiable His residue at position 33; His26 is buried within the protein and therefore not accessible to modification.[21] As expected, DEPC modification of native horse heart cyt *c* indicated the presence of exactly 1 accessible His residue (see Figure 3.11 for representative data). In contrast, both bands IV and V of the native cyt *c* modification reaction possess 1.5 modifiable His residues. The indication of the presence of a fractional His present may be due to the contribution of absorption of a concurrently formed 220 nm band at 240 nm., making it difficult to determine the precise absorption at 240 nm. Band III yielded 0.3 modifiable His residues and band II appeared to have 0.2 to 0.4 surface His resides. However, in band II the 220 nm band was quite intense, and it was again difficult to accurately determine the change in absorption at 240 nm. Overall, the DEPC modification results are in agreement with bands II and III being Ru-modified at position 33 and bands IV and V modified at His26, although the presence of an additional adduct at 220 nm in the $Ru(bpy)_2(im)^{2+}$-modified proteins makes it impossible to definitively assign the position of the $Ru(bpy)_2(im)^{2+}$ label from DEPC modification data alone.

5. Circular Dichroism Measurements : Melting Transition and Evidence for Δ and Λ Isomers

Comparison of the CD spectra in the far UV region of native cyt *c* and modification products bands II and III indicate that the $Ru(bpy)_2(im)^{2+}$ modification of cyt *c* at position 33 results in negligible perturbation of secondary structure (Figure 3.12). CD data obtained at the Kansas State University by Prof. L. Anderson on bands IV and V (His26-modified products) are also nearly identical with native, indicating negligible

Figure 3.11 Time course of the DEPC modification reaction with native cyt *c* at the conditions described in the text. Protein concentration is 21 μM. The traces that grow with time monitor absorption at 236, 238, 240, and 242 nm. The time independent trace is a control monitoring absorption at 410 nm (Soret). The change in absorption corresponds to one modifiable His residue per protein.

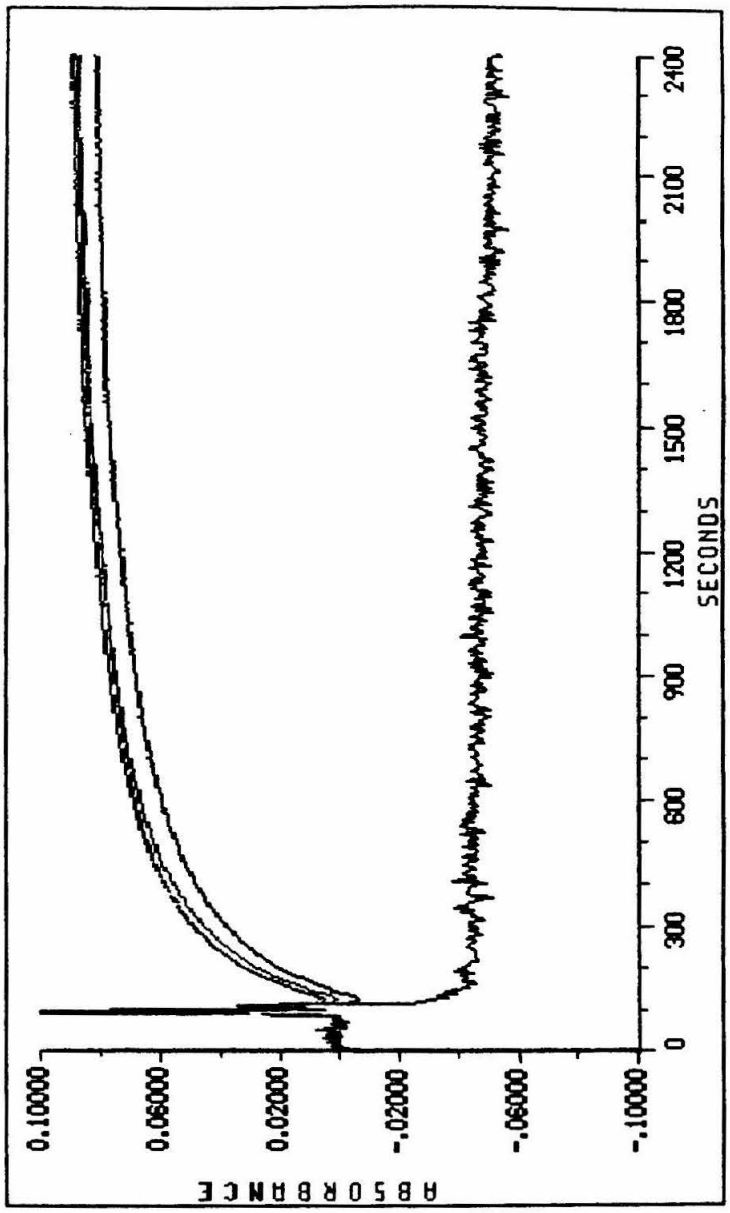
0.10000
0.06000
0.02000
-.02000
-.06000
-.10000
ABSORBANCE
0
300
600
900
1200
1500
1800
2100
2400
SECONDS

Figure 3.12 Far-UV circular dichroism spectra of native horse heart ferric cyt *c* (····), $Ru(bpy)_2$(im)His33 ferric cyt *c* (band II) (——), and $Ru(bpy)_2$(im)His33 ferric cyt *c* (band III) (used for ET experiments) (—···—···) in 25 mM NaPi, pH 7.0. Sample concentrations were 11 - 12 μM and spectra were obtained in a 0.1 cm pathlength cell on the 20 mdeg sensitivity scale at ambient temperature.

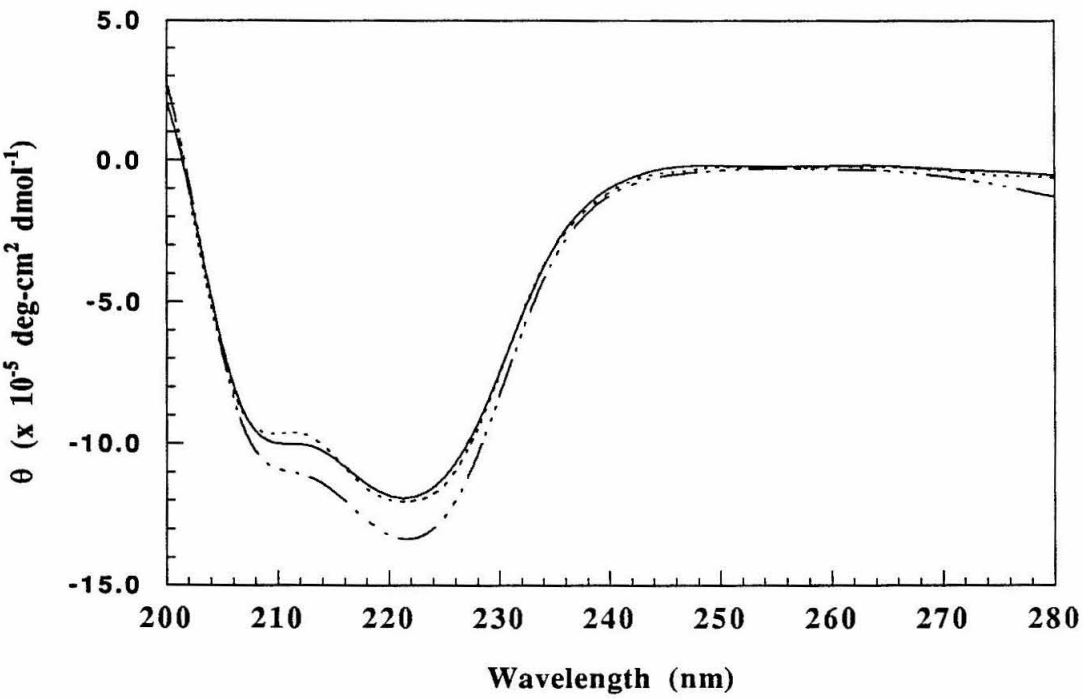
5.0
0.0
-5.0
-10.0
-15.0
θ (x 10-5 deg-cm2 dmol-1)
200
210
220
230
240
250
260
270
280
Wavelength (nm)

secondary structural alterations in these modified proteins. The melting transition of ferric $Ru(bpy)_2(im)$His33 cyt *c* (band III) was determined to be 80° C by temperature-dependent CD at 222 nm, slightly lower than the native transition at 87° C. The melting transition is reversible, *i.e.*, the helical secondary structure is recovered upon returning to room temperature.

An interesting effect was noted[25] in the CD spectrum in the region of the bipyridyl π - π^* absorption. A positive Cotton effect was observed at ~296 nm for bands III and V and a negative Cotton effect in bands II and IV at this wavelength (Figure 3.13 A and B). This observation implies that the four singly modified products correspond to the delta and lambda isomers formed at position 33 and 26. The two possible stereoisomers of the *cis*-$Ru(bpy)_2(im)_2^{2+}$ complex are illustrated in Figure 3.14. While unexpected, it is conceivable that the overall surface charge distribution on the Δ-$Ru(bpy)_2(im)$His33 cyt *c isomer* differs enough from that of Λ-$Ru(bpy)_2(im)$His33 cyt *c* to accommodate separation by cation-exchange chromatography. Based on previous CD work on Δ and Λ isomerism in tris-phenathroline and bipyridyl complexes,[26] band II is tentatively assigned as Δ-$Ru(bpy)_2(im)$His33 cyt *c*, band III (used for electron transfer) Λ-$Ru(bpy)_2(im)$His33 cyt *c*, band IV as Δ-$Ru(bpy)_2(im)$His26 cyt *c*, and band V as Λ-$Ru(bpy)_2(im)$His26 cyt *c*.

6. 2-D COSY NMR Studies

In an effort to ascertain if $Ru(bpy)_2(im)^{2+}$ modification of cyt *c* perturbs the protein structure, intensive NMR investigations were conducted on the Δ and Λ isomers of ferric $Ru(bpy)_2(im)$His33^{2+} cyt *c* in collaboration with Prof. Peter E. Wright and Dr. Dimitrios Morikis of the Scripps Research Institute. A comparison of amide N-H and C_α-H proton shifts obtained from double quantum COSY experiments with native cyt *c*, Δ-$Ru(bpy)_2(im)$His33 cyt *c* and Λ-$Ru(bpy)_2(im)$His33 cyt *c* (2 - 4 mM protein in 90%/10% H_2O/D_2O, 100 mM NaPi, 150 mM NaCl, pH 5.7, 293 K) indicate there is no

Figure 3.13 (A) Circular dichroism spectra in the near-UV region of $Ru(bpy)_2(im)$His33 ferric cyt *c* (band II)(——), and $Ru(bpy)_2(im)$His33 ferric cyt *c* (band III) (used for ET experiments) (—···—···) in 25 mM NaPi, pH 7.0. Sample concentrations were 11 - 12 μM and spectra were obtained in a 0.1 cm pathlength cell on the 20 mdeg sensitivity scale at ambient temperature. (B) Circular dichroism spectra in the near-UV region of native horse heart cyt *c* (———), $Ru(bpy)_2(im)$His26 ferric cyt *c* (band IV) (- - - - -), and $Ru(bpy)_2(im)$His26 ferric cyt *c* (band V) (·····) in 20 mM NaPi, pH 6.9. Sample concentrations were 46 - 60 μM. Data collected by Prof. Laura Anderson at Kansas State University.[25]

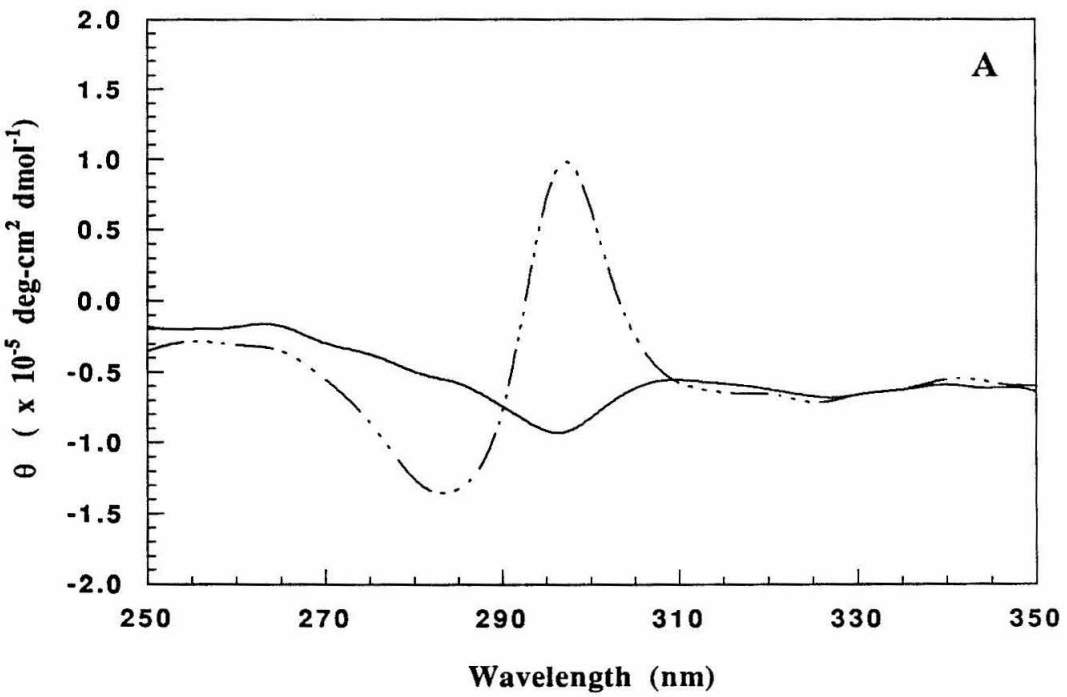
A
2.0
1.5
1.0
0.5
0.0
-0.5
-1.0
-1.5
-2.0
θ (x 10-5 deg-cm2 dmol-1)
250
270
290
310
330
350
Wavelength (nm)

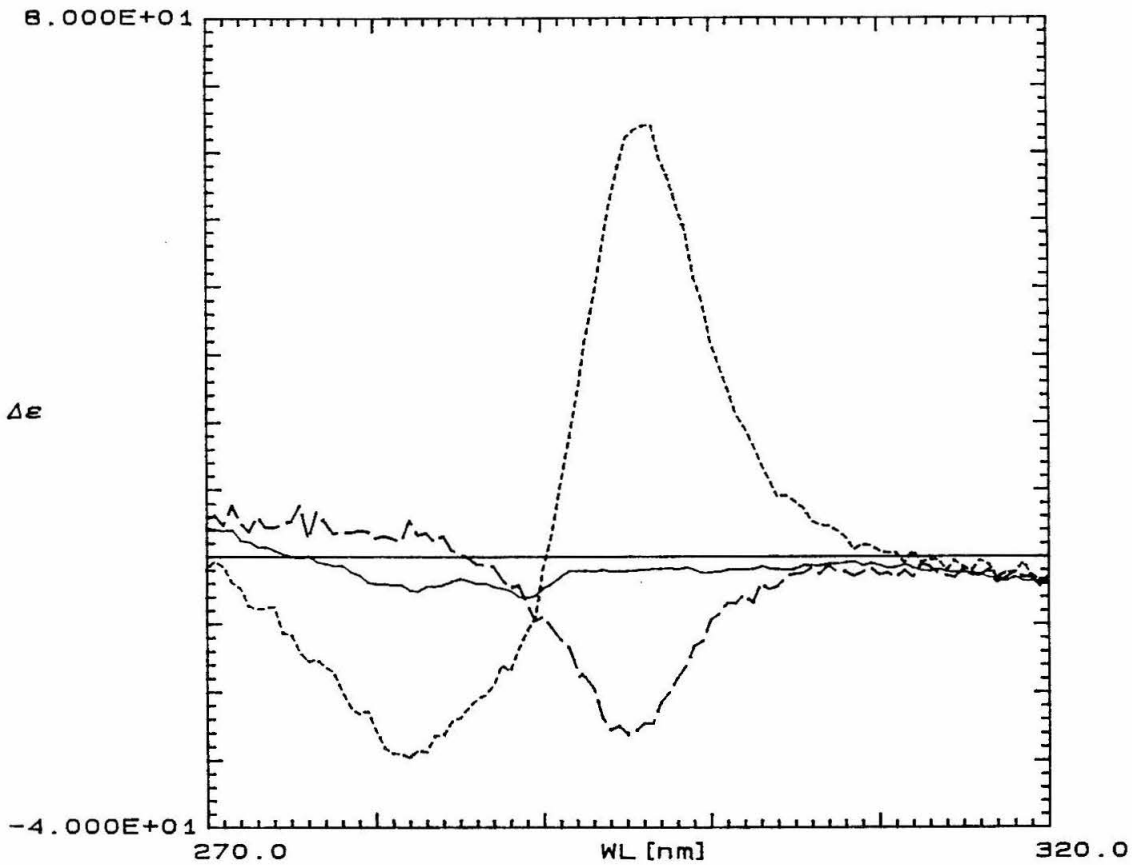
8.000E+01
Δε
-4.000E+01
270.0
WL [nm]
320.0

Figure 3.14 Illustration of the Δ and Λ isomers of $Ru(bpy)_2(im)_2^{2+}$.

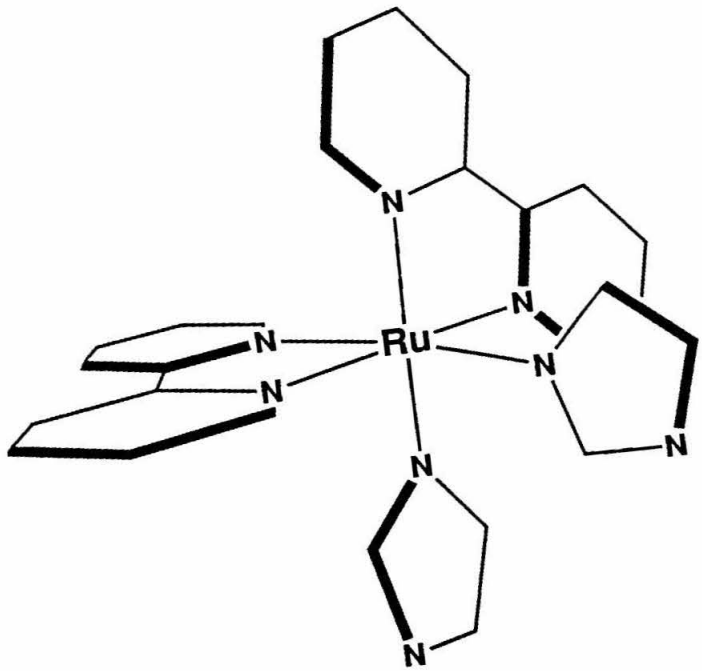

Δ

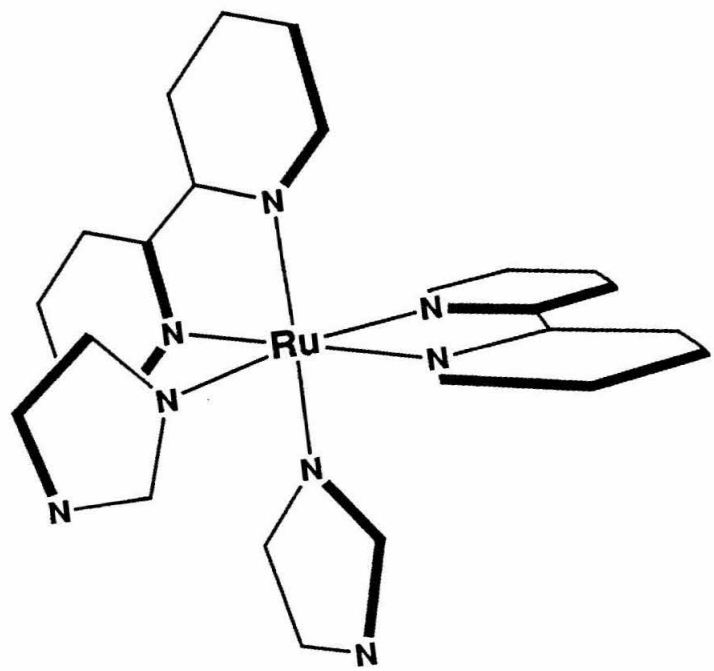

Λ

significant perturbation of the protein structure. The "fingerprint" region (C_α-H to N-H proton-proton *J*-coupled crosspeaks), assigned by Englander and coworkers,[27] was scrutinized, and the experimental results are detailed in Appendix A. Spectra obtained for Δ-$Ru(bpy)_2(im)$His33 cyt *c* and Λ-$Ru(bpy)_2(im)$His33 cyt *c* were similar, implying that the $Ru(bpy)_2(im)^{2+}$ label does not interact appreciably with the protein surface. Interestingly, differences between the two isomers were observed in the region of the C-terminal helix. 85% of the assignments made for the native protein could be transferred to the $Ru(bpy)_2(im)$His33 modified proteins (*i.e.*, resonances were within 0.1 ppm of the native assignment). Changes in chemical shift were noted between residues 90 - 100, indicating either small structural changes in the vicinity of the label or shifts due to contact interactions or ring-current effects with the aromatic rings of the Ru ligands. In other regions of the protein, resonances either were not observed (due to significant shifting or lack of sensitivity) or shifted, however no pattern of structural changes was discerned.

7. *EPR Spectroscopy*

The EPR spectrum of ferric Λ-$Ru(bpy)_2(im)$His33 cyt *c* at 6.8 K in 50 mM HEPES, 50% glycerol, pH 7.0 was virtually identical with the spectrum of the native horse heart protein.

C. *$Ru(bpy)_2(im)$His72 cyt c (semisynthetic horse heart)*

The semisynthesis, characterization and pentaammine modification of His72 cyt *c* is described in Chapter 2. Extension of this work using the $Ru(bpy)_2(im)^{2+}$-modification technique is presented here.

1. $Ru(bpy)_2(im)^{2+}$-Modification Reaction

The modification reaction was conducted as described in General Methods. To characterize the modification reaction, a trial reaction was conducted to monitor the time-dependent growth of modified protein products. Aliquots removed during the course of the reaction were analyzed, following imidazole treatment, by analytical cation-exchange chromatography (FPLC Mono S 5/5). Four singly modified bands grow in that elute at an ionic strength slightly higher than the native protein, exactly analogous to products observed in the $Ru(bpy)_2(im)^{2+}$-modification reaction of native horse heart cyt *c*. Therefore, these products were identified as His33 and His26 modified proteins Three additional singly modified products grow in at higher ionic strength and in higher yield than any other $Ru(bpy)_2(im)^{2+}$-modified cyt *c* product (analogous to the pentaammineruthenium-modification reaction, refer to Chapter 2). These products were tentatively assigned as His72 singly modified species. A representative chromatogram of the modification reaction after imidazole treatment is given in Figure 3.15. The product elution profile by cation-exchange chromatography is nearly identical if the reaction products are separated prior to imidazole treatment, implying that the $Ru(bpy)_2(H_2O)$HisX cyts *c* have identical elution times with the $Ru(bpy)_2(im)$HisX cyts *c* and cannot be distinguished by cation-exchange chromatography.

Of the three His72-labeled products (labeled A, B, and C), only band B was used for ET studies. While bands A and B appear to possess absorption spectra identical with that given in Figure 3.10, close analysis reveals that band C does not possess a 695 nm band. Therefore, Met80 ligation must be altered in this species. It is possible that the Met residue is displaced by an imidazole during imidazole treatment since the pH at which that reaction is usually performed is near the pKa for the alkaline transition in horse heart cyt *c* (pKa ~9.3).[28] In this transition, the Met axial ligand is displaced by a strong-field ligand. Band A was typically recovered in too low yield for extensive study, although it has been characterized by CD (*vide infra*) and possesses a typical

Figure 3.15 Typical cation-exchange (FPLC Mono S 10/10, flow rate of 3.5 ml/min) chromatogram for the semisynthetic His72 cyt *c* modification reaction with $Ru(bpy)_2(CO_3)$ reaction products in 25 mM NaPi, pH 7.0. Gradient represents the concentration of NaCl in mM. The first main band corresponds to unmodified protein, bands labeled A, B, and C represent the three singly $Ru(bpy)_2(im)^{2+}$-modified cyt *c* products not observed in the modification reaction with native horse heart cyt *c*. Detection is on the 1.0 absorbance scale at 405 nm.

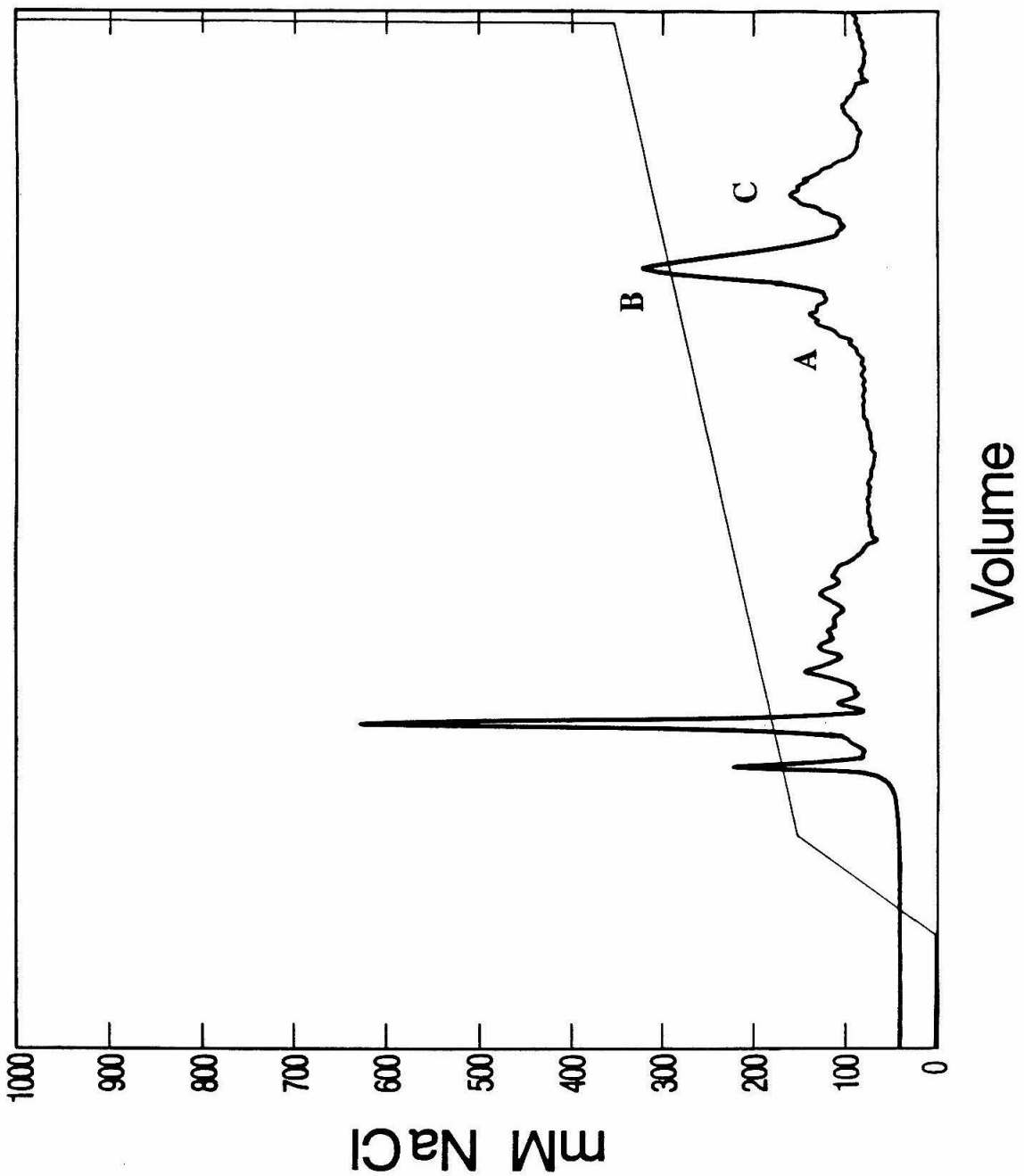
mM NaCl
1000
900
800
700
600
500
400
300
200
100
0
A
B
C
Volume

luminescence decay lifetime. Bands that elute at higher ionic strength correspond to multiply modified products.

Typical modification reactions were 0.2 mM purified His72 cyt *c*, 2.0 mM $Ru(bpy)_2(CO_3)$ in 25 mM NaPi, pH 7.0 and were quenched after 15 hours of reaction. Incubation in 2M imidazole was conducted at room temperature for 48 hours. Imidazole was removed by gel filtration prior to FPLC purification. The modified protein was repurified before use.

2. Tryptic Mapping

To confirm that band B used for subsequent ET studies was indeed modified at position 72, a tryptic digest analysis was conducted. Trypsin is a protease that catalyzes the hydrolysis of peptide bonds, and specifically cleaves on the carboxy side of Lys and Arg residues. Cleavage sites in the protein and the anticipated peptide-fragment products are given in Figure 3.16.[29] In this analysis, the tryptic fragments are isolated by reversed-phase chromatography and the peptide containing the Ru label is identified by UV/vis absorption spectroscopy. Microsequencing affords identification of the Ru-containing peptide and thus the site of modification can be unambiguously determined.

A 0.52 mg sample of native horse cyt *c* in 260 µl and a 0.1 mg sample of $Ru(bpy)_2$(im)His72 cyt *c* in 120 µl of 0.1 M NH_4CO_3, pH 8.5 were incubated with trypsin (2 mg/ml in 0.001 M HCl, added in two separate aliquots at T = 0 and T = 4 hours for a total of 4% trypsin by weight) at 37° C for 24 hours. The reaction was quenched by addition of dilute HCl to adjust the digestion solutions to pH 2.0. The digested samples were lyophilized and analyzed by reversed-phase chromatography detected at 280 nm (FPLC PepRPC HR 5/5 with a linear gradient of 0% to 40% CH_3CN with 0.1% trifluoroacetic acid in 0.1% aqueous trifluoroacetic acid) (Figure 3.17 A and B). UV/vis analysis of the fractions indicated the presence of two new bands in the $Ru(bpy)_2$(im)His72 cyt *c* digest not present in the native digest (indicated by * and **,

Figure 3.16 Amino acid sequence of His72 cyt *c* (new His residue marked by capitalization) with the sites of cleavage by trypsin[29] and the anticipated peptide products indicated.

1 **Ac - Gly - Asp - Val - Glu - Lys - Gly - Lys - Lys - Ile - Phe**
<----------T1----------><----T2----> <----------

11 **Val - Gln - Lys - Cys - Ala - Gln - Cys - His - Thr - Val**
--T3----------><----------T4----------

21 **Glu - Lys - Gly - Gly - Lys - His - Lys - Thr - Gly - Pro**
----------><--------T5-------><----T6----><----------

31 **Asn - Leu - His - Gly - Leu - Phe - Gly - Arg - Lys - Thr**
----------T7----------><----

41 **Gly - Gln - Ala - Pro - Gly - Phe - Thr - Tyr - Thr - Asp**
----------T8----------

51 **Ala - Asn - Lys - Asn - Lys - Gly - Ile - Thr - Trp - Lys**
----------><----T9----><----------T10---------->

61 **Glu - Glu - Thr - Leu - Met - Glu - Tyr - Leu - Glu - Asn**
<----------T11----------

71 **Pro - HIS- Lys - Tyr - Ile - Pro - Gly - Thr - Lys - Met**
----------><----------T12----------><-----

81 **Ile - Phe - Ala - Gly - Ile - Lys - Lys - Lys - Thr - Glu**
----------T13----------><----T14---><-------T15-

91 **Arg - Glu - Asp - Leu - Ile - Ala - Tyr - Leu - Lys - Lys**
----->><----------T16----------><----T17---><----

101 **Ala - Thr - Asn - Glu -OH**
----------T18---------->

Figure 3.17 Tryptic digest maps of (A) native and (B) $Ru(bpy)_2(im)$His72 cyt *c* obtained by reversed-phase chromatography (FPLC PepRPC HR 5/5, flow rate of 0.7 ml/min). Gradient represents the concentration of solution B (CH_3CN with 0.1% trifluoroacetic acid) in A (0.1% aqueous trifluoroacetic acid). Bands denoted by an * or ** correspond to peptides not observed in the digest of native horse heart cyt *c*. Detection is on the (A) 0.1 and (B) 0.05 absorbance scales at 280 nm.

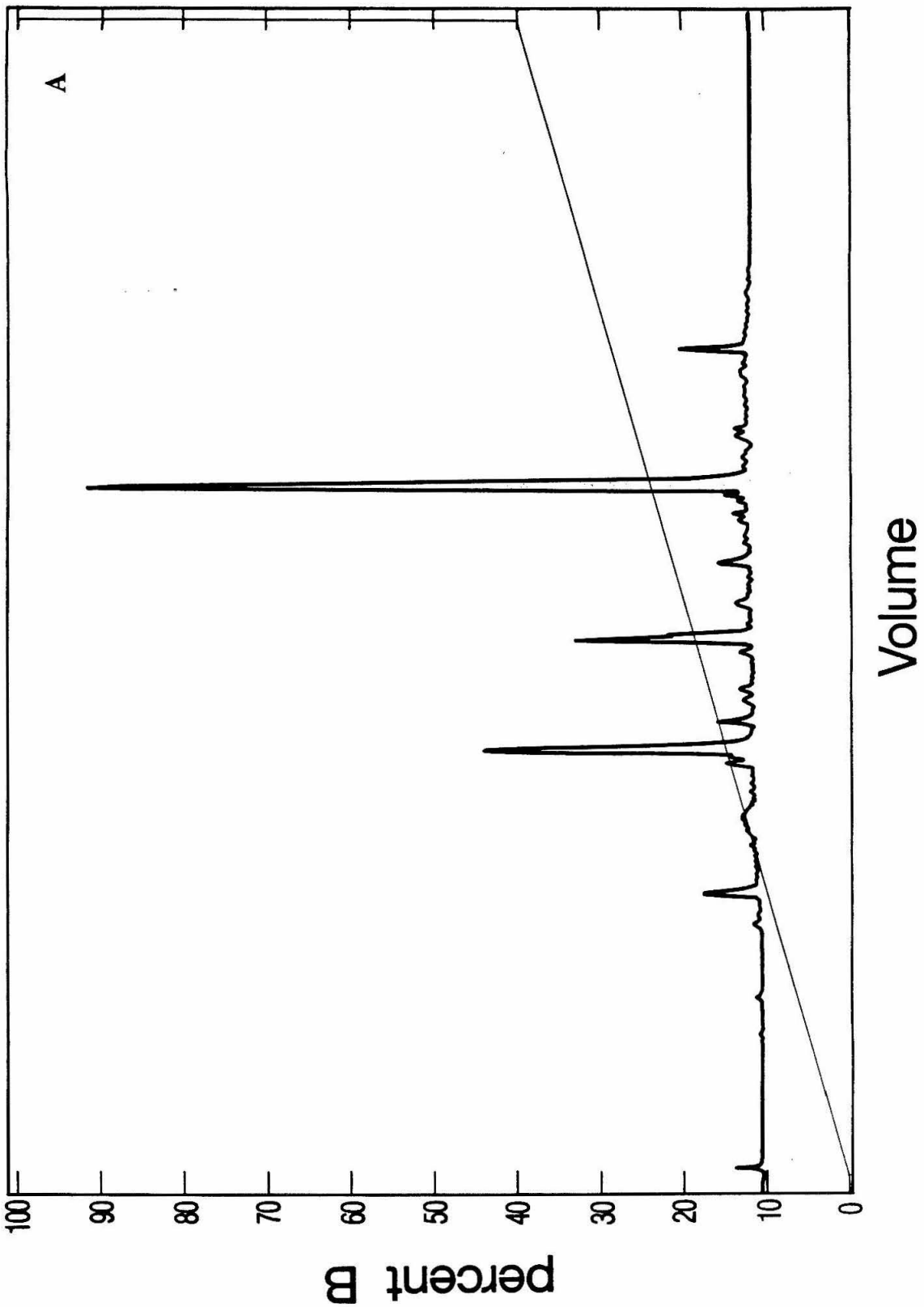
A
100
90
80
70
60
50
40
30
20
10
0
percent B
Volume

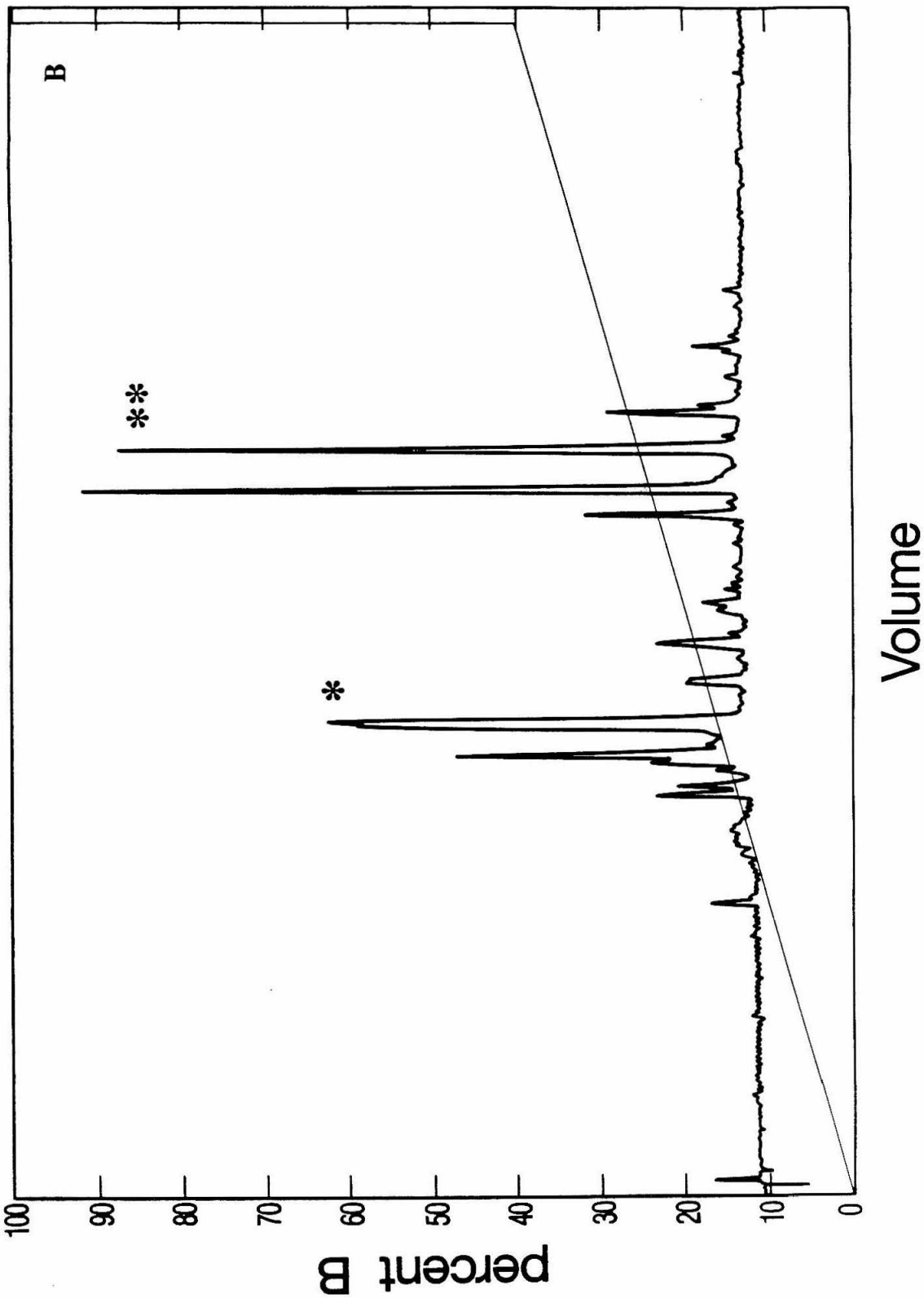
B
**
*
100
90
80
70
60
50
40
30
20
10
0
percent B
Volume

Figure 3.17 B) that contained the $Ru(bpy)_2(im)$HisX chromophore. Microsequencing (at the Caltech Biopolymer Synthesis and Analysis Resource Center) of the band marked by ** indicated the sequence Glu-Glu-Thr-Leu-Met-Glu-Tyr-Leu-Glu-Asn-Pro-His-Lys, corresponding to fragment T11 and confirming the site of modification at position 72. The band marked by * was recovered in far lower yield than the T11 peptide and only the first four N-terminal residues could be sequenced. The sequence, Leu-Glu-Asn-Pro, corresponds to an uncharacteristic secondary cleavage within the T11 peptide, perhaps due to overdigestion. This sequence is unique to the T11 peptide.

3. *Diethylpyrocarbonate Modification*

DEPC-modification studies of His72 cyt *c*, carried out as previously described, indicated the presence of approximately 2.5 solvent-accessible His residues. Modification of $Ru(bpy)_2(im)$His72 cyt *c* with DEPC indicated the presence of only one surface His residue. The analysis of the absorption data was again complicated due to concurrent growth of a 220 nm band that is only observed in the $Ru(bpy)_2(im)^{2+}$-modified proteins. Therefore, while the results of the DEPC-modifcation studies are consistent with the introduction of a new surface His residue in the His72 cyt *c* protein and the modification of a surface His residue with a Ru species as anticipated, they should only be considered as supporting evidence and not definitive proof. The absorption spectrum provides a more accurate assessment of the degree of $Ru(bpy)_2(im)^{2+}$ modification of a given derivative; spectra of bands A and B indicate unambiguously that these proteins are singly modified.

4. *Circular Dichroism Measurements : Melting Transition and Evidence for Δ and Λ Isomers*

Comparison of the CD spectra in the far UV region of native cyt *c* and His72 cyt *c* modification product bands A and B indicate that $Ru(bpy)_2(im)^{2+}$ modification of cyt *c* at

Figure 3.18 Far-UV circular dichroism spectra of native horse heart ferric cyt *c* (——), ferric Ru(bpy)$_2$(im)His72 cyt *c* (band A)(— · · · — · · ·), and ferric Ru(bpy)$_2$(im)His72 cyt *c* (band B) (used for ET experiments) (· · · · ·) in 25 mM NaPi, pH 7.0. Sample concentrations were 11 - 12 μM and spectra were obtained in a 0.1 cm pathlength cell on the 20 mdeg sensitivity scale at ambient temperature.

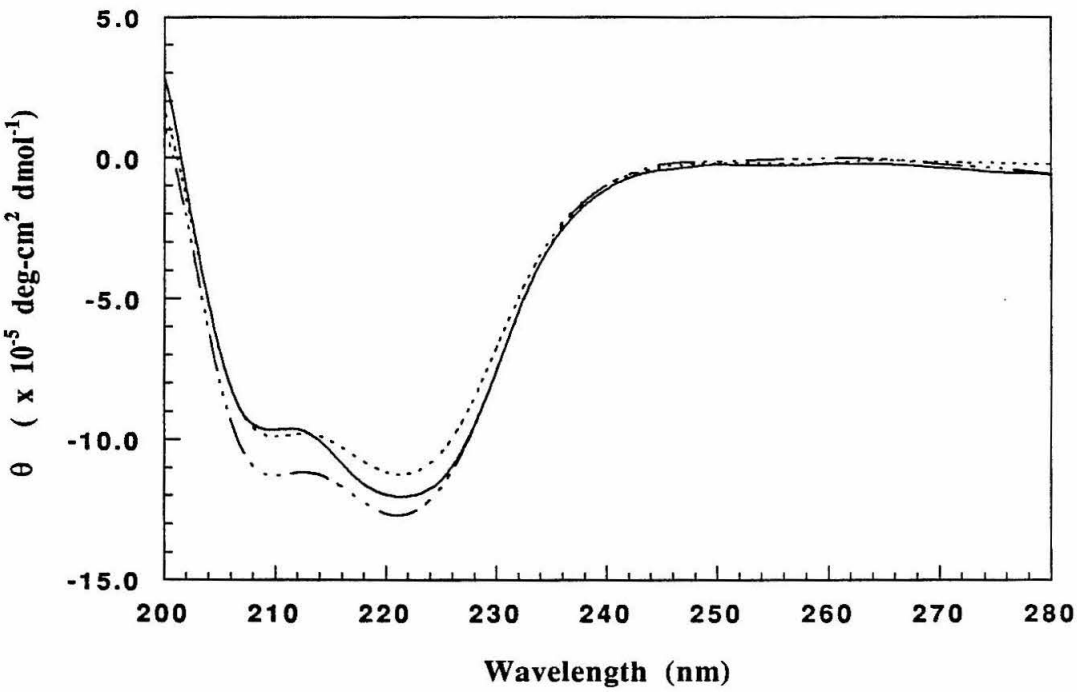
5.0
0.0
-5.0
-10.0
-15.0
θ (x 10-5 deg-cm2 dmol-1)
200
210
220
230
240
250
260
270
280
Wavelength (nm)

Figure 3.19 Circular dichroism spectra in the near-UV region of ferric $Ru(bpy)_2$(im)His72 cyt *c* (band A)(—···—···) , and ferric $Ru(bpy)_2$(im)His72 cyt *c* (band B) (used for ET experiments) (———) in 25 mM NaPi, pH 7.0. Sample concentrations were 11 - 12 μM and spectra were obtained in a 0.1 cm pathlength cell on the 20 mdeg sensitivity scale at ambient temperature.

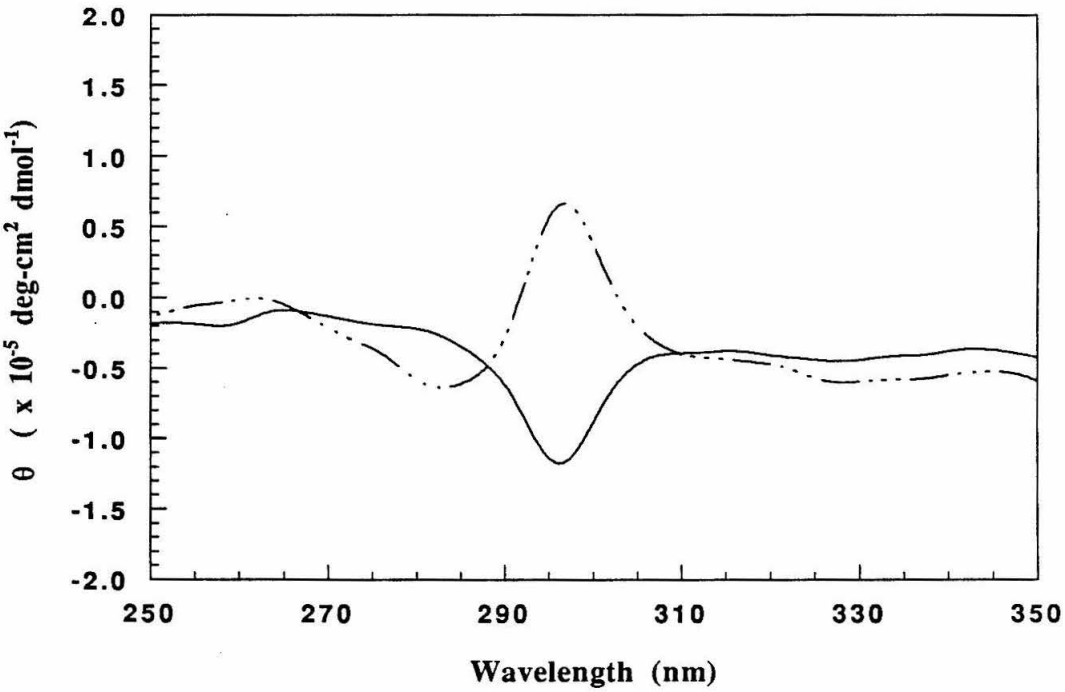
2.0
1.5
1.0
0.5
0.0
-0.5
-1.0
-1.5
-2.0
θ (x 10-5 deg-cm2 dmol-1)
250
270
290
310
330
350
Wavelength (nm)

position 72 causes negligible disruption of the protein secondary structure (Figure 3.18). The melting transition of ferric $Ru(bpy)_2(im)$His72 cyt *c* (band B) was determined by temperature-dependent CD at 222 nm and is ~80° C in 25 mM NaPi, pH 7.0, similar to the transition of ferric $Ru(bpy)_2(im)$His 33 cyt *c* and slightly lower than the unmodified His72 cyt *c* melting transition at 87° C. The measured melting transition was broader than normally observed, however this may be due to an experimental artifact present in the instrument at this time because the instrument baseline was sensitive to temperature. α-helical secondary structure was recovered upon cooling the denatured sample to 25° C, indicating that the melting transition is also reversible, as observed with the His33 modified protein.

The CD spectrum observed in the 280 nm region for the two His72-modified proteins suggests that they are related stereoisomers, as concluded for the His33-modified proteins. A positive Cotton effect was observed at ~296 nm for band A and a negative Cotton effect for band B at this wavelength (Figure 3.19). Therefore, based on the previous discussion, band A is assigned as the Λ-$Ru(bpy)_2(im)$His72 cyt *c* isomer and band B (used for ET studies) as the Δ-$Ru(bpy)_2(im)$His72 cyt *c* isomer. Future references to $Ru(bpy)_2(im)$His72 cyt *c* refer to the Δ isomer unless otherwise indicated.

5. *Electron-Transfer Studies*

The steady-state emission spectrum of ferric $Ru(bpy)_2(im)$His72 cyt *c* was measured at room temperature in 50 mM NaPi, pH 7.0 (Figure 3.20). The luminescence was weak and not detectable by eye. The uncorrected emission maximum at 670 nm corresponds well with that observed in the $Ru(bpy)_2(im)_2^{2+}$ model compound.[10b]

Luminescence decay and transient absorption measurements on the $Ru(bpy)_2(im)$His72 labeled derivative were made as discussed in General Methods. The excited state lifetimes, as fit from the luminescence decay data at 650 nm, were essentially identical in each redox state, $k_d = 1.40(5) \times 10^7\ s^{-1}$ ($\tau = 71$ ns) for both ferric

Figure 3.20 Steady-state emission spectrum of ferric $Ru(bpy)_2(im)$His72 cyt *c* (band B), 35 μM in 50 mM NaPi, pH 7.0, 27° C ((uncorrected (——); corrected (- - - -)). The excitation wavelength was 436 nm with the Hg/Xe lamp. The sensitivity was 0.050 mV, the time constant was 1.0 s, taken with 1 nm resolution.

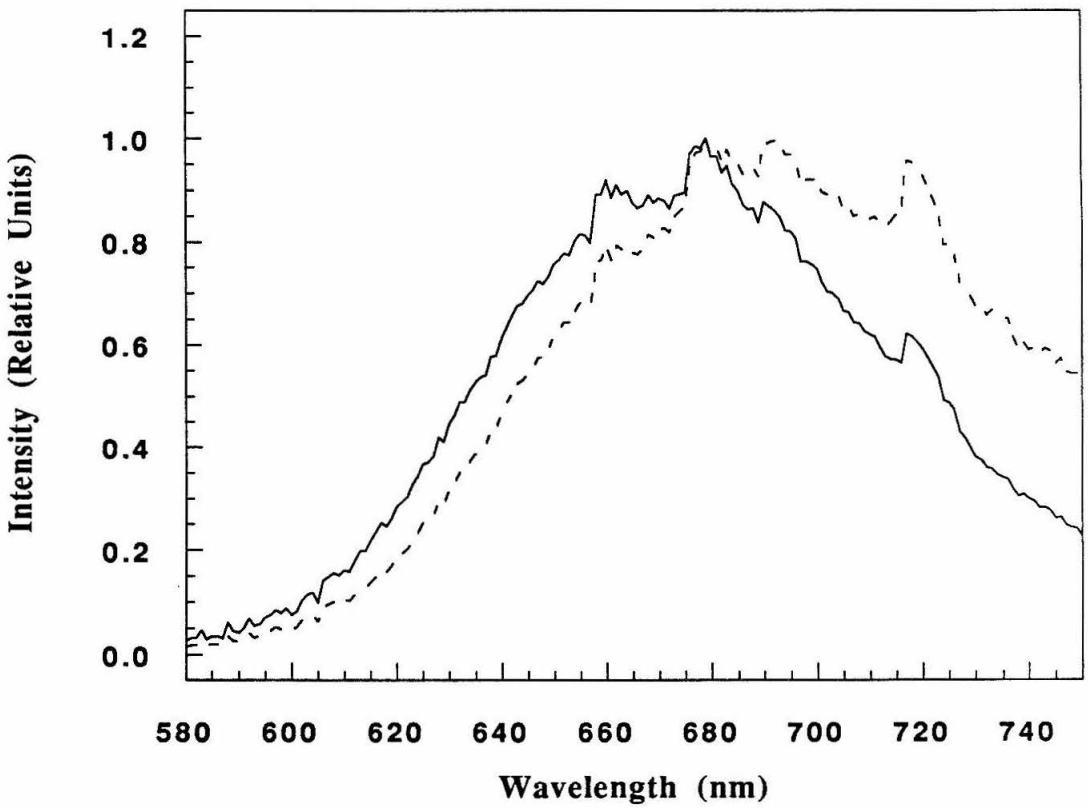
Intensity (Relative Units)
1.2
1.0
0.8
0.6
0.4
0.2
0.0
580
600
620
640
660
680
700
720
740
Wavelength (nm)

and ferous Ru(bpy)$_2$(im)His72 cyt *c*. The convolved fit of the luminescence decay data for the ferric protein is shown in Figure 3.21.

Flash / quench and photoinduced techniques were used to acquire data for the determination of the Fe^{2+} to Ru^{3+} (k_{ET}^{mm}) ET rate. A control experiment was performed to insure that the Ru(bpy)$_2$(im)His72^{3+} species formed by Rua_6^{3+} redox quenching of the *Ru(bpy)$_2$(im)His72 excited state was stable in the absence of an ET pathway with the heme. In Figure 3.22, transient absorption data obtained at 504 nm is presented for a sample of *ferric* Ru(bpy)$_2$(im)His72^{2+} cyt *c* (11.3 μM in 50 mM NaPi, pH 7.0) with 20 mM Rua_6^{3+}. As demonstrated by the flat trace, the Ru(bpy)$_2$(im)His72^{3+} species generated by the excited state redox quenching does not react with any other site on the protein, and is entirely stable on the timescale of observed ET kinetics. Recovery of the ferrous Ru(bpy)$_2$(im)$^{2+}$-modified protein on a long timescale is achieved by the bimolecular Rua_6^{2+} to ferric protein ET, which is retarded due to the low concentration of these species.

A full analysis of 16 data sets from both the direct photoinduced and flash / quench experiments at 550 and 395 (or 400) nm fit to both single and double exponentials (to fit the fast minor component due to excited state decay) led to the calculation of a Fe^{2+} to Ru^{3+} ET rate of 9.0(3) x 10^5 s^{-1}. Identical kinetics were observed in the flash / quench experiment at wavelengths corresponding to $Ru^{3+/2+}$ (504 and 306 nm) and heme ET. Data obtained at 550, 504, and 395 nm for the flash / quench experiments are shown in Figure 3.23. Data from the photoinduced experiments and at 550, 395 and 306 nm are presented in Figure 3.24.

The rate for photoinduced ET (k_{ET}*) was calculated as described from three full data sets (transient absorption at 370, 395, and 550 nm). The data obtained at 370 nm used to calculate the concentration of excited state obtained was fit convolved with the laser pulse (Figure 3.25). Kinetic measurements at 306 nm confirmed that identical ET

Figure 3.21 Luminescence decay of a 15 μM sample of ferrous $Ru(bpy)_2(im)$His72 cyt *c* in 50 mM NaPi, pH 7.0 observed at 650 nm following excitation at 480 nm (2 mJ pulse). The smooth line is the fit to a single exponential decay function convolved with the instrument response (shown); $k_d = 1.40(5) \times 10^7\ s^{-1}$.

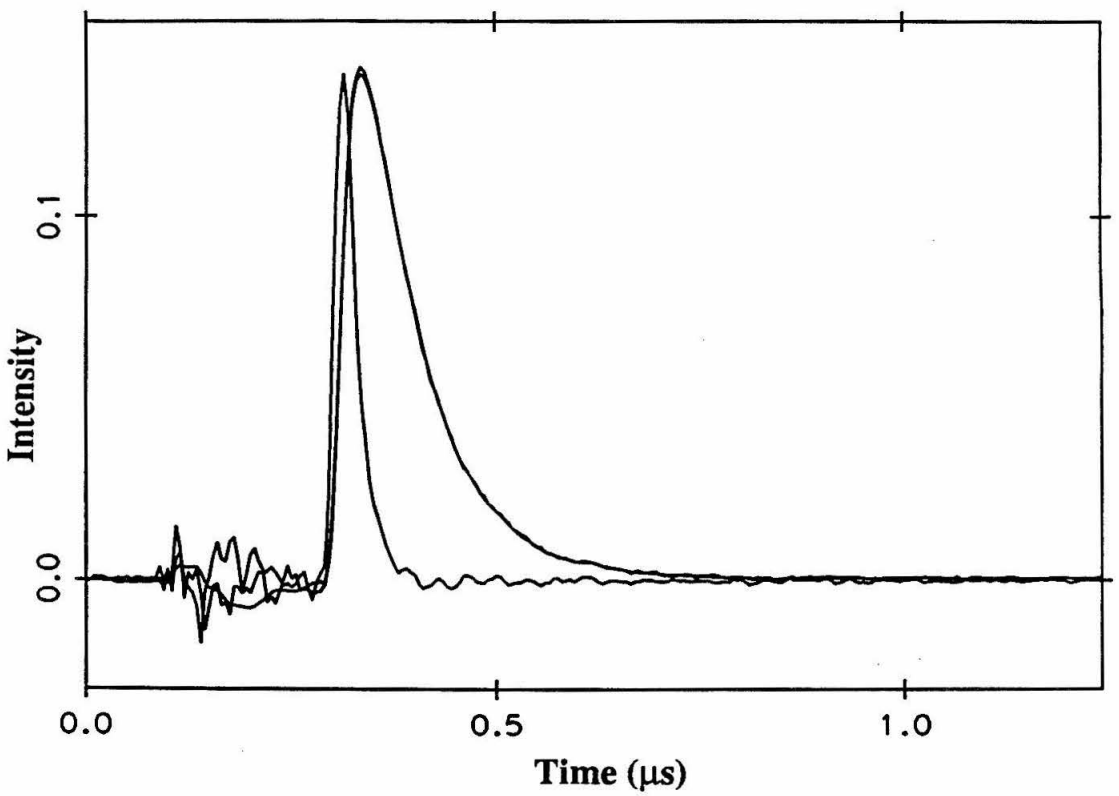
Intensity
0.1
0.0
0.0
0.5
1.0
Time (μs)

Figure 3.22 Transient absorption kinetics at 504 nm following laser flash excitation (480 nm, 25 ns, 2 mJ) of $Ru(bpy)_2(im)His72^{2+}$ - Fe^{3+} cyt *c* (11 μM) and Rua_6^{3+} (20 mM) in 50 mM NaPi, pH 7.0, at room temperature. The transiently generated $Ru(bpy)_2His72^{3+}$ - Fe^{3+} cyt *c* species is present in solution for up to 0.1 s before bimolecular back reaction to the initial redox states can begin to be detected.

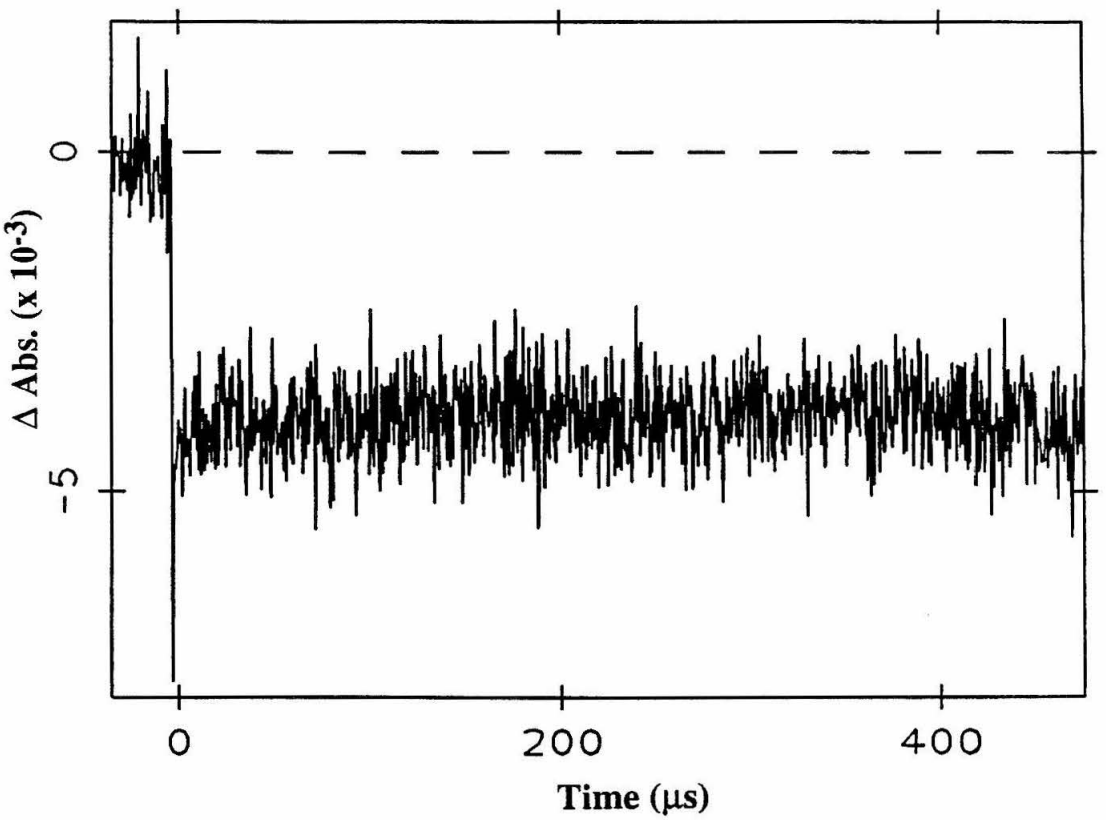
0
-5
Δ Abs. (x 10-3)
0
200
400
Time (μs)

Figure 3.23 Transient absorption kinetics at various wavelengths following laser flash excitation (480 nm, 25 ns, 2 mJ) of $Ru(bpy)_2(im)His72^{2+}$-Fe^{2+} cyt *c* with Rua_6^{3+} in 50 mM NaPi, pH 7.0, at room temperature. The decay corresponds to the production of $Ru(bpy)_2(im)His72^{2+}$ - Fe^{3+} cyt *c* due to intramolecular ET from Fe^{2+} to Ru^{3+} at a rate of 9.0×10^5 s^{-1}. Smooth lines correspond to fits to either a single (k_{ET}^{mm} (k_1) = 9.0×10^5 s^{-1}) or biexponential decay function (k_{ET}^{mm} (k_1) = 9.0×10^5 s^{-1} and $k_d = k_2$ (k_d = ~1.7×10^7 s^{-1} due to the presence of excited-state quencher). The sample concentration and coefficients for the rate terms are given. (A) 550 nm, 13.9 μM protein, 5 mM Rua_6^{3+}, c_1 = 0.0095, c_2 = -0.019. (B) 395 nm, 13.9 μM protein, 5 mM Rua_6^{3+}, c_1 = -0.019, c_2 = 0.033. (C) 504 nm, 13.9 μM protein, 5 mM Rua_6^{3+}, c_1 = -0.0041, c_2 = -0.046.

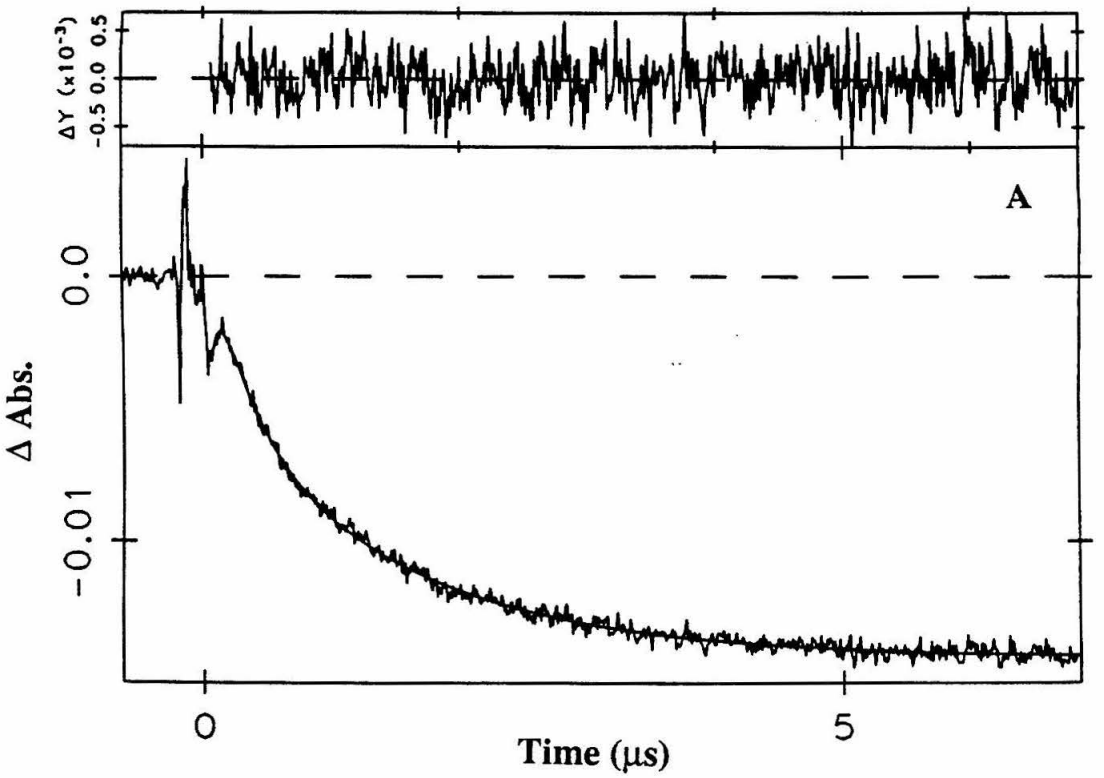
ΔY (x10⁻³)
-0.5 0.0 0.5
A
0.0
-0.01
Δ Abs.
0
5
Time (μs)

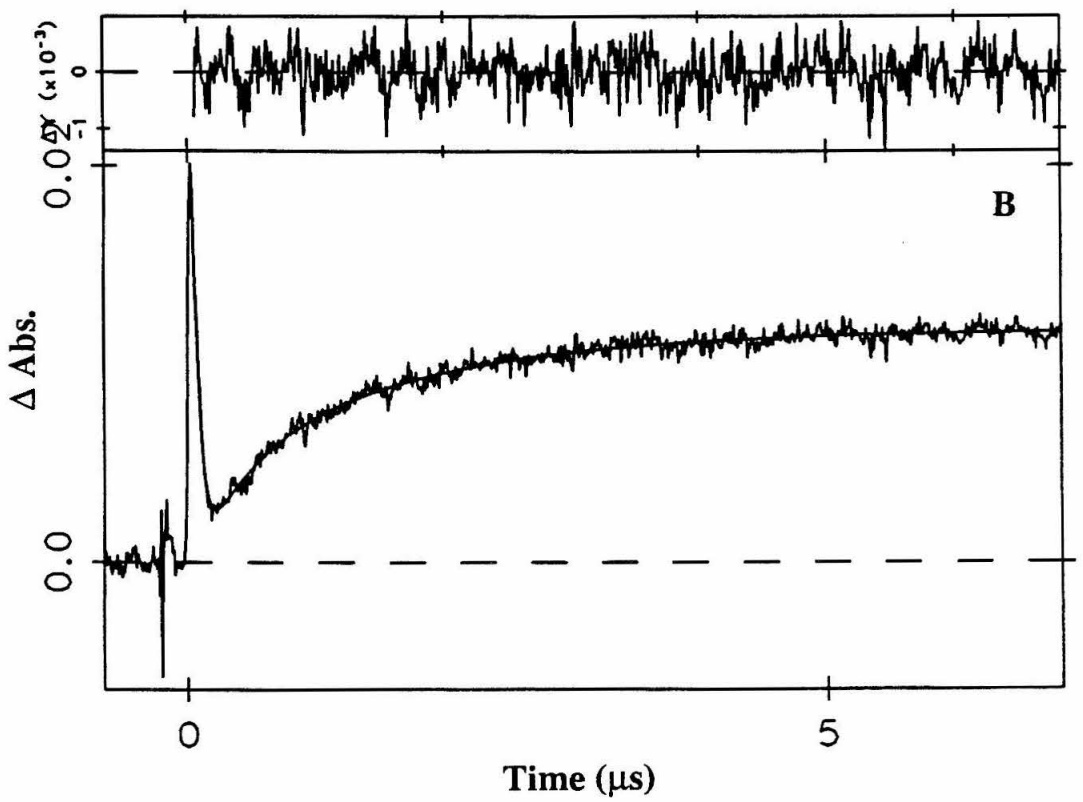
ΔY (x10⁻³)
0
-1
B
0.02
0.0
Δ Abs.
0
5
Time (μs)

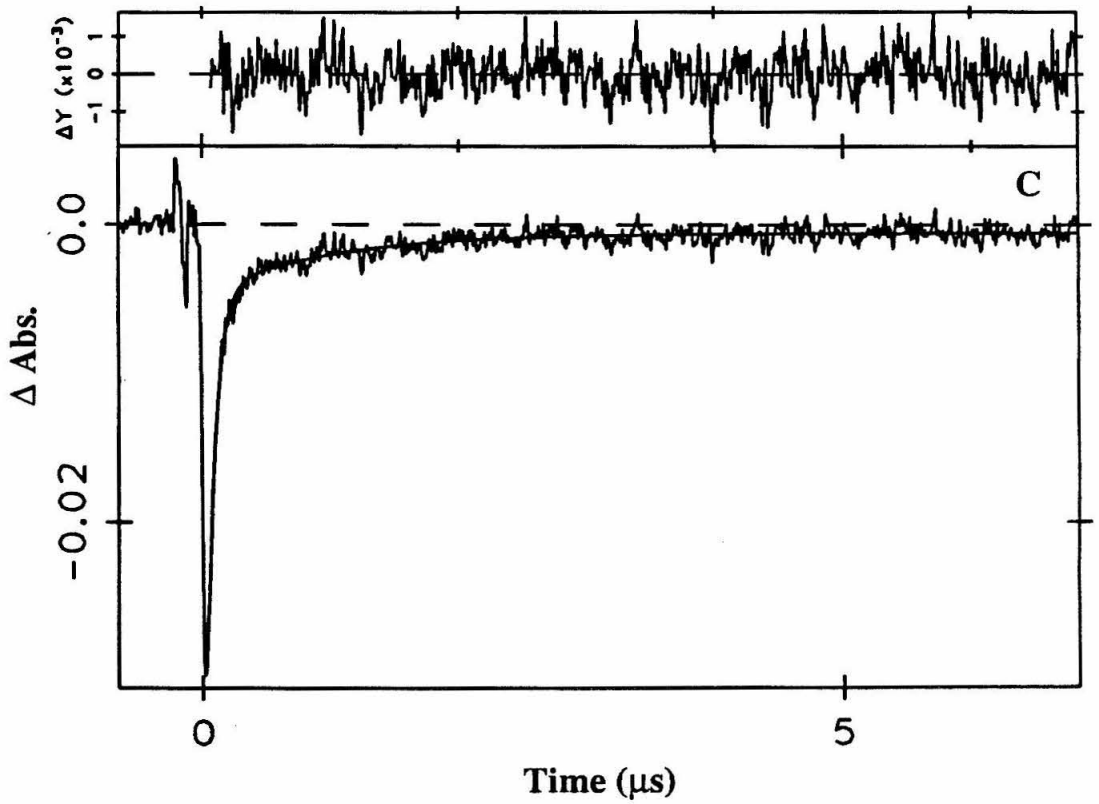
ΔY (x10⁻³)
-1
0
1
C
0.0
Δ Abs.
-0.02
0
5
Time (μs)

Figure 3.24 Transient absorption kinetics at various wavelengths following laser flash excitation (480 nm, 25 ns, 2 mJ) of $Ru(bpy)_2(im)His72^{2+}$ - Fe^{3+} cyt *c* in 50 mM NaPi, pH 7.0, at room temperature. The rise corresponds to production of ferrous cyt *c* due to photoinduced ET (at 306 nm, also due to excited-state formation). The decay corresponds to the production of $Ru(bpy)_2(im)His72^{2+}$ - Fe^{3+} cyt *c* due to intramolecular ET from Fe^{2+} to Ru^{3+} at a rate of 9.0×10^5 s^{-1}. Smooth lines correspond to fits to a biexponential decay function (k_{ET}^{mm} (k_1) = 9.0×10^5 s^{-1} and k_d (k_2) = 1.40×10^7 s^{-1}). The sample concentration and coefficients for the rate terms are given. (A) 550 nm, 12.2 μM protein, $c_1 = 0.0028$, $c_2 = -0.0039$. (B) 395 nm, 12.2 μM protein, $c_1 = -0.0025$, $c_2 = 0.020$. (C) 306 nm, 12.2 μM protein, $c_1 = 0.0029$, $c_2 = 0.035$.

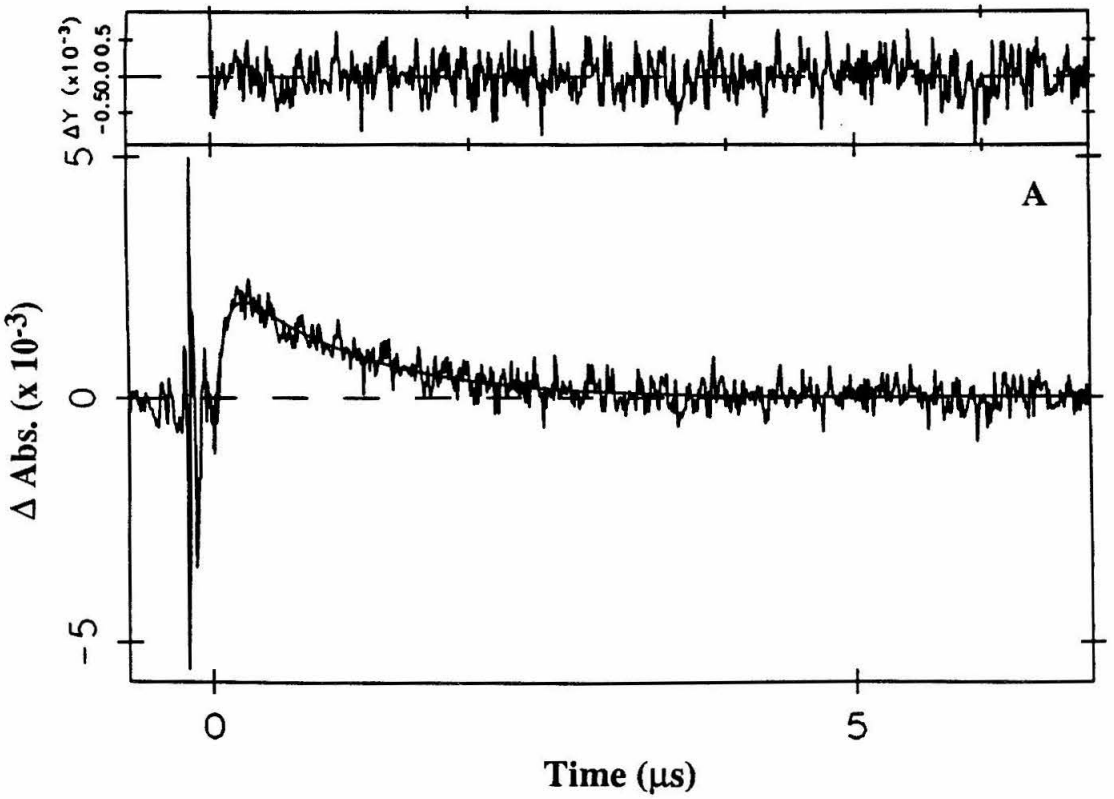
ΔY (x10⁻³)
5
-0.5 0.0 0.5
A
Δ Abs. (x 10⁻³)
5
0
-5
0
5
Time (μs)

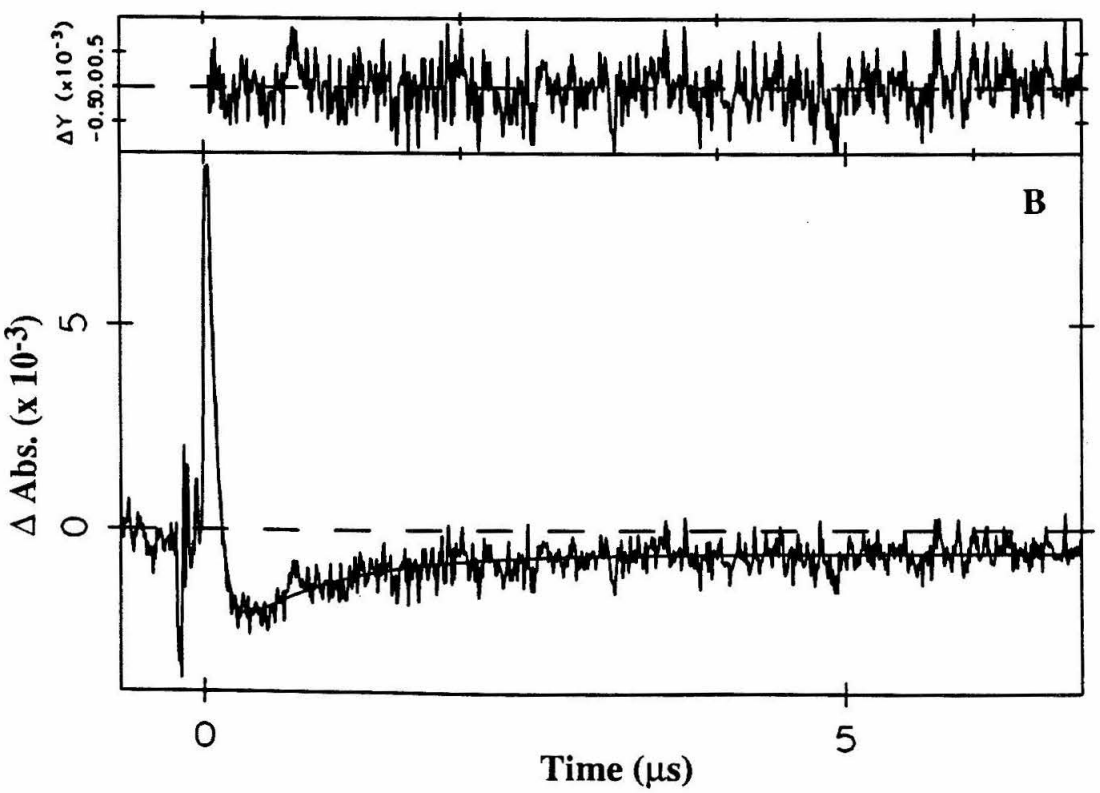
ΔY (x10⁻³)
-0.5 0.0 0.5
B
Δ Abs. (x 10⁻³)
5
0
0
5
Time (μs)

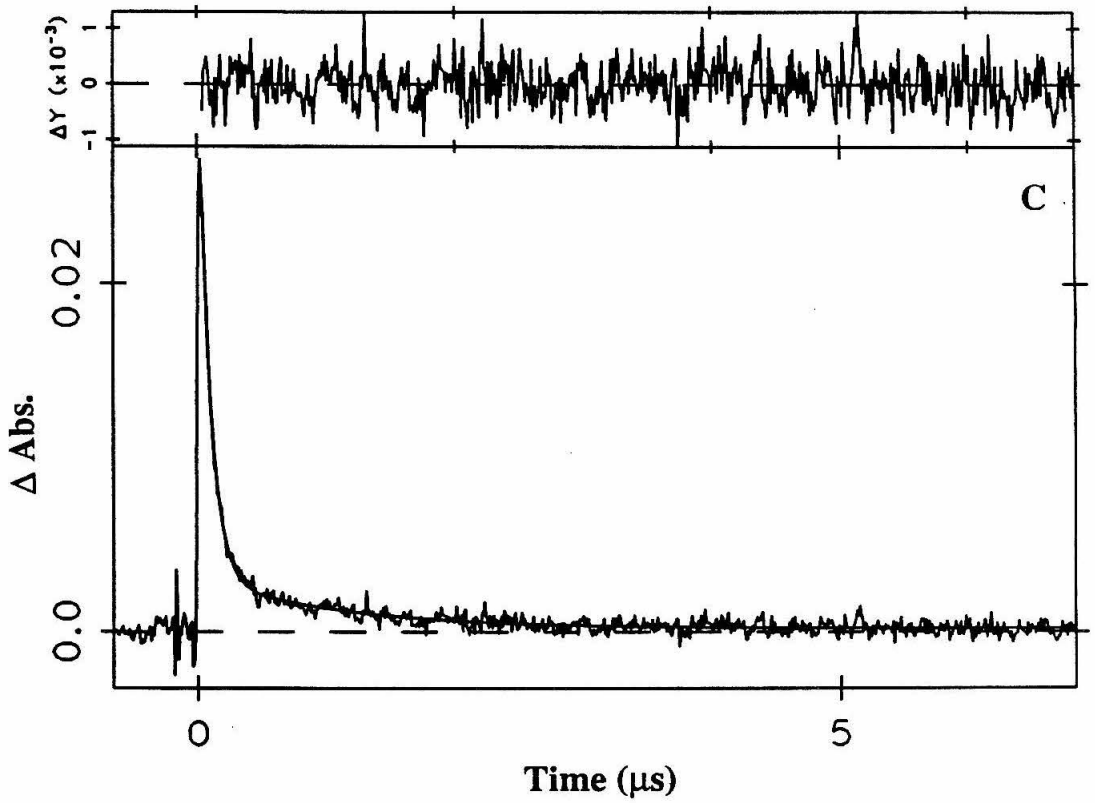
ΔY (x10⁻³)
1
0
-1
C
0.02
0.0
Δ Abs.
0
5
Time (μs)

Figure 3.25 Transient absorption kinetics at 370 nm following laser flash excitation (480 nm, 25 ns, 2 mJ) of $Ru(bpy)_2(im)His72^{2+}$ - Fe^{3+} cyt *c*, 12.2 μM in 50 mM NaPi, pH 7.0, at room temperature. The smooth line is the fit to a single exponential decay function convolved with the instrument response. The decay corresponds to the decay of the $*Ru(bpy)_2(im)His72^{2+}$ excited state ($k_d = 1.40 \times 10^7\ s^{-1}$, $c_1 = 0.067$).

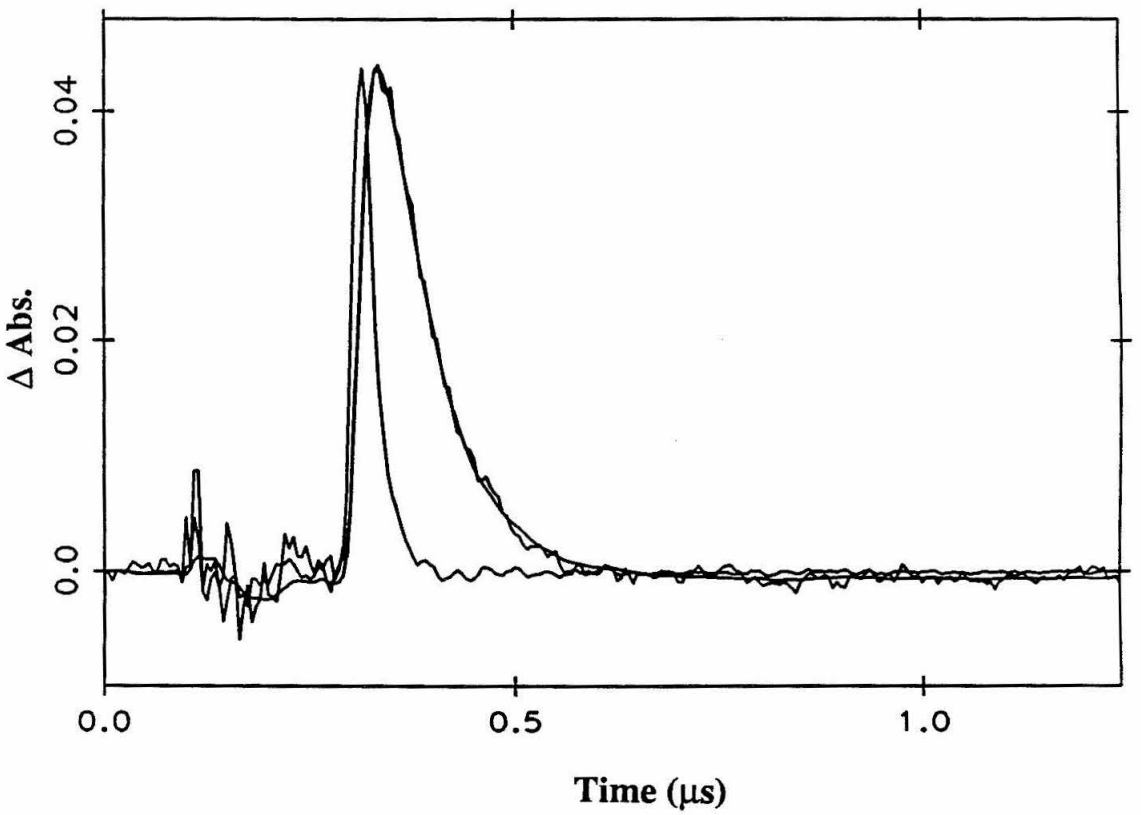
Δ Abs.
0.04
0.02
0.0
0.0
0.5
1.0
Time (μs)

kinetics are observed for Ru^{3+} reduction. Based on these data, a rate constant for $*Ru^{2+}$ to Fe^{3+} ET of 3.4(7) x 10^5 s^{-1} is calculated.

The metal-to-metal Fe^{2+} to Ru^{3+} ET rate was studied using the flash / quench methodology as a function of applied hydrostatic pressure in collaboration with Prof. Rudi van Eldik of the University of Witten / Herdecke. The experimental set up for transient absorption is identical with that described for the experiments at atmospheric pressure except the sample cell is replaced with a cylindrical 2 cm quartz pathlength pillbox cell contained in a thermostated high pressure vessel constructed with titanium sapphire windows .[30] Pressures of up to 1500 atm can be applied to the sample using a hydraulic pressure apparatus. ET measurements were made at four pressures (1, 500, 1000, and 1500 atm), allowing the sample to equilibrate at each new pressure for 45 minutes. The pressure cell scattered significantly more laser light than the standard precision cuvettes, necessitating the use of a 550 nm interference filter for detection thereby limiting data collection to this wavelength. The scattered light also complicated data analysis.

Parallel flash / quench studies conducted by Dr. I-Jy Chang measuring k_{ET}^{mm} in $Ru(bpy)_2(im)His33$ cyt *c* showed negligible pressure dependence of observed rate constant in the 1 - 1500 atm regime. The redox potential of horse heart cyt *c* increases monotonically as a function of applied pressure, and at 1500 atm is 40 mV higher than at atmospheric pressure.[31] However, this slight change in driving force has an insubstantial effect on the observed rate constant. The results obtained with $Ru(bpy)_2(im)His33$ cyt *c* are in contrast to results obtained in Ru_5His33 cyt *c* using pulse radiolysis to initiate ET.[32] In the Ru_5His33 cyt *c* system, the volume of activation ($\Delta V^{\ddagger}$) associated with the ET is -16 to -18 cm^3/mole. However, this activation volume could be almost entirely attributed to the $\Delta V^{\ddagger}$ of the Ru_5His label due to an increase in solvent electrostriction around the ruthenium center. The Fe^{2+} to $Ru(bpy)_2(im)His72$ ET rate showed a weak

pressure dependence; Figure 3.26 shows fits of kinetic traces at increasing pressures. Data are summarized in Table 3.3 and plotted in Figure 3.27 A.

Table 3.3. Summary of Fe^{2+} to $Ru(bpy)_2(im)His72^{3+}$ ET rates as a function of applied pressure (20 μM protein in 50 mM NaPi, 7 mM Rua_6^{3+}, 25° C).

Pressure (atm)	Rate (s^{-1})
1	1.03×10^6
500	1.12×10^6
1000	1.35×10^6
1500	1.43×10^6

Although a linear relationship between applied pressure and rate is observed, the effect is small (a factor of 1.5 in rate constant) and the inherent error in the fits precludes serious interpretation of the data beyond the conclusion of a weak pressure dependence in the ferrous heme to $Ru(bpy)_2(im)His72^{3+}$ ET rate that is not observed in the ferrous heme to $Ru(bpy)_2(im)His33^{3+}$ ET rate. An the activation volume can be calculated from:[33]

$$\left(\frac{\partial \ln k_{ET}}{\partial P}\right)_T = \frac{-\Delta V^{\ddagger}}{RT}$$

P is pressure in atm, T is temperature in K, and R is the gas constant. A plot of $\ln k_{ET}$ as a function of pressure is presented in Figure 3.27 B. A linear least squares fit (correlation coefficient = 0.98) gives an apparent value of $\Delta V^{\ddagger} = -6(2)$ cm^3/mole. Since a negative $\Delta V^{\ddagger}$ is exactly opposite to that expected on the basis of a decrease in electrostriction during reduction of the ruthenium moiety, the increase in rate constant is attributed to a pressure-mediated increase in electronic coupling due to compression of the protein structure with pressure. The rate increase corresponds to a 0.1 Å increase in the space jumps of the His72-heme tunneling pathway (*vide infra*).

Figure 3.26 Transient absorption kinetics at 550 nm following laser flash excitation (480 nm, 25 ns, 2 mJ) of 20 μM $Ru(bpy)_2(im)His72^{2+}$ - Fe^{2+} cyt *c* with 7 mM Rua_6^{3+} in 50 mM NaPi, pH 7.0, 25° C, as a function of applied pressure. The decay corresponds to the production of $Ru(bpy)_2(im)His72^{2+}$ - Fe^{3+} cyt *c* due to intramolecular ET from Fe^{2+} to Ru^{3+} (k_{ET}^{mm}). Smooth lines correspond to fits to a biexponential decay function ($k_{ET}^{mm} = k_1$ and $k_2 = 3.0 \times 10^7$ s^{-1}, due to excited state decay and scattered light). The applied pressure, Fe^{2+} to Ru^{3+} rate constant, and coefficients for the rate terms are given. (A) 1 atm, 1.03×10^6 s^{-1}, $c_1 = 0.012$, $c_2 = -0.022$. (B) 500 atm, 1.12×10^6 s^{-1}, $c_1 = 0.012$, $c_2 = -0.029$. (C) 1000 atm, 1.35×10^6 s^{-1}, $c_1 = 0.013$, $c_2 = -0.038$. (D) 1500 atm, 1.43×10^6 s^{-1}, $c_1 = 0.012$, $c_2 = -0.072$.

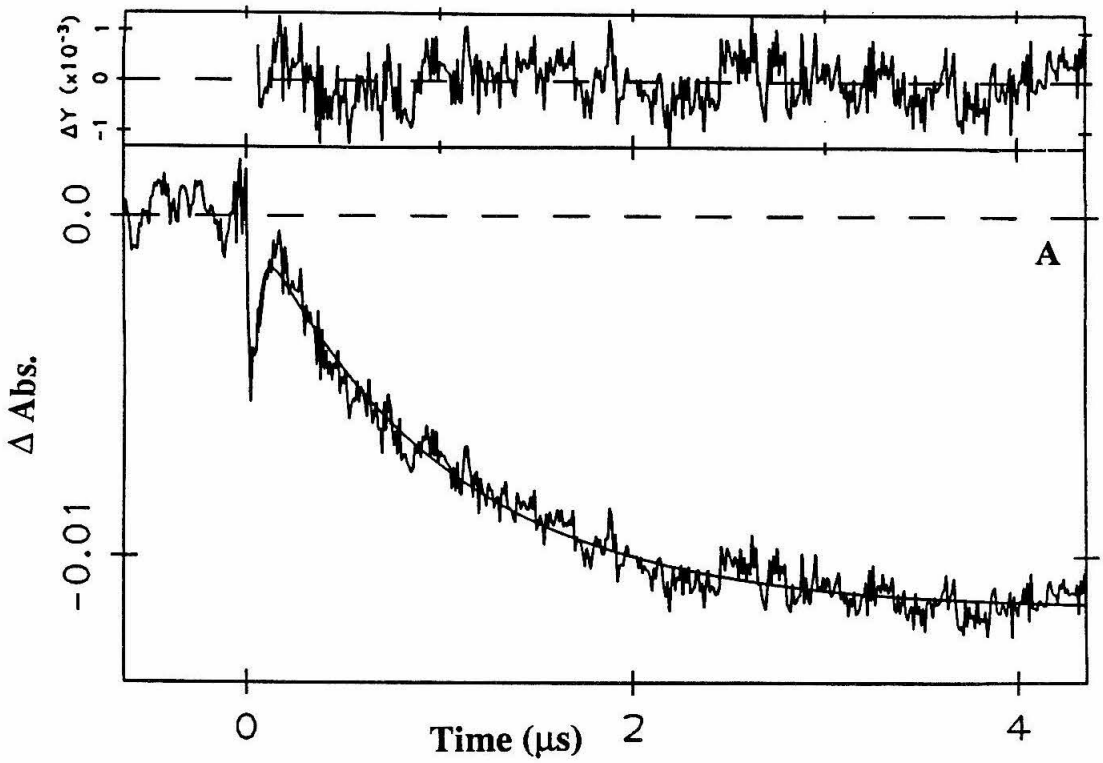
ΔY (x10⁻³)
1
0
-1
0.0
A
Δ Abs.
-0.01
0
Time (μs)
2
4

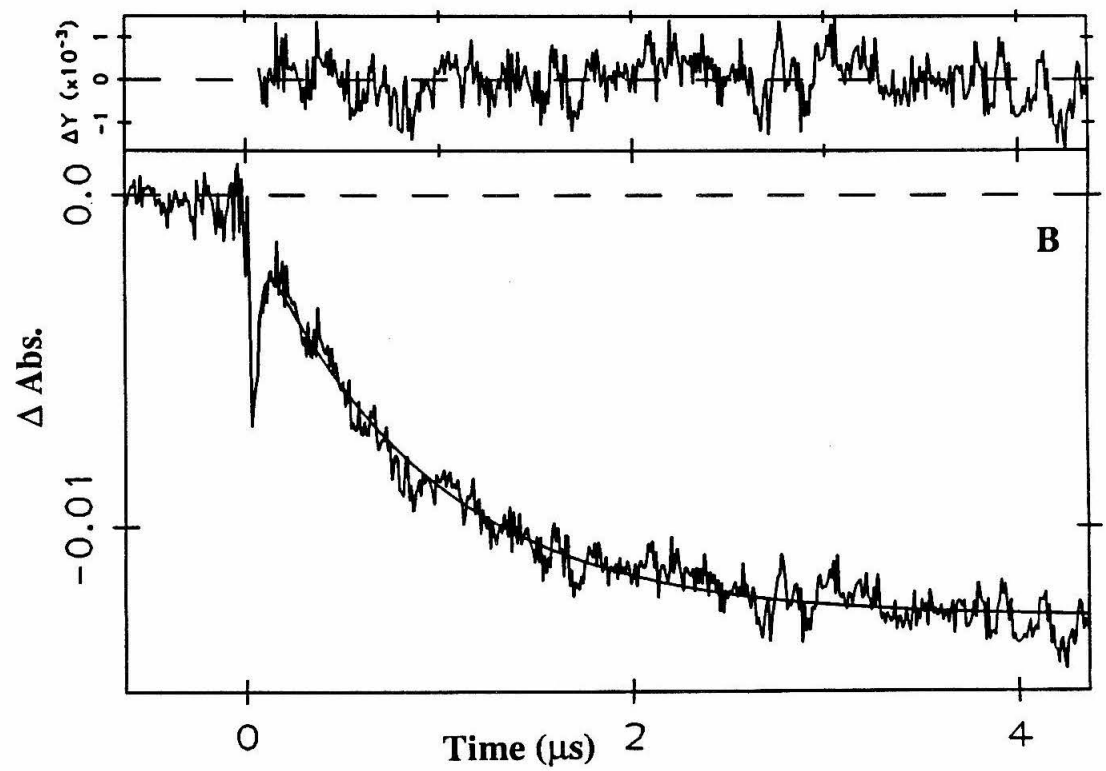
ΔY (x10⁻³)
1
0
-1
0.0
B
Δ Abs.
-0.01
0
Time (μs)
2
4

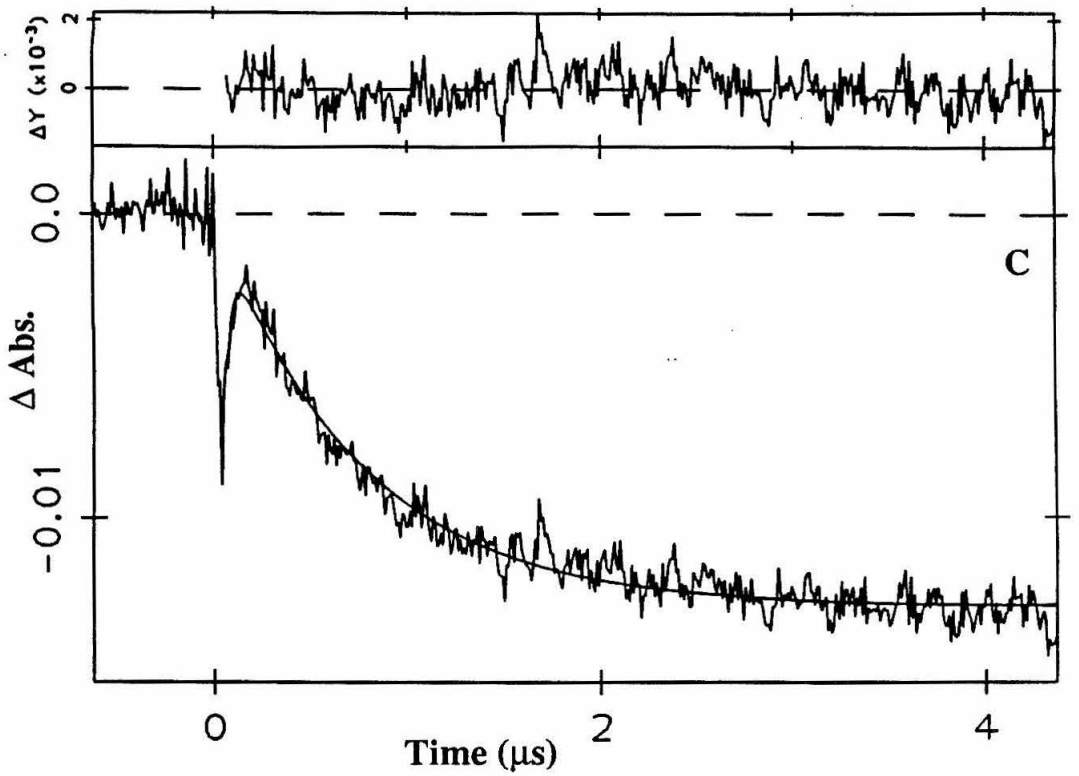
ΔY (x10⁻³)
2
0
0.0
C
Δ Abs.
-0.01
0
2
4
Time (μs)

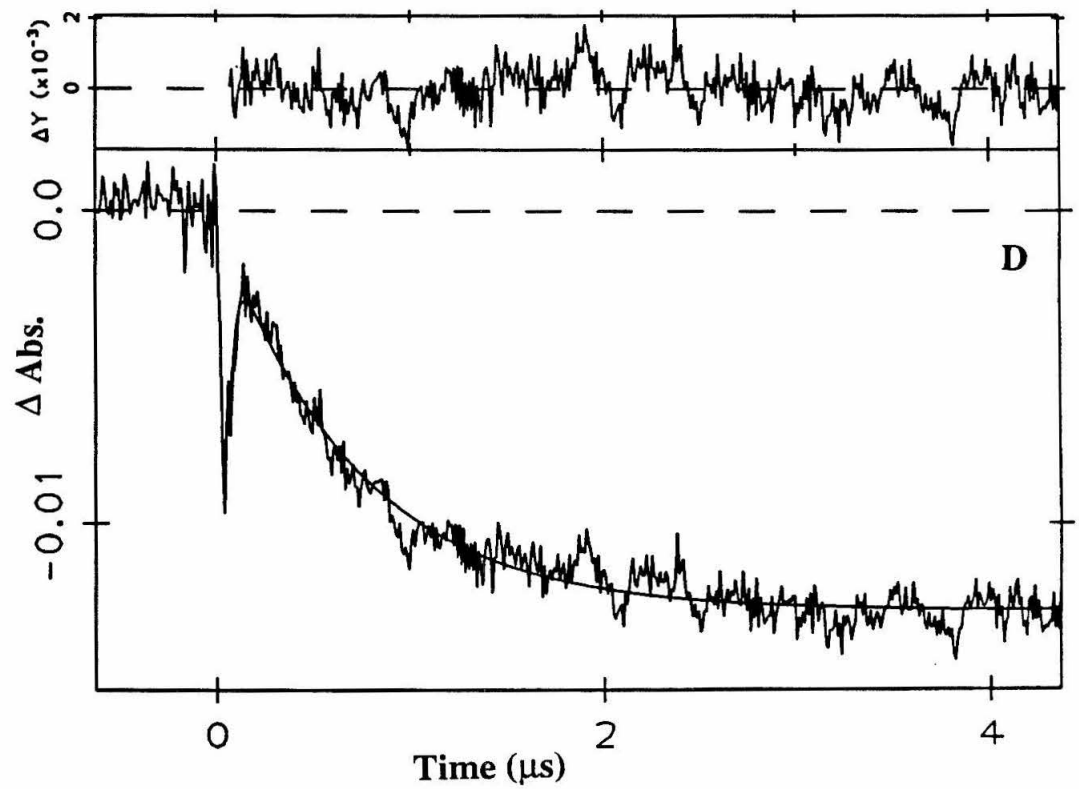
ΔY (x10⁻³)
2
0
0.0
D
Δ Abs.
-0.01
0
2
4
Time (μs)

Figure 3.27 (A) Plot of Fe^{2+} to Ru^{3+} ET rates in $Ru(bpy)_2(im)His72$ cyt *c* as a function of applied pressure. (B) Plot and linear least squares fit of ln k_{ET}^{mm} as a function of pressure.

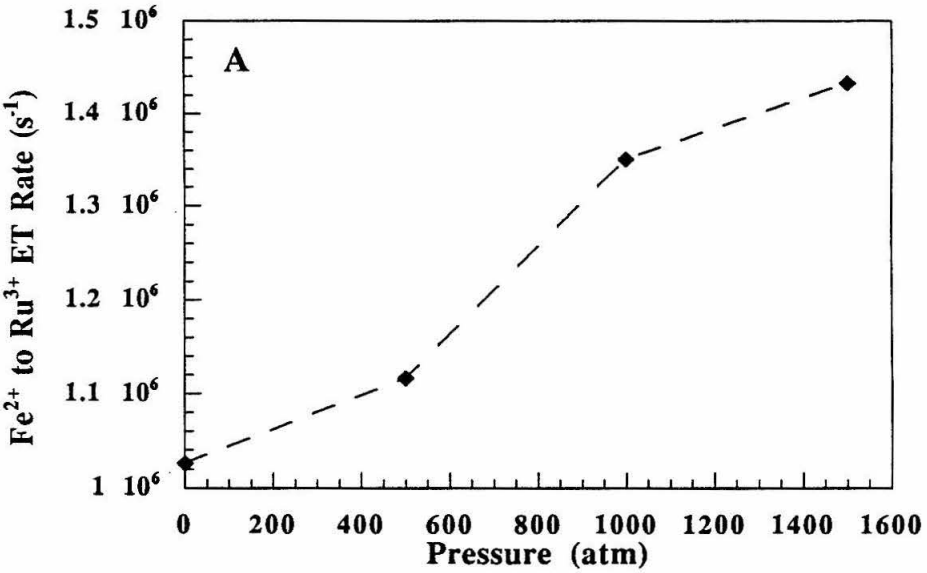
A
1.5 10^6
1.4 10^6
1.3 10^6
1.2 10^6
1.1 10^6
1 10^6
Fe2+ to Ru3+ ET Rate (s-1)
0
200
400
600
800
1000
1200
1400
1600
Pressure (atm)

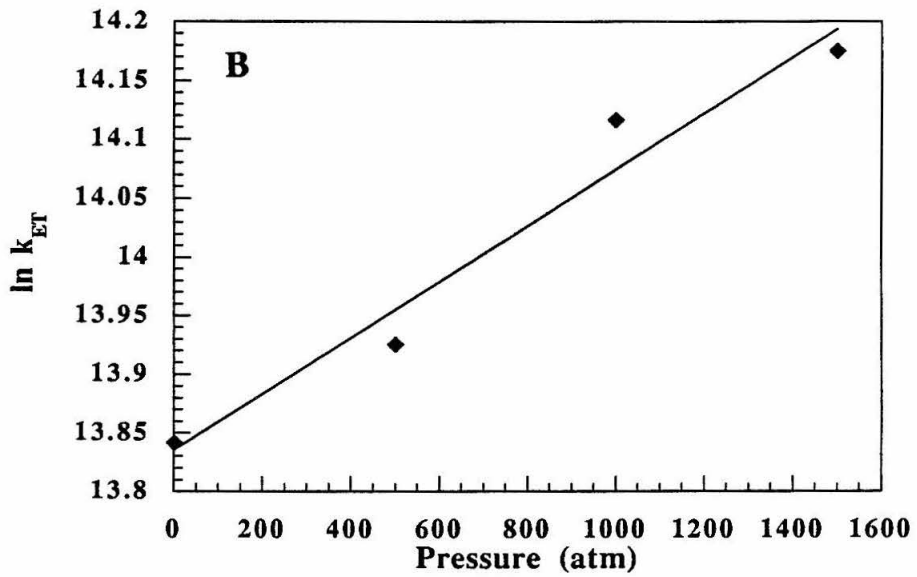
B
14.2
14.15
14.1
14.05
14
13.95
13.9
13.85
13.8
ln kET
0
200
400
600
800
1000
1200
1400
1600
Pressure (atm)

D. Ru(bpy)$_2$(im)His39 cyt c (Candida krusei)

Native *C. k.* cyt *c* was modified with Ru(bpy)$_2$(im)$^{2+}$ at position 39 and electron transfer studies carried out in collaboration with Dr. Morten J. Bjerrum, a Carlsberg Foundation Scholar visiting the Beckman Institute for 1990 -1991.

1. Ru(bpy)$_2$(im)$^{2+}$-Modification Reaction

Typically, 0.5 mM purified protein in 25 mM NaPi, pH 7.0 was reacted with 2 mM Ru(bpy)$_2$(CO_3) following the protocol detailed in the General Methods section. For the first reaction, aliquots were removed and analyzed, following imidazole treatment, by analytical cation-exchange chromatography (FPLC Mono S 5/5). Only one singly modified band was observed to develop at early reaction times, followed at long reaction times by two multiply modified protein products. A representative chromatogram is presented in Figure 3.28 The first band, eluting at the column void volume, is Co(EDTA)$^-$, added to fully oxidize the protein. The subsequent bands correspond to unmodified protein, singly modified protein (major product), followed by the two multiply modified products. Based on prior results obtained from ruthenium ammine modifications of the *C. k.* native and Zn porphyrin proteins indicating that His39 is far more reactive to modification than His33,[5] the singly modified product was identified as Ru(bpy)$_2$(im)His39 cyt *c*. Optimal reaction time for obtaining singly modified product is 15 hours, followed by 48 hours of treatment with 2M imidazole prior to purification. The product was purified to homogeneity prior to laser experiments. The Δ and Λ isomers of yeast Ru(bpy)$_2$(im)HisX cyts *c* do not appear to be separable by cation-exchange chromatography (an observation consistent with the work of Danilo R. Casimiro[34]).

2. Electron-Transfer Studies

Luminescence decay and transient absorption measurements were made as

Figure 3.28 Typical cation-exchange (FPLC Mono S 16/10, flow rate of 6.0 ml/min) chromatogram for the *C. k.* His39 cyt *c* modification reaction with $Ru(bpy)_2(CO_3)$ reaction products in 25 mM NaPi, pH 7.0. Gradient represents the concentration of NaCl in mM. The first band, eluting at the column void volume, is $Co(EDTA)^-$. The subsequent bands correspond to unmodified protein, singly modified protein (major product), and two multiply modified products. Detection is on the 2.0 absorbance scale at 405 nm.

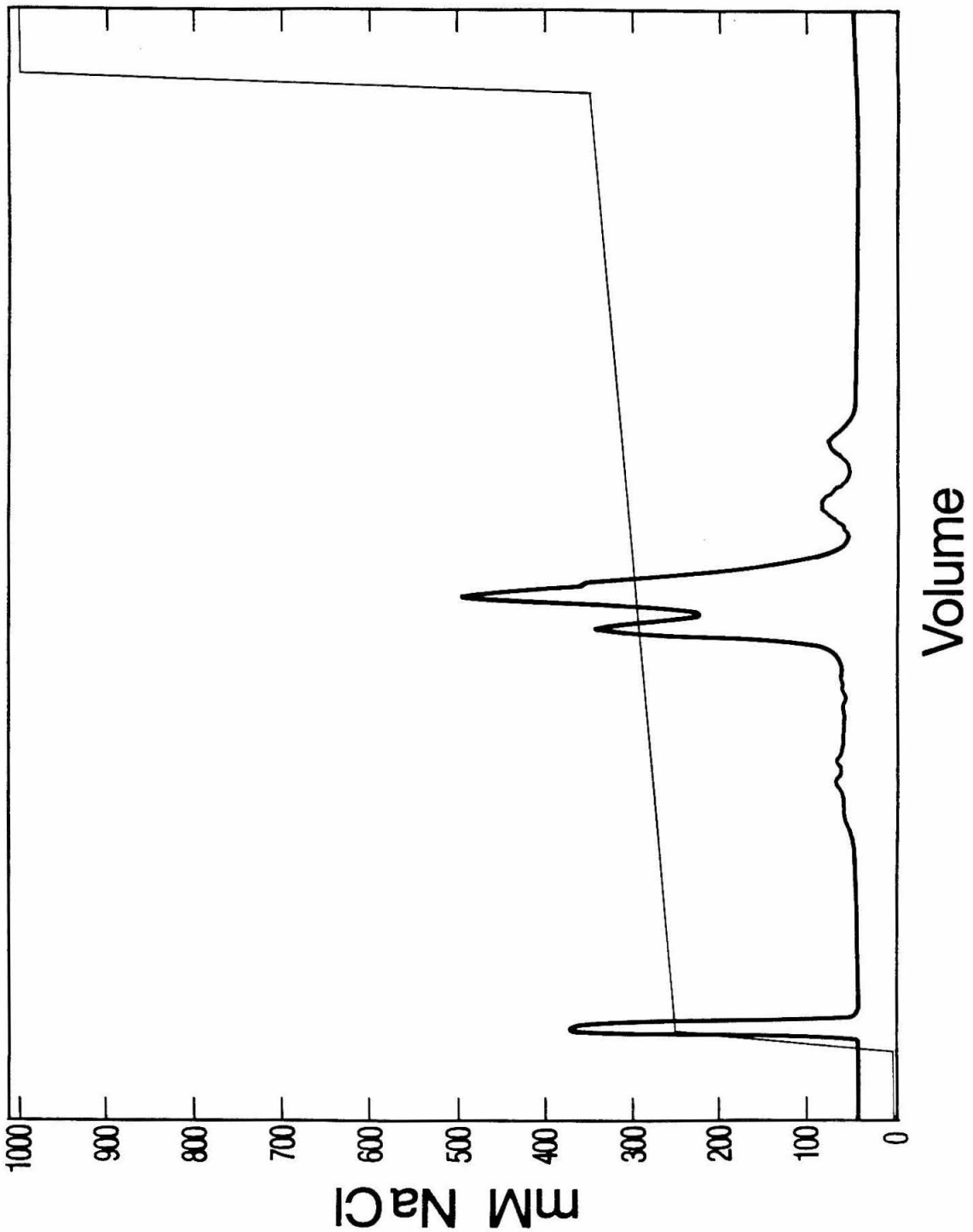
mM NaCl
1000
900
800
700
600
500
400
300
200
100
0
Volume

discussed in General Methods. The excited state lifetimes, as determined from the luminescence decay data at 650 nm, were 1.35(5) x10^7 s^{-1} (τ = 74 ns) for ferric $Ru(bpy)_2$(im)His39 cyt *c* and 1.20(5) x10^7 s^{-1} (τ = 83 ns) for ferrous $Ru(bpy)_2$(im)His39 cyt *c*. These values were used in subsequent fits. Luminescence decay data obtained with the modified ferric protein fit convolved with the laser pulse are shown in Figure 3.29.

Flash / quench and photoinduced techniques were used to acquire data for the determination of k_{ET}^{mm}. A full analysis of 12 data sets at both 550 and 400 nm fit to both single and double exponentials (to fit the fast minor component due to excited state decay) resulted in a measured ET rate of 3.2(4) x 10^6 s^{-1}. Identical kinetics were observed at wavelengths corresponding to $Ru^{3+/2+}$ (526 and 504 nm) and heme ET. Data obtained at 550 and 400 nm are shown in Figure 3.30 (flash / quench) and at 550 and 425 nm in Figure 3.31 (photoinduced).

The rate for photoinduced ET (k_{ET}*) was calculated as described from four full data sets (transient absorption at 370, 400, and 550 nm). Data obtained at 370 nm was used to calculate the excited state yield (Figure 3.32). Based on these data, the calculated rate constant for *Ru^{2+} to Fe^{3+} ET is 1.4(5) x 10^6 s^{-1}. This rate of photoinduced ET is unusually high for $Ru(bpy)_2$(im)His-modified proteins, however it is consistent with the small yet reproducible difference in excited state lifetimes of the oxidized and reduced proteins.

E. Ru(bpy)$_2$(im)His62 cyt c (Saccharomyces cerevisae)

1. Ru(bpy)$_2$(im)$^{2+}$-Modification Reaction

A 0.20 mM purified protein solution in 25 mM NaPi, pH 7.0 was reacted with 2 mM $Ru(bpy)_2(CO_3)$ following the protocol detailed in the General Methods section. In a trial reaction, aliquots were removed and analyzed following imidazole treatment by analytical cation-exchange chromatography (FPLC Mono S 5/5). Two singly modified

Figure 3.29 Luminescence decay of a 20 μM sample of ferric $Ru(bpy)_2(im)$His39 cyt *c* in 50 mM NaPi, pH 7.0 observed at 650 nm following excitation at 480 nm (4 mJ pulse). The smooth line is the fit to a single exponential decay function convolved with the instrument response (shown); $k_d = 1.35(5) \times 10^7\ s^{-1}$.

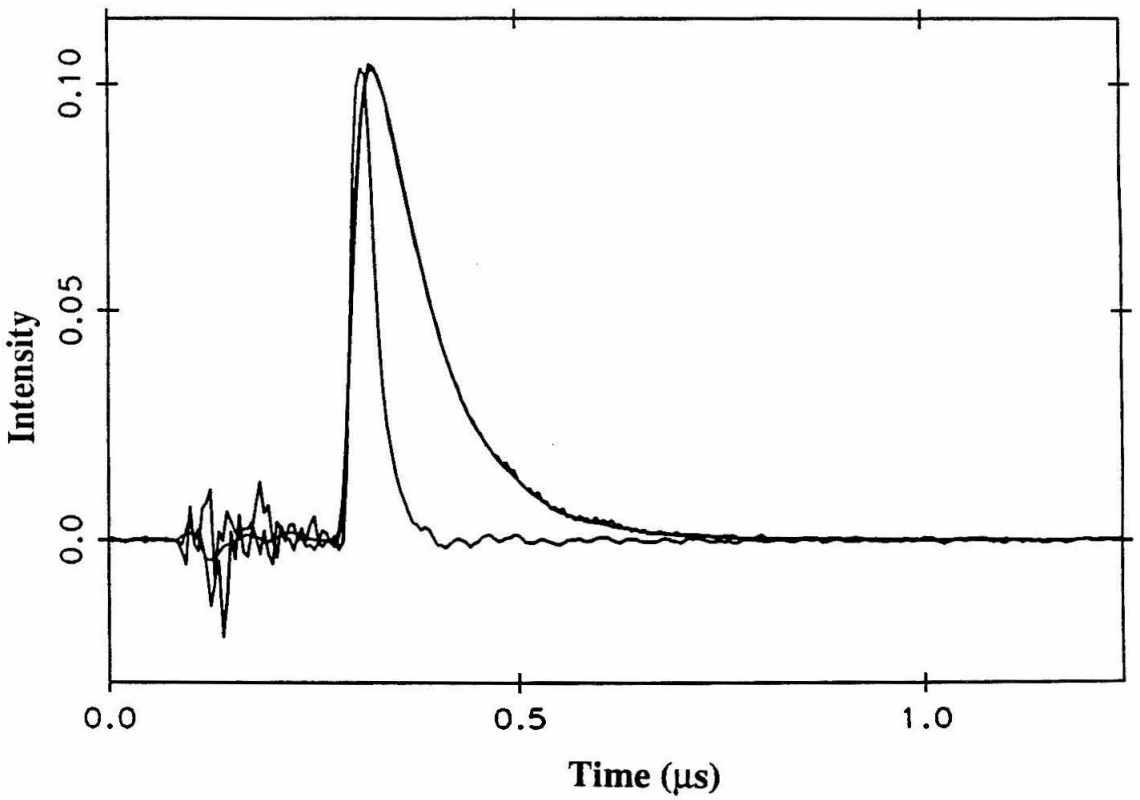
Intensity
0.10
0.05
0.0
0.0
0.5
1.0
Time (μs)

Figure 3.30 Transient absorption kinetics at various wavelengths following laser flash excitation (480 nm, 25 ns, 4 mJ) of $Ru(bpy)_2(im)His39^{2+}$ - Fe^{2+} cyt *c* with Rua_6^{3+} in 50 mM NaPi, pH 7.0, at room temperature. The decay corresponds to the production of $Ru(bpy)_2(im)His39^{2+}$ - Fe^{3+} cyt *c* due to intramolecular ET from Fe^{2+} to Ru^{3+} at a rate of 3.2×10^6 s^{-1}. Smooth lines correspond to fits to either a single (k_{ET}^{mm} (k_1) = 3.2×10^6 s^{-1}) or biexponential decay function (k_{ET}^{mm} (k_1) = 3.2×10^6 s^{-1} and $k_d = k_2$ (k_d = ~2×10^7 s^{-1} due to the presence of excited-state quencher). The sample concentration and coefficients for the rate terms are given. (A) 550 nm, 20 μM protein, 8 mM Rua_6^{3+}, c_1 = 0.026, c_2 = -0.017. (B) 400 nm, 20 μM protein, 8 mM Rua_6^{3+}, c_1 = -0.019, c_2 = 0.060.

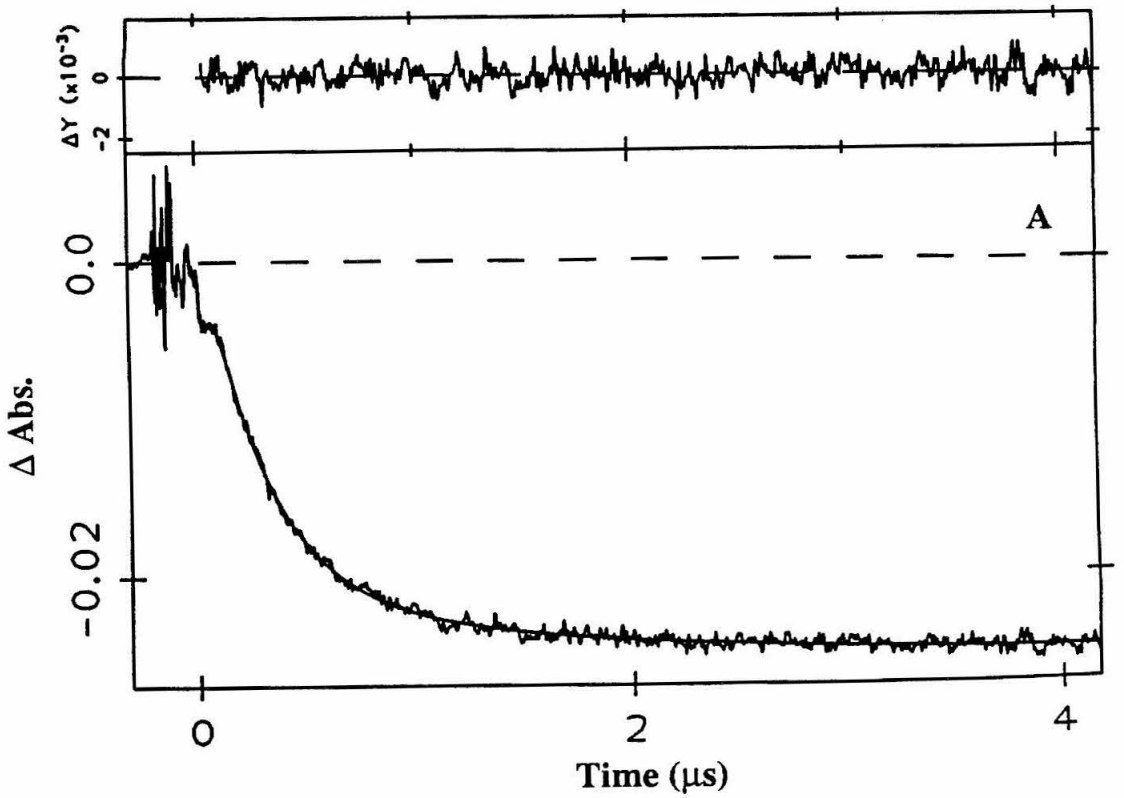
ΔY (x10⁻³)
0
-2
A
0.0
-0.02
Δ Abs.
0
2
4
Time (μs)

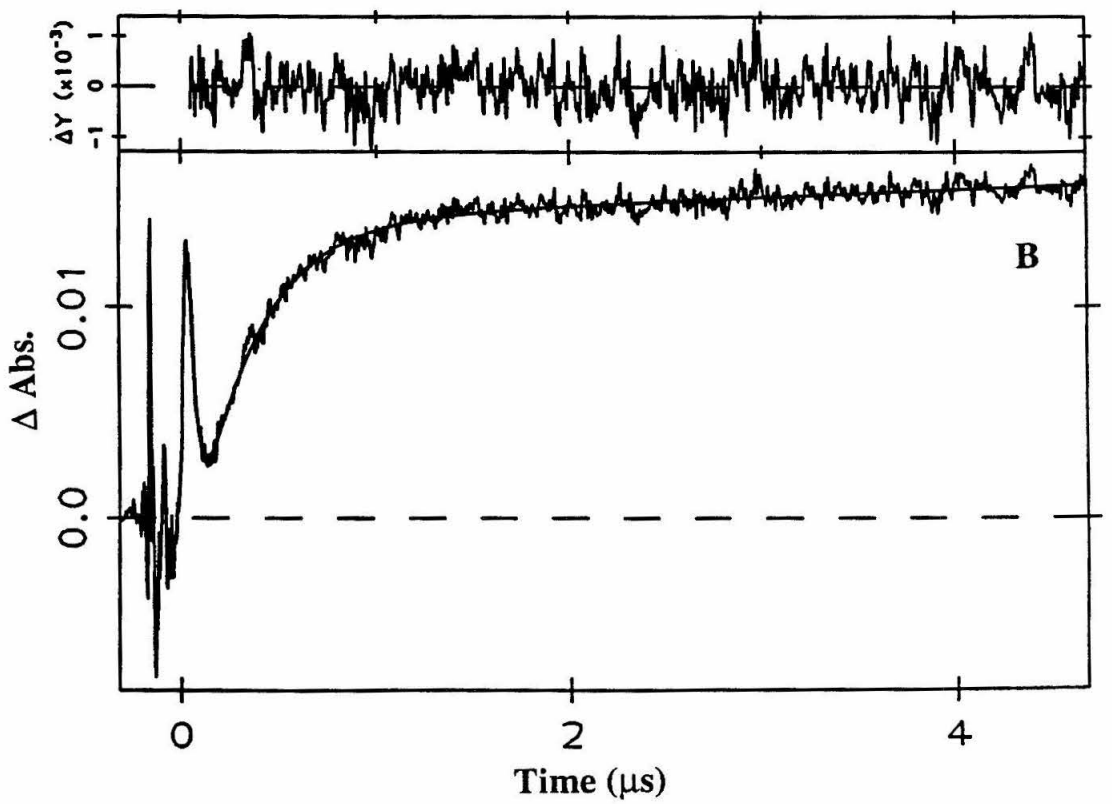
ΔY (x10⁻³)
1
0
-1
B
0.01
0.0
Δ Abs.
0
2
4
Time (μs)

Figure 3.31 Transient absorption kinetics at various wavelengths following laser flash excitation (480 nm, 25 ns, 4 mJ) of $Ru(bpy)_2(im)His39^{2+}$ - Fe^{3+} cyt *c* in 50 mM NaPi, pH 7.0, at room temperature. The rise corresponds to production of ferrous cyt *c* due to photoinduced ET. At 425 nm (B), there is additionally a contribution due to formation of the excited state in the signal rise. The decay corresponds to the production of $Ru(bpy)_2(im)His39^{2+}$ - Fe^{3+} cyt *c* due to intramolecular ET from Fe^{2+} to Ru^{3+} at a rate of 3.2×10^6 s^{-1}. Smooth lines correspond to fits to either a biexponential (k_{ET}^{mm} (k_1) = 3.2×10^6 s^{-1} and k_d (k_2)= 1.35×10^7 s^{-1})(A) or a single exponential decay function (k_{ET}^{mm} (k_1) = 3.2×10^6 s^{-1})(B). The sample concentration and coefficients for the rate terms are given. (A) 550 nm, 20 μM protein, $c_1 = 0.011$, $c_2 = -0.023$. (B) 425 nm, 20 μM protein, $c_1 = -0.0046$.

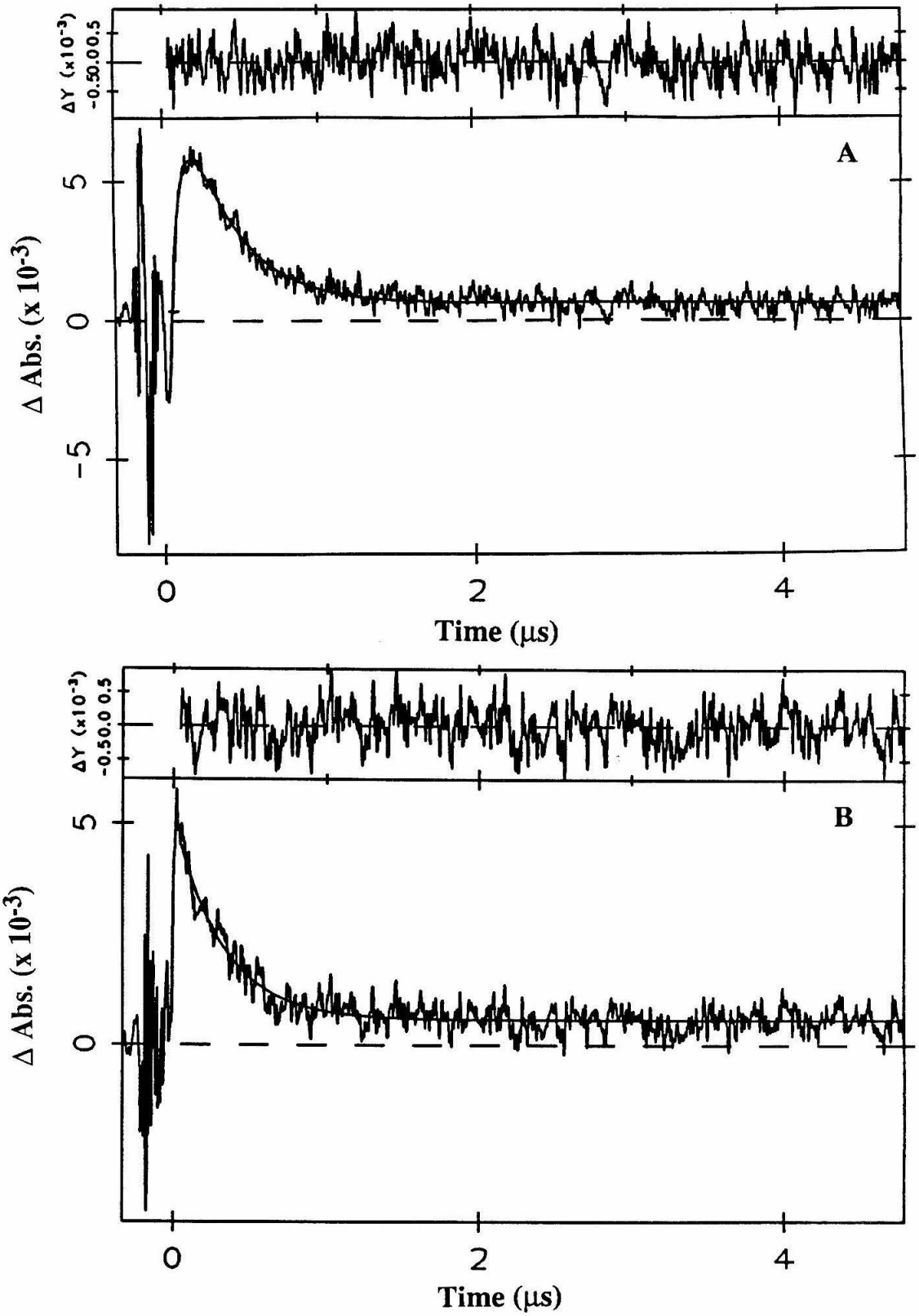
ΔY (x10⁻³)
-0.5 0.0 0.5
A
5
0
−5
Δ Abs. (x 10⁻³)
0
2
4
Time (μs)
ΔY (x10⁻³)
-0.5 0.0 0.5
B
5
0
Δ Abs. (x 10⁻³)
0
2
4
Time (μs)

Figure 3.32 Transient absorption kinetics at 370 nm following laser flash excitation (480 nm, 25 ns, 4 mJ) of $Ru(bpy)_2(im)His39^{2+}$ - Fe^{3+} cyt *c*, 5 μM in 50 mM NaPi, pH 7.0, at room temperature. The smooth line is the fit to a single exponential decay function convolved with the instrument response. The decay corresponds to the decay of the $*Ru(bpy)_2(im)His72^{2+}$ excited state ($k_d = 1.35 \times 10^7\ s^{-1}$, $c_1 = 0.026$).

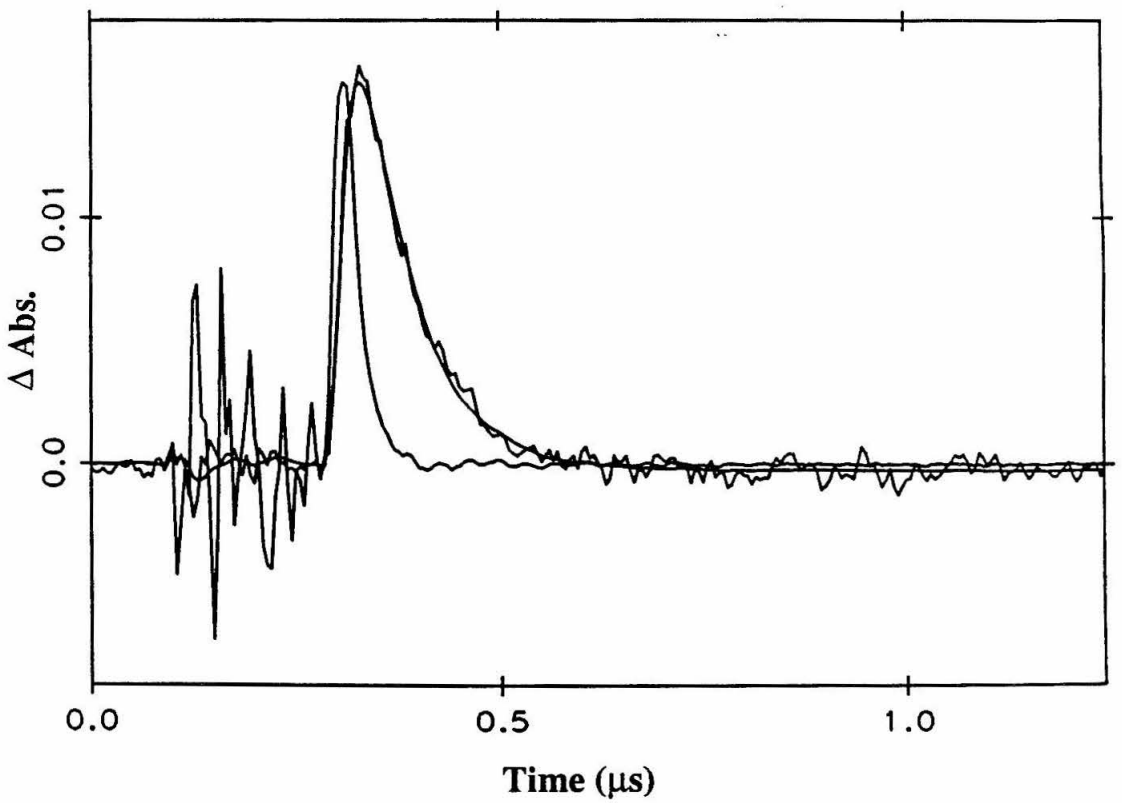
Δ Abs.
0.01
0.0
0.0
0.5
1.0
Time (μs)

protein bands were observed to form at early reaction times, followed at later reaction times by multiply modified products. Figure 3.33 illustrates a typical cation-exchange chromatogram of the reaction. The first main band corresponds to unmodified protein, the second and third are singly modified protein products, with the multiply modified species in the final high salt wash. Previous studies of the ruthenium ammine modification of the native and Zn porphyrin proteins indicate that the His62 residue of this mutant is far more reactive to modification than His33,[6] therefore the first (lower yield) singly modified product was tentatively assigned as $Ru(bpy)_2$(im)His33 cyt *c* and the second (higher yield) singly modified product assigned as $Ru(bpy)_2$(im)His62 cyt *c*. ET rate determinations in both derivatives strongly support this assignment. Optimal reaction time for isolation of singly modified product is 13.5 hours, followed by 24 - 48 hours of treatment with 2M imidazole prior to purification. Only pure product (by cation exchange) was used in laser experiments. As previously noted, the Δ and Λ isomers of yeast $Ru(bpy)_2$(im)HisX cyts *c* do not appear to be separable by cation-exchange chromatography.

2. *Electron-Transfer Studies*

Luminescence decay and transient absorption measurements on the $Ru(bpy)_2$(im)His62 derivative were made as discussed in General Methods. The excited state lifetimes, as determined from the luminescence decay data at 650 nm, were nearly identical in both redox states, $k_d = 1.05(5) \times 10^7\ s^{-1}$ (τ =95 ns) for ferric and ferrous $Ru(bpy)_2$(im)His62 cyt *c*. Figure 3.34 shows the convolved fit of the luminescence decay data.

Flash / quench and photoinduced techniques were used to acquire data for the determination of the Fe^{2+} to Ru^{3+} (k_{ET}^{mm}) ET rate. The position of His62 in the protein results in weak electronic coupling with the heme (Chapter 4), thus the Fe^{2+} to Ru^{3+} rate is significantly slower than in other derivatives and the yield of photoinduced ET

Figure 3.33 Typical cation-exchange (FPLC Mono S 10/10, flow rate of 3.5 ml/min) chromatogram for the *S. c.* His62 cyt *c* modification reaction with $Ru(bpy)_2(CO_3)$ reaction products in 25 mM NaPi, pH 7.0. Gradient represents the concentration of NaCl in mM. The first main band corresponds to unmodified protein, the second and third are singly modified protein products, with the multiply modified species in the high NaCl salt wash. Detection is on the 1.0 absorbance scale at 405 nm.

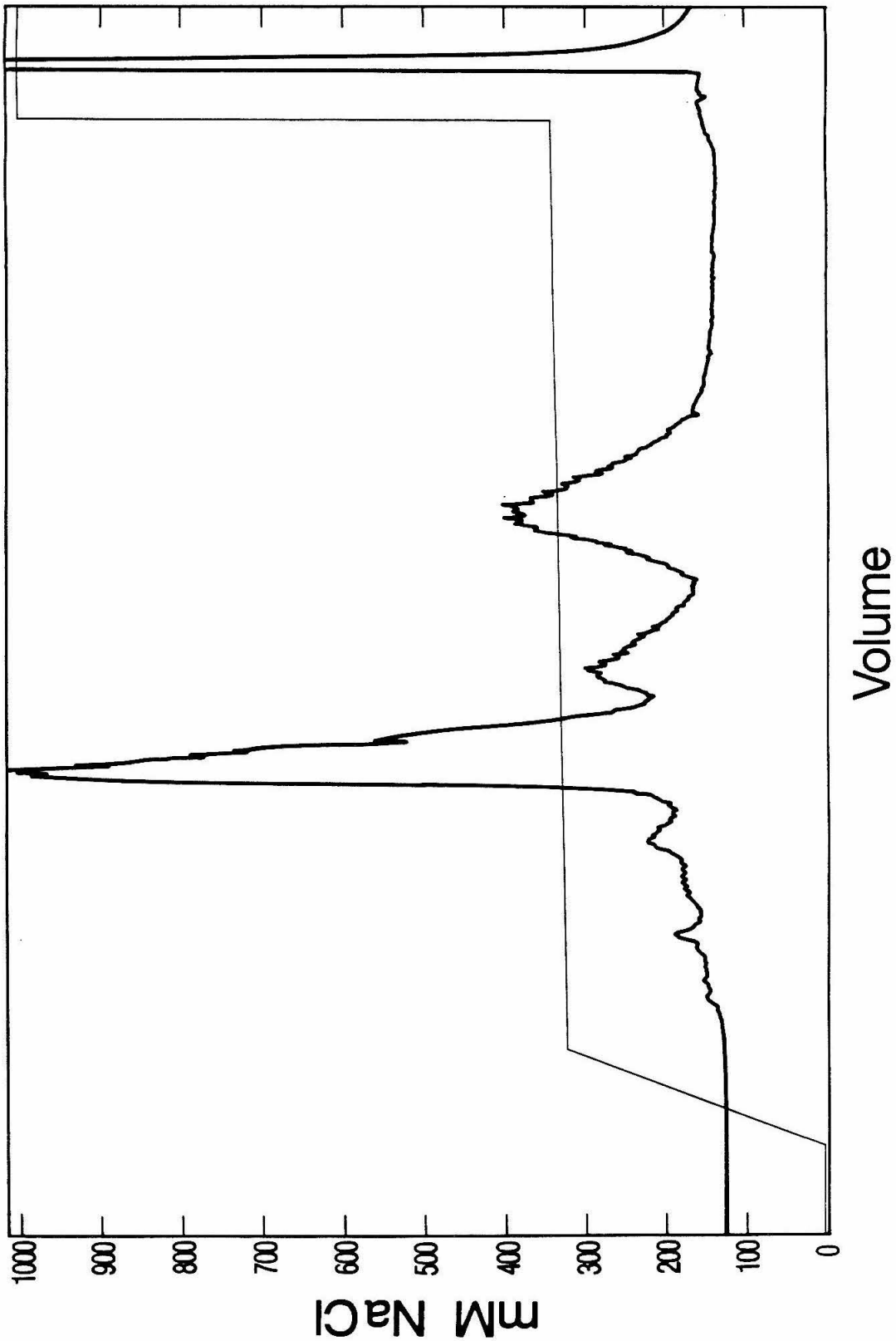
1000
900
800
700
600
500
400
300
200
100
0
mM NaCl
Volume

Figure 3.34 Luminescence decay of a 19.3 μM sample of ferrous $Ru(bpy)_2(im)His62$ cyt *c* in 50 mM NaPi, pH 7.0 observed at 650 nm following excitation at 480 nm (2 mJ pulse). The smooth line is the fit to a single exponential decay function convolved with the instrument response (shown); $k_d = 1.05(5) \times 10^7\ s^{-1}$.

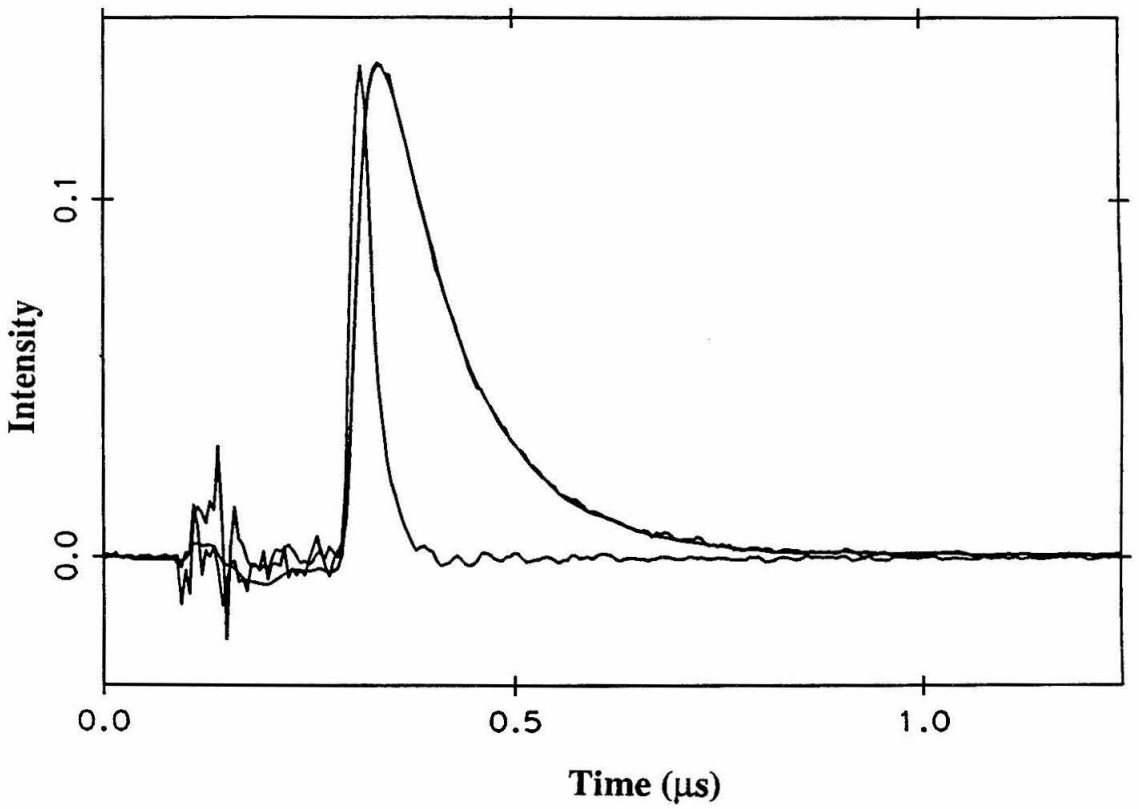
Intensity
0.1
0.0
0.0
0.5
1.0
Time (μs)

extremely low (it was anticipated that none would be observed). A full analysis of 12 data sets at 550 and 390 (or 393) nm fit to a single exponential (the fast minor component due to excited state decay is not resolved on this timescale) resulted in a rate of 1.0(2) x 10^4 s^{-1}. Identical kinetics were observed in the flash / quench experiment at wavelengths corresponding to $Ru^{3+/2+}$ (504 nm) and the heme ET. Data obtained at 550, 504, 425, and 390 nm for the flash / quench experiments are shown in Figure 3.35. Data from the photoinduced experiments at 550 and 393 nm are presented in Figure 3.36. A small long-lived kinetic component is observed and attributed to a ferric impurity. Attempts to remove this component by addition of a trace amount of *in situ*-generated Rua_6^{2+} were not successful.

The rate for photoinduced ET (k_{ET}*) was calculated as described from four full data sets (transient absorption at 370, 393, and 550 nm). Data obtained at 370 nm used to calculate the excited state yield was fit convolved with the laser pulse (Figure 3.37). The low yield of photoinduced ET product precluded data collection at wavelengths used to investigate Ru^{3+} reduction. Based on heme data, the calculated rate constant $*Ru^{2+}$ to Fe^{3+} is 1.1(2) x 10^5 s^{-1}, an order of magnitude larger than k_{ET}^{mm}.

ET was investigated in the secondary singly modified product obtained in the modification reaction. In a flash / quench experiment, a fast (~3 x 10^6 s^{-1}) (Figure 3.38) rate was observed, with no absorbance changes noted on longer timescales. This rate is consistent with that measured in horse heart $Ru(bpy)_2$(im)His33 cyt *c* supporting the proposed assignment of this product. Similar results were noted in the ruthenium pentaammine modification work, with the minor modification product also identified as the His33-labeled protein from ET measurements.[35]

Figure 3.35 Transient absorption kinetics at various wavelengths following laser flash excitation (480 nm, 25 ns, 2 mJ) of $Ru(bpy)_2(im)His62^{2+}$ - Fe^{2+} cyt *c* with Rua_6^{3+} in 50 mM NaPi, pH 7.0, at room temperature. The decay corresponds to the production of $Ru(bpy)_2(im)His62^{2+}$ - Fe^{3+} cyt *c* due to intramolecular ET from Fe^{2+} to Ru^{3+} at a rate of $1.0 \times 10^4\ s^{-1}$. Smooth lines correspond to fits to a single exponential decay function (k_{ET}^{mm} (k_1) = $1.0 \times 10^4\ s^{-1}$); the excited-state lifetime is insignificant on this timescale. The sample concentration and coefficients for the rate terms are given. (A) 550 nm, 18.4 μM protein, 7 mM Rua_6^{3+}, $c_1 = 0.017$. (B) 390 nm, 18.4 μM protein, 7 mM Rua_6^{3+}, $c_1 = -0.015$. (C) 425 nm, 18.4 μM protein, 7 mM Rua_6^{3+}, $c_1 = 0.016$. (D) 504 nm, 18.8 μM protein, 7 mM Rua_6^{3+}, $c_1 = -0.0049$.

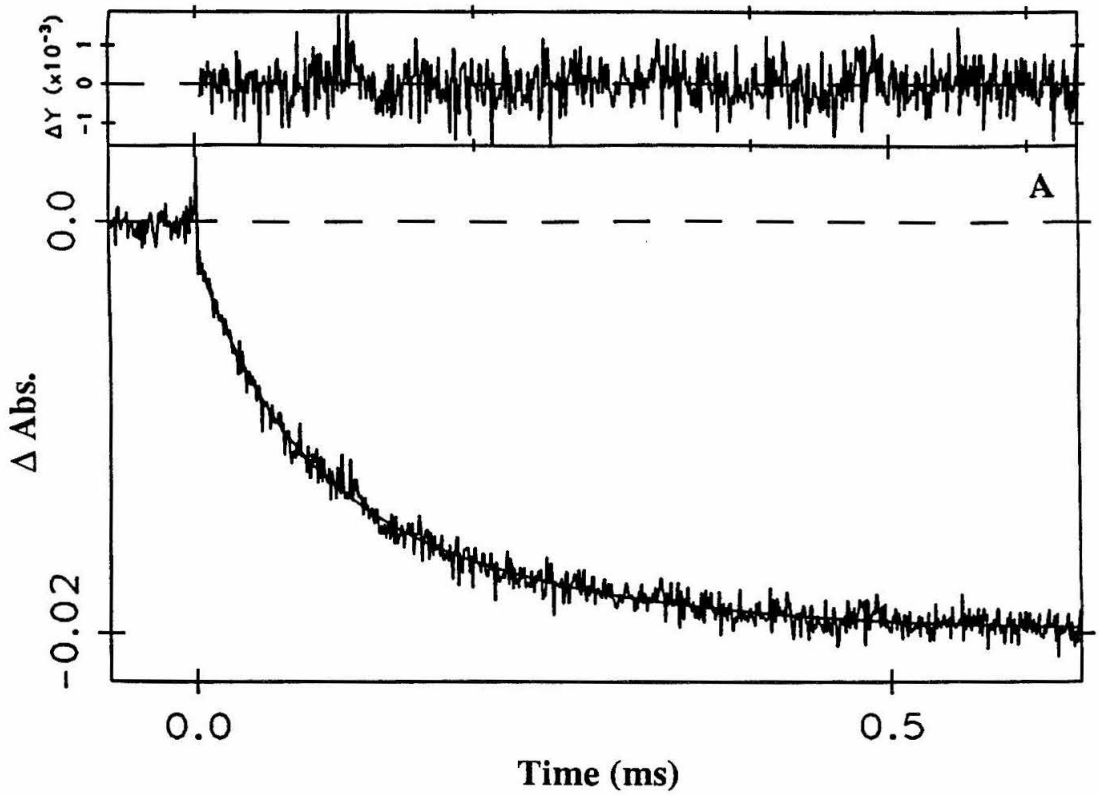
ΔY (x10⁻³)
-1
0
1
A
0.0
Δ Abs.
-0.02
0.0
0.5
Time (ms)

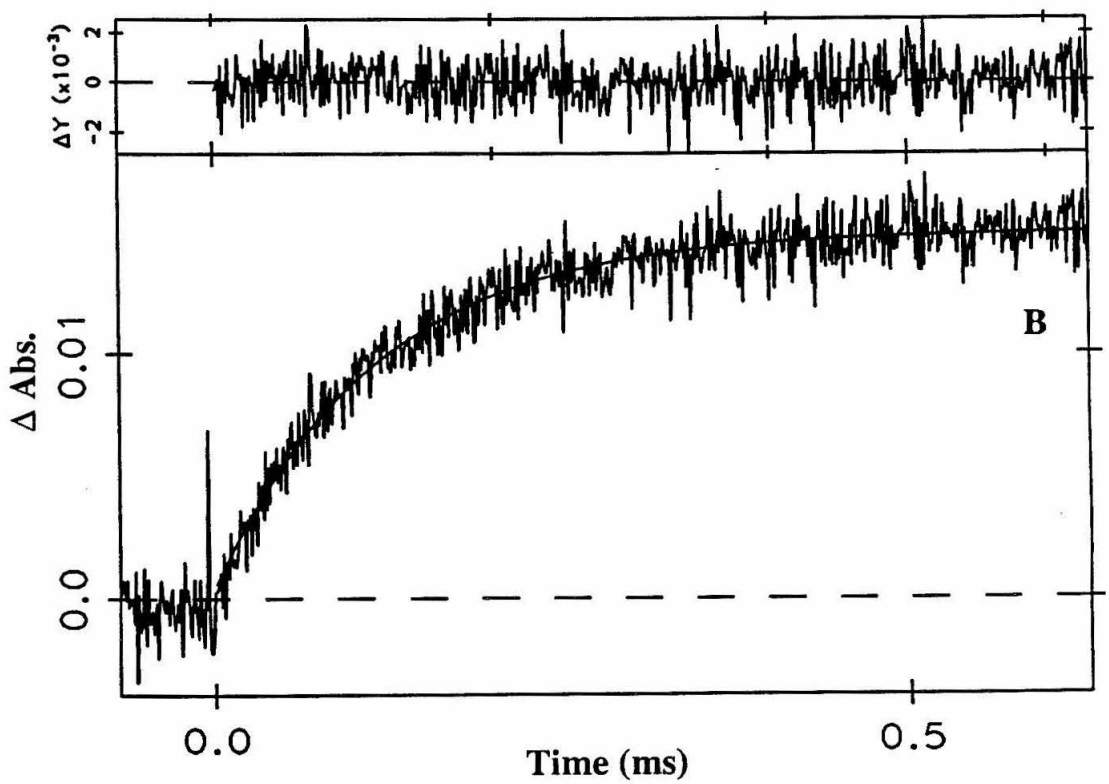
ΔY (x10⁻³)
-2
0
2
B
Δ Abs.
0.01
0.0
0.0
0.5
Time (ms)

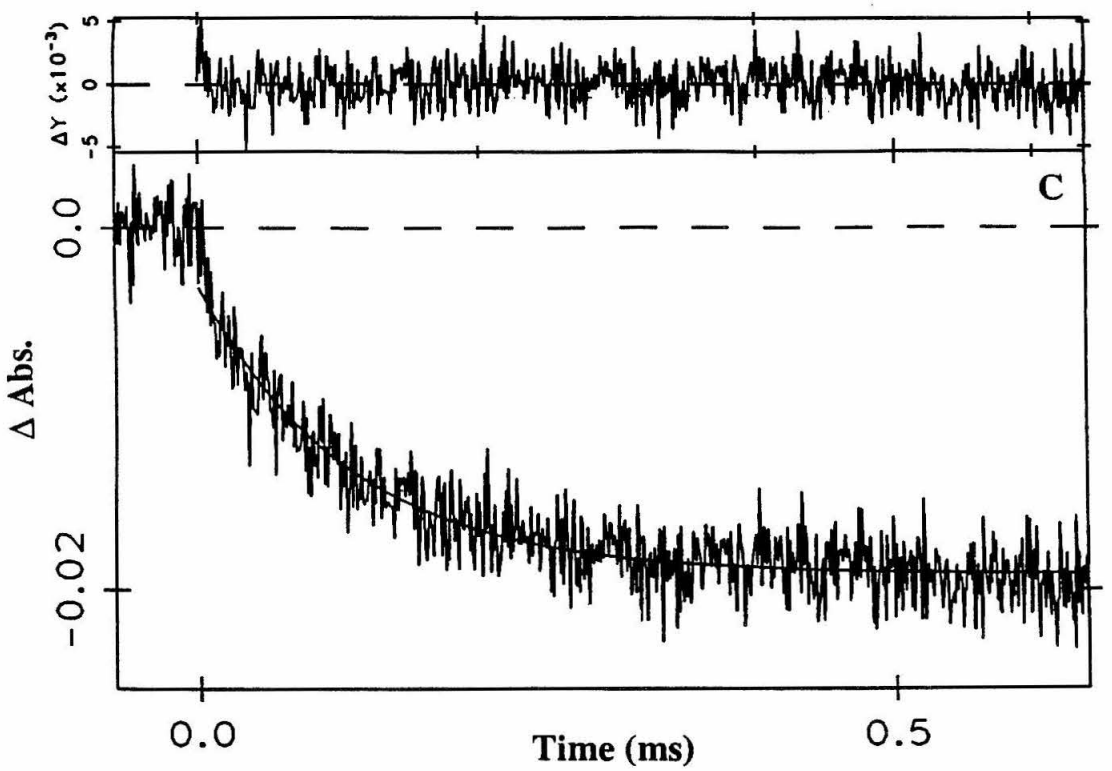
ΔY (x10⁻³)
5
0
-5
C
0.0
Δ Abs.
-0.02
0.0
0.5
Time (ms)

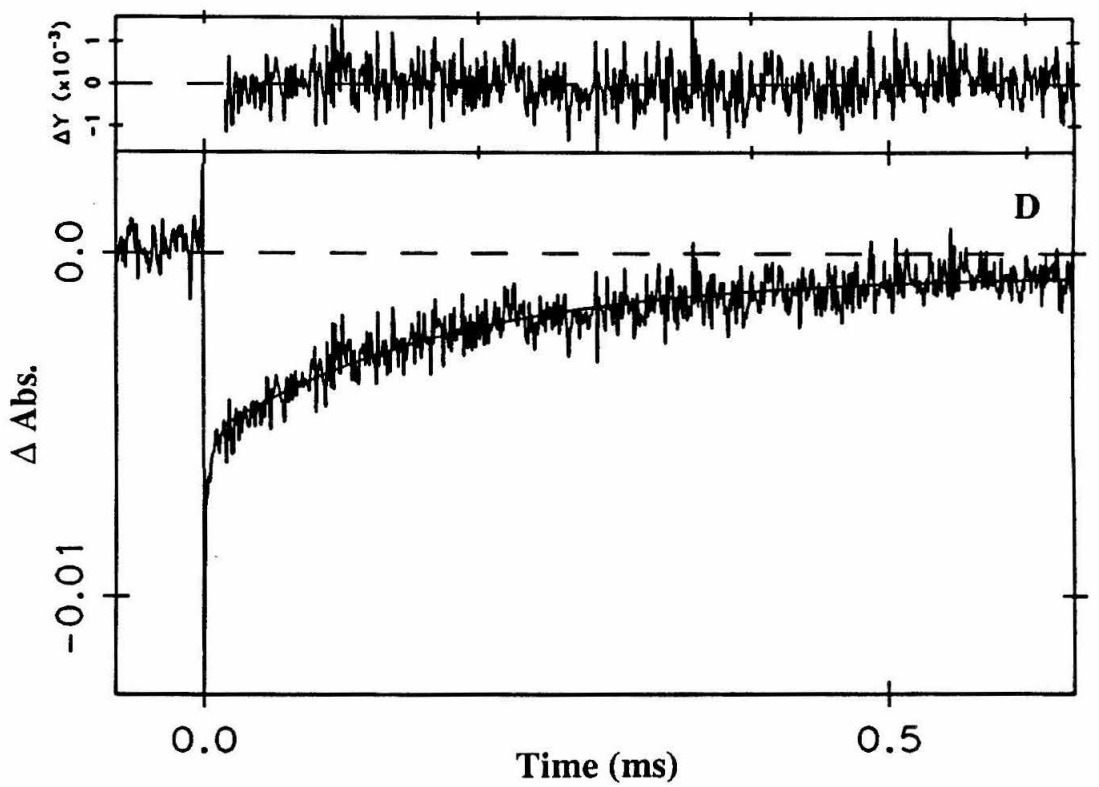
ΔY (x10⁻³)
1
0
-1
D
0.0
Δ Abs.
-0.01
0.0
0.5
Time (ms)

Figure 3.36 Transient absorption kinetics at various wavelengths following laser flash excitation (480 nm, 25 ns, 2 mJ) of $Ru(bpy)_2(im)His62^{2+}$ - Fe^{3+} cyt *c* in 50 mM NaPi, pH 7.0, at room temperature. The rise corresponds to production of ferrous cyt *c* due to photoinduced ET. The decay corresponds to the production of $Ru(bpy)_2(im)His62^{2+}$ - Fe^{3+} cyt *c* due to intramolecular ET from Fe^{2+} to Ru^{3+} at a rate of 1.0×10^4 s^{-1}. Smooth lines correspond to fits to a biexponential decay function (k_{ET}^{mm} (k_1) = 1.0×10^4 s^{-1} and k_d (k_2)= 1.05×10^7 s^{-1}). The sample concentration and coefficients for the rate terms are given. (A) 550 nm, 16.1 μM protein, $c_1 = 0.0012$, $c_2 = -0.011$. (B) 393 nm, 7.5 μM protein, $c_1 = -0.0035$, $c_2 = 2.4$.

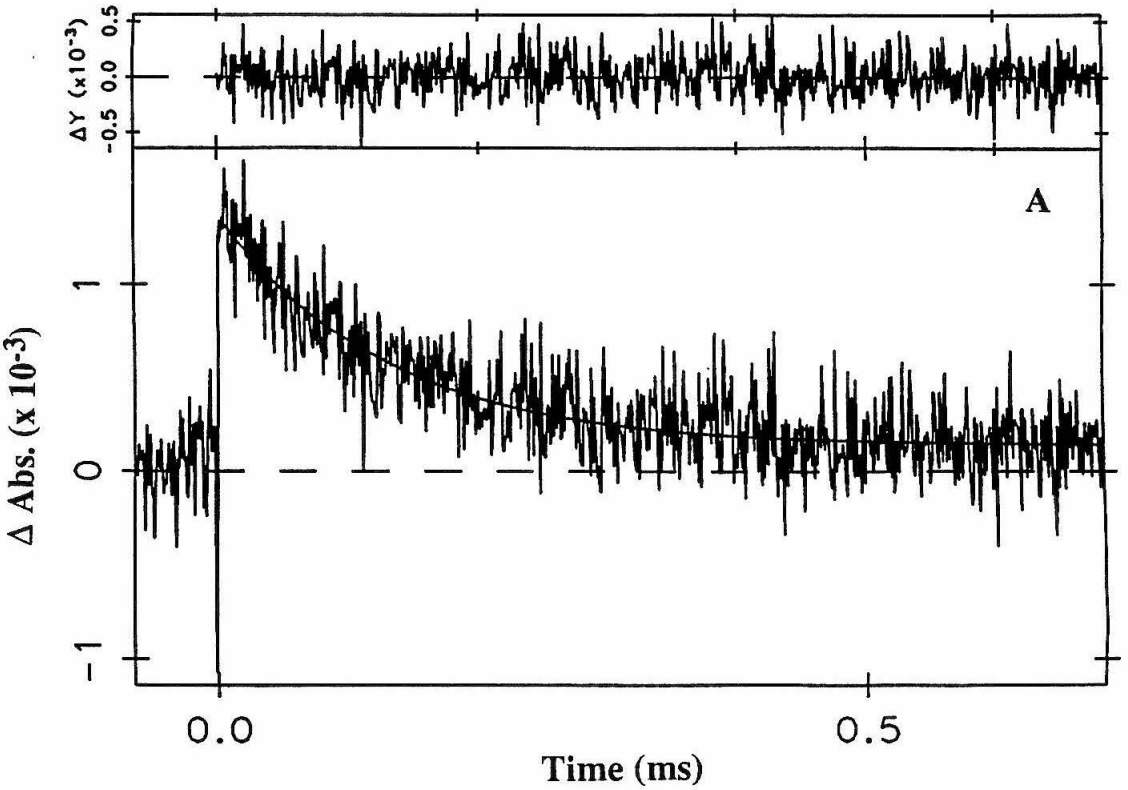
ΔY (x10⁻³)
-0.5 0.0 0.5
A
Δ Abs. (x 10⁻³)
1
0
−1
0.0
0.5
Time (ms)

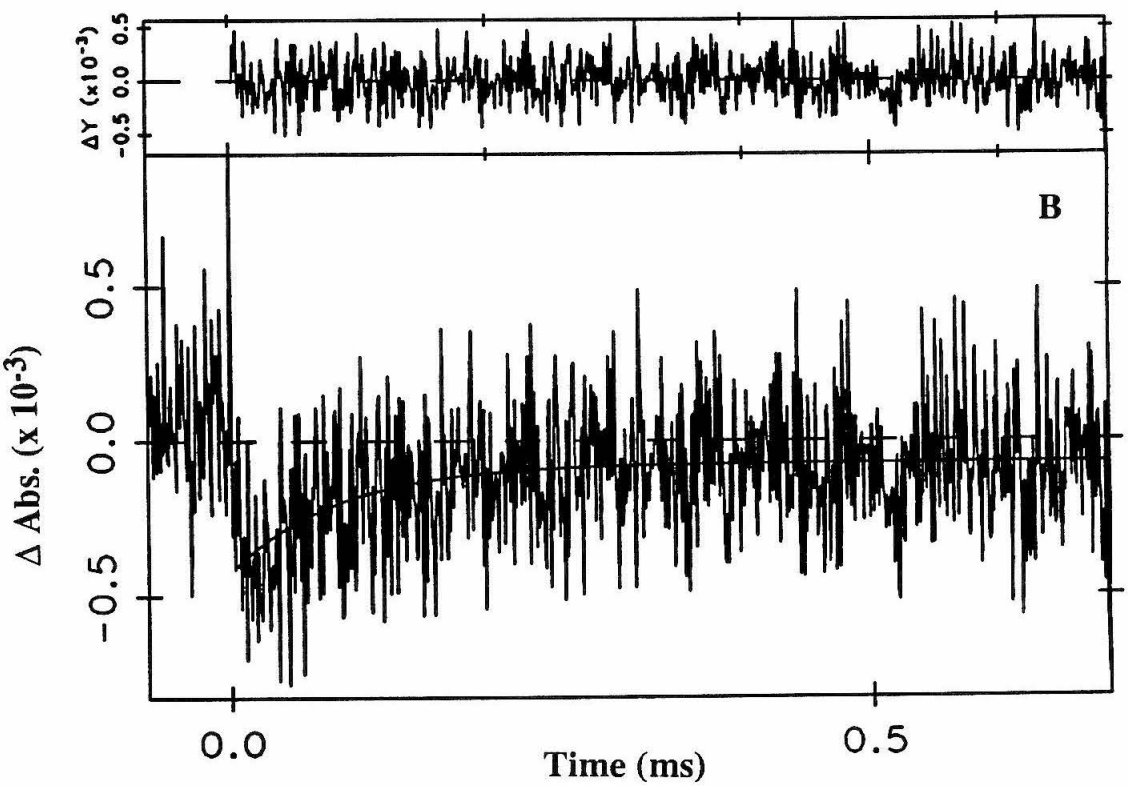
ΔY (x10⁻³)
-0.5 0.0 0.5
B
Δ Abs. (x 10⁻³)
0.5
0.0
−0.5
0.0
0.5
Time (ms)

Figure 3.37 Transient absorption kinetics at 370 nm following laser flash excitation (480 nm, 25 ns, 2 mJ) of $Ru(bpy)_2(im)His62^{2+}$ - Fe^{3+} cyt *c*, 16.6 μM in 50 mM NaPi, pH 7.0, at room temperature. The smooth line is the fit to an exponential decay function convolved with the instrument response. The decay corresponds to the decay of the $*Ru(bpy)_2(im)His72^{2+}$ excited state ($k_d = 1.05 \times 10^7\ s^{-1}$, $c_1 = 0.067$).

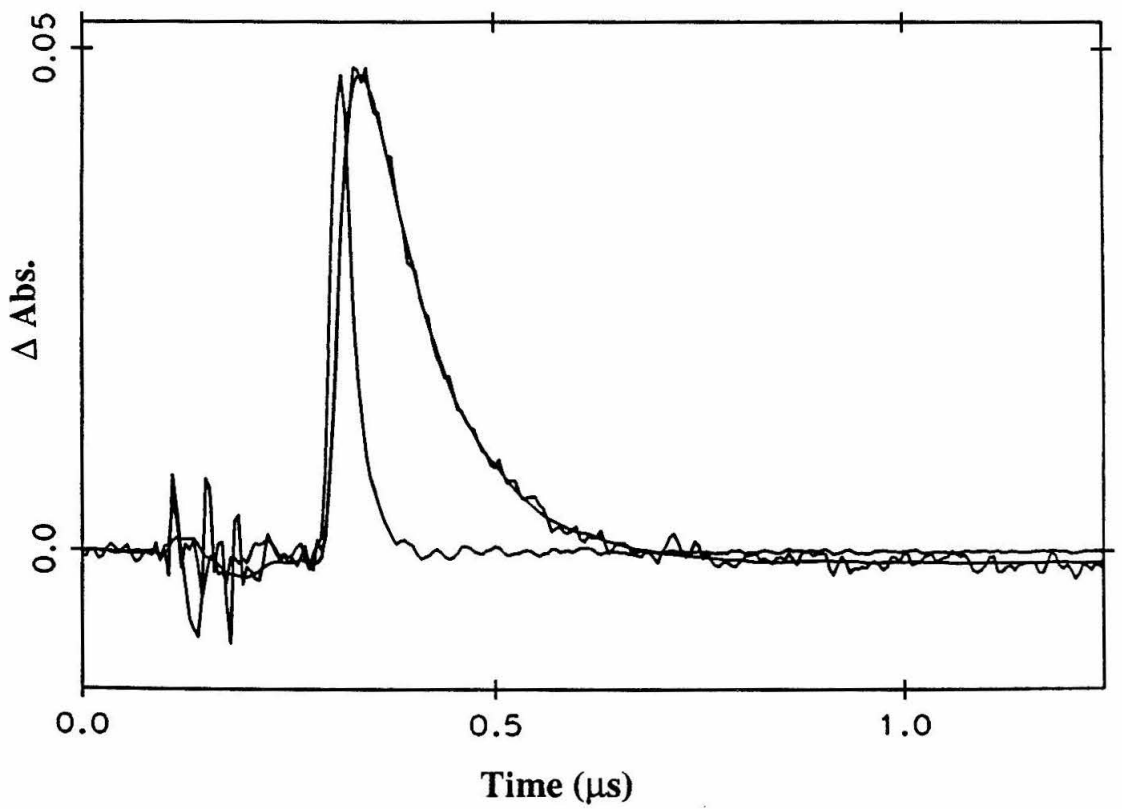
0.05
0.0
Δ Abs.
0.0
0.5
1.0
Time (μs)

Figure 3.38 Transient absorption kinetics at 550 nm following laser flash excitation (480 nm, 25 ns, 2 mJ) of 21 μM *S. c.* $Ru(bpy)_2(im)His33^{2+}$ - Fe^{2+} cyt *c* with 5 mM Rua_6^{3+} in 50 mM NaPi, pH 7.0, at room temperature. The decay corresponds to the production of $Ru(bpy)_2(im)His33^{2+}$ - Fe^{3+} cyt *c* due to intramolecular ET from Fe^{2+} to Ru^{3+} at a rate of 2.6×10^6 s^{-1}. Smooth lines correspond to a fit to a single exponential (k_{ET}^{mm} (k_1) = 3.5×10^6 s^{-1} (c_1 = 0.003). The rate is over two orders of magnitude faster than the His62 derivative.

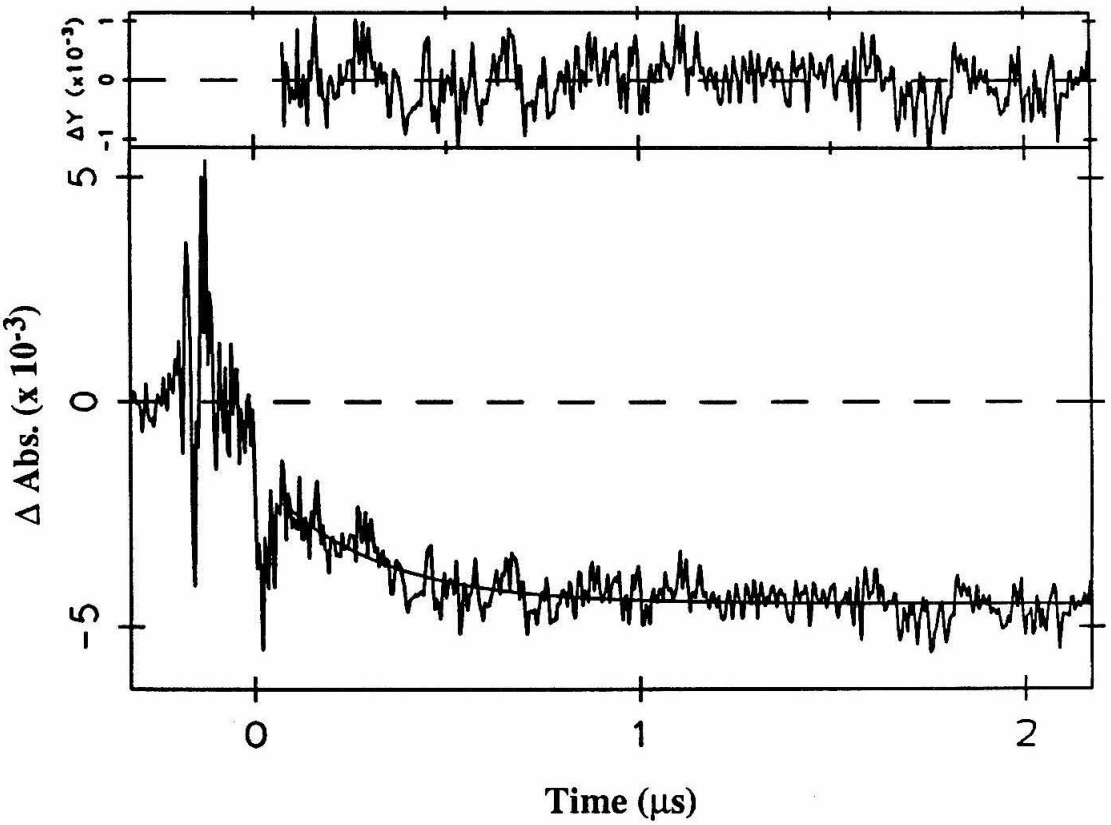
ΔY (x10⁻³)
1
0
-1
5
0
-5
Δ Abs. (x 10⁻³)
0
1
2
Time (μs)

IV. Conclusion

Intramolecular ET rates have been measured in a series of structurally engineered $Ru(bpy)_2(im)HisX^{2+}$ cyts *c* [X =33 (horse heart)[13], 39 (*C. k.*), 62 (recombinant *S. c.* Asn62 to His), and 72 (semisynthetic horse heart)] by direct photoinduced and flash / quench methodologies. Luminescence decay (k_d) and electron transfer rates obtained (k_{ET}^{mm} and k_{ET}*) are summarized in Table 3.4.

Table 3.4. ET parameters for $Ru(bpy)_2(im)HisX$ cyts *c*. Numbers in parentheses indicate uncertainties in the preceding digits.

X	k_d s^{-1}	k_{ET}* (*Ru^{2+} to Fe^{3+}) s^{-1}	k_{ET}^{mm} (Fe^{2+} to Ru^{3+}) s^{-1}
39	Fe^{2+}: 1.20(5) x 10^7 Fe^{3+}: 1.35(5) x 10^7	1.4(5) x 10^6	3.2(4) x 10^6
33[13]	Fe^{3+}: 1.25 x 10^7	2.0(5) x 10^5	2.6(3) x 10^6
72	Fe^{2+}: 1.40(5) x 10^7 Fe^{3+}: 1.40(5) x 10^7	3.4(7) x 10^5	9.0(3) x 10^5
62	Fe^{2+}: 1.05(5) x 10^7 Fe^{3+}: 1.05(5) x 10^7	1.1(2) x 10^5	1.0(2) x 10^4

The difference in excited state lifetimes between derivatives may be due to distance-dependent (*e.g.*, Förster type) energy transfer quenching by the heme. The interpretation of the ET rate data collected from these mapping studies is discussed in the following chapter.

V. References

1. Reviewed in (a) Winkler, J. R.; Gray, H. B. *Chem. Rev.* **1992**, *92*, 369. (b) Gray, H. B.; Winkler, J. R. *Pure & Appl. Chem.* **1992**, *64*, 1257. (c) Mayo, S. L.; Ellis, W. R.; Crutchley, R. J.; Gray, H. B. *Science,* **1986**, *233*, 948.

2. (a) Winkler, J. R.; Nocera, D. G.; Yocum, K. B.; Bordignon, E.; Gray, H. B. *J. Am. Chem. Soc.* **1982**, *104*, 5798. (b) Nocera, D. G.; Winkler, J. R.; Yocum, K. M.; Bordgnon, E.; Gray, H. B. *J. Am. Chem. Soc.* **1984**, *106*, 5145.

3. Meade, T. J.; Gray, H. B.; Winkler, J. R. *J. Am. Chem. Soc.* **1989**, *111*, 4353.

4. Elias, H.; Chou, M. H.; Winkler, J. R. *J. Am. Chem. Soc.* **1988**, *110*, 429.

5. (a) Therien, M. J.; Selman, M.; Gray, H. B.; Chang, I-J.; Winkler, J. R. *J. Am. Chem. Soc.* **1990**, *112*, 2420. (b) Selman, M. A. Ph. D. Thesis, California Institute of Technology, **1989**. A lower limit of 170 s^{-1} was placed on the $Ru^{2+}a_5$His39 to Fe^{3+} ET rate compared to 30 s^{-1} measured in the analagous horse heart His33 cyt *c* derivative.[2]

6. Bowler, B. E.; Meade, T. J.; Mayo, S. L.; Richards, J. H.; Gray, H. B. *J. Am. Chem. Soc.* **1989**, *111*, 8757. Therien, M. J.; Bowler, B. E.; Selman, M. A.; Gray, H. B.; Chang, I-J.; Winkler, J. R. In *ACS Advances in Chemistry Series,* Bolton, J. R., Mataga, N., McLendon, G., Eds.; (American Chemical Society: Washington DC) 1991; No. 228, pp 191 - 200.

7. Bushnell, G. W.; Louie, G. V.; Brayer, G. D. *J. Mol. Biol.* **1990**, *214*, 585. Louie, G. V.; Brayer, G. D. *J. Mol. Biol.* **1990**, *214*, 527. Berghuis, A. M.; Brayer, G. D. *J. Mol. Biol.* **1992**, *223*, 959.

8. The properties of $Ru(bpy)_3^{2+}$ are reviewed in Juris, A.; Balzani, V.; Barigelletti, F.; Campagna, S.; Belser, P.; von Zelewsky, A. *Coord. Chem. Rev.* **1988**, *84*, 85.

9. Durham, B.; Pan, L. P.; Long, J. E.; Millett, F. *Biochemistry* **1989**, *28*, 8659. Pan, L. P.; Durham, B.; Wolinska, J.; Millet, F. *Biochemistry* **1988**, *27*, 7180.

10. (a) Durham, B. D.; Pan, L. P.; Hahm, S.; Long, J.; Millett, F. In *ACS Advances in Chemistry Series*; Johnson, M. K., King, R. B., Kurtz, D. M., Kutal, C., Norton, M. L., Scott, R. A. Eds.; (American Chemical Society: Washington DC) 1990; Vol. 226, pp. 181 - 193. (b) Millett, F.; Durham, B. In *Metals in Biological Systems*; Sigel, H., Sigel A. Eds. (Dekker : New York) 1991; Vol. 27, pp 223 - 264. (c) Pinnick, D. V.; Durham, B. *Inorg. Chem.* **1984**, *23*, 1440.

11. Geren, L.; Hahm, S.; Durham, B. *Biochemistry* **1991**, *30*, 9450.

12. Willie, A.; Stayton, P. S.; Sligar, S. G.; Durham, B.; Millett, F. *Biochemistry* **1992**, *31*, 7237.

13. Chang, I-J.; Gray, H. B.; Winkler, J. R. *J. Am. Chem. Soc.* **1991**, *113*, 7056.

14. Brown, G. M.; Sutin, N. *J. Am. Chem. Soc.* **1979**, *101*, 883.

15. Marcus, R. A.; Sutin, N. *Biochim. Biophys. Acta* **1985**, *811*, 265.

16. Dixon, D. W.; Xong, X. *Adv. Chem. Ser.* **1990**, *226*, 161.

17. Chang, I-J.; Winkler, J. R.; Gray, H. B., unpublished results.

18. Scott, J. A.; Willie, A.; McLean, M.; Stayton, P. S.; Sligar, S. G.; Durham, B.; Millett, F. *J. Am. Chem. Soc.* **1993**, *115,* 6820.

19. Johnson, E. C.; Sullivan, B. P.; Salmon, D. J.; Adeyemi, S. A.; Meyer, T. J. *Inorg. Chem.* **1978**, *17*, 2211.

20. Long, C.; Vos, J. G. *Inorg. Chim. Acta* **1984**, *89*, 125.

21. Rice, S. F.; Gray, H. B. *J. Am. Chem. Soc.* **1983**, *105*, 4571. Bailey, J. A.; Hill, M. J.; Marsh, R. E.; Miskowski, V. M.; Schaefer, W. P; Gray, H. B., in preparation.

22. Jackman, M. P.; Lim, M.-C.; Osvath, P.; Harshani de Silva, D. G. A.; Sykes, G. A. *Inorg. Chim. Acta* **1988**, *153*, 205.

23. Bjerrum, M. J., unpublished results.

24. Taylor, J. R. *An Introduction to Error Analysis*, (University Science: Mill Valley, CA) 1982.

25. This observation was first made by Prof. Laura Anderson of the Kansas State University, Manhattan, Kansas, on samples sent to her laboratory for MCD studies.

26. Mason, S. F.; Peart, B. J. *J. Chem. Soc. Dalton Trans.* **1973**, 949. Daul, C.; Schlaepfer, C. W. *J. Chem. Soc. Dalton Trans.* **1988**, 393. Barton, J. K.; Lolis, E. *J. Am. Chem. Soc.* **1985**, *107*, 708. Braterman, P. S.; Noble, B. C.; Peacock, R. D. *J. Phys. Chem.* **1986**, *90*, 4913. Hiort, C.; Nordén, B.; Rodger, A. *J. Am. Chem. Soc.* **1990**, *112*, 1971.

27. Feng, Y.; Roder, H.; Englander, S. W. *Biochemistry* **1989**, *28*, 195.

28. Barker, P. D.; Mauk, A. G. *J. Am. Chem. Soc.* **1992**, *114*, 3619.

29. Brautigan, D. L.; Ferguson-Miller, S.; Tarr, G. E.; Margoliash, E. *J. Biol. Chem.* **1978**, *253*, 140.

30. Spitzer, M.; Gärtig, F.; van Eldik, R. *Rev. Sci. Instrum.* **1988**, *59*, 2092.

31. Cruanes, M. T.; Rodgers, K. K.; Sligar, S. G. *J. Am. Chem. Soc.***1992**, *114*, 9660.

32. Wishart, J. F.; van Eldik, R.; Sun, J.; Su, C.; Isied, S. *Inorg. Chem*, **1992**, *31*, 3986.

33. van Eldik, R.; Asano, T.; Le Noble, W. J. *Chem. Rev.* **1989**, *89*, 549.

34. Casimiro, D. R. Ph. D. Thesis, California Institute of Technology, **1994**.

35. Bowler, B. E., unpublished results.

Chapter 4

Experimental and Theoretical Electronic Couplings in $Ru(bpy)_2(im)HisX$ Cytochromes *c* (X = 33, 39, 62, 72)

I. Introduction

Both theoretical[1-13] and experimental[14-28] studies have indicated that variations in distant electronic couplings play a major role in controlling the rates of ET through proteins. A main goal of the work on $Ru(bpy)_2(im)HisX$ cyts *c* (X = 33, 39, 62, 72) is to develop an experimentally validated coupling map for this protein. Intramolecular ET rates from Fe^{2+} to $Ru(bpy)_2(im)HisX^{3+}$ were measured by time-resolved absorption spectroscopy (Chapter 3). The positions relative to the heme of the four His sites are illustrated in the composite cyt *c* structure in Figure 4.1. The experimentally derived electronic couplings are evaluated in the context of different theoretical formulations to provide insight into the nature of redox center coupling in biological electron transfer.

II. Experimental Electronic Couplings

Electronic couplings (H_{AB}s) can be extracted from the ET rate data and compared if the nuclear factor in the Marcus expression for ET is assumed to be constant in the systems studied. This is not an unreasonable assumption, for in the cyts *c* studied, the redox potential of the heme is invariant (native horse heart cyt *c* = 265 mV, His72 cyt *c* = 255 mV, native *C. k.* cyt *c* = 264 mV,[29] and *S. c.* His62 cyt *c* 268 mV[30] *vs.* NHE) and does not change significantly upon modification with $Ru(bpy)_2(im)^{2+}$ (Chapter 3). The chemical nature of the appended redox probe is conserved, and the solvation environments of both the heme group (evidenced by similar redox potentials) and the protein surface $Ru(bpy)_2(im)^{2+}$ label are similar within the series addressed. Therefore, the driving forces and reorganization energies are expected to be nearly identical in the $Ru(bpy)_2(im)HisX$ cyts *c* studied.

To compare electronic couplings with other systems, it is useful to estimate the activationless rate k_{max}, the anticipated rate constant at $-\Delta G^o = \lambda$. Because the experimental Fe^{2+} to Ru^{3+} ET reactions are nearly activationless, the maximum ET rates are estimated to be nearly the same as the experimental rates. Using a value of $-\Delta G^o$ =

Figure 4.1 Composite figure of His surface residues in cyt *c* illustrating the four regions of the protein reported on, with relative positions of the HisX groups and the heme unit. The heme is red, the polypeptide backbone is blue, and the His sites of $Ru(bpy)_2(im)^{2+}$ attachment are yellow. Counterclockwise from the top, the residues are: His33 (native, horse heart), His39 (native, *C.k.*), His62 (genetically engineered *S. c.*), His72 (semisynthetic horse heart).

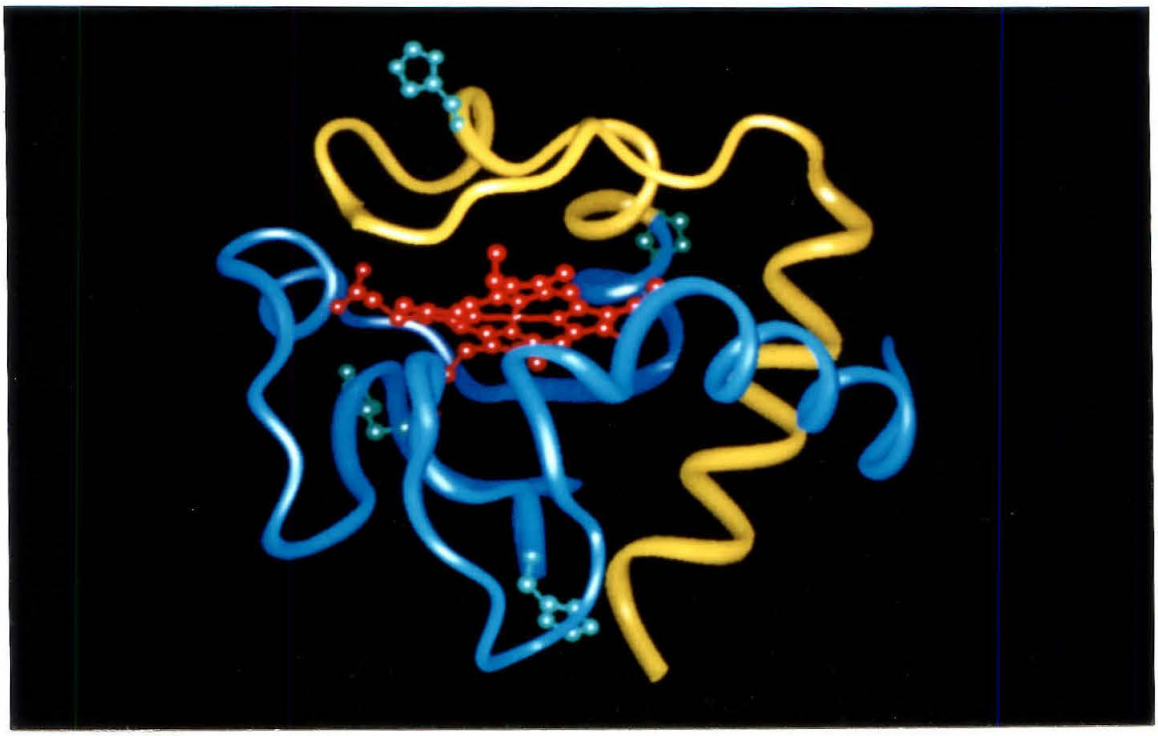

0.74 eV for the ET reaction and estimating λ at 0.80 eV (refer to discussion in Chapter 3), k_{max} and H_{AB} values can be calculated using the semiclassical Marcus expression (for nonadiabatic ETs at fixed distance and medium between donor and acceptor):[1]

$$k_{ET} = \sqrt{\frac{4\pi^3}{h^2 \lambda k_b T}} [H_{AB}]^2 \exp\left(\frac{-(\Delta G^o + \lambda)^2}{4\lambda k_b T}\right)$$

where k_b is Boltzmann's constant, T is temperature, h is Planck's constant, H_{AB} is the matrix element that couples reactants and products at the transition state, ΔG^o is the change in free energy for the reaction, and λ is the sum of the inner and outer sphere contributions to the reorganization energy. Activationless (maximum) rates are therefore limited by the electronic factor:

$$k_{max} = \sqrt{\frac{4\pi^3}{h^2 \lambda k_b T}} [H_{AB}]^2$$

The results of calculations of k_{max} and H_{AB} for the Fe^{2+} to Ru^{3+} (metal to metal) ET rates (k_{ET}^{mm}) are set out in the Table 4.1.

Table 4.1. Experimental ET parameters for $Ru(bpy)_2(im)HisX$ cyts *c*. Numbers in parentheses indicate uncertainties in the preceding digit.

X	k_{ET}* (*Ru^{2+} to Fe^{3+}) s^{-1}	k_{ET}^{mm} (Fe^{2+} to Ru^{3+}) s^{-1}	k_{max} (Fe^{2+} to Ru^{3+}) s^{-1}	H_{AB} (Fe^{2+} to Ru^{3+}) cm^{-1}
39	1.4(5) x 10^6	3.2(4) x 10^6	3.3 x 10^6	0.11
33	2.0(5) x 10^5	2.6(3) x 10^6	2.7 x 10^6	0.097
72	3.4(7) x 10^5	9.0(3) x 10^5	9.4 x 10^5	0.057
62	1.1(2) x 10^5	1.0(2) x 10^4	1.0 x 10^4	0.0060

Rates for the excited-state ET reactions are also given in Table 4.1. In the photoinduced ET reaction, the electron donor in the $*Ru(bpy)_2(im)His^{2+}$ charge-transfer excited state is a bipyridyl radical anion Therefore, these reactions involve ET from the coordinated bipyridyl radical anion at the protein surface. They are highly exoergic ($-\Delta G >> \lambda$). The estimated order of H_{AB} values ($62 \sim 33 \sim 72 < 39$) for the bpy anion to Fe^{3+} ET reactions differs from that derived from the Fe^{2+} to Ru^{3+} rates. No interpretation of these couplings is offered; among the many uncertainties are the nature and magnitude of donor (bpy anion) couplings to groups on the protein surface and the exact position of the bipyridyl ligands with respect to the protein surface and heme-group. The relatively high rates of these reactions are of interest, because the ability to rapidly inject electrons into internal protein redox centers with laser pulses could provide a novel method for studying highly reactive species that often are encountered (or proposed as intermediates) in the catalytic reaction of metalloenzymes. Rapid photoinjection of electrons can also serve as a trigger for the study of protein-folding events on the submicrosecond timescale.

III. Distance-Dependent Model

Most biologically relevant ETs are nonadiabatic and occur at donor-acceptor distances that preclude direct overlap of the donor and acceptors wavefunctions (refer to Chapter 1 for further discussion). Therefore a formulation for electronic couplings *via* the protein medium is necessary. Semiclassical theory predicts that electronic couplings, and thus k_{max} values, will fall off exponentially with distance.[1] This simple formulation of H_{AB} in biological systems assumes the intervening polypeptide is entirely homogeneous and can be treated as a square barrier through which the electron tunnels. The medium serves to lower the barrier height with respect to a vacuum. This model[3] leads to the following formulation of H_{AB}:

$$H_{AB} = H_{AB}^{o} \exp [-1/2\beta (R - R_o)]$$

with H_{AB}^{o} as the electronic coupling at donor / acceptor contact, R is the donor-acceptor distance, and R_o is the donor-acceptor distance at close contact (3 Å), and β is the scaling factor for the rate dropoff with distance.

Dutton and coworkers have evaluated maximum ET rates from a variety of protein and covalently linked donor-acceptor systems as a function of intervening distance.[12] They have found that observed rates in covalently linked systems of the porphyrin / quinone, biphenyl / acceptor, and iridium dimer / pyridinium type with both saturated and unsaturated bridge can be adequately described using a universal β of 0.7 $Å^{-1}$. Similar treatment of rates obtained in photosynthetic reaction centers and in Ru(ammine)-modified heme proteins leads to a monotonic rate dependence on intervening distance, characterized by a β of 1.4 $Å^{-1}$. However, the apparent agreement in the case of the modified heme proteins is somewhat misleading. Firstly, some of the donor-acceptor distances used for the Ru-modified protein are not the ones reported in the original literature. Secondly, the nature of log k_{ET} *vs.* distance plots makes deviations from the fit line by as much as two orders of magnitude less conspicuous.

To evaluate the experimental electronic couplings in terms of a strictly distance-dependent model, donor-acceptor distances in $Ru(bpy)_2$(im)HisX cyts *c* were obtained from $Ru(bpy)_2$(im)HisX cyt *c* structures constructed by combining crystallographic information with molecular modeling. The appropriate crystal structure (ferric horse heart cyt *c* (1.94 Å resolution)[31] for His33 and His72 cyts *c* and ferrous *S. c.* cyt *c* (1.23 Å resolution)[32] for native *C. k.* His39 and *S. c.* His62 cyt *c*) was modified with a $Ru(bpy)_2(im)^{2+}$ fragment modeled from the $Ru(bpy)_2Cl_2$ crystal structure.[33] In the case of genetically (His62) or semisynthetically (His72) produced mutants, the native side chain was replaced with a His residue and these structures locally minimized.[22a] In modeling $Ru(bpy)_2(im)^{2+}$-modified proteins, only the side chain was allowed to move

(*i.e.*, no backbone perturbations). Based on NMR and CD data that indicate the bipyridyl ligands do not interact significantly with the protein and negligible perturbation of secondary structure accompanies $Ru(bpy)_2(im)^{2+}$ modification. The position of the Ru label was minimized with respect to van der Waals contacts with the protein (< 3 Å) by rotation about the C_α-C_β and C_β-C_γ bonds. It was found that energy minimization of each structure did not significantly change any of the measured edge-edge distances compared with the original orientation of the imidazole side chain. The distances measured within a series of low-energy conformers differed by less than 0.2 Å.

Using these structures, the series of donor-acceptor distances set out in Table 4.2 was obtained.

Table 4.2. Summary of distance measurements based on modeling of the $Ru(bpy)_2(im)^{2+}$ label on crystallographically defined protein structures. Minimum edge-edge distances are underlined.

Site	heme to im (Å)	im to axial ligand (Å)	Ru to Fe (Å)	im to Fe (Å)	bpy to heme (Å)
39	<u>12.3</u>	16.1	20.3	15.6	14.6
33	12.8	<u>11.1</u>	17.9	14.8	12.2
72	10.1	<u>8.4</u>	13.8	10.5	11.3
62	<u>14.8</u>	17.8	21.0	18.5	14.4

"Heme," "im," and "bpy" refer to the closest carbon or nitrogen atoms of the conjugated porphyrin, imidazole, and bipyridyl ring(s) (*i.e.*, excluding the heme ring substituents). Axial ligand refers to either the sulfur atom of Met80 or any position on the conjugated ring of His18.

Although different conventions for calculating the distance between the $Ru(bpy)_2(im)$HisX and heme redox centers give different distances (Table 4.2), the *trends*

in these distances are similar regardless of the standard used. We define edge-edge distance as the nearest point on the imidazole ring (usually Cγ) of the Ru label to the nearest point on the coupled heme chromophore (including the conjugated porphyrin ring or axial ligand substituents). Shortest distances using this definition are underlined in Table 4.2. A summary figure of the His side-chain position and heme-His distances is presented in Figure 4.2. Analyses are also presented throughout using metal-metal distances to demonstrate that the interpretation of the electronic coupling data is independent of the donor-acceptor distance measurement convention chosen. However, in the absence of crystal structures of the $Ru(bpy)_2(im)^{2+}$-modified proteins, the metal-metal distance measurements are known to less accuracy than the edge-edge distances because the flexibility of the His side chain prevents determination of the exact position of the Ru metal center.

Plots of log k_{max} as a function of edge-edge distance shows that the ET rates measured in cyt *c do not* correlate with edge-edge or metal-metal distance (Figure 4.3 A and B). (Distances are plotted as R - R_o, where the contact distance R_o = 3 Å.) Furthermore, if a maximum ET rate of 3 x 10^{12} s^{-1} at close contact (3 Å) is assumed, the edge-edge distance dependences for covalently coupled donor-acceptor complexes are represented adequately by lines with slopes of 0.8 to 1.2 $Å^{-1}$ (Figure 4.4).[34] Because the maximum ET rates for all the $Ru(bpy)_2(im)$HisX-modified cyts *c* lie well below these lines, it is apparent that the Fe^{2+} to Ru^{3+} electronic couplings are weaker than the corresponding donor-acceptor interactions in purely covalently coupled systems. If we draw a best fit line through the Fe^{2+} to Ru^{3+} points (dotted line, Figure 4.4), its 3 Å intercept (1.6 x 10^8 s^{-1}) is much smaller than that expected for a system in which the terminal atoms of the bridging group are covalently bonded to the donor [(Fe^{2+} (heme *c*)] and the acceptor [Ru^{3+} (HisX)]. Thus couplings through the protein medium are significantly weaker and decrease more rapidly with distance than covalently bound donor-acceptor systems.

Figure 4.2 Summary of minimum edge-edge distances for the $Ru(bpy)_2(im)HisX$ cyts *c* studied as defined in the text.

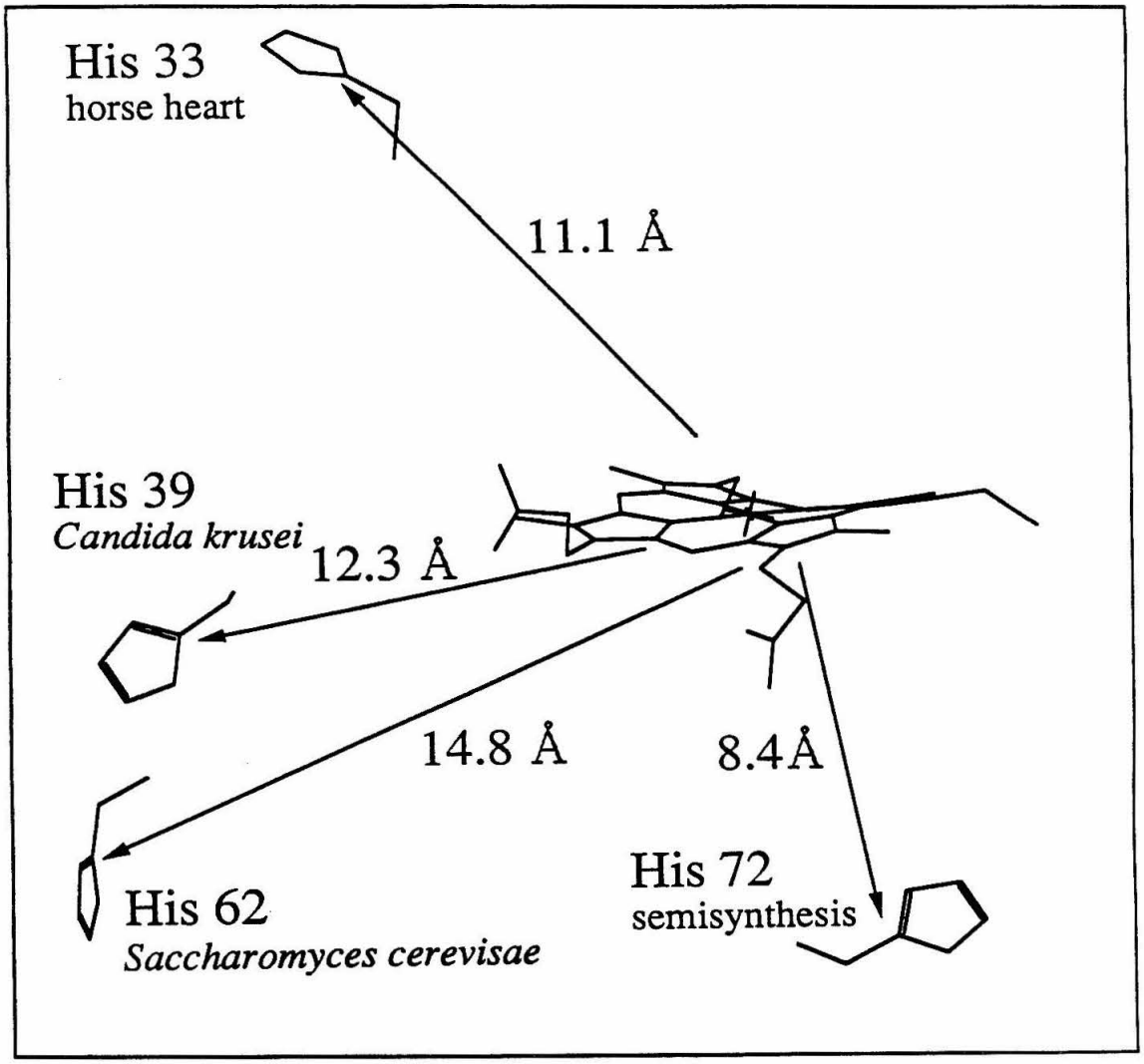
His 33
horse heart
11.1 Å
His 39
Candida krusei
12.3 Å
14.8 Å
8.4Å
His 62
Saccharomyces cerevisae
His 72
semisynthesis

Figure 4.3 Maximum ET rates for the Fe^{2+} to Ru^{3+} ET reaction versus (A) edge-edge and (B) metal-metal distance. Distances are those measured from $Ru(bpy)_2(im)HisX$ cyt *c* structures minus a contact distance, R_o, of 3 Å.

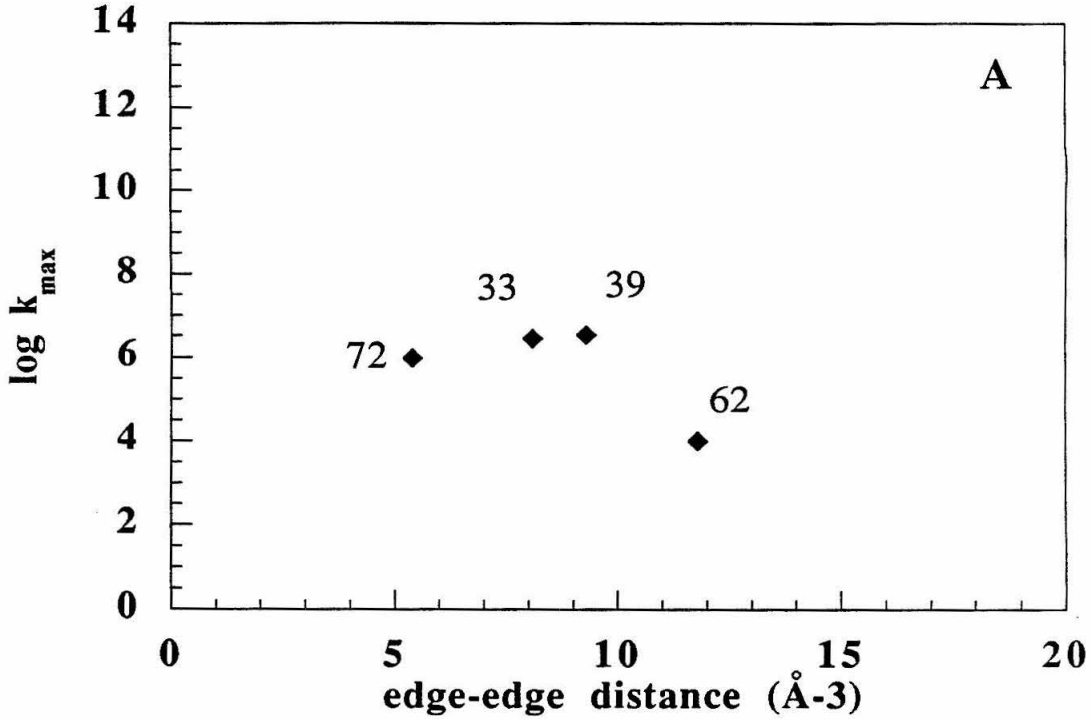
A
log k_{max}
14
12
10
8
6
4
2
0
0
5
10
15
20
edge-edge distance (Å-3)
72
33
39
62

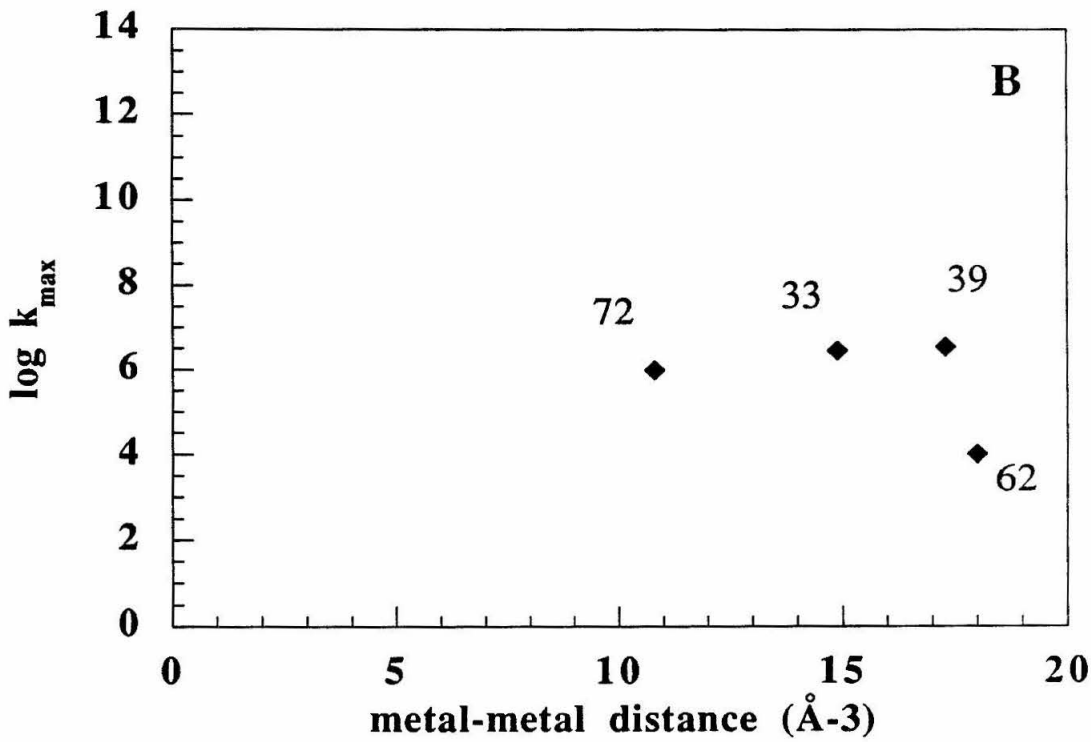
B
log k_{max}
14
12
10
8
6
4
2
0
0
5
10
15
20
metal-metal distance (Å-3)
72
33
39
62

Figure 4.4 Maximum ET rates (X = 33, 39, 62, and 72) versus edge-edge distance minus 3 Å (van der Waals contact). Exponential-decay lines: slope 1.0 $Å^{-1}$ (solid line); 0.8 to 1.2 $Å^{-1}$ (dashed lines); intercept 3 x 10^{12} s^{-1}. Best fit (dotted) line: slope = 0.66 $Å^{-1}$; intercept 1.6 x 10^{8} s^{-1}.

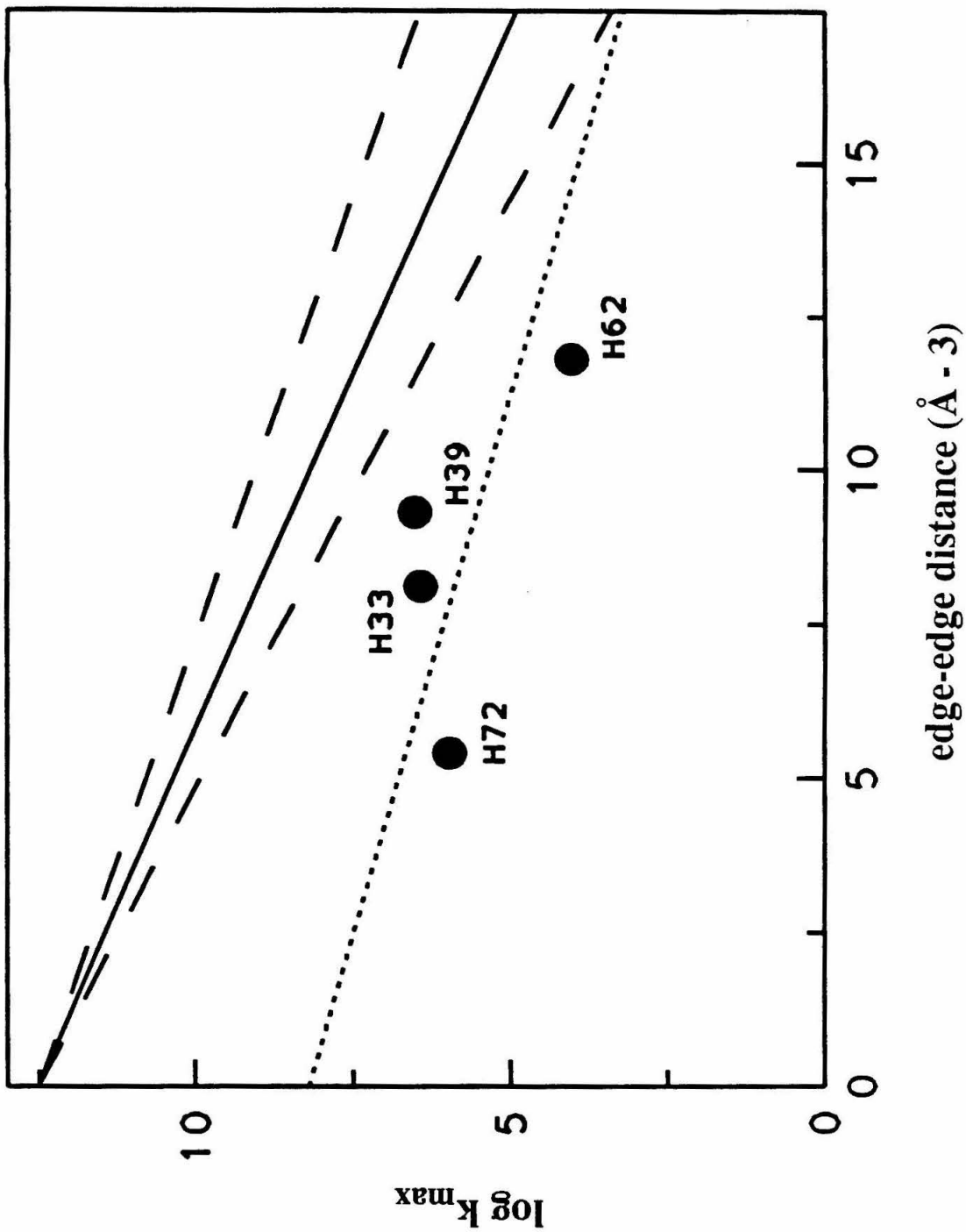
log k_{max}
10
5
0
0
5
10
15
edge-edge distance (Å - 3)
H62
H39
H33
H72

Activationless intraprotein ET spanning twelve orders of magnitude in rate and nearly 19 Å in redox-site separation has been interpreted in terms of edge-edge exponential decay with a 1.4 $Å^{-1}$ slope and a 1 x 10^{13} s^{-1} intercept.[12] Implicit in this interpretation is the assumption that the intervening polypeptide can be treated as a homogeneous medium. This correlation, then, serves as a reference line; deviations from this line indicate situations in which inhomogeneities must be considered. The cyt *c* activationless rate data as a function of both edge-edge and metal-metal distances are plotted coincident with the $\beta = 1.4$ $Å^{-1}$, 1 x 10^{13} s^{-1} intercept line in Figure 4.5 A and B. Because one of the measured k_{max} values (X = 72) lies four orders of magnitude below this edge-edge exponential-decay line, and two others (X = 33, 62) deviate from the line by more than a factor of 50, analysis in terms of the intervening medium is called for. Thus, it is readily apparent that there is no correlation with donor-acceptor distance and none of the exponential-decay models satisfactorily explains the experimental data.

IV. Medium-Dependent Models

With the failure of a simple distant-dependent model to account for observed rates in $Ru(bpy)_2(im)HisX$-modified cyts *c*, mechanisms[4,5,10] that allow the specific character of the intervening wavefunctions to mediate the electronic coupling between donor and acceptor were investigated. In these formulations, there are no "intermediates" in which the electron resides at some point within the intervening medium, however the specific HOMO and/or LUMO orbitals of the medium are used to couple the donor and acceptor in the ET reaction, thus effectively lowering the tunneling barrier. These treatments differ from the distance-dependent formulations, which also invoke distant electronic coupling *via* the medium, in that medium-dependent formulations propose that specific interactions within the medium enhance or attenuate coupling at a given donor-acceptor distance.[35]

Figure 4.5 Maximum ET rates (X = 33, 39, 62, and 72) versus (A) edge-edge and (B) metal-metal distance minus 3 Å (van der Waals contact). Exponential decay line with 1 x 10^{13} s^{-1} intercept and 1.4 $Å^{-1}$ slope.

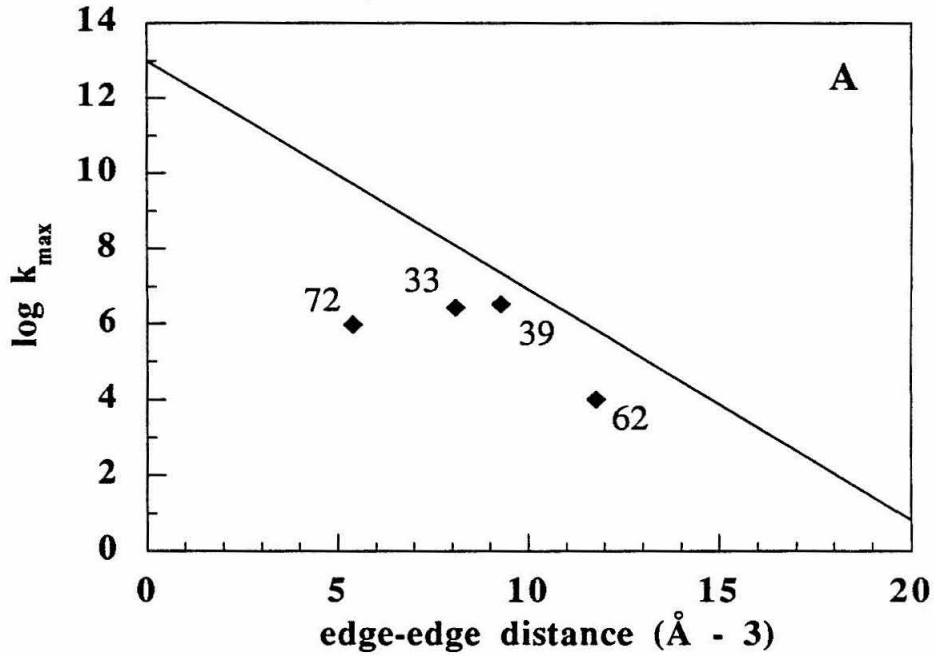
A
log k_{max}
14
12
10
8
6
4
2
0
72
33
39
62
0
5
10
15
20
edge-edge distance (Å - 3)

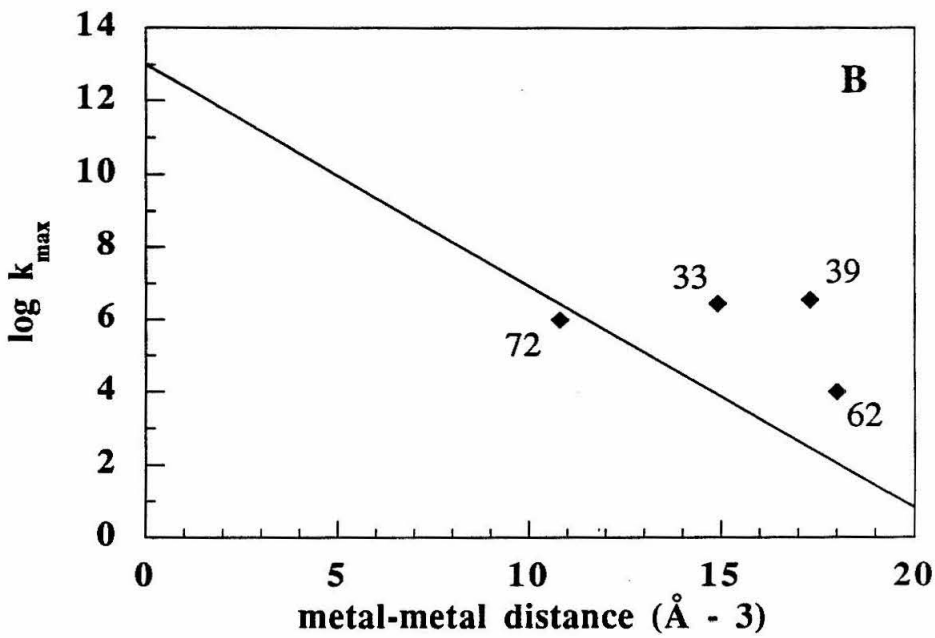
B
log k_{max}
14
12
10
8
6
4
2
0
33
39
72
62
0
5
10
15
20
metal-metal distance (Å - 3)

Initial work investigating medium dependence in biological long-range ET focused on the role of intervening aromatic residues, due to energetic accessibility of the low energy LUMO and high energy HOMO orbitals. However, following some initial indications to the contrary,[19] it has been demonstrated that the mere presence of an aromatic group in the intervening medium is not sufficient for enhanced couplings.[20,26] (Coupling *via* aromatic moieties may be important in appropriately oriented systems, *e.g.*, the role of the intervening chlorophyll between the special pair and the pheophytin in the photosynthetic reaction centers may be to couple the initial ET step through a superexchange mechanism. Alternatively, the chlorophyll may serve as the site of a transiently populated ET intermediate.[36])

A. σ-Bond-Tunneling Pathway Model

1. Theory and Algorithm

In a first-order approach for including the composition of the protein medium in electronic coupling predictions, David Beratan and José Onuchic formulated the coupling properties of the intervening in terms of three simple elements.[4] Each element is assigned an intrinsic coupling value, and the total coupling between donor and acceptor is equal to the product of the intervening coupling elements. While empirical, this approach allows direct evaluation of electronic couplings in terms of the chemical nature of the intervening medium.

In analogy to covalently bonded donor-acceptor systems, one might attempt to evaluate electronic couplings by following the direct covalent connectivities between the donor and acceptor species. In proteins, however, the complex fold of the polypeptide generally makes these direct routes far too long and circuitous mediate the measured couplings. Therefore, while sigma-bond hole-tunneling through covalent bonds is the basis of the pathway model, two other types of molecular interactions are considered to facilitate electronic couplings within the polypeptide structure, albeit less strongly than

the coupling assigned to a full covalent bond. The dominant coupling pathway can then "shortcut" a circuitous covalent pathway through either a hydrogen bonding (H-bond) interaction or, if favorable, a through-space interaction. These weaker coupling interactions will only be important if their net coupling is larger than the coupling afforded by the all covalently bonded route connecting the donor and acceptor species.

The coupling due to a σ-bond tunneling pathway is partitioned into the product of the individual coupling elements along a pathway linking the donor and acceptor. The coupling is expressed as:

$$H_{AB} \propto \prod_i \varepsilon_C(i) \prod_j \varepsilon_H(j) \prod_k \varepsilon_S(k)$$

ε are the decay factors for i covalently bonded interactions, j H-bonded interactions, and k through-space jumps in the pathway. The numerical values assigned to each type of interaction are discussed below.[4a]

Inspection of the literature on experimentally derived couplings in donor-acceptor systems indicates a coupling per bond of 0.7 to 0.4.[7b] A consensus value of 0.6 was therefore selected for ε_C, the coupling decay per covalent bond.[4f] Note that this treatment does not distinguish between types of covalent bonds or address orientation effects. Relative to the differences between the three types of coupling interactions, the effects due to the orientation and variation in the types of covalent bond assume a secondary role in determining coupling.

Through-space interactions are treated as bonds attenuated by tunneling through a barrier. A rapid exponential decay through space of 1.7 $Å^{-1}$ was proposed based on the penetration of a one-dimensional square barrier by a 5 - 10 eV electron.[4a] The tunneling distance is taken as the atom-to-atom distance minus one covalent bond (average value = 1.4 Å). The exponential decay term is divided by a factor of 2 in order to account for unfavorable orientation effects.

Since H-bonding interactions bring lone pair and bonding orbitals in close proximity in a weakly bonding interaction, they are treated as two "stretched" covalent bonds. H-bond interactions are treated as a covalent bond attenuated through space by the same decay factor used for through-space interactions. However, the attenuation distance is now the atom-to-atom distance minus two covalent bonds (2.8 Å). Potential H-bonding interactions in the protein structure are evaluated computationally because H-atom positions are not crystallographically defined.

To summarize, each individual coupling interaction will be numerically evaluated as:

$$\varepsilon_C = 0.6$$

$$\varepsilon_H = \varepsilon_C^2 \exp [-1.7 (R - 2.8)]$$

$$\varepsilon_S = (0.5) \varepsilon_C \exp [-1.7 (R - 1.4)]$$

with R as the atom-to-atom distance (not including hydrogen atoms). It is important to note that the results of the pathway analysis of couplings are *qualitative* and only relative H_{AB} values are calculated. Thus the calculated couplings cannot be directly compared to the experimental H_{AB} values.

An algorithm based on graph theory[37] has been written that searches all potential pathways between defined donor and acceptor atoms in crystal structures using the principles described.[4b] The details of the program design and operation are discussed in Reference 4a. Pathways more weakly coupled than a predefined cutoff value are discarded and the remaining pathways presented in order of decreasing couplings. A text file describing each pathway step by step as well as a vector file to be used in conjunction with the input structure file for visualizing the pathway on a graphics terminal are output from the program.

All pathway calculations were performed with the FORTRAN program Pathways, V 2.2 written by J. N. Betts, D. N. Beratan, and J. N. Onuchic on Biograf-formatted $Ru(bpy)_2(im)HisX$-modified structure files with heteroatom hydrogen atoms added. The program was run on Silicon Graphics Personal IRIS and INDIGO workstations. The following parameters were used:

radius_limit1:	0.00
radius_limit2:	5.00
guess_limit:	0.00
search_limit:	1.00E-06
range_limit:	1.00E-19
cv_dist:	1.40
cv_hab:	0.60
ts_scale:	0.50
beta:	1.70
slop:	0.90
srch_slop:	0.50
hbond_limit:	3.50
hbond_hab:	0.36
hbond_dist:	2.90
hbond_exp:	1.70
hbond_angle:	90.00

The pathway program has been used to calculate a coupling map for cyt *c* that color codes each atom in the protein's structure according to the intensity of the predicted pathway coupling relative to the distance-dependent coupling for that atom.[4d] This map allows identification of regions where pathway-dependent and distance-dependent predictions of coupling differ. "Hot" regions are positions in the structure where the pathway coupling is stronger than expected given the donor-acceptor separation, while "cold" regions represent sites where the pathway coupling redox centers is unusually poor relative to the donor-acceptor distance. His33 and His62 correspond to sites where the pathway and distance analysis predict similar results. His39 is a "hot" spot, with enhanced coupling predicted due to the medium, while His72 is "cold", since the medium is predicted to inhibit coupling. As will be seen, these predictions are consistent with the experimentally derived couplings.

2. Dominant σ-Tunneling Pathways in Cytochrome c

σ-Tunneling pathways were calculated as described using the modeled $Ru(bpy)_2(im)HisX$ cyt *c* structures constructed for the donor-acceptor distance analysis. The results for the HisX-modified proteins are summarized below. As a check on the search algorithm, pathways were searched both using the iron atom as donor and C_γ of the labeled His residue as acceptor and *visa versa.* The same results were obtained regardless of the direction of the search. The C_γ atom of the labeled His residue was selected as the point of attachment since the position of the $Ru(bpy)_2(im)^{2+}$ ligands with respect to the protein surface is not known. Therefore pathways involving space-jumps from the Ru ligands to other residues on the protein surface were considered irrelevant. However, pathways calculated using the Ru atom as the terminal atom contained none of these potential artifactual pathways. Families of pathways were commonly found. They are composed of a series of nearly equivalent pathways that take slightly different atomic steps through essentially the same amino acids, *e.g.*, coupling through one side of a His ring or the other, or backtracking through a neighboring residue. Only the best pathway for each family is described.

His33: The best pathway for His33 has 11 covalent bonds and one hydrogen bond (3.16 Å) and is illustrated in Figure 4.6. Coupling is from His33 through the backbone through Leu32 to Asn31 to Pro30 followed by a H-bond jump from the Pro30 backbone carbonyl oxygen to the δN of His18; calculated coupling: $\varepsilon_T = 8.45 \times 10^{-4}$. Other pathways found with couplings within an order of magnitude of the dominant pathway are (atomic connections are covalent unless otherwise indicated):

1. His33 - Leu32 - Asn31 - (H-bond, 3.42 Å) - Arg38 - (H-bond, 2.76 Å) - heme propionate. 12 covalent bonds, 2 H-bonds: $\varepsilon_T = 1.47 \times 10^{-4}$.
2. His33 - Leu32 - (H-bond, 2.70 Å) - Thr19 - His18. 14 covalent bonds, 1 H-bond: $\varepsilon_T = 3.97 \times 10^{-4}$.

Figure 4.6 Dominant σ-tunneling pathway from His33 to the heme. The path extends from His33 through the backbone through Leu32 to Asn31 to Pro30 followed by a H-bond (3.16 Å) jump from the Pro30 backbone carbonyl oxygen to the δN of His18. Covalent bonds are represented by lines and the hydrogen bond by a dashed line.

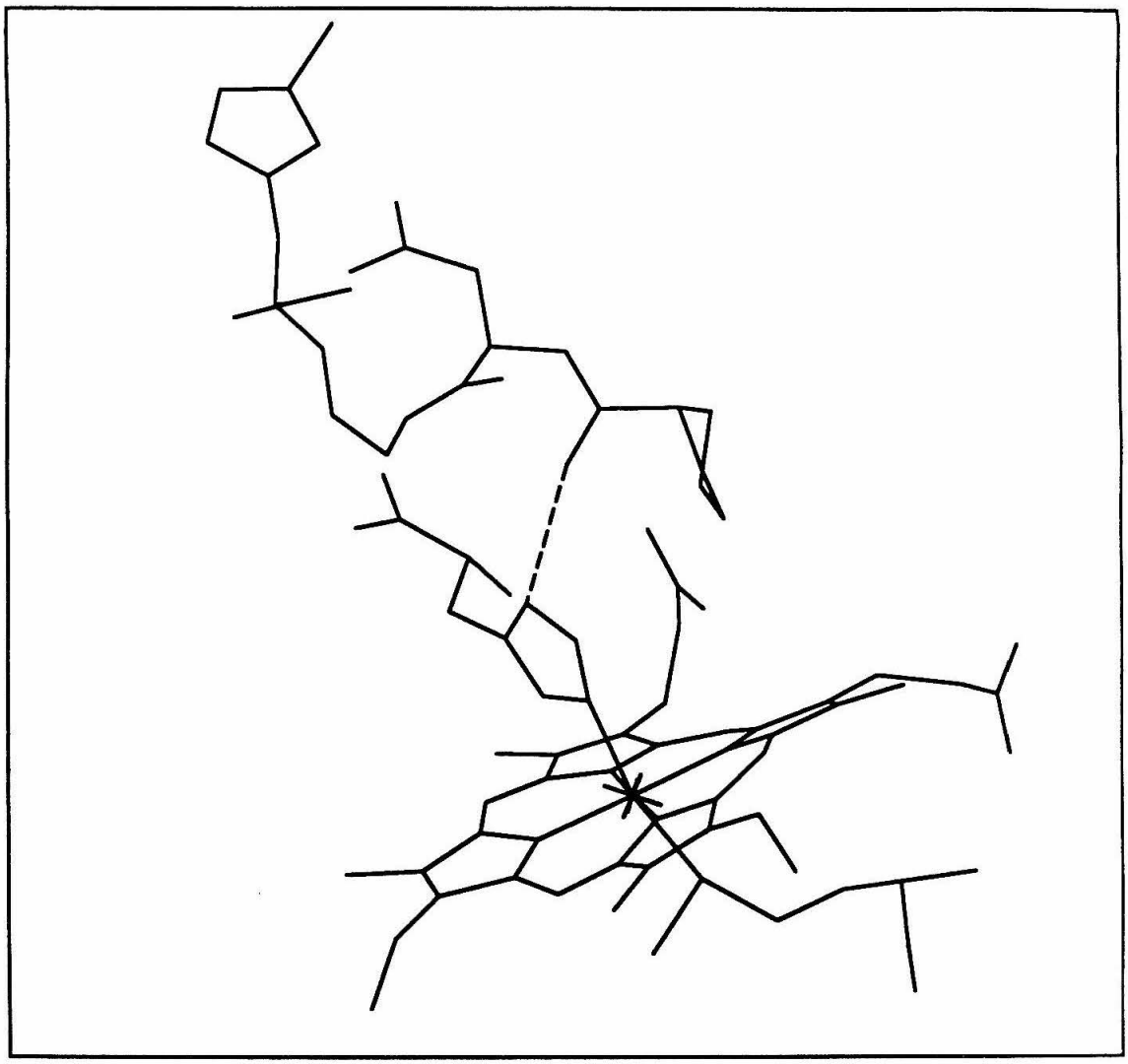

3. His33 - Leu32 - (space jump, 3.79 Å) - heme. 8 covalent bonds, 1 space jump: $\varepsilon_T = 8.61 \times 10^{-5}$.

His39: The best His39 pathway also has 11 covalent bonds and 1 hydrogen bond and is illustrated in Figure 4.7. The pathway follows covalent linkages from His39 to Ser40 to Gly41, followed by a H-bond (3.21 Å) from the N of the amide backbone to the heme propionate; $\varepsilon_T = 7.65 \times 10^{-4}$. Pathways found that utilized a crystallographically defined water molecule were discarded, because the dynamics of these water molecules in the solution structures are not understood. No other well-coupled pathways were found.

His62: The dominant His62 pathway includes 16 covalent bonds and 2 H-bonds. The pathway is covalently linked from His62 to the backbone followed by a 2.91 Å H-bond from His62 NH to the Asp60 carbonyl oxygen. The path is again all covalently linked through to the εN of Trp59 followed by a H-bond to the heme propionate; $\varepsilon_T = 2.60 \times 10^{-5}$. A nearly equivalent pathway exists for His62 that consists of 12 covalent bonds and space jump of 3.6 Å.[22] This pathway traces the backbone from His62 to Asn63 to Met64 through the Met64 side chain and ends with a 3.64 Å through-space jump from the sulfur to the heme edge; $\varepsilon_T = 1.46 \times 10^{-5}$. The two dominant pathways are shown in Figure 4.8. Many pathways related to the dominant ones were found for this weakly coupled system. Others are:

1. His62 - (H-bond, 2.91 Å) - Asp60 - (H-bond, 3.08 Å) - Met64 - (space jump, 3.64 Å) - heme. 8 covalent bonds, 2 H-bonds, 1 space jump: $\varepsilon_T = 1.06 \times 10^{-5}$.
2. His62 - (H-bond, 2.96 Å) - Ser 65 - Met64 - (H-bond, 2.95 Å) - Leu68 - (space jump, 4.02 Å) - heme. 10 covalent bonds, 2 H-bonds, 1 space jump: $\varepsilon_T = 2.30 \times 10^{-6}$.
3. One set of calculated pathways, His62 to Asn63 - (H-bond, 2.72 Å) - Tyr67 - (H-bond, 3.25 Å) - S (Met80), 14 covalent bonds, 2 H-bonds, were discarded because

Figure 4.7 Dominant σ-tunneling pathway from His39 to the heme. The path extends from His39 to Ser40 to Gly41, followed by a H-bond (3.21 Å) from the N of the amide backbone to the heme propionate. Covalent bonds are represented by lines and the hydrogen bond by a dashed line.

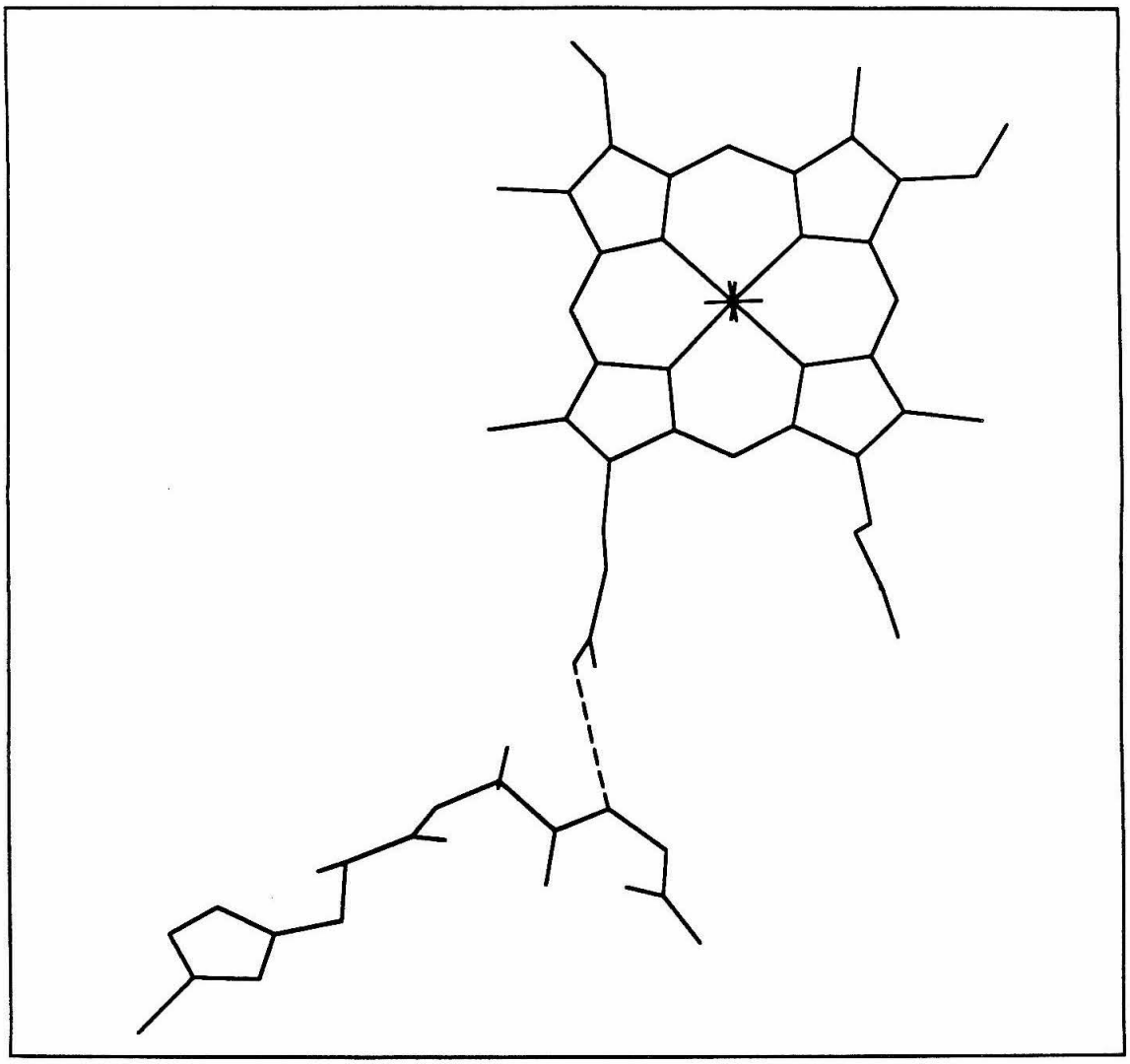

Figure 4.8 The two dominant σ-tunneling pathways from His62 to the heme. The first pathway starts with covalent linkages from His62 to the backbone followed by a 2.91 Å H-bond from His62 NH to the Asp60 carbonyl oxygen. The path is covalently linked through to the εN of Trp59 followed by a H-bond to the heme propionate. The second path traces the backbone from His62 to Asn63 to Met64 through the Met64 side chain and ends with a 3.64 Å through-space jump from the sulfur to the heme edge. Covalent bonds are represented by lines, hydrogen bonds by dashed lines, and the space jump by a dotted line.

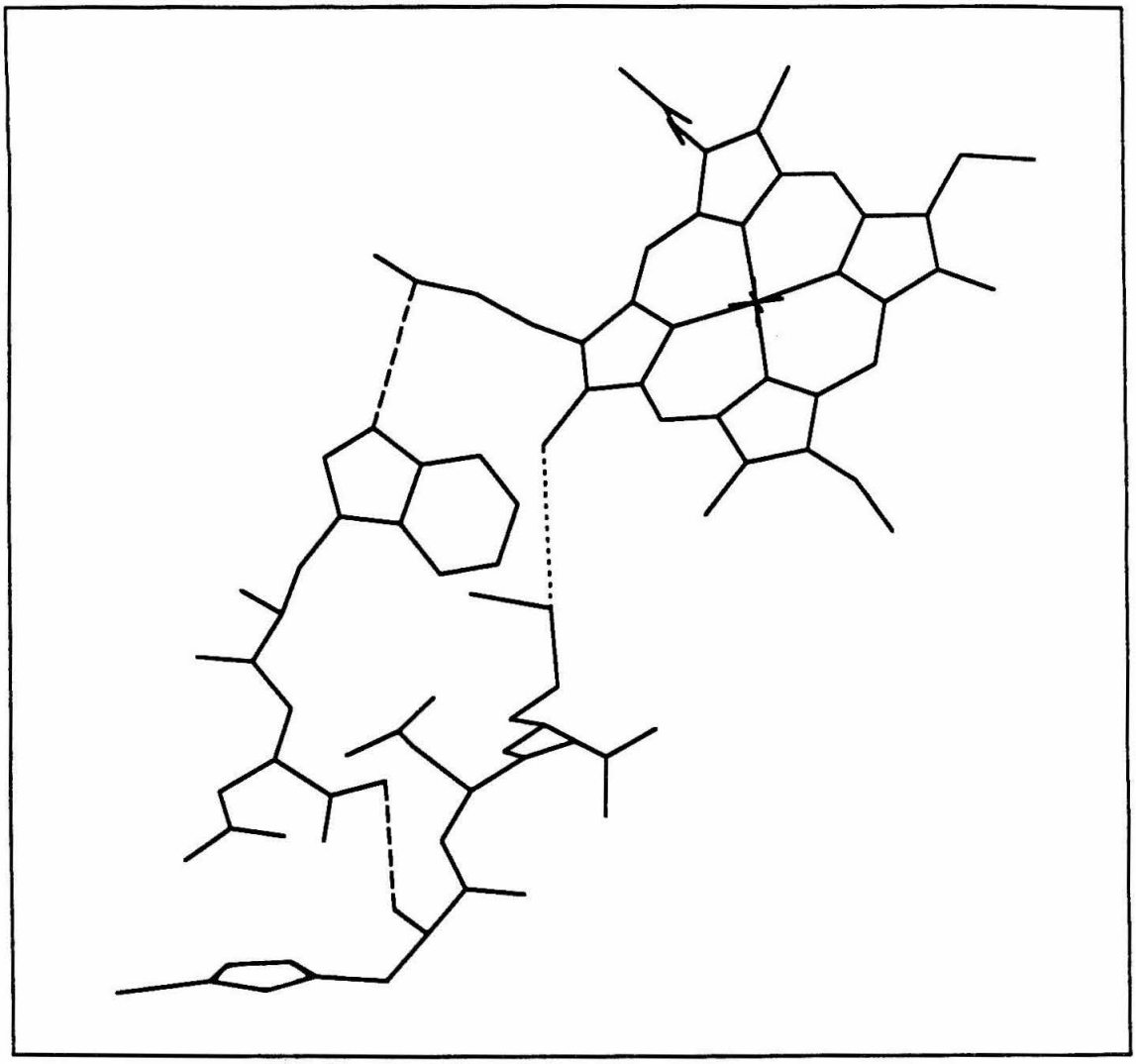

the proposed long-range H-bonding interaction is not present in the protein; the Tyr OH-group is involved in a H-bond interaction with a crystallographically defined water molecule. Treatment of this interaction as a through-space jump gives this pathway an $\varepsilon_T = 5.00 \times 10^{-6}$.

His72: Of special interest is the finding that there are no good routes to couple His72 to the heme, even though this site has the shortest edge-edge distance in the series studied. The Met80 side of the heme has predominantly through-space contacts with the helix containing His72, and the best pathway extends from His72 through Pro71 with a 3.88 Å through-space jump from Pro C_β to Met80 C_ε (Figure 4.9). Although there are only 8 covalent bonds in this path, the through-space jump adds the equivalent of 10.6 bond units to the σ-tunneling length; ($\varepsilon_T = 1.23 \times 10^{-4}$). The Pro71 to Met80 space jump pathway was represented in several slightly different pathways. Other families of pathways that were within an order of magnitude are:

1. His72 - Pro71 - (H-bond, 3.03 Å) - Ile75 - (H-bond, 2.97 Å) - Thr78 - (H-bond, 2.56 Å) - heme propionate. 15 covalent bonds, 3 H-bonds: $\varepsilon_T = 2.80 \times 10^{-5}$.
2. His72 - Pro71 - Asn70 - (H-bond, 2.53 Å) - Tyr67 - (H-bond, 3.32 Å) - Met80. 17 covalent bonds, 2 H-bonds: $\varepsilon_T = 2.00 \times 10^{-5}$.

The dominant σ-tunneling pathways obtained based on the above calculations are shown in the composite cyt *c* structure in Figure 4.10.

The couplings obtained from the calculated pathways are converted to effective bond lengths (n_{eff}) using a one-bond decay of 0.6. For example, a H-bond of 3.25 Å has an ε_H of 0.20, which equals $(0.6)^n$, therefore that H bond is equal to n = 3.2 bond units. Generally, an average H-bonding interaction is equivalent to 2 - 3 covalent bonds in the pathway model. Through-space interactions are less favorable, with a 3.88 Å space jump the equivalent of 10.6 bond units. Multiplying the effective number of bonds by 1.4 Å

Figure 4.9 Dominant σ-tunneling pathway from His72 to the heme. The path extends from His72 to Pro71 via covalent linkages, followed by a critical 3.88 Å through-space jump from Pro C_β to Met80 C_ε. Covalent bonds are represented by lines and the space jump by a dotted line.

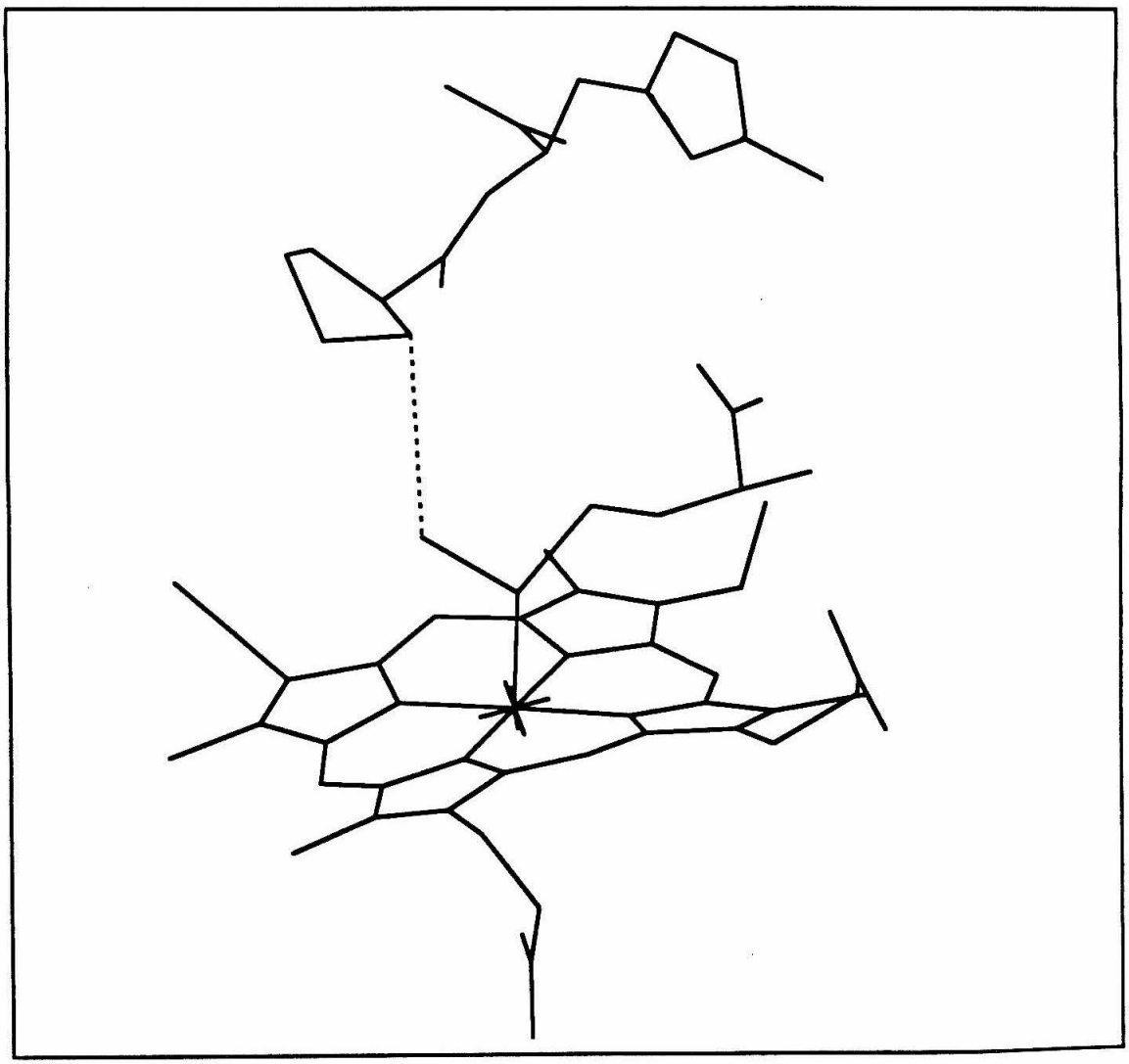

Figure 4.10 Dominant σ-tunneling pathways from the imidazole to the heme based on the σ-tunneling pathway model of Beratan, Betts and Onuchic.[4] Covalent bonds are represented by lines, hydrogen bonds by dashed lines and the space jump by a dotted line.

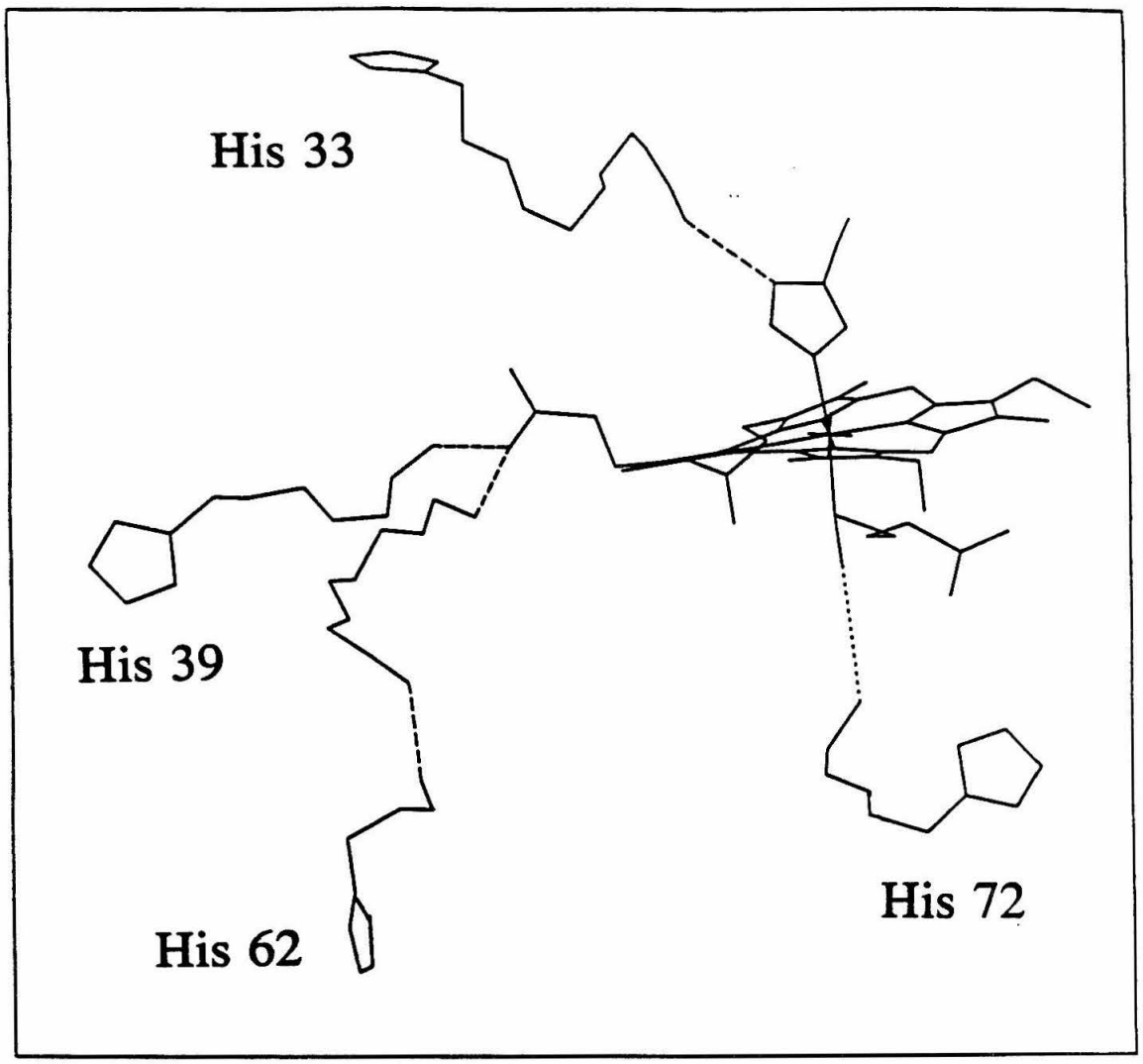
His 33
His 39
His 62
His 72

per bond gives σ-tunneling lengths (σl) for the four pathways. Edge-edge distances, n_{eff}s and σls for the four pathways considered are summarized in Table 4.3.

Table 4.3. Experimental couplings, edge-edge distances, and edge-edge sigma-tunneling pathlengths for $Ru(bpy)_2(im)HisX$ cyts *c*.

X	H_{AB} (Fe^{2+} to Ru^{3+}) (cm^{-1})	$d_{edge\text{-}edge}$ (Å)	n_{eff}	$\sigma l_{edge\text{-}edge}$ (Å)
39	0.11	12.3	14.0 (11 C) (1 H)	19.6
33	0.097	11.1	13.9 (11 C) (1 H)	19.5
72	0.057	8.4	17.6 (7 C) (1 S)	24.6
62	0.0060	14.8	20.6 (16 C) (2 H)	28.8

C = covalent bond, H = hydrogen bond, and S = space jump.

We find that the maximum ET rates correlate with a bond-length scale that takes into account the weaker couplings associated with hydrogen bonds and through-space jumps in dominant pathways. The maximum ET rates correlate well with σ-tunneling lengths (one-bond limit set at 3×10^{12} s^{-1}; slope of 0.71 $Å^{-1}$) (Figure 4.11). This correlation is particularly striking when directly compared to the edge-edge distance plot with a line representing $\beta = 1.4$ $Å^{-1}$, intercept of 10^{13} s^{-1} from Dutton's distance analysis (Figure 4.12).

It is interesting to address the effect on the correlation of k_{max} with the σ-tunneling lengths if the metal-to-metal pathways and multiple edge-edge pathways are used. Metal-metal pathways are essentially the edge-edge pathways with the appropriate number of covalent bonds added. Only the His72 point is affected because the bond count for this site increases by only four bonds whereas the bond counts for the other

Figure 4.11 Maximum ET rates (X = 33, 39, 62, and 72) versus σ-tunneling length (σl): slope 0.71 $Å^{-1}$; intercept 3 x 10^{12} s^{-1}. The fit β-value of 0.71 $Å^{-1}$ correlates well with the theoretically predicted value of 0.73 $Å^{-1}$, assuming ε = 0.6 for a 1.4 Å covalent bond ($\beta = \frac{2\ln(0.6)}{1.4Å}$).

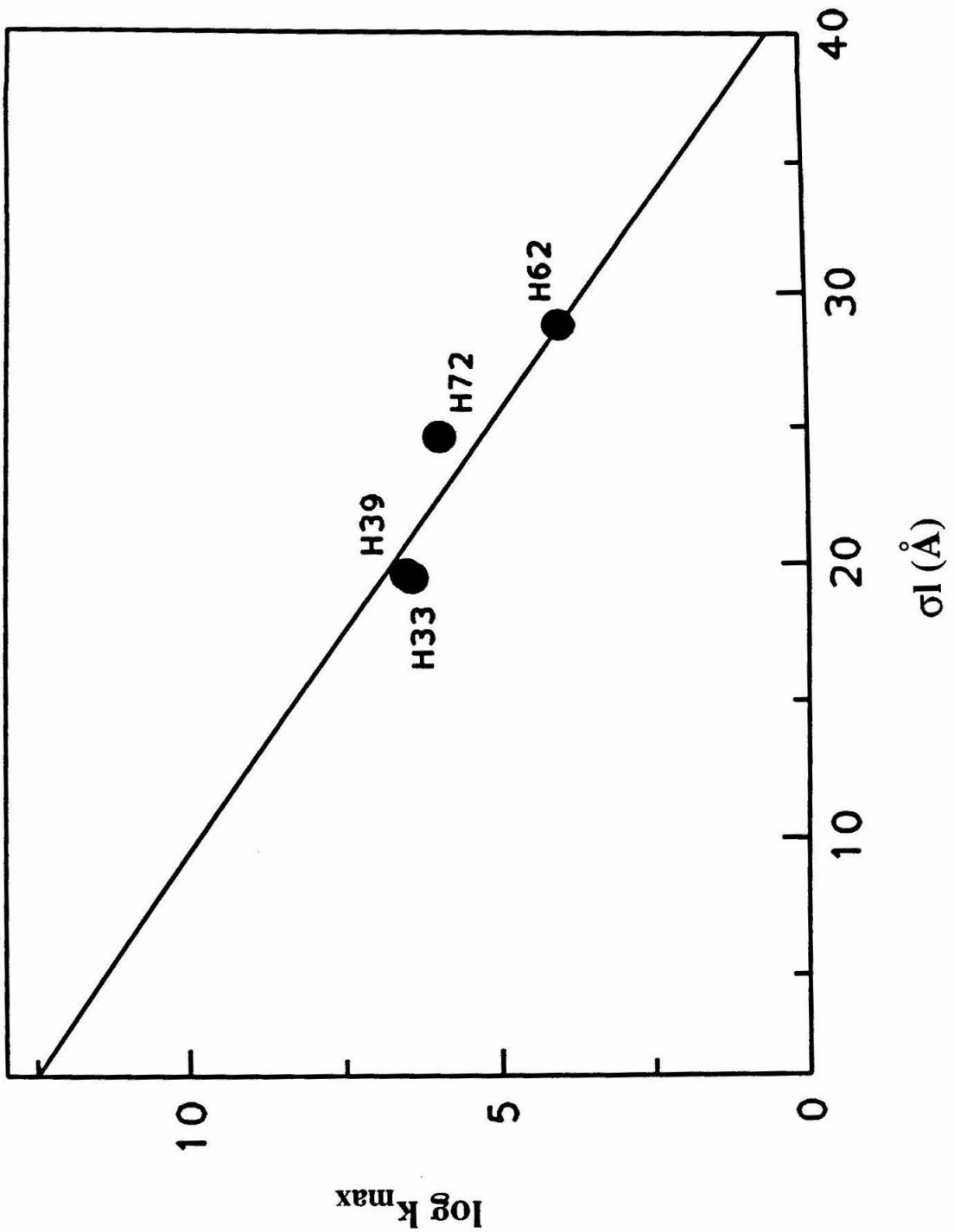
log k_{max}
10
5
0
40
30
20
10
σI (Å)
H62
H72
H39
H33

Figure 4.12 (A) Maximum ET rates (X = 33, 39, 62, and 72) versus edge-edge distance minus 3 Å (van der Waals contact). Exponential decay line with 1 x 10^{13} s^{-1} intercept and 1.4 $Å^{-1}$ slope. (B) Maximum ET rates (X = 33, 39, 62, and 72) versus σ-tunneling length (σl): slope 0.71 $Å^{-1}$; intercept 3 x 10^{12} s^{-1}.

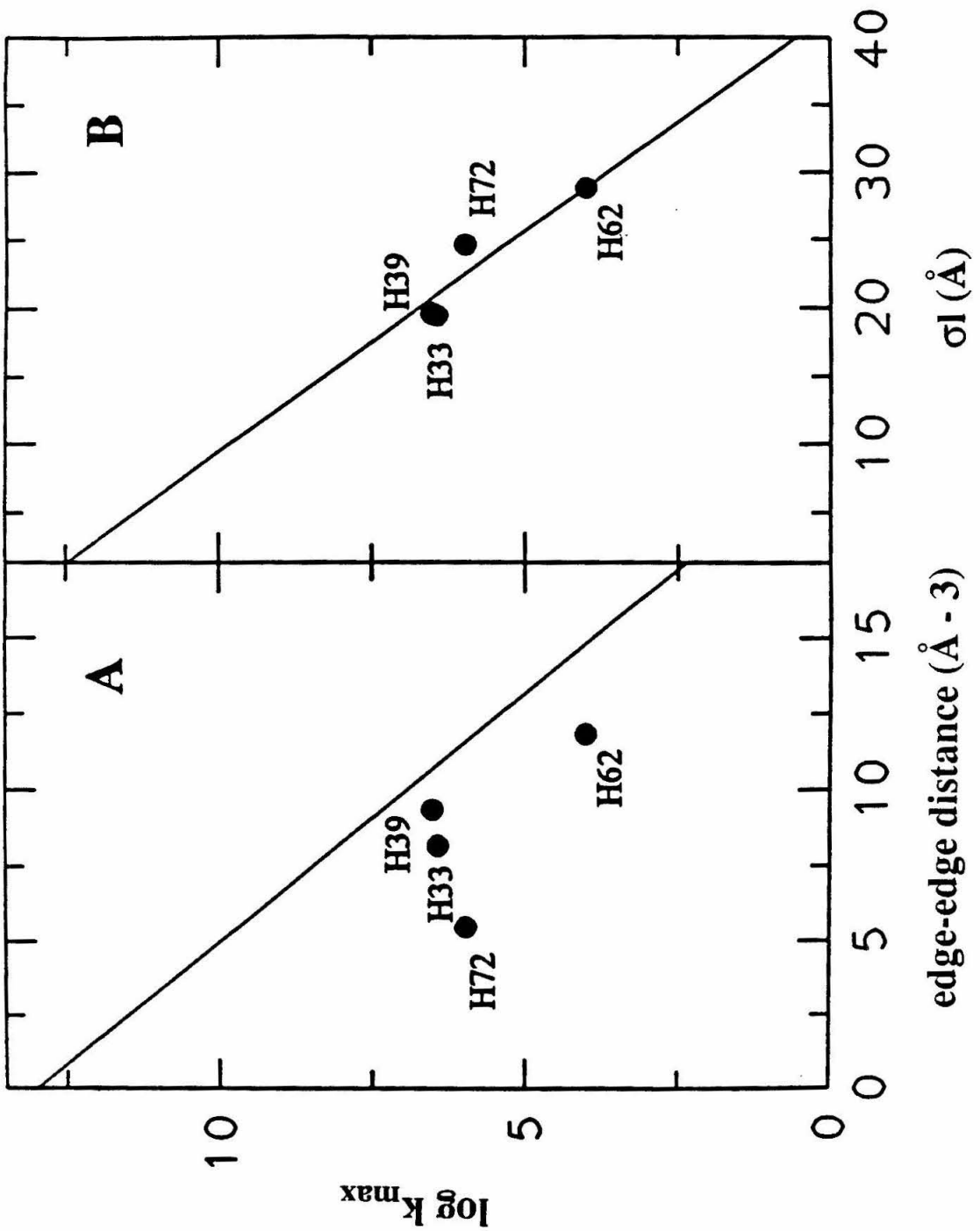
A
B
H72
H39
H33
H62
log kmax
edge-edge distance (Å - 3)
σl (Å)
0
5
10
15
20
30
40

sites increase by six bonds. Metal-metal σ-tunneling pathway parameters are summarized in Table 4.4.

Table 4.4. Experimental couplings, metal-metal distances, and metal-metal σ-tunneling pathlengths for $Ru(bpy)_2(im)HisX$ cyts *c*.

X	H_{AB} (Fe^{2+} to Ru^{3+}) (cm^{-1})	$d_{metal\text{-}metal}$ (Å)	n_{eff}	$\sigma l_{metal\text{-}metal}$ (Å)
39	0.11	20.3	20.0 (17 C) (1 H)	28.0
33	0.097	17.9	19.9 (17 C) (1 H)	27.9
72	0.057	13.8	21.6 (10 C) (1 S)	30.2
62	0.0060	21.0	26.6 (22 C) (2 H)	37.2

C = covalent bond, H = hydrogen bond, and S = space jump.

Multiple edge-edge σ-tunneling pathways were calculated using the sum of all pathways (n) within an order of magnitude of the dominant pathway, including all representatives of a given pathway family (n = 1 (His39), 5 (His33), 11 (His72) and 10 (His62).[23] Table 4.5 is a summary of the σ-tunneling pathlengths for the edge-edge, metal-metal, and multiple edge-edge formulations.

Plots of k_{max} as a function of σl and fits of these points to a line (with no fixed intercept) are shown in Figures 4.13 (edge-edge pathways) and 4.14 (metal-metal and multiple edge-edge pathways). All treatments are satisfactory in that they result in roughly linear correlations that are qualitatively better than the distance analysis. The metal-metal correlation is slightly better and the multiple paths analysis significantly worse than the edge-edge correlation. Although strong conclusions can not be drawn

Figure 4.13 Maximum ET rates (X = 33, 39, 62, and 72) versus edge-edge σ-tunneling length. Exponential decay line with 2.7 x 10^{11} s^{-1} intercept and 0.57 $Å^{-1}$ slope (correlation coefficient = 0.935).

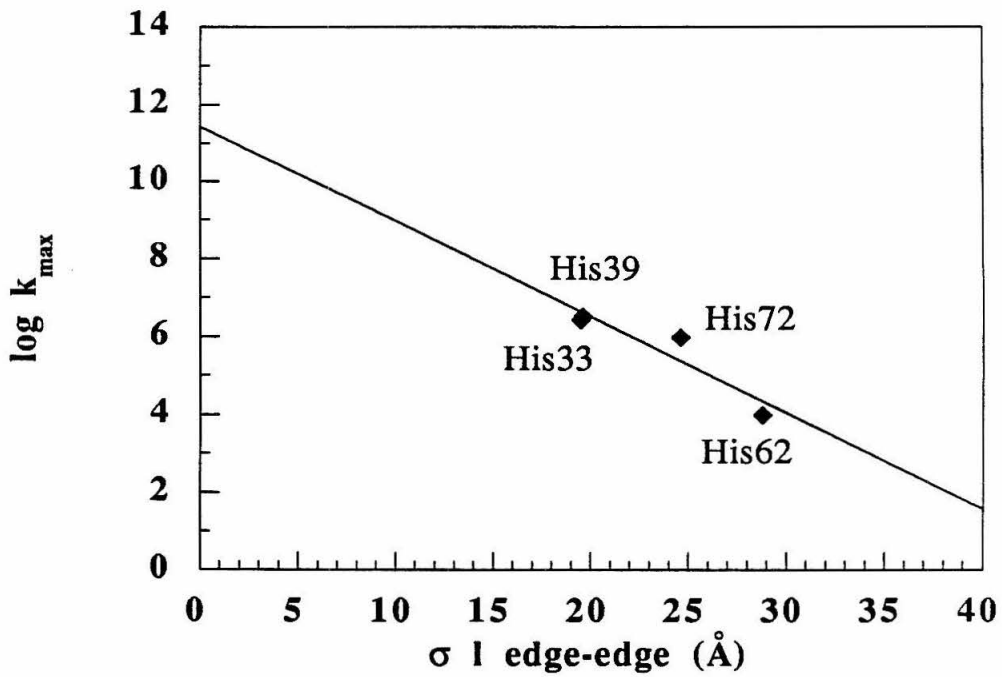
14
12
10
8
6
4
2
0
log k max
His39
His72
His33
His62
0
5
10
15
20
25
30
35
40
σ I edge-edge (Å)

Figure 4.14 (A) Maximum ET rates (X = 33, 39, 62, and 72) versus metal-metal σ-tunneling length. Exponential decay line with 1.0×10^{14} s^{-1} intercept and 0.62 $Å^{-1}$ slope (correlation coefficient = 1.0). (B) Maximum ET rates (X = 33, 39, 62, and 72) versus multiple edge-edge σ-tunneling length. Exponential decay line with 3.5×10^{12} s^{-1} intercept and 0.80 $Å^{-1}$ slope (correlation coefficient = 0.79).

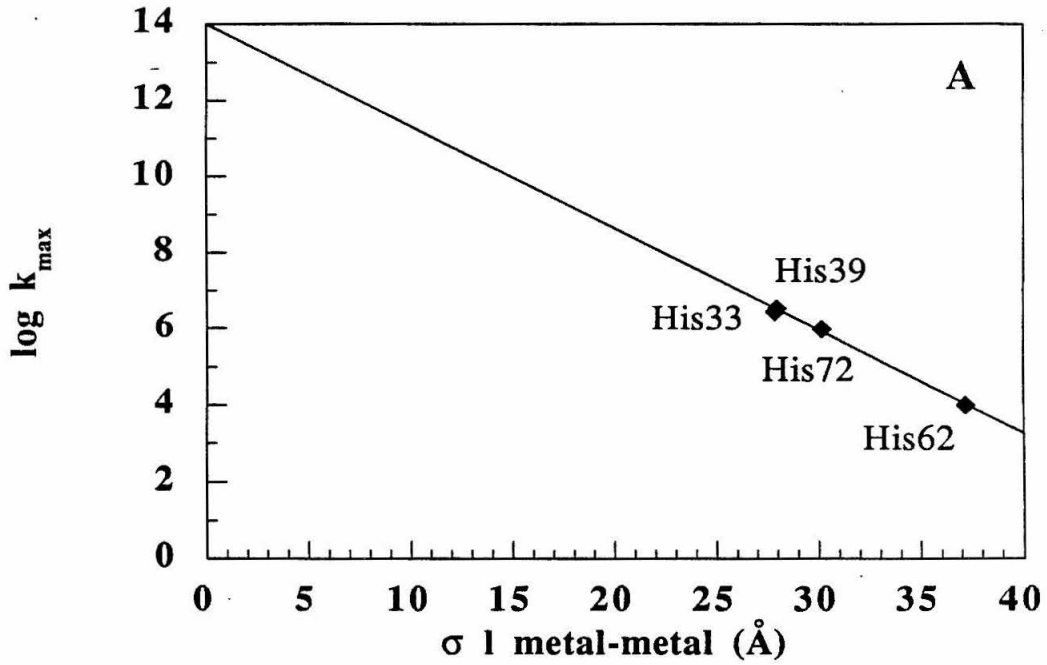
A
log k_{max}
14
12
10
8
6
4
2
0
His39
His33
His72
His62
0
5
10
15
20
25
30
35
40
σ l metal-metal (Å)

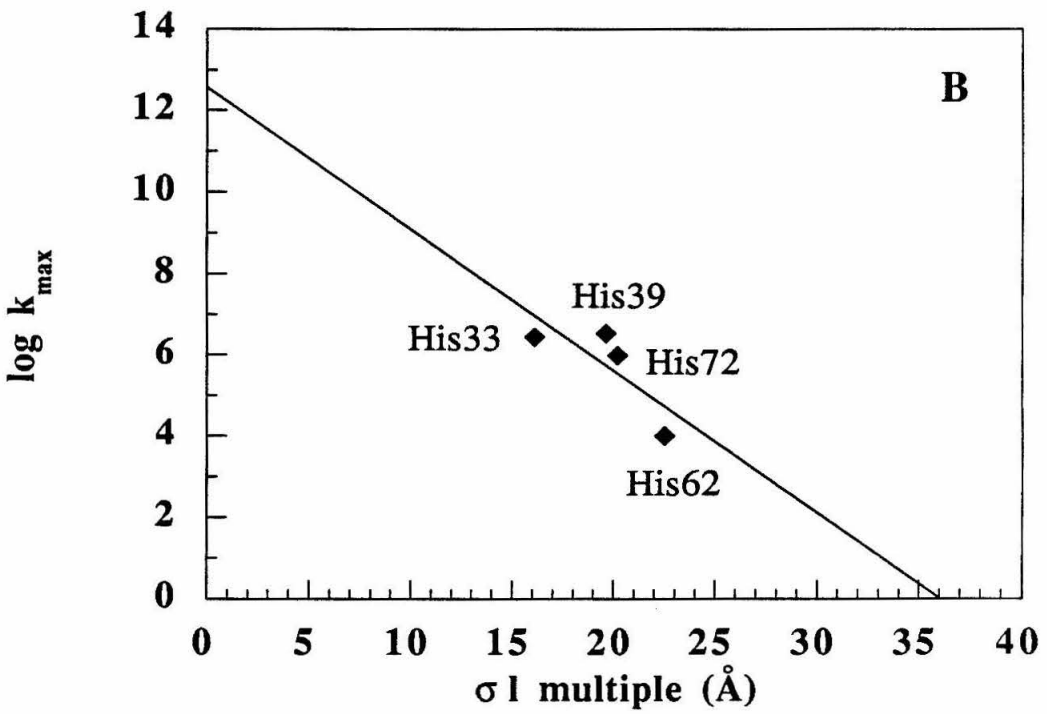
B
log k_{max}
14
12
10
8
6
4
2
0
His39
His33
His72
His62
0
5
10
15
20
25
30
35
40
σ l multiple (Å)

from the limited data set, a better approach is clearly necessary to account for the presence of multiple potential pathways.

Table 4.5. Summary of all possible σl formulations for $Ru(bpy)_2(im)HisX$ cyts *c*.

X	H_{AB} (Fe^{2+} to Ru^{3+}) (cm^{-1})	$\sigma l_{metal\text{-}metal}$ (Å)	$\sigma l_{edge\text{-}edge}$ (Å)	$\sigma l_{multiple}$ (Å)
39	0.11	28.0	19.6	19.6
33	0.097	27.9	19.5	16.1
72	0.057	30.2	24.6	20.2
62	0.0060	37.2	28.8	22.6

C = covalent bond, H = hydrogen bond, and S = space jump.

3. *Conclusions from the σ-Tunneling Pathway Analysis*

Maximum ET rates measured in $Ru(bpy)_2(im)HisX$ cyts *c* correlate more closely with the empirical σ-tunneling pathway analysis than they do with a simple distance-dependent model. This conclusion is most dramatically illustrated by His72, whose measured rate deviates by four orders of magnitude from that predicted from a distance-dependent treatment.[38] The pathway analysis is attractive because it attributes this effect to a readily apparent structural feature of the protein, the lack of direct covalent or H-bonded connectivity between the redox centers, and thus dramatically emphasizes the point that chemical nature of the intervening protein medium has some significant effect on the electronic coupling of redox centers. It can be misleading, however, to interpret electronic couplings in terms of single pathways. For example, Ru-heme couplings in myoglobin cannot be adequately explained using the single pathway approach.[23] The following section describes predictions of electronic couplings in $Ru(bpy)_2(im)HisX$ cyts *c* that treat the relevant portion of the intervening polypeptide structure explicitly.

The linear correlation of rates with couplings predicted by the pathway analysis illustrates a few key points. The weak coupling of His62 to the heme demonstrates that intervening aromatic or polarizable groups do not necessarily enhance electronic couplings. It should be noted that, in the absence of the His72 data points, a roughly linear correlation of rate with distance is observed. This effect is neither surprising, nor is it evidence refuting the pathway model. Since the pathway model scales couplings with bonding interactions between redox centers, it is anticipated that, in general, as donor-acceptor distances increase the σ-bond tunneling length will also increase. The point, illustrated emphatically with His72, is that chemical composition of the intervening medium is able to exert an influence of at least two orders of magnitude in coupling strength over the general distant dependent trend. Figure 4.15,[4i] illustrates σ-tunneling pathway couplings as a function of distance for all the nonhydrogen atoms in cyt *c*. Though the general trend of a decrease in couplings with distance is found, at a *given* donor-acceptor distance, scatter over two orders in magnitude of coupling (thus four in rate) is anticipated due to differences in the composition of the intervening protein structure.

B. Extended Hückel Calculations

Marcus and coworkers have developed[5] an approach for the calculation of electronic couplings in Ru-modified proteins that combines an extended Hückel calculation with an artificial intelligence search to select intervening amino acids that most likely participate in coupling redox centers. This diminished data set representing the intervening medium is used to calculate relative H_{AB}s.[5a,c]

The extended Hückel approach has been applied successfully to covalently linked donor-acceptor model systems, where good agreement with experimentally measured couplings (in the range 250 to 10 cm^{-1}) and β-values (in the range 1.1 to 0.6 $Å^{-1}$) was found in four separate series of bridged systems (bridge = saturated hydrocarbons,

Figure 4.15[4i] Calculated σ-tunneling pathway couplings as a function of donor-acceptor distance for all non-hydrogen atoms in cyt *c*. Note the two orders of magnitude scatter in coupling at a given distance.

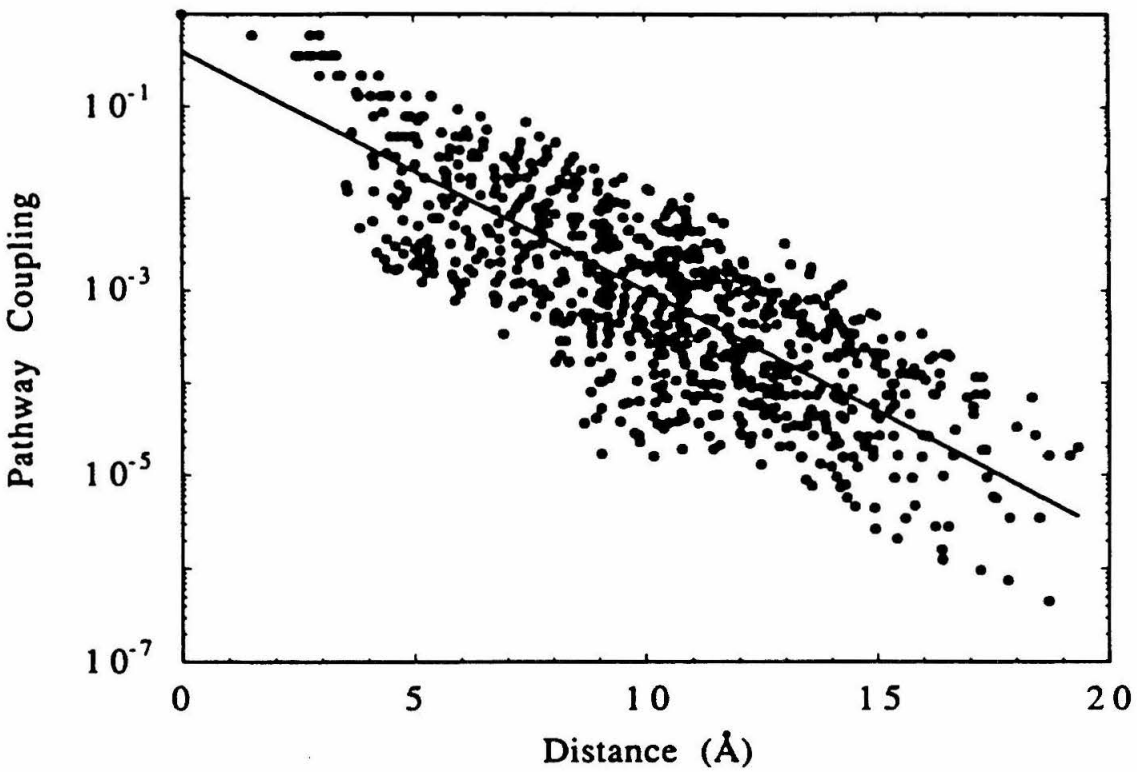
Pathway Coupling
10^-1
10^-3
10^-5
10^-7
0
5
10
15
20
Distance (Å)

norbornyl groups, dithiaspiro rings, and polyproline).[5a] These calculations supported the experimental observation that the chemical nature of the bridge between donor and acceptor is critical in determining electronic couplings.

Applying this methodology to a large protein system is a formidable task due to the sheer size of the data set (even a small protein such as cyt *c* contains nearly 1000 non-hydrogen atoms). However, it is unlikely that atoms and bonds distant from the region between the donor and acceptor can contribute significantly to couplings. Therefore, an artificial intelligence (AI) search was introduced to identify the 10 - 20 amino acids likely to participate in coupling, thus generating a computationally tractable problem.[5d] This informed search, using a simplified electronic coupling potential for each atom, combines the advantages of depth-first and breadth-first approaches. Searches were conducted from both donor to acceptor and acceptor to donor to ensure no directional bias. Amino acids containing atoms identified in the search were selected for the extended Hückel calculations. These amino acids were identified for $Ru(bpy)_2(im)HisX$ cyts *c* by an AI search (Table 4.6) on the same structure files used for the σ-tunneling pathway calculations.

Table 4.6. Critical amino acids for electronic coupling between heme and $Ru(bpy)_2(im)HisX$ identified by an artificial intelligence search.[5d] Residues in bold were used in the "single-path" calculations.

His33	His39	His72	His62
Tyr67	Met80	**Met80**	**Met64**
Met80	**Asn52**	Phe82	**Asp60**
Leu32	Val57	Cys17	Pro30
Pro30	Leu58	Lys79	Asn31
Asn31	Tyr67	Ile81	Leu32
His26	Trp59	Pro71	Ile35
His33	Phe82	Asn70	Phe36
Trp59	**Gly41**	**His72**	Trp59
His18	**Asn56**	**Thr78**	Asn63
Thr19	Pro71		**His62**
Cys14	Ser40		Tyr74
Ala15	**His39**		Val57
Lys22	Ile35		
Gly34	Thr78		
Leu35	Lys55		
Arg38			
Gly24			
Gly23			
Glu21			
Lys25			

The positions of the single path intervening residues with respect to the heme and the $Ru(bpy)_2(im)HisX$ label are depicted in Figure 4.16 for X = 33, 39, 62, and 72. As anticipated, the amino acids identified in the search are spatially situated in the region between the Ru-label and the heme group.

Figure 4.16 Illustration of the amino acids selected by the artificial intelligence search that may contribute to heme-Ru(bpy)$_2$(im)HisX (donor-acceptor, in bold) coupling (Table 4.6). Only side chains are shown for clarity. (A) X = 33; (B) X = 39; (C) X = 62; (D) X = 72.

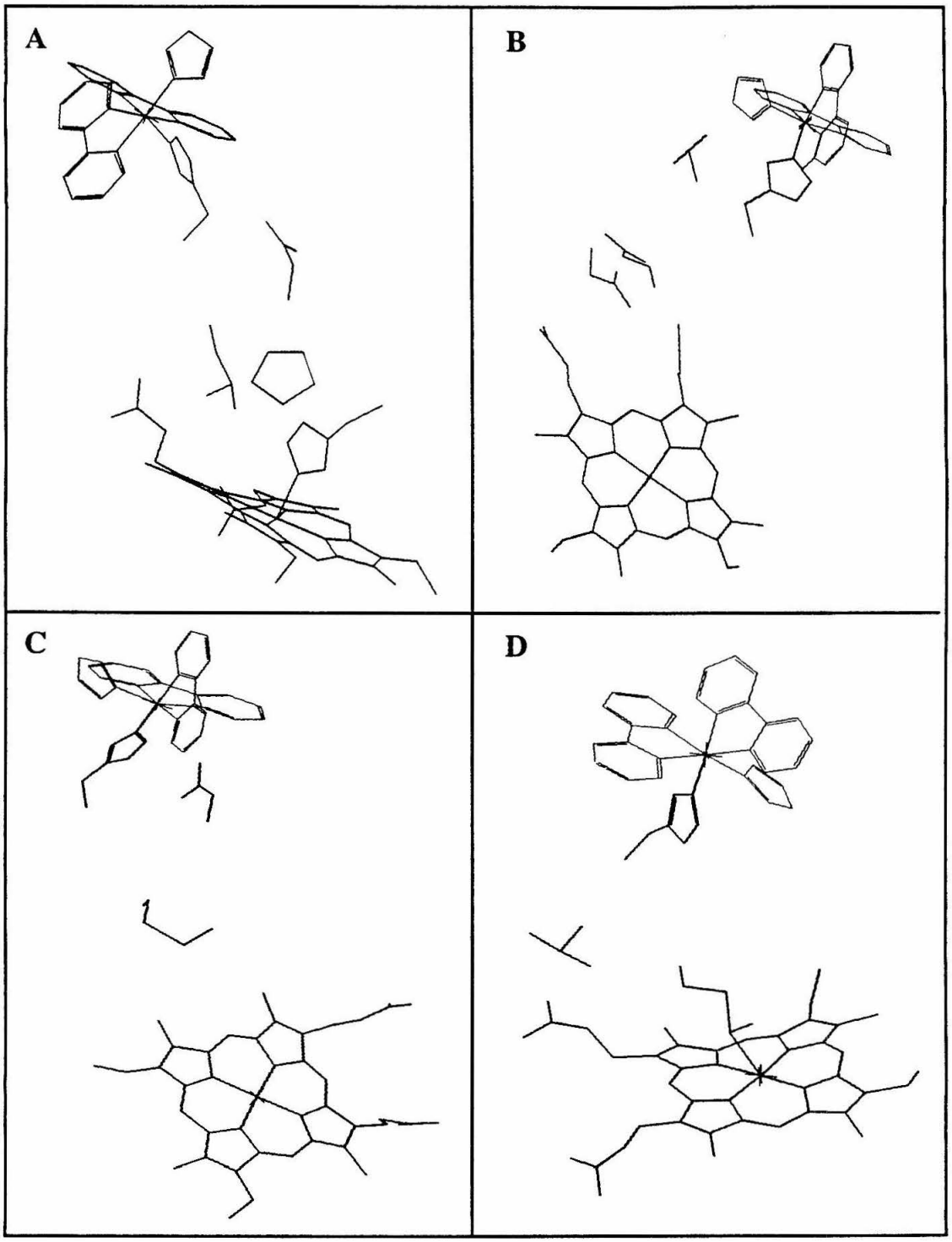
A
B
C
D

The abbreviated intervening medium is treated as the bridge for extended Hückel calculations as described in Reference 5d. Second-order perturbation theory is applied to the diagonalized bridge orbitals to evaluate relative H_{AB}s according to:

$$H_{AB} = T_D T_A \sum_l \left(\frac{C_{D_l} C_{A_l}}{E_x - E_l} \right)$$

where T_D and T_A are the matrix elements for the donor and acceptor with the bridge, $C_{D(A)l}$ is the coefficient of the l^{th} bridge orbital obtained from extended Hückel theory, E_l is the energy of the l^{th} molecular orbital, also obtained from extended Hückel theory, and E_x is the energy of the molecular orbital of the donor at the transition state.[5d] Energies for the donor and acceptor in the transition state were obtained from optical charge transfer energies.

Calculations were performed for each protein using two data sets, one containing the complete set of amino acids identified in the artificial intelligence search (designated full) and a second with only the amino acids selected for the "best" path (most highly coupled) in the AI search. The H_{AB}s calculated for each set of the series of $Ru(bpy)_2(im)HisX$ cyts *c* are given in Table 4.7.

Table 4.7. Experimental and calculated Fe^{2+} to Ru^{3+} electronic couplings using extended Hückel theory for full data set and single paths in $Ru(bpy)_2(im)HisX$ cyt *c* derivatives.

X	H_{AB} (exp) (cm^{-1})	H_{AB}(full) (cm^{-1})	H_{AB}(single) (cm^{-1})	$H_{AB}/H_{AB(His33)}$ (full)	$H_{AB}/H_{AB(His33)}$ (single)
33	0.097	0.01	0.007	1	1
39	0.11	0.01	0.007	1	1
72	0.057	0.007	0.003	0.7	0.4
62	0.0060	0.002	0.001	0.2	0.14

Plots of k_{max} as a function of calculated H_{AB}s from both the full and single path data sets are presented in Figure 4.17 A and B. As with the σ-tunneling pathway calculations, good agreement is observed with the calculated relative H_{AB}s and the experimental rates (and derived couplings). His33 and His39 are predicted to possess identical couplings, consistent with experimental values and the σ-tunneling pathway analysis. His62 is predicted to be weakly coupled, consistent with all other analyses. Significantly, the anomalously small coupling measured in the His72 derivative, whose rate is poorly described by the donor-acceptor distance model, is predicted using the AI / extended Hückel approach. The weak coupling is attributed to a specific structural feature, the presence of a 2.7 Å cavity between $Ru(bpy)_2(im)$His72 and the heme, similar to the coupling-crippling through-space jump identified in the σ-tunneling pathway analysis.

Somewhat better correlations of measured activationless rates with calculated H_{AB}s are found using the full data set of intervening amino acids obtained from the AI search rather than just the "best" path amino acids, although the results are similar (notably, weak His72 coupling is predicted even if only the "best" path is used). This result, essentially the opposite of what was found for the σ-tunneling pathway analysis, implies that more sophisticated calculations employing very large intervening medium data sets may be required for accurate H_{AB} predictions, perhaps at the sacrifice of readily visualized (if oversimplified) descriptions of the electronic coupling.[39] It is interesting to note that the residues selected by the AI search for the best path do not necessarily correspond to the dominant pathways found in the σ-tunneling pathway analysis. For example, in the His72 pathway, Thr78 is chosen for the best pathway in the AI search yet appears only in a secondary σ-tunneling pathway. It is remarkable that despite the significant differences between the two medium-dependent models, for both approaches excellent correlation between activationless rates and calculated couplings is found.

Figure 4.17 (A) Maximum ET rates (X = 33, 39, 62, and 72) versus relative H_{AB} calculated with a full intervening medium data set using extended Hückel theory for evaluating energies and orbital coefficients. Fit line with 3.2×10^3 s^{-1} intercept and 310 per cm^{-1} slope, correlation coefficient = 0.98. (B) Maximum ET rates (X = 33, 39, 62, and 72) versus H_{AB} calculated with a single path intervening medium data set using extended Hückel theory for evaluating energies and orbital coefficients. Line fitted with 1.4×10^4 s^{-1} intercept and 350 per cm^{-1} slope, correlation coefficient = 0.89.

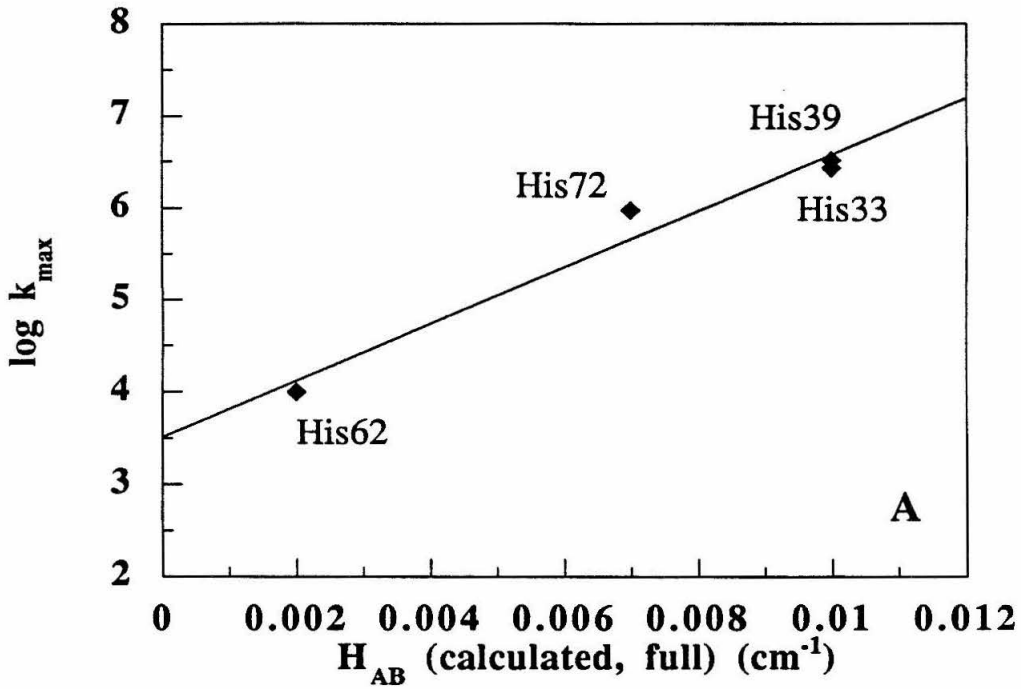
8
7
6
5
4
3
2
log k_{max}
His39
His72
His33
His62
A
0
0.002
0.004
0.006
0.008
0.01
0.012
H_{AB} (calculated, full) (cm^{-1})

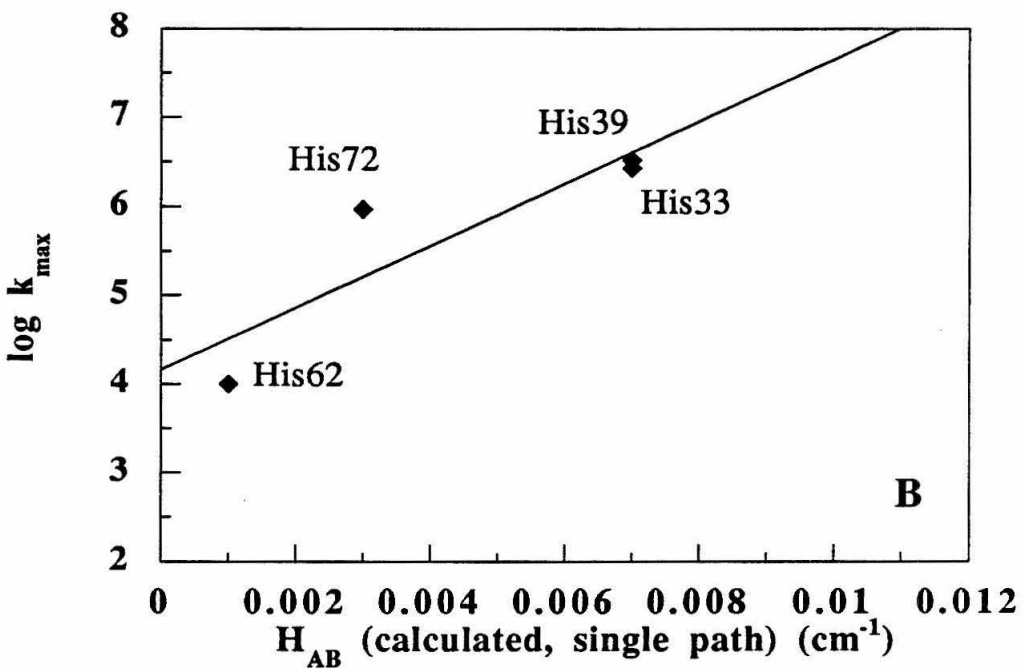
8
7
6
5
4
3
2
log k_{max}
His39
His72
His33
His62
B
0
0.002
0.004
0.006
0.008
0.01
0.012
H_{AB} (calculated, single path) (cm^{-1})

C. Inhomogeneous Aperiodic Lattice Model

A new quantum-molecular formulation of medium-dependent electronic couplings devised by Kuki and coworkers accommodates the calculation of *absolute* H_{AB} values using inhomogeneous aperiodic lattice (IAL) theory.[10] Ionization potentials and triple resonance integrals are used to devise an accurate IAL Hamiltonian matrix, then a nonperturbative Green's function calculation is made to numerically evaluate charge resonance energies. Advantages of the IAL method are that the *full* protein structure is used in the calculation accompanied by no simplifying assumptions and that interference effects are accounted for.

This approach has been recently applied to the Ru(ammine) modified HisX Zn cyts *c* (X = 33, 39, 62) and good agreement was found with experimentally derived values.[10c] Residues distant from the direct line joining donor and acceptor were unexpectedly found to contribute significantly to the net coupling. Preliminary calculations have been made on the series of $Ru(bpy)_2(im)$HisX cyts *c* studied here, using a donor-acceptor energy of -6.5 eV.[40] An attempt was made to specifically include the redox-active *d*-orbital on the iron atom. The results of these calculations are summarized in Table 4.8.

Table 4.8. Preliminary calculations of H_{AB} values in $Ru(bpy)_2(im)$HisX cyts *c* using IAL theory.[40]

X	H_{AB} (Fe^{2+} to Ru^{3+}) (cm^{-1})	H_{AB} (IAL) (cm^{-1})	H_{AB} (IAL, with *d*-orbital) (cm^{-1})
33	0.11	0.095	0.072
39	0.097	0.062	0.26
72	0.057	0.14	0.18
62	0.0060	0.0030	0.032

The calculated H_{AB}s generally agree within a factor of 3 of measured values (the d-orbital calculation with His62 is the one exception). However, the trends observed, particularly with respect to the weakly coupled His72, do not correlate well with the experimental data. It is likely that more accurate orbital energies and dynamics considerations are needed to obtain quantitatively accurate results. It will be interesting to see if the IAL method will successfully predict absolute values for H_{AB}; the small electronic couplings observed in long-range biological ET make this a formidable task.

V. Conclusion

Distant Fe^{2+} - Ru^{3+} electronic couplings have been extracted from intramolecular electron-transfer rates in $Ru(bpy)_2(im)HisX$ (where X = 33, 39, 62, and 72) derivatives of cyt *c*. The couplings increase according to 62 (0.0060) < 72 (0.057) < 33 (0.097) < 39 (0.11 cm^{-1}); however, this order is incongruent with histidine to heme edge-edge distances [62 (14.8) > 39 (12.3) > 33 (11.1) > 72 (8.4 Å)]. Intervening aromatic or polarizable atoms do not enhance electronic couplings. The rates (and couplings) correlate with the lengths of σ-tunneling pathways comprised of covalent bonds, hydrogen bonds and through-space jumps from the histidines to the heme group. Space jumps greatly decrease couplings: one from Pro71 to Met80 extends the σ-tunneling length of the His72 pathway by roughly 10 covalent bond units. Experimental couplings also correlate well with those calculated using extended Hückel theory to evaluate the contribution of the intervening protein medium. Thus, while a distance-dependent formulation of electronic coupling in nonadiabatic electron transfer describes qualitatively trends observed in rates measured in $Ru(bpy)_2(im)$-modified cyts *c*, the chemical nature of the intervening medium needs to be considered for a more precise evaluation of couplings.

VI. References

1. Marcus, R. A.; Sutin, N. *Biochim. Biophys. Acta* **1985**, *811*, 265. Marcus, R. A. *J. Chem. Phys.* **1956**, *24*, 966. Marcus, R. A. *J. Chem. Phys.* **1965**, *43*, 679.

2. Bertrand, P. *Struct. Bond.* **1991**, *75*, 1.

3. (a) Halpern, J.; Orgel, L. E. *Discussion Faraday Soc.* **1960**, *29*, 32. (b) McConnell, H. M. *J. Chem. Phys.* **1961**, *35*, 508. (c) Hopfield, J. J. *Proc. Natl. Acad. Sci. USA* **1974**, *71*, 3640. (d) Jortner, J. *J. Chem. Phys.* **1976**, *64*, 4860. (e) DeVault, D. *Quantum-mechanical tunneling in biological systems* (Cambridge University Press: Cambridge) 1984.

4. (a) Onuchic, J. N.; Beratan, D. N.; Winkler, J. R.; Gray, H. B. *Annu. Rev. Biophys. Biomol. Struct.* **1992**, *21*, 349. (b) Beratan, D. N.; Onuchic, J. N.; Betts, J. N.; Bowler, B. E.; Gray, H. B. *J. Am. Chem. Soc.* **1990**, *112*, 7915. (c) Beratan, D. N.; Onuchic, J. N.; Hopfield, J. J. *J. Phys. Chem.* **1987**, *86*, 4488. (d) Beratan, D. N.; Betts, J. N.; Onuchic, J. N. *Science* **1991**, *252*, 1285. (e) Onuchic, J. N.; Andrade, P. C. P.; Beratan, D. N. *J. Chem. Phys.* **1991**, *95*, 1131. (f) Onuchic, J. N.; Beratan, D. N. *J. Chem. Phys.* **1990**, *92*, 722. (g) Beratan, D. N.; Onuchic, J. N. *Photosynth. Res.* **1989**, *22*, 173. (h) Betts, J. N.; Beratan, D. N.; Onuchic, J. N. *J. Am. Chem. Soc.* **1991**, *113*, 4043. (i) Beratan, D. N.; Betts, J. N.; Onuchic, J. N. J. *Phys. Chem.* **1992**, *96*, 2852.

5. (a) Siddarth, P; Marcus, R. A. *J. Phys. Chem.* **1990**, *94*, 2985. (b) Siddarth, P.; Marcus, R. A. *J. Phys. Chem.* **1990**, *94*, 8430. (c) Siddarth, P.; Marcus, R. A. *J. Phys. Chem.* **1992**, *96*, 3213. (d) Siddarth, P.; Marcus, R. A. *J. Phys. Chem.* **1993**, *97*, 2400. (e) Siddarth, P.; Marcus, R. A. *J. Phys. Chem.* **1993**, *97*, 6111. (f) Siddarth, P.; Marcus, R. A. *J. Phys. Chem.* **1993**, in press.

6. Christensen, H. E. M.; Conrad, L. S.; Mikkelsen, K. V.; Nielsen, M. K.; Ulstrup, J. *Inorg. Chem.* **1990**, *29*, 2808. Christensen, H. E. M.; Conrad, L. S.; Hammerstad-Pedersen, J. M; Ulstrup, J. *FEBS Lett.* **1992**, *296*, 141. Christensen, H. E. M.; Conrad, L. S.; Mikkelsen, K. V.; Ulstrup, J. *J. Phys. Chem.* **1992**, *96*, 4451.

7. (a) Mikkelsen, K. V.; Ratner, M. A. *Chem. Rev.* **1988**, *87*, 113. (b) Ratner, M. A. *J. Phys. Chem.* **1990**, *94*, 4877. (c) Todd, M. D.; Nitzan, A.; Ratner, M. A. *J. Phys. Chem.* **1993**, *97*, 29.

8. Goldman, C. *Phys. Rev. A* **1991**, *43*, 4500.

9. Larsson, S. *J. Am. Chem. Soc.* **1981**, *103*, 4034. Broo, A.; Larsson, S. *J. Phys. Chem.* **1991**, *95*, 4925. Broo, A. *Chem. Phys.* **1993**, *169*, 135. Broo, A. *Chem. Phys.* **1993**, *169*, 152.

10. (a) Kuki, A. in *Structure and Bonding* (Verlag: New York) 1991, Vol. 75, pp. 49-83. (b) Gruschus, J. M.; Kuki, A. *Chem. Phys. Lett.* **1992**, *192*, 205. (c) Gruschus, J. M.; Kuki, A. *J. Phys. Chem.* **1993**, *97*, 5581.

11. Newton, M. D. *Chem. Rev.* **1991**, *91*, 767.

12. Moser, C. C.; Keske, J. M.; Warncke, K.; Farid, R. S.; Dutton, P. L. *Nature* **1992**, *355*, 796. Farid, R. S.; Moser, C. C.; Dutton, P. L. *Curr. Opin. Struct. Biol.* **1993**, *3*, 225.

13. Kuki, A.; Wolynes, P. G. *Science* **1987**, *236*, 1647.

14. Sigel, H; Sigel, A. Eds. *Metal Ions in Biological Systems* (Dekker: New York) 1991, Vol. 27.

15. Bowler, B. E.; Raphael, A. L.; Gray, H. B. *Prog. Inorg. Chem.* **1990**, *38*, 259. Therien, M. J.; Chang, J.; Raphael, A. L.; Bowler, B. E.; Gray, H. B. *Struct. Bond.* **1991**, *75*, 109.

16. Canters, G. W.; van de Kamp, M. *Curr. Opin. Struct. Biol.* **1992**, *2*, 859.

17. McLendon, G. *Acc. Chem. Res.* **1988**, *21*, 160.

18. (a) Winkler, J. R.; Gray, H. B. *Chem. Rev.* **1992**, *92*, 369. (b) Gray, H. B.; Winkler, J. R. *Pure & Appl. Chem.* **1992**, *64*, 1257.

19. Liang, N.; Pielak, G.; Mauk, A. G.; Smith, M.; Hoffman, B. M. *Proc. Natl. Acad. Sci. USA* **1987**, *84*, 1249. Liang, N.; Mauk, A. G.; Pielak, G; Johnson, J. A; Smith, M.; Hoffman, B. M. *Science* **1988**, *240*, 311.

20. Wallin, S. A.; Stemp, E. D. A.; Everest, A. M.; Nocek, J. M.; Netzel, T. L.; Hoffman, B. M. *J. Am. Chem. Soc.* **1991**, *113*, 1842. Everest, A. M.; Wallin, S. A.; Stemp, E. D. A.; Nocek, J. M.; Mauk, A. G.; Hoffman, B. A. *J. Am. Chem. Soc.* **1991**, *113*, 4337.

21. Therien, M. J.; Selman, M.; Gray, H. B.; Chang, I-J.; Winkler, J. R. *J. Am. Chem. Soc.* **1990**, *112*, 2420. Selman, M. A. Ph. D. Thesis, California Institute of Technology, **1989**.

22. (a) Bowler, B. E.; Meade, T. J.; Mayo, S. L.; Richards, J. H.; Gray, H. B. *J. Am. Chem. Soc.* **1989**, *111*, 8757. (b) Therien, M. J.; Bowler, B. E.; Selman, M. A.; Gray, H. B.; Chang, I-J.; Winkler, J. R. In *ACS Advances in Chemistry Series*, Bolton, J. R., Mataga, N., McLendon, G., Eds.; (American Chemical Society: Washington DC) 1991; No. 228, pp. 191 - 200.

23. Casimiro, D. R.; Wong L.-L.; Colón, J. L.; Zewert, T. E.; Richards, J. H.; Chang, I-J.; Winkler, J. R.; Gray, H. B. *J. Am. Chem. Soc.* **1993**, *115*, 1485.

24. Jacobs, B. A.; Mauk, M. R.; Funk, W. D.; MacGillivray, R. T. A.; Mauk, A. G.; Gray, H. B. *J. Am. Chem. Soc.* **1991**, *113*, 4390.

25. Wuttke, D. S.; Bjerrum, M. J.; Winkler, J. R.; Gray, H. B. *Science* **1992**, *256*, 1007. Wuttke, D. S.; Bjerrum M. J.; Chang, I-J.; Winkler, J. R.; Gray, H. B. *Biochim. Biophys. Acta* **1992**, *1101*, 168.

26. Casimiro, D. R.; Richards, J. H.; Winkler, J. R.; Gray, H. B. *J. Phys. Chem.*, in press.

27. Farver, O.; Pecht, I. *FEBS Lett.* **1989**, *244*, 376. Farver, O.; Pecht, I. *FEBS Lett.* **1989**, *244*, 379. Farver, O.; Skov, L. K.; van de Kamp, M.; Canters, G. W.; Pecht, I. *Eur. J. Biochem.* **1992**, *210*, 399. Farver, O.; Pecht, I. *J. Am. Chem. Soc.* **1992**, *114*, 5764.

28. Govindaraju, K.; Christensen, H. E. M.; Lloyd, E.; Olsen, M.; Salmon, G. A.; Tomkinson, N. P.; Sykes, A. G. *Inorg. Chem.* **1993**, *32*, 40. Sykes, A. G. *Struct. Bond.* **1991**, *75*, 175.

29. Margalit, R.; Schejter, A. *Eur. J. Biochem.* **1973**, *32*, 492.

30. Bowler, B. E., determined by differential pulse polarography at a 4,4'-bipyridine modified gold electrode, unpublished results.

31. Bushnell, G. W.; Louie, G. V.; Brayer, G. D. *J. Mol. Biol.* **1990**, *214*, 585.

32. Louie, G. V.; Brayer, G. D. *J. Mol. Biol.* **1990**, *214*, 527.

33. Eggleston, D. S.; Goldsby, K A.; Hodgson, D. J.; Meyer, T. J. *Inorg. Chem.* **1985**, *24*, 4573. Kimura, T.; Sakurai, T.; Shima, M. *Acta Cryst.* **1982**, *B38*, 112. The modeled orientation of the bipyridyl and imidazole ligands is in good agreement with the recent structural characterization of $[Ru(bpy)_2(im)_2]SO_4 \cdot 10\ H_2O$. Connick, W. B.; Henling, L. M; Di Bilio, A. G.; Gray, H. B., in preparation.

34. Closs, G. L.; Miller, J. R. *Science* **1988**, *240*, 440.

35. The term superexchange has been coined to describe electronic couplings mediated by the intervening medium between distant donor - acceptor species. This mechanism is invoked in both distance and medium dependent formulations of matrix coupling elements because, in both treatments, the medium serves to lower the tunneling barrier.

36. Recently reviewed in DiMagno, T. J.; Wang, Z.; Norris, J. R. *Curr. Opin. Struct. Biol.* **1992**, *2*, 836.

37. Buckley, F.; Harary, F. *Distance in graphs* (Addison Wesley: Reading, Mass.) 1990.

38. It is tempting to use the pressure dependence observed in Fe^{2+} to $Ru(bpy)_2(im)His72^{3+}$ k_{ET}^{mm} rates absent in the same experiments withRu(bpy)$_2$(im)His33-labeled protein to support the pathway model (*i.e.*, compressing the space jump). However, these data are also consistent with a shortening of the His72-heme edge-edge distance with applied pressure. The only conclusion to be drawn from a

comparison of the His72 and His33 pressure-dependent rates is that Fe^{2+} to Ru^{3+} electronic coupling is enhanced from position His72 with applied pressure while no effect is observed from position His33.

39. Good correlations have also been found between experimentally determined maximum ET rates (and couplings) and calculated relative H_{AB}s found using the AI / extended Hückel approach in Ru-ammine modified myoglobins,[5e,23] and also His58, His66, and His66(Phe67) $Ru(bpy)_2(im)$-modified cyts *c*.[5f,26]

40. Gruschus, J. M., private communication.

Chapter 5

Semisynthesis of Bipyridyl-Alanine Cytochrome *c* Mutants: Novel Proteins with Enhanced Electron-Transfer Properties[1]

I. Introduction

Naturally occurring proteins possess desirable properties in that their diverse functions, accompanied by well defined supramolecular structures, provide almost limitless opportunities for the construction of new devices. Although site-directed mutagenesis has allowed specific alteration of protein architecture, it is a technique that relies upon the cell's biosynthetic machinery, and is therefore limited to the encoded amino acids. It would be advantageous to include unnatural amino acids into protein ensembles to augment existing structures, or to introduce new functionalities altogether.[2] Both *in vitro* expression of chemically acylated suppressor tRNA[3,4] and total chemical synthesis[5] methodologies have been employed to incorporate unnatural amino acids into protein sequences. However, the former technique suffers from low throughput of protein, while the latter is limited to sequence lengths that can be built by employing solid phase peptide synthesis technology. In contrast, the semisynthetic methodology (refer to Chapter 2),[6] in which fragments of native protein are fused with synthetically prepared peptides to form complete protein sequences, can provide a means for facile generation of proteins containing unnatural amino acids in large quantities. To date, the semisynthetic technique has been limited to those proteins that are naturally amenable to facile cleavage and religation; however, the use of genetic engineering should provide a means for more general application of semisynthesis in the future. In addition, the recent developments in synthetic methods for production of novel, optically pure amino acids[7] and advances in solid phase peptide synthesis[8] now allow the assembly of peptides in essentially infinite variety. With these tools in hand, the stage is now set for the general manipulation of proteins well beyond the constraints set by nature.

In developing strategies for the construction of novel electron-transfer proteins[9-12] in relatively large (milligram) quantities, semisynthesis has been selected for the incorporation of unnatural amino acids directly into polypeptide backbones. An example of the power of this approach is the semisynthetic construction of two horse heart cytochrome *c* (cyt *c*) mutants containing chelating π-acceptor side chains, (S)-2-amino-3-(2,2'-bipyrid-6-

yl)-propanoic acid (6Bpa)[13] (**1**) and (S)-2-amino-3-(2,2'-bipyrid-4-yl)-propanoic acid (4Bpa)[14] (**2**) (Figure 5.1), at position 72 in the native protein sequence. Because the bipyridyl ligands have a high affinity for metal cations and can be placed site-specifically on the polypeptide backbone,[15] they are ideal for building versatile biological electron-transfer (ET) systems. Importantly, the bipyridyl amino acid mutations allow the assembly of a $Ru(bpy)_3^{2+}$ center[16] at a defined site on the protein surface, which is expected to increase markedly the efficiency of photoinduced ET from an electronically excited ($*Ru^{2+}$) surface site to the protein metal center relative to that of a $Ru(bpy)_2$(im)His-modified protein (Chapters 3 and 4).[11,17] Enhanced photoinduced ET is used to study ET in the conformationally perturbed alkaline form of cyt *c* and can also be used to study ET in other unfolded or partially folded states. In addition, the two mutant proteins differ only in the regioisomer of the bipyridyl amino acid employed, thereby allowing a sensitive probe of the effects of ligand orientation on metal coordination.

II. Experimental

The semisynthetic methodology and experimental protocols for protein reconstitution, purification and general handling are given in Chapter 2. Details of the absorption, CD, EPR, isoelectric focusing, and differential pulse polarography measurements are described in the experimental section of Chapter 2. Steady-state luminescence and excitation spectra, and time-resolved luminescence decay and transient absorption measurements were obtained as described in the experimental section of Chapter 3, unless otherwise indicated. Sodium dodecyl sulfate polyacrylamide gel electrophoresis (SDS-PAGE) was performed by T. J. Mizoguchi using standard protocols.

A. Amino Acid Synthesis

6Bpa (**1**) and 4Bpa (**2**) were synthesized as described in References 13 (6Bpa) and 14 (4Bpa).[18] Reaction schemes are given in Figure 5.2 A, B and C. The 6Bpa amino acid

Figure 5.1 (*S*)-2-amino-3-(2,2'-bipyrid-6-yl)-propanoic acid (6Bpa) (**1**) and (*S*)-2-amino-3-(2,2'-bipyrid-4-yl)-propanoic acid (4Bpa) (**2**).

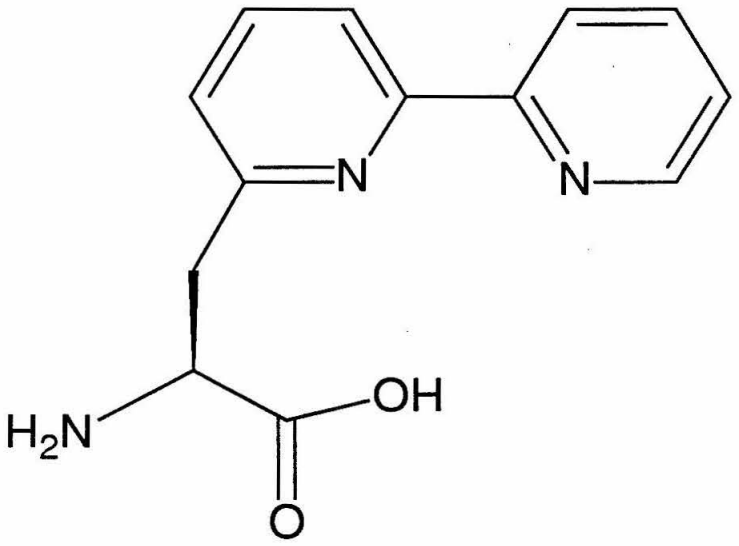

1

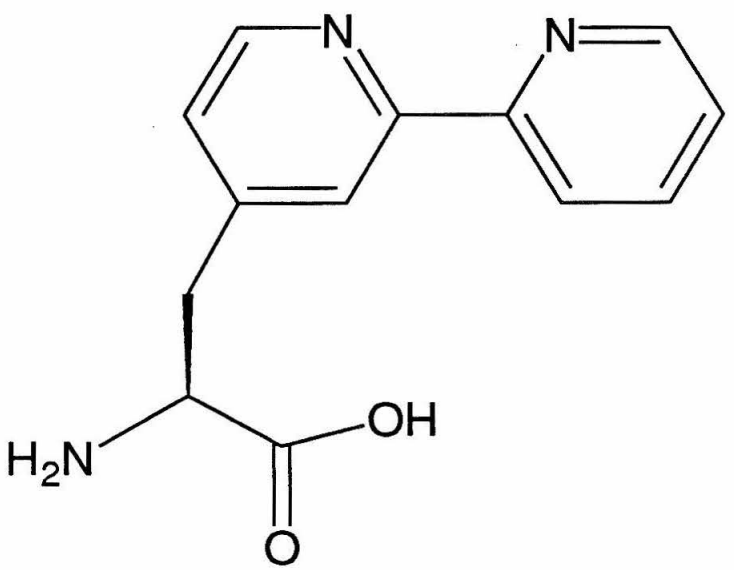

2

Figure 5.2 Reaction schemes for (A) the stereoselective synthesis of 6Bpa, (B) racemic synthesis of 4Bpa, and (C) enantiomeric resolution of 4Bpa using enzymatic hydrolysis.

A

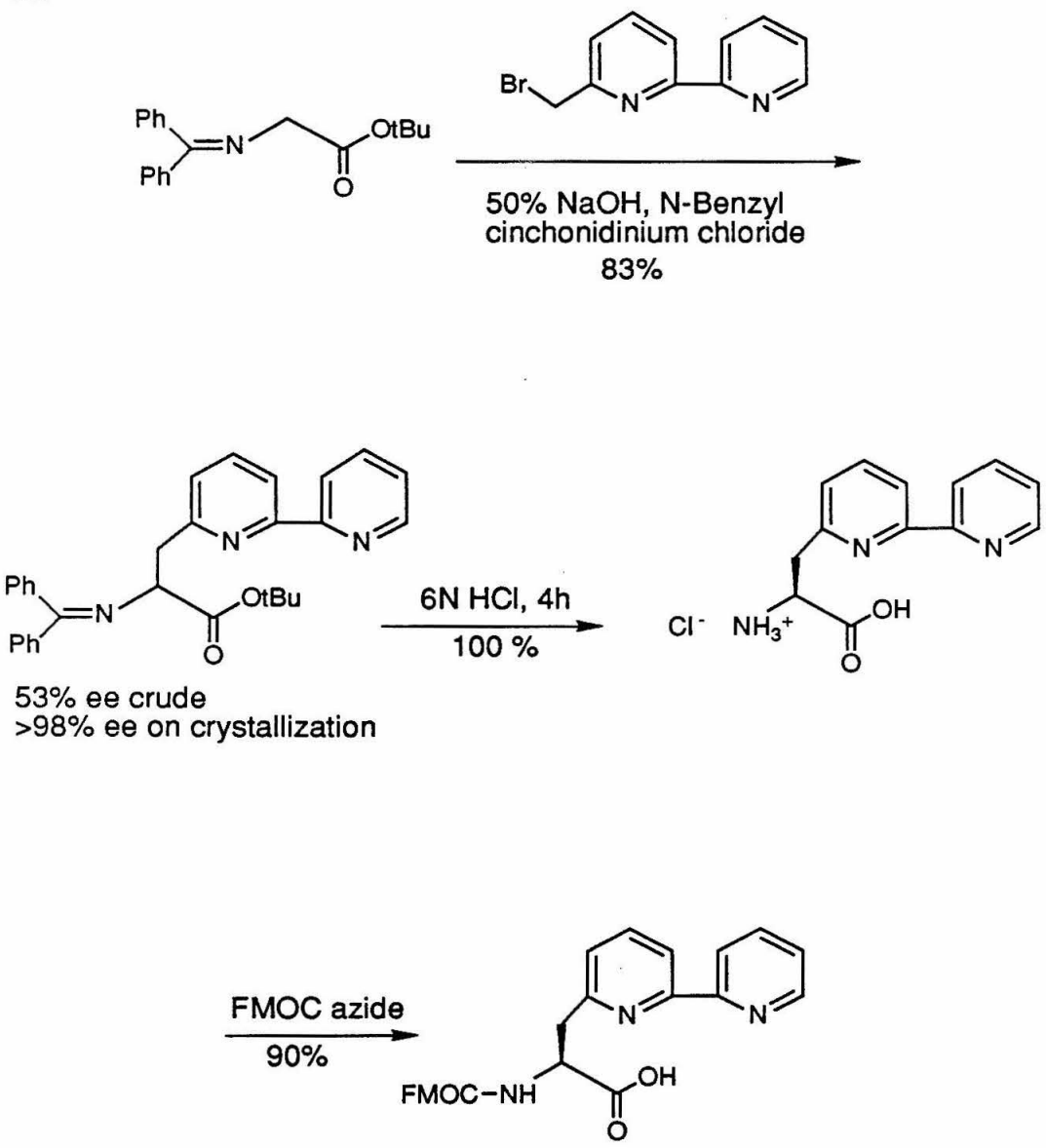
Ph
Ph
N
OtBu
O
Br
N
N
50% NaOH, N-Benzyl
cinchonidinium chloride
83%
Ph
Ph
N
OtBu
O
6N HCl, 4h
100 %
Cl⁻
NH3+
OH
O
53% ee crude
>98% ee on crystallization
FMOC azide
90%
FMOC–NH
OH
O

B

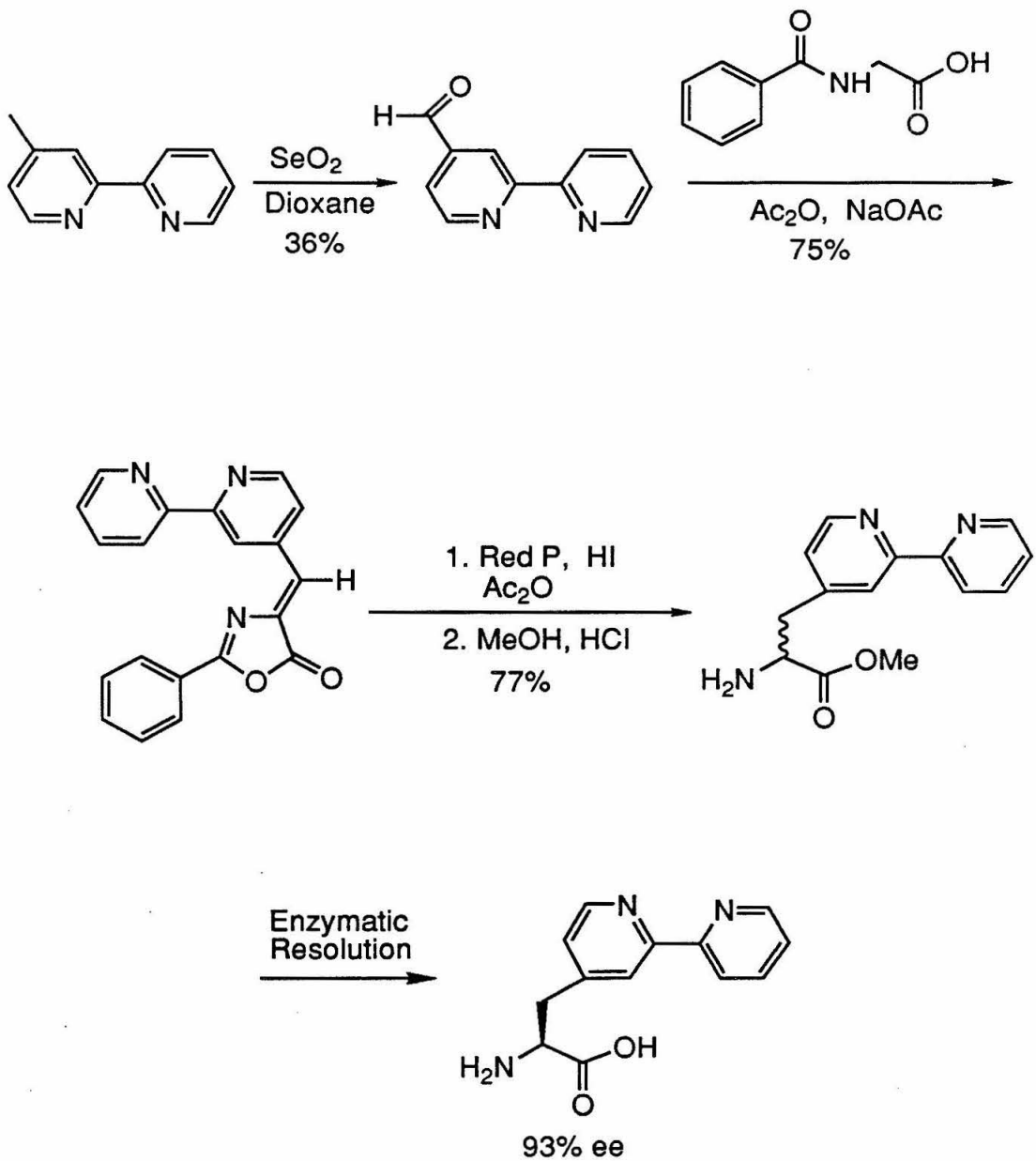
SeO2
Dioxane
36%
Ac2O, NaOAc
75%
1. Red P, HI
Ac2O
2. MeOH, HCl
77%
Enzymatic
Resolution
93% ee

C

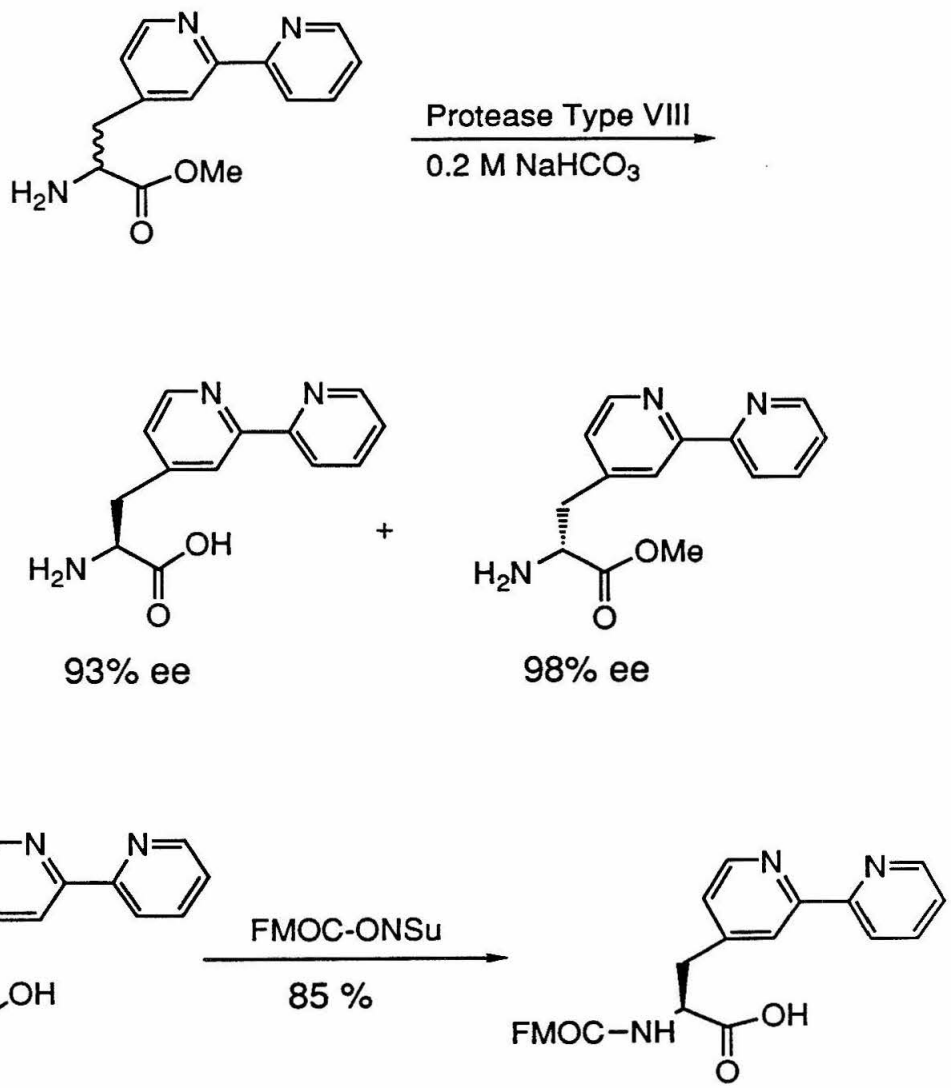

was prepared by the asymmetric alkylation of *N*-(diphenylmethlyene) glycine *tert*-butyl ester with 6-(bromomethyl)-2,2'-bipyridine in the presence of a phase transfer catalyst, *N*-benzyl cinchonidinium.[19] This reaction afforded the L-enantiomer in 53% enantiomeric excess (ee), which was subsequently enriched to >98% by selective crystallization of the racemic material. The product was deprotected by hydrolysis with 6N HCl and subsequently protected with 9-fluorenylmethyl carbamate (FMOC) succinate to yield the FMOC derivative compatible with solid phase peptide synthetic protocols. The synthetic strategies outlined by Erlenmeyer were employed for the synthesis of the *racemic* methyl ester of 4Bpa, as illustrated in Figure 5.2 B; 4-(methyl)-2,2'-bipyridine was oxidized to the corresponding aldehyde with selenium dioxide and condensed with hippuric acid to afford the 4-bipyridineazlactone. Reduction with red phosphorus and hydroiodic acid followed by esterification in methanol yielded the desired methyl ester of 4Bpa. Resolution of the enantiomers was achieved by extraction of the D-enantiomer methyl ester following selective hydrolysis of the L-enantiomer. Protease type VIII (subtilisin) hydrolyzes the L-enantiomer more readily than the D-enantiomer. This method is under kinetic control and affords the D- and L-enantiomers in high ee: L = 93% ee; D = 98% ee.

B. Peptide Synthesis

All peptides were synthesized on a 0.1 mmol scale using solid phase FMOC-amino protection and BOP/HOBT activated-ester chemistry on a Milligen 9050 peptide synthesizer.[18] PAL resin (Milligen) was used to afford amides at the carboxy terminus. For the naturally occurring amino acids, 4.0-8.0 equivalents were used per coupling; 2.50 amino acid equivalents were employed for the bipyridyl amino acids. Activated esters were prepared *in situ* with BOP and HOBT in 0.451 M *N*-methyl-morpholine/DMF. Double and triple couplings were employed when needed. Acylation times varied from 0.75 to 2 hours depending upon coupling efficiency of the particular amino acid. Deprotection of FMOC-protected amine groups was performed using a seven minute 20% piperidine/DMF

wash. The peptides were cleaved from the resin using Reagent R as described by Milligen and lyophilized from water. The crude peptide mixtures were purified using P2 gel filtration chromatography with 50 mM acetic acid eluent and semi-preparative reversed-phase HPLC. Peptide-containing fractions were identified by TLC and HPLC methods (H_2O:CH_3CN mixtures; UV 256, 228 nm detection), and concentrated by lyophilization. Pure peptides were stored at -20° C. Final purity was assessed by mass spectrometry and amino acid sequencing, although the presence of the bipyridyl amino acid obstructed sequencing past that point. Final yield of the full peptide was ~40%; half of that material was recovered as the Met80-sulfoxide (*vide infra*).

C. Protein Reconstitution

4(6)Bpa72 cyt *c* was reconstituted using 0.15 to 0.35 mM 1-65 lactone with 0.8 equivalents 66-104 (4(6)Bpa72) peptide in 25 mM NaPi, pH 6.8 to 7.0. The reaction solution was thoroughly degassed and the reaction carried out under anaerobic conditions (in an inert atmosphere box). Reduction was achieved using 1 to 1.5 equivalents of freshly prepared sodium dithionite and the reaction allowed to proceed for ~40 hours. The products were purified by cation-exchange chromatography (FPLC Mono S 10/10 column) in 25 mM NaPi, pH 7.0, with a 0.1 to 0.4 M NaCl gradient. The semisynthetic proteins eluted at similar volumes as native cyt *c*. Using this methodology ~20 milligrams of 4(6)Bpa72 cyt *c* was isolated. Protein yields could not be directly assessed due to aggregation and impurities in the peptide.

D. $Ru(bpy)_2^{2+}$ Modification of 4(6)Bpa72 Cytochrome c

$Ru(bpy)_2$(4Bpa72)cyt *c* was prepared by reaction of 0.2 mM protein and 2 mM $Ru(bpy)_2CO_3$ in 25 mM NaPi, pH 6.5 - 7.0, under anaerobic conditions. The modification reaction was monitored by absorption spectroscopy and terminated by gel filtration at a $Ru(bpy)_3^{2+}$ to heme ratio of 1:1. Treatment with imidazole facilitated separation of the

His33 modified derivative. The products were purified by cation-exchange chromatography (FPLC 10/10 Mono S column) in 25 mM NaPi, pH 7.0, with a 0.1 to 0.4 M NaCl gradient. Final yield was ~20%.

E. $Ru(bpy)_2^{2+}$ Modification of Model Peptides Containing 4(6)Bpa

Two peptides of the general sequence Ac-Bpa-Thr-Pro-D-Ala-Val-Phe-NH_2, where Bpa is either **1** or **2**, were synthesized and characterized.[18] The $Ru(bpy)_2^{2+}$-modification reaction was performed with 1.0 mM peptide and 3.8 mM $Ru(bpy)_2CO_3$ in 25 mM NaPi, pH 7.0, under anaerobic conditions in the absence of light. The modification reaction was monitored by absorption spectroscopy and terminated by addition of excess imidazole after 5.5 hours of reaction. Initial purification was by gel filtration chromatography (BioGel P2 200-400 mesh column) in 50 mM acetic acid, a yellow band was recovered as product. Final purification was by reversed-phase liquid chromatography. Similar yields of the $Ru(bpy)_2^{2+}$-modified 4Bpa and 6Bpa peptides were obtained. Modified peptides were characterized by NMR, absorption and emission spectroscopy, mass spectrometry, and luminescence decay measurements.

F. Time-Resolved Measurements

ET rates were determined on 5 - 20 μM protein samples. No concentration dependence was observed. $*Ru^{2+}$ to Fe^{3+} and Fe^{2+} to Ru^{3+} ET rates were measured by direct excitation of $Ru(bpy)_2(4Bpa72)^{2+}$ - Fe^{2+}cyt *c*. Using the flash / quench technique (refer to Chapter 3) metastable $Ru(bpy)_2(4Bpa72)^{3+}$ - Fe^{2+}cyt *c* was generated in less than 100 ns by quenching a small fraction of $*Ru(bpy)_2(4Bpa72)^{2+}$ - cyt *c* with $Ru(NH_3)_6^{3+}$. In both flash / quench and direct photoinduced experiments intramolecular ET was readily observable at 550 and 395 nm ($Fe^{3+/2+}$), 434 nm ($Ru^{3+/2+}$), and 370 nm ($*Ru^{2+}$) after 480 nm excitation (~25 ns pulse width). Fe^{2+} to Ru^{3+} ET rates (k_{ET}^{mm}) were determined from both flash / quench and photoinduced data sets. Rates of intramolecular $*Ru^{2+}$ to Fe^{3+} ET

(k_{ET}*) were determined from *Ru^{2+} kinetics and extracted from the yield of $Ru(bpy)_2(4Bpa72)^{3+}$ - Fe^{2+}cyt *c* (Chapter 3 contains an in-depth discussion of these calculations). The photoinduced ET rate (k_{ET}*) in $Ru(bpy)_2$(4Bpa72)cyt *c* based on a calculation of the quantum yield of photoinduced ET products corresponds closely to the difference in excited-state lifetime between the Fe^{2+} (1.6×10^7 s^{-1}) and the Fe^{3+} (1.9×10^7 s^{-1}) proteins (Table 5.1); however, this difference is only an estimate of the ET rate as it does not distinguish between other quenching mechanisms in the ferrous and ferric proteins.

G. Molecular Modeling

A qualitative appraisal of the low energy conformers was performed[18] for the unnatural amino acid side chain at position 72 in horse heart cyt *c* (based on the native crystal structure).[20] Low energy conformers were selected from a Ramachandran map generated for χ_1 and χ_2 using Insight II v.2.1.0 Modeling Package (Biosym Technologies) on a Silicon Graphics Personal Iris 4D/25TG with the Discover force field. In all cases the chelating nitrogens of 6Bpa72 cyt *c* were directed towards the protein structure.

II. Results and Discussion

A. Amino Acid and Peptide Synthesis and Characterization[18]

The 39-mer peptides were prepared by standard FMOC solid phase peptide synthesis with no difficulties encountered due to the inclusion of the unnatural amino acids. The stereoselective syntheses of **1** and **2** allow for exclusive incorporation of the L-enantiomer into peptides.

Difficulties were encountered in the purification of the peptides due to the oxidation of the Met residue to the corresponding sulfoxide (confirmed by mass spectrometry and reversed-phase chromatographic analysis of the reduced peptides). In addition, the peptides were highly insoluble in aqueous solvents and buffers following reversed-phase

chromatographic purification. This property hindered purification and eventually crude peptide was used directly in reconstitution reactions, resulting in higher net recovery of Bpa-containing proteins.

B. Protein Reconstitution

The unnatural amino-acid containing proteins were assembled through the coupling of two protein segments representing residues 1-65 and 66-104 of the complete horse heart cyt *c* primary sequence. Native fragment 1-65, containing the covalently bound heme and a homoserine (Hse) lactone at the carboxy terminus, was obtained through cyanogen bromide cleavage of native horse heart cyt *c* at Met65 under denaturing conditions, followed by purification of the heme-containing fragment using cation-exchange chromatography (refer to Chapter 2 for details). Peptides 66-104 with the bipyridyl amino acids incorporated at position 72 were prepared by solid phase peptide synthesis utilizing *N*-9-fluorenyl-methoxycarbonyl (FMOC) amino protection strategy.[18] The synthetic peptides were purified by reversed-phase HPLC and characterized by electrospray mass spectrometry. Reconstitution of the protein was effected through incubation of the two purified fragments under neutral reducing conditions, thereby allowing reaction of the Hse65 lactone and the amino terminus of 66-104, to form a peptide bond. The renatured, fully-formed protein was then purified using cation-exchange chromatography (Figure 5.3). The reconstitution reaction is extremely selective; reaction of crude peptide 66-104 with purified fragment 1-65 resulted in similar yields of protein in slightly lower purity. This remarkable selectivity most likely due to favorable secondary structure interactions between the two peptide fragments prior to amide bond formation.

Figure 5.3 Typical cation-exchange chromatogram (FPLC Mono S 10/10, flow rate 3.5 ml/min) for the 4(6)Bpa reconstitution reaction in 25 mM NaPi, pH 7.0. Gradient shows the concentration of NaCl in mM. Products eluting at low ionic strength correspond to the reduced and oxidized forms of the reconstituted protein. The 1-65 fragment starting material is indicated. Detection is on the 2.0 absorbance scale at 280 nm.

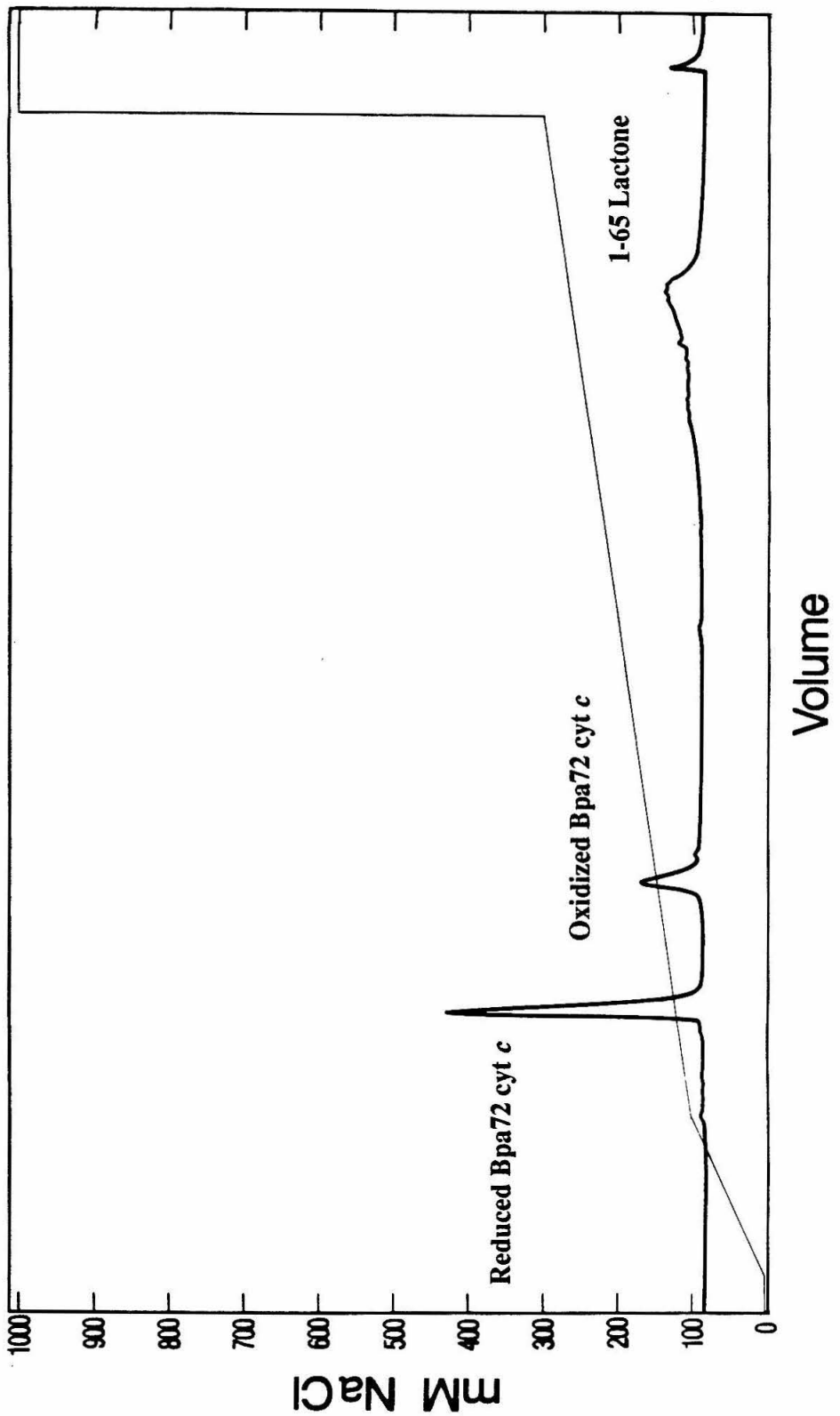
mM NaCl
1000
900
800
700
600
500
400
300
200
100
0
Volume
Reduced Bpa72 cyt *c*
Oxidized Bpa72 cyt *c*
1-65 Lactone

C. Protein Characterization

1. Absorption Spectroscopy

The 4Bpa72 cyt *c* (also 6Bpa72 cyt *c*, not shown) absorption spectrum in 50 mM NaPi, pH 7.0, at room temperature overlays nearly identically with that of native cyt *c* in both the ferric and ferrous states, with the anticipated addition of a 290 nm band due to the bipyridine absorption[14] (ε_{bpy} = 13300 M^{-1} cm^{-1}; $\varepsilon_{cyt\ c}$ = 19500 M^{-1} cm^{-1}). Spectra for the ferric state are presented in Figure 5.4 A. In addition, the 695 nm band, indicative of proper Met80 ligation to the heme, is unperturbed in the ferric Bpa72 proteins relative to the native protein (Figure 5.4 B).

2. Circular Dichroism Spectroscopy

Circular dichroism spectra of the semisynthetic and native ferric proteins in the far UV region in 50 mM NaPi, pH 7.0, at 25° C are superposable (Figure 5.5). Variable temperature CD studies in this spectral region on the ferric 6Bpa variant demonstrated that the protein denatured at approximately 85-90° C, nearly identical with the native ferric horse heart protein melting temperature of 87° C (Figure 5.6). Thus, the overall secondary structure and thermodynamic stability of the protein is unaffected by the replacement of Lys72 with either of the bipyridyl amino acids.

3. Electrochemistry

The reduction potential of the mutant protein, a useful probe of the heme center environment and ligand geometry, was found to be nearly identical (within experimental error) with the native protein as measured by differential pulse polarography at a 4,4'-bipyridyl-modified gold electrode. The reduction potentials of the semisynthetic and native proteins are: native cyt *c* = 0.265(5) V, 6Bpa72 cyt *c* = 0.265(5) V, 4Bpa72 cyt *c* = 0.258(5) V *vs.* NHE. Data are shown for 4Bpa72 cyt *c* in Figure 5.7.

Figure 5.4 Electronic absorption spectra of 4Bpa72 (· · · ·) and native horse heart cyt *c* (——). Spectra were recorded using a 1 cm cell in 50 mM NaPi, pH 7.0, at room temperature. The 4Bpa72 cyt *c* (as well as the 6Bpa72 cyt *c*, not shown) spectrum overlays identically with native cyt *c* with the addition of a 290 nm band due to the bipyridine absorption (ε_{bpy} = 13300 M^{-1} cm^{-1}; $\varepsilon_{cyt\,c}$ = 19500 M^{-1} cm^{-1}), including the 695 nm band indicative of Met ligation. (A) 250 - 700 nm region. (B) 600 - 800 nm region. Proteins were oxidized with Na[Co(EDTA)] prior to purification.

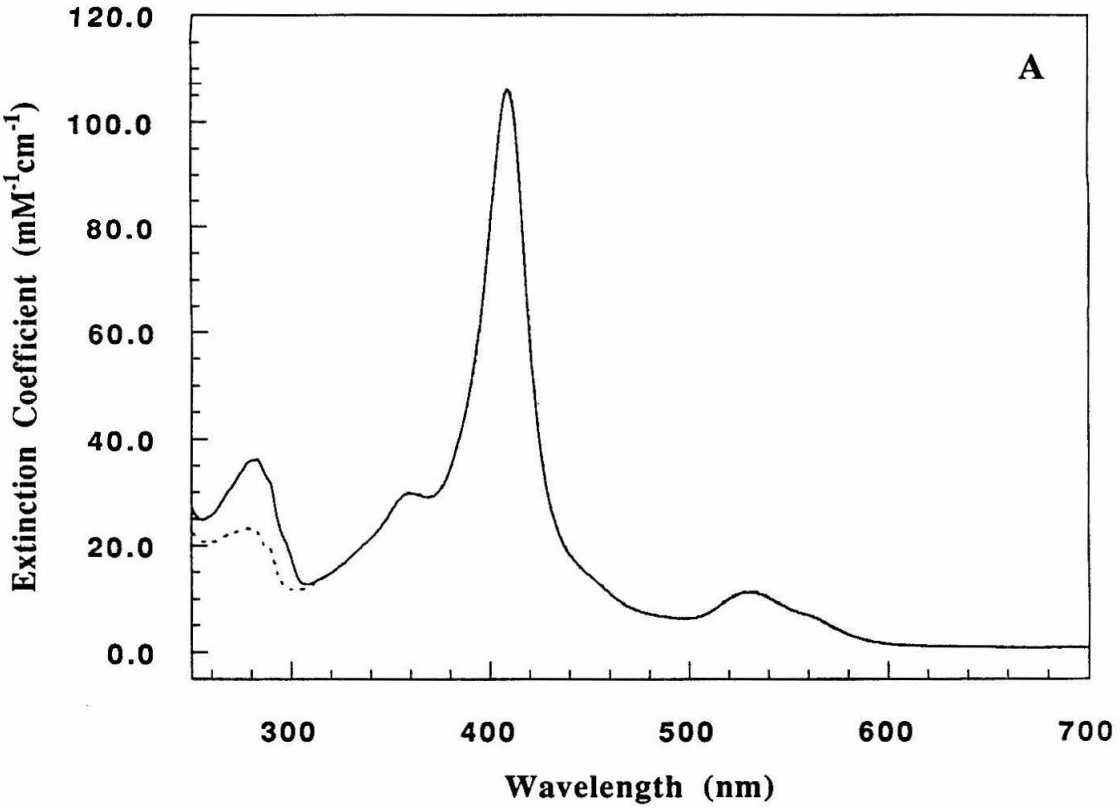
A
120.0
100.0
80.0
60.0
40.0
20.0
0.0
Extinction Coefficient (mM-1cm-1)
300
400
500
600
700
Wavelength (nm)

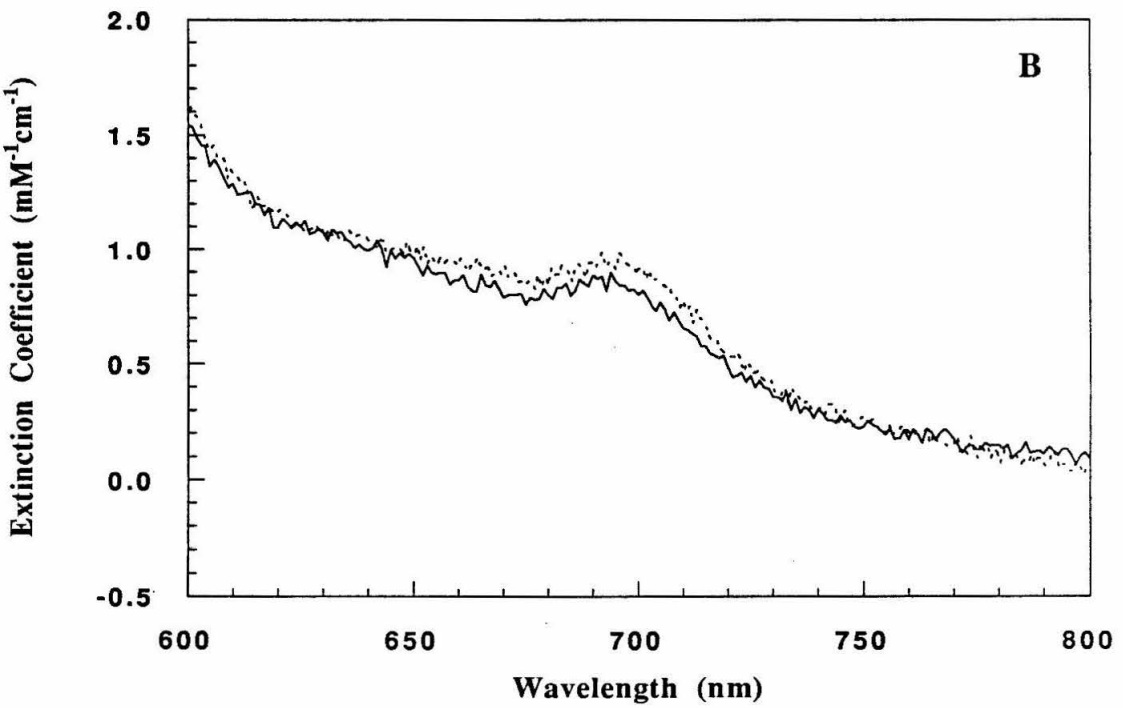
B
2.0
1.5
1.0
0.5
0.0
-0.5
Extinction Coefficient (mM-1cm-1)
600
650
700
750
800
Wavelength (nm)

Figure 5.5 Circular dichroism spectra in the far UV region of ferric cyts *c* : native horse heart cyt *c* (——), 6Bpa72 cyt *c* (- - -), 4Bpa72 cyt *c* (· – · – · – ·). Sample concentrations were ~13 μM. Spectra were recorded using a 0.10 cm cell on the 20 mdeg sensitivity scale in 50 mM NaPi, pH 7.0, at 25° C.

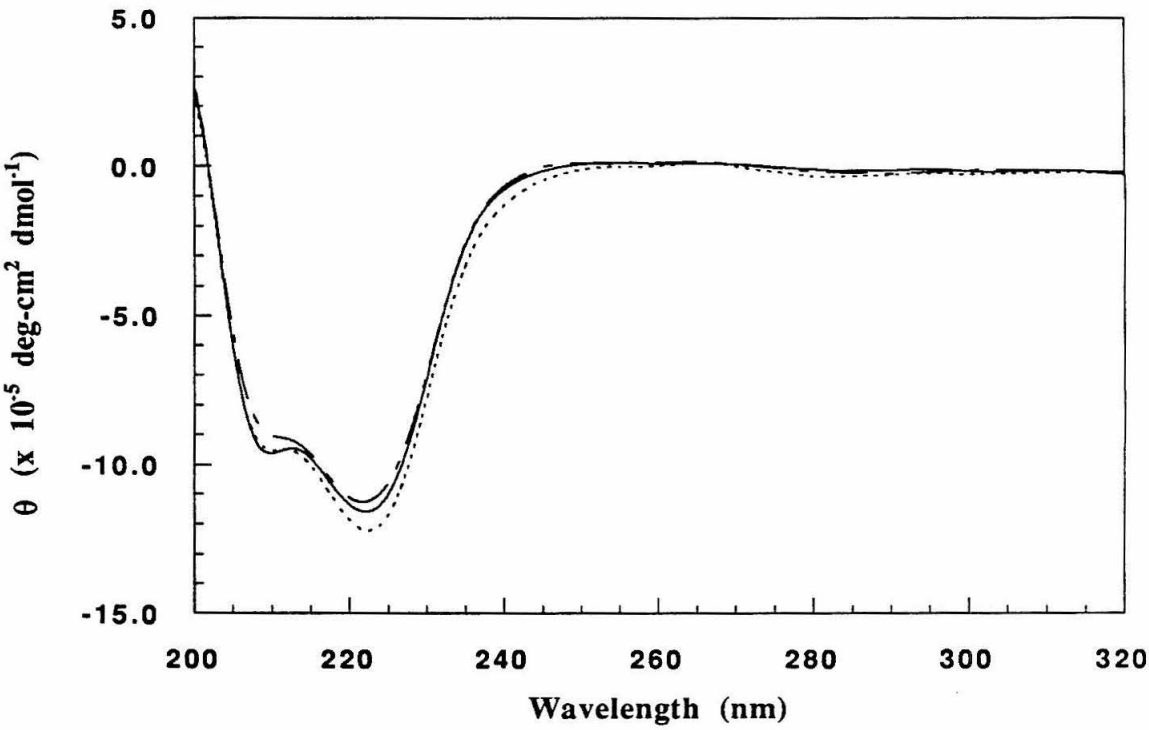
5.0
0.0
-5.0
-10.0
-15.0
θ (x 10-5 deg-cm2 dmol-1)
200
220
240
260
280
300
320
Wavelength (nm)

Figure 5.6 Melting curves for (A) native cyt *c* and (B) 6Bpa72 cyt *c* in 50 mM NaPi, pH 7.0. The intensity of the 222 nm signal of the CD spectrum is plotted as a function of temperature. The native and mutant melting curves superimpose exactly.

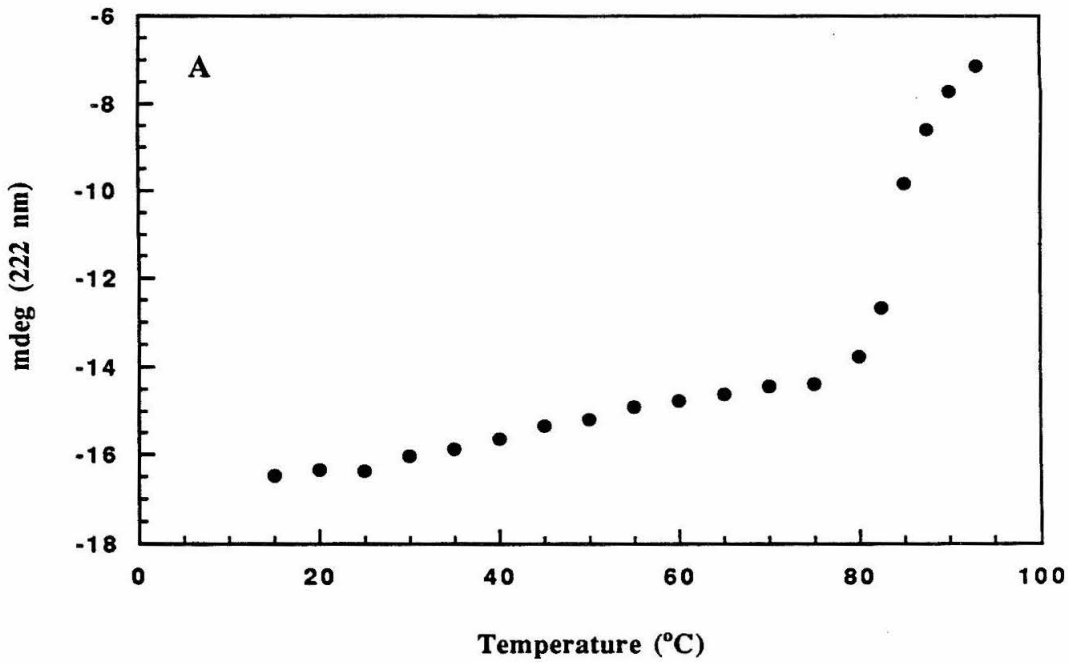
A
mdeg (222 nm)
-6
-8
-10
-12
-14
-16
-18
0
20
40
60
80
100
Temperature (°C)

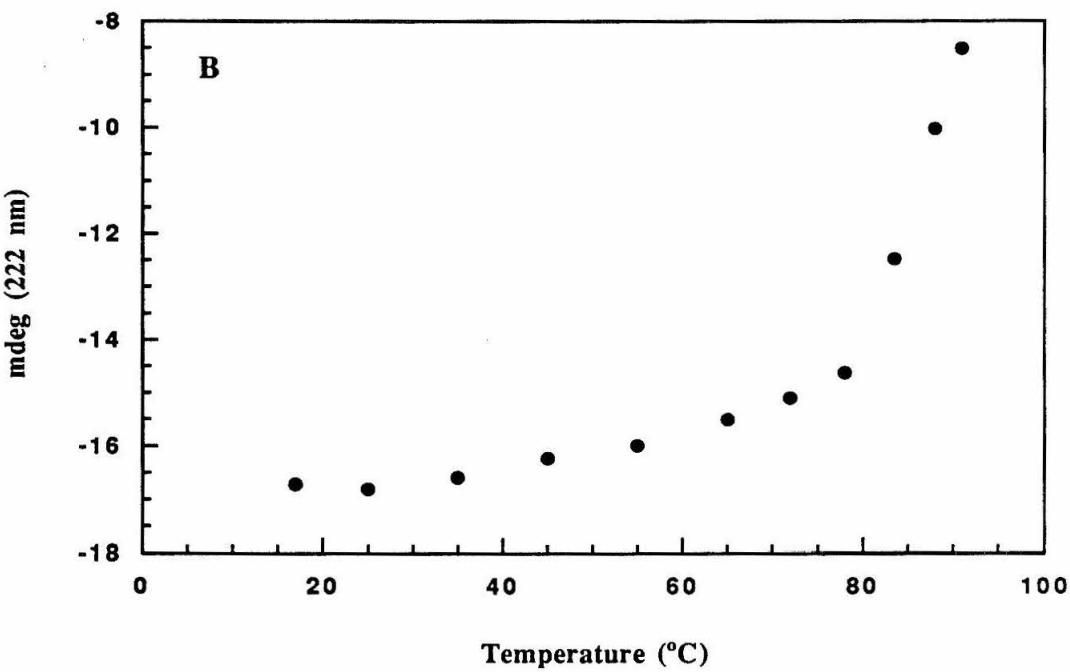
B
mdeg (222 nm)
-8
-10
-12
-14
-16
-18
0
20
40
60
80
100
Temperature (°C)

Figure 5.7 Differential pulse polarogram of 4Bpa72 cyt *c* in 50 mM NaPi, 10 mM 4,4'-bipyridine at a gold electrode, scan rate = 0.5 mV/s, drop rate 0.5 s^{-1}, modulation amplitude = 25 mV. $E^{o'}$ = 258 mV *vs.* NHE.

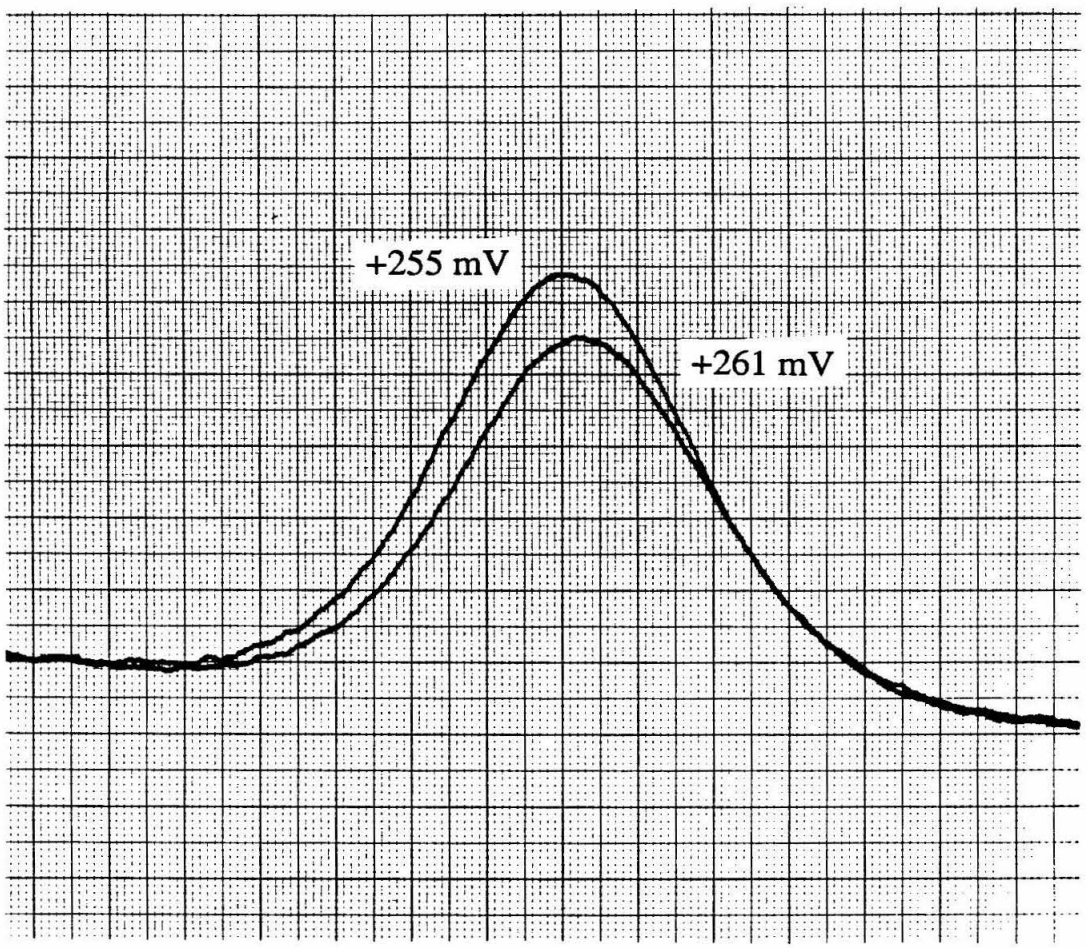
+255 mV
+261 mV

4. EPR Spectroscopy

The EPR spectrum of ferric 6Bpa72 cyt *c* at 6.8 K was virtually identical with that of the native protein (Figure 5.8). This observation indicates analogous ligand environments of the heme groups in the native and semisynthetic proteins since the *g*-values are extremely sensitive to the electronic character of the heme ligands. Measured values are: $g = 3.03$, 2.21 and 1.21 for both horse cyt *c* and 6Bpa72 cyt *c*, literature values for cyt *c* are $g = 3.06$, 2.24 and 1.24 at slightly difference conditions.[21] The reason for the small discrepancy between reported and measured values is not known. Spectra were obtained in 50 mM HEPES, 50% glycerol, pH 7.0 on an ESP-300 Bruker spectrometer equipped with a helium cryostat in the laboratories of Prof. David Goodin.

5. Mass Spectrometry

High resolution thermospray mass spectrometry of the mutant proteins produced peaks at 12426(12) amu (6Bpa72 cyt *c*) and 12439(12) amu (4Bpa72 cyt *c*), as compared to the native protein which produced a peak at 12385(12) amu. This change is consistent with an anticipated nominal difference of 66 amu for the Lys to bipyridyl and Met to homoserine mutations (native calculated = 12364; 4(6)Bpa72 cyt *c* calculated = 12430 amu). Raw and deconvoluted data for 4Bpa72 cyt *c* and 6Bpa72 cyt *c* are presented in Figure 5.9. Lower mass forms probably correspond to deamidated species. Samples were prepared in 20 mM ammonium bicarbonate buffer (pH=7.6), diluted with 1N acetic acid. Spectra were recorded on a Vestec Thermospray LC-Mass Spectrometer and analyzed using deconvolution algorithms developed at the laboratories of Prof. Curtis Monig.

6. Electrophoresis

IEF gel analysis shows the mutant proteins to have a slightly lower isoelectric point relative to the native protein, consistent with the substitution of bipyridinelysine for lysine at

Figure 5.8 EPR spectrum of (A) native ferric horse heart cyt *c* and (B) ferric 6Bpa72 cyt *c* at 6.8 K in 50 mM HEPES, 50% glycerol, pH 7.0, g = 3.03, 2.21 and 1.21. Spectrum obtained on an ESP-300 Bruker spectrometer equipped with a helium cryostat in the laboratories of Prof. David Goodin.

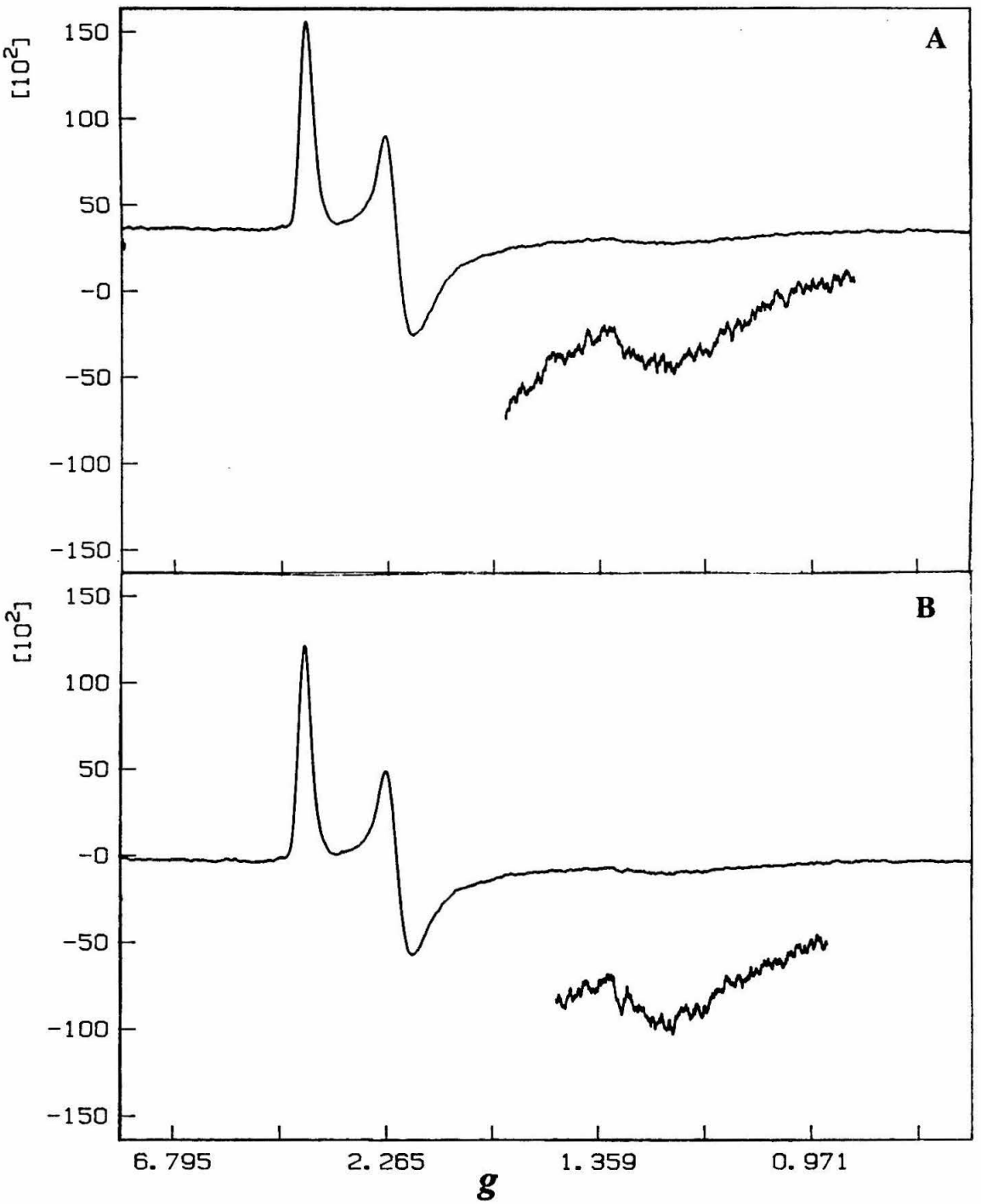
A
B
[10²]
150
100
50
-0
-50
-100
-150
6.795
2.265
1.359
0.971
g

Figure 5.9 Thermospray mass spectra ((A) raw data, (B) deconvoluted data) of 6Bpa72 cyt *c* (first page) and 4Bpa72 cyt *c* (second page). Samples were prepared in 20 mM ammonium bicarbonate buffer (pH=7.6), diluted with 1N acetic acid. Spectra were recorded on a Vestec Thermospray LC-Mass Spectrometer and analyzed using deconvolution algorithms developed at the laboratories of Prof. Curtis Monig.

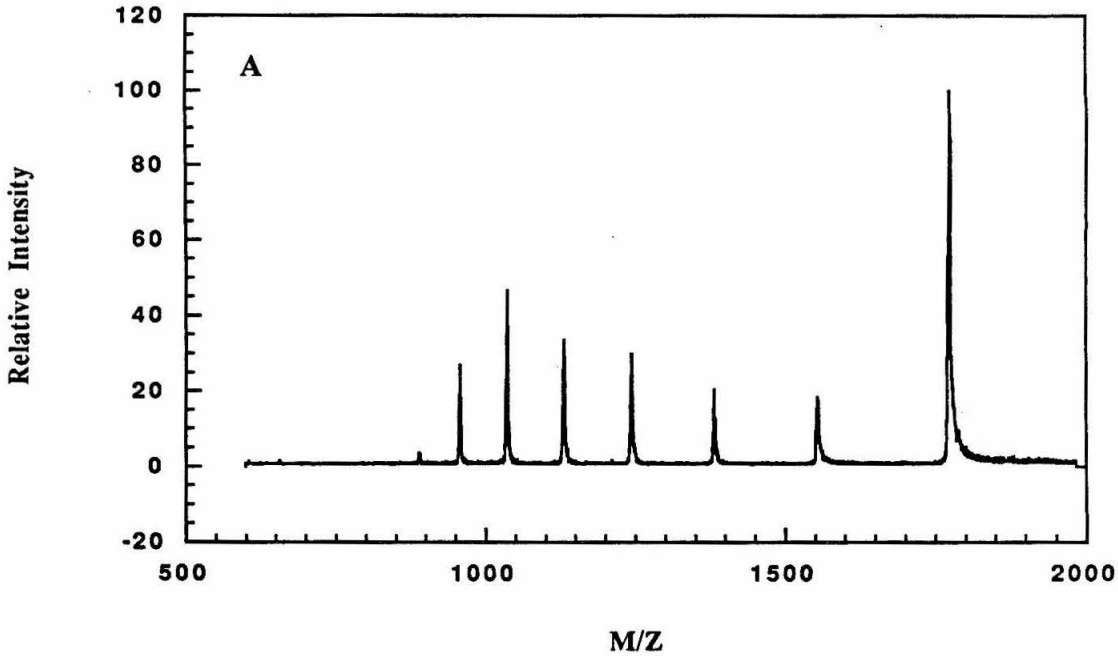
A
Relative Intensity
120
100
80
60
40
20
0
-20
500
1000
1500
2000
M/Z

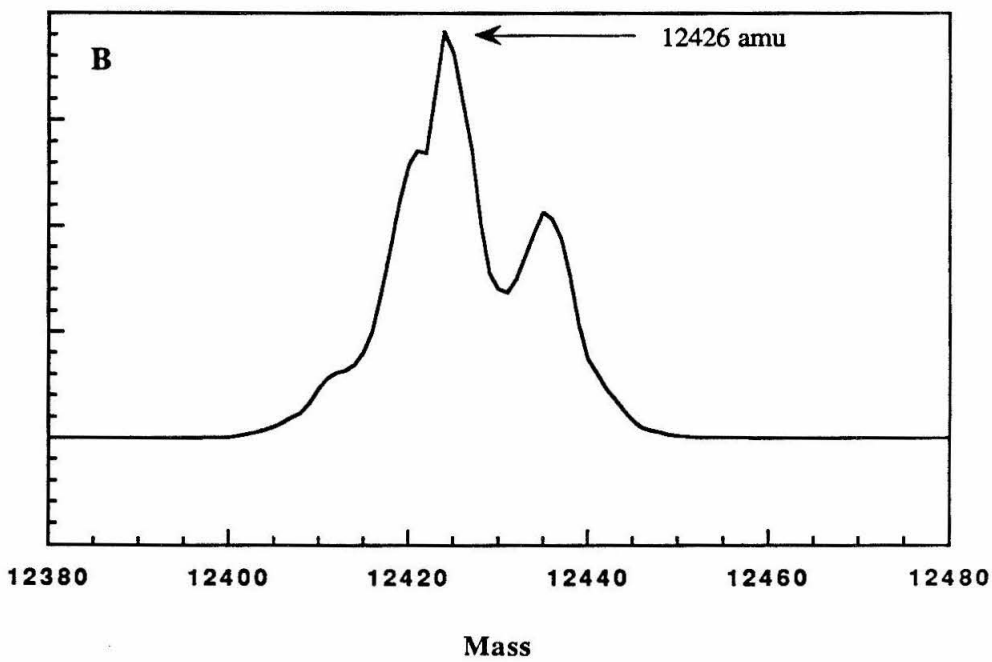
B
12426 amu
12380
12400
12420
12440
12460
12480
Mass

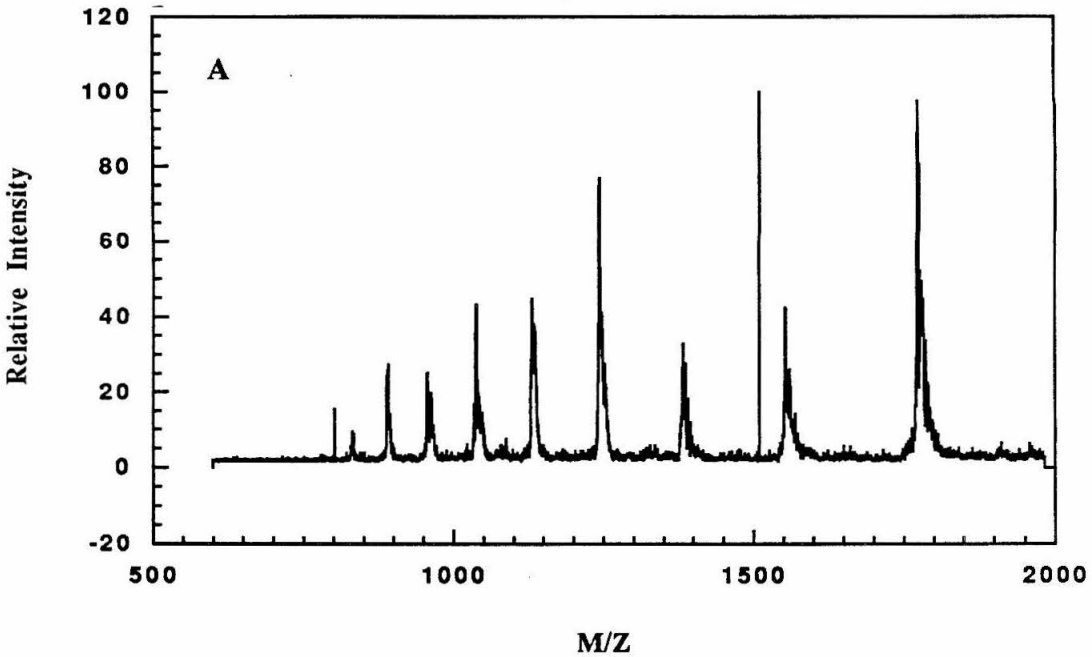
A
Relative Intensity
120
100
80
60
40
20
0
-20
500
1000
1500
2000
M/Z

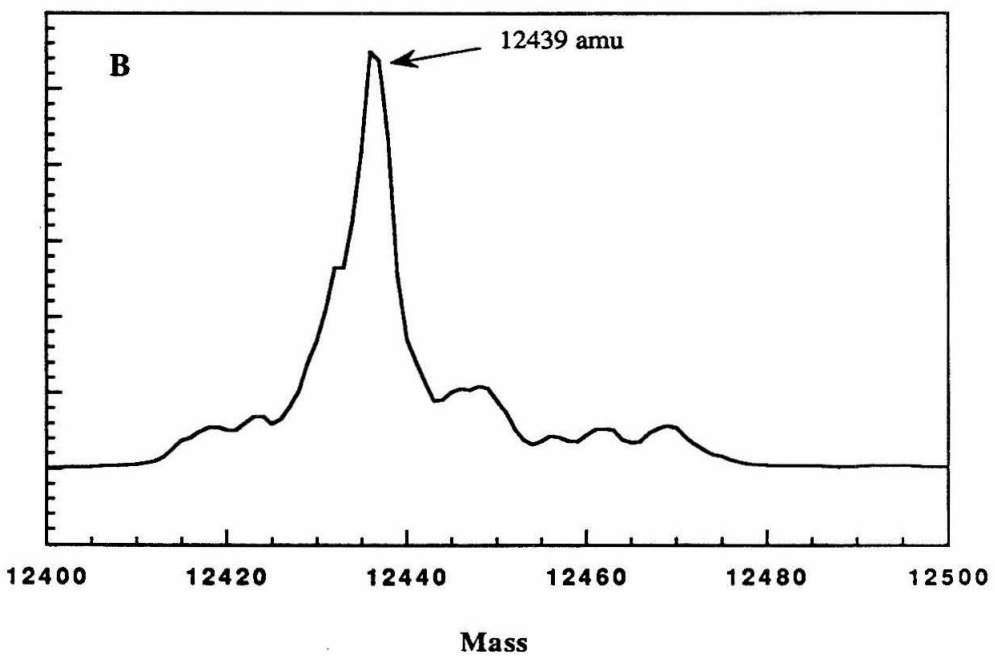
B
12439 amu
12400
12420
12440
12460
12480
12500
Mass

position 72. Gel shifts from SDS-PAGE (denaturing polyacrylamide gel electrophoresis) and elution profiles from cation-exchange chromatography are consistent with the proposed structure.

These characterization data indicate that the unnatural amino acids have been successfully integrated into the polypeptide structure and that incorporation of the bipyridyl amino acids does not affect the structural integrity of the proteins. A model of the protein structure with the unnatural amino acid incorporated at position 72 is shown in Figure 5.10.

D. $Ru(bpy)_2^{2+}$ Modification and Characterization of 4(6)Bpa72 cyt c

Modification of the 4Bpa and 6Bpa proteins with a redox-active unit was achieved *via* incubation with excess $Ru(bpy)_2CO_3$ (refer to Chapter 3 and Reference 17). Singly modified derivatives were purified to homogeneity by cation-exchange chromatography (Figure 5.11). Bpa72-modified protein was unambiguously distinguished from the His33-modified form by absorption and emission spectroscopy (see Table 5.1 for comparisons).

The modification reaction proceeded somewhat more slowly than anticipated, and unwanted modification at His33 represented a major side reaction. Lowering the pH to 6.5 to protonate this His residue did not significantly impede the side reaction.

Interestingly, only 4Bpa72 cyt *c* could be modified at the surface bipyridyl residue. Molecular modeling of the two regioisomers indicates that the chelating nitrogens of the bipyridine are more accessible to solvent in the 4Bpa protein. Model peptide studies (following section) indicate that this regiospecificity cannot be attributed to an intrinsic property of the bipyridyl ligand and is most likely due to constraints at the 6Bpa72 site due to the protein structure.

The UV-Vis absorption spectra of $Ru(bpy)_2$(4Bpa72) cyt *c* corresponds exactly to the sum of the component protein and $Ru(bpy)_3^{2+}$ species (Figure 5.12 A). Note the distinctive shift in the Ru^{2+} to bipyridyl MLCT band from 490 nm in the

Figure 5.10 Model of 4Bpa72 cyt *c* based on the crystal structure of ferric horse heart cyt *c*.[20] The blue tube is the 1-65 native fragment backbone; the yellow tube is the 66-104 backbone constructed by solid phase peptide synthesis; red indicates the heme group; and purple is the 4(6)Bpa72 residue. In the 6Bpa protein the chelating bipyridyl nitrogen atoms are facing into the protein; in the 4Bpa protein the chelating bipyridyl nitrogens are likely to be solvent accessible.

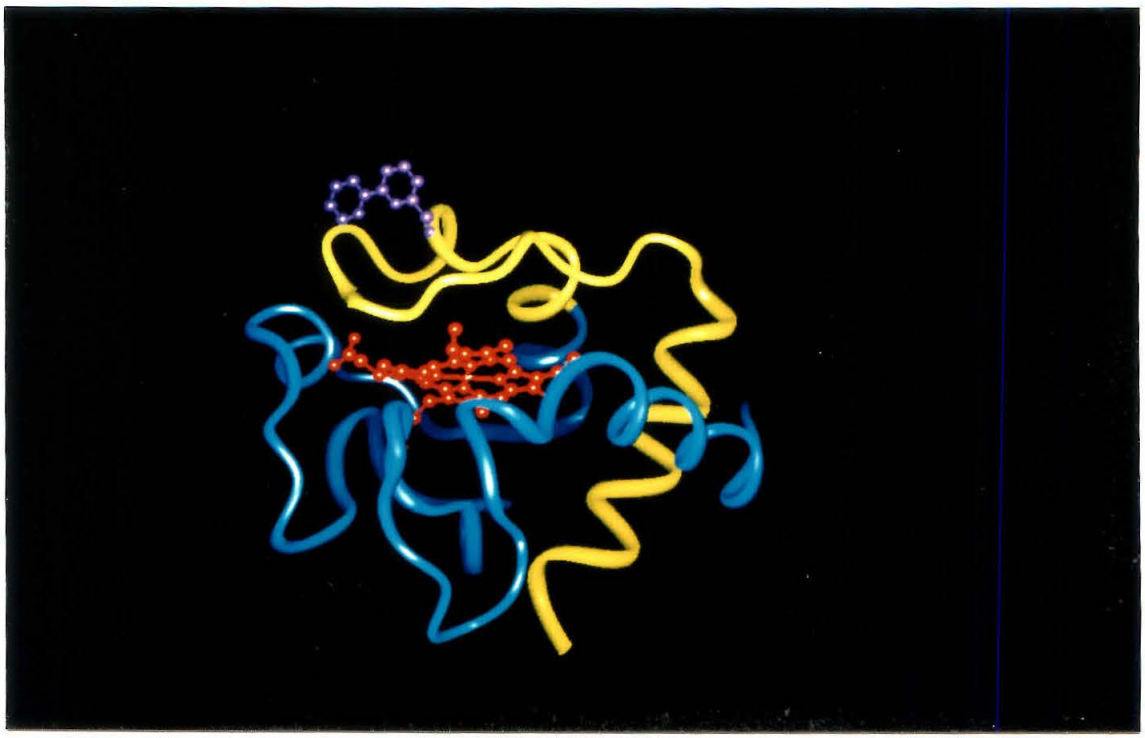

Figure 5.11 Typical cation-exchange chromatogram (FPLC Mono S 10/10, flow rate 3.5 ml/min) for the products of the 4Bpa cyt *c* modification reaction with $Ru(bpy)_2(CO_3)$ in 25 mM NaPi, pH 7.0. Gradient represents the concentration of NaCl in mM. The product eluting at low ionic strength is unmodified protein, immediately followed by $Ru(bpy)_2$(im)HisX-derivatized proteins. The product with the spectroscopic characteristics indicative of a $Ru(bpy)_3^{2+}$-modified protein is denoted by the *. Detection is on the 1.0 absorbance scale at 405 nm.

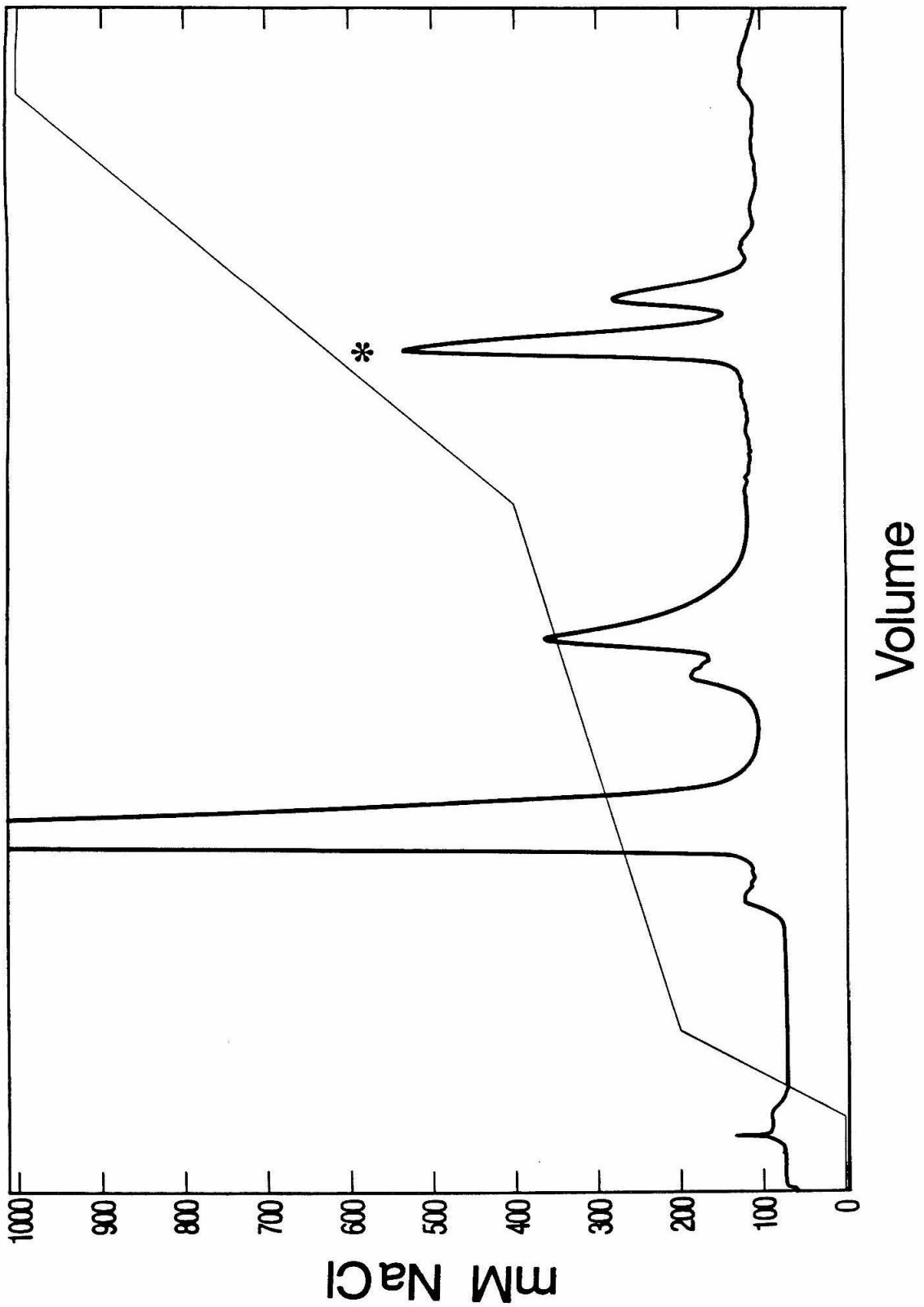
mM NaCl
1000
900
800
700
600
500
400
300
200
100
0
*
Volume

Figure 5.12 Electronic absorption spectra of cyts *c*: (····) native horse heart cyt *c*; (——) 4Bpa72 cyt *c*; (·–·–·–·) $Ru(bpy)_2$(4Bpa72)cyt *c*. Spectra were recorded using a 1 cm cell in 50 mM NaPi, pH 7.0, at room temperature. The $Ru(bpy)_2$(4Bpa72)cyt *c* spectrum corresponds to that of native cyt *c* plus $Ru(bpy)_3^{2+}$ with no additional spectral perturbations observed. (A) 250 - 700 nm region. (B) 600 - 800 nm region (native spectrum deleted for clarity).

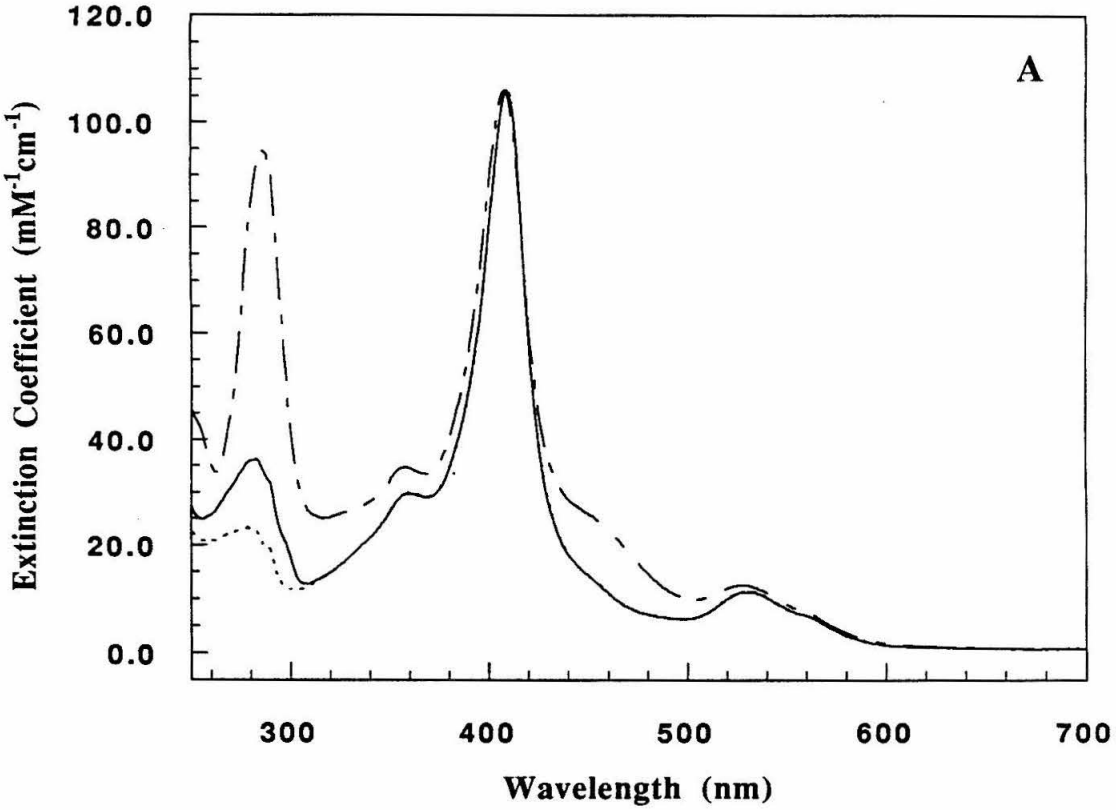
A
120.0
100.0
80.0
60.0
40.0
20.0
0.0
Extinction Coefficient (mM-1cm-1)
300
400
500
600
700
Wavelength (nm)

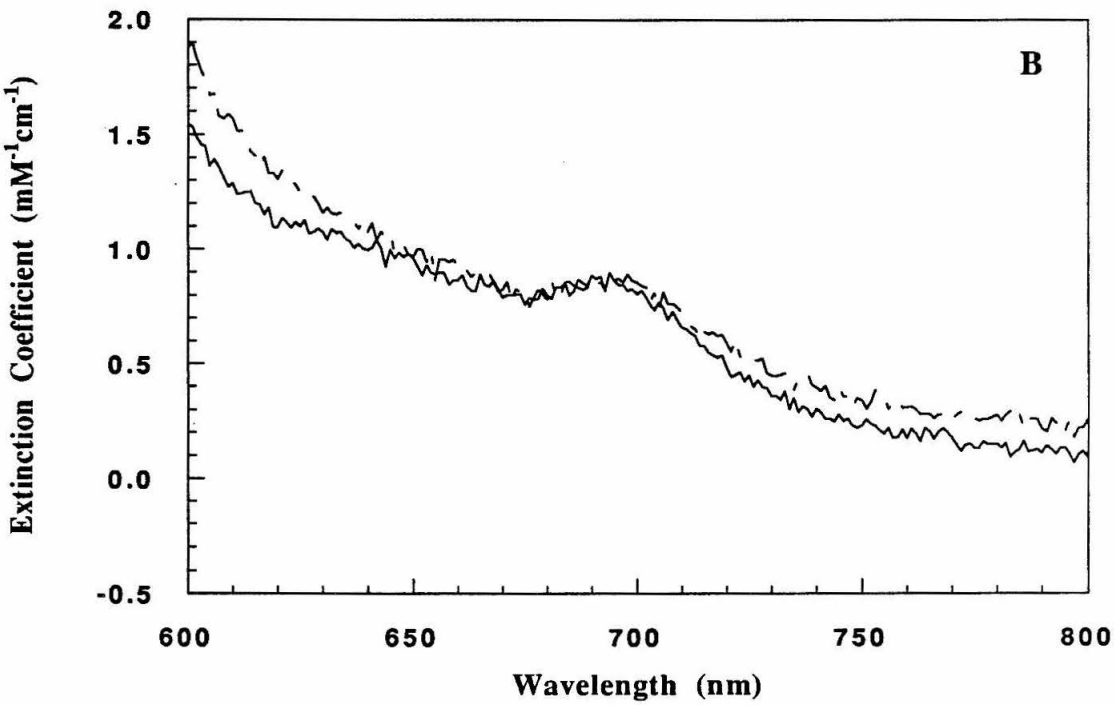
B
2.0
1.5
1.0
0.5
0.0
-0.5
Extinction Coefficient (mM-1cm-1)
600
650
700
750
800
Wavelength (nm)

$Ru(bpy)_2(im)His^{2+}$ cyt *c* derivatives (Figure 3.10) to 452 nm due to the presence of a $Ru(bpy)_3^{2+}$ chromophore. The 695 band is present in the $Ru(bpy)_2^{2+}$-modified protein (Figure 5.12 B). The maxima of the emission spectra of both oxidized and reduced $Ru(bpy)_2$(4Bpa72)cyt *c* (ferrous form, Figure 5.13) are clearly indicative of a $Ru(bpy)_3^{2+}$ (λ_{max} = 617 nm) rather than a $Ru(bpy)_2(im)_2^{2+}$ species (λ_{max} = 670 nm). The excitation spectrum confirms that the origin of the luminescence is the $Ru(bpy)_3^{2+}$ MLCT state (Figure 5.14) because it mirrors the absorption spectrum of $Ru(bpy)_3^{2+}$. The excited state lifetimes were determined for $Ru(bpy)_2$(6Bpa72)cyt *c* in both the ferrous (k_d = 1.61(5) x 10^7 s^{-1}; τ = 62 ns) and ferric (k_d = 1.91(5) x 10^7 s^{-1}; τ = 52 ns) states in 50 mM NaPi, pH 7.0, (Figure 5.15) (λ_{ex} = 480 nm, λ_{obs} = 620 nm). The dramatic quenching of the excited state lifetime of the $Ru(bpy)_3^{2+}$ species (612 ns at these conditions) upon attachment to either the ferrous or ferric protein can not be attributed to covalent attachment to a polypeptide (refer to the model peptide studies) and is probably due to energy transfer quenching. Similar excited state quenching in both protein redox states has been reported when a $Ru(bpy)_3^{2+}$ moiety is covalently attached to surface Lys residues of cyt *c*.[22] The spectroscopic properties of $Ru(bpy)_2^{2+}$-modified proteins and related model compounds are set out in Table 5.1.

Table 5.1. Spectroscopic properties of $Ru(bpy)_2L^{2+}$ model compounds (L = bpy, im_2) and $Ru(bpy)_2$-modified Bpa72 proteins. For $Ru(bpy)_3^{2+}$ data, refer to Reference 16; $Ru(bpy)_2(im)_2^{2+}$; refer to Chapter 3. λ_{em} values are from the uncorrected spectra.

	λ_{abs} (MLCT) (nm)	λ_{em} (nm)	τ (ns)
$Ru(bpy)_2$(4Bpa72) cyt *c* (pH 7.0)	452	617	Fe^{2+}: 62 Fe^{3+}: 52
$Ru(bpy)_3^{2+}$	454	615	612
$Ru(bpy)_2$(im)His72 cyt *c* (pH 7.0)	~490	670	Fe^{2+}: 71 Fe^{3+}: 71
$Ru(bpy)_2(im)_2^{2+}$	492	670	66

Figure 5.13 Uncorrected (——) and corrected (- - - -) room temperature emission spectra of ferrous $Ru(bpy)_2(4Bpa72)$cyt *c*, 5.3 μM in 50 mM NaPi, pH 7.0. Excitation was 436 nm from a Hg/Xe lamp, with a 446 nm cutoff filter. Detection sensitivity was 0.200 mV with 5 mm slits.

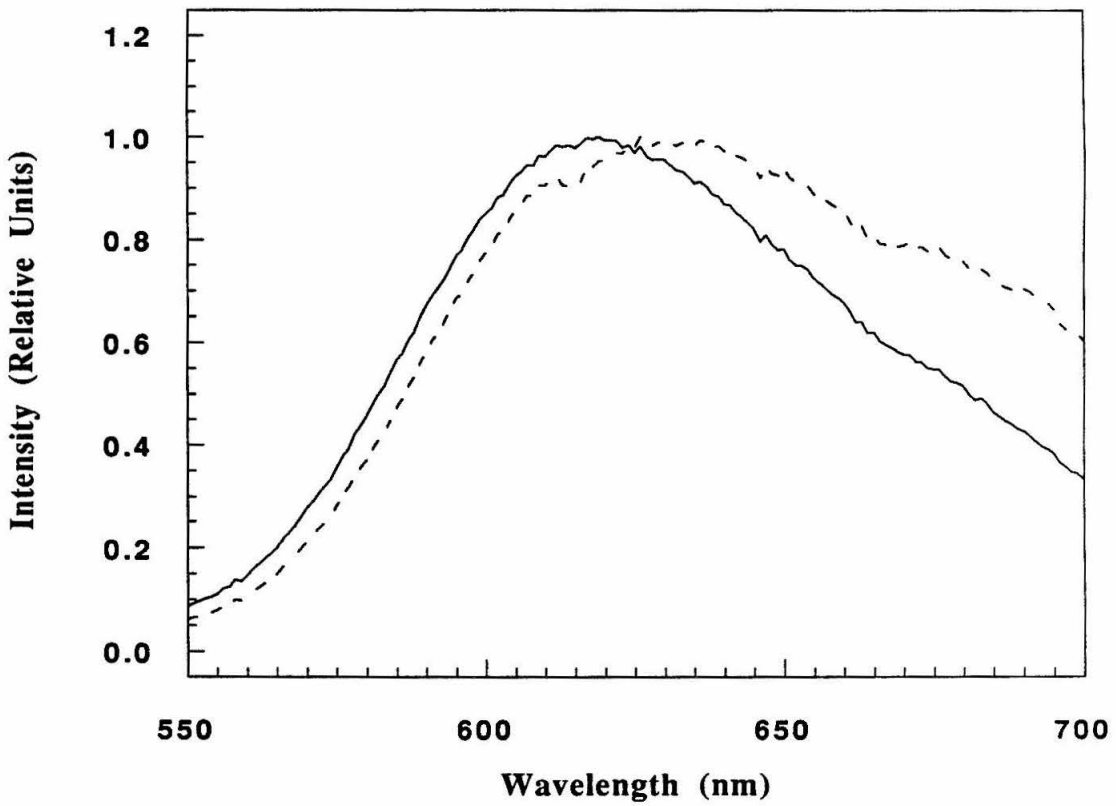
Intensity (Relative Units)
1.2
1.0
0.8
0.6
0.4
0.2
0.0
550
600
650
700
Wavelength (nm)

Figure 5.14 Room temperature excitation spectrum of ferrous $Ru(bpy)_2(4Bpa72)$cyt *c*, 4.2 μM in 50 mM NaPi, pH 7.0. Excitation was with a Xe lamp. Detection was at 620 nm (586 nm cutoff filter) with 0.100 mV sensitivity and 5 mm monochrometer slits.

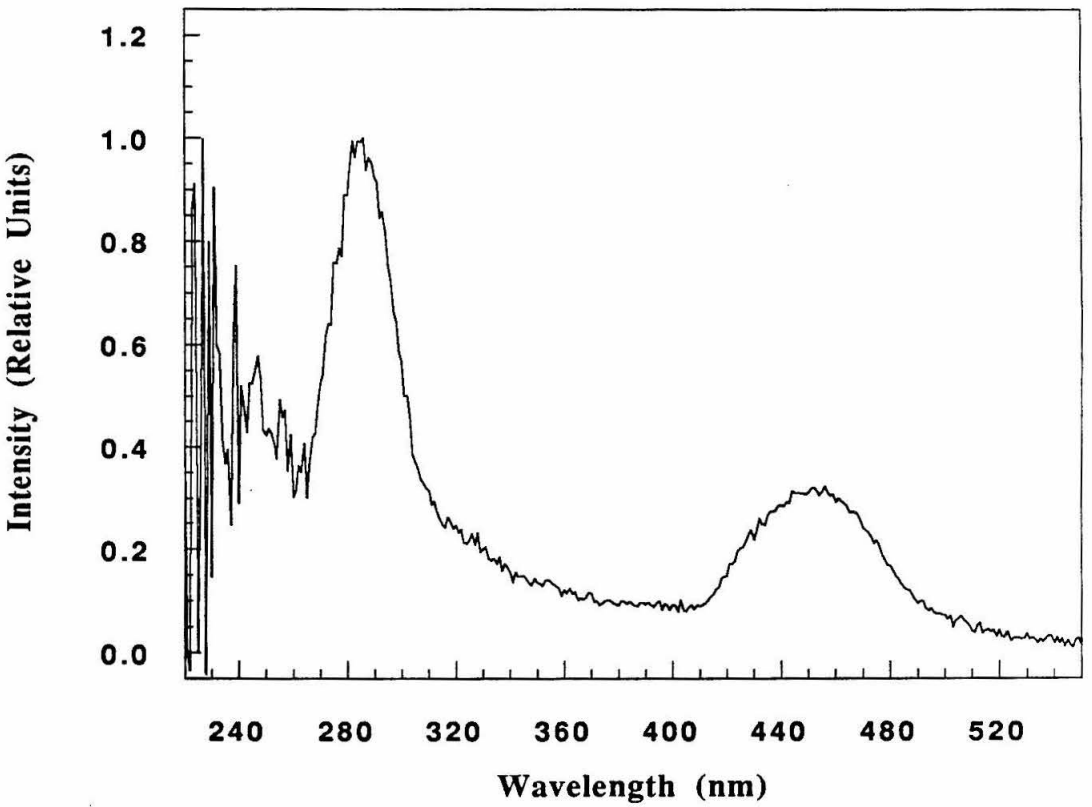
Intensity (Relative Units)
1.2
1.0
0.8
0.6
0.4
0.2
0.0
240
280
320
360
400
440
480
520
Wavelength (nm)

Figure 5.15 (A) Luminescence decay of a 10.5 μM sample of ferric $Ru(bpy)_2$(4Bpa72)cyt *c* in 50 mM NaPi, pH 7.0, observed at 620 nm following excitation at 480 nm (2 mJ pulse). The smooth line is the fit to a single exponential decay function convolved with the instrument response (shown); $k_d = 1.91(5) \times 10^7\ s^{-1}$, c = 0.147. (B) Luminescence decay of a 7.0 μM sample of ferrous $Ru(bpy)_2$(4Bpa72)cyt *c* in 50 mM NaPi, pH 7.0, observed at 620 nm following excitation at 480 nm (2 mJ pulse). The smooth line is the fit to a single exponential decay function convolved with the instrument response (shown); $k_d = 1.61(5) \times 10^7\ s^{-1}$, c = 0.161.

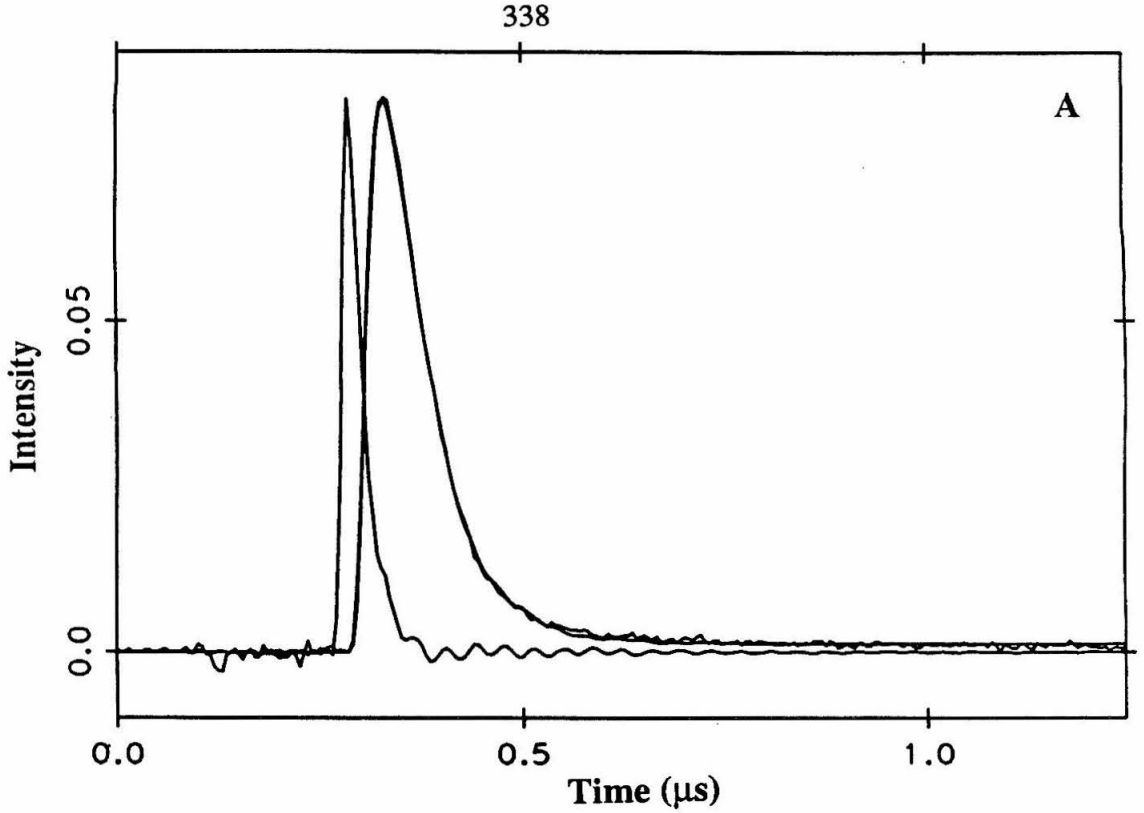
A
Intensity
0.05
0.0
0.0
0.5
1.0
Time (μs)

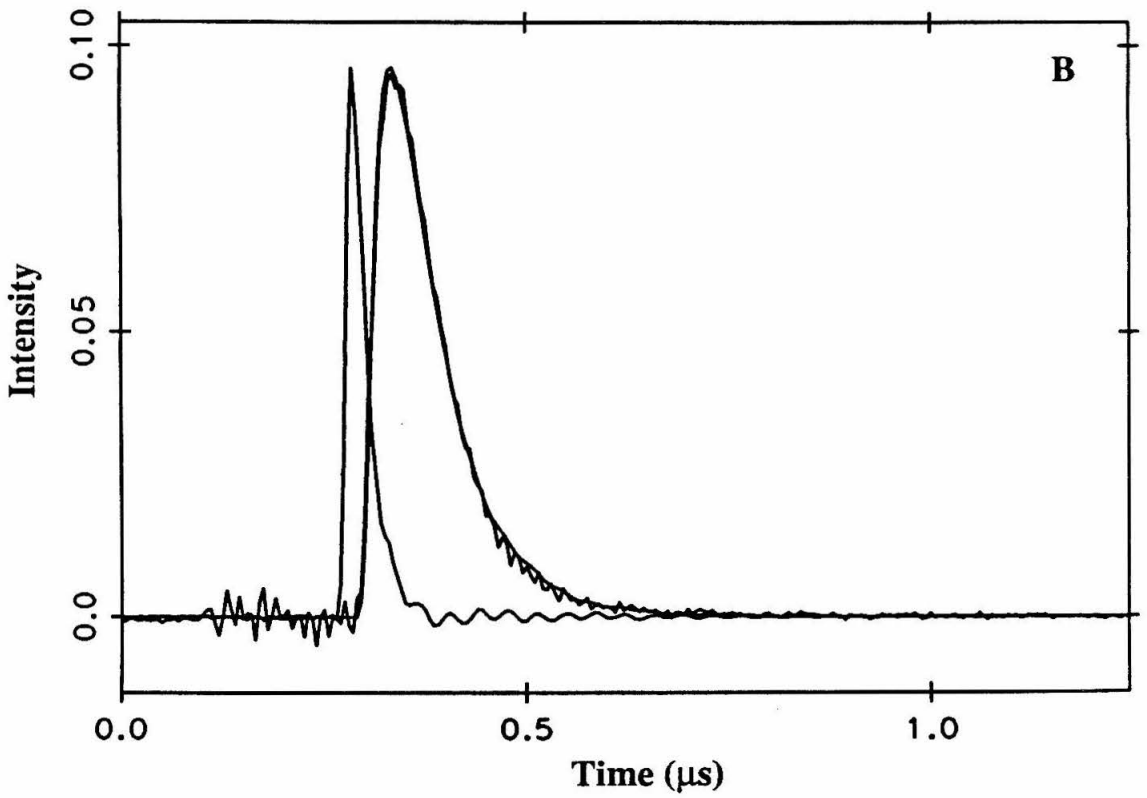
B
Intensity
0.10
0.05
0.0
0.0
0.5
1.0
Time (μs)

Comparison of the circular dichroism spectra of $Ru(bpy)_2$(4Bpa72)cyt *c* and 4Bpa cyt *c* indicate minimal perturbation of secondary structure upon $Ru(bpy)_2^{2+}$ modification (Figure 5.16). The CD in the near UV region indicates that the species isolated is predominantly the Λ-isomer. Formation of the Δ-isomer was not observed. Based on the spectroscopic data presented, a model in which the $Ru(bpy)_2^{2+}$ label does not interact with the protein structure was constructed and is shown in Figure 5.17.

E. Model Peptide Studies

Two peptides of the general sequence Ac-Bpa-Thr-Pro-D-Ala-Val-Phe-NH_2, where Bpa is either **1** or **2**, were synthesized, characterized[18] and modified by $Ru(bpy)_2CO_3$ in high yield to afford derivatives with electronic-absorption and steady-state-emission properties characteristic of $Ru(bpy)_3^{2+}$. The emission spectra for the 4Bpa and 6Bpa modified peptides and $Ru(bpy)_3^{2+}$ model complexes are presented in Figure 5.18. These data indicate that the regiospecificity observed in the protein modification reaction is not due to any intrinsic difference in the reactivity of the bipyridyl amino acid within a peptide structure.

However, while the $*Ru^{2+}$ lifetime of the $Ru(bpy)_2$(4Bpa) peptide is nearly identical with that of $Ru(bpy)_3^{2+}$ (τ=612 ns for $Ru(bpy)_2$(4Bpa) peptide, τ=644 ns for $Ru(bpy)_3^{2+}$ in aqueous solution), the $*Ru^{2+}$ lifetime of the $Ru(bpy)_2$(6Bpa) peptide is significantly shorter (τ< 6 ns). The luminescence decay data and fit are shown in Figure 5.19. The quantum yield for emission is also correspondingly lower (Figure 5.18). Similar observations have been reported in other $Ru(bpy)_3^{2+}$ complexes substituted at the 6-position of the bipyridyl ligand. For example, $Ru(bpy)_2$(6-methyl-bpy)$^{2+}$ has an MLCT excited-state lifetime of 8 ns in ethanol ($Ru(bpy)_3^{2+}$ = 670 ns) at 298 K, and a $Ru(bpy)_2$(bpy-Ni^{2+}-cyclam)$^{4+}$ complex, in which the cyclam ring is linked to the bipyridyl ligand *via* a methylene chain attached at the 6-position, exhibits an excited-state lifetime < 2 ns at room temperature.[23] The excited-state deactivation in 6-substituted derivatives has

Figure 5.16 Circular dichroism spectra in the far UV region of ferric cyts *c*: native horse heart cyt *c* (——), 4Bpa72 cyt *c* (·–·–·–·), $Ru(bpy)_2$(4Bpa72)cyt *c* (- - - -). Sample concentrations were ~13 μM, except for $Ru(bpy)_2$(4Bpa72)cyt *c*, 3.8 μM. Spectra were recorded using a 0.10 cm cell on the 20 mdeg sensitivity scale in 50 mM NaPi, pH 7.0, at 25° C.

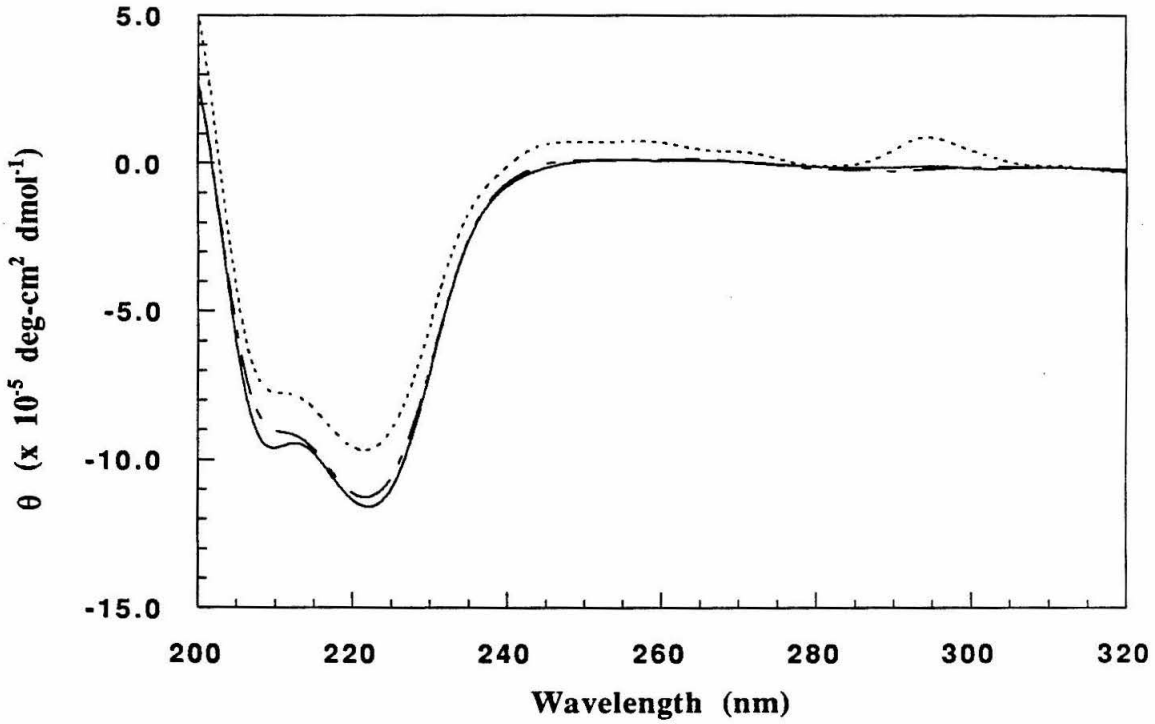
5.0
0.0
-5.0
-10.0
-15.0
θ (x 10-5 deg-cm2 dmol-1)
200
220
240
260
280
300
320
Wavelength (nm)

Figure 5.17 Model of $Ru(bpy)_2(4Bpa72)$cyt *c* based on the crystal structure of ferric horse heart cyt *c*.[20] The blue tube is the 1-65 native fragment backbone; the yellow tube is the 66-104 backbone constructed by solid phase peptide synthesis; red indicates the heme group; and purple indicates the $Ru(bpy)_3^{2+}$ unit.

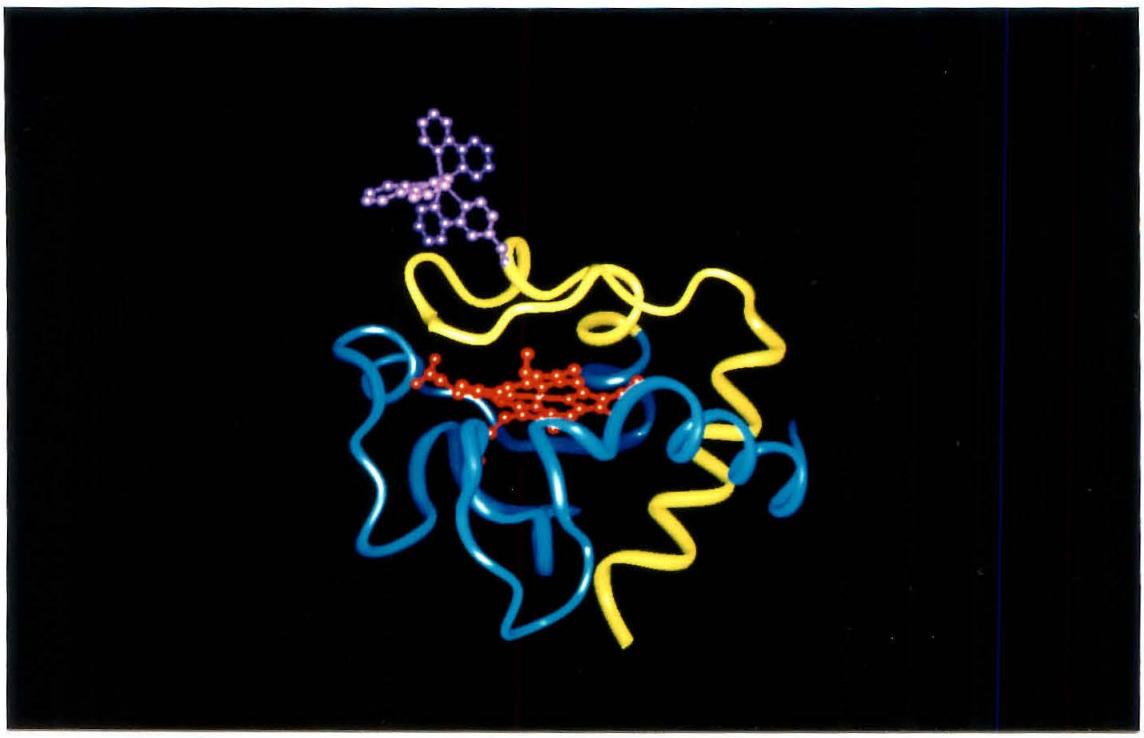

Figure 5.18 Uncorrected (——) and corrected (- - - -) room temperature emission spectra of (A) $Ru(bpy)_2$(4Bpa)-peptide, 27.0 μM in 25 mM NaPi, pH 7.0, sensitivity = 5.0 mV, (B) $Ru(bpy)_2$(6Bpa)-peptide, 15.4 μM in 25 mM NaPi, pH 7.0, sensitivity = 0.010 mV, and (C) $Ru(bpy)_3Cl_2$ 16.6 μM in 25 mM NaPi, pH 7.0, sensitivity = 2.0 mV. Excitation was 436 nm from the Hg/Xe lamp, with a 446 nm cutoff filter. 5 mm slits were used.

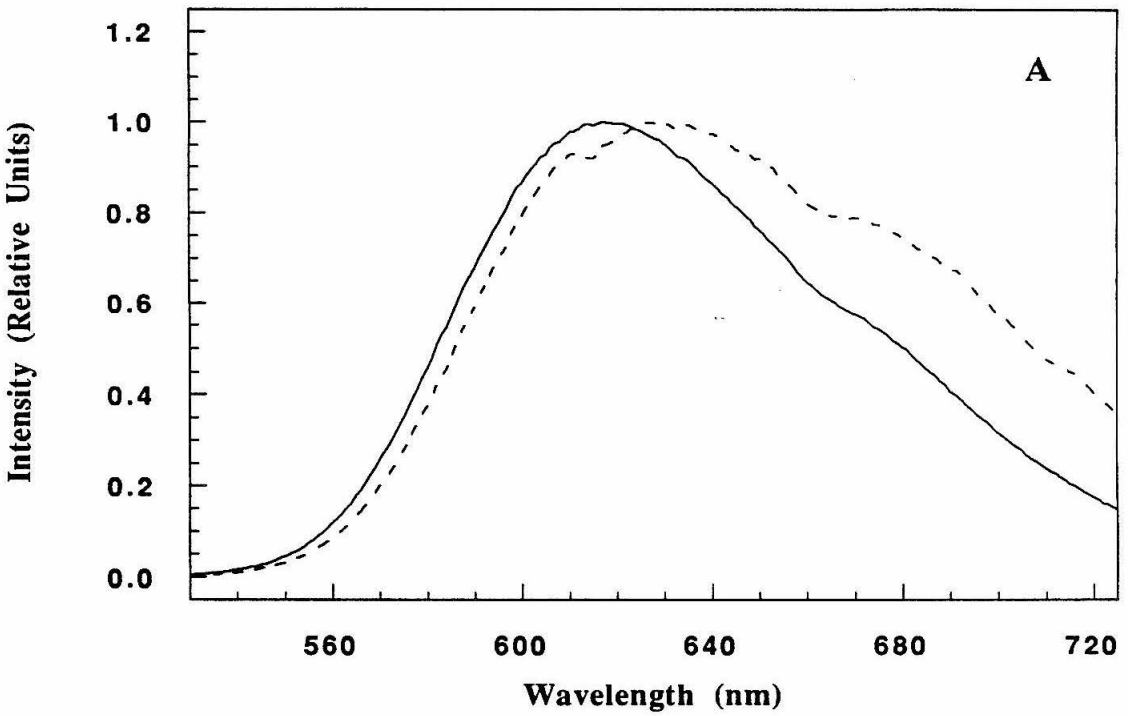
A
Intensity (Relative Units)
1.2
1.0
0.8
0.6
0.4
0.2
0.0
560
600
640
680
720
Wavelength (nm)

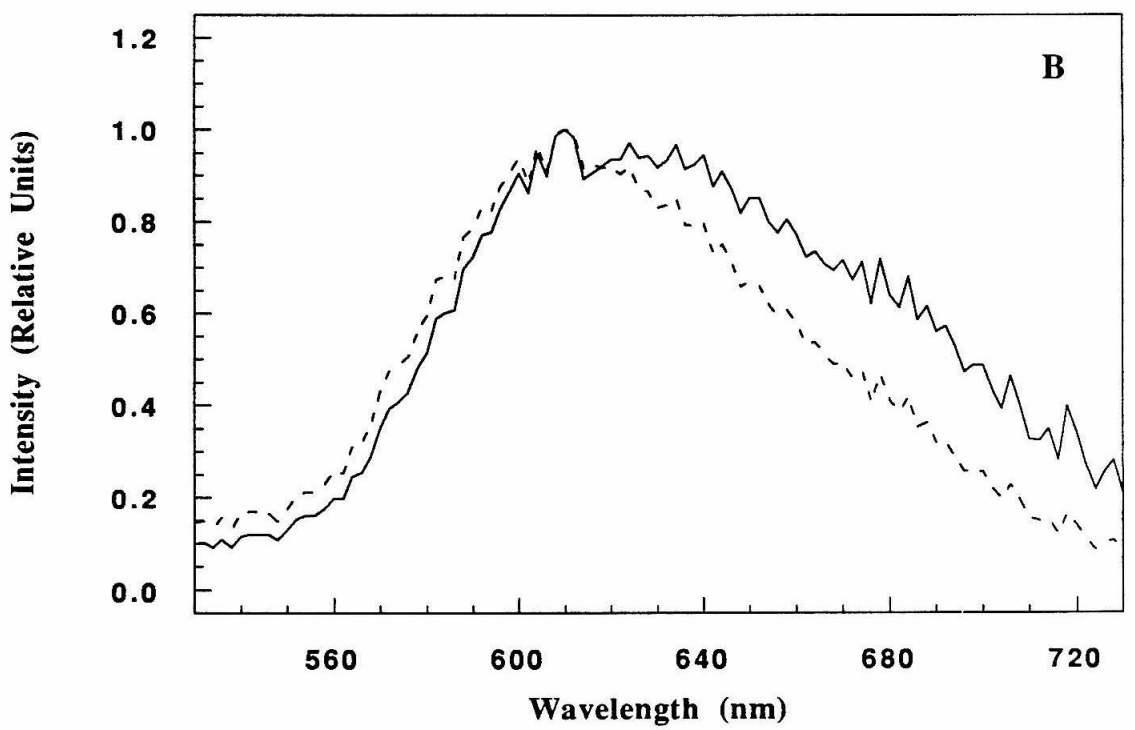
B
Intensity (Relative Units)
1.2
1.0
0.8
0.6
0.4
0.2
0.0
560
600
640
680
720
Wavelength (nm)

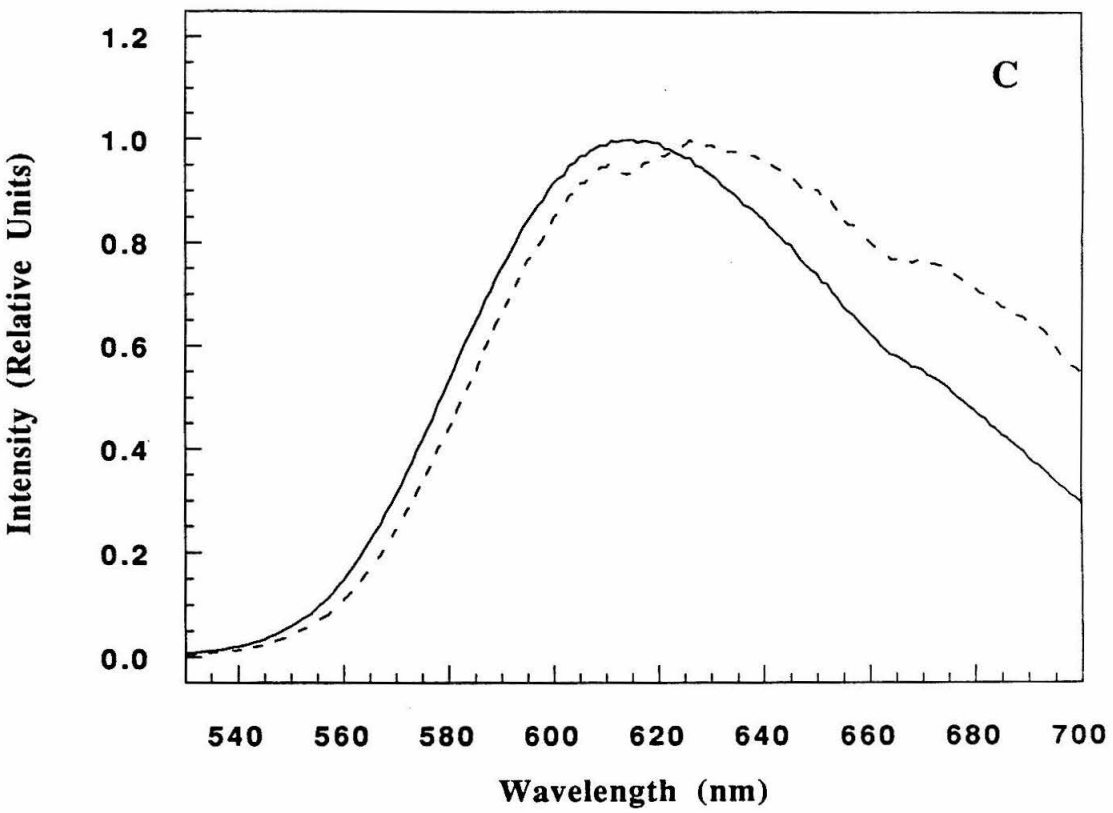
C
1.2
1.0
0.8
0.6
0.4
0.2
0.0
Intensity (Relative Units)
540
560
580
600
620
640
660
680
700
Wavelength (nm)

Figure 5.19 (A) Luminescence decay of a 27.0 μM sample of $Ru(bpy)_2$(4Bpa)-peptide in 25 mM NaPi, pH 7.0, observed at 620 nm following excitation at 480 nm (2 mJ pulse). The smooth line is the fit to a single exponential decay function convolved with the instrument response (shown); $k_d = 1.55(5) \times 10^6\ s^{-1}$, c = 0.24. (B) Luminescence decay of a 15.4 μM sample of $Ru(bpy)_2$(6Bpa)-peptide, in 25 mM NaPi, pH 7.0, observed at 620 nm following excitation at 480 nm (2 mJ pulse). The smooth line is the fit to a single exponential decay function convolved with the instrument response (shown); $k_d > 10^8\ s^{-1}$, c = 0.23. (C) Luminescence decay of a 16.6 μM sample of $Ru(bpy)_3Cl_2$, in 25 mM NaPi, pH 7.0, observed at 620 nm following excitation at 480 nm (2 mJ pulse). The smooth line is the fit to a single exponential decay function convolved with the instrument response (shown); $k_d = 1.63(5) \times 10^6\ s^{-1}$, c = 0.18.

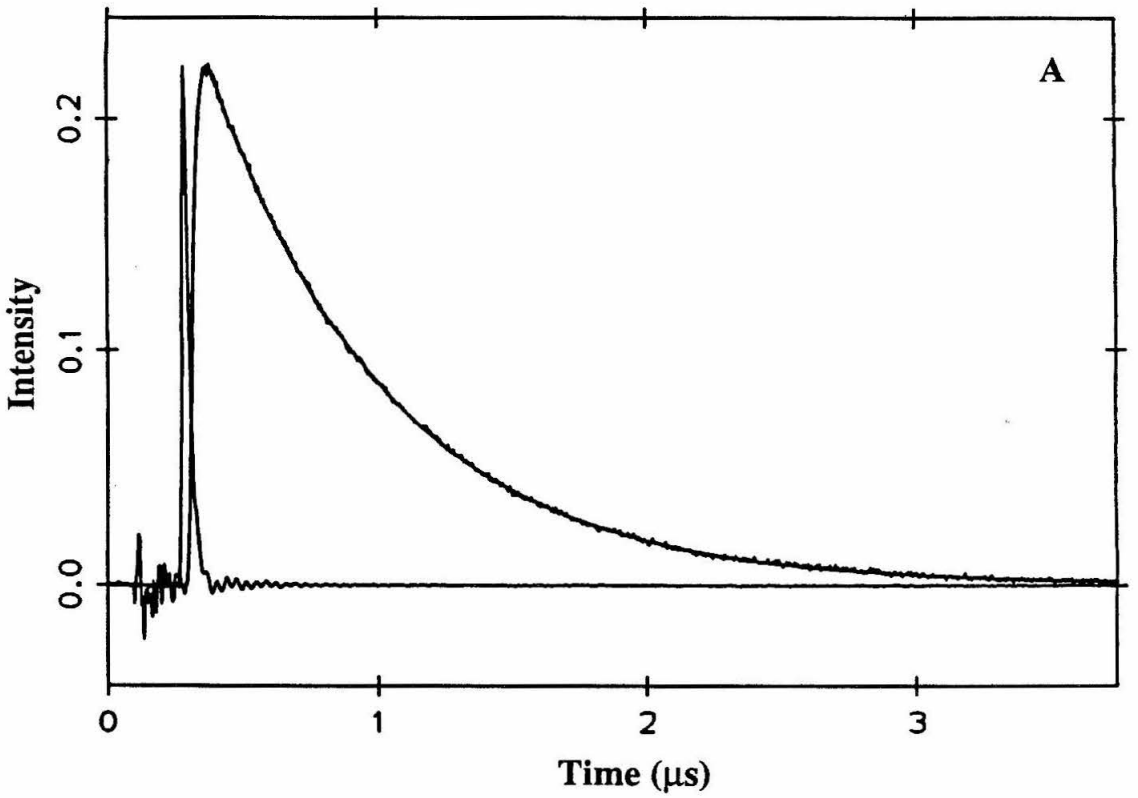
A
Intensity
0.0
0.1
0.2
0
1
2
3
Time (μs)

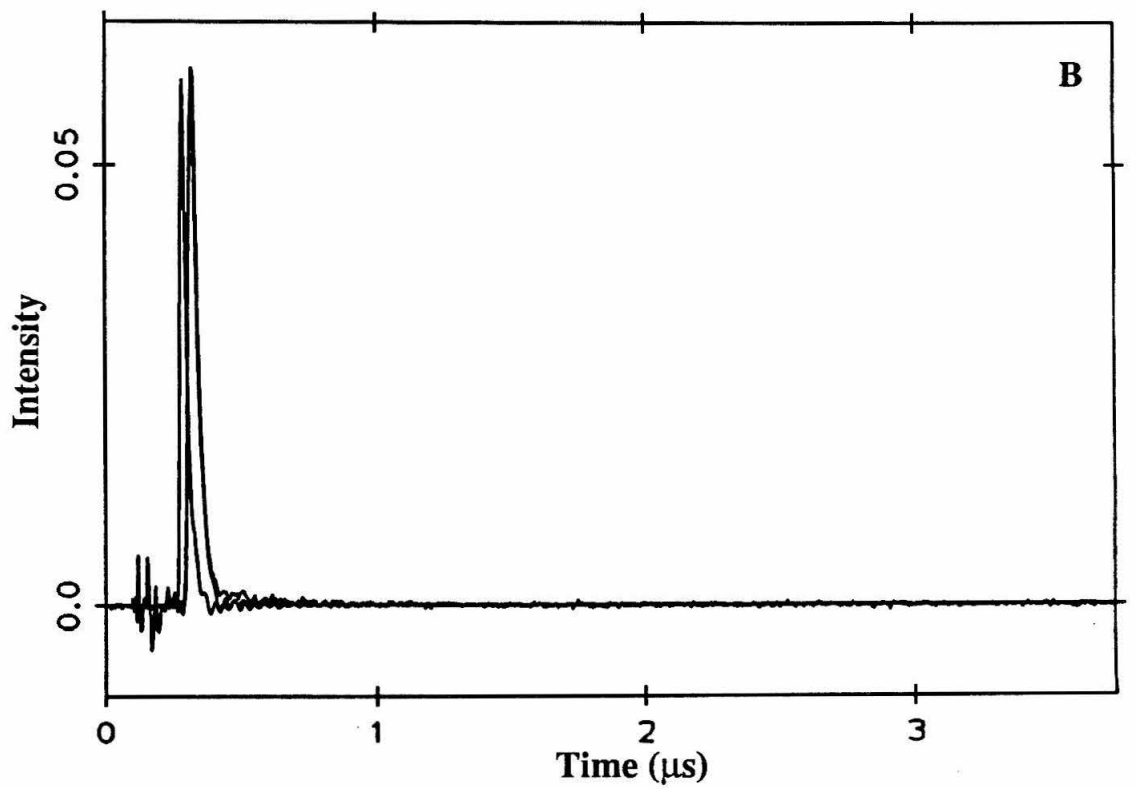
B
Intensity
0.0
0.05
0
1
2
3
Time (μs)

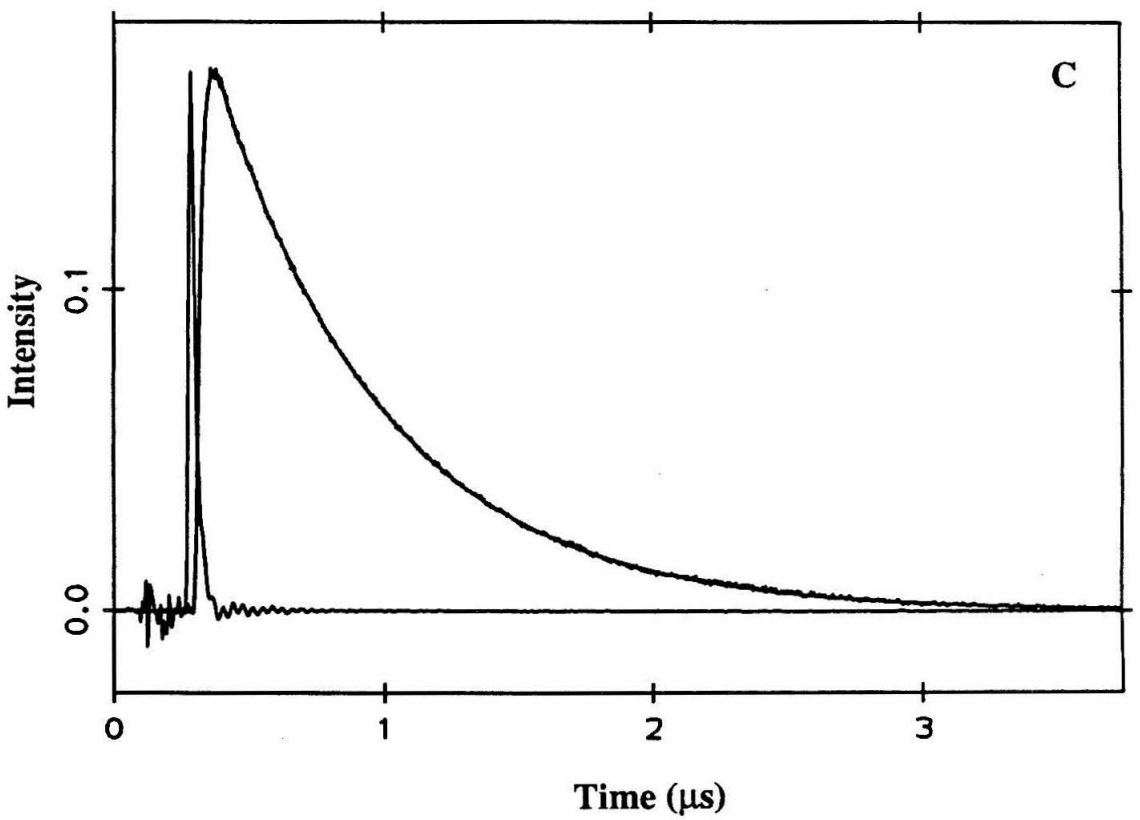
C
Intensity
0.1
0.0
0
1
2
3
Time (μs)

been attributed to the sterically induced increase in the Ru-N(6Bpa) bond length upon substitution at the 6-position (Ru-N = 2.056 Å in $Ru(bpy)_3^{2+}$;[24] one Ru-N bond (to the substituted bipyridyl ligand) = 2.143 Å (average = 2.072 Å) in $Ru(bpy)_2(bpy\text{-}Ni^{2+}\text{-}cyclam)^{4+}$).[25] This structural change is proposed to reduce the ligand field strength, thus stabilizing low-lying deactivating ligand field states in the vicinity of the lowest ^{3}MLCT state.

Table 5.2. Spectroscopic properties of $Ru(bpy)_2L^{2+}$ model compounds (L = bpy, im_2) and $Ru(bpy)_2^{2+}$-modified peptides. ($Ru(bpy)_3^{2+}$, Reference 16; $Ru(bpy)_2(im)_2^{2+}$, refer to Chapter 3).

	λ_{abs} (MLCT) (nm)	λ_{em} (nm)	τ (ns)	Ru-N (Å)
$Ru(bpy)_3^{2+}$	454	615	612	2.056
$Ru(bpy)_2(im)_2^{2+}$	492	670	66	
$Ru(bpy)_2$ (4Bpa-peptide)	454	617	644	
$Ru(bpy)_2$ (6Bpa-peptide)	448	610	(6.8)*	2.143**

* Lifetime is at the detection limit.
** Reported distance in a related $Ru(bpy)_2(bpy\text{-}Ni^{2+}\text{-}cyclam)^{4+}$ complex.[25]

F. Electron-Transfer Studies at pH 7.0: Enhanced Electronic Couplings

Direct-photoinduced and flash-quench techniques (refer to Chapter 3) were employed to obtain the rate constants for electron transfer in $Ru(bpy)_2$(4Bpa72)cyt *c*. The spectral features of the $Ru(bpy)_3^{2+}$ label are similar and slightly blue-shifted relative to $Ru(bpy)_2(im)_2^{2+}$. The pertinent difference spectra (*i.e.*, $*Ru^{2+}$ - Ru^{2+} and Ru^{3+} - Ru^{2+}) have been previously reported.[16] The $Ru(bpy)_3^{3+}$ spectrum has a maximum at ~420 nm. The Ru^{3+} - Ru^{2+} difference spectrum exhibits a significant bleach at 434 nm ($\Delta\varepsilon$ ~-4500 $M^{-1}\,cm^{-1}$), a Fe^{2+}/Fe^{3+} isosbestic wavelength, although a bleach due to the excited state ($\Delta\varepsilon$ ~-12000 $M^{-1}\,cm^{-1}$) dominates at this wavelength. The $*Ru^{2+}$ - Ru^{2+} difference spectrum

exhibits a maximum absorption at ~370 nm ($\Delta\varepsilon$ = 18500 M^{-1} cm^{-1}) and a large bleach centered at 450 nm ($\Delta\varepsilon$ = -12000 M^{-1} cm^{-1}). The relevant electrochemical potentials used for calculating driving forces are set out in Table 5.2. Potentials for $Ru(bpy)_3^{2+}$ are used as models for $Ru(bpy)_2$(4Bpa72)cyt *c* since the ambient temperature emission and MLCT absorption properties of these two species are virtually identical.[26]

Table 5.3. Summary of relevant reduction potentials for the calculation of driving forces in aqueous solution. $Ru(bpy)_3^{2+}$ data are from Reference 16; cyt *c* (pH 11.0) from Reference 27.

Redox Couple	Reduction Potential (V *vs.* NHE)
cyt *c* ($Fe^{3+/2+}$) (pH 7.0)	0.265
cyt *c* ($Fe^{3+/2+}$) (pH 11.0)	-0.200
$Ru(bpy)_3^{3+/2+}$	1.26
$Ru(bpy)_3^{3+/*2+}$	-0.86

The Fe^{2+} to Ru^{3+} ET rate constant (k_{ET}^{mm}) was determined from nine flash / quench (Q = $[Ru(NH_3)_6]Cl_3$) and photoinduced data sets at 550 and 395 nm fit to both single and double exponential decay functions as described in Chapter 3. A rate constant of 6.5(5) x 10^6 s^{-1} was calculated. Identical kinetics were observed at 504 and 434 nm corresponding to Ru^{3+}/Ru^{2+} ET. Data obtained at 550 and 395 nm for the flash / quench experiments fit convolved with the laser pulse are shown in Figure 5.20. Data from the photoinduced experiments at 550, 434 and 395 nm are presented in Figure 5.21. The rate constant for photoinduced ET (k_{ET}*) was calculated as 6(2) x10^6 s^{-1} from two full data sets (550, 395 and 370 nm). Representative data obtained at 370 nm used to calculate the excited state concentration are fit convolved with the pulse in Figure 5.22 (note the addition

Figure 5.20 Transient absorption kinetics at various wavelengths following laser flash excitation (480 nm, 25 ns, 2 mJ) of ferrous $Ru(bpy)_2(4Bpa72)$cyt *c* in 50 mM NaPi, pH 7.0, with ~5 mM $[Rua_6]Cl_3$, at room temperature. The decay corresponds to the production of ferric $Ru(bpy)_2(4Bpa72)$cyt *c* due to intramolecular ET from Fe^{2+} to Ru^{3+} at a rate of 6.5×10^6 s^{-1}. Smooth lines correspond to fits to a biexponential decay function, $k_1 = k_{ET}^{mm}$ (6.5×10^6 s^{-1}), $k_2 = k_d = 2 \times 10^7$ s^{-1} (due to the presence of excited-state quencher). The wavelength, sample concentration and coefficients for the rate terms are given. (A) 550 nm, 14.0 μM protein, $c_1 = 0.041$, $c_2 = -0.051$. (B) 395 nm, 14.0 μM protein, $c_1 = -0.020$, $c_2 = -0.017$.

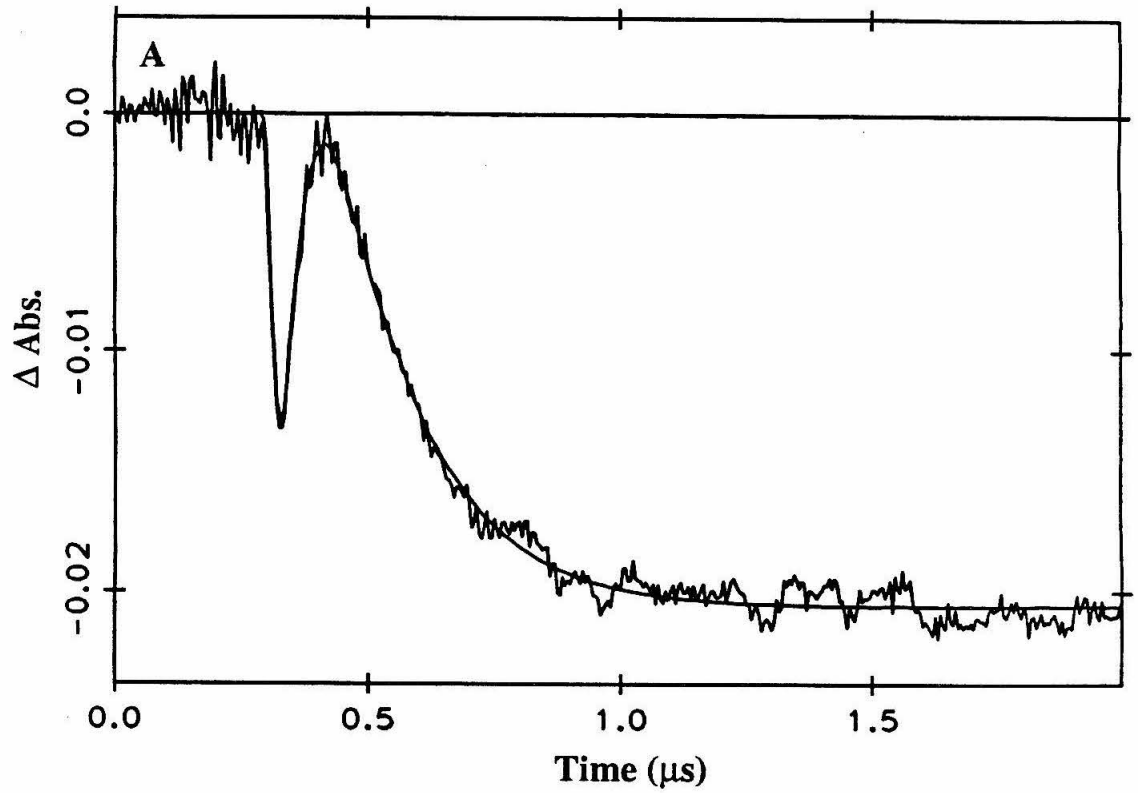
A
0.0
-0.01
-0.02
Δ Abs.
0.0
0.5
1.0
1.5
Time (μs)

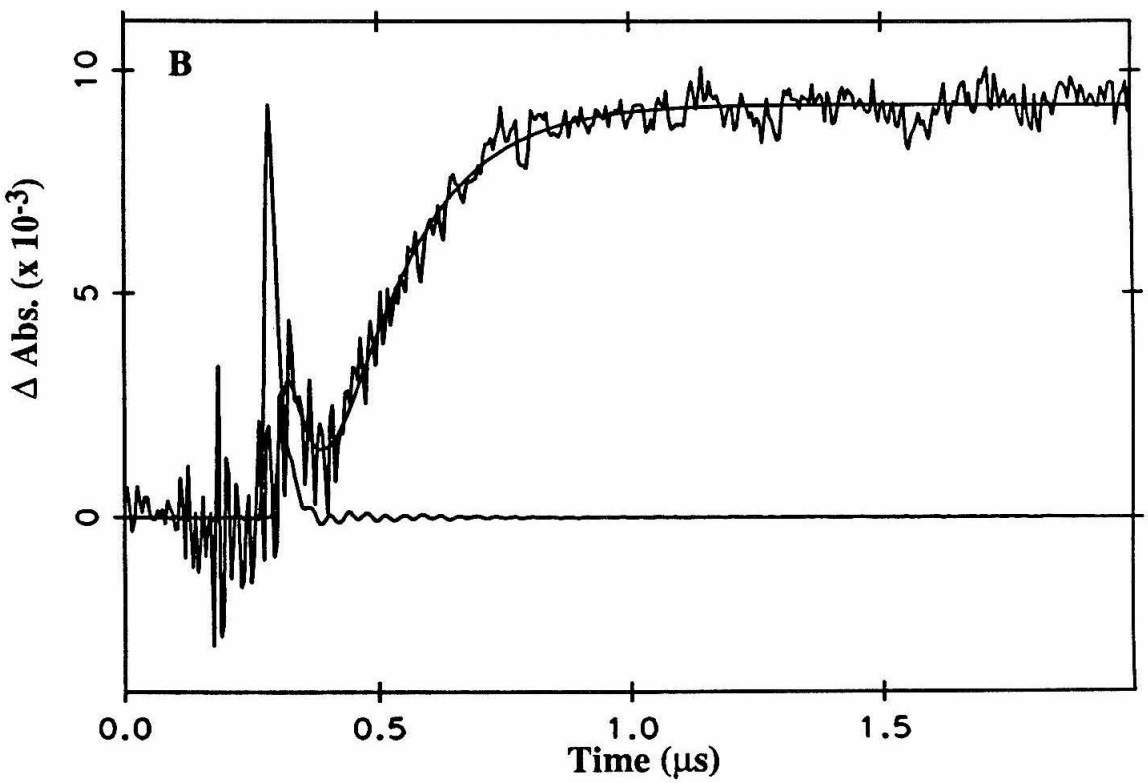
B
10
5
0
Δ Abs. (x 10-3)
0.0
0.5
1.0
1.5
Time (μs)

Figure 5.21 Transient absorption kinetics at various wavelengths following laser flash excitation (480 nm, 25 ns, 2 mJ) of ferric $Ru(bpy)_2$(4Bpa72)cyt *c* in 50 mM NaPi, pH 7.0, at room temperature. The rise corresponds to production of ferrous cyt *c* due to photoinduced ET. The decay corresponds to the production of ferric $Ru(bpy)_2$(4Bpa72)cyt *c* due to intramolecular ET from Fe^{2+} to Ru^{3+} at a rate of 6.5×10^6 s^{-1}. Smooth lines correspond to fits to a biexponential decay function, $k_1 = k_{ET}^{mm}$ (6.5×10^6 s^{-1}), $k_2 = k_d$ = ~3×10^7 s^{-1} (5.8×10^8 s^{-1} at 434 nm, due to the *generation* of excited state with the pulse, decay fit only to Ru^{3+} decay). The wavelength, sample concentration and coefficients for the rate terms are given. (A) 550 nm, 11.2 μM protein, $c_1 = 0.058$, $c_2 = -0.066$. (B) 395 nm, 11.2 μM protein, $c_1 = -0.067$, $c_2 = -0.075$. (C) 434 nm, 11.2 μM protein, $c_1 = -0.059$, $c_2 = -0.061$.

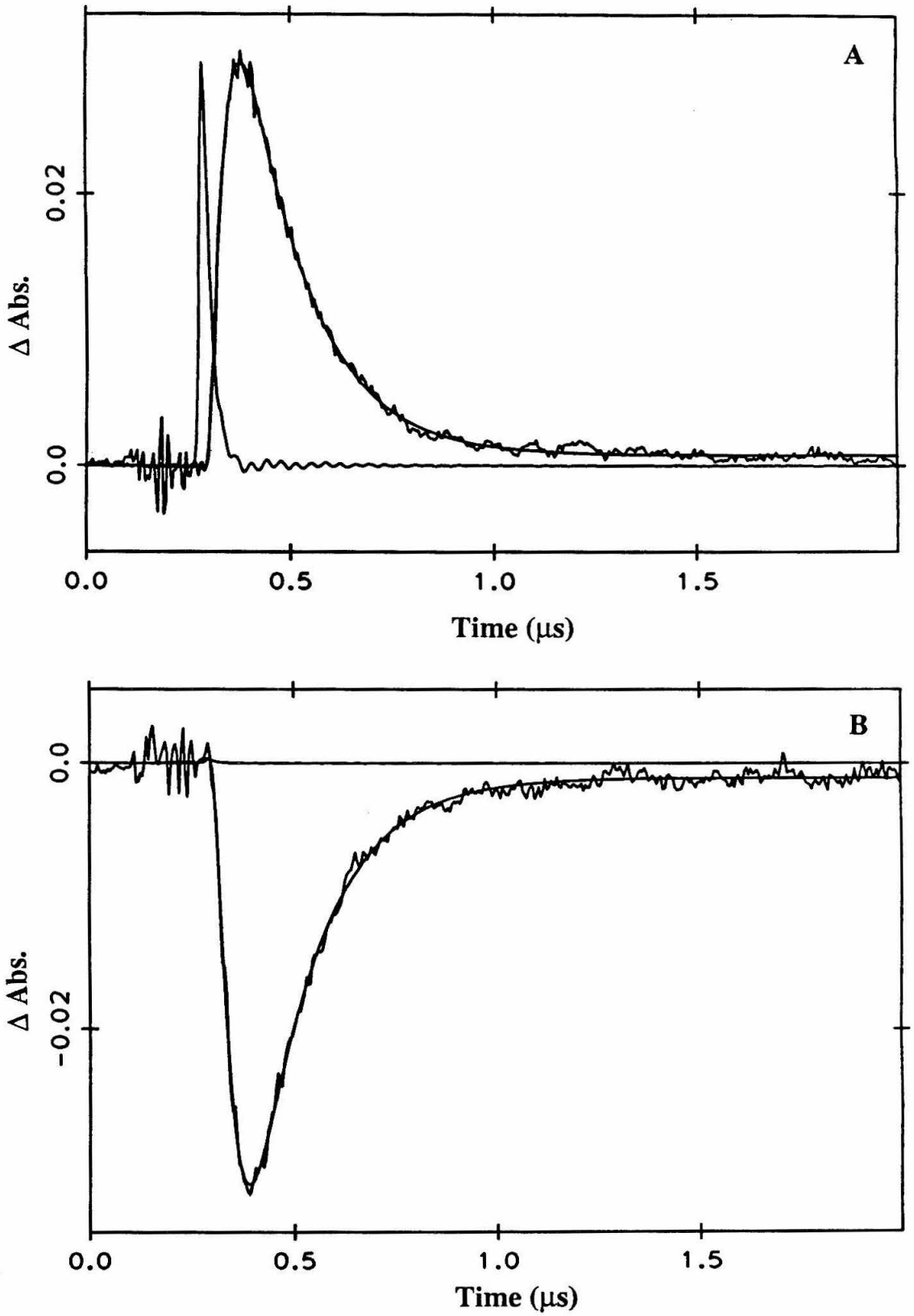
A
0.02
0.0
Δ Abs.
0.0
0.5
1.0
1.5
Time (μs)
B
0.0
-0.02
Δ Abs.
0.0
0.5
1.0
1.5
Time (μs)

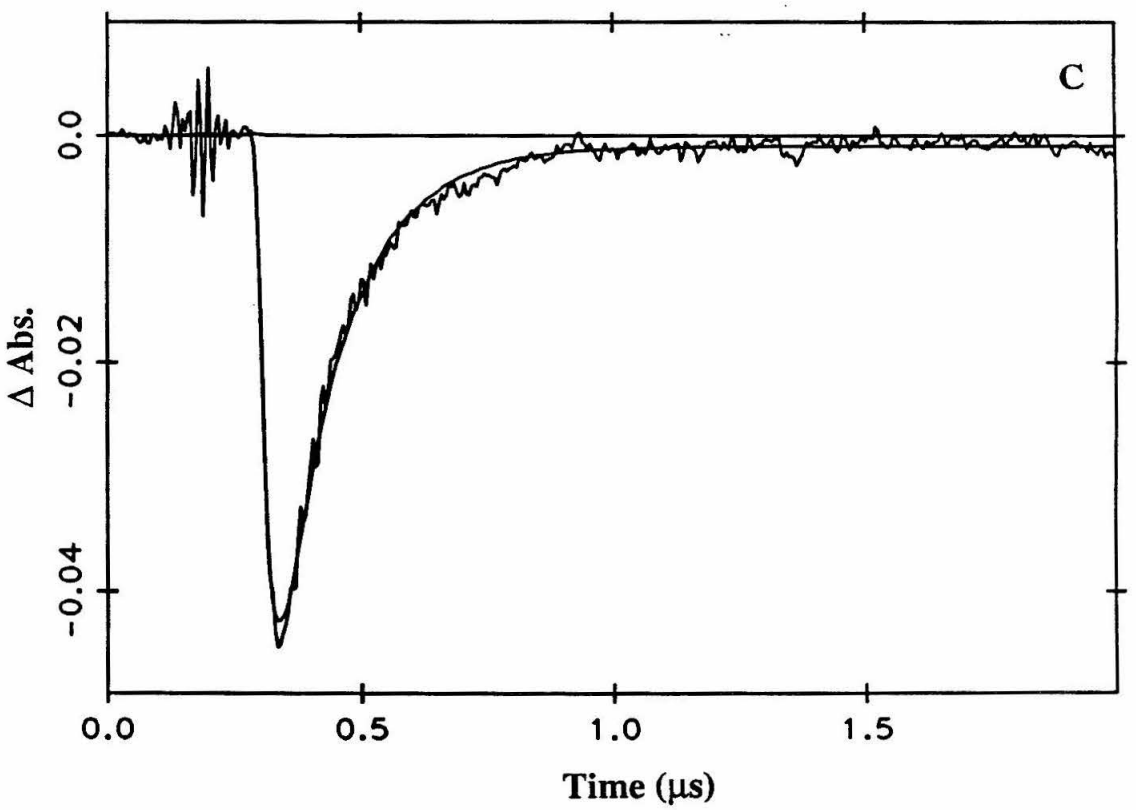
C
0.0
-0.02
-0.04
Δ Abs.
0.0
0.5
1.0
1.5
Time (μs)

Figure 5.22 Transient absorption kinetics at 370 nm following laser flash excitation (480 nm, 25 ns, 2 mJ) of an 11.2 μM sample of ferric $Ru(bpy)_2(4Bpa72)$cyt *c* in 50 mM NaPi, pH 7.0, at room temperature. The smooth line is the fit to a biexponential decay function convolved with the instrument response. The signal is the excited state decay at 1.9×10^7 s^{-1} ($c_1 = 0.183$) followed by transient generation of ferrous protein, $k_2 = 6.5 \times 10^6$ s^{-1}, $c_2 = -0.059$.

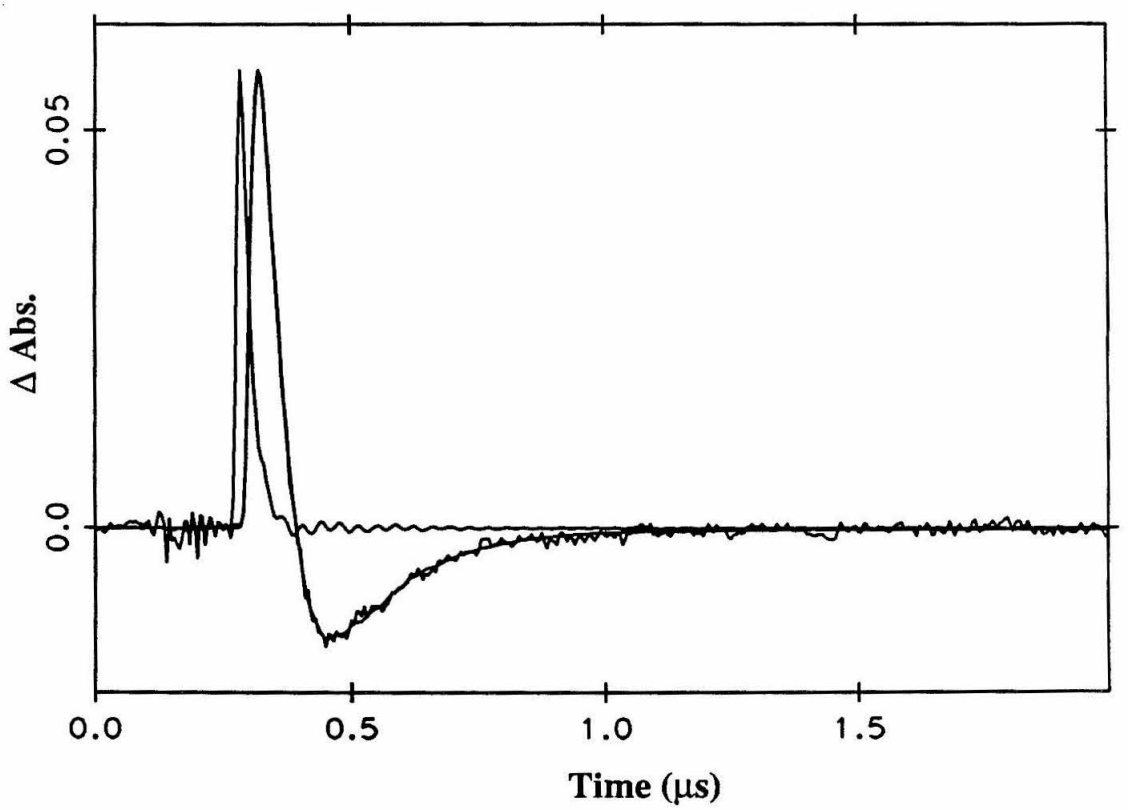
0.05
0.0
Δ Abs.
0.0
0.5
1.0
1.5
Time (μs)

slow transient due to Fe^{2+}/Fe^{3+} ET). The value of k_{ET}* calculated from the yield of ET products corresponds qualitatively to the difference in excited state lifetime of the ferrous and ferric states. High photoinduced ET rates also have been observed in cyt *c* derivatives with a $Ru(bpy)_2$(dicarboxybipyridine) species tethered directly to a surface lysine. A rate constant of 1.4×10^7 s^{-1} has been reported for *$Ru(bpy)_2$(dcbpy)Lys72 to ferric heme ET. However, the flexible nature of the Ru linkage to the protein precludes the comparison of these data with the His72 and Bpa72 derivatives in the context of electronic coupling models. Laser-induced electron photoinjection with Lys-modified derivatives has been used to initiate thermal ET within protein:protein complexes [*e.g.*, $Ru(bpy)_3$LysX cyt *c*:cyt *c* peroxidase, X = 13, 25, 27, 72].[28]

The rate constants for both Fe^{2+} to Ru^{3+} and *Ru^{2+} to Fe^{3+} ET are much higher than in the corresponding $Ru(bpy)_2$(im)His72 cyt *c* protein (Table 5.4). Since the intrinsic decay rates of the His72 and 4Bpa72 modified proteins are comparable (Table 5.1), the photoinduced ET rates (k_{ET}*) are proportional to ET product yield. The increased yield of photoinduced ET products (~30%) in the 4Bpa72 protein relative to the His72 (2.3%)[11] protein may be understood in terms of the nature of the photoinduced ET reaction. The electron transfer originates from MLCT excitation, and the effective electron donor, a bipyridyl-based anion radical, is built directly into the polypeptide backbone in $Ru(bpy)_2$(4Bpa72)cyt *c*, in contrast to being at some undefined location with respect to the protein surface in $Ru(bpy)_2$-modified His72 cyt *c*. We conclude that the bipyridyl side chain enhances the distant donor-acceptor electronic coupling by effectively shortening the tunneling pathway between the Ru and heme redox units in position-72 modified proteins. The σ-tunneling pathway approach[29] employed in the analysis of $Ru(bpy)_2$(im)His-modified cyts *c* (refer to Chapter 4) predicts enhanced electronic coupling of approximately the magnitude observed in the photoinduced ET reaction of the Ru-modified 4Bpa72 cyt *c* relative to His72 cyt *c* if one assumes the pathway is effectively four bonds longer in $Ru(bpy)_2$(im)His72 cyt *c* than $Ru(bpy)_2$(4Bpa)cyt *c*.[30] The four additional bonds are due

to the electron tunneling pathway from the bpy anion radical to the Ru metal through the His72 imidazole ring to within one bond of C_β. In $Ru(bpy)_2(4Bpa)$cyt *c*, the MLCT excitation effectively transfers the electron directly to within one bond of C_β. This simple pathway explanation does not take into account alternate pathways that may be available for the $*Ru(bpy)_2(im)$His72 to heme ET, and valid pathways for the photoinduced ET step can not be evaluated in the absence of precise structural information. The Fe^{2+} to Ru^{3+} ET reaction is most likely in the inverted region ($-\Delta G^o$ = 1.0 eV, λ = 0.8 eV); $k_{max} = 1.06 \times 10^7$ s^{-1} if λ = 0.8 eV. This ~10-fold enhancement in rate constant relative to the His72-modificed protein can also be attributed to an increase in Ru-heme electronic coupling.

Table 5.4. Summary of electron-transfer parameters for $Ru(bpy)_2(4Bpa72)$cyt *c* and $Ru(bpy)_2(im)$His72 cyt *c*.

	$*Ru^{2+}$ to Fe^{3+} $k_{ET}*$ (s^{-1})	$-\Delta G^o$ (eV)	Fe^{2+} to Ru^{3+} k_{ET}^{mm} (s^{-1})	$-\Delta G^o$ (eV)
$Ru(bpy)_2(4Bpa72)$ cyt *c* (pH 7.0)	6(2) x 10^6	1.1	6.5(5) x 10^6	1.00
$Ru(bpy)_2(His72)$ cyt *c* (pH 7.0)	3.4(7) x 10^5	1.2	9.0(3) x 10^5	0.74

G. Electron-Transfer Studies of the Alkaline Form

The enhanced ET properties of $Ru(bpy)_2(4Bpa72)$cyt *c* can be employed to probe conformationally perturbed states of the protein. For example, at high pH (p*Ka* ~9.3),[27,31] ferric cyt *c* exists in a low-potential state (the midpoint potential is roughly -200 mV)[27] with altered ligation, while at identical conditions the ferrous state has a native-like (pH 7.0) ligation and polypeptide conformation. The alkaline form has been proposed to consist of two strong-field alternate axially ligated species;[32,33] recent site-directed mutagenesis studies identify Lys79 and Lys73 as the sixth ligands replacing Met80.[34] Due to the large quantum yield and fast electron-transfer rates of $Ru(bpy)_2(4Bpa72)$cyt *c* at pH 7.0, photoinduced ET experiments at pH 11 will allow the rapid (< 60 ns, 480 nm-excitation)

generation of ferrous protein in the ferric alkaline conformation. The flash / quench methodology is not applicable at high pH because of the low redox potential of the alkaline form.

Photoinduced ET experiments conducted on the alkaline form show an unexpectedly high yield of ET from *Ru(bpy)$_2$(4Bpa72) to the heme (Figure 5.23). The subsequent Fe^{2+} to Ru^{3+} ET kinetics are comprised of at least two components (1.2(5) x 10^7, 1.0(5) x 10^6 s^{-1}). The excited state lifetimes are nearly identical at pH 11.0 and pH 7.0, k_d = 1.95(10) x 10^7 s^{-1} (51 ns) (Figure 5.24). Data were analyzed from two separate preparations, and reported rate constants determined from two full data sets (550, 504, 434, 395, 370 nm). Figure 5.25 shows data from 550 and 395 nm, Figure 5.26 is data obtained at 370 nm. Values of $\Delta\varepsilon$ for Fe^{2+}/Fe^{3+} [35] at pH 11.0 and $Ru^{2+}/*Ru^{2+}$ are similar to those at pH 7.0, therefore their values at pH 7.0 were used. Some difficulties were encountered in the determination of the photoinduced ET rate constant. The rapid Fe^{2+} to Ru^{3+} ET rate constants warranted biexponential data fits convolved with the pulse. Small changes in the 10^7 s^{-1} decay term, due to small fitting adjustments to factors such as the pretrigger noise in the data set, affected the extracted c_n terms by as much as a factor of two. Thus, it is difficult to determine the k_{ET}* rate constant to higher accuracy (and precision) than 9(3) x 10^6 s^{-1}. The high pH environment is not expected to change the $Ru^{3+/2+*}$ potential; the $Ru^{3+/2+}$ potential is identical at pH 7.0, 9.5 and 11.0 in 50 mM NaPi.[36] Values for these potentials of -0.86 V and 1.26 were therefore used, respectively, for the calculation of driving forces at high pH.

The two Fe^{2+} to Ru^{3+} ET components (~1 x 10^7, ~1 x 10^6 s^{-1}) (Figure 5.26) are both much faster than estimates of the Met80 religation rate (40 to 1 s^{-1}).[27,33,37] Our finding of two distinct decay pathways for the intramolecular oxidation of the photogenerated high-pH ferrous protein accords with other evidence indicating that alkaline ferricytochrome *c* is a mixture of at least two different conformers.[33,34] These experiments are only possible using the enhanced electron coupling afforded by the incorporation of the

Figure 5.23 (A) Transient absorption kinetics at 550 nm following laser flash excitation (480 nm, 25 ns, 2 mJ) of $Ru(bpy)_2$(4Bpa72)cyt *c*, 11.2 μM in 50 mM NaPi, pH 7.0, at room temperature. The smooth line is the fit to a biexponential decay function convolved with the instrument response (shown). The rise corresponds to production of ferrous cyt *c* due to photoinduced ET. The decay corresponds to Fe^{2+} to Ru^{3+} ET at 6.5×10^6 s^{-1}. (B) Transient absorption kinetics at 550 nm following laser flash excitation (480 nm, 25 ns, 2 mJ) of $Ru(bpy)_2$(4Bpa72)cyt *c*, 15.8 μM in 50 mM NaPi, pH 10.8, at room temperature. The smooth line is a fit to a 3-exponential decay function convolved with the instrument response (shown). The rise corresponds to production of ferrous cyt *c* due to direct photoinduced ET. The decay corresponds to Fe^{2+} to Ru^{3+} ET at 1.2×10^7 and 1.0×10^6 s^{-1}. Virtually identical kinetics were observed at pH 9.85.

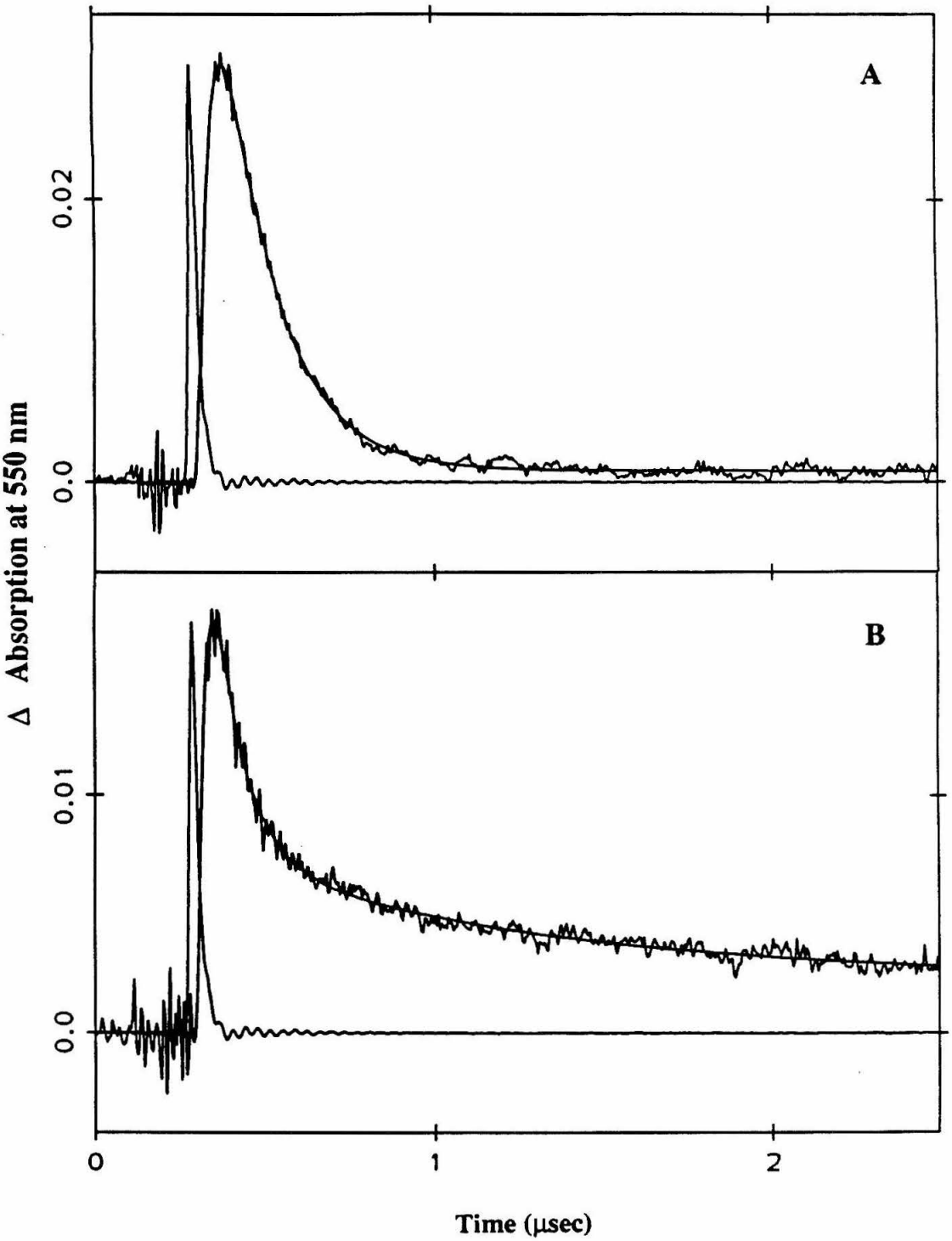
A
B
0.02
0.0
0.01
0.0
Δ Absorption at 550 nm
0
1
2
Time (μsec)

Figure 5.24 Luminescence decay of a 7.1 μM sample of ferric $Ru(bpy)_2(4Bpa72)$cyt *c* in 50 mM NaPi, pH 9.9, observed at 620 nm following excitation at 480 nm (2 mJ pulse). The smooth line is the fit to a single exponential decay function convolved with the instrument response (shown); $k_d = 1.95(10) \times 10^7\ s^{-1}$, c = 0.2152.

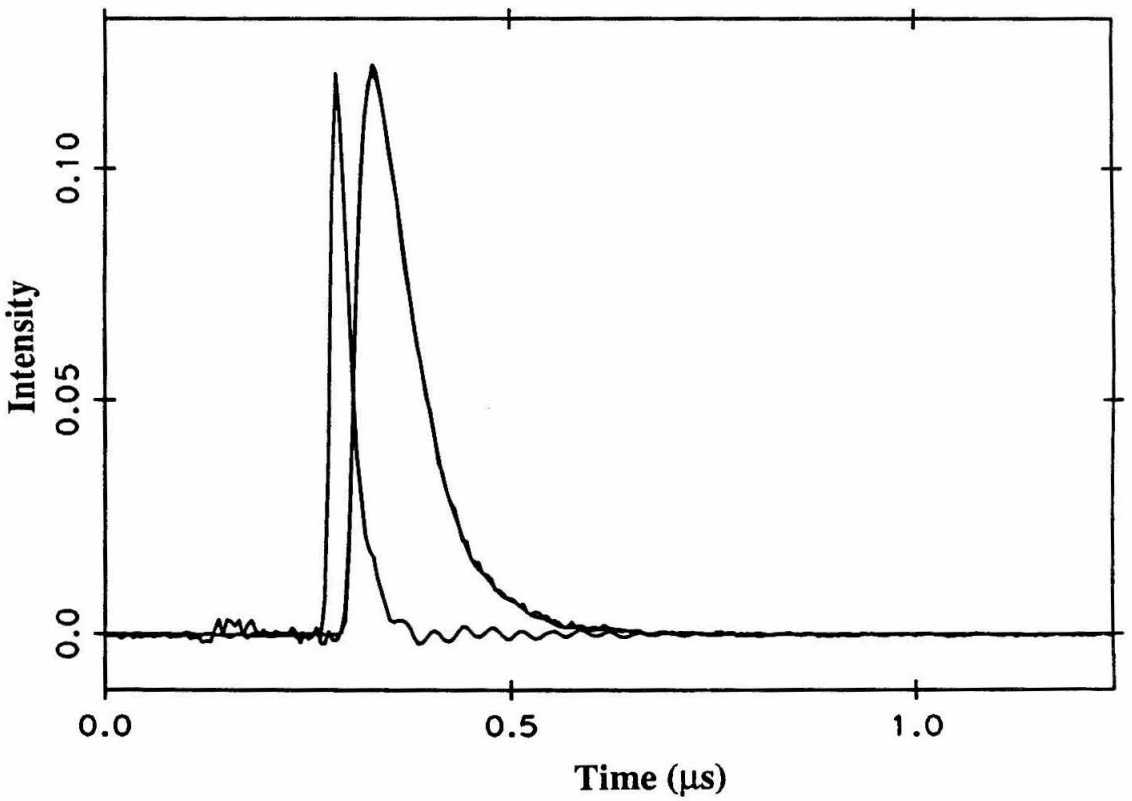
Intensity
0.0
0.05
0.10
0.0
0.5
1.0
Time (μs)

Figure 5.25 Transient absorption kinetics at various wavelengths following laser flash excitation (480 nm, 25 ns, 2 mJ) of ferric $Ru(bpy)_2(4Bpa72)$cyt *c* in 50 mM NaPi, pH 10.8, at room temperature. The rise corresponds to production of ferrous cyt *c* due to photoinduced ET. The decay corresponds to the production of ferric $Ru(bpy)_2(4Bpa72)$cyt *c* due to biphasic intramolecular ET from Fe^{2+} to Ru^{3+} at rates of 1.0×10^6 s^{-1} and 1.2×10^7 s^{-1}. Smooth lines correspond to fits to a three-exponential decay function, $k_1 = k_{ET}^{mm}$ (1.0×10^6 s^{-1}), $k_2 = k_{ET}^{mm}$ (1.2×10^7 s^{-1}), $k_3 = k_d = \sim 1 \times 10^8$ s^{-1}. The wavelength, sample concentration and coefficients for the rate terms are given. (A) 550 nm, 15.8 μM protein, $c_1 = 0.0051$, $c_2 = 0.018$, $c_3 = -0.039$. (B) 395 nm, 15.8 μM protein, $c_1 = -0.0068$, $c_2 = -0.031$, $c_3 = 0.073$.

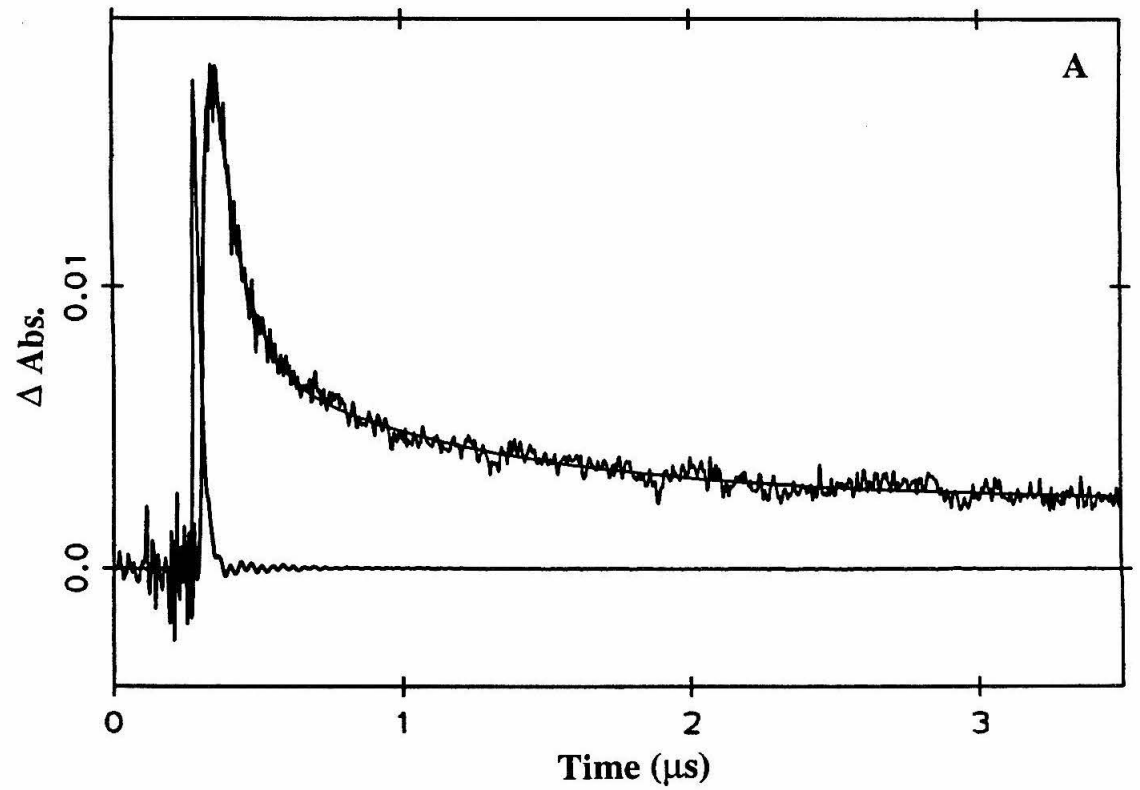
A
Δ Abs.
0.01
0.0
0
1
2
3
Time (μs)

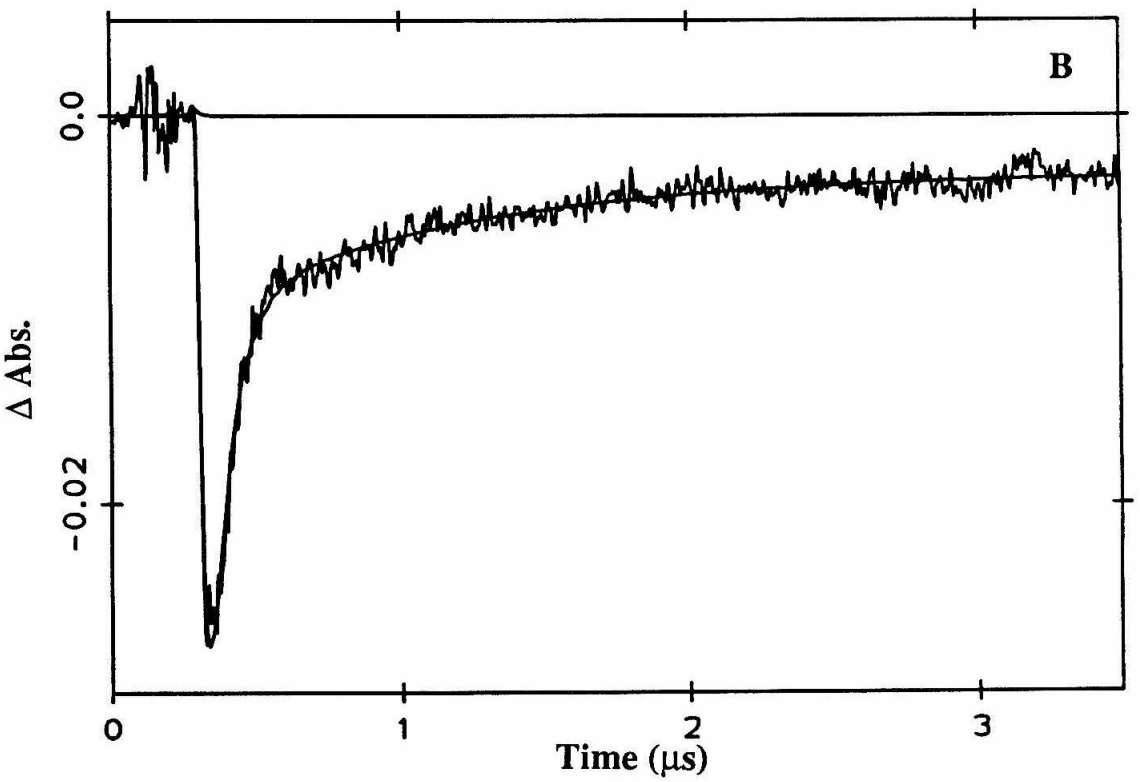
B
Δ Abs.
0.0
-0.02
0
1
2
3
Time (μs)

Figure 5.26 Transient absorption kinetics at 370 nm following laser flash excitation (480 nm, 25 ns, 2 mJ) of a 15.8 μM sample of ferric $Ru(bpy)_2(4Bpa72)$cyt *c* in 50 mM NaPi, pH 10.8, at room temperature. The smooth line is the fit to a biexponential decay function convolved with the instrument response. The signal is the excited state decay at 1.9×10^7 s^{-1} ($c_1 = 0.052$) followed by transient generation of ferrous protein, k_2 (fit) = 1.7×10^6 s^{-1}, $c_2 = -0.024$.

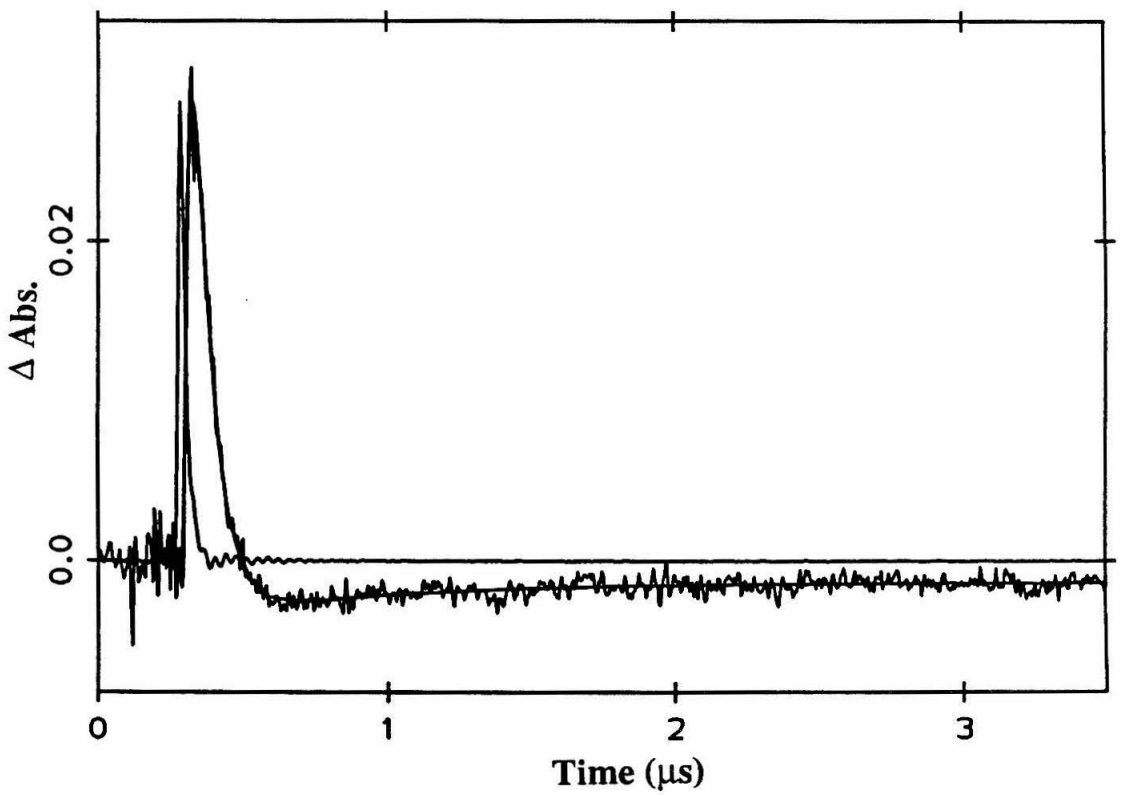
Δ Abs.
0.02
0.0
0
1
2
3
Time (μs)

bipyridyl amino acid; at high pH, Ru(bpy)$_2$(im)His72 cyt *c* possesses a slightly shorter luminescence decay lifetime (58 ns), however, upon excitation of the Ru-chromophore no transiently generated ET products could be detected.

Table 5.5. Electron-transfer parameters for Ru(bpy)$_2$(4Bpa72)cyt *c* and Ru(bpy)$_2$(im)His72 cyt *c*.

	$*Ru^{2+}$ to Fe^{3+} $k_{ET}*$ (s^{-1})	$-\Delta G^o$ (eV)	Fe^{2+} to Ru^{3+} k_{ET}^{mm} (s^{-1})	$-\Delta G^o$ (eV)
Ru(bpy)$_2$(4Bpa72) cyt *c* (pH 7.0)	6(2) x 10^6	1.1	6.5(5) x 10^6	1.00
Ru(bpy)$_2$(4Bpa72) cyt *c* (pH 11.0)	9(3) x 10^6	0.66	1.2(5) x 10^7 1.0(5) x 10^6	1.46
Ru(bpy)$_2$(His72) cyt *c* (pH 7.0)	3.4(7) x 10^5	1.2	9.0(3) x 10^5	0.74
Ru(bpy)$_2$(His72) cyt *c* (pH 11.0)	-	0.75	-	1.20

The ability to photogenerate reduced cyt *c* rapidly with high quantum efficiency in conformationally altered forms opens the way for studies of submicrosecond protein-folding events. The use of laser excitation rather than traditional "rapid" mixing techniques will allow spectroscopic measurements to be made in the time domain that is considered critical for the understanding of folding dynamics.[38]

IV. Conclusion

Two horse heart cytochrome *c* (cyt *c*) variants incorporating the unnatural amino acids (*S*)-2-amino-3-(2,2'-bipyrid-6-yl)-propanoic acid (6Bpa) (**1**) and (*S*)-2-amino-3-(2,2'-bipyrid-4-yl)-propanoic acid (4Bpa) (**2**) at position 72 have been prepared using semisynthetic protocols. Negligible perturbation of the protein structure results from this introduction of unnatural amino acids. Redox-active Ru(2,2'-bipyridine)$_2^{2+}$ binds to

4Bpa72 cyt *c* but not to the 6Bpa protein. Enhanced ET rate constants were observed in the $Ru(bpy)_2^{2+}$-modified 4Bpa72 cyt *c* relative to the analogous His72 derivative (k ($*Ru^{2+}$ to Fe^{3+}) = 9(3) x 10^6 s^{-1} in $Ru(bpy)_2$(4Bpa72)cyt *c*, 3.4(7) x 10^5 s^{-1} in $Ru(bpy)_2$(im)His72 cyt *c*; k (Fe^{2+} to Ru^{3+}) = 6.5(5) x 10^6 s^{-1} in $Ru(bpy)_2$(4Bpa72)cyt *c*, 9.0(3) x 10^5 s^{-1} in $Ru(bpy)_2$(im)His72 cyt *c*). The rapid (< 60 nanosecond) photogeneration of ferrous Ru-modified 4Bpa72 cyt *c* in conformationally altered states demonstrates that laser-induced electron transfer can be employed to study submicrosecond protein-folding events.

V. References

1. The work presented in this chapter was conducted in collaboration with Prof. B. Imperiali and S. L. Fisher of the California Institute of Technology. They were responsible for the synthesis of both bipyridyl alanine amino acids and the 39-mer peptides used for semisynthesis.

2. Reviewed in Balaram, P. *Curr. Opin. Struct. Biol.* **1992**, *2*, 845.

3. Noren, C. J.; Anthony-Cahill, S. J.; Griffith, M. C.; Schultz, P. G. *Science* **1989**, *244*,182. Mendel, D.; Ellman, J. A.; Schultz, P. G. *J. Am. Chem. Soc.* **1991**, *113*, 2758. Ellman, J.; Mendel, D.; Anthony-Cahill, S.; Noren, C. J. *Meth. Enzymol.* **1991**, *202*, 301. Ellman, J. A.; Mendel, D.; Schultz, P. G. *Science* **1992**, *255*, 197. Mendel, D.; Ellman , J. A.; Chang, Z.; Veenstra, D. L.; Kollman, P. A.; Schultz, P. G. *Science* **1992**, *256*, 1798. Ellman, J. F.; Volkman, B. F.; Mendel, D.; Schultz, P. G.; Wemmer, D. E. *J. Am. Chem. Soc.* **1992**, *114*, 7959. Chung, H. H.; Benson, D. R.; Schultz, P. G. *Science* **1993**, *259*, 806. Judice, J. K.; Gamble, T. R.; Murphy, E. C.; de Vos, A. M.; Schultz, P. G. *Science* **1993**, *261*, 1578.

4. Bain, J. D.; Glabe, C. G.; Dix, T. A.; Chamberlin, A. R. *J. Am. Chem. Soc.* **1989**, *111*, 8013. Bain, J. D.; Switzer, C.; Chamberlin, A. R.; Benner, S. A. *Nature* **1992**, *356*, 537. Bain, J. D.; Diala, E. S.; Glabe, C. G.; Wacker, D. A.; Lyttle, M. H.; Dix, T. A. *Biochemistry* **1992**, *30*, 5411.

5. deL. Milton, R. C.; Milton, S. C. F.; Kent, S. B. H. *Science* **1992**, *256*, 1445. Schnölzer, M.; Kent, S. B. H. *Science* **1992**, *256*, 221. Muir, T. W.; Kent, S. B. H. *Curr. Opin. Biotech.* **1993**, *4*, 420. Zawadzke, L. E.; Berg, J. M. *J. Am. Chem. Soc.* **1992**, *114*, 4002.

6. Raphael, A. L.; Gray, H. B. *J. Am. Chem. Soc.* **1991**, *113*, 1038. Frauenhoff, M. M.; Scott, R. A. *Proteins* **1992**, *14*, 202. Wallace, C. J. A. *FASEB J.* **1993**, *7*, 505.

Humphries, J.; Offord, R. E.; Smith, R. A. G. *Curr. Opin. Biotech.* **1991**, *2*, 539. Chaiken, I. M. *CRC Critical Reviews in Biochemistry* **1981**, 255. Offord, R. E. *Semisynthetic Proteins* (John Wiley and Sons, New York) 1980.

7. Williams, R. M. *Synthesis of Optically Active α-Amino Acids* (Pergamon Press, New York) 1989.

8. Kent, S. B. H. *Ann. Rev. Biochem.* **1988**, *57*, 957. Stewart, J. M.; Young, J. D. *Solid Phase Peptide Synthesis* (Pierce Chemical Co., Rockford, Illinois) 2nd ed, 1984.

9. Winkler, J. R.; Gray, H. B. *Chem. Rev.* **1992**, *92*, 369.

10. Bowler, B. E.; Meade, T. J.; Mayo, S. L.; Richards, J. H.; Gray, H. B. *J. Am. Chem. Soc.* **1989**, *111*, 8757.

11. (a) Wuttke, D. S.; Bjerrum, M. J.; Winkler, J. R.; Gray, H. B. *Science* **1992**, *256*, 1007. (b) Wuttke, D. S.; Bjerrum, M. J.; Chang, I-J.; Winkler, J. R.; Gray, H. B. *Biochim. Biophys. Acta* **1992**, *1101*, 168.

12. Casimiro, D. R.; Wong L.-L.; Colón, J. L.; Zewert, T. E.; Richards, J. H.; Chang, I-J.; Winkler, J. R.; Gray, H. B. *J. Am. Chem. Soc.* **1993**, *115*, 1485.

13. Imperiali, B.; Fisher, S. L. *J. Org. Chem.* **1992**, *57*, 757.

14. Imperiali, B.; Prins, T. J.; Fisher, S. L. *J. Org. Chem.* **1993**, *58*, 1613.

15. Imperiali, B.; Fisher, S. L. *J. Am. Chem. Soc.* **1991**, *113*, 8527. Smith, R. M.; Martell, A. E. *Critical Stability Constants Vol. 2, Amines* (Plenum Press: New York) 1975, pp. 235-262.

16. Juris, A.; Balzani, V.; Barigelletti, F.; Campagna, S.; Belser, P.; von Zelewsky, A. *Coord. Chem. Rev.* **1988**, *84*, 85. Kalyanasundaram, K. *Coord. Chem. Rev.* **1982**, *46*, 161.

17. Chang, I-J.; Gray, H. B.; Winkler, J. R. *J. Am. Chem. Soc.* **1991**, *113*, 7056.

18. Fisher, S. L., Ph. D. Thesis, California Institute of Technology, **1993**.

19. O'Donnell. M. J.; Bennett, W. D.; Wu, S. *J. Am. Chem. Soc.* **1983**, *22*, 171.

20. Bushnell, G. W.; Louie, G. V.; Brayer, G. D. *J. Mol. Biol.* **1990**, *214*, 585.

21. Salmeen, I.; Palmer, G. *J. Chem. Phys.* **1968**, *48*, 2049.

22. Pan, L. P.; Durham, B.; Wolinska, J.; Millett, F. *Biochemistry* **1988**, *27*, 7180. Durham, B.; Pan, L. P.; Long, J. E.; Millett, F. *Biochemistry* **1989**, *28*, 8659.

23. Fujita, E.; Milder, S. J.; Brunschwig, B. S. *Inorg. Chem.* **1992**, *31*, 2079.

24. Rillema, D. P.; Jones, D. S.; Levy, H. A. *J. Chem. Soc., Chem. Commun.* **1979**, 849.

25. Kimura, E.; Wada, S.; Shionoya, M.; Takahashi, T.; Iitaka, Y. *J. Chem. Soc., Chem. Commun.* **1990**, 397.

26. The electrochemical redox potential of $Ru(bpy)_2(4,4'\text{-dimethyl-}2,2'\text{-bpy})^{2+}$ is 40 mV lower that $Ru(bpy)_3^{2+}$ in acetonitrile (Mabrouk, P. A.; Wrighton, M. S. *Inorg. Chem.*

1986, *25*, 526). Thus, the change in potential of $Ru(bpy)_2(4Bpa)^{2+}$ relative to $Ru(bpy)_3^{2+}$ is anticipated to be < 20 mV. Because negligible perturbation is observed in the spectroscopic features of $Ru(bpy)_2(4Bpa)^{2+}$ relative to $Ru(bpy)_3^{2+}$, the $Ru(bpy)_3^{2+}$ potentials are used to calculate $-\Delta G^o$. Insufficient material was obtained for direct electrochemical measurements on the modified protein.

27. Barker, P. D.; Mauk, A. G. *J. Am. Chem. Soc.* **1992**, *114*, 3619.

28. Hahm, S; Durham, B.; Millett, F. *Biochemistry* **1992**, *31*, 3472.

29. Onuchic, J. N.; Beratan, D. N.; Winkler, J. R.; Gray, H. B. *Annu. Rev. Biophys. Biomol. Struct.* **1992**, *21*, 349. Refer to Chapter 4 for an in-depth discussion.

30. Beratan, D. N., private communication.

31. Theorell, H; Åkesson, Å. *Science* **1939**, *90*, 67. Theorell, H; Åkesson, Å. *J. Am. Chem. Soc.* **1941**, *63*, 1812.

32. Reviewed in Moore, G. R.; Pettigrew, G. W. *Cytochromes c. Evolutionary, Structural and Physiochemical Aspects* (Verlag: Berlin) 1990, pp. 190 - 196.

33. Hong, X; Dixon, D. W. *FEBS Lett.* **1989**, *246*, 105.

34. Ferrer, J. C.; Guillemette, J. G.; Bogumil, R.; Inglis, S. C.; Smith, M.; Mauk, A. G. *J. Am. Chem. Soc.* **1993**, *115*, 7507. Ferrer, J. C.; Guillemette, J. G.; Bogumil, R.; Inglis, S. C.; Smith, M.; Mauk, A. G., Poster B040 presented at the 6th International Conference on Bioinorganic Chemistry, August 23 - 27, 1993, La Jolla, California.

35. The alkaline form absorption spectrum differs only slightly from that of the native form (Nall, B. T.; Zuniga, E. H.; White, T. B.; Wood, L. C.; Ramdas, L. *Biochemistry* **1989**, *28*, 9834). The Soret blue shifts by 2 nm and increases slightly in intensity (~5%). A small decrease (< 5%) in intensity is observed at 550 nm. The resulting changes in $\Delta\varepsilon$ (Fe^{2+}/Fe^{3+}) (the reduced form is unaffected by this change in pH) at pH 11.0 do not affect the calculated photoinduced rate constant; the rates calculated using 395 nm and 550 nm are essentially identical (within experimental error) and exhibit no differences due to a systematic error. The pKa for the alkaline transition in 4Bpa72 cyt *c* is identical with that of the native protein. No evidence for an altered high spin form of the alkaline form of 4Bpa72 cyt *c* or $Ru(bpy)_2$(4Bpa72)cyt *c* was detected spectroscopically, an additional 600 nm band has been noted in the alkaline form of a Lys72-derivatized cyt *c* (Smith, H. T.; Millett, F. *Biochemistry* **1980**, *19*, 1117).

36. Hill, M. J.; Wuttke, D. S., unpublished results. It is difficult to measure the $Ru^{2+/1+}$ potential at high pH due to interference by the reduction of water.

37. Hasumi, H. *Biochim. Biophys. Acta* **1980**, *626*, 265. Hodges, H. L.; R. A. Holwerda, R. A.; Gray, H. B. *J. Am. Chem. Soc.* **1974**, *96*, 3132. Land, E. J.; Swallow, A. J. *Arch. Biochem. Biophys.* **1971**, *145*, 365. Pecht, I; Faraggi, M. *Proc. Natl. Acad. Sci. USA*

1972, *69*, 902. Lambeth, D. O.; Campbell, K. L.; Zand, R.; Palmer, G. *J. Biol. Chem.* **1973**, *248*, 8130.

38. Karplus, M.; Shakhnovich, E. *Protein Folding*; W. H. Freeman and Company: New York, 1992; pp. 127 - 195.

Appendix A

2-D Double Quantum COSY NMR Studies of His72 and $Ru(bpy)_2(im)His33$ Cytochromes *c*

In collaboration with Prof. P. E. Wright and Dr. Dimitrios Morikis, 2-D proton NMR studies were conducted in an effort to elucidate the specific structural effects of $Ru(bpy)_2(im)^{2+}$ modification of surface His residues and the replacements of Lys72 with His and Met80 with Cys. Data were collected on both isolated derivatives of $Ru(bpy)_2(im)$His cyt *c* to determine if the two proposed stereochemical isomers differ structurally. NMR was selected to probe protein structure due to the difficulty of obtaining crystals of the horse species of cyt *c*.[1]

The proton NMR spectra of ferrous[1] and ferric[2] horse heart cyt *c* have been fully assigned by S. W. Englander and coworkers. The availability of these assignments facilitates interpretation of data collected on mutants; if chemical shift perturbations are minimal, resonances of the cyt *c* derivatives can be readily assigned. The observation of significant shifts relative to native cyt *c* indicate either structural perturbations at that site or, in the case of the $Ru(bpy)2(im)^{2+}$-modified proteins, a new interaction with a neighboring aromatic ring causing contact or ring-current shifts. Patterns observed in chemical shifts would allow the mapping of structural perturbations onto the crystal structure.[4] Thus, the goal of these experiments is not to solve the solution structures, but to identify regions, if any, of the proteins studied that undergo conformational change, since the analyses presented in this thesis rely on the crystal structure of native horse heart cyt *c*. Since NMR specifically reports on each residue individually, it is superior to macroscopic techniques, such as CD, that can only report on the overall protein structure.

For preliminary analysis, the "fingerprint" region of the spectrum was targeted. This region, consisting of C_α-H to N-H proton-proton *J*-coupled crosspeaks, affords the chemical shifts of the C_α-H to N-H protons and is sensitive to changes in either. The chemical shifts of these protons are extremely sensitive to protein conformation, and this region is commonly studied to ascertain the homogeneity of the sample. To ensure that the literature assignments could be transferred to the proteins studied, data were collected native horse heart cyt *c* at nearly identical conditions with those reported (90% D_2O/10%

H_2O,100 mM NaPi, 150 mM NaCl, pH 5.7, 293 K). The ferric form was selected for study to avoid experimental complications using dithionite. In the ferric derivative, the paramagnetic center may amplify small shifts due to conformational changes. Representative data from this region are presented in Figure A.1.

Data were collected on freshly prepared samples, oxidized fully with Na[Co(EDTA)] and purified to homogeneity by cation-exchange chromatography as described. Double quantum COSY spectra were collected rather than COSY spectra to move resonances away from the T_1 noise generated by the water signal. The only manifestation of this change in the spectra obtained is that $\omega_2 = \omega_2$ and $\omega_{1obs} = \omega_1 + \omega_2$. Spectra were collected at 293 K on a Brucker AMX 500.13 MHz NMR spectrometer using standard Brucker software with a 8333.33 Hz sweep width and 4 K real points in ω_2 and a doubled sweep width and 1 K real points in ω_1. Data were processed using FELIX on a SPARC workstation. Prior to Fourier transform the data were multiplied by a sine bell shifted 90° in F2 and a 55° sine bell in F1 and zero filled to 2K complex points. Samples were 2-4 mM in 90% D_2O/10% H_2O, 100 mM NaPi, 150 mM NaCl. Final pHs (uncorrected for the isotope effect) were: native cyt *c*, 5.73; His72 cyt *c*, 5.74; $Ru(bpy)_2$(im)His33 cyt *c* (ET band), 5.73; $Ru(bpy)_2$(im)His33 cyt *c* (not ET band), 5.75; Cys80His72 cyt *c*, 5.74.

Assignments made from comparison with published data are set out in Table A.1. There was a systematic shift of -0.05 ppm from published values, attributable to differences in referencing procedures.[5] Most of the assigned C_αH-NH crosspeaks were identified in the native sample. Fourteen of the 100 anticipated crosspeaks were not found, mostly Gly residues (which have two crosspeaks and thus weaker signals) and paramagnetically shifted resonances. Resonances in the cyt *c* derivatives were tentatively assigned, if a resonance was not observed it could be due to either a lack of sensitivity or a chemical shift from its original value large enough to preclude assignment by comparison. The designations "ET band" and "not ET band" on the $Ru(bpy)_2$(im)His33

cyt *c* derivatives refer to Band III (tentatively assigned at the Λ-isomer, with which ET studies were performed) and Band II (tentatively assigned at the Δ-isomer), respectively, as described in Chapter 3. The 1-D ^{1}H spectrum of His72 cyt *c* indicated the presence of a small impurity with slightly shifted resonances in the 10 - 40 ppm region; it was not observed in earlier 1-D ^{1}H NMR studies. Good 1-D ^{1}H NMR spectra were obtained on a sample of Ru(bpy)$_2$(im)His72 cyt *c*, however, the sample was too dilute for 2-D studies.

In all the proteins studied, except Cys80His72 cyt *c*, most of the resonances could be readily assigned by comparison with the native spectrum. This good correlation indicates negligible perturbation of the overall protein structure, with certain regions of the derivatives identical with the native structure. In the Cys80 axial mutant protein high quality data were obtained, however the *g*-tensor of the unpaired electron differs so drastically from that of the Met80 ligated proteins that there is no correlation between the chemical shifts of the native and His72Cys80 protein due to significantly different paramagnetic interactions (Appendix B). Bar graphs are presented following the assignment table that illustrate the C_αH and NH proton chemical shifts as a function of amino acid residue of the derivatives studied. Blank spots correspond to unassigned resonances. Following the assignment graphs are bar graphs of the difference in chemical shifts between relevant cyt *c* derivatives. Offscale bars represent resonances that were assigned in one derivative and not in the other. These difference graphs pinpoint regions where small structural perturbations may have occurred.

References

1. Brayer, G. D.; Lo, T. P., private communication.

2. Wand, A. J.; Di Stefano, D. L.; Feng, Y.; Roder, H.; Englander, S. W. *Biochemistry* **1989**, *28*, 186.

3. Feng, Y.; Roder, H.; Englander, S. W.; Wand, A. J.; Di Stefano, D. L. *Biochemistry* **1989**, *28*, 195.

4. An NMR-generated structure of cyt *c* has not been reported, although NMR data suggest that the structure in solution is analogous to the crystal structure.

5. Spectra referenced to the HDO signal. Published spectra referenced to Na 3-(trimethylsilyl)[2,2,3,3-$^{2}H_4$] propionate.

Figure A.1 Representative data of the fingerprint region obtained from 2-D double quantum COSY NMR experiments.

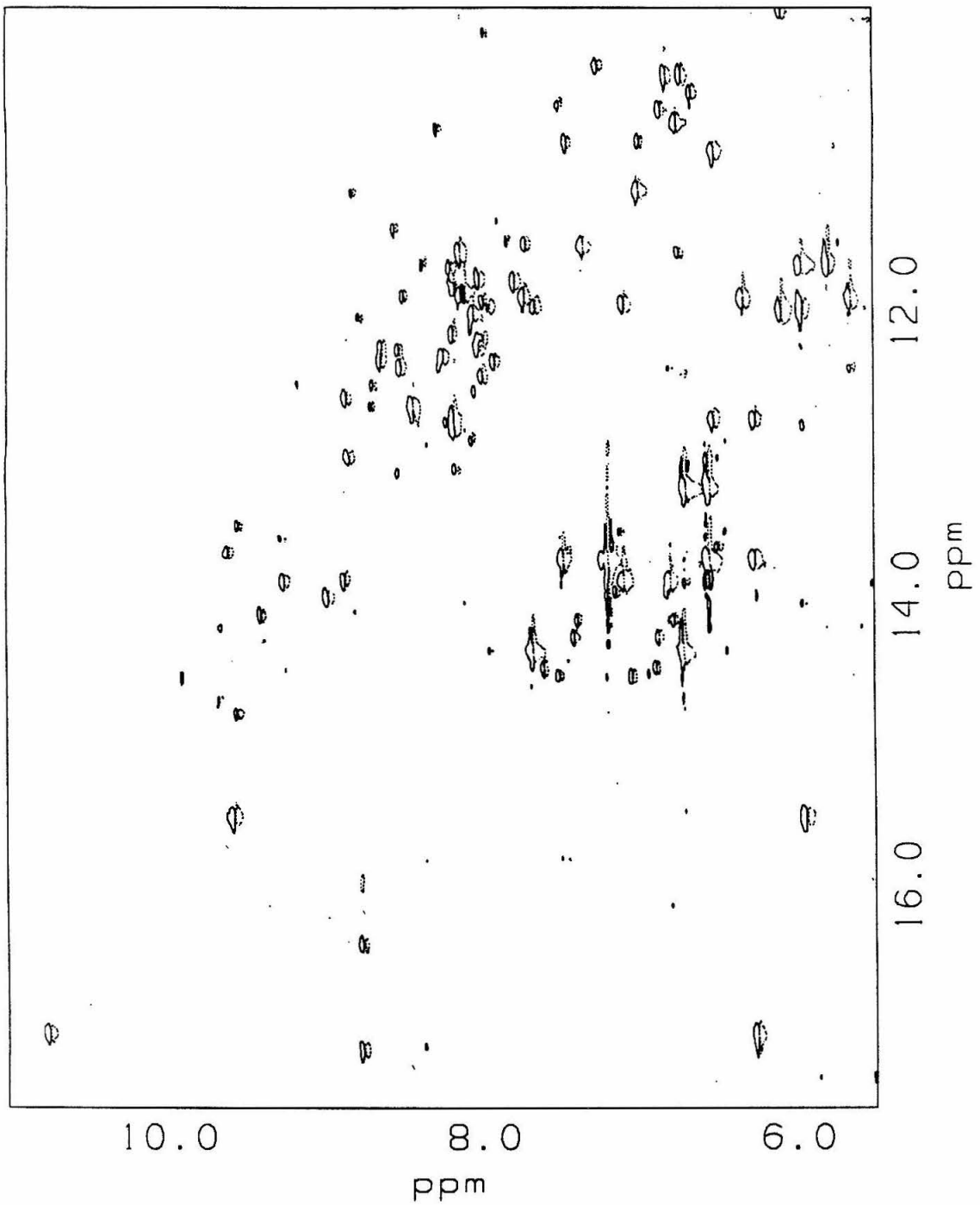
10.0
8.0
6.0
ppm
12.0
14.0
16.0
ppm

	nat cyc-NH	nat cyc-Ca	H72 cyc-NH	NH:H72-nat	residue number	H72 cyc-Ca
1	8.1050	3.5300	8.1250	0.020000	1.0000	3.5450
2	9.2150	4.6300	9.2450	0.030000	2.0000	4.6550
3	8.4630	3.4470	8.4850	0.021999	3.0000	3.4750
4	8.0250	4.0200	8.0450	0.020000	4.0000	4.0350
5	8.0100	3.8500	8.0050	-0.0050001	5.0000	3.8450
6	8.6500	3.1700	8.6800	0.030001	6.0000	3.1850
7	7.9750	2.2000	7.9650	-0.0099998	7.0000	2.2050
8	6.8500	3.8300	6.8550	0.0050001	8.0000	3.8400
9	7.4350	3.4500	7.4500	0.015000	9.0000	4.4650
10	8.3520	3.3680	8.3600	0.0079994	10.000	3.3800
11	8.8450	3.8000	8.8500	0.0050001	11.000	3.8000
12	7.7800	4.0950	7.7800	0.0000	12.000	4.0900
13	8.4200	4.3000	8.4300	0.010000	13.000	4.2850
14	8.0270	4.3730	8.0050	-0.022000	14.000	4.1050
15	8.0900	5.9650	8.0900	0.0000	15.000	5.9550
16	9.8930	4.6920	9.8800	-0.013000	16.000	4.6800
17	9.6450	6.0050	9.5650	-0.080001	17.000	5.9550
18	10.960	9.1100	0.0000	-10.960	18.000	0.0000
19	10.710	6.2400	10.740	0.030000	19.000	6.2700
20	8.9450	5.0050	8.9700	0.025001	20.000	5.0350
21	0.0000	0.0000	0.0000	0.0000	21.000	0.0000
22	9.1450	3.3850	9.1450	0.0000	22.000	3.4050
23	9.4550	4.0300	9.4650	0.010000	23.000	4.0450
24	0.0000	0.0000	0.0000	0.0000	24.000	0.0000
25	8.8200	4.2100	8.8300	0.010000	25.000	4.2250
26	8.8570	5.0030	8.8650	0.0079994	26.000	5.0200
27	8.1550	4.7000	8.1550	0.0000	27.000	4.7000
28	8.0750	0.0000	0.0000	-8.0750	28.000	0.0000
29	0.0000	0.0000	0.0000	0.0000	29.000	0.0000
30	0.0000	0.0000	0.0000	0.0000	30.000	0.0000
31	0.0000	0.0000	0.0000	0.0000	31.000	0.0000
32	9.6140	5.0110	9.6450	0.031000	32.000	5.0700
33	0.0000	0.0000	0.0000	0.0000	33.000	0.0000
34	0.0000	0.0000	0.0000	0.0000	34.000	0.0000
35	0.0000	0.0000	0.0000	0.0000	35.000	0.0000
36	8.6500	3.6580	8.6750	0.025001	36.000	3.8900
37	9.2870	4.3380	9.2550	-0.032000	37.000	4.3600
38	8.1550	4.6050	8.1550	0.0000	38.000	4.6050
39	0.0000	0.0000	0.0000	0.0000	39.000	0.0000
40	7.4450	4.1950	0.0000	-7.4450	40.000	0.0000
41	0.0000	0.0000	0.0000	0.0000	41.000	0.0000
42	7.6870	4.3680	7.6500	-0.037000	42.000	4.3750
43	8.0350	4.5650	8.0250	-0.010000	43.000	4.5750
44	0.0000	0.0000	0.0000	0.0000	44.000	0.0000
45	8.9500	4.2600	0.0000	-8.9500	45.000	0.0000

	nat cyc-NH	nat cyc-Ca	H72 cyc-NH	NH:H72-nat	residue number	H72 cyc-Ca
46	6.8100	3.6400	6.8200	0.010000	46.000	3.6400
47	6.7200	3.7250	6.7250	0.0050001	47.000	3.7300
48	7.9650	4.0100	7.9800	0.015000	48.000	4.0150
49	9.5800	4.1100	9.5950	0.015000	49.000	4.1100
50	8.8500	4.1950	8.8300	-0.020000	50.000	4.2250
51	8.0700	4.1170	8.0700	0.0000	51.000	4.1170
52	8.5500	4.6700	8.5150	-0.035000	52.000	4.6250
53	8.6350	3.7150	8.6350	0.0000	53.000	3.8900
54	8.0700	4.8550	8.0500	-0.020000	54.000	4.8800
55	6.8000	4.4550	0.0000	-6.8000	55.000	0.0000
56	0.0000	0.0000	0.0000	0.0000	56.000	0.0000
57	6.5300	4.4300	6.5150	-0.015000	57.000	4.4550
58	8.2550	4.1200	8.2350	-0.020000	58.000	4.1300
59	8.7050	4.6400	8.6900	-0.015000	59.000	4.6050
60	7.9425	4.2625	7.9800	0.037500	60.000	4.2650
61	0.0000	0.0000	0.0000	0.0000	61.000	0.0000
62	9.4600	4.0300	9.5350	0.075000	62.000	3.9850
63	7.0000	4.3100	6.9900	-0.010000	63.000	4.2600
64	8.4700	3.7700	8.5200	0.050000	64.000	3.8050
65	0.0000	0.0000	0.0000	0.0000	65.000	0.0000
66	6.6000	4.0400	6.6600	0.060000	66.000	3.9150
67	0.0000	0.0000	0.0000	0.0000	67.000	0.0000
68	8.0730	2.5220	8.2700	0.19700	68.000	2.5550
69	6.7550	3.7250	6.9900	0.23500	69.000	3.9250
70	6.6470	4.8680	6.7330	0.086000	70.000	4.9270
71	0.0000	0.0000	0.0000	0.0000	71.000	0.0000
72	9.4850	5.2350	9.5400	0.055000	72.000	5.2770
73	7.8050	4.4450	7.9100	0.10500	73.000	4.4900
74	0.0000	0.0000	0.0000	0.0000	74.000	0.0000
75	9.4680	4.7870	9.3900	-0.078000	75.000	4.7400
76	0.0000	0.0000	0.0000	0.0000	76.000	0.0000
77	9.3700	4.5800	9.3700	0.0000	77.000	4.5650
78	9.0500	5.2150	0.0000	-9.0500	78.000	0.0000
79	0.0000	0.0000	0.0000	0.0000	79.000	0.0000
80	0.0000	0.0000	0.0000	0.0000	80.000	0.0000
81	8.5700	5.1150	0.0000	-8.5700	81.000	0.0000
82	9.0300	4.5400	0.0000	-9.0300	82.000	0.0000
83	8.4750	4.2500	0.0000	-8.4750	83.000	0.0000
84	0.0000	0.0000	0.0000	0.0000	84.000	0.0000
85	7.9500	3.8150	7.7150	-0.23500	85.000	4.2500
86	8.4300	3.9050	8.3050	-0.12500	86.000	4.1350
87	8.1830	4.1140	8.1750	-0.0079994	87.000	4.2200
88	8.9050	3.4450	8.8400	-0.065000	88.000	3.4100
89	8.1350	3.8520	8.1250	-0.010000	89.000	3.8250
90	6.0230	3.9220	6.0850	0.062000	90.000	3.9350

	nat cyc-NH	nat cyc-Ca	H72 cyc-NH	NH:H72-nat	residue number	H72 cyc-Ca
91	7.0900	3.1350	7.2500	0.16000	91.000	3.1450
92	8.2180	3.5170	8.1900	-0.028001	92.000	3.5700
93	8.2100	3.9800	8.1750	-0.035000	93.000	4.0350
94	7.8180	3.8020	7.8250	0.0070000	94.000	3.7550
95	8.3850	3.0030	8.5400	0.15500	95.000	2.9750
96	7.7800	3.8850	7.7100	-0.070000	96.000	3.9000
97	7.8800	4.0900	7.9400	0.060000	97.000	4.0950
98	8.7230	3.3000	8.7700	0.047001	98.000	3.3400
99	8.8450	2.4100	8.8100	-0.035000	99.000	2.4450
100	6.7200	4.0050	6.7550	0.035000	100.00	4.0300
101	8.6400	3.9950	8.6900	0.049999	101.00	4.0150
102	7.9050	4.5100	7.9850	0.080000	102.00	4.5100
103	7.0800	4.9050	7.0850	0.0050001	103.00	4.9250
104	7.3450	4.2650	7.3400	-0.0049996	104.00	4.2850

	Ca:H72-native	NH:Ru33ET	NH:ET-natcyt c	Ca:Ru33ET	Ca:ET-nat cyc	NH:Ru33NET
1	0.015000	8.1200	0.015000	3.5400	0.0100000	8.1200
2	0.025000	9.2200	0.0050001	4.6450	0.015000	9.2150
3	0.028000	8.4700	0.0070000	3.4500	0.0030000	8.4650
4	0.015000	8.0300	0.0050001	4.0200	0.0000	8.0250
5	-0.0049999	8.0300	0.020000	3.8400	-0.0100000	8.0200
6	0.015000	8.6500	0.0000	3.1800	0.0100000	0.0000
7	0.0049999	7.9800	0.0050001	2.2050	0.0049999	0.0000
8	0.0100000	6.8500	0.0000	2.8300	-1.0000	6.8500
9	1.0150	7.4250	-0.0099998	3.4600	0.0100000	7.4250
10	0.012000	8.3600	0.0079994	3.3700	0.0019999	8.3520
11	0.0000	8.8370	-0.0080004	3.8030	0.0030000	8.8400
12	-0.0049996	7.7850	0.0049996	4.0850	-0.0099998	7.7850
13	-0.015000	8.4250	0.0050001	4.2950	-0.0050001	8.4250
14	-0.26800	8.0200	-0.0070000	4.3400	-0.033000	8.0200
15	-0.010000	0.0000	-8.0900	0.0000	-5.9650	0.0000
16	-0.012000	0.0000	-9.8930	0.0000	-4.6920	9.8930
17	-0.050000	9.5500	-0.095000	5.9600	-0.045000	9.6450
18	-9.1100	0.0000	-10.960	0.0000	-9.1100	0.0000
19	0.030000	10.740	0.030000	6.2550	0.015000	10.715
20	0.030000	8.9250	-0.020000	4.9150	-0.090000	8.9400
21	0.0000	0.0000	0.0000	0.0000	0.0000	0.0000
22	0.020000	0.0000	-9.1450	0.0000	-3.3850	0.0000
23	0.015000	0.0000	-9.4550	0.0000	-4.0300	0.0000
24	0.0000	0.0000	0.0000	0.0000	0.0000	0.0000
25	0.015000	8.7800	-0.040000	4.2500	0.040000	8.8250
26	0.017000	8.8650	0.0079994	5.0000	-0.0029998	8.8600
27	0.0000	8.1050	-0.050000	4.7650	0.065000	8.1500
28	0.0000	0.0000	-8.0750	0.0000	0.0000	0.0000
29	0.0000	0.0000	0.0000	0.0000	0.0000	0.0000
30	0.0000	0.0000	0.0000	0.0000	0.0000	0.0000
31	0.0000	0.0000	0.0000	0.0000	0.0000	0.0000
32	0.059000	0.0000	-9.6140	0.0000	-5.0110	0.0000
33	0.0000	0.0000	0.0000	0.0000	0.0000	0.0000
34	0.0000	0.0000	0.0000	0.0000	0.0000	0.0000
35	0.0000	0.0000	0.0000	0.0000	0.0000	0.0000
36	0.23200	8.7250	0.075001	3.7700	0.11200	8.6500
37	0.022000	0.0000	-9.2870	0.0000	-4.3380	0.0000
38	0.0000	8.1450	-0.0099993	4.5700	-0.035000	8.1550
39	0.0000	0.0000	0.0000	0.0000	0.0000	0.0000
40	-4.1950	0.0000	-7.4450	0.0000	-4.1950	7.5200
41	0.0000	0.0000	0.0000	0.0000	0.0000	0.0000
42	0.0070000	7.6850	-0.0019999	4.3750	0.0070000	7.6900
43	0.0099998	0.0000	-8.0350	0.0000	-4.5650	0.0000
44	0.0000	0.0000	0.0000	0.0000	0.0000	0.0000
45	-4.2600	0.0000	-8.9500	0.0000	-4.2600	0.0000

	Ca:H72-native	NH:Ru33ET	NH:ET-natcyt c	Ca:Ru33ET	Ca:ET-nat cyc	NH:Ru33NET
46	0.0000	6.8550	0.045000	3.6400	0.0000	6.8150
47	0.0050001	6.7250	0.0050001	3.7300	0.0050001	6.7250
48	0.0049996	7.9850	0.020000	4.0150	0.0049996	7.9750
49	0.0000	9.5950	0.015000	4.1150	0.0049996	9.5850
50	0.030000	8.8600	0.0099993	4.2050	0.0099998	8.8550
51	0.0000	8.0650	-0.0050001	4.1400	0.023000	8.0600
52	-0.045000	8.5550	0.0050001	4.6600	-0.010000	8.5500
53	0.17500	8.6350	0.0000	3.6800	-0.035000	8.6450
54	0.025000	0.0000	-8.0700	0.0000	-4.8550	0.0000
55	-4.4550	0.0000	-6.8000	0.0000	-4.4550	0.0000
56	0.0000	0.0000	0.0000	0.0000	0.0000	0.0000
57	0.025000	6.5950	0.065000	4.4950	0.065000	6.5400
58	0.010000	8.2500	-0.0050001	4.1650	0.045000	8.2550
59	-0.035000	0.0000	-8.7050	0.0000	-4.6400	0.0000
60	0.0025001	7.9550	0.012500	4.1900	-0.072500	7.9550
61	0.0000	0.0000	0.0000	0.0000	0.0000	0.0000
62	-0.045000	9.4750	0.015000	3.9250	-0.10500	9.4700
63	-0.050000	7.0100	0.010000	4.3100	0.0000	7.0100
64	0.035000	8.4950	0.025000	3.7750	0.0050001	8.4950
65	0.0000	0.0000	0.0000	0.0000	0.0000	0.0000
66	-0.12500	6.6050	0.0050001	4.0550	0.015000	6.6050
67	0.0000	0.0000	0.0000	0.0000	0.0000	0.0000
68	0.033000	8.0650	-0.0080004	2.5200	-0.0020001	8.0750
69	0.20000	6.7600	0.0050001	3.8050	0.080000	6.7600
70	0.059000	6.6550	0.0080004	4.8600	-0.0079999	6.6550
71	0.0000	0.0000	0.0000	0.0000	0.0000	0.0000
72	0.042000	9.4700	-0.014999	5.2350	0.0000	9.4800
73	0.045000	7.8100	0.0050001	4.4550	0.0099998	7.8100
74	0.0000	0.0000	0.0000	0.0000	0.0000	0.0000
75	-0.047000	9.4700	0.0019999	4.7950	0.0079999	9.4700
76	0.0000	0.0000	0.0000	0.0000	0.0000	0.0000
77	-0.015000	9.3850	0.015000	4.5500	-0.030000	9.3800
78	-5.2150	9.0550	0.0050001	5.1950	-0.020000	9.0500
79	0.0000	0.0000	0.0000	0.0000	0.0000	0.0000
80	0.0000	0.0000	0.0000	0.0000	0.0000	0.0000
81	-5.1150	0.0000	-8.5700	0.0000	-5.1150	0.0000
82	-4.5400	9.0350	0.0050001	4.6100	0.070000	9.0350
83	-4.2500	8.5350	0.059999	4.1850	-0.065000	8.4750
84	0.0000	0.0000	0.0000	0.0000	0.0000	0.0000
85	0.43500	7.9650	0.015000	3.8250	0.0100000	7.9600
86	0.23000	8.4450	0.014999	3.9100	0.0050001	8.4400
87	0.10600	8.1900	0.0070000	4.1300	0.016000	8.1900
88	-0.035000	8.9200	0.015000	3.4250	-0.020000	8.9050
89	-0.027000	8.1350	0.0000	3.8600	0.0079999	8.1100
90	0.013000	6.0350	0.012000	3.9350	0.013000	6.0300

	Ca:H72-native	NH:Ru33ET	NH:ET-natcyt c	Ca:Ru33ET	Ca:ET-nat cyc	NH:Ru33NET
91	0.0100000	7.1000	0.0099998	3.1450	0.0100000	7.0900
92	0.053000	8.2250	0.0070000	3.5300	0.013000	8.2150
93	0.055000	8.2200	0.010000	3.9950	0.015000	8.2100
94	-0.047000	7.8850	0.067000	3.7500	-0.052000	7.8180
95	-0.028000	8.3800	-0.0050001	3.0350	0.032000	8.3700
96	0.015000	7.8050	0.025000	3.8900	0.0050001	7.7750
97	0.0049996	7.9050	0.025000	4.1100	0.020000	0.0000
98	0.040000	8.7100	-0.013000	3.3300	0.030000	0.0000
99	0.035000	8.7800	-0.065001	2.4900	0.080000	0.0000
100	0.025000	6.7200	0.0000	4.0400	0.035000	6.7200
101	0.020000	8.6500	0.0099993	3.9800	-0.015000	0.0000
102	0.0000	0.0000	-7.9050	0.0000	-4.5100	7.9100
103	0.020000	7.1300	0.050000	4.9250	0.020000	7.0450
104	0.020000	7.3450	0.0000	4.2750	0.010000	7.3400

	NH:NET-nat cyc	NH:NET-ET	Ca:Ru33NET	Ca:NET-cyc	Ca:NET-ET
1	0.015000	0.0000	3.5350	0.0050001	-0.0049999
2	0.0000	-0.0050001	4.6450	0.015000	0.0000
3	0.0019999	-0.0050001	3.4250	-0.022000	-0.025000
4	0.0000	-0.0050001	4.0150	-0.0050001	-0.0050001
5	0.010000	-0.0099993	3.8400	-0.0100000	0.0000
6	-8.6500	-8.6500	0.0000	-3.1700	-3.1800
7	-7.9750	-7.9800	0.0000	-2.2000	-2.2050
8	0.0000	0.0000	3.8300	0.0000	1.0000
9	-0.0099998	0.0000	3.4450	-0.0050001	-0.015000
10	0.0000	-0.0079994	3.3680	0.0000	-0.0019999
11	-0.0050001	0.0030003	3.7950	-0.0049999	-0.0079999
12	0.0049996	0.0000	4.0850	-0.0099998	0.0000
13	0.0050001	0.0000	4.2950	-0.0050001	0.0000
14	-0.0070000	0.0000	4.3650	-0.0080004	0.025000
15	-8.0900	0.0000	0.0000	-5.9650	0.0000
16	0.0000	9.8930	4.6920	0.0000	4.6920
17	0.0000	0.095000	6.0050	0.0000	0.045000
18	-10.960	0.0000	0.0000	-9.1100	0.0000
19	0.0050001	-0.025000	6.2350	-0.0049996	-0.020000
20	-0.0050001	0.014999	5.0050	0.0000	0.090000
21	0.0000	0.0000	0.0000	0.0000	0.0000
22	-9.1450	0.0000	0.0000	-3.3850	0.0000
23	-9.4550	0.0000	3.9200	-0.11000	3.9200
24	0.0000	0.0000	0.0000	0.0000	0.0000
25	0.0050001	0.045000	4.2100	0.0000	-0.040000
26	0.0029993	-0.0050001	4.9900	-0.013000	-0.010000
27	-0.0050001	0.045000	4.7000	0.0000	-0.065000
28	-8.0750	0.0000	0.0000	0.0000	0.0000
29	0.0000	0.0000	0.0000	0.0000	0.0000
30	0.0000	0.0000	0.0000	0.0000	0.0000
31	0.0000	0.0000	0.0000	0.0000	0.0000
32	-9.6140	0.0000	0.0000	-5.0110	0.0000
33	0.0000	0.0000	0.0000	0.0000	0.0000
34	0.0000	0.0000	0.0000	0.0000	0.0000
35	0.0000	0.0000	0.0000	0.0000	0.0000
36	0.0000	-0.075001	3.8950	0.23700	0.12500
37	-9.2870	0.0000	0.0000	-4.3380	0.0000
38	0.0000	0.0099993	4.6100	0.0050001	0.040000
39	0.0000	0.0000	0.0000	0.0000	0.0000
40	0.075000	7.5200	4.1950	0.0000	4.1950
41	0.0000	0.0000	0.0000	0.0000	0.0000
42	0.0030003	0.0050001	4.3750	0.0070000	0.0000
43	-8.0350	0.0000	0.0000	-4.5650	0.0000
44	0.0000	0.0000	0.0000	0.0000	0.0000
45	-8.9500	0.0000	0.0000	-4.2600	0.0000

	NH:NET-nat cyc	NH:NET-ET	Ca:Ru33NET	Ca:NET-cyc	Ca:NET-ET
46	0.0050001	-0.040000	3.6300	-0.0100000	-0.0100000
47	0.0050001	0.0000	3.7300	0.0050001	0.0000
48	0.0099998	-0.010000	4.0050	-0.0050001	-0.0099998
49	0.0050001	-0.010000	4.1100	0.0000	-0.0049996
50	0.0049992	-0.0050001	4.2100	0.015000	0.0050001
51	-0.0099993	-0.0049992	4.0450	-0.072000	-0.095000
52	0.0000	-0.0050001	4.6700	0.0000	0.010000
53	0.010000	0.010000	3.6900	-0.025000	0.0100000
54	-8.0700	0.0000	0.0000	-4.8550	0.0000
55	-6.8000	0.0000	0.0000	-4.4550	0.0000
56	0.0000	0.0000	0.0000	0.0000	0.0000
57	0.0099998	-0.055000	4.4700	0.040000	-0.025000
58	0.0000	0.0050001	4.1350	0.015000	-0.030000
59	-8.7050	0.0000	0.0000	-4.6400	0.0000
60	0.012500	0.0000	4.2650	0.0025001	0.075000
61	0.0000	0.0000	0.0000	0.0000	0.0000
62	0.010000	-0.0050001	3.9250	-0.10500	0.0000
63	0.010000	0.0000	4.3050	-0.0050001	-0.0050001
64	0.025000	0.0000	3.7700	0.0000	-0.0050001
65	0.0000	0.0000	0.0000	0.0000	0.0000
66	0.0050001	0.0000	4.0450	0.0050001	-0.0099998
67	0.0000	0.0000	0.0000	0.0000	0.0000
68	0.0019999	0.010000	2.5400	0.018000	0.020000
69	0.0050001	0.0000	3.8000	0.075000	-0.0050001
70	0.0080004	0.0000	4.8700	0.0019999	0.0099998
71	0.0000	0.0000	0.0000	0.0000	0.0000
72	-0.0050001	0.0099993	5.2400	0.0049996	0.0049996
73	0.0050001	0.0000	4.4500	0.0049996	-0.0050001
74	0.0000	0.0000	0.0000	0.0000	0.0000
75	0.0019999	0.0000	4.7950	0.0079999	0.0000
76	0.0000	0.0000	0.0000	0.0000	0.0000
77	0.010000	-0.0050001	4.5750	-0.0050001	0.025000
78	0.0000	-0.0050001	5.2150	0.0000	0.020000
79	0.0000	0.0000	0.0000	0.0000	0.0000
80	0.0000	0.0000	0.0000	0.0000	0.0000
81	-8.5700	0.0000	0.0000	-5.1150	0.0000
82	0.0050001	0.0000	4.5450	0.0050001	-0.065000
83	0.0000	-0.059999	4.2500	0.0000	0.065000
84	0.0000	0.0000	0.0000	0.0000	0.0000
85	0.010000	-0.0050001	3.8150	0.0000	-0.0100000
86	0.0099993	-0.0050001	3.9050	0.0000	-0.0050001
87	0.0070000	0.0000	4.1250	0.011000	-0.0050001
88	0.0000	-0.015000	3.4450	0.0000	0.020000
89	-0.025001	-0.025001	3.8900	0.038000	0.030000
90	0.0070004	-0.0049996	3.9250	0.0030000	-0.0100000

	NH:NET-nat cyc	NH:NET-ET	Ca:Ru33NET	Ca:NET-cyc	Ca:NET-ET
91	0.0000	-0.0099998	3.1450	0.0100000	0.0000
92	-0.0030003	-0.010000	3.5450	0.028000	0.015000
93	0.0000	-0.010000	3.9850	0.0049999	-0.0100000
94	0.0000	-0.067000	3.8020	0.0000	0.052000
95	-0.015000	-0.010000	2.9950	-0.0080001	-0.040000
96	-0.0050001	-0.030000	3.8600	-0.025000	-0.030000
97	-7.8800	-7.9050	0.0000	-4.0900	-4.1100
98	-8.7230	-8.7100	0.0000	-3.3000	-3.3300
99	-8.8450	-8.7800	0.0000	-2.4100	-2.4900
100	0.0000	0.0000	4.0100	0.0050001	-0.030000
101	-8.6400	-8.6500	0.0000	-3.9950	-3.9800
102	0.0049996	7.9100	4.5050	-0.0050001	4.5050
103	-0.035000	-0.085000	4.8750	-0.030000	-0.050000
104	-0.0049996	-0.0049996	4.2650	0.0000	-0.010000

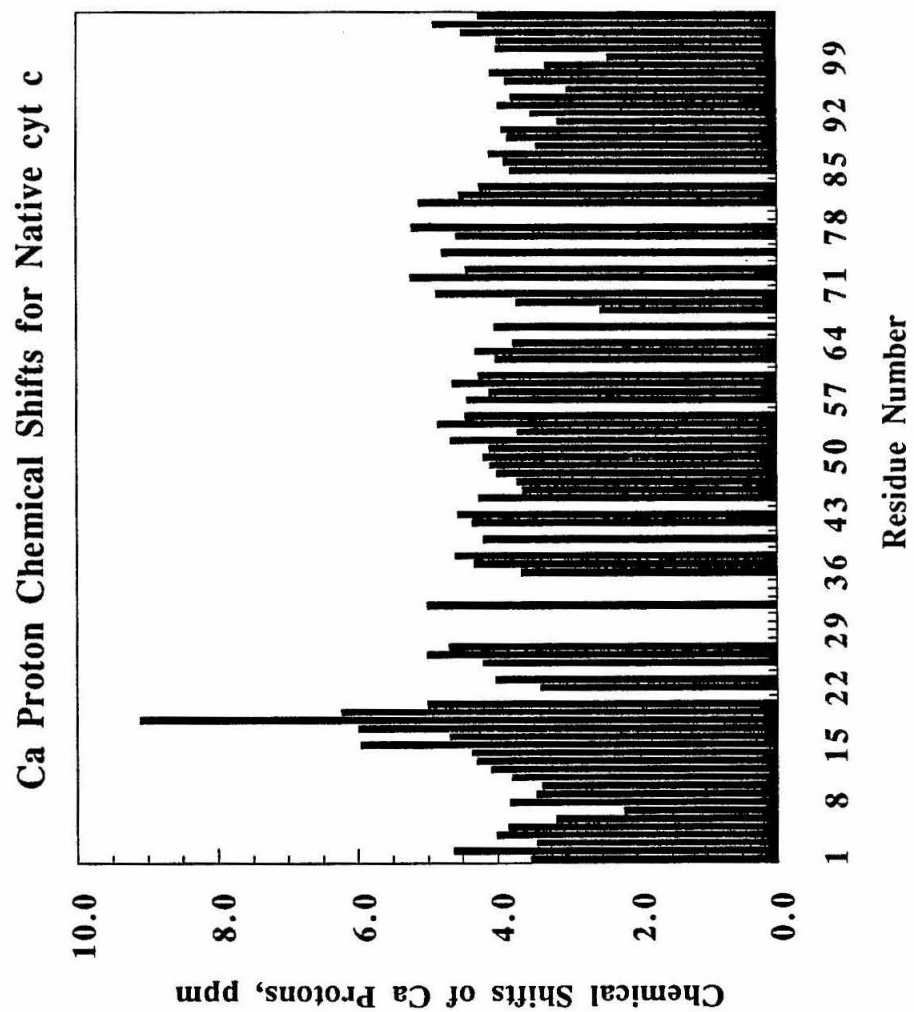
Ca Proton Chemical Shifts for Native cyt c
Chemical Shifts of Ca Protons, ppm
10.0
8.0
6.0
4.0
2.0
0.0
1 8 15 22 29 36 43 50 57 64 71 78 85 92 99
Residue Number

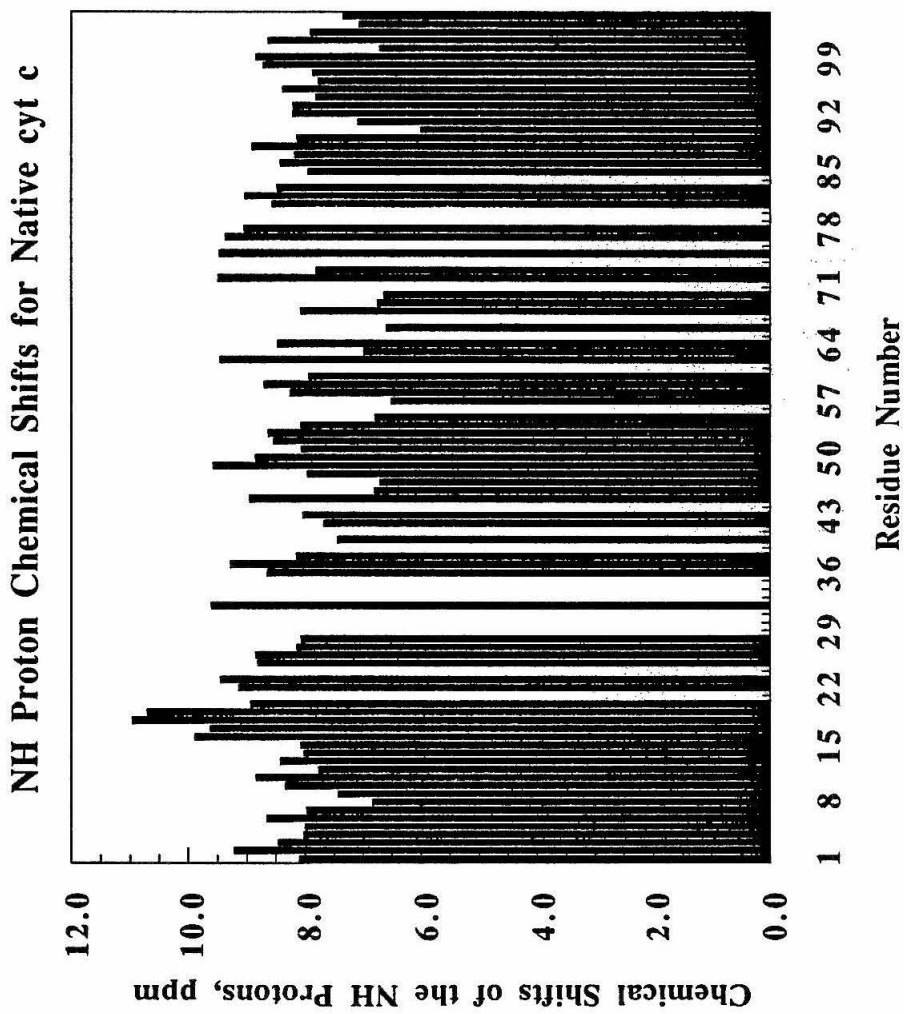
NH Proton Chemical Shifts for Native cyt c
Chemical Shifts of the NH Protons, ppm
12.0
10.0
8.0
6.0
4.0
2.0
0.0
1 8 15 22 29 36 43 50 57 64 71 78 85 92 99
Residue Number

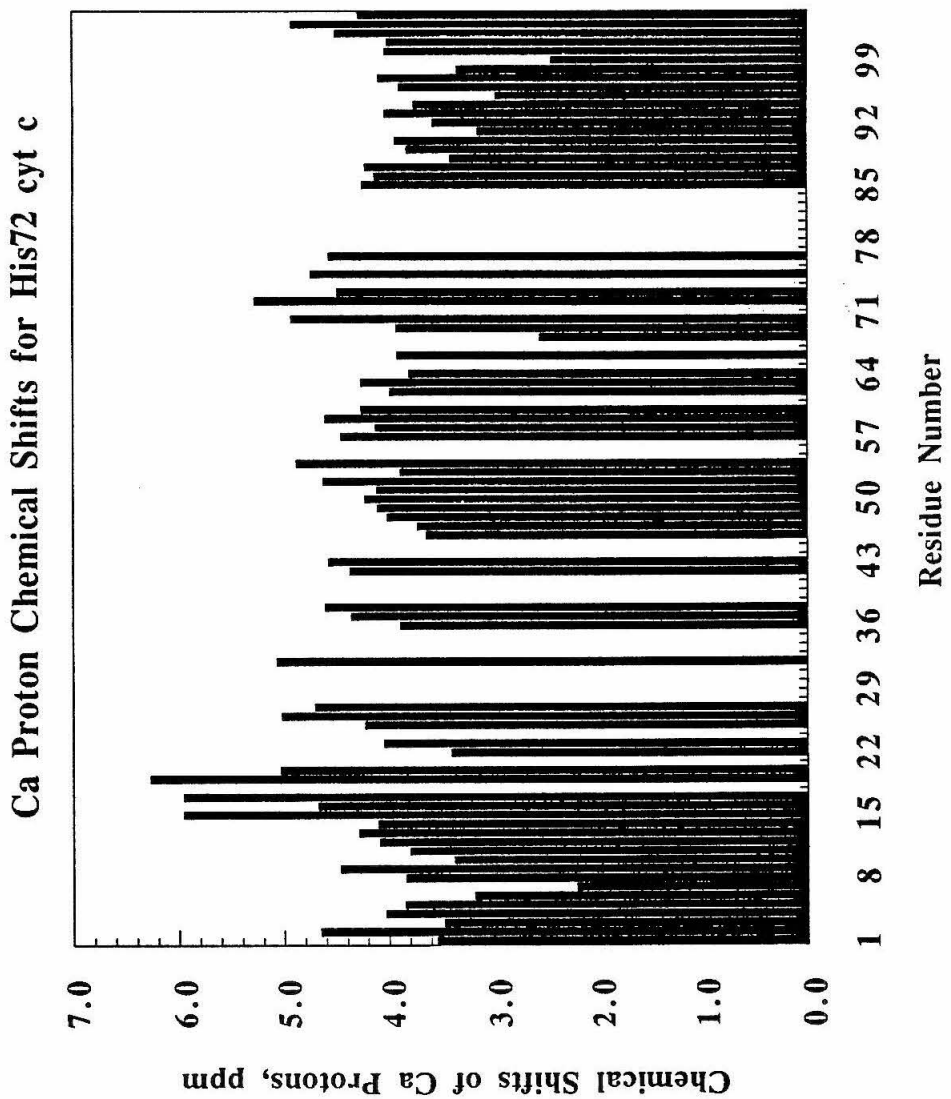
Ca Proton Chemical Shifts for His72 cyt c
Chemical Shifts of Ca Protons, ppm
7.0
6.0
5.0
4.0
3.0
2.0
1.0
0.0
1 8 15 22 29 36 43 50 57 64 71 78 85 92 99
Residue Number

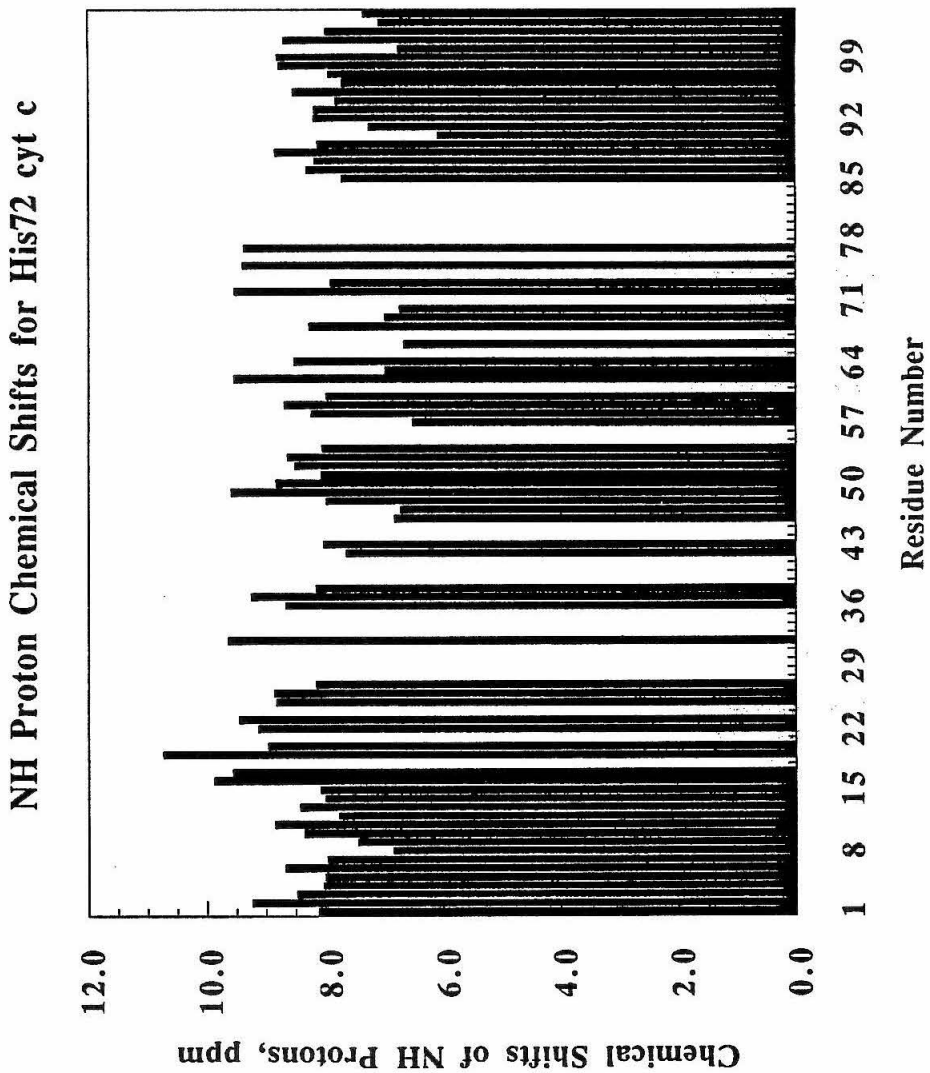
NH Proton Chemical Shifts for His72 cyt c
Chemical Shifts of NH Protons, ppm
12.0
10.0
8.0
6.0
4.0
2.0
0.0
1 8 15 22 29 36 43 50 57 64 71 78 85 92 99
Residue Number

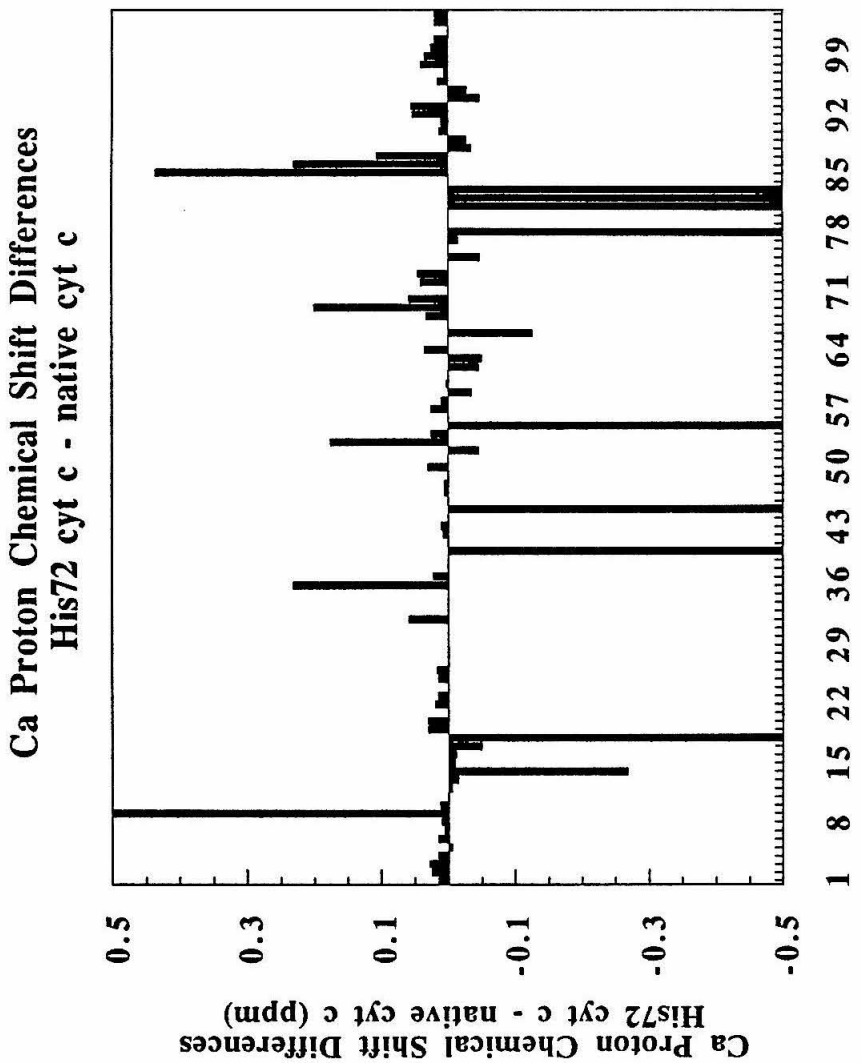
Ca Proton Chemical Shift Differences
His72 cyt c - native cyt c
0.5
0.3
0.1
-0.1
-0.3
-0.5
1 8 15 22 29 36 43 50 57 64 71 78 85 92 99
Residue Number
Ca Proton Chemical Shift Differences
His72 cyt c - native cyt c (ppm)

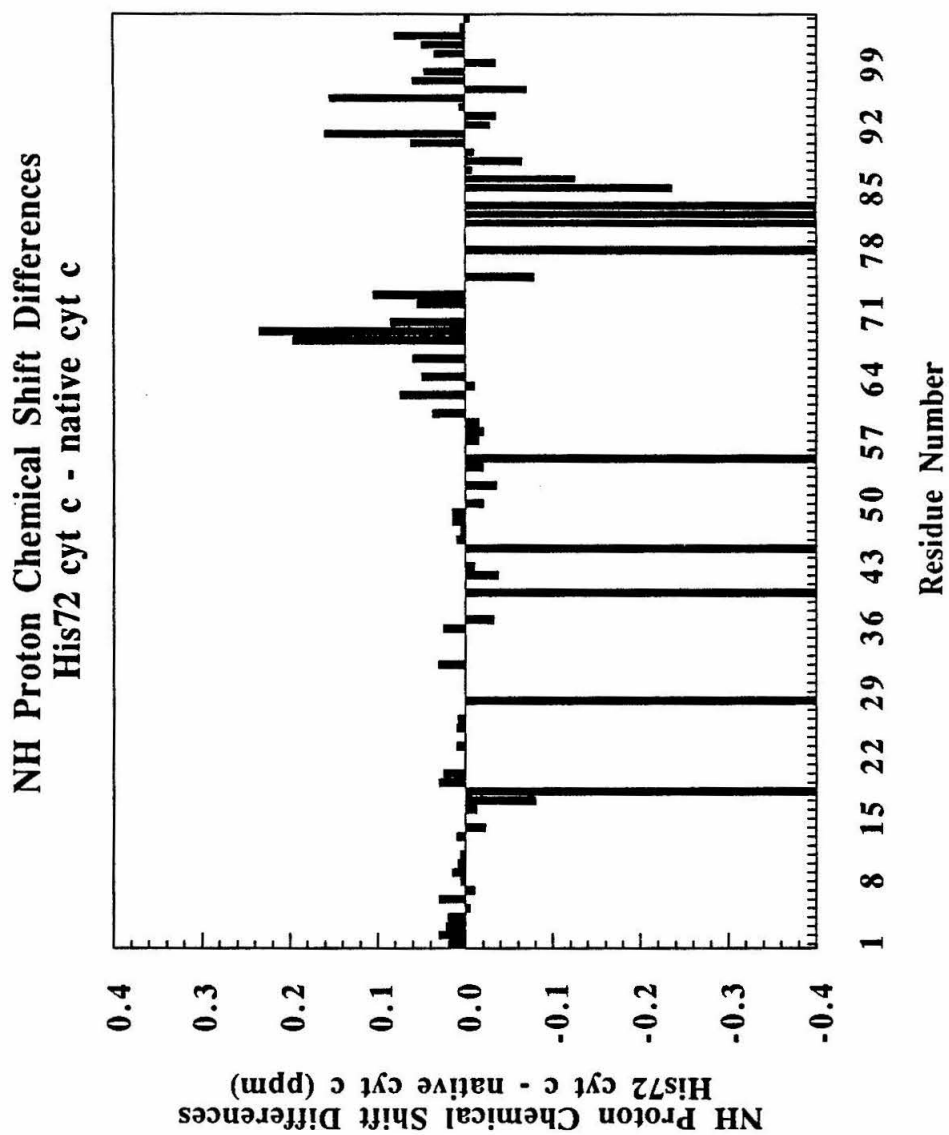
NH Proton Chemical Shift Differences
His72 cyt c - native cyt c
NH Proton Chemical Shift Differences
His72 cyt c - native cyt c (ppm)
0.4
0.3
0.2
0.1
0.0
-0.1
-0.2
-0.3
-0.4
1 8 15 22 29 36 43 50 57 64 71 78 85 92 99
Residue Number

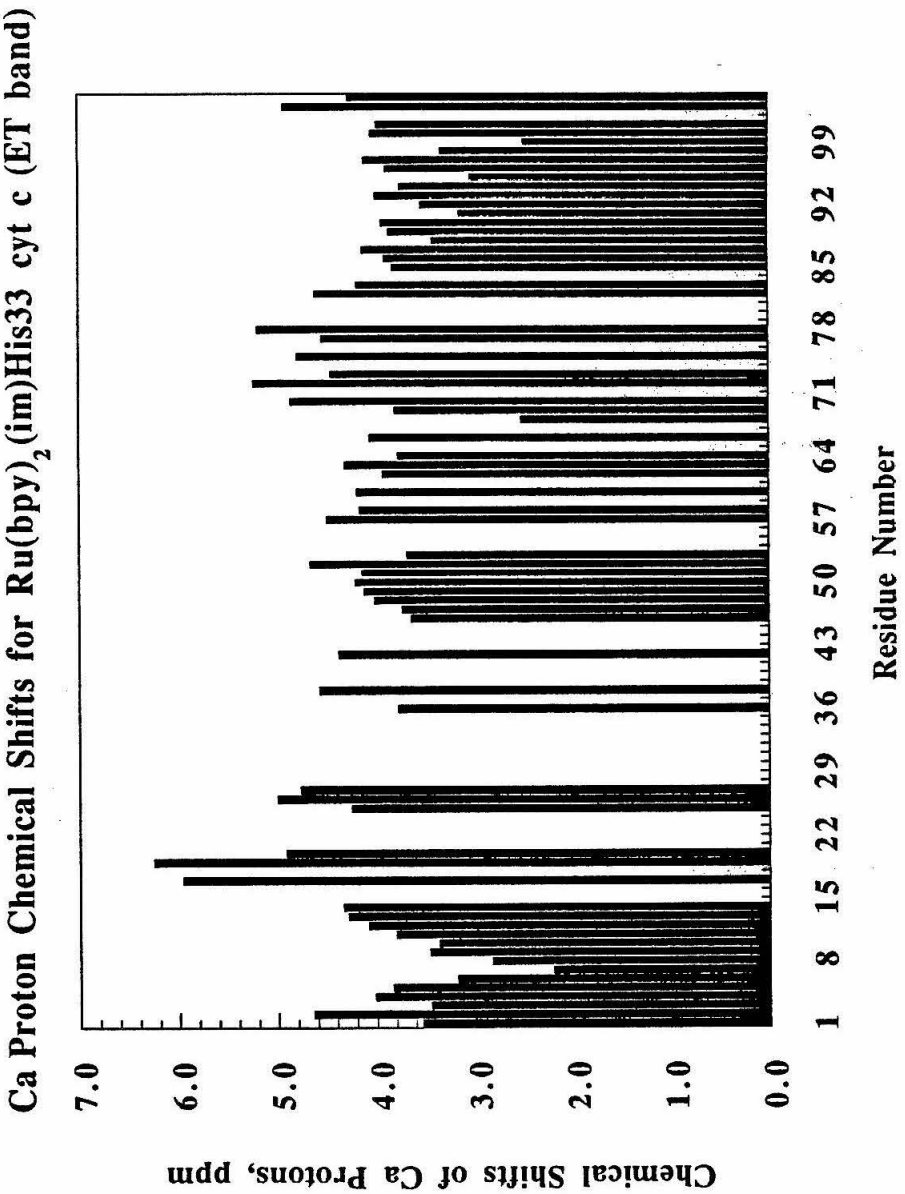
Ca Proton Chemical Shifts for Ru(bpy)2(im)His33 cyt c (ET band)
Chemical Shifts of Ca Protons, ppm
7.0
6.0
5.0
4.0
3.0
2.0
1.0
0.0
1 8 15 22 29 36 43 50 57 64 71 78 85 92 99
Residue Number

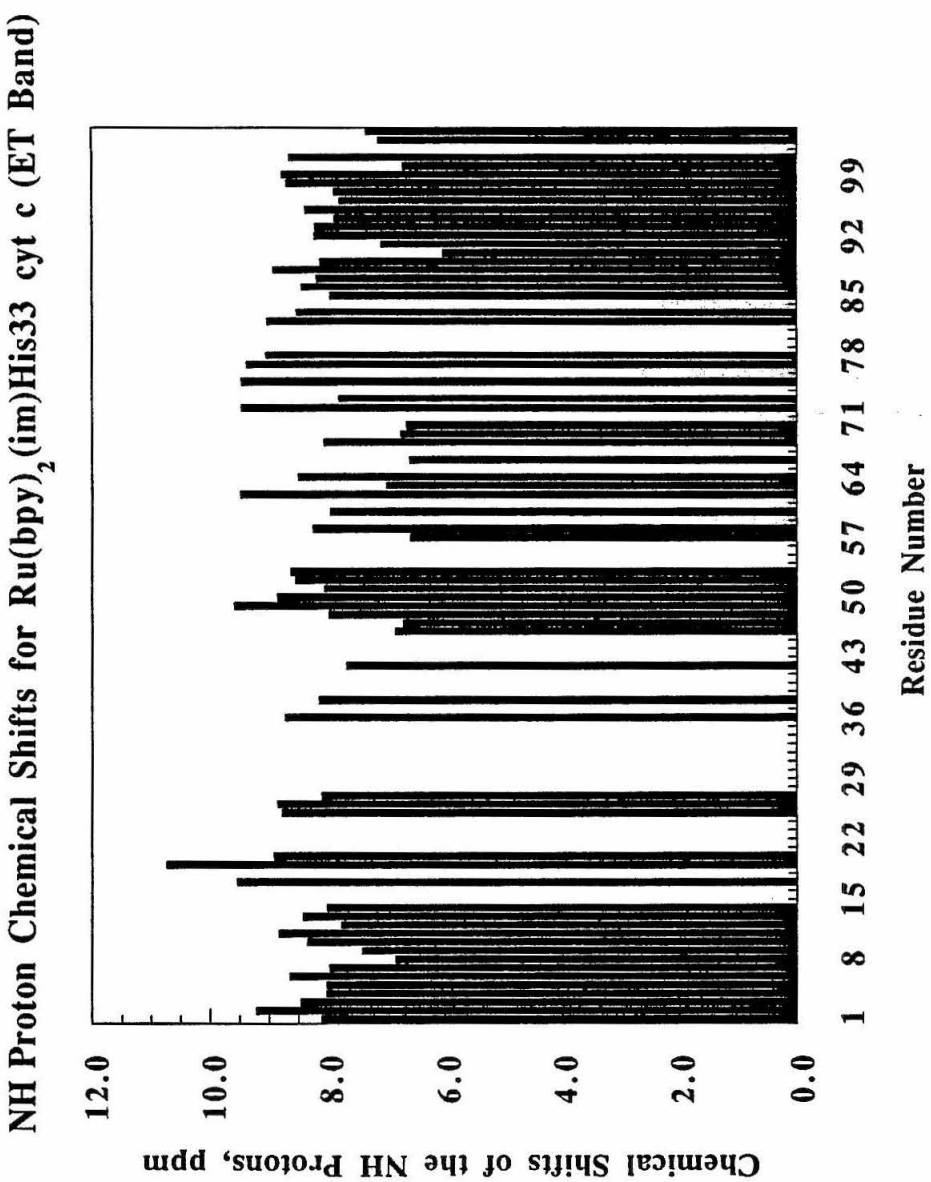
NH Proton Chemical Shifts for Ru(bpy)2(im)His33 cyt c (ET Band)
Chemical Shifts of the NH Protons, ppm
12.0
10.0
8.0
6.0
4.0
2.0
0.0
1 8 15 22 29 36 43 50 57 64 71 78 85 92 99
Residue Number

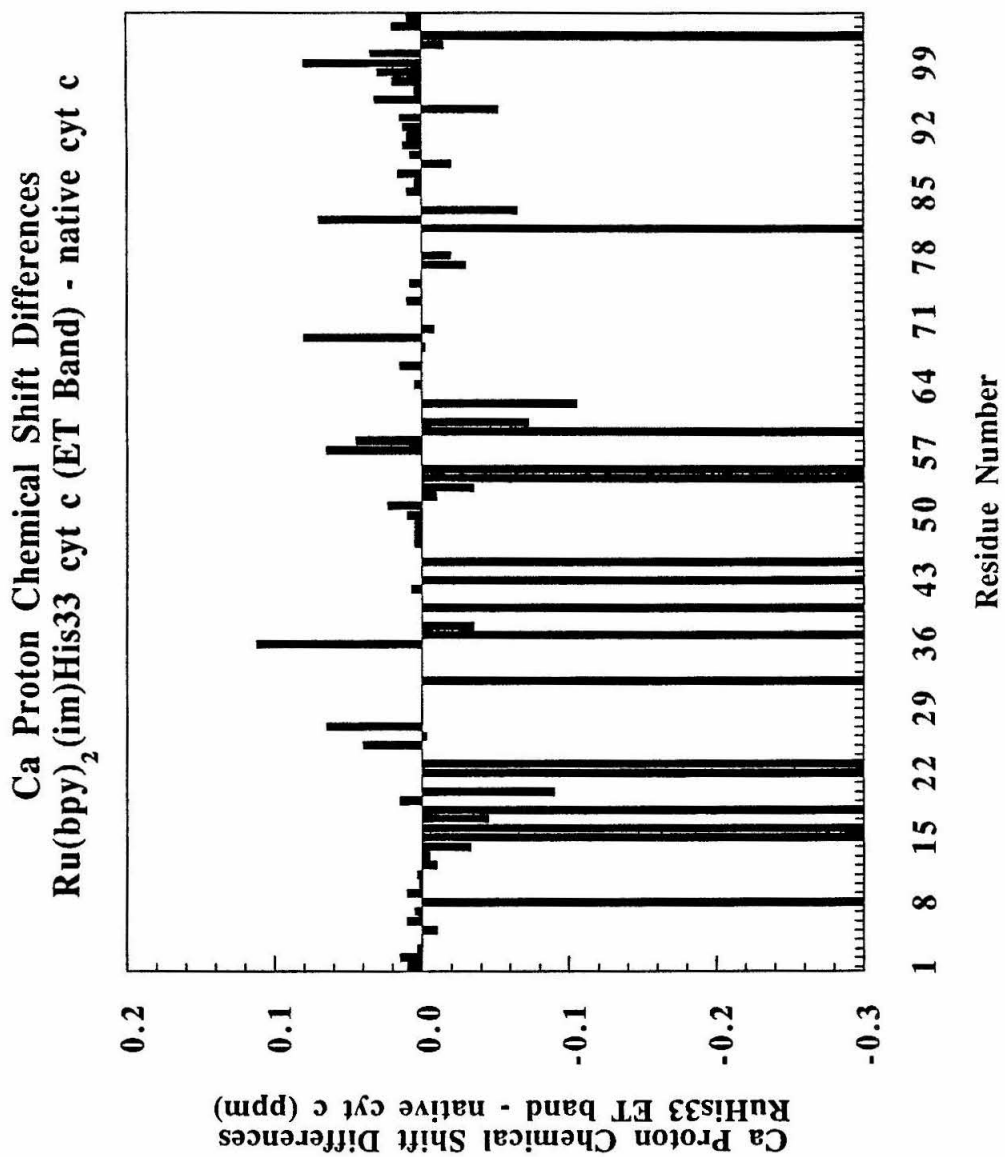
Ca Proton Chemical Shift Differences
Ru(bpy)2(im)His33 cyt c (ET Band) - native cyt c
Ca Proton Chemical Shift Differences
RuHis33 ET band - native cyt c (ppm)
0.2
0.1
0.0
-0.1
-0.2
-0.3
1 8 15 22 29 36 43 50 57 64 71 78 85 92 99
Residue Number

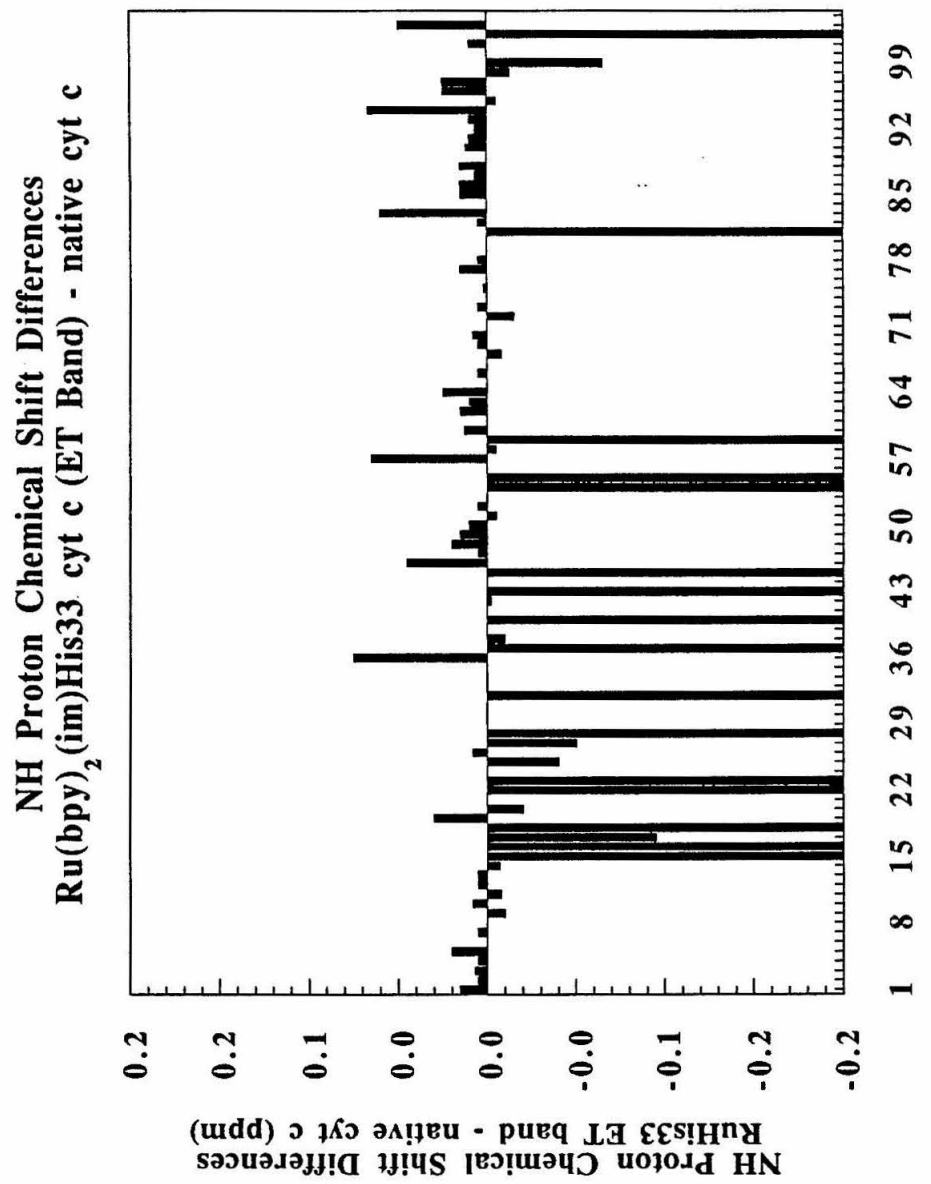
NH Proton Chemical Shift Differences
Ru(bpy)2(im)His33 cyt c (ET Band) - native cyt c
NH Proton Chemical Shift Differences
RuHis33 ET band - native cyt c (ppm)
0.2
0.2
0.1
0.0
0.0
-0.0
-0.1
-0.2
-0.2
1 8 15 22 29 36 43 50 57 64 71 78 85 92 99
Residue Number

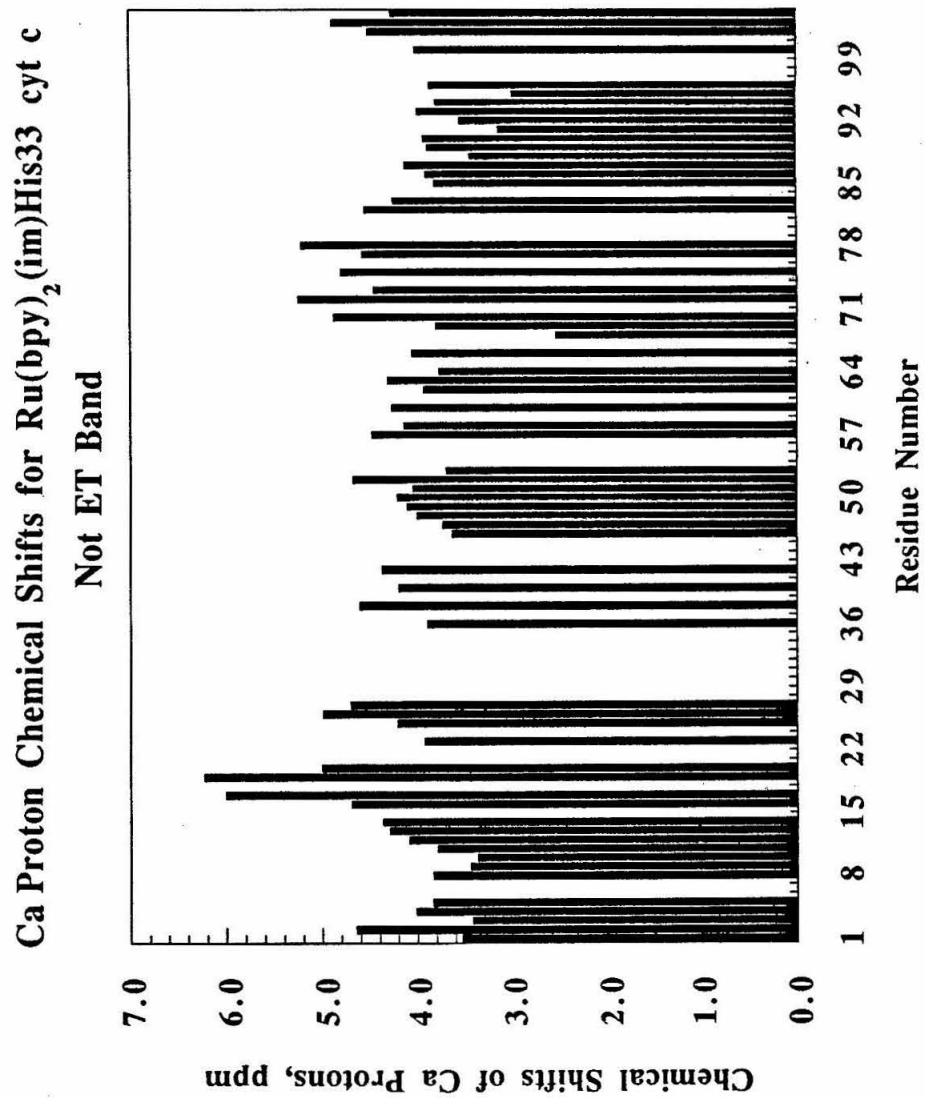
Ca Proton Chemical Shifts for Ru(bpy)2(im)His33 cyt c
Not ET Band
Chemical Shifts of Ca Protons, ppm
7.0
6.0
5.0
4.0
3.0
2.0
1.0
0.0
1 8 15 22 29 36 43 50 57 64 71 78 85 92 99
Residue Number

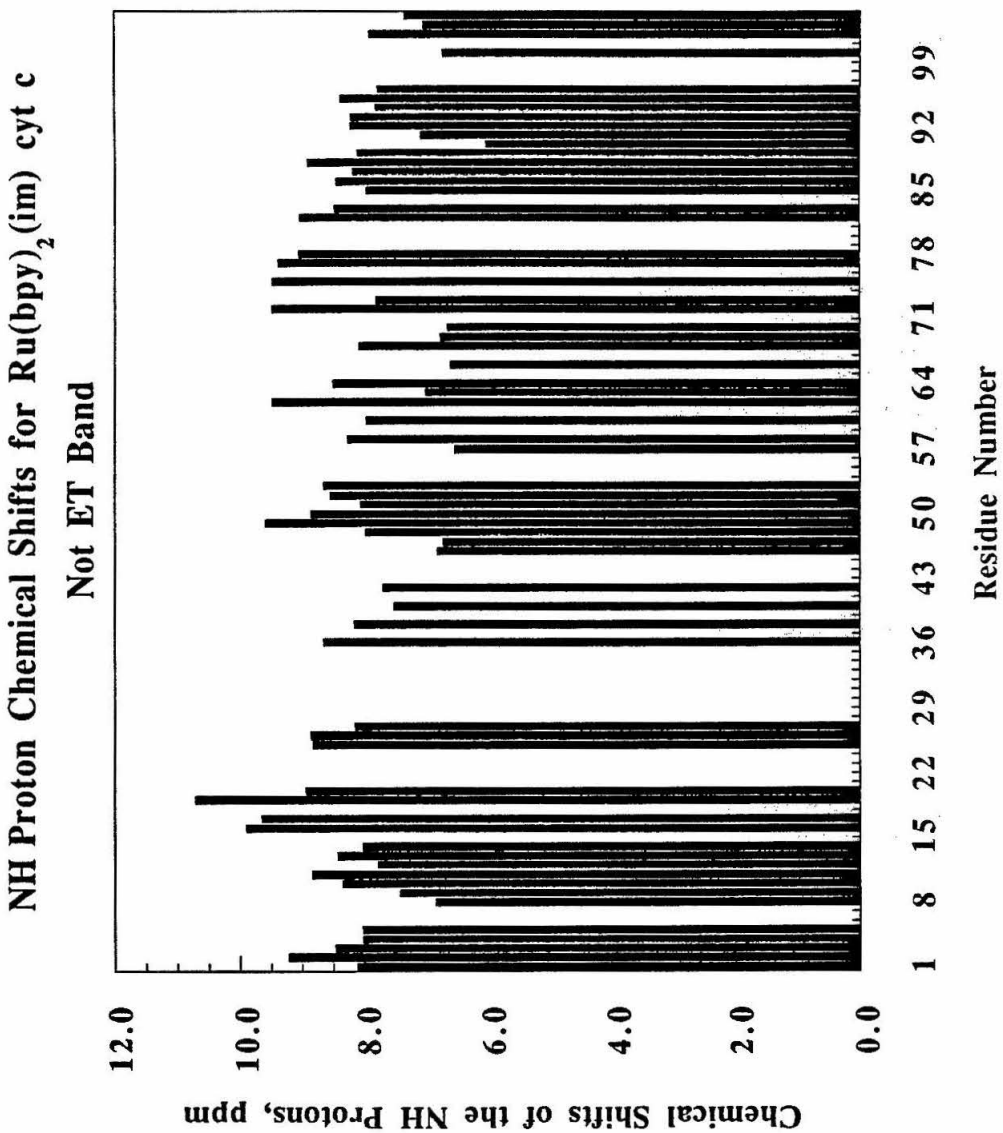
NH Proton Chemical Shifts for Ru(bpy)2(im) cyt c
Not ET Band
Chemical Shifts of the NH Protons, ppm
12.0
10.0
8.0
6.0
4.0
2.0
0.0
1 8 15 22 29 36 43 50 57 64 71 78 85 92 99
Residue Number

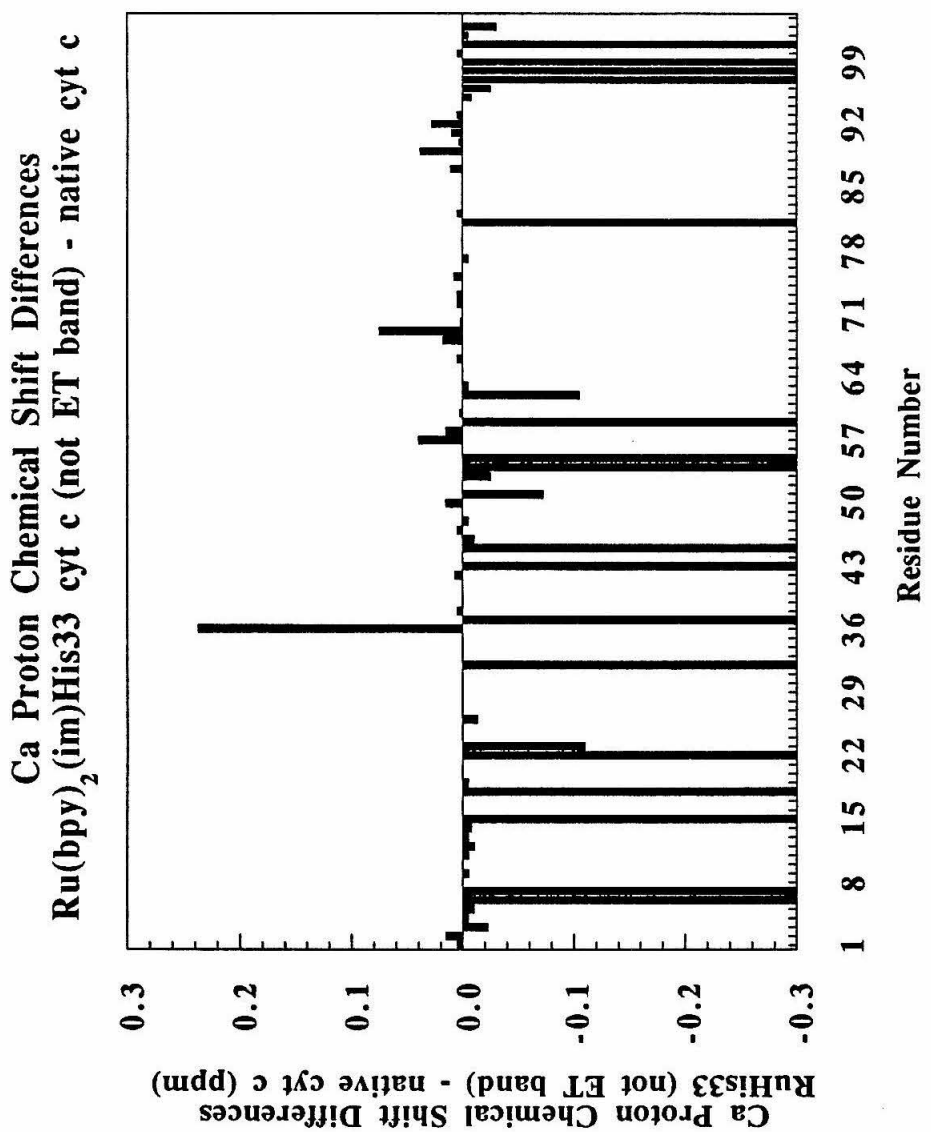
Ca Proton Chemical Shift Differences
Ru(bpy)2(im)His33 cyt c (not ET band) - native cyt c
Ca Proton Chemical Shift Differences
RuHis33 (not ET band) - native cyt c (ppm)
0.3
0.2
0.1
0.0
-0.1
-0.2
-0.3
1 8 15 22 29 36 43 50 57 64 71 78 85 92 99
Residue Number

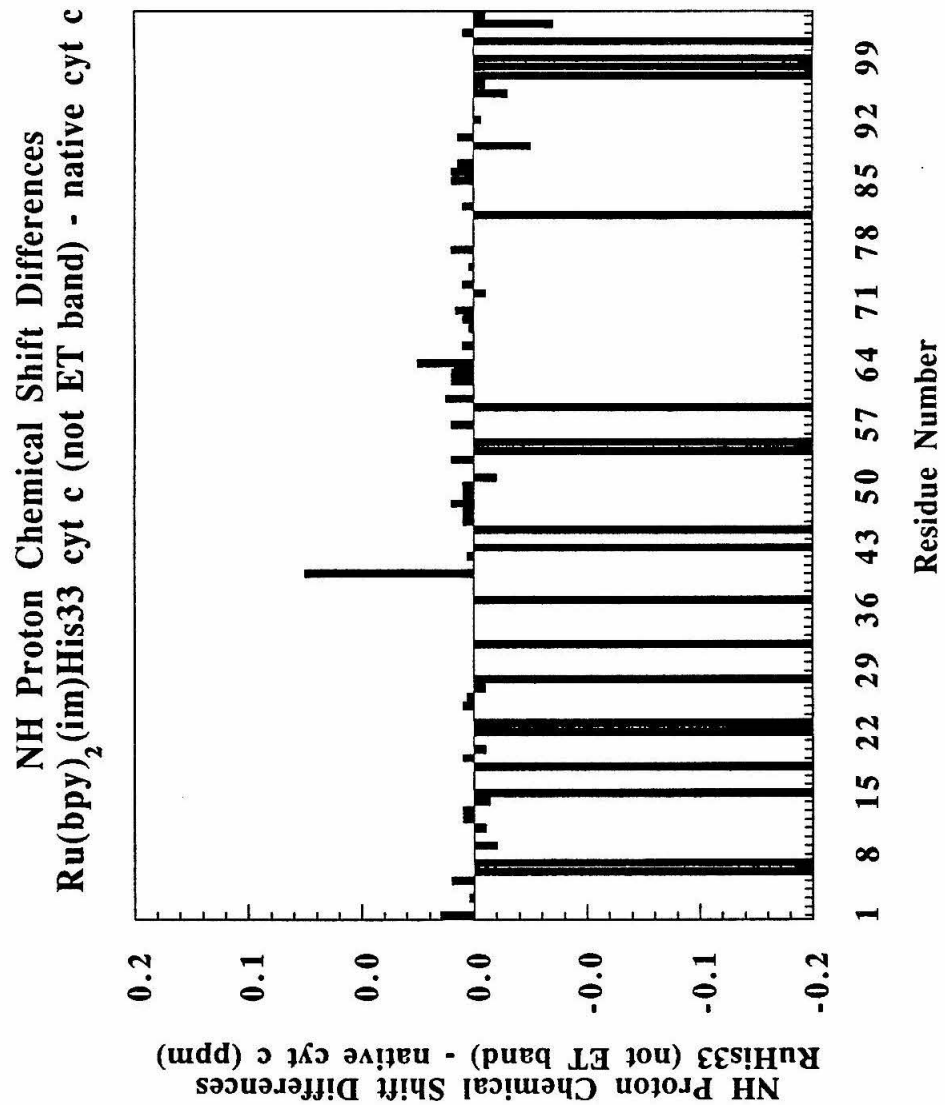
NH Proton Chemical Shift Differences
Ru(bpy)2(im)His33 cyt c (not ET band) - native cyt c
NH Proton Chemical Shift Differences
RuHis33 (not ET band) - native cyt c (ppm)
0.2
0.1
0.0
0.0
-0.0
-0.1
-0.2
1 8 15 22 29 36 43 50 57 64 71 78 85 92 99
Residue Number

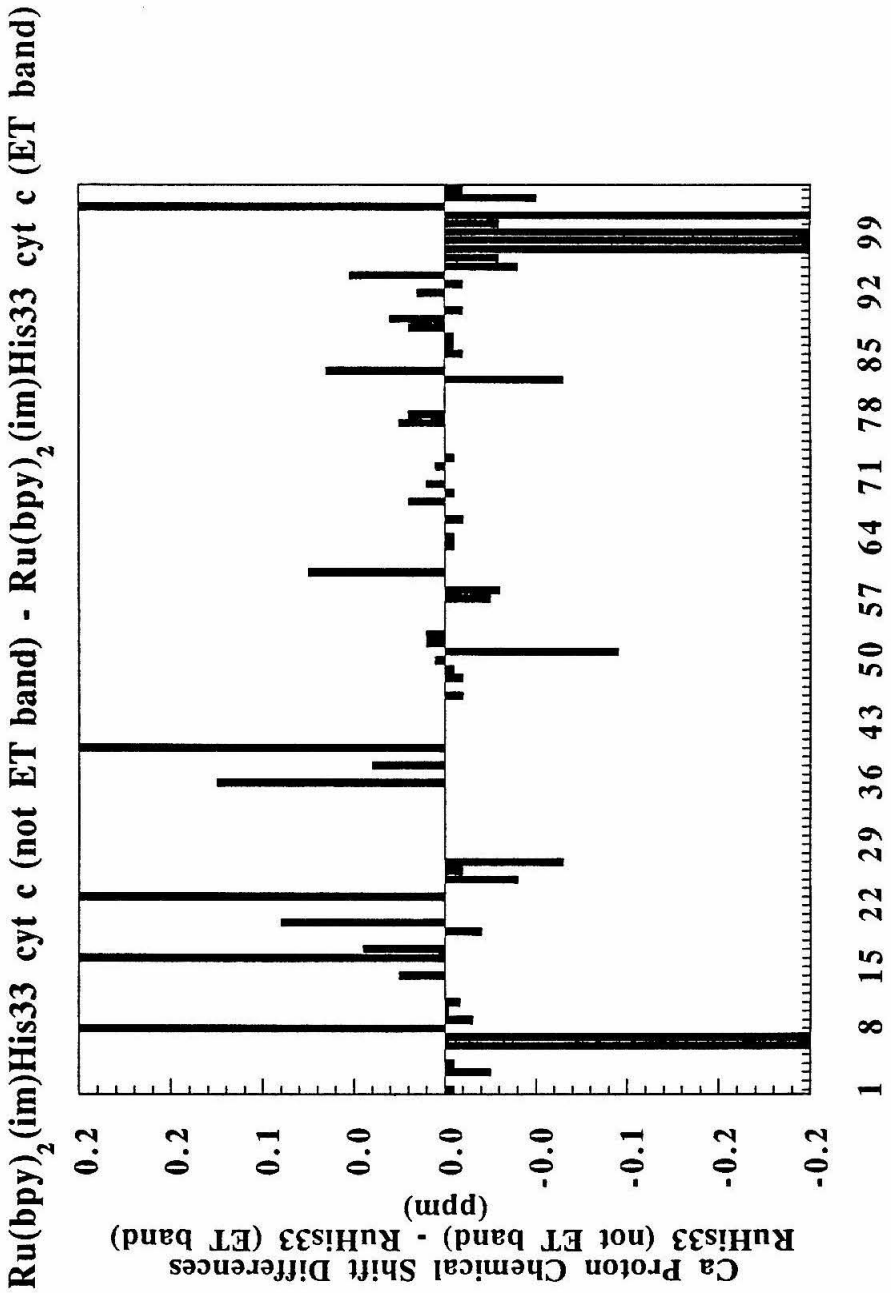
Ca Proton Chemical Shift Differences
Ru(bpy)2(im)His33 cyt c (not ET band) - Ru(bpy)2(im)His33 cyt c (ET band)
Ca Proton Chemical Shift Differences
RuHis33 (not ET band) - RuHis33 (ET band)
(ppm)
0.2
0.2
0.1
0.0
0.0
-0.0
-0.1
-0.2
-0.2
1 8 15 22 29 36 43 50 57 64 71 78 85 92 99
Residue Number

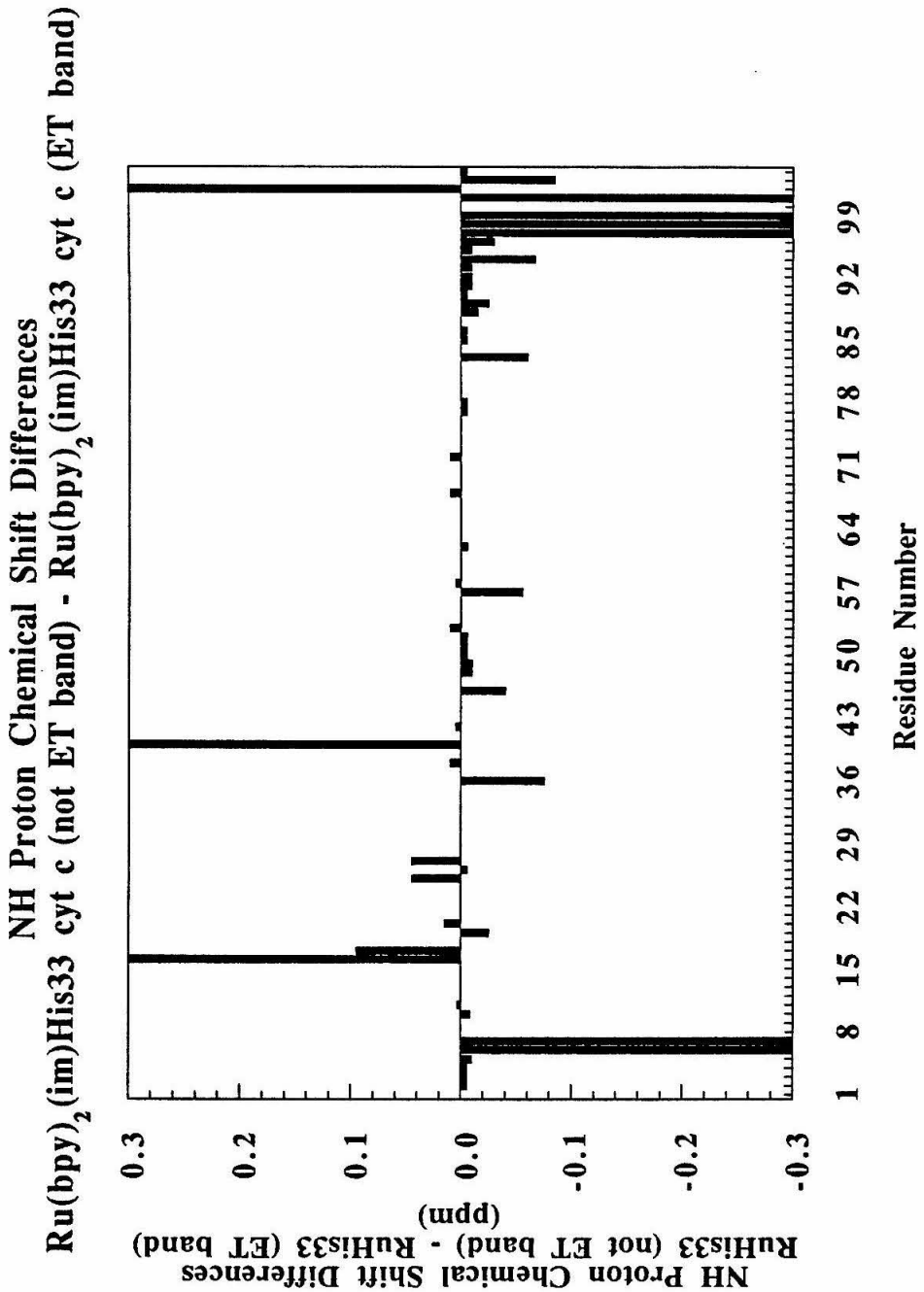
NH Proton Chemical Shift Differences
Ru(bpy)2(im)His33 cyt c (not ET band) - Ru(bpy)2(im)His33 cyt c (ET band)
NH Proton Chemical Shift Differences
RuHis33 (not ET band) - RuHis33 (ET band)
(ppm)
0.3
0.2
0.1
0.0
-0.1
-0.2
-0.3
1 8 15 22 29 36 43 50 57 64 71 78 85 92 99
Residue Number

Appendix B

Spectroscopic Characterization of an Axial Ligand Mutant:
His72Cys80 Cytochrome *c*

It has been previously demonstrated in this group that the semisynthetic methodology could be employed for the generation of axial ligand mutants at position 80 of cyt *c*.[1] Specifically, high yields of a Met80 to Cys mutant were obtained. This axial ligand replacement dramatically altered the spectroscopic and electrochemical features of the protein. The Soret and α,β bands of the ferric absorption spectrum are red-shifted to 416 and 540 nm, respectively, and two new charge transfer bands are observed at 635 and 740 nm. The spectrum of the ferric state closely resembles that of ferric cytochrome P450, implying intact Cys ligation. The absorption spectrum of ferrous Cys80 cyt *c*, however, is nearly identical with ferrous native cyt *c*, implying loss of cysteine ligation upon reduction. The reduced state is dramatically destabilized; the protein reduction potential is shifted over half of an electron volt relative to native cyt *c* to - 390 mV *vs.* NHE.[1] The MCD spectrum of ferric Cys80 cyt *c* in the visible region (300 - 750 nm) correlates well with the imidazole adduct of cytochrome P450, supporting the model of intact Cys/His ligation in ferric Cys80 cyt *c*.

In an effort to exploit the ET potential of this variant, a Cys80 His72 mutant was constructed semisynthetically following the protocols described previously (Chapter 2). The reconstitution reaction afforded a high yield of the axial ligand mutant. EPR, ^{1}H NMR, CD, and mass spectrometry measurements were made on this variant. His72Cys80 cyt *c* was subsequently derivatized with $Ru(bpy)_2(CO_3)$ using the protocols outlined in Chapter 3. The His72-modified protein was identified by analogy with the His72 cyt *c* cation-exchange chromatograms and used for ET studies. The results of these investigations are detailed below.

EPR

The EPR spectrum of His72Cys80 cyt *c* was measured at 33K in 50 mM HEPES, 50% glycerol, pH 7.0. The spectrum obtained (Figure B.1) differed dramatically from that of native cyt *c* (Figure 2.17). *g*-values were 2.563, 2.274 and 1.846. These values

correlate well with those reported for the imidazole adduct of cytochrome P450[3]; g = 2.56, 2.27, 1.87. Inclusion of this point on the heme "truth table"[4] (rhombicity (V / Δ) *vs.* tetragonal field (Δ / λ)) places it directly in the region of Cys-ligated hemes.

NMR

The ^{1}H NMR spectrum of His72Cys80 cyt *c* exhibits perturbed chemical shifts of the paramagnetically shifted resonances in the far upfield and downfield regions of the spectrum (Figure B.2 A, refer to Figure 2.21 for native cyt *c*). The experimental conditions are discussed in Appendix A, T = 315 K. Note the extremely broadened peaks and the lack of sharp hypershifted resonances. Due to the altered paramagnetic properties of the unpaired electron, the ^{1}H NMR spectrum in the normal region (Figure B.2 B) could not be assigned by comparison with the native spectrum.

Circular Dichroism

The circular dichroism spectrum of His72Cys80 cyt *c* in the far UV region indicates approximately equivalent or slightly greater α-helicity than native cyt *c* (Figure B.3 A). Since the precise extinction coefficients for the mutant are not known, a direct comparison between the native and mutants proteins can not be made. Spectra were collected at progressively higher temperatures to determine the melting transition temperature, however, the protein did not exhibit significant loss of α-helicity even at 93° C. The melting temperature of the His72Cys80 variant must be higher than 100° C.

MCD

John Dawson's group continued work on the Cys80 mutants with His72Cys80 cyt *c*. Sufficient sample could be provided to investigate the MCD signal in the near-IR region of the spectrum. This region is thought to be more diagnostic for axial ligand assignments than the visible region of the spectrum. The His72Cys80 cyt *c* protein

exhibits a near-IR MCD spectrum virtually identical with that of 1-methylimidazole cytochrome P450 (1-methyl imidazole P450 possesses signals at 736 and 1148 nm; His72Cys80 cyt c possesses signals at 734 and 1148 nm) and differs from His/His, His/Met and His/H_2O ligated proteins. These data provide further evidence for the Cys/His ligation assignment in the ferric state. A combination of the EPR, MCD and charge-transfer band data from a series of heme proteins can be used to unambiguously assign the ligation state.[5]

Mass Spectrometry

Thermospray mass spectra were obtained on a Vestec Thermospray LC-Mass Spectrometer in the laboratories of Prof. C. Monig. The measured results were consistent with calculated masses. Masses obtained were: native horse heart cyt *c*, 12380(12) (calculated, 12364); His72Cys80 cyt *c*, 12333(12) (calculated, 12315).

Electron-Transfer Studies

The $Ru(bpy)_2(im)His72^{2+}$ - Cys80 cyt *c* derivative was isolated in high yield. The luminescence decay was measured at 650 nm, $k_d = 1.7 \times 10^7\ s^{-1}$ (60 ns). In the absence of quencher, no transiently generated products due to photoinduced ET were observed in the transient absorption traces collected at wavelengths corresponding to large $\Delta\varepsilon$ for the Fe^{3+} / Fe^{2+} states. This is not unexpected, as the driving force for photoreduction is low ($-\Delta G^o = -0.56$ eV). It was believed that the $Fe^{4+/3+}$ couple may be accessible, however addition of an oxidative quencher, $[Rua_6]Cl_3$, to transiently form a $Ru(bpy)_2(im)His72^{3+}$ species on the protein surface perhaps capable of oxidizing the Fe^{3+} heme did not produce any transients other than those expected for the $Ru(bpy)_2(im)His72^{3+}$ species. This mutant is not amenable to ET studies with the techniques developed thus far.

References

1. Raphael, A. L.; Gray, H. B. *J. Am. Chem. Soc.* **1991**, *113*, 1038.

2. Rux, J. J.; Dawson, J. H. *FEBS Lett.* **1991**, *1-2*, 49.

3. Lipscomb, J. D. *Biochemistry* **1980**, *9*, 3590. Dawson, J. H.; Andersson, L. A.; Sono, M. *J. Biol. Chem.* **1982**, *257*, 3606.

4. Blumberg, W. E.; Peisach, J. in *Probes of Structure and Function in Macromolecules and Membranes* Chance, B.; Yonetani, T.; Mildvan, A. S. Eds. (Academic Press: New York) 1969, pp. 215 - 227.

5. Gadsby, P. M.; Thomson, A. J. *J. Am. Chem. Soc.* **1990**, *112*, 5003.

Figure B.1 EPR spectrum of His72Cys80 cyt *c* obtained in 50 mM HEPES, 50% glycerol, pH 7.0 glass at 33 K.

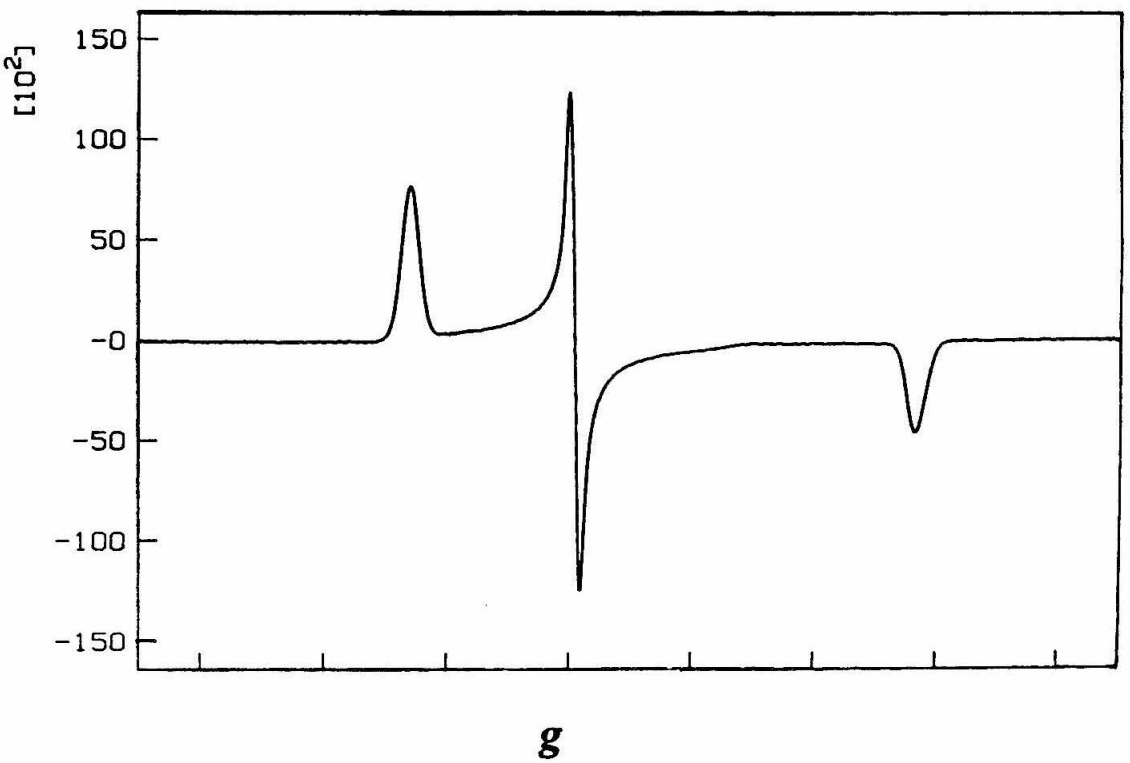
150
100
50
-0
-50
-100
-150
[10²]
g

Figure B.2 ^{1}H NMR spectrum of His72Cys80 cyt *c* obtained in 90% D_2O/ 10% H_2O, 100 mM NaPi, 150 mM NaCl, pH 5.74 at 315 K; (A) hyperfine-shifted region and (B) normal region of the spectrum.

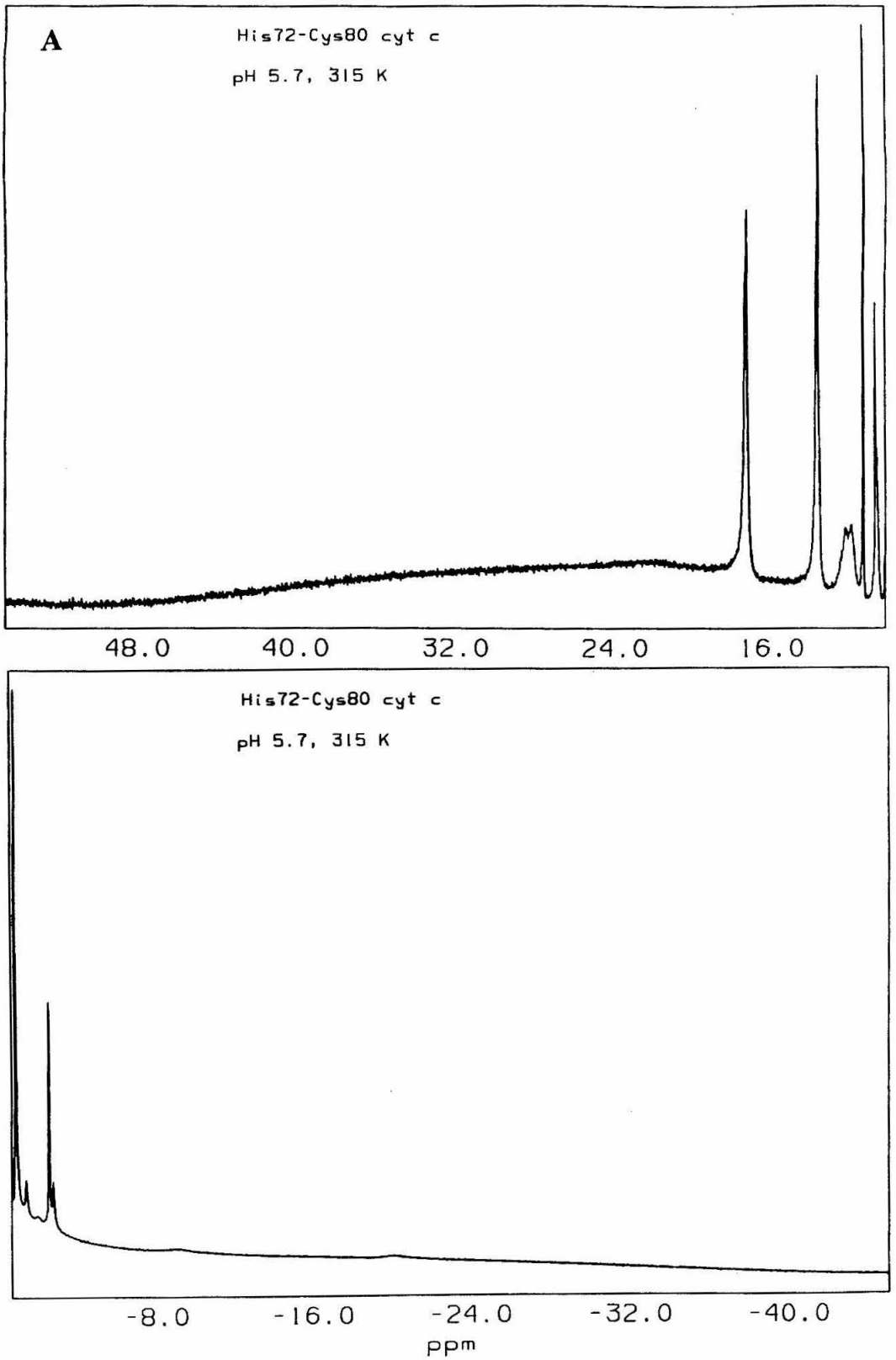
A
His72-Cys80 cyt c
pH 5.7, 315 K
48.0
40.0
32.0
24.0
16.0
His72-Cys80 cyt c
pH 5.7, 315 K
-8.0
-16.0
-24.0
-32.0
-40.0
ppm

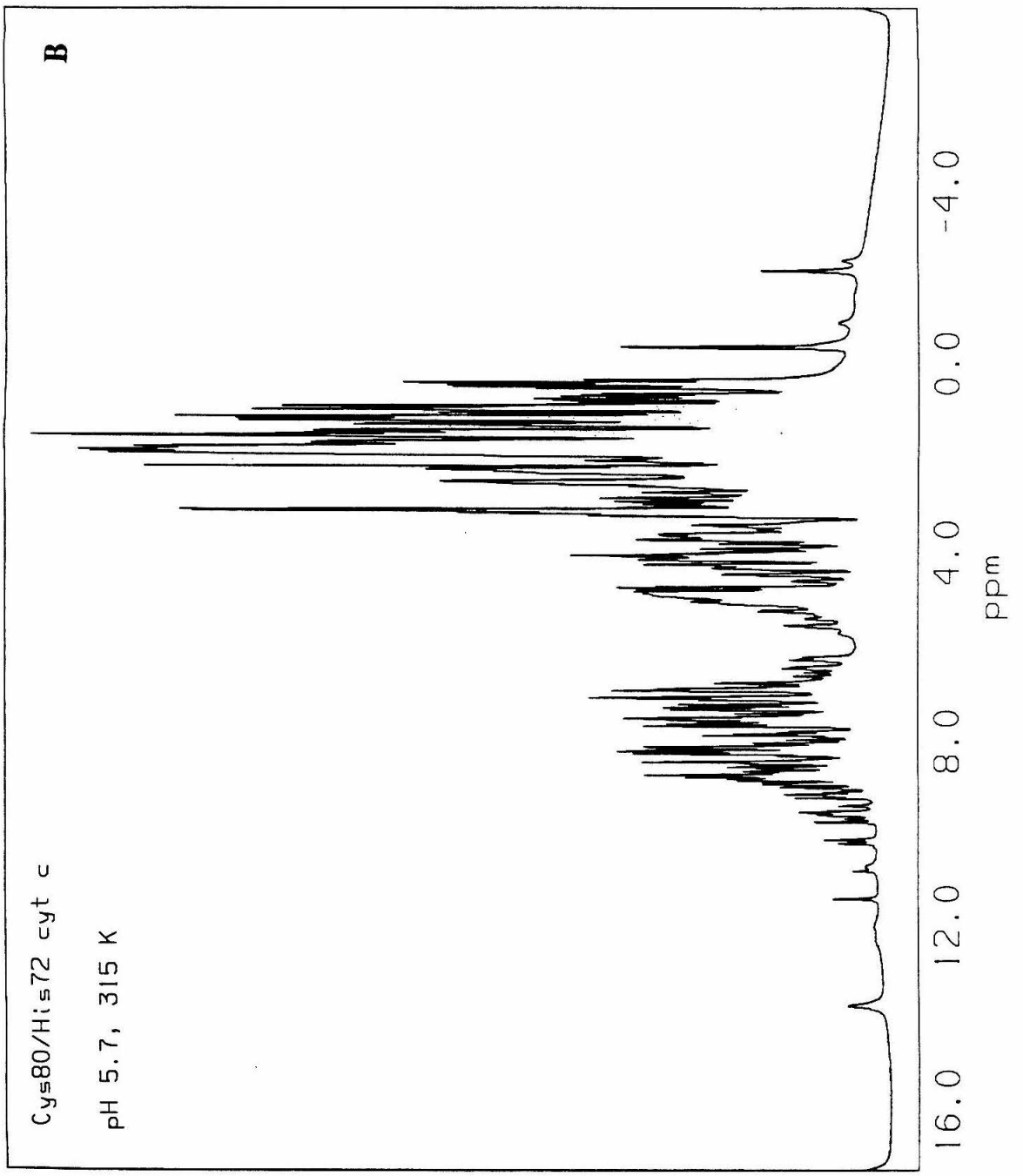
B
Cys80/His72 cyt c
pH 5.7, 315 K
16.0
12.0
8.0
4.0
0.0
-4.0
ppm

Figure B.3 Circular dichroism data obtained with a ~10 μM sample of His72Cys80 cyt *c* in 50 mM NaPi, pH 7.0; (A) far UV region of the spectrum at ambient temperature and (B) signal at 222 nm as a function of temperature. The signal should be ~-8 mdeg for the random-coil form.

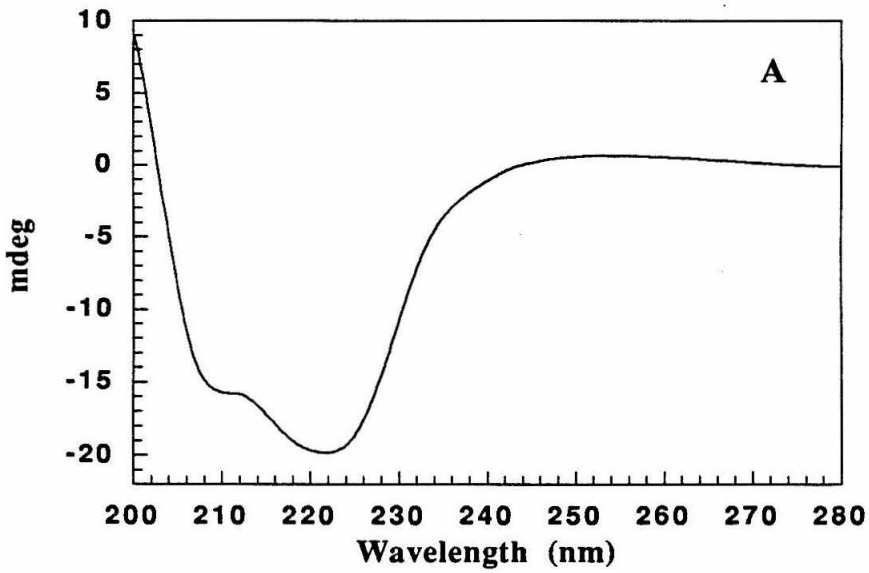
A
10
5
0
-5
-10
-15
-20
mdeg
200
210
220
230
240
250
260
270
280
Wavelength (nm)

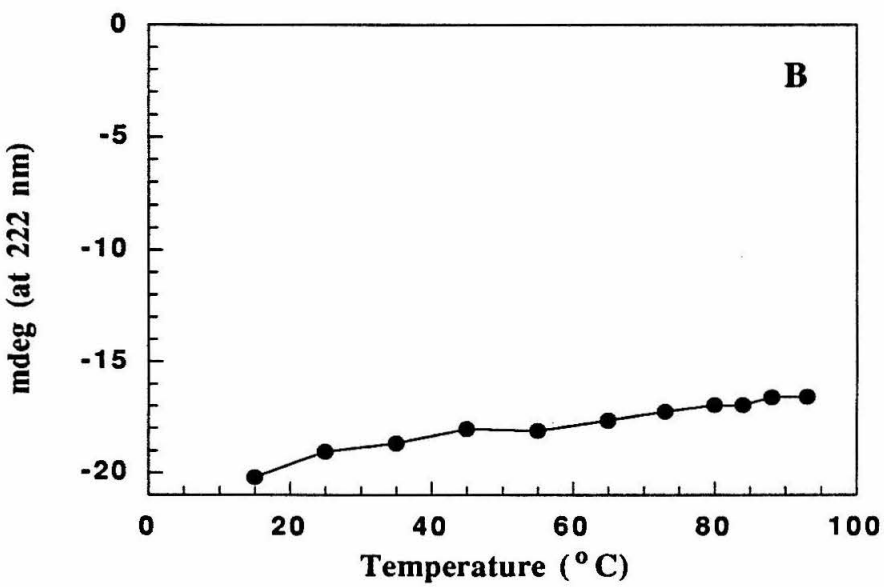
B
0
-5
-10
-15
-20
mdeg (at 222 nm)
0
20
40
60
80
100
Temperature (°C)